OKLAHOMA GEOLOGICAL SURVEY
Charles J. Mankin, *Director*

CIRCULAR 100

ISSN 0078-4397

Ames Structure in Northwest Oklahoma and Similar Features: Origin and Petroleum Production (1995 Symposium)

KENNETH S. JOHNSON AND JOCK A. CAMPBELL
Editors

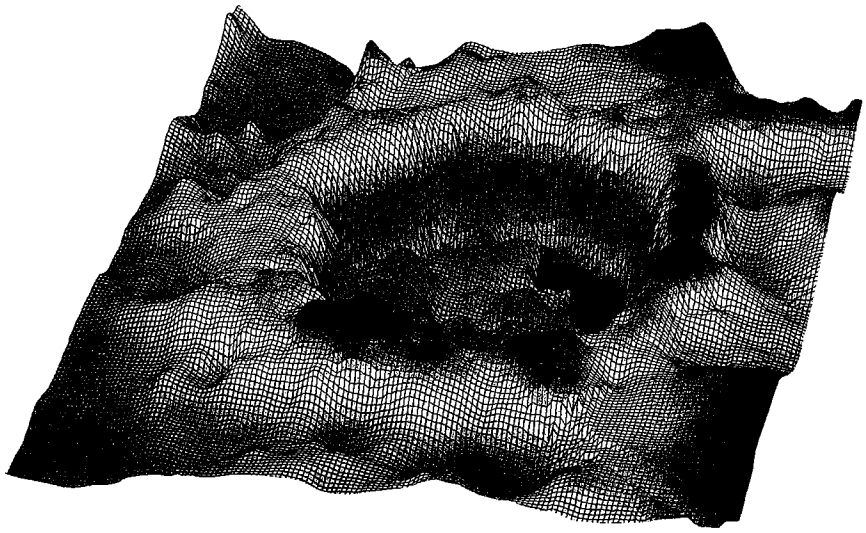

Proceedings of a symposium held March 28–29, 1995, in Norman, Oklahoma.

Co-sponsored by:
Oklahoma Geological Survey
and
Bartlesville Project Office,
U.S. Department of Energy

The University of Oklahoma
Norman
1997

ERRATA

Oklahoma Geological Survey Circular 100

Ames Structure Symposium

Page 10, right column, line 13 — "3,440 MMCF" should read "3.44 MMCF"

General Note: The D. & J. Oil Company no. 1-20 Gregory was the first oil well drilled within the Ames crater. Drilling started in October 1991 and was completed in November 1991.

OKLAHOMA GEOLOGICAL SURVEY

CHARLES J. MANKIN, *Director*
KENNETH S. JOHNSON, *Associate Director*

SURVEY STAFF

JAMES H. ANDERSON, *Cartographic Draftsperson III*
RICHARD D. ANDREWS, *Geologist III*
LARRY T. AUSTIN, *Log Library Assistant*
BETTY D. BELLIS, *Word-Processing Operator II / Technical Typist*
TOM L. BINGHAM, *Geologist II*
MITZI G. BLACKMON, *Clerk-Typist I*
RAYMON L. BROWN, *Geophysicist*
JOCK A. CAMPBELL, *Petroleum Geologist IV*
BRIAN J. CARDOTT, *Geologist IV*
JAMES R. CHAPLIN, *Geologist IV*
JANISE L. COLEMAN, *Office Assistant IV*
CHRISTIE L. COOPER, *Editor*
TAMMIE K. CREEL, *Secretary II*
CHARLES R. DYER III, *Drilling Technician*
WALTER C. ESRY, *Manager, Core and Sample Library*
ROBERT O. FAY, *Geologist IV*
T. WAYNE FURR, *Manager of Cartography*
PATRONALIA M. HANLEY, *Chemist*
LEROY A. HEMISH, *Coal Geologist IV*
JOHN HUMPHREY, *Operations Assistant I*
SHIRLEY A. JACKSON, *Research Specialist I*
PRISCILLA A. JOHNSON, *Office Assistant IV*
JAMES E. LAWSON, JR., *Chief Geophysicist*
CHARLOTTE C. LLOYD, *Cartographic Draftsperson II*
KENNETH V. LUZA, *Engineering Geologist IV*
TODD S. MCCORMICK, *Electronic Technician*
MICHAEL J. MERCER, *Manager, Log Library*
RICHARD G. MURRAY, *Copy Center Operator*
SUE M. PALMER, *Office Assistant II*
TRACY P. PEETERS, *Associate Editor*
DAVID O. PENNINGTON, *Operations Assistant II*
JUDY A. SCHMIDT, *Office Manager*
CONNIE G. SMITH, *Promotion and Information Specialist*
PAUL E. SMITH, *Supervisor, Offset Press Copy Center*
JOYCE A. STIEHLER, *Chief Clerk*
MICHELLE J. SUMMERS, *Technical Project Coordinator*
NEIL H. SUNESON, *Stratigrapher / Geologist IV*
JANE L. WEBER, *Coordinator, Departmental Computer Systems*
STEPHEN J. WEBER, *Chief Chemist*

Title-Page Illustration

Three-dimensional, computer-generated diagram of the Ames structure, based on a second-order residual map drawn on top of the Sylvan Shale. Viewed toward the south-southeast, from an elevation of 40° above the horizon. Prepared by Rick A. Carlson, DLB Oil and Gas, Inc., Oklahoma City.

♻ *printed on recycled paper*

This publication, printed by the Oklahoma Geological Survey, is issued by the Oklahoma Geological Survey as authorized by Title 70, Oklahoma Statutes, 1981, Sections 231–238. 1,500 copies have been prepared for distribution at a cost of $18,175 to the taxpayers of the State of Oklahoma. Copies have been deposited with the Publications Clearinghouse of the Oklahoma Department of Libraries.

PREFACE

The transfer of technical information will aid in the search for, and production of, our oil and gas resources. To facilitate this technology transfer, the Oklahoma Geological Survey (OGS) and the Bartlesville Project Office of the U.S. Department of Energy (BPO-DOE) cosponsored a symposium dealing with the search for, and production of, oil and gas resources from meteorite-impact craters. The focus of the symposium was on the Ames structure, an Early Ordovician circular structure formed in northwestern Oklahoma by meteorite impact, volcanic activity, or dissolution and collapse. The structure is 6–10 mi across, is buried by 9,000 ft of younger sedimentary units, and is a prolific source of oil and gas. Information also was presented on similar features elsewhere in the world. The symposium was held on March 28–29, 1995, at the Oklahoma Center for Continuing Education, The University of Oklahoma, Norman. This volume contains the proceedings of that symposium.

Research reported upon at the symposium focused on meteorite-impact craters, exploration, hydrocarbon occurrences, reservoir characterization, geochemistry, remote sensing, recognition criteria, and alternative interpretations for the origin of the Ames structure. In describing the Ames structure and similar features, and their related petroleum reservoirs, the researchers have increased our understanding of how the geologic history of an area can affect reservoir heterogeneity and our ability to efficiently recover the hydrocarbons they contain. We hope that the symposium and these proceedings will bring such research to the attention of the geoscience and energy-research community and will help foster exchange of information and increased research interest by industry, university, and government workers.

Twenty-four papers were presented orally at the symposium, and they are presented here as full papers or abstracts. An additional 17 reports were given as posters, and they are presented here as short reports or abstracts. In each of the two parts of this volume, papers are arranged as follows: (1) general papers on impact craters, (2) the Ames structure, and (3) similar features elsewhere in North America. About 225 persons attended the symposium. Stratigraphic nomenclature and age determinations used by the various authors in this volume do not necessarily agree with those of the OGS.

This is the eighth symposium in as many years dealing with topics of major interest to geologists and others involved in petroleum-resource development in Oklahoma and adjacent states. These symposia are intended to foster the exchange of information that will improve our ability to find and recover our nation's oil and gas resources. Earlier symposia covered the Anadarko basin (published as OGS Circular 90), Late Cambrian–Ordovician geology of the southern Midcontinent (OGS Circular 92), source rocks in the southern Midcontinent (OGS Circular 93), petroleum-reservoir geology in the southern Midcontinent (OGS Circular 95), structural styles in the southern Midcontinent (OGS Circular 97), fluvial-dominated deltaic reservoirs in the southern Midcontinent (OGS Circular 98), and Simpson and Viola Groups in the southern Midcontinent (OGS Circular 99).

Persons involved in the organization and planning of the Ames structure symposium include Kenneth Johnson, Jock Campbell, and Charles Mankin of the OGS and Tom Wesson, Michael Ray, and Herb Tiedemann of BPO-DOE. Other personnel who contributed include Michelle Summers and Tammie Creel, Registration Co-Chairs; LeRoy Hemish, Poster-Session Chair; Connie Smith, Publicity Chair; and Judy Schmidt, Exhibits Coordinator. Technical editing of this volume was done by Mary Eberle, Wordrite, Boulder, Colorado; layout and production was done by Sandra Rush, Rush Services, Denver, Colorado. Appreciation is expressed to each of them and to the many authors who worked toward a highly successful symposium.

KENNETH S. JOHNSON and
JOCK A. CAMPBELL
General Chairmen

CONTENTS

PART I

PAPERS PRESENTED ORALLY AT THE SYMPOSIUM

Terrestrial Impact Structures: Basic Characteristics and Economic Significance, with Emphasis on Hydrocarbon Production

Richard A. F. Grieve
Continental Geoscience Division
Geological Survey of Canada
Ottawa, Canada

ABSTRACT.—An introduction is provided to the literature on terrestrial impact structures and their economic, particularly hydrocarbon, deposits. The basic morphologic and morphometric characteristics of terrestrial impact structures are illustrated, along with the criteria for their recognition. Some progenetic and syngenetic examples of associated economic deposits are summarized, including world-class deposits in the Witwatersrand basin, South Africa (gold and uranium) and at Sudbury, Canada (copper, nickel, platinum-group elements). Hydrocarbon deposits in impact structures are epigenetic and occur generally in the central uplifted area of complex impact structures and in the rim area of both complex and simple impact structures. In some cases, the impact structure not only hosts the reservoir rocks, it also provides the central topographic basin in which the organic-rich postimpact sediments are deposited that then become source rocks. Examples of hydrocarbon-bearing impact structures, mostly from North America, are illustrated. It is also noted that much of the oil production from the Campeche fields, Gulf of Mexico, may be linked to the formation of breccia reservoir rocks by the Chicxulub impact event, which occurred at the Cretaceous/Tertiary boundary.

INTRODUCTION

The current awareness of the nature and occurrence of terrestrial impact structures is such that new discoveries are being made by members of the general geoscience community just as often as by specialists in the study of impact structures. Some well-known economic deposits are located within impact structures. Of the almost 160 known terrestrial impact structures (Grieve and Shoemaker, 1994), ≈35 have some form of potentially economic deposits. The number currently, or in the relatively recent past, producing some form of economic resources is ≈20. Economic deposits related to impact structures can be subdivided into progenetic, syngenetic, and epigenetic deposits and are considered in some detail in Grieve and Masaitis (1994). They are summarized here, with emphasis on hydrocarbon-bearing impact structures. Prior to this summary, a context is provided by describing some of the salient characteristics of known terrestrial impact craters.

Richard A. F. Grieve, Continental Geoscience Division, Geological Survey of Canada, 1 Observatory Crescent, Ottawa, Ontario K1A OY3, Canada.

BASIC CHARACTERISTICS OF TERRESTRIAL IMPACT CRATERS

Terrestrial impact craters are often degraded or modified by terrestrial geologic processes. In some cases, erosion has removed the entire crater form. In such cases, there is no longer a crater, and the feature is more correctly referred to as an impact structure. To avoid having to define when a crater ceases to be a crater, all impact features are referred to here by the more generic term *impact structures*. Despite the effects of erosion, the terrestrial impact record illustrates the basic morphological progression with size observed on other planets. On Earth, simple structures occur up to diameters of ≈2 km, if the target rocks are sedimentary, and up to ≈4 km, if the target rocks are crystalline. Above these respective diameters, terrestrial impact structures generally have a complex form. Because of the effects of terrestrial processes, particularly erosion, there are a number of

Grieve, R. A. F., 1997, Terrestrial impact structures: basic characteristics and economic significance, with emphasis on hydrocarbon production, *in* Johnson, K. S.; and Campbell, J. A. (eds.), Ames structure in northwest Oklahoma and similar features: origin and petroleum production (1995 symposium): Oklahoma Geological Survey Circular 100, p. 3–16.

biases in the known terrestrial impact record. These include temporal, size-frequency, and spatial biases. They are discussed in detail in Grieve and Shoemaker (1994), along with estimates of the terrestrial cratering rate, and are not repeated here.

Simple Structures

Simple structures consist of a bowl-shaped depression with a structurally uplifted and locally overturned rim area. The best-known terrestrial simple structure is Barringer or Meteor Crater (Fig. 1; Table 1). Most other terrestrial simple structures are not as well preserved as Meteor Crater, which still retains its overturned flap of bedrock on the rim and part of its exterior ejecta blanket. Drilling at Meteor Crater, and other simple structures, indicates that the apparent floor is underlain by a breccia lens, which is approximately parabolic in cross section. This lens consists of brecciated target material and is contained in the fractured, but essentially autochthonous, target rocks of the floor and wall of the so-called true crater. Although the breccia lens contains some highly shocked materials, the bulk (≈90%) bears little or no diagnostic evidence of shock. So-called shock-metamorphic effects in the autochthonous target rocks are restricted to the floor of the true crater, where maximum shock pressures on the order of 25 GPa (250 kilobars) are recorded and attenuate rapidly with depth (Robertson and Grieve, 1977).

Various levels of detail on the mechanics of simple crater formation can be found in Dence and others (1977), Croft (1980), Grieve and Garvin (1984), and other references. At its maximum growth, the initial so-called transient cavity, which is formed by excavation and displacement of target material set in motion by the impact is parabolic in cross section and reaches a depth approximately ⅓ of its diameter. The walls and floor of this cavity are, in part, lined with melted and shocked materials set in motion and driven down into the expanding cavity. The transient cavity, however, is highly unstable during its late-stage growth, and its walls collapse inward. This

Figure 1. Oblique aerial view of the simple Barringer or Meteor Crater, Arizona, United States. The hummocky material exterior to the structurally uplifted rim is the ejecta blanket.

TABLE 1. — PRINCIPAL CHARACTERISTICS OF IMPACT STRUCTURES MENTIONED IN TEXT

Name	Location	Latitude	Longitude	Age (Ma)	Diameter (km)
Ames	Oklahoma, USA	N36°15′	W98°12′	470 ± 30	16
Avak	Alaska, USA	N71°15′	W156°38′	>95	12
Barringer	Arizona, USA	N35°2′	W111°1′	0.049 ± 0.003	1.19
Boltysh	Ukraine	N48°45′	E32°10′	88 ± 3	24
Bosumtwi	Ghana	N6°30′	W1°25′	1.03 ± 0.02	10.5
Calvin	Michigan, USA	N41°50′	W85°57′	≈430	8.5
Carswell	Saskatchewan, Canada	N58°27′	W109°30′	115 ± 10	39
Chicxulub*	Yucatan, Mexico	N21°20′	W89°30′	64.98 ± 0.05	170
Clearwater West	Quebec, Canada	N56°13′	W74°30′	290 ± 20	36
Kara	Russia	N69°12′	E65°0′	73 ± 3	65
Manicouagan	Quebec, Canada	N51°23′	W68°42′	214 ± 1	100
Marquez	Texas, USA	N31°17′	W96°18′	58 ± 2	13
Newporte	North Dakota, USA	N48°58′	W101°58′	<500	3
Popigai	Russia	N71°30′	E111°0′	35 ± 5	100
Puchezh-Katunki	Russia	N57°6′	E43°35′	175 ± 3	80
Red Wing	North Dakota, USA	N47°36′	W103°33′	200 ± 25	9
Ries	Germany	N48°53′	E10°37′	15 ± 1	24
Siljan	Sweden	N61°2′	E14°52′	368.0 ± 1.1	52
Steen River	Alberta, Canada	N59°30′	W117°38′	95 ± 7	25
Steinheim	Germany	N48°2′	E10°4′	15 ± 1	3.8
Sudbury	Ontario, Canada	N46°36′	W81°11′	1850 ± 3	250
Ternovka	Ukraine	N48°1′	E33°5′	≈350	15
Tookoonooka	Queensland, Australia	S27°7′	E142°50′	128 ± 5	55
Viewfield**	Saskatchewan, Canada	N49°35′	W103°5′	≈190	2.8
Vredefort	South Africa	S27°0′	E27°30′	2018 ± 14	300
Zapadnaya	Ukraine	N49°44′	E29°0′	169 ± 5	4

* In several cases, diameter estimates are poorly constrained or debatable. Chicxulub is an exceptional case, with other diameter estimates ranging up to ≈300 km (Sharpton and others, 1993).
** Impact origin not confirmed.

collapse enlarges the final rim diameter slightly compared to the transient-cavity diameter and partly fills the final simple structure with brecciated, but largely unshocked material from the transient-cavity wall, i.e., the observed breccia lens.

Simple structures with the best available data yield the following depth:diameter relationship:

$$d_a = 0.13D^{1.06}$$

and

$$d_t = 0.28D^{1.02},$$

where D is final rim diameter, d_a and d_t are apparent and true depth (defined as the maximum depth from the original ground surface to the top and bottom of the breccia lens, respectively), and units are in kilometers. Target rock type does not appear to have a major effect on d:D relationships for simple structures, as the sample used includes structures in both crystalline and sedimentary targets.

Complex Structures

Complex impact structures are characterized by an uplifted central area, occurring as a central topographic peak and/or ring. This is surrounded by an annular depression and a normally faulted structural rim area. Examples of the morphological subgroups of complex craters, which are more clearly observed on other planetary bodies (Wood and Head, 1976), can be found in the terrestrial record. With increasing diameter, these subgroups are *central-peak craters* (e.g., Steinheim, Fig. 2; Table 1), *central-peak basins* with both a central peak and a surrounding ring (e.g., Clearwater West, Table 1), *peak-ring basins* with only a ring (e.g., Popigai, Table 1), and possibly *multi-ring basins* with several rings (e.g., Chicxulub, Table 1).

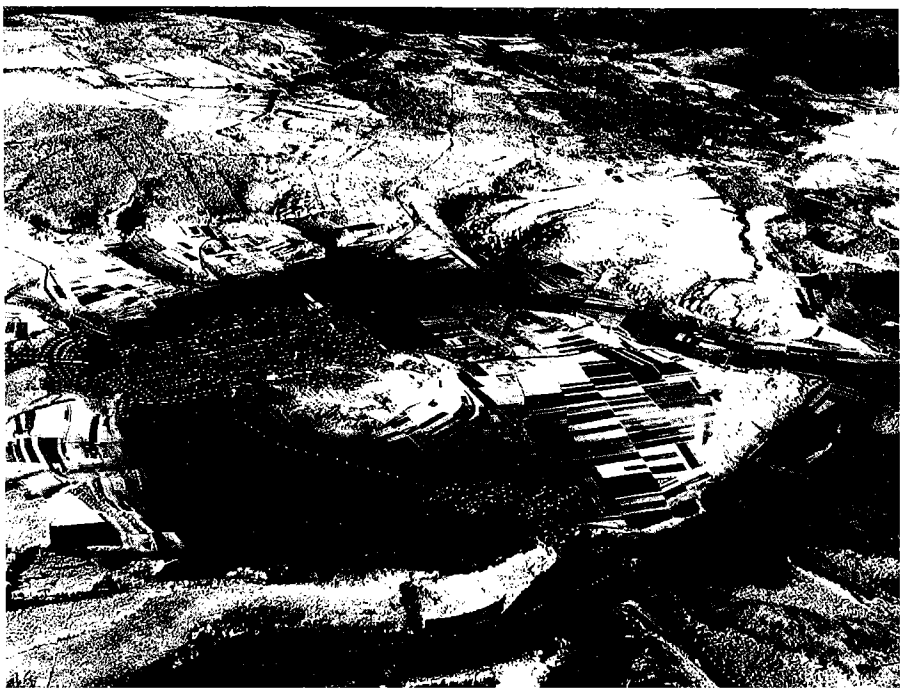

Figure 2. Oblique aerial view of the complex Steinheim structure, Germany. The main features are a rim area, annular trough, and central peak.

Geologic observations indicate that the central structures consist of shocked target rocks stratigraphically uplifted to their present position. The surrounding annular depression is partially filled by allochthonous target material, in the form of polymict breccia and/or impact-melt rocks. The volume of impact-melt rocks can be significant. For example, the present thickness of the annular impact-melt sheet at the 100-km-diameter Manicouagan structure (Table 1) reaches ≈250 m over an area of 2000 km^2, with an estimated original volume of ≈1000 km^3. This allochthonous material—breccia or melt rock or a mixture—overlies the target rocks of the true floor of the structure, which rises through a series of normal faults to form the structurally complex rim area.

The modification or collapse of the transient cavity is considerably more severe in complex compared to simple structures, resulting in much smaller d:D ratios for the final structure. Transient-cavity modification at complex structures involves a volume of target material well beyond the limit of the transient-cavity diameter. Stratigraphic observations and determinations of the level of shock (≈30–40 GPa) (Robertson and Grieve, 1977; Stöffler and others, 1988) in the target rocks of the central structures indicate that they correspond to the uplifted floor of the transient cavity. Some indication of the status of knowledge of cratering mechanics at complex impact structures can be found in papers in Schultz and Merrill (1981) and in Melosh (1989); however, many of the details are the focus of on-going research (e.g., Ivanov, 1994). The differences in the transition diameters from simple to complex forms between crystalline and weaker sedimentary targets indicate a role for the strength of the target in the modification process. This is also reflected in the fact that complex structures are shallower in sedimentary targets than in crystalline ones. The relationships for apparent depth are

$$d_a = 0.12D^{0.30}$$

and

$$d_a = 0.15D^{0.43},$$

for sedimentary and crystalline targets, respectively. These relationships are based on few data and have considerable uncertainty, particularly as erosion affects d:D ratios more severely at the relatively shallower complex craters than at simple craters. The general form, however, of the relationships is similar to $d \propto D^{0.3}$ for complex structures on the Moon (Pike, 1977).

The amount of structural uplift (U_s) in the central structures at complex terrestrial impact structures can be measured, where the subsurface stratigraphy is known. The relationship is

$$U_s = 0.06D^{1.1},$$

where U_s is the amount of stratigraphic uplift undergone by the deepest lithology now uplifted and exposed at the surface in the center (Grieve and others, 1981). Drilling and geophysical data indicate, however, that complex impact structures are inherently near-surface features, with residual structural disturbance in the center extending to depths of only $\approx 1.5U_s$ to $2.0U_s$.

RECOGNITION OF IMPACT STRUCTURES

Planetary (i.e., extraterrestrial) impact craters are recognized by their morphology. Terrestrial impact structures are recognized primarily by the physical effects of impact. Although a crater form, with the appropriate morphometric relationships, is an excellent indicator of an impact origin, a near-pristine form is restricted in the terrestrial environment to impact structures that are either very young or were buried and protected from erosion very soon after formation. In addition to the modifying effects of erosion on morphology, the highly active terrestrial geologic environment results in a number of processes that can produce circular or quasi-circular geologic features. Approximately 30% of known terrestrial impact structures are buried. They were recognized initially as geophysical anomalies. There are a number of distinctive geophysical characteristics associated with impact structures, which are detailed in Pilkington and Grieve (1992). Such anomalies are characteristic but not diagnostic of an impact origin. An impact origin can only be proven through drilling and sample examination. The criterion for the recognition of terrestrial impact structures is the occurrence of shock-metamorphic effects in the target rocks. Details of shock-metamorphic effects can be found in papers in French and Short (1968) and Roddy and others (1977) and in Stöffler (1972,1974) and references therein. They are only briefly summarized here.

Shock-Metamorphic Effects in Autochthonous Lithologies

The only megascopic indicator of shock metamorphism is the occurrence of shatter cones (Dietz, 1968). They are best developed in fine-grained, structurally isotropic lithologies, such as carbonates and quartzites. Shatter cones are generally developed at relatively low shock pressures. The most common shock-metamorphic effect is the occurrence of microscopic, so-called planar deformation features (PDFs) in tectosilicates, in particular, in quartz. When fresh, the majority of PDFs in quartz are filled with glass (Engelhardt and Bertsch, 1969). At older impact structures, they are annealed and are manifest as linear chains of microscopic inclusions. Such features are called decorated PDFs. A recent, comprehensive review of shock metamorphism in quartz is given in Stöffler and Langenhorst (1994), which documents changes in optical properties and other physical properties that parallel the progressive development of PDFs in the shock-pressure range 7.5–35 GPa.

At pressures in excess of ≈30 GPa and ≈35 GPa, shock-induced disorder is sufficient to render feldspar and quartz, respectively, to a glass. These are solid-state glasses with properties distinct from fusion glasses (Stöffler and Langenhorst, 1994). They are referred to as diaplectic glasses. Shock can also generate high-pressure mineral polymorphs, e.g., stishovite and coesite from quartz and diamond from graphite.

Because of attenuation, subsolidus shock-metamorphic effects in parautochthonous rocks are limited in radial extent (Robertson and Grieve, 1977). They occur only in the central area of the impact structures, i.e., at the base of the true crater, in simple structures and in the central uplifted area at complex structures. They diminish in intensity with radial distance from the center of the structure and with depth.

Shock-Metamorphic Effects in Allochthonous Lithologies

A variety of breccias occur at impact structures, from polymict breccias containing a wide range of shock-metamorphosed clasts, known as suevites, to relatively unshocked monomict breccias. They occur as allochthonous bodies, exterior ejecta, and dikes within the target rocks and as parautochthonous bodies in the target rocks of the crater floor. There is evidence for multigenerations, with some breccias being formed during cavity excavation and others during cavity modification (e.g., Lambert, 1981; Müller-Mohr, 1992). Pseudotachylite also occurs at impact structures and was first described at the Vredefort structure (Table 1). Pseudotachylite and breccias, however, can occur as the result of endogenic geologic processes. To be ascribed to impact and used for the identification of impact structures, they must contain shock-metamorphosed clasts.

Upon release from shock pressures above ≈50 GPa, individual minerals begin to thermally decompose or melt (Stöffler, 1972,1974), leading to the production of mixed-mineral melts. Above ≈60 GPa, the heat released on shock decompression is sufficient to cause whole-rock melting. The resulting impact melts occur as glass bombs in crater ejecta (Engelhardt, 1990), as glassy to crystalline masses within the breccia fill, or as coherent annular sheets lining the floor of complex structures in crystalline targets (Grieve and others, 1977). The rocks of impact-melt sheets tend to be heavily charged with clastic debris, some of which displays subsolidus shock-metamorphic effects, toward their lower and upper contacts. The chemistry of impact-melt rocks is governed by melting some mix of target rocks. Parameters such as $^{87}Sr/^{86}Sr$

and $^{143}Nd/^{144}Nd$ ratios reflect the preexisting target rocks, whereas isochron dating methods indicate much younger crystallization ages related to the impact (e.g., Faggart and others, 1985). In some cases, enrichments above target-rock levels in trace siderophile and platinum-group elements, and sometimes chromium, have been identified in impact-melt rocks (Palme, 1982). These are due to an admixture of up to a few percent of meteoritic projectile material. Osmium isotopic anomalies, in particular, low $^{187}Os/^{188}Os$ ratios, can also indicate an admixture of meteoritic material (e.g., Koeberl and others, 1994).

ECONOMIC DEPOSITS ASSOCIATED WITH IMPACT STRUCTURES

The types of economic deposits within impact structures can be classified according to their time of formation. *Progenetic deposits* originate prior to the impact. The effect of the impact has been to spatially redistribute these deposits. *Syngenetic deposits* originate during the impact, or immediately afterward, owing to the energy deposition of the impact, resulting in phase changes and melting. *Epigenetic deposits* result from postimpact processes, including hydrothermal alteration, restricted sedimentation in an enclosed topographic basin, and the flow of fluids into the structural trap formed by the impact structure. Details of these types of deposits can be found in Grieve and Masaitis (1994). Progenetic and syngenetic deposits are only summarized here, where the emphasis is on epigenetic deposits of hydrocarbons.

Progenetic Deposits

In many cases, progenetic deposits are relatively small. The larger deposits, however, include iron, uranium, and gold at the Carswell, Ternovka, and Vredefort structures (locations, ages, and sizes given in Table 1).

Carswell is a deeply eroded complex structure. It has an ≈20-km-diameter basement core, surrounded by units of the unmetamorphosed Proterozoic Athabasca Group: sandstones and conglomerates of the William River Subgroup, sandstones and siltstones of the Douglas Formation, and dolomites of the Carswell Formation. Known uranium mineralization is concentrated along the south to southwest contact between the basement core and the William River Subgroup, with an estimated 46,500 tonnes of uranium originally being present in the currently known deposits (Harper, 1982); the mineralization occurs in both the basement core and the William River Subgroup. Details of the ore deposits can be found in papers in Lainé and others (1985). It was the uplift of the basement core by >2 km (Harper, 1982), during the formation of a complex structure, that brought the ores to their present high and exploitable levels.

Iron and uranium ores occur in the crater floor at the highly eroded Ternovka complex structure (Nikolsky and others, 1982), which was formed in the Krivoj Rog iron ore basin. The ores are due to hydrothermal and metasomatic action, which occurred during the Early Proterozoic. Postimpact hydrothermal alteration led to remobilization and the formation of veins of pitchblende. The production of uranium ceased in 1967, but iron ore is still extracted from two main open pits: Annovsky and Pezromaisk. The total reserves at Pezromaisk are estimated at 74 million tonnes, with additional reserves of lower-grade deposits estimated at ≈675 million tons. Because of brecciation, blocks of ore are mixed with barren blocks, which causes difficulties in evaluating the reserves.

The Witwatersrand basin in South Africa is a world-class gold and uranium mining camp. At the center of the basin is the Vredefort dome. The dome and immediately surrounding structure consist of an uplifted, ≈44-km-diameter, central core of predominantly Archean granites, an ≈18-km-wide collar of steeply dipping to overturned Proterozoic supracrustal rocks of the Witwatersrand and Ventersdorp Supergroups and an outer, ≈28-km-wide synclinorium of Proterozoic supracrustal rocks of the Transvaal sequence. Although the origin of Vredefort has been somewhat contentious, recent TEM (transmission electron microscope) investigations have confirmed the presence of annealed PDFs in quartz, coesite, and stishovite (White, 1993; Leroux and others, 1994). If the entire crustal section exposed to the center is ≈36 km in thickness (Hart and others, 1991), then the relationship for the amount of structural uplift at complex impact craters suggests that the original diameter was on the order of 335 km. Using other spatial arguments, Therriault and others (1993) suggested that the original rim diameter may have been ≈300 km. Additional arguments for an original diameter of ≈300 km are given in Grieve and Masaitis (1994). With this diameter, the Vredefort structure encompasses a series of post-Transvaal anticlinal and synclinal structures surrounding the central core, identified by McCarthy and others (1986) as being related to Vredefort (Fig. 3). These concentric structures are the cause of the preservation from erosion of much of the Central Rand Group in the Witwatersrand basin (McCarthy and others, 1990).

The major gold deposits of the Witwatersrand basin occur in an ≈180° arc at the outer edge of the outcrop of the Central Rand Group. Unlike Carswell, where the ores are exposed owing to the central uplift, the ores at Vredefort are preserved because they were downdropped within the annular trough (Fig. 3). The goldfields have been mined for more than 100 years, with total production, as of 1985, being >40,500 tonnes; associated uranium production for the same time period is >136,500 tonnes (Pretorius, 1986). Current revenues from mining of gold and uranium are of the order of $7

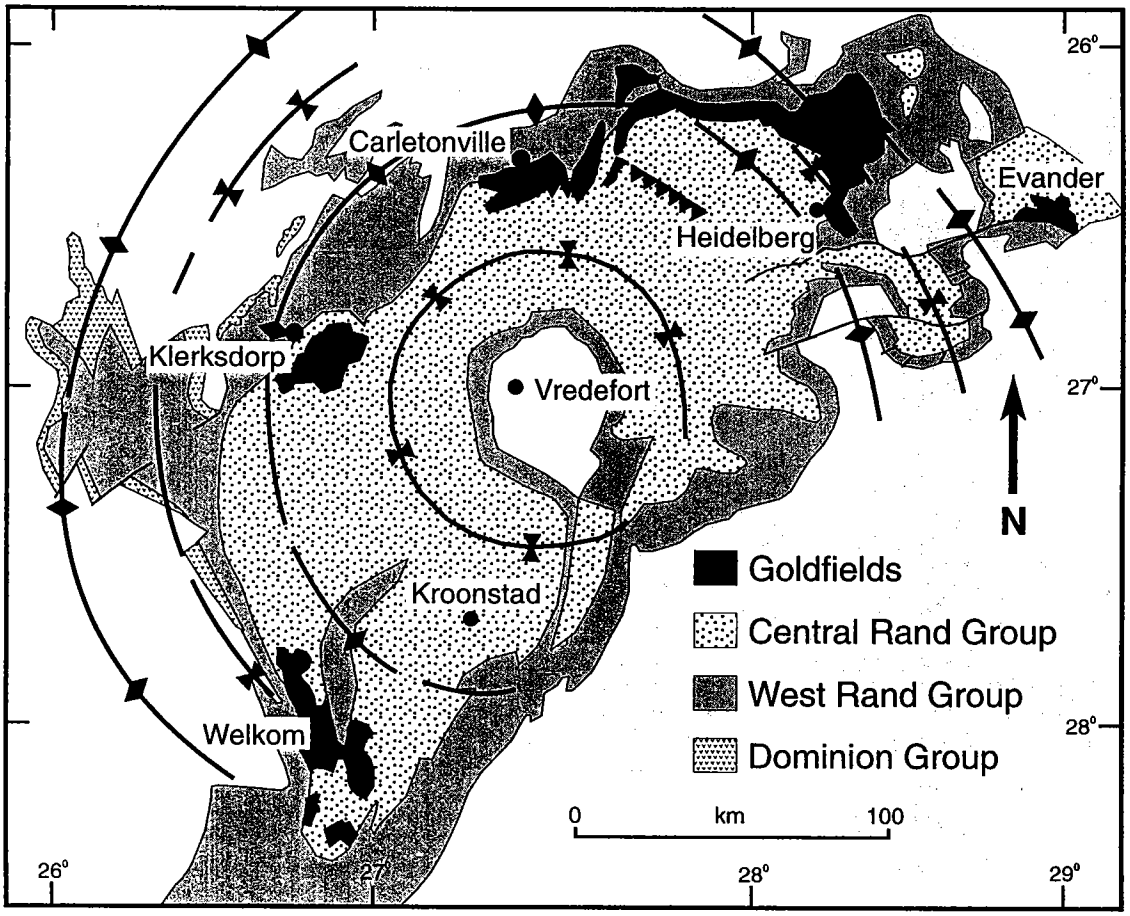

Figure 3. Geologic sketch map of the Witwatersrand basin, South Africa, showing the main gold and uranium fields of the Central Rand. Also shown are the concentric structures associated with the ≈300-km Vredefort impact structure. See text for details.

billion per year. There are indications that there was lead loss and redistribution of uranium and gold at ca. 2 Ga; the cause was probably a hydrothermal event, which may have been related to the Vredefort impact (Frimmel and others, 1993).

Syngenetic Deposits

Syngenetic economic deposits include impact diamonds, copper-nickel and platinum-group elements in sulfides, and other metals. The occurrence and nature of impact diamonds are discussed in Masaitis (1989,1993) and Grieve and Masaitis (1994) and are only briefly summarized here.

Workers in the former Soviet Union discovered the existence of impact diamonds. They are known to occur at a number of impact structures, e.g., Kara, Puchezh-Katunki, Ries, Ternovka, and Zapadnaya (Table 1), and are most common as inclusions in impact-melt rocks and in melt clasts in suevite breccias, where they are present at the level 10 ppb or more. The distribution of diamonds within individual impact-melt and suevite bodies can be irregular. They tend to be concentrated in rays or zones emanating from areas where the original carbon-bearing lithologies are most abundant (Masaitis, 1993). They also tend to be radially restricted. Closer to the centers of the structures, high postshock temperatures caused oxidation of the diamonds; at some critical distance from the centers, the shock pressures were too low to result in the phase transformation of carbon to diamond.

The origin of the 1.85 Ga Sudbury Igneous Complex has been controversial, and a considerable literature exists concerning aspects of Sudbury geology (e.g., papers in Pye and others, 1984; Lightfoot and Naldrett, 1994). For the most recent arguments and conclusions regarding the impact model for the Sudbury structure, the reader is referred to Grieve (1994) and Stöffler and others

(1994). Their major conclusions are listed here: (1) all breccia and melt lithologies can be explained by impact; (2) there is no requirement for additional magmatic components derived from the mantle at 1.85 Ga in the Sudbury Igneous Complex, other associated melt bodies, or the ore deposits; and (3) the Sudbury structure represents an eroded and heavily tectonized remnant of an originally 200–250-km-diameter, possibly multiring, impact basin. Reflection seismic data indicate that the Sudbury Igneous Complex has been highly tectonized and subjected to northwest-southeast shortening during the Penokean orogeny (Wu and others, 1994). This picture of thrusting is consistent with structural observations indicating that ductile deformation was followed by thrusting (Shanks and Schwerdtner, 1991; Hirt and others, 1993). Thus, the present configuration of the Sudbury structure, expressed as an elliptical outcrop pattern, is the result of tectonic modification.

The copper-nickel and platinum-group-element ores at Sudbury are world class; the deposit consists of an estimated 1.65×10^9 tonnes of 1.2% Ni and 1.05% Cu. Over the past five years, the value of these ores extracted averaged ≈$2 billion per year. The complex association of the ores at Sudbury results from postimpact hydrothermal activity and Penokean tectonic and metamorphic processes. The overall commonality to all the ore deposits is that they lie at the base or just beneath the Sudbury Igneous Complex. Sulfide immiscibility resulted from the combination of lithologies that was melted to form the impact melt (yielding the Sudbury Igneous Complex), producing a liquid with an initial composition that was high in SiO_2 (≈64%). The crustal source of the ores, as well as the associated silicates, is indicated by their Re-Os and Nd-Sm isotopic compositions (Dickin and others, 1992).

Epigenetic Deposits

Epigenetic deposits include hydrothermal deposits, hydrocarbons, oil shales, organic and chemical sediments, as well as waters. Here, hydrocarbon deposits, at mainly North American structures, are discussed. Other types of economic occurrences are discussed in more detail in Grieve and Masaitis (1994).

The Ames Structure

The Ames structure (Table 1) is buried by ≈3 km of Ordovician to Holocene sedimentary deposits (Carpenter and Carlson, 1992). During recent oil exploration, a local structure, known as the Hunton graben was recognized as part of a much larger complex impact structure (Roberts and Sandridge, 1992). A variety of shock-metamorphic effects have been observed, including PDFs in quartz and impact-melt rocks (Koeberl and others, 1995a). The rim of the structure is defined by the structurally high Lower Ordovician Arbuckle dolomite, and >600 m of Cambrian-Ordovician strata and some underlying basement are missing in the center of the structure because of excavation. The structure is covered by ≈60 m of postimpact Middle Ordovician shale, which forms a seal (Kuykendall and others, 1994).

The first oil and gas discoveries were from an ≈500-m-thick section of Lower Ordovician Arbuckle dolomite, which has local porosity due to impact-induced fracturing and karst formation (Roberts and Sandridge, 1992). The DLB no. 27-4 Cecil well, drilled in 1991 into the rim of the Ames structure, had drill-stem rates of 3,440 MMCF (million cubic feet) of gas and 300 BOPD (barrels of oil per day) (Roberts and Sandridge, 1992). Wells in the center of the structure failed to encounter the Arbuckle and bottomed in granite breccia of the central uplift or in granite-dolomite breccia. These wells include the D. & J. no 1-20 Gregory, which is the most productive oil well from a single pay zone in Oklahoma. It encountered an ≈80 m section of highly porous granite breccia below the Oil Creek shale. A drill-stem test of the zone flowed at ≈1,300 BOPD, with an estimate of primary recovery of 10 MMBO (million barrels of oil) from this single well (B. N. Carpenter, written communications, 1994; Kuykendall and others, 1994). Currently, estimates of reserves are 50 MMBO and 20 BCFG (billion cubic feet of gas). The source of the hydrocarbons is the lower section of postimpact Oil Creek shale, which has not been recognized outside of the structure (Castaño and others, 1994). At Ames, the impact not only produced the required reservoir rocks but also the paleoenvironment for the deposition of postimpact oil shales that, upon subsequent burial and maturation, provided oil and gas.

Red Wing Creek

Red Wing Creek (Table 1) is a 9-km-diameter complex structure, with a central peak, in which strata have been uplifted ≈1 km (Fig. 4; Brenan and others, 1975). The presence of fragments of shatter cones was the first indication of shock metamorphism (Brenan and others, 1975), and, more recently, PDFs in quartz and melt breccias have been identified (Koeberl and Reimold, 1995). The structure is formed in Silurian to Triassic carbonates with minor sandstones and evaporites and is buried by ≈1.5 km of Jurassic to Neogene postimpact sedimentary units. Shell Oil drilled the northwest flank of the central uplift in 1965 and the annular trough in 1968. Both were dry holes. However, True Oil redrilled what was later recognized as the center of the central uplift in 1972 and discovered ≈820 m of oil column, with considerable structural complexity and brecciation and a net pay of ≈490 m. These intervals are in contrast to the surrounding area, with ≈30 m oil columns. The large oil column is due to the structural repetition of the Mississippian Mission Canyon Formation in

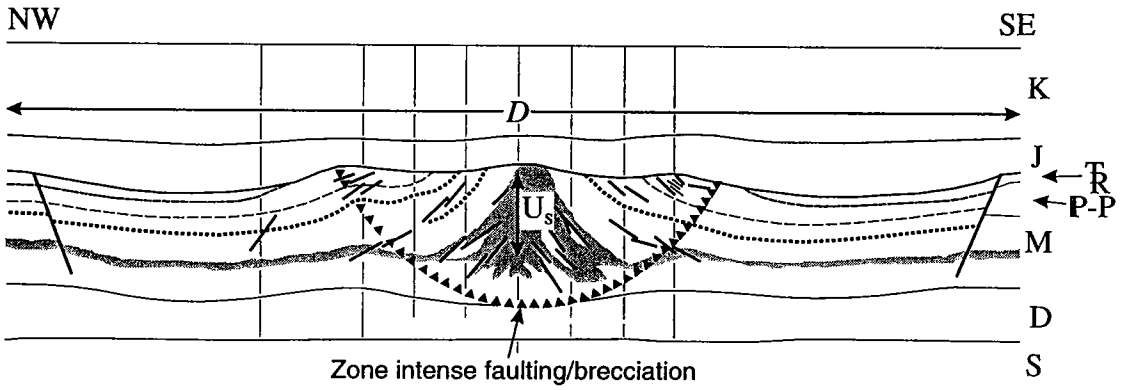

Figure 4. Geologic cross section of the complex Red Wing Creek structure, North Dakota, United States, with limit of structural disturbance and amount of structural uplift (U_s) indicated. Diameter of structure (D) is 9 km. Hydrocarbons are produced from the central uplift. See text for details. Constructed from data in Brennan and others (1975).

the central uplift (Brenan and others, 1975). Impact-induced porosity and permeability result in relatively high flow rates of over 1,000 BOPD; cumulative production, since discovery, has been ≈13 MMBO and ≈16 BCFG (Pickard, 1994). It is estimated that the brecciated central uplift contains over 130 MMBO, and primary and secondary recoverable reserves may exceed 70 MMBO (Donofrio, 1981; Pickard, 1994). The natural gas reserves are estimated at 100 BCF. Virtually all the oil has been discovered within a diameter of ≈3 km, corresponding to the central uplift, with the wells having the highest cumulative productivity per square kilometer of any in North Dakota, if not the United States.

Newporte

Newporte (Table 1) has the form of a simple impact structure. It is buried by ≈3 km of sedimentary deposits and was first explored for hydrocarbons in the late 1970s (Clement and Mayhew, 1979). At that time, its origin was unknown, although a possible impact origin was suggested (Donofrio, 1981). Recent microscopic investigations of breccia materials indicate the presence of PDFs in quartz and feldspar (Gerlach and others, 1994; Koeberl and others, 1995b). Although a simple structure, there are some similarities with Ames. The present cumulative production of ≈120,000 barrels of oil is from Cambrian Deadwood sandstone, which appears as the lowermost unit of the postimpact sedimentary fill, and brecciated granite of the rim area. As at Ames, the source rock appears to be a locally developed lithology (Castaño and others, 1994).

Avak

Avak (Table 1) is buried by late Pleistocene and Quaternary deposits, affects Ordovician-Silurian to Cretaceous rocks, and has the form of a complex impact structure (Kirschner and others, 1992). Listric faults define a rim area, and it has an annular trough and central uplift, where the Lower-Middle Jurassic Kingak Shale and Barrow Sand are uplifted 500 m from their regional levels. The Avak 1 well, drilled to a depth of 1,225 m in the central uplift, penetrated the general succession of the area: Lower Cretaceous "Pebble Shale," Jurassic Kingak Shale, Lower Jurassic Barrow Sand, and Ordovician Frankilian argillite. Shock-metamorphic features (Therriault and Grantz, 1995), breccia, repetition of beds, and out-of-sequence beds are encountered (Collins, 1961; Kirschner and others, 1992). Oil shows in Avak 1 are not commercial. Indeed, Kirschner and others (1992) suggested that, within the area of Avak, hydrocarbon accumulations may have been disrupted and lost due to the formation of the structure. The South Barrow, East Barrow, and Sikulik gas field, however, are due to listric faults in the crater rim, which have placed Lower Cretaceous Torok shales against the Lower Jurassic Barrow Sand, creating an effective updip gas seal. The South and East Barrow fields are currently in production, and primary recoverable gas is estimated at ≈37 BCF (Lantz, 1981).

Steen River

The Steen River complex structure (Table 1) is buried by ≈180 m of Quaternary and Lower Cretaceous Loon River shale. It was first drilled in 1963 by Imperial Oil, who encountered Precambrian basement some 760 m above the expected regional level and also "pyroclastics." The target rocks consist of ≈1.4 km of Devonian carbonates, evaporites, and shales, overlying Precambrian granitic gneiss basement. In the center, ≈185 m of Loon River shale is followed by ≈120 m of suevite breccia, ex-

hibiting a range of shock-metamorphic features (Carrigy, 1968). Oil is produced from two wells in fractured dolomite of the Keg River Formation on the northern rim at ≈600 BOPD, with a cumulative production of ≈300,000 barrels. The structure is relatively isolated, and operations are currently limited to winter months, when the ground is frozen (Tooth and Stewart, 1994).

Campeche

The oil fields of the Campeche Bank off southern Mexico are world class. They may, in part, be linked to impact. In the 10 fields described by Santiago and Baro (1990), 9 have hydrocarbon production from Cretaceous/Tertiary (K/T) breccias, and, in some cases, the breccias are the sole or main producers (Fig. 5). The fields are generally associated with anticlinal structures. The K/T breccias, with their average porosity of ≈10%, are the reservoir rocks. Individual wells produce over 20,000 BOPD and 20 MMCFGPD, although the average is closer to 6,000 barrels and several million cubic feet (Santiago and Baro, 1990). The thicknesses of the K/T breccia units range from 125 to 275 m, but the production interval can be less (Camargo and Quezada, 1992). Although these breccias are temporally linked to the K/T boundary, the question is whether they are genetically linked to the ≈170-km-diameter Chicxulub structure (Table 1; Hildebrand and others, 1991), ≈300 km to the northwest, which is generally believed to be the K/T boundary impact structure. At least in the case of the K/T Lomas Triste breccia deposits in the Campeche Bank, shocked quartz has been reported from the upper portion of the breccias and linked to Chicxulub (Limon and others, 1994). The breccia deposits, however, are too thick to represent solely impact ejecta. They are largely local material and may represent the results of seismic and tsunami activity associated with the K/T impact event. Similar high-energy breccia deposits are known in currently onshore locations in and around the Gulf of Mexico and into the southern United States (e.g., Smit and others, 1992).

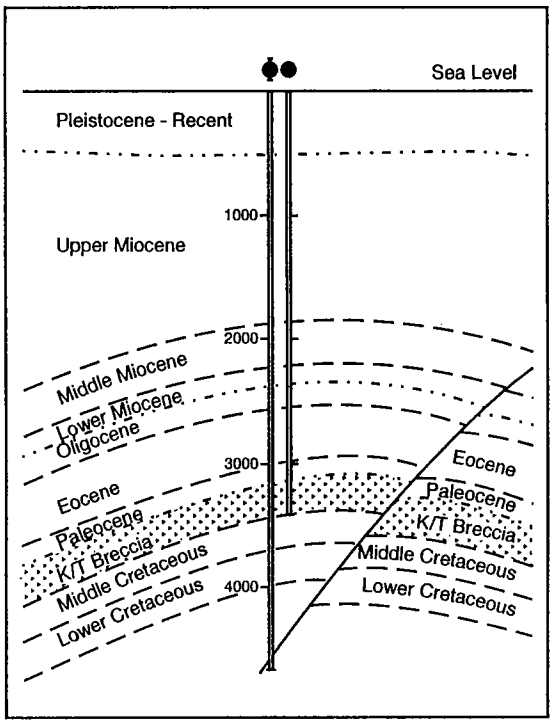

Figure 5. Geologic cross section of Ek oil field, Campeche Bank, Gulf of Mexico. The reservoir rocks are K/T breccias, probably associated genetically with the formation of the Chicxulub impact structure. Modified from Santiago and Baro (1990).

Boltysh

Oil shales are known to occur in the post-impact sediments at a number of structures in the Ukraine (Grieve and Masaitis, 1994). The most significant are at the Boltysh structure (Table 1), which is buried by >0.5 km of upper Mesozoic and Cenozoic sedimentary units and where there are an estimated 4.5 billion tonnes of oil shales. They are the result of biological activity in the isolated topographic basin formed by the impact structure. The situation is analogous to that of Ames. Unlike Ames, however, burial has been insufficient to result in maturation.

Bosumtwi

The starting point for hydrocarbon accumulation at Boltysh and Ames may be somewhat analogous to the situation at Bosumtwi (Table 1). The topographic basin resulting from the impact structure has no outside drainage, and the structure is partly filled by a lake. The lake sediments are richly organic and anoxic, and they actively generate methane gas, which gives rise to occasional periods of bubbling at the surface, accompanied by a sulfurous smell (Junner, 1937). Jones (1983) has suggested that 250 BCF of methane could be trapped in breccias and fractured rocks of the central uplift.

Other Structures

Other impact structures contain hydrocarbons. Gas is produced at the 13-km-diameter Marquez structure (Table 1). There may be a zone of potential stratigraphic trapping within the Tookoonooka structure (Table 1). More important for hydrocarbon exploration, Tookoonooka has created a shadow zone to hydrocarbon migration from the Eromanga basin depocenter in Australia, since the Early Cretaceous (Gorter and others, 1989). In the case of Siljan (Table 1), hydrocarbon exploration

was undertaken because it was an impact structure. The exploration, which was highly controversial, was aimed at abiogenic hydrocarbons from the mantle that were channeled into Siljan as a result of impact-induced fracturing (Gold, 1988). There are also a number of structures that may be of impact origin, such as Viewfield, (Table 1), that produce hydrocarbons. Like Newporte, Viewfield has the form of a simple structure. Shock-metamorphic effects, however, have not been identified to date. The recoverable reserves associated with Viewfield are estimated to be 20 MMBO (Isaac and Stewart, 1993). Over 500,000 barrels of oil have been produced since 1978 from the Calvin structure (Table 1), which is an 8.5-km-diameter complex structure (Milstein, 1988). In addition, a number of seismic targets have been identified that have hydrocarbon potential and the characteristics of impact structures (e.g., Gudlaugsson, 1993).

CONCLUDING REMARKS

Given the relatively small number of known impact structures, it would seem that, as a class of geologic features, impact structures have considerable economic potential overall and make worthwhile exploration targets. From an exploration point of view, impact structures have the disadvantage of being random in both space and time. They can be formed anywhere, at any time. The geologic and geophysical characters of impact structures are well documented; thus, recognition is relatively straightforward. Impact structures also have a general property that is an advantage in exploration. At a large scale, they tend to have fixed morphometric and structural relationships for a given diameter. Once a structure is known to be of impact origin, it is possible to make considerable predictions as to the structural and lithological character of the feature as a whole. Such predictions are generally not possible for most endogenic geologic features. The development of an exploration or exploitation strategy based on these relationships is most notably illustrated by the drilling for hydrocarbons, where the central uplift and the rim area are obvious targets. Donofrio (1981) proposed that major oil and gas deposits may occur in brecciated basement rocks of impact structures. If these structures also generate conditions favorable for source-rock development, such as at Bosumtwi, Boltysh, and Ames, their potential could not only be considerable, but they could occur in geologic environments generally not considered as potential sources for hydrocarbons.

ACKNOWLEDGMENTS

I thank M. Ford for manuscript preparation on a very short time schedule and A. Hildebrand for critically reviewing an earlier version of the manuscript. I acknowledge contributions from the Geological Survey of Canada.

REFERENCES CITED

Brenan, R. L.; Peterson, B. L.; and Smith, H. J., 1975, The origin of Red Wing Creek structure, McKenzie County, North Dakota: Wyoming Geological Association Earth Science Bulletin 8, p. 1–41.

Camargo, Z. A.; and Quezada, M. J., 1992, Analysis of economic geology of areas of the Gulf of Mexico with hydrocarbon potential [in Spanish]: Boletín de la Asociación Mexicana de Géologos Petroleros, v. 41, p. 1–32.

Carpenter, B. N.; and Carlson, R., 1992, The Ames impact crater: Oklahoma Geology Notes, v. 52, p. 208–223.

Carrigy, M. A., 1968, Evidence of shock metamorphism in rocks from the Steen River structure, Alberta, *in* French, B. M.; and Short, N. M. (eds.), Shock metamorphism of natural materials: Mono Book Corp., Baltimore, p. 367–378.

Castaño, J. R.; Clement, J. H.; Kuykendall, M. D.; and Sharpton, V. L., 1994, Source rock potential of impact craters [abstract]: American Association of Petroleum Geologists Annual Convention Official Program, p. 118.

Clement, J. H.; and Mayhew, T. E., 1979, Newporte discovery opens new pay: Oil and Gas Journal, v. 77, p. 165–172.

Collins, F. R., 1961, Core test and test wells, Barrow area, Alaska: U.S. Geological Survey Professional Paper 305-K, p. 569–644.

Croft, S. K., 1980, Cratering flow fields: implications for the excavation and transient expansion stages of crater formation: Lunar and Planetary Science Conference, 11th, Proceedings, Houston, Texas, p. 2347–2378.

Dence, M. R.; Grieve, R. A. F.; and Robertson, P. B., 1977, Terrestrial impact structures: principal characteristics and energy considerations, *in* Roddy, D. J.; Pepin, R. O.; and Merrill, R. B. (eds.), Impact and explosion cratering: Pergamon Press, New York, p. 247–275.

Dickin, A. P.; Richardson, J. M.; Crocket, J. H.; McNutt, R. H.; and Peredery, W. V., 1992, Osmium isotope evidence for a crustal origin of platinum group elements in the Sudbury nickel ore, Ontario, Canada: Geochimica et Cosmochimica Acta, v. 56, p. 3531–3537.

Dietz, R. S., 1968, Shatter cones in cryptoexplosion structures, *in* French, B. M.; and Short, N. M. (eds.), Shock metamorphism of natural materials: Mono Book Corp., Baltimore, p. 267–285.

Donofrio, R. R., 1981, Impact craters: implications for basement hydrocarbon production: Journal of Petroleum Geology, v. 3, p. 279–302.

Engelhardt, W. v., 1990, Distribution, petrography and shock metamorphism of the ejecta of the Ries crater in Germany—a review: Tectonophysics, v. 171, p. 259–273.

Engelhardt, W. v.; and Bertsch W., 1969, Shock induced planar deformation structures in quartz from the Ries crater, Germany: Contribu-

tions to Mineralogy and Petrology, v. 20, p. 203–234.

Faggart, B. E., Jr.; Basu, A. R.; and Tatsumoto, M., 1985, Origin of the Sudbury complex by meteoritic impact: neodymium isotopic evidence: Science, v. 230, p. 436–439.

Frimmel, H. E.; Le Roex, A. P.; Knight, J.; and Minter, W. E. L., 1993, A case study of the post depositional alteration of the Witwatersrand basal reef gold placer: Economic Geology, v. 88, p. 249–265.

French, B. M.; and Short, N. M. (eds.), 1968, Shock metamorphism of natural materials: Mono Book Corp., Baltimore, 644 p.

Gerlach, T. R.; Forsman, N. F.; and Anderson, N. L., 1994, Evidence for an impact origin of the Newporte structure, Renville County, North Dakota [abstract]: Geological Society of America Abstracts with Programs, v. 26, no. 7, p. 425.

Gold, T., 1988, The deep earth gas theory with respect to the results from the Gravberg-1 well, *in* Bodén, A.; and Eriksson, K. G. (eds.), Deep drilling in crystalline bedrock: Springer-Verlag, Berlin, v. 1, p. 18–27.

Gorter, J. D.; Gostin, V. A.; and Plummer, P. S., 1989, The enigmatic sub-surface Tookoonooka complex in southwest Queensland: its impact origin and implications for hydrocarbon accumulations, *in* O'Neil, B. J. (ed.), The Cooper and Eromanga basins, Australia: Petroleum Exploration Society of Australia, Adelaide, p. 441–456.

Grieve, R. A. F., 1994, An impact model of the Sudbury structure, Ontario, *in* Lightfoot, P. C.; and Naldrett, A. J. (eds.), Proceedings of the Sudbury-Noril'sk Symposium: Ontario Geological Survey Special Volume 5, Ontario Ministry of Northern Development and Mines, Toronto, p. 119–132.

Grieve, R. A. F.; and Garvin, J. B., 1984, A geometric model for excavation and modification at terrestrial simple impact craters: Journal of Geophysical Research, v. 89, p. 11561–11572.

Grieve, R. A. F.; and Masaitis, V. L., 1994, The economic potential of terrestrial impact craters: International Geology Review, v. 36, p. 105–151.

Grieve, R. A. F.; and Shoemaker, E. M., 1994, The record of past impacts on Earth, *in* Gehrels, T. (ed.), Hazards due to comets and asteroids: University of Arizona Press, Tucson, p. 417–462.

Grieve, R. A. F.; Dence, M. R.; and Robertson, P. B., 1977, Cratering processes: as interpreted from the occurrence of impact melts, *in* Roddy, D. J.; Pepin, R. O.; and Merrill, R. B. (eds.), Impact and explosion cratering: Pergamon Press, New York, p. 791–814.

Grieve, R. A. F.; Robertson, P. B.; and Dence, M. R., 1981, Constraints on the formation of ring impact structures, based on terrestrial data, *in* Schultz, P. H.; and Merrill, R. B. (eds.), Multi-ring basins: Pergamon Press, New York, p. 37–57.

Gudlaugsson, S. T., 1993, Large impact crater in the Barents Sea: Geology, v. 21, p. 291–294.

Harper, C. T., 1982, Geology of the Carswell structure, central part: Saskatchewan Geological Survey Report 214, p. 1–6.

Hart, R. J.; Andreoli, M. A. G.; Reimold, W. U.; and Tredoux, M., 1991, Aspects of the dynamic and thermal metamorphic history of the Vredefort cryptoexplosion structure: implications for its origin: Tectonophysics, v. 192, p. 313–331.

Hildebrand, A. R.; Penfield, G. T.; Kring, D. A.; Pilkington, M.; Camargo, A. Z.; Jacobsen, S. B.; and Boynton, W. V., 1991, Chicxulub crater: a possible Cretaceous/Tertiary boundary impact crater on the Yucatan Peninsula, Mexico: Geology, v. 19, p. 867–871.

Hirt, A. M.; Lowrie, W.; Clendenen, W. S.; and Kligfield, R., 1993, Correlation of strain and the anisotropy of magnetic susceptibility in the Onaping Formation: evidence for a near-circular origin of the Sudbury basin: Tectonophysics, v. 225, p. 231–254.

Isaac, J. H.; and Stewart, R. R., 1993, 3D seismic characterization of possible meteorite impact structure [abstract]: Canadian Geophysical Union Program and Abstracts, p. 28.

Ivanov, B. A., 1994, Geochemical models of impact cratering, *in* Dressler, B. O.; Grieve, R. A. F.; and Sharpton, V. L. (eds.), Large meteorite impacts and planetary evolution: Geological Society of America Special Paper 293, p. 81–92.

Jones, W. B., 1983, A proposed gas pool in the Pleistocene Bosumtwi crater, Ghana: Journal of Petroleum Geology, v. 5, p. 315–318.

Junner, N. R., 1937, The geology of the Bosumtwi caldera and surrounding country: Gold Coast Geological Survey Bulletin, v. 8, p. 5–46.

Kirschner, C. E.; Grantz, A.; and Mullen, M. W., 1992, Impact origin of the Avak structure, Arctic Alaska, and genesis of the Barrow gas fields: American Association of Petroleum Geologists Bulletin, v. 76, p. 651–679.

Koeberl, C.; and Reimold, W. U., 1995, Shock metamorphism at Red Wing Creek structure, North Dakota: confirmation of an impact origin [abstract]: Lunar and Planetary Science, v. 26, p. 769–770.

Koeberl, C.; Shirey, S. B.; and Reimold, W. U., 1994, Re-Os isotopics as a diagnostic tool for the study of impact craters [abstract], *in* New developments regarding the K/T event and other catastrophes in earth history: Lunar and Planetary Institute Contributions, v. 825, p. 61–63.

Koeberl, C.; Reimold, W. U.; Dallmeyer, R. D.; and Powell, R. A., 1995a, Petrology, mineralogy, geochemistry and age of impact melt rocks from the Ames structure, Oklahoma [abstract]: Lunar and Planetary Science, v. 26, p. 775–776.

Koeberl, C.; Reimold, W. U.; and Bromdt, D., 1995b, The Newporte impact structure, North Dakota: shock metamorphism in breccias [abstract]: Lunar and Planetary Science, v. 26, p. 773–774.

Kuykendall, M. D.; Johnson, C. L.; and Carlson, R. A., 1994, Reservoir characterization of a complex impact crater: "Ames crater," northern shelf, Anadarko basin [abstract]: American Association of Petroleum Geologists Annual Convention Official Program, p. 191.

Lainé, R.; Alonso, D.; and Svab, M. (eds.), 1985, The Carswell structure uranium deposits, Saskat-

chewan: Geological Association of Canada Special Paper 29, 230 p.
Lambert, P., 1981, Breccia dikes: geological constraints on the formation of complex craters, *in* Schultz, P. H.; and Merrill, R. B. (eds.), Multi-ring basins: Pergamon Press, New York, p. 59–78.
Lantz, R., 1981, Barrow gas fields—N. Slope, Alaska: Oil and Gas Journal, v. 79, p. 197–200.
Leroux, H.; Reimold, W. U.; and Doukhan, J.-C., 1994, A TEM investigation of shock metamorphism in quartz from the Vredefort dome, South Africa: Tectonophysics, v. 230, p. 223–239.
Lightfoot, P. C.; and Naldrett, A. J. (eds.), 1994, Proceedings of the Sudbury-Noril'sk Symposium: Ontario Geological Survey Special Volume 5, Ontario Ministry of Northern Development and Mines, Toronto, 423 p.
Limon, M.; Cedillo, E.; Quezada, J. M.; Grajales, J. M.; Alvarez, W.; Hildebrand, A. R.; Sanchez, M. A.; Rosales, C.; and Gonzalez, V., 1994, Cretaceous-Tertiary boundary sedimentary breccias from southern Mexico: normal sedimentary deposits or impact-related breccias? [abstract]: American Association of Petroleum Geologists Annual Convention Official Program, p. 199.
Masaitis, V. L., 1989, The economic geology of impact craters: International Geology Review, v. 31, p. 922–933.
_____ 1993, Diamantiferous impactites, their distribution and petrogenesis [in Russian]: Regional Geology and Metallogeny, v. 1, p. 121–134.
McCarthy, T. S.; Charlesworth, E. G.; and Stanistreet, I. G., 1986, Post-Transvaal structural features of the northern portion of the Witwatersrand basin: Transactions of the Geological Society of South Africa, v. 89, p. 311–324.
McCarthy, T. S.; Stanistreet, I. G.; and Robb, L. J., 1990, Geological studies related to the origin of the Witwatersrand basin and its mineralization—an introduction and a strategy for research and exploration: South African Journal of Science, v. 93, p. 1–4.
Melosh, H. J., 1989, Impact cratering: a geologic process: Oxford University Press, New York, 245 p.
Milstein, R. L., 1988, The Calvin 28 structure: evidence for impact origin: Canadian Journal of Earth Sciences, v. 25, p. 1524–1530.
Müller-Mohr, V., 1992, Breccias in the basement of a deeply eroded impact structure, Sudbury, Canada: Tectonophysics, v. 216, p. 219–226.
Nikolsky, A. P.; Naumov, V. P.; Mashchak, M. S.; and Masaitis, V. L., 1982, Shock metamorphosed rocks and impactites of Ternovka astrobleme [in Russian]: Transactions of Vsesoyuznogo Nauchno-Issledovatel'skogo Geologicheskogo Instituta (VSEGEI), Moscow, v. 238, p. 132–142.
Palme, H., 1982, Identification of projectiles of large terrestrial impact craters and some implications for the interpretation of Ir-rich Cretaceous/Tertiary boundary layers, *in* Silver, L. T.; and Schultz, P. T. (eds.), Geological implications of impacts of large asteroids and comets on the Earth: Geological Society of America Special Paper 190, p. 223–233.
Pickard, C. F., 1994, Twenty years of production from an impact structure, Red Wing Creek field, McKenzie County, North Dakota [abstract]: American Association of Petroleum Geologists Annual Convention Official Program, p. 234.
Pike, R. J., 1977, Size-dependence in the shape of fresh impact craters on the moon, *in* Roddy, D. J.; Pepin, R. O.; and Merrill, R. B. (eds.), Impact and explosion cratering: Pergamon Press, New York, p. 489–509.
Pilkington, M.; and Grieve, R. A. F., 1992, The geophysical signature of terrestrial impact craters: Review of Geophysics, v. 30, p. 161–181.
Pretorius, D. A., 1986, The gold fields of the Witwatersrand basin, *in* Anhaeusser, C. R.; and Maske, S. (eds.), Mineral deposits of southern Africa: Geological Society of South Africa, Johannesburg, v. 1, p. 489–493.
Pye, E. G.; Naldrett, A. J.; and Giblin, P. E. (eds.), 1984, The geology and ore deposits of the Sudbury structure: Ontario Geological Survey Special Volume 1, Ontario Ministry of Northern Development and Mines, Toronto, 604 p.
Roberts, C.; and Sandridge, B., 1992, The Ames hole: Shale Shaker, v. 42, p. 118–121.
Robertson, P. B.; and Grieve, R. A. F., 1977, Shock attenuation at terrestrial impact structures, *in* Roddy, D. J.; Pepin, R. O.; and Merrill, R. B. (eds.), Impact and explosion cratering: Pergamon Press, New York, p. 687–702.
Roddy, D. J.; Pepin, R. O.; and Merrill, R. B. (eds.), 1977, Impact and explosion cratering: Pergamon Press, New York, 1301 p.
Santiago, J.; and Baro, A., 1990, Mexico's giant fields, *in* Halbouty, M. T. (ed.), Giant oil and gas fields of the decade 1978–1988: American Association of Petroleum Geologists, Tulsa, p. 73–99.
Schultz, P. H.; and Merrill, R. B. (eds.), 1981, Multiring basins: Pergamon Press, New York, 295 p.
Shanks, W. S.; and Schwerdtner, W. M., 1991, Structural analysis of the central and southwestern Sudbury structure, Southern province, Canadian Shield: Canadian Journal of Earth Sciences, v. 28, p. 411–430.
Sharpton, V. L.; Burke, K.; Camarago-Zanoguerra, A.; Hall, S. A.; Lee, D. S.; Marin, L. F.; Suarez-Reynoso, G.; Quezada-Muneton, J. M.; Spudis, P. D.; and Urrita-Fucugauchi, J., 1993, Chicxulub impact basin: size and other characteristics derived from gravity analysis: Science, v. 261, p. 1564–1567.
Smit, J.,; Montonari, A.; Swinburne, N. H. M.; Alvarez, W.; Hildebrand, A. R.; Margolis, S. V.; Claeys, P.; Lowrie, W.; and Asaro, F., 1992, Tektite-bearing, deep-water clastic unit at the Cretaceous-Tertiary boundary in northeastern Mexico: Geology, v. 20, p. 99–103.
Stöffler, D., 1972, Deformation and transformation of rock-forming minerals by natural and experimental shock processes; I. Behavior of minerals under shock compression: Fortschritte der Mineralogie, v. 49, p. 50–113.
_____ 1974, Deformation and transformation of rock-forming minerals by natural and experimental

shock processes; II. Physical properties of shocked minerals: Fortschritte der Mineralogie, v. 51, p. 256–289.

Stöffler, D.; and Langenhorst, F., 1994, Shock metamorphism of quartz in nature and experiment; 1. Basic observation and theory: Meteoritics, v. 29, p. 155–181.

Stöffler, D.; Bischoff, L.; Oskierski, W.; and Weist, B., 1988, Structural deformation, breccia formation, and shock metamorphism in the basement of complex terrestrial impact craters: implications for the cratering process, *in* Bodén, A.; and Eriksson, K. G. (eds.), Deep drilling in crystalline bedrock: Springer-Verlag, Berlin, v. 1, p. 277–297.

Stöffler, D.; Deutsch, A.; Avermann, M.; Bischoff, L.; Brockmeyer, P.; Buhl, D.; Lakomy, R.; and Müller-Mohr, V., 1994, The formation of the Sudbury structure, Canada: towards a unified impact model, *in* Dressler, B. O.; Grieve, R. A. F.; and Sharpton, V. L. (eds.), Large meteorite impact and planetary evolution: Geological Society of America Special Paper 293, p. 303–318.

Therriault, A. M.; and Grantz, A., 1995, Planar deformation features in quartz grains from mixed breccia of the Avak structure, Alaska [abstract]: Lunar and Planetary Science, v. 26, p. 1403–1404.

Therriault, A. M.; Reid, A. M.; and Reimold, W. U., 1993, Original size of the Vredefort structure, South Africa [abstract]: Lunar and Planetary Science, v. 24, p.1419–1420.

Tooth, J.; and Stewart, R. R., 1994, The Steen River structure: geology and oil production [abstract]: American Association of Petroleum Geologists Annual Convention Official Program, p. 272.

White, J. C., 1993, Shock induced melting and silica polymorph formation, Vredefort structure, South Africa, *in* Boland, J. A.; and Fitz Gerald, J. D. (eds.), Defects and processes in solid state: geoscience applications: Elsevier, New York, p. 69–84.

Wood, C. A.; and Head, J. W., 1976, Comparison of impact basins on Mercury, Mars and the moon: Lunar and Planetary Science Conference, 7th, Proceedings, Houston, Texas, p. 3629–3651.

Wu, J.; Milkereit, B.; and Boerner, D., 1994, Timing constraints on deformation history of the Sudbury impact structure: Canadian Journal of Earth Sciences, v. 31, p. 1654–1660.

Survey of Hydrocarbon-Producing Impact Structures in North America: Exploration Results to Date and Potential for Discovery in Precambrian Basement Rock

Richard R. Donofrio
Consulting Geologist
Oklahoma City, Oklahoma

ABSTRACT.—Seventeen confirmed impact structures occur in petroliferous areas of North America, nine of which are being exploited for commercial hydrocarbons. Production comes from impact-affected granites, carbonate rocks, and sandstones yielding from 30 BOPD to over 2 MMBOPD (million barrels of oil per day), plus over 1.4 BCFGPD (billion cubic feet of gas per day). Reservoirs are found in central uplifts, rims, slump terraces, and ejecta and probably in subcrater fracture zones. Disrupted rocks in proximity to impact structures, such as Chicxulub, also contain hydrocarbon deposits. In some cases hydrothermal activity attending impact events can diminish reservoir quality, and talus deposits resulting from erosion of the central uplift and rim afford alternative drilling targets. The drilling success rates for new field wildcats and total wells into confirmed astroblemes are about 21 and 77%, respectively. These figures approximate the industry's success rates for wells drilled during the past five years. Roughly 50% of confirmed astroblemes and astrobleme anomalies in petroleum provinces are commercial oil and gas fields.

Outstanding statistics include a 7,200 BOPD well test in the Ames impact structure, a 4.3 BCFGPD calculated well test at the Sierra Madera astrobleme, and a well having a 2,850 ft oil column (1,600 ft of net pay) in the Red Wing Creek impact structure. Reserves are also impressive, ranging from 3 million barrels of oil at Steen River to 30 BBO (billion barrels of oil) and 15 TCFG (trillion cubic feet of gas) associated with Chicxulub. The current estimated gross income of oil and gas production from confirmed impact events in North America is $16 billion per year. To determine the hypothetical hydrocarbon potential from undiscovered or unrecognized astroblemes in U.S. petroleum basins, the exercise of overlaying the distribution pattern of Canadian Shield astroblemes onto the lower 48 states was performed. The results suggest, intuitively at least, the presence in basement rocks of impact structures with potential reserves ranging from 5 BBO to over 105 BBO.

INTRODUCTION

Twenty-five years have passed since the Red Wing Creek discovery revealed the prolific hydrocarbon potential of meteorite-impact craters (astroblemes and impact structures). Commercial oil and gas discoveries in other impact structures, as well as recognition that certain existing fields resulted from impact, have provided a small but interesting database for such esoteric structures. Included in the database are astrobleme anomalies. These are curious circular structures that lack evidence of shock metamorphism but may be of impact origin. In this paper, these anomalies include buried structures that mimic impact craters, such as calderas.

To bring organization and currency to information on producing impact structures, it was apparent that the data needed to be compiled and updated. Accordingly, I have reduced drilling results of producing impact structures and other related anomalies into table form, which should provide useful information for the profession. This review of drilling results includes a discussion of astrobleme features, drilling odds, hydrothermal considerations, and impact probability rates and concludes with an attempt to estimate the potential reserves in impact craters in the basement.

Richard R. Donofrio, 6106 North Meridian, Oklahoma City, OK 73112.

Donofrio, R. R., 1997, Survey of hydrocarbon-producing impact structures in North America: exploration results to date and potential for discovery in Precambrian basement rock, *in* Johnson, K. S.; and Campbell, J. A. (eds.), Ames structure in northwest Oklahoma and similar features: origin and petroleum production (1995 symposium): Oklahoma Geological Survey Circular 100, p. 17–29.

PRODUCING ASTROBLEMES

North American onshore and offshore petroleum provinces include nine confirmed impact structures that are commercial oil and gas fields: Ames, Avak, Calvin, Chicxulub, Marquez, Newporte, Red Wing Creek, Sierra Madera, and Steen River (Table 1). Marquez and Sierra Madera produce from below the base of their structures, but they are included here because of possible impact effects at depth. Calvin is included as confirmed on the basis of studies by Milstein (1994); Chicxulub, a confirmed astrobleme (Koeberl and others, 1994), is considered to be a producing impact event on the basis of the nature of the areal oil fields that lie beyond the crater's outer rim. Also included for reference are two producing astrobleme anomalies: Viewfield and Lyles Ranch. Of these, the origin of Lyles Ranch (also known as Bee Bluff or the Uvalde structure) is the most controversial (Sharpton and Nielson, 1988).

The structures in Table 1 are shown with locations, diameters, impact ages, discovery year of hydrocarbons, various well counts, reservoir rock, producing depths, daily production, and primary (recoverable) reserves. Data were obtained from operators, participants, government and private organizations, and consultants with direct access to well information. Although some operators were unable or reluctant to release reserve figures, estimates for these fields are provided.

Over 1,000 wells, including stratigraphic tests, dry holes, injection wells, and producers, have been drilled to date to delineate the structures in Table 1. Some of the more salient results of these drilling efforts are briefly noted below.

Impact Ages

Producing impact structures range in impact age from Cambrian–Ordovician for Newporte (Forsman and others, 1996) to late Tertiary for Lyles Ranch (LeVie, 1985). Within this time span, the ages of the structures are concentrated in the early Paleozoic, Mesozoic, and Cenozoic; as Table 1 shows, there is an absence of producing impact structures in the middle and late Paleozoic—a gap of more than 200 m.y. during which hydrocarbon-prolific Pennsylvanian and Mississippian source beds were deposited in large areas of the North American craton. Although Red Wing Creek produces from disrupted Mississipian beds, the impact event there is not Mississippian in age but occurred later—in the Jurassic–Triassic in this case. Impact craters formed in middle and late Paleozoic time have been found elsewhere but are apparently absent in petroliferous regions. It could be argued that certain oil and gas fields have not yet been recognized as having an impact origin and that undiscovered hydrocarbon-bearing impact craters are also present (Donofrio, 1976).

Discovery Year

None of the structures in Table 1 was interpreted as an astrobleme when it was initially drilled. Of the 11 structures listed, hydrocarbons were discovered in 6 between 1972 and 1978. The year 1972 is significant because it marks the phenomenal oil discovery at Red Wing Creek. The 1977 discovery of Sierra Madera hydrocarbons was in the Sierra Madera gas field below the structure's central uplift. Hydrocarbons had been discovered earlier in fields partially encompassing Sierra Madera, and the dates are provided in Table 1 notes.

Hydrocarbon discoveries and astrobleme confirmation lags have narrowed significantly because geologists now know what to look for. Avak, for example, was discovered in 1948 and is Alaska's oldest producing field (Lantz, 1981). Over 40 years later, shock metamorphism was recognized in its cores (Kirschner and others, 1992). Avak remains the first gas-producing confirmed impact structure. Its counterpart for oil is Steen River in northwest Alberta, where oil was discovered in 1968. This discovery was unrelated to shock-metamorphic studies in 1966, which were published in 1968 by Carrigy and Short.

Discovery of commercial hydrocarbons at Ames in 1991 preceded evidence for confirmed astrobleme status by about one year. Oil and gas fields older than Avak and those more recent than Ames may also be recognized as impact structures.

Producing Depths

The producing depths of astroblemes range from 200 ft at Lyles Ranch to over 17,000 ft at Chicxulub (Table 1). Excluding Chicxulub, Sierra Madera has wells approaching 13,500 ft and is the deepest. Both Sierra Madera and Lyles Ranch are unique gas fields in Texas. A search of available data showed that Lyles Ranch, which has a distinct surface expression, is the shallowest commercial gas field in Texas. It may be the shallowest overall, but this conclusion requires further study. LeVie (1985) noted that the field is anomalous in a regional trend that includes serpentine intrusions. If Lyles Ranch were excluded from Table 1, then the Calvin structure in Michigan, with commercial oil at 800 ft, becomes the shallowest-producing confirmed astrobleme.

Flow Rates and Reserves

Sierra Madera also has a distinct surface expression (Wilshire and others, 1972) that is frequently referred to as the Sierra Madera disturbance. Geologic complexities resulting from the impact event and regional tectonics appear to have affected gas reservoirs at depth. A gas well below the crater's south rim area, the Texas Pacific no. 6 Montgomery-Fulk drilled in 1975, held the state record for many years for calculated absolute

open-flow potential (S. Melzer, personal communication, 1995). Actual flow is generally about one-third of calculated flow. PI (Petroleum Information Corporation, 1975) records indicate a calculated rate of 4.3 BCFGPD (billion cubic feet of gas per day). In comparison, the average gas well in the Texas-Oklahoma area produces about 200 MCFGPD (thousand cubic feet of gas per day), whereas the average gas consumption of a typical southwestern community consisting of 10,000 dwellings is about 1 BCF per year.

Also, records are held by Red Wing Creek in North Dakota and Ames in Oklahoma. Red Wing Creek's 2,850 ft oil column (1,600 ft of net pay) in True Oil Company's no. 22-27 Burlington Northern well (Brenan and others, 1975) is unmatched in North Dakota and apparently elsewhere in the United States. An estimated 120 MMBO (million barrels of oil) are in place within Red Wing Creek's <2-mi-diameter reservoir area. P. Page (personal communication, 1994), the well-site geologist on the D. & J. no. 1-20 Gregory well in the Ames impact structure, observed an unreported *open-flow* DST (drill-stem test) in the upper 60 ft of a 204-ft pay zone that yielded over 100 barrels of oil in 20 min with no apparent drop in pressure (7,200 BOPD [barrels of oil per day]). This is the highest DST rate from a granite reservoir in North America and may be the highest worldwide. Comparable flow rates in similar lithology could not be found in the literature. Estimated reserves for this well are over 5 million barrels, assuming that its 500 BOPD allowable is a prudent production rate. With the exception of Chicxulub, Ames is the most prolific astrobleme at 2,600 BOPD plus 3.1 MMCFGPD (million cubic feet of gas per day). Of the 40 producing wells, however, 6 completed in brecciated granite account for over half the daily oil production.

The most recent studies by V. Sharpton (personal communication, 1997) put the maximum diameter of the Chicxulub structure in Mexico's Yucatan Peninsula at about 180 mi. The reservoir rock is primarily dolomitized breccia (Santiago and Baro, 1990), which is believed to have originated in part by interaction of impact-generated subsea seismic waves with platform carbonates (J. Rosenfeld; G. Penfield, personal communication, 1995). This producing breccia occurs in (proposed) postimpact structural traps about 90 mi (within two crater radii) southwest of the outer rim in the offshore Bay of Campeche. As of January 1995, remaining (proved) reserves for this area were estimated by PEMEX at 27.2 BBO (billion barrels of oil) (including condensate) and 11.3 TCFG (trillion cubic feet of gas) (E. Gonzalez, personal communication, 1995). Of interest is that, about the same date, U.S. reserves were 22.9 BBO and 162.4 TCFG. Thus, the oil reserves believed to be associated with the Chicxulub impact event exceed those of the entire onshore and offshore U.S. reserves, including Alaska's Prudhoe Bay. Current production from the Bay of Campeche is about 2.1 MMBOPD (million barrels of oil per day) (including condensate) and about 1.4 BCFGPD. This area constitutes the major part of Mexico's 2.8 MMBOPD production. Chicxulub also accounts for mostly all of the estimated $16 billion per year gross income from hydrocarbon production associated with North American impact structures.

ASTROBLEME FEATURES

Figure 1 shows the astrobleme features where reservoirs can develop, and Table 2 lists producing examples. Four such producing features have been confirmed to date: central uplift, rim, slump terraces and/or listric faults, and ejecta. Listric faults are combined with slump terraces because this type of faulting, which is curvilinear and concave upward, usually produces slump terraces. Indirectly, sedimentary units draped over certain astrobleme features, such as the central uplift, may also form reservoirs. A possible example needing further study is the producing Heidt anomaly in Stark County, North Dakota (*Oil and Gas Journal*, 1996).

Five of the producing astrobleme examples in Table 2 disrupted Precambrian rock. Of these, Ames, Calvin, Steen River, and Chicxulub are complex-type structures with central uplifts, and Newporte is a simple bowl-shaped structure. Ames and Newporte produce from both crystalline and sedimentary rock. At Ames, the central uplift produces from brecciated Precambrian granite; the rim and ejecta produce from Ordovician dolomites. At Newporte, the rim rocks of Cambrian sandstones and brecciated Precambrian granite provide the reservoirs. Chicxulub, Calvin, and Steen River have central uplifts of basement rock underlying sedimentary units but do not produce from the Precambrian. Steen River produces from overturned and fractured Devonian dolomites in the rim (G. Robertson, personal communication, 1995), and Chicxulub produces from Cretaceous dolomitized breccia affected outside of the crater. Avak has a central uplift of metamorphic basement rock—a Paleozoic argillite—underlying sedimentary rocks. However, the structure produces from Jurassic sandstones in the rim area that were displaced by listric faults (Kirschner and others, 1992). Another example of this type of faulting is found at the Calvin impact structure, where listric faults resulted in slump terraces. The reservoir rock is a Devonian dolomitized algal mat, some areas of which have open flow channels 2 to 3 in. wide (T. Kuhns, personal communication, 1995). The configuration of the structure following impact influenced the depositional environment for reefal-type development.

Subcrater fracture-zone production has not been confirmed, but Marquez and Sierra Madera

TABLE 1.—PRODUCING IMPACT

Name*	Location	Diameter (mi)	Diameter (km)	Impact age	Hydrocarbon discovery year	Wells required for discovery	Active producing wells**
(1) **Ames**	Major County, Oklahoma	8	13	E. Ordovician	1991	1	40
(2) Avak	Point Barrow, Alaska	7.5	12	Cretaceous-Tertiary	1949	2	10
(3) **Calvin**	Cass County, Michigan	3	4.8	L. Ordovician	1978	2	30
(4) **Chicxulub**	Yucatan Peninsula, Mexico	180	300	Cretaceous-Tertiary	1974	6	453
(5) Marquez	Leon County, Texas	7.9	12.7	E. Tertiary	1977	5?	6
(6) **Newporte**	Renville County, North Dakota	2	3.2	Cambrian-Ordovician	1977	1	2
(7) Red Wing Creek	McKenzie County, North Dakota	5.6	9	Jurassic-Triassic	1972	3	14
(8) Sierra Madera	Pecos County, Texas	8	13	L. Cretaceous	1977	4	20
(9) **Steen River**	N.W. Alberta, Canada	15.5	25	M. Cretaceous	1968	7	2
(A) Lyles Ranch	Zavala County, Texas	2.5	4	L. Tertiary	1979	2	4
(B) Viewfield	S.E. Saskatchewan, Canada	2	3.2	E. Jurassic	1969	2	50

*(1)–(9) are confirmed impact structures. (A) Lyles Ranch and (B) Viewfield lack diagnostic shock metamorphism and are classified as astrobleme anomalies. Structures disrupting Precambrian basement rock are in bold. Success rates usually are determined by more than one operator. Refer to text and references for details of structures and reservoir rocks.

**Production and well-count figures are through March 1995, unless stated otherwise.

Sources and notes correspond to listed order of structures:
(1) Continental Resources, Inc.; Petroleum Information Corp. Production and well count figures are through August 1996. The strong natural water drive is affecting optimum production and recovery.
(2) Alaska Oil and Gas Conservation Commission.
(3) Michigan Geological Survey; Center Junction Corp.
(4) PEMEX. Early well records are unclear relative to penetration of key Lomas Tristes breccia or fractured interval. Apparently five deep wells were required for onshore discovery prior to exploration in adjacent offshore Bay/Gulf of Campeche, where hydrocarbons were discovered on the first well. Data shown, including discovery year, are for Bay of Campeche fields. Well count is through December 1994. Production figures are through November 1995. Production is from outside of outer rim within a distance of two crater radii to the southwest.

appear to be suitable candidates. The best gas production in both areas is either directly below the crater (Marquez) or below the peripheral rim area (Sierra Madera). Marquez produces from Early Cretaceous fluvial sandstones and shales, and Sierra Madera produces from Early Paleozoic fractured carbonates.

Briefly, some of the other impact features include rim-flank pinchout resulting from eroded rim rocks and marine transgressive deposits on a rim or rim arc's basinward flank, breccia lens pinchout created where the breccia lens abuts the crater wall updip, radial faults resulting from radial tension fractures (analogous to spokes on a

Structures in North America

Dry holes	Total wells	Success rate	Reservoir rock	Producing depth (ft)	Daily production BOPD	Daily production CFGPD	Primary reserves BO	Primary reserves CFG
49	98	50%	Granite, carbonates	8,400–9,500	2,600	3.1 MM	25 MM	15 B
7	18	61%	Sandstones	2,600–2,800		1.3 MM		39 B
25	91	73%	Carbonates	800–900	110		3 MM	
93	658	86%	Carbonates	8,300–17,000+ (11,500 avg)	2.1 MM	1.4 B	30 B	15 T
4	10	60%	Sandstones	9,000 avg	30	1.8 MM	100–150 M	5–7 B
3	7	57%	Granite, sandstones	9,150–9,600	280		15 MM	
14	34	58%	Carbonates	8,000–9,700	960	2.3 MM	20 MM	25 B
10	65	84%	Carbonates	12,000–13,500		7.7 MM		270 B
25	29	14%	Carbonates	4,265–4,500	550		3–5 MM+	
5	14?	64%	Sandstones	200–500		68 M		2 B
24	137	82%	Carbonates	4,160–4,300	575	260 M	10.5 MM	4.5 B

(5) Texas Railroad Commission; Marathon Oil Co. Production is from below base of crater. Reserves not available; estimated. Diameter is from recent gravity studies by Wong (1994).
(6) North Dakota Geological Survey; Eagle Operating Co. Production and well count figures are through November 1996. One recompleted well in Cambrian sandstones yields mostly all production.
(7) North Dakota Geological Survey; True Oil Co. Secondary recovery using miscible hydrocarbon flooding was begun in 1982, prior to depletion of primary reserves. Total reserves not available. Using 120 MMBOIP (million barrels of oil in place), the field may recover 35–60 MMBO and 45–80 BCFG.
(8) University of Texas of the Permian Basin; Melzer Exploration Co. Reserves are from four fields believed to be linked in part to the impact event. Names and discovery years of fields are Elsinore, 1958; Pikes Peak East, 1972; GMW, 1976; Sierra Madera, 1977. Production is from below base of crater and rim area.
(9) Mercantile Canada Energy, Inc. Structure is oblate, actual dimensions are 14.5 × 15.5 mi (23 × 26.5 km). Significant potential. Needs more exploration.
(A) Texas Railroad Commission. Production figures are through December 1994.
(B) Saskatchewan Energy and Mines. 700 MBO remaining for primary recovery. Secondary recovery, if initiated, is limited and may yield an additional 1–3 MMBO. The two pay zones already have a partial natural water drive.

wheel), simultaneous and overlapping craters resulting from multiple impacts or impact overprinting, and elongate or "butterfly"-shaped craters formed by low-angle impacts. As with conventional reservoirs, these features require source, seal, and trap. Unlike conventional reservoirs, geochemical studies by Castaño and others (1994) suggest that meteorite impacts can create closed basins that are favorable for the deposition of hydrocarbon source rocks. Producing examples appear to be Ames and Newporte.

It is proposed that almost all of the features in Table 2 are capable of producing hydrocarbons from basement rock. The exception is the sub-

TABLE 2.—IMPACT STRUCTURE RESERVOIRS

Impact feature	Producing example
Central uplift	Ames, Calvin, Red Wing Creek
Rim	Ames, Avak, Calvin, Newporte, Steen River, Lyles Ranch*, Viewfield*
Ejecta	Ames, Chicxulub(?)
Slump terraces and/or listric faults	Avak, Calvin
Radial faults	Ames(?)
Drapeover	Heidt*(?)
Subcrater fracture zone	Marquez(?), Sierra Madera(?)
Marine impact	Chicxulub breccia(?), North Sea turbidites(?)
Brecca lens pinchout	Not yet recognized
Rim-flank pinchout	Not yet recognized
Simultaneous and/or overlapping craters	Not yet recognized
Elongate or "butterfly" craters	Not yet recognized

*Impact origin not yet confirmed.

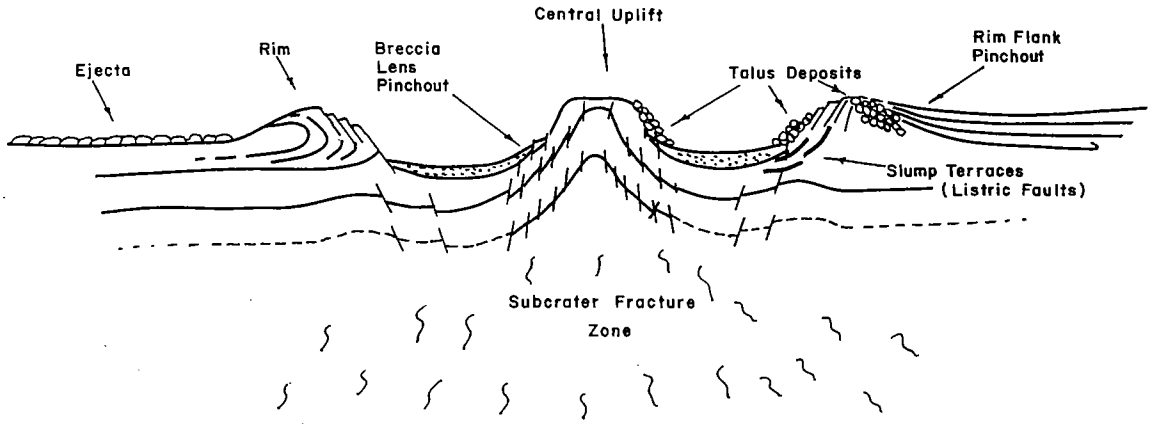

Figure 1. Diagrammatic cross section of a complex-type impact structure showing composite (ideally symmetrical) reservoir features. Radial faults not included. Modified from Donofrio (1981) and Brenan and others (1975).

crater fracture zone below the base of the crater. This feature is limited to whatever sedimentary column may be present because conventional source beds are not present beneath otherwise undisturbed Precambrian crystalline rock (Donofrio and others, 1984).

NONPRODUCING ASTROBLEMES

Other impact events are known to have occurred in oil- and gas-prone areas. However, the timing for hydrocarbon sourcing, sealing, and trapping has not been conducive to formation of commercial deposits in some structures.

Within North American offshore and onshore petroleum provinces there are eight confirmed impact structures where commercial hydrocarbons have not been reported. These are Montagnais, Scotian Shelf (L. Jansa, personal communication, 1993); Eagle Butte, Alberta; Flynn Creek and Wells Creek, Tennessee; Kentland, Indiana; Middlesboro, Kentucky; Serpent Mound, Ohio; and Kilmichael, Mississippi. The latter is tentatively included here as a confirmed astrobleme because, subsequent to studies by Robertson and Butler (1982), diagnostic shock-metamorphic features in quartz have reportedly been found. Verification is currently underway.

One of these structures may prove to have commercial potential. According to the Kentucky Geological Survey, the 3.6-mi-diameter Middlesboro structure in Bell County, Kentucky, has a 15

MCFGPD shut-in well completed in Mississippian siltstones at 3,200 ft. Two other wells were dry, but additional drilling may be forthcoming. The remaining astroblemes identified above were either dry, had shows, or may not have been adequately explored.

OTHER ANOMALIES

Other structures exist that lack shock-metamorphic evidence but meet other geologic and geophysical criteria for astroblemes. Some examples are Haswell hole, Colorado (Gay, 1997); Panther Mountain, New York (Isachsen and others, 1994); Chimney prospect, Montana (Plawman and Hagar, 1983); Hartney, Manitoba; Elbow and Dumas, Saskatchewan (Sawatsky, 1977); and Lamont and Selmon, Oklahoma. Byler (1992) showed numerous intact and discontinuous circular anomalies in North America, some of which may be remnant impact scars. Overviews and/or references for numerous astroblemes and astrobleme anomalies can also be found in Grieve and Masaitis (1994), Grieve and others (1995), and Koeberl and Anderson (1996). An intriguing and controversial paper on the meteorite-impact theory as a viable alternative to plate-tectonics theory can be found in Butler (1996). The list of astrobleme anomalies continues to expand, and candidate structures will be confirmed as information warrants.

DRILLING ODDS

The tentative and limited information on confirmed impact structures in petroleum provinces indicates that 9 of 17 astroblemes (53%) are commercial oil and gas fields. However, it required about 42 wells into the 17 structures to establish which were commercial. These numbers give a new field wildcat success rate of about 21% (9 hits out of 42 wells). Other wells into the 9 commercial astroblemes can be difficult to classify as exploratory or development. For example, most operators consider that drilling in the Ames impact structure is primarily exploration regardless of the separation distances among wells. Therefore, the success rates in Table 1 are given for each structure as a percentage of all wells for that particular structure. For example, a total of 7 wells were drilled at Newporte, of which 3 were dry holes. Thus, 4 wells out of 7 (regardless of the categories) were successful, which gives a success rate of about 57%. Of the 4 completions, 2 are currently active.

The drilling success rates for producing astroblemes range from 14% at the remote Steen River structure to 86% at Chicxulub. The average success rate for total wells into all producing astroblemes is about 77%. Excluding Chicxulub, which accounts for two-thirds of the total wells into producing astrobleme areas, the average success rate is about 58%. In most cases, the success rates would have been higher if operators had been aware of what they were drilling from the outset. In comparison, the success rates for 127,253 U.S. wells drilled from 1990 through 1994 were about 20% for new field wildcats and 74% for all wells (PI, 1995).

As previously noted, 53% of confirmed astroblemes in petroleum provinces are commercial oil and gas fields. Of the 9 commercial impact structures, Table 1 reveals that 5 required between 1 and 3 wells for hydrocarbon discovery. The other 4 craters needed between 4 and 7 wells. Considering the hydrocarbon potential of astroblemes, the drilling success rates are quite favorable. However, all producing astrobleme discoveries to date have been by accident, and the potential rewards of wildcat drilling come with a "Catch-22."

The drilling success rates are for confirmed astroblemes in petroleum provinces, not for astrobleme anomalies, which may or may not be bona fide astroblemes (e.g., solution collapse features, calderas). Unless the objective is confirmed as an astrobleme prior to or during drilling, the well may be headed into an anomaly having a lower (or zero) chance of success. Impact craters having surface expressions may display shock metamorphism and can be studied prior to drilling. But buried structures require drilling, and the exploration may find that the objective is not a confirmed astrobleme.

What are the chances of finding commercial hydrocarbons in astrobleme anomalies? Based on a preliminary check of published material, 6 of 12 curious circular structures in North American petroleum provinces are commercial oil and gas fields. All but one, a circular depression in Texas County, Oklahoma (*Oil and Gas Journal,* 1993), were previously mentioned in this paper. This tentative list suggests that 50% of astrobleme anomalies have been drilled successfully. The chances of hitting pay on the first well calculate at about 25% or better for anomalies of decreasing diameters. Combining confirmed astroblemes and astrobleme anomalies gives a total of (at least) 29 circular structures in North American onshore and offshore petroleum provinces. Of these, 15 are commercial oil and gas fields (about 52%). These figures could differ if relevant unpublished drilling prospects were included.

HYDROTHERMAL CONSIDERATIONS

In rare cases high-temperature hydrothermal activity can enhance reservoir quality by rupturing overlying rocks. An example of hydrothermal rupture is the Blackburn oil field in Nevada, where carbonates overlying an ancient magmatic heat source were possibly fractured and brecciated by explosive hydrothermal action, i.e., ground

water contacting a pluton became superheated and overpressured owing to the overburden (Hulen and others, 1990). This porosity-creating mechanism, however, is quite different from conditions at meteorite-impact sites.

Following an impact event, hydrothermal circulation is initiated within the target rocks. A boiling water table forms below the impact-melt sheet and steam and water escape mainly at the rim in simple craters and in both the rim and central uplift of complex craters (Newsom, 1980). There is negligible pressure buildup, however, and the net effect of circulation activity is to plug fractures with mineral deposits.

Hydrothermal effects following impact events have not been duplicated in the laboratory, but experiments directed at understanding fault-zone sealing may afford insight into hydrothermal processes. Moore and others (1994) studied the hydrothermal effects on a typical granite composed of plagioclase, quartz, and feldspar. Extrapolation of data from fractured samples subjected to temperatures of 300 to 500 °C showed that permeability reductions of almost three orders of magnitude (1,000 times less) can occur within a few years in crystalline basement areas such as the Canadian Shield. These permeability decreases are most likely caused by hydrothermal-related solution-transfer processes that redistribute minerals in rock and can result in negligible fluid flow approaching that of intact granite.

At the Ries crater in Germany, Pohl (1977) calculated that some of the suevite took about 2,000 years to cool from 600 to 100 °C. Hydrothermal activity measured there has been documented at other terrestrial impact structures, with estimated postimpact temperatures ranging from 100 to 700 °C (Koeberl and others, 1989). Hydrothermal alteration of target rocks can occur in a fraction of the time it takes for temperatures at impact sites to reach ambient levels, and this alteration is invariably detrimental to reservoir quality.

Hydrothermal activity at impact sites can produce economic deposits of zinc minerals, for example (Grieve and Masaitis, 1994), but for potential hydrocarbon reservoirs, the fractured rock needs to remain open. As a general rule, hydrocarbon reservoirs are unproductive (or uneconomic) below a porosity of about 5%. The permeability threshold for gas reservoirs is about 0.1 md (millidarcies) and about 0.5 md for oil reservoirs. Values near the threshold, however, can be offset by large pay zones.

Both porosity and permeability are affected by hydrothermal activity, but the reductions in porosity are not as consequential as the reductions in permeability. An example of hydrothermal effects across a basement astrobleme is given in Donofrio (1981) for the 8-mi-diameter Deep Bay structure on the Canadian Shield. The rim core had a porosity of 8.5% and a permeability of 0.01 md; breccia off the flank of the central uplift (possibly talus) had 21.4% and 13.7 md; and the central uplift had 14.9% and 0.05 md. All three areas had adequate porosities, but only one area had adequate permeability.

Hydrothermal effects thus place constraints on drilling locations in impact structures, particularly those in basement rock. Moderate crater erosion prior to burial can enhance reservoir quality and form talus deposits on the flanks of central highs and peripheral rims, thus offsetting permeability reductions due to hydrothermal activity. The most productive reservoir at Ames, for example, is a relithified granodiorite that is frequently referred to as brecciated granite or a rubble pile. This rubble condition may have resulted from exposure of the central uplift to subaerial weathering and erosion (Roberts and Sandridge, 1992). Similar material (probably talus) may form the carbonate rubble of the productive rim at the Viewfield structure (Donofrio, 1981).

The central uplift at the Steen River basement astrobleme was penetrated near the center and found to be of competent, tight igneous rocks initially misidentified as volcanic rocks (Winzer, 1972). The central-uplift flanks at Steen River also need to be explored, and hydrothermal studies, including fluid-inclusion analysis, need to be undertaken at both it and Ames. Determining the hydrothermal effects in sedimentary astroblemes and astrobleme anomalies such as Red Wing Creek and the Chimney prospect, respectively, would also be informative. Until more information is forthcoming, geologists should use the Ames experience when planning an exploration program for similar structures in basement rock (Donofrio, 1994).

RANDOM OR NONRANDOM IMPACTS?

Impact events are assumed to be random in time and space. Impact probability rates of Cannon (1995), for example, using the density of Earth-crossing asteroids and cratering rates on other planetary bodies, suggest that at least 500 astroblemes the size of Ames should have been created in the conterminous states since the beginning of the Cambrian. The number preserved to the present will be considerably less, however.

Shaw (1994) argued against the random nature of impact events and sampling bias and called attention to the ordered age grouping and positioning of craters on North America, Eurasia, and Australia. Shaw noted three spatial nodes that have persisted since the late Precambrian. These nodes represent the loci of mutual overlap of all age groups of known impact events and mark the intersection points of cratering swaths that encircle the Earth. For example, the cratering nodes of North America, Eurasia, and Australia can be connected by a nearly circular swath during the Phanerozoic, suggesting that bolides are impacting limited areas. A possible explanation is that

the orbital parameters of bolides are influenced by gravitational variations within the Earth. Of interest is that the crater-age overlap forming the node for North America embraces mostly all petroleum provinces. If Shaw is correct, an abundance of astroblemes unpredicted by cratering estimates may exist in oil- and gas-prone areas.

POTENTIAL RESERVES OF BASEMENT ASTROBLEMES

While the random vs. nonrandom issue is debated, an intuitive approach might be used to estimate the reserves in undiscovered or unrecognized U.S. impact structures in basement rocks. Figure 2 shows the location of astroblemes on the Canadian Shield and several of the larger petroleum basins in the United States. For illustrative purposes, the petroliferous areas are shown in their present-day configuration. Crater names and dimensions can be found in Grieve and Robertson (1989). All of these astroblemes are developed in crystalline basement rock and range in impact age from Precambrian to Tertiary, with the majority dated as Paleozoic. Diameters range from 1.2 to over 84 mi, with half approaching or exceeding the 14 mi diameter of the Ries impact structure in Germany. The Ries is mentioned because it illustrates the penetration effects of large bolides. Pohl and others (1977) noted that the Ries crater was created by the impact of a 3,300-ft-diameter stony meteorite that penetrated about 2,000 ft of sedimentary rocks and continued for another 2,100 ft into crystalline basement. Seismic surveys have revealed that basement rock at the crater center has been brecciated and fractured down to about 20,000 ft. Impact events forming craters of this diameter or larger could penetrate deeply into petroleum basins and affect basement rock.

The impact structures in Figure 2 have been studied in detail by the Geological Survey of Canada. From geologic and geophysical data, which include core studies, the volume of brecciated and fractured rock can be estimated and adjustments made for hydrothermal effects. If it is assumed that the Canadian Shield astrobleme distribution is a fair representation of impact density for the larger, more resistant structures, the question to be answered is, "What would the potential reserves of these craters be if the impacts had of occurred in petroleum basins?" The following parameters are used: a 50% crater erosional level before preservation by overlying sedimentary deposits; a threshold sedimentary cover of about 7,000 ft to provide the geothermal conditions for hydrocarbon generation; proper timing of impact event, source rock, and seal; and an oil-recovery factor of 100 barrels per acre-foot.

To evaluate the potential reserves, the Canadian Shield astrobleme cluster was shifted about 15° south (Fig. 3). Initially, this shift was selected because it is the point at which the most northerly crater of the cluster contacts the requisite overburden in a U.S. petroliferous area, the Michigan basin. Likewise, Figure 3 shows that such a shift displaces numerous astroblemes into onshore and offshore petroliferous areas. Potential reserves for this scenario are about 50 BBO, an extraordinary figure more than double current U.S. reserves. If we control (or subtract) the reserves in all basement rock, including granite washes, the drop in potential reserves is less than 1%. This result suggests that the volume of undiscovered basement hydrocarbons may be significantly higher than known basement reserves.

At first glance the practicing exploration geologist may reason that such fanciful superpositions are meaningless in the real world of exploration, but one cannot ignore impact densities of large astroblemes or the geographic distribution of petroleum provinces. The only real challenge may come from optimistic geologists who claim that impact structures remain undiscovered and that they occur in greater numbers than are shown here. Of interest is that no matter to what degree or how far and wide the Canadian Shield astrobleme cluster is shifted or rotated into the area of U.S. petroleum basins, the potential reserves range from a low of 5 BBO to a high of over 105 BBO.

The conditions leading to giant hydrocarbon accumulations in conventional reservoir rocks such as sandstones and carbonates appear to be fortuitous, but they do occur. According to one estimate, worldwide exploration has revealed that giants constitute only 0.6% of significant oil fields yet they contain 84% of the reserves (Hobson and Tiratsoo, 1981). Giants within the U.S. usually are defined as having at least 100 MM barrels of recoverable oil or 1 TCF of recoverable gas. Before excluding the lower 48 states from such potential, geologists should consider Van Der Loop's (1996) resource base study where she has noted, "although the biggest fields in any trend are usually the first ones found . . . if you do find something in a lower 48 frontier area, the chances that it will be big enough to keep are better than if you had found something in a mature trend."

For astrobleme anomalies, those chances could be much higher than the 4% or less success rate for conventional prospects in lower 48 frontier areas. As I stated over 15 years ago (Donofrio, 1981), "suspicious gravity, seismic, and magnetic anomalies in basement should be penetrated and tested where drilling depth permits. These anomalies include elevated areas of basement as well as synclines. . . . Detection of astroblemes by geophysical or geologic methods means that fractured reservoirs have been located. . . . Unquestionably with some deep-basement impacts the capital expenditures will be considerable but the possible rewards can be enormous." Clearly such structures are of strategic importance to the United States (Donofrio, 1983).

The Canadian Shield cluster displacement

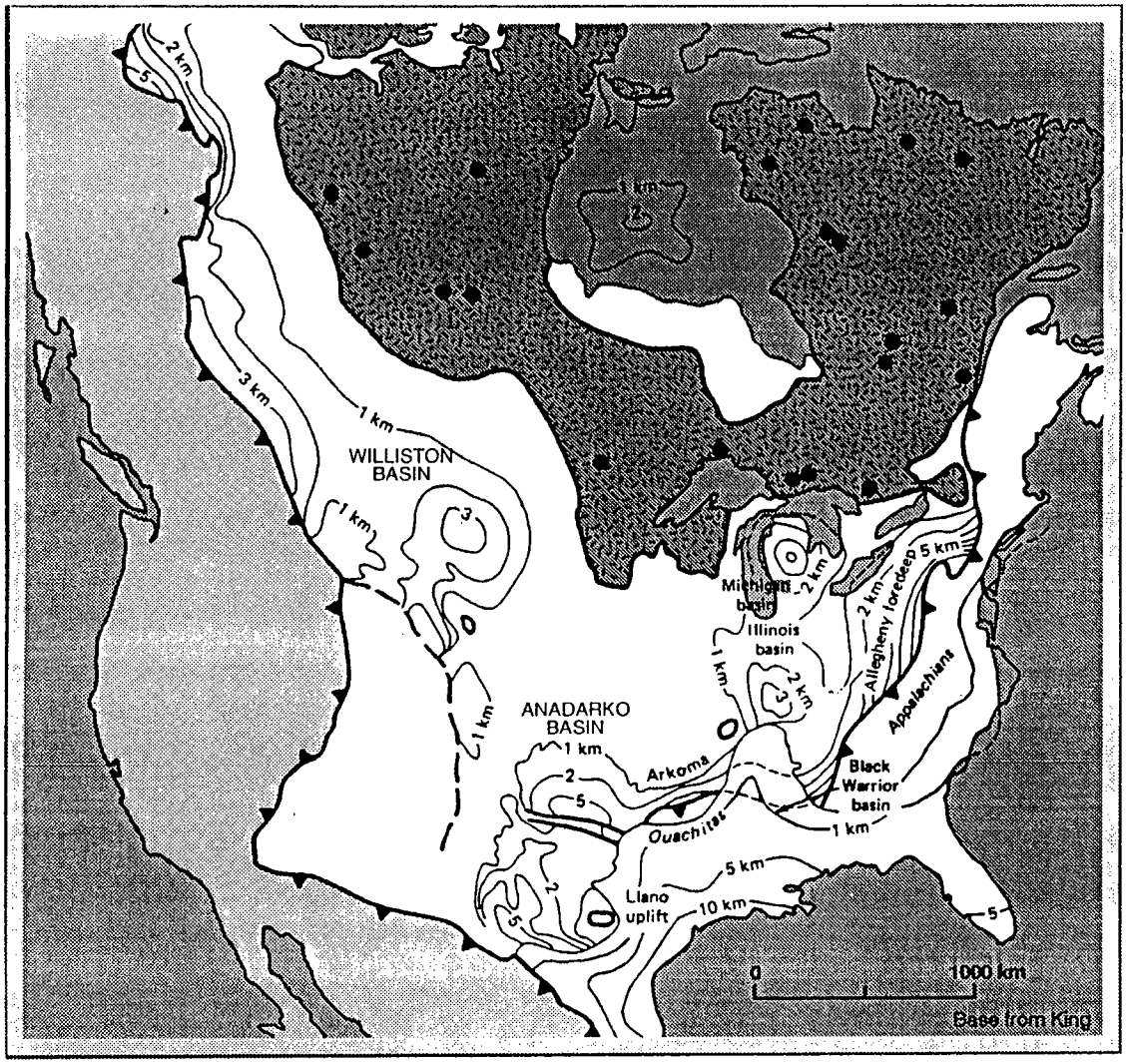

Figure 2. Distribution of astroblemes on the exposed Precambrian Canadian Shield. Contours show the approximate depth below sea level of the unconformity between Precambrian basement rock and sedimentary cover. The contours in the Gulf Coast and Atlantic coastal margin show the depth to Paleozoic basement rocks. Base map modified from Suppe (1986) and King and Edmonston (1972).

exercise (Fig. 3) suggests that the potential for hydrocarbon reserves in impact craters in basement rocks may be significant and that, like conventional oil and gas fields, most of the reserves will be found in only a few large structures.

Thus far, the largest producing confirmed astrobleme in the United States is Ames with a diameter of about 8 mi. Nonproducing confirmed impact craters larger than Ames have not yet been recognized in U.S. petroleum provinces. In U.S. areas outside petroleum provinces, the largest confirmed impact structure is the 54-mi-diameter Chesapeake Bay crater in Virginia.

Where are the other large-scale impact structures comparable to those on the Canadian Shield?

CONCLUSIONS

The drilling record to date shows that, although producing impact structures are few in number, they have a disproportionate share of significant characteristics. These include (1) the ability to form (or enhance) structure, reservoir rock, and possibly source rock independent of the regional geology; (2) exceptional reservoir thickness, high yields, and flow rates; (3) production (and potential production) from numerous types of reservoirs

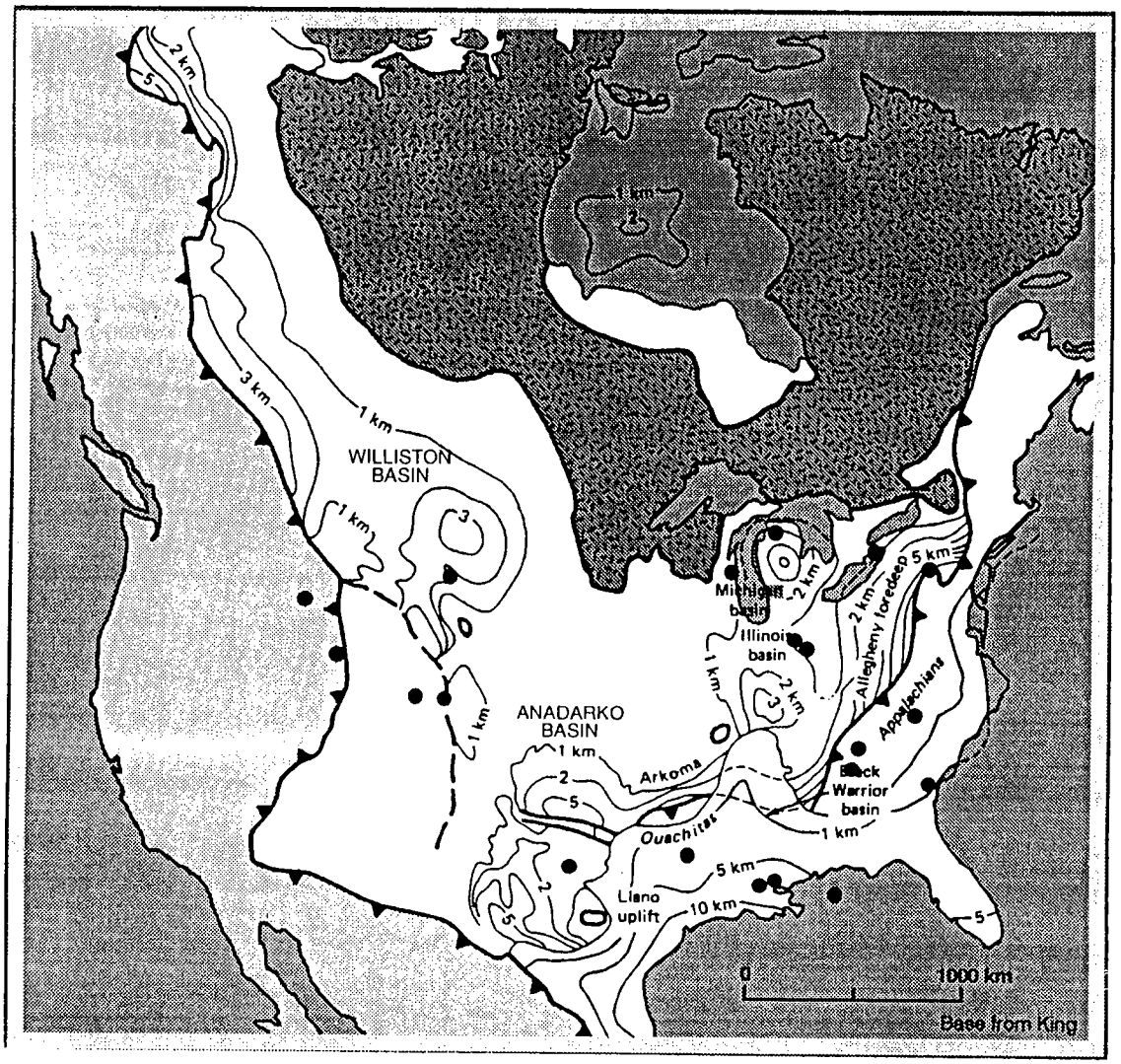

Figure 3. Canadian Shield astroblemes shifted 15° south. Note the impact structures within petroleum provinces. Any shift or rotation of this astrobleme cluster into U.S. petroleum basins results in potential reserves ranging from 5 BBO to over 105 BBO.

within, below, above, and beyond the structure; and (4) reservoirs that include crystalline basement rock.

The drilling success rates in confirmed astroblemes for new field wildcats and total wells are 21 and 77%, respectively. These rates approximate the industry's average of 20 and 74% for the same categories. The similarity in figures is not surprising considering that all producing astroblemes to date were found by accident with conventional exploration models and practices. After hydrocarbons were discovered came the realization that the structures had an impact origin. To use astroblemes as an exploration concept, geologists need to reverse the sequence.

About half the confirmed astroblemes and astrobleme anomalies in petroleum provinces are commercial oil and gas fields and, on average, these structures required about 2–4 wildcats to find the pay. The number of wildcats appears to reflect the dimensions of included anomalies in this initial study. Like confirmed astroblemes, the database for astrobleme anomalies is small and inconclusive.

The least explored horizon and final frontier for the petroleum geologist is crystalline basement. Two producing impact structures have already proven that this lithology can be a viable reservoir. Undiscovered basement (and sedimentary rock) astroblemes certainly exist and are capable of

hosting giant oil and gas fields. The known and potential dimensions of impact events need to be realized. Large-scale impact structures (or their remnants) approach linearity relative to regional geologic and geophysical coverage used in an exploration program. Recognition of a feature such as a rim arc is a challenge to explorationists, and I propose that the basinward flank of a large-scale rim segment is where a giant field awaits discovery.

ACKNOWLEDGMENTS

I offer my appreciation to D. Groff for his critical review of this manuscript and helpful suggestions and to K. Mauk for his computer assistance with Table 1.

REFERENCES CITED

Brenan, R. L.; Peterson, B. L.; and Smith, H. J., 1975, The origin of the Red Wing Creek structure, McKenzie County, North Dakota: Wyoming Geological Association Earth Science Bulletin, v. 8, 41 p.

Butler, M. D., 1996, the MI Theory: a reply and further comments: The Leading Edge, v. 15, p. 383–391.

Byler, W. H., 1992, Evidence of large horizontal earth movements, *in* Mason, K. (ed.), Basement tectonics 7: Kluwer Academic Publishers, Dordrecht, Netherlands, p. 33–48.

Cannon, J., 1995, The frequency and distribution of terrestrial impact craters [abstract]: Society of Independent Professional Earth Scientists Annual Convention, p. 9.

Carrigy, M.; and Short, N. M., 1968, Evidence of shock metamorphism in rocks from the Steen River structure, Alberta, *in* French, B. M.; and Short, N. M. (eds.), Shock metamorphism of natural materials: Baltimore, Mono Book Corp., p. 135–158.

Castaño, J. R.; Clement, J. H.; Kuykendall, M. D.; and Sharpton, V. L., 1994, Source rock potential of impact craters [abstract]: American Association of Petroleum Geologists, 1994 Annual Convention Official Program, p. 118.

Donofrio, R. R., 1976, The challenges of exploration: impact craters: Ultramar Quarterly, no. 3, p. 8.

_____ 1981, Impact craters: implications for basement hydrocarbon production: Journal of Petroleum Geology, v. 3, p. 279–302.

_____ 1983, The strategic importance of detecting subsurface hydrocarbon-bearing astroblemes [abstract]: U.S. Department of Energy Small Business Innovative Research Program: Contract Awards, DOE-ER-0181, p. 18.

_____ 1994, Petroleum exploration strategies for impact features [abstract]: American Association of Petroleum Geologists, 1994 Annual Convention Official Program, p. 138.

Donofrio, R. R.; Olsen, K. H.; Vlierboom, F. W.; Witschard, F.; and Petersson, G., 1984, Deep gas, Swedish premises: the Siljan Ring project—independent expert evaluation: Vattenfall, Stockholm, Sweden, 63 p.

Forsman, N. F.; Gerlach, T. R.; and Anderson, N. L., 1996, Impact origin of the Newporte structure, Williston basin, North Dakota: American Association of Petroleum Geologists Bulletin, v. 80, p. 721–730.

Gay, S. P., Jr., 1997, "Haswell hole," a previously unknown impact structure in southeast Colorado, *in* Johnson, K. S.; and Campbell, J. A. (eds.), Ames structure in northwest Oklahoma and similar features: origin and petroleum production (1995 symposium): Oklahoma Geological Survey Circular 100 [this volume], p. 272–276.

Grieve, R. A. F.; and Masaitis, V. L., 1994, The economic potential of terrestrial impact craters: International Geology Review, v. 36, p. 105–151.

Grieve, R. A. F.; and Robertson, P. B., 1989, Terrestrial impact structures (Geological Survey of Canada map), *in* American Association of Petroleum Geologists, AAPG Explorer, April 1989, p. 16.

Grieve, R. A. F.; Rupert, J.; Smith, J.; and Therriault, A., 1995, The record of terrestrial impact cratering: GSA Today, v. 5, p. 189–196.

Hobson, G. D.; and Tiratsoo, E. N., 1981, Introduction to petroleum geology: Scientific Press Ltd., Beaconsfield, England, 352 p.

Hulen, J. B.; Bereskin, S.; and Bortz, L. C., 1990, High-temperature hydrothermal origin for fractured carbonate reservoirs in the Blackburn oil field, Nevada: American Association of Petroleum Geologists Bulletin, v. 74, p. 1262–1272.

Isachsen, Y. W.; Wright, S. F.; and Revetta, F. A., 1994, The Panther Mountain feature possibly hides a buried impact crater: Northeastern Geology, v. 16, p. 123–136.

King, P. B.; and Edmonston, G. J., 1972, Generalized tectonic map of North America: U.S. Geological Survey Map I-688, scale 1:5,000,000, 1 sheet.

Kirschner, C. E.; Grantz, A.; and Mullen, M. W., 1992, Impact origin of the Avak structure, Arctic Alaska, and genesis of the Barrow gas fields: American Association of Petroleum Geologists Bulletin, v. 76, 651–679.

Koeberl, C.; and Anderson, R. R., 1996, Manson and company: impact structures in the United States, *in* Koeberl, C.; and Anderson, R. R. (eds.), The Manson impact structure, Iowa: anatomy of an impact crater: Geological Society of America Special Paper 302, 476 p.

Koeberl, C.; Fredrickson, K.; Gotzinger, M.; and Reimold, W. U., 1989, Anomalous quartz from the Roter Kamm impact crater, Namibia: evidence for post-impact hydrothermal activity?: Geochimica et Cosmochimica Acta, v. 53, p. 2113–2118.

Koeberl, C.; Sharpton, V. L.; Schuraytz, B. C.; Shirley, S. B.; Blum, J. D.; and Marin, L. E., 1994, Evidence for a meteoritic component in impact melt rocks from the Chicxulub structure: Geochimica et Cosmochimica Acta, v. 58, p. 1679–1684.

Lantz, R. J., 1981, Barrow gas fields—North Slope, Alaska: Oil and Gas Journal, v. 79, p. 197–200.

LeVie, D. S., 1985, Lyles Ranch field, south Texas:

production from an astrobleme?: Transactions of the Gulf Coast Association of Geological Societies, v. 35, p. 179–187.
Milstein, R., 1994, The Calvin impact crater, Cass County, Michigan: identification and analysis of a subsurface Ordovician astrobleme: Oregon State University unpublished Ph.D. dissertation, 114 p.
Moore, D. E.; Lockner, D. A.; and Byerlee, J. D., 1994, Reduction of permeability in granite at elevated temperatures: Science, v. 265, p. 1558–1561.
Newsom, H. E., 1980, Hydrothermal alteration of impact melt sheets with implications for Mars: Icarus, v. 44, p. 207–216.
Oil and Gas Journal, 1993, v. 91, p. 62.
Oil and Gas Journal, 1996, v. 94, p. 81.
Petroleum Information Corporation (PI), 1975, Scout Card for Texas Pacific Oil Co., Inc., no. 6 Montgomery-Fulk, Sec. 87, Blk A, Pecos County, West Texas.
Petroleum Information Corporation (PI), 1995, Resume 1994, section 2, p. 8: Petroleum Information Corporation, Denver, Colorado.
Plawman, T. L.; and Hagar, P. I., 1983, Impact structure, *in* Bally, A. W. (ed.), Seismic expression of structural styles: American Association of Petroleum Geologists, Studies in Geology Series no. 15, v. 1, p. 1.4.1–1.4.3.
Pohl, J., 1977, Paleomagnetics of the Ries Crater: Geologica Bavarica, v. 75, p. 329–438.
Pohl, J.; Stöffler, D.; Gall, H.; and Ernston, K., 1977, The Ries impact crater, *in* Roddy, D. J.; Pepin, P. O.; and Merrill, R. B. (eds.), Impact and explosion cratering: Pergamon Press, New York, p. 343–404.
Roberts, C.; and Sandridge, B., 1992, The Ames hole: Shale Shaker, v. 42, no. 5, p. 118-121.
Robertson, P. B.; and Butler, M. D., 1982, The Kilmichael structure, Mississippi: evidence for a meteorite impact origin: Journal of Geology, v. 90, p. 589–601.
Santiago, J.; and Baro, A., 1990, Mexico's giant fields, *in* Halbouty, M. T. (ed.), Giant oil and gas fields of the decade 1978–1988: American Association of Petroleum Geologists Memoir 54, p. 73–99.
Sawatsky, H. B., 1977, Buried impact craters in the Williston basin and adjacent area, *in* Roddy, D. J.; Pepin, P. O.; and Merrill, R. B. (eds.), Impact and explosion cratering: Pergamon Press, New York, p. 461–480.
Sharpton, V. L.; and Nielson, D. C., 1988, Is the Bee Bluff structure in south Texas an impact crater?, *in* Ryder, G., and Sharpton, V. L. (eds.), Proceedings of the 19th Lunar and Planetary Science Conference: Cambridge University Press, Cambridge, and the Lunar and Planetary Institute, Houston, v. 19, p. 1065–1066.
Shaw, H. R., 1994, Craters, cosmos, and chronicles: a new theory of Earth: Stanford University Press, Stanford, California, 688 p.
Suppe, J., 1986, Principles of structural geology: Prentice-Hall, Englewood Cliffs, New Jersey, 535 p.
Van Der Loop, M., 1996, Is there a resource base in lower 48 frontiers?: Houston Geological Society Bulletin, v. 38, p. 18–21.
Wilshire, H. G.; Offield, T. W.; Howard, K. A.; and Cummings, D., 1972, Geology of the Sierra Madera cryptoexplosion structure, Pecos County, Texas: U.S. Geological Survey Professional Paper 599-H, 42 p.
Winzer, S. R., 1972, The Steen River astrobleme, Alberta, Canada: 24th International Geological Congress, Montreal, section 14, p. 148–156.
Wong, A. M., 1994, The subsurface character of Marquez dome impact structure, Texas, as determined by well log and gravity analysis: University of Houston unpublished M.S. thesis, 103 p.

Impact Cratering: The Mineralogical and Geochemical Evidence

Christian Koeberl
University of Vienna
Vienna, Austria

ABSTRACT.—Over the past 15 years, new studies related to the events that caused the extinction of the majority of life on Earth at the end of the Cretaceous Period have led to the hypothesis that a large-scale asteroid or comet impact occurred at 65 Ma. In the past, impact cratering as a geologic process has not been much appreciated by the general geological community, despite the fact that, on all other planets and satellites with a solid surface, impact cratering is the most important process that alters the surface at the present time as well as during most of the history of the solar system. Detailed studies, mainly since the 1960s, have led to the recognition of about 150 impact structures on Earth. Here, some fundamental mineralogical and geochemical properties of impact-derived rocks that are used to recognize impact craters are reviewed. The formation of impact craters leads to pressure and temperature conditions in the target rocks that are significantly different from those reached during any internal terrestrial process. Among the most characteristic changes induced by the impact-generated shock waves are irreversible changes in the crystal structure of rock-forming minerals, such as quartz and feldspar. These shock-metamorphic effects are characteristic of impact and do not occur in natural materials formed by any other process. In addition, geochemical methods are used to find traces of the meteoritic projectile in impact-melt rocks and glasses. A complete and diligent mineralogical, petrological, and geochemical study is necessary before any conclusions regarding an impact origin of geologic structures can be reached.

INTRODUCTION

During the 1980s and early 1990s, a lively debate was held in the geological community regarding the cause of the mass extinction that marks the end of the Cretaceous Period, at the Cretaceous/Tertiary (K/T) boundary (see, e.g., Silver and Schultz, 1982; Sharpton and Ward, 1990). Interest in the events at the K/T boundary was renewed by a publication by Alvarez and others (1980), who found that the concentrations of the rare platinum-group elements (PGEs: Ru, Rh, Pd, Os, Ir, and Pt) and other siderophile elements (e.g., Co, Ni) are enriched by up to four orders of magnitude in the thin clay layer marking the K/T boundary compared to their concentrations in normal terrestrial crustal rocks. These observations were interpreted by Alvarez and others (1980) as the result of a large asteroid or comet impact, which caused extreme environmental stress. This hypothesis was later strongly supported by the finding of shocked minerals in the K/T boundary layer by Bohor and others (1984,1987). It turned out that one of the main problems impeding the acceptance of the theory that a large impact took place at 65 Ma was a lack of detailed knowledge of impact cratering and shock-metamorphic processes in the general geological community. Similar debates—regarding impact vs. internal origin—have been held in discussing the origin of a variety of "unusual" structures around the world, including the Ames structure in Oklahoma. Thus, it seems useful to briefly review the basic knowledge of terrestrial impact craters and shock metamorphism. The discussion of general properties of impact craters is the topic of the paper by Grieve (1997), and here I will review mainly mineralogical and geochemical aspects of impact structures.

Historically, the concept of impact cratering on Earth has not been much accentuated in classical geological studies. The concept of classical Huttonian and Lyellian geology is that slow, endogenic

Christian Koeberl, Institute of Geochemistry, University of Vienna, Althanstrasse 14, A-1090 Vienna, Austria.

Koeberl, Christian, 1997, Impact cratering: the mineralogical and geochemical evidence, *in* Johnson, K. S.; and Campbell, J. A. (eds.), Ames structure in northwest Oklahoma and similar features: origin and petroleum production (1995 symposium): Oklahoma Geological Survey Circular 100, p. 30–54.

processes lead to gradual changes in the geologic record. In this uniformitarian view, internal forces are preferred over seemingly more exotic processes to explain geologic phenomena that often give the impression of occurring over very long periods of time. In contrast, impact appears as an exogenic, relatively rare, violent, and unpredictable event, which violates every tenet of uniformitarianism. The explanation of craters on the Moon or Earth as being of impact origin has been opposed by many geologists over much of this century. It is almost ironical that it was Alfred Wegener who published a little-known study (Wegener, 1921), in which he concluded that the craters on the Moon are of meteorite-impact origin. The history of study and acceptance of impact cratering over this century is somewhat similar to the record of the acceptance of plate tectonics (for a historical account of impact-crater studies, see, e.g., Mark, 1987; Hoyt, 1987; Marvin, 1990; and Glen, 1994).

Planetary exploration and extensive lunar research in the second half of the 20th century led to the conclusion that essentially all craters visible on the Moon (and many on Mercury, Venus, and Mars) are of impact origin. Therefore, it has to be concluded that, over its history, the Earth was subjected to a larger number of impact events than the Moon. Part of the reason why this conclusion was not widely accepted among geologists may be that terrestrial processes (weathering, plate tectonics, etc.) effectively work to obliterate the surface expression of these structures on Earth. Through studies of the orbits of asteroids and comets, astronomers have a relatively good understanding of the rate with which these objects strike the Earth (e.g., Shoemaker and others, 1990; Weissman, 1990). For example, minor objects in the solar system with diameters of ≥1 km (mainly asteroids) collide with the Earth at a frequency of about 4.3 impacts per million years (Shoemaker and others, 1990), and each such impact forms a crater ≥10 km in diameter. Impactors of about 2 km in diameter collide with the Earth about every 1 to 2 million years. Impact of Earth-orbit crossing asteroids dominate the formation of craters on Earth that are smaller than about 30 km in diameter, whereas comet impact probably forms the majority of craters that are larger than about 50 km in diameter (Shoemaker and others, 1990). However, the orbits of asteroids are better known than those of comets, because many of the latter have such long periodicities that no appearance has yet been observed during the time of human civilization.

In an important historical and sociological evaluation of the K/T boundary debates, Glen (1994, p. 52) found that "resistance to the [impact] hypothesis seemed inverse to familiarity with impacting studies." Thus, planetary scientists, astronomers, and meteoriticists have grown accustomed to view "large-body impact as a normal geological phenomenon—something to be expected throughout Earth history—but another group, the paleontologists, is confounded by what appears to be an ad hoc theory about a nonexistent phenomenon" (D. M. Raup in Glen, 1994, p. 147). Thus, it may be concluded that one scientist's uniformitarianism is another scientist's *deus ex machina*.

However, it may be important to consider the time scales involved in this discussion. What geologists have called "uniformitarianism" is the result of integrating individual catastrophes of various magnitudes over a sufficiently long time span. Earthquakes, volcanic eruptions, landslides, etc., are locally devastating if time spans of maybe 20 to 100 yr are concerned, but if the whole world and longer time spans are concerned, these "catastrophes" become part of the "uniformitarian" process of explosive volcanism, earthquake history, or erosion. The bias in what is considered uniformitarian is related to the life span of humans and the human civilization. As large meteorite impacts have not been observed during the last few millennia (with rare exceptions, such as the Tunguska event, which occurred in a remote tundra location of Siberia in 1908—but even this event was too small to produce a crater), such events tend to be neglected when constructing the "uniformitarian" history of the Earth. The falls of small meteorites have been observed quite frequently. There is no real conflict between uniformitarianism and meteorite impact. We just have to learn to apply the same principle that is being used for extrapolating the frequency of volcanic eruptions and earthquakes to the scaling of meteorite impacts—the large and devastating ones occur less often than the small events.

About 150 impact structures are currently known on Earth (e.g., Grieve and Shoemaker, 1994; Grieve, 1997). However, it is somewhat embarrassing that almost two thirds of the confirmed or probable impact craters in the United States have only been studied superficially (see Koeberl and Anderson, 1996). Considering that some impact events severely affected the geologic and biological evolution on Earth and that even small impacts can disrupt the biosphere and lead to local devastation (Chapman and Morrison, 1994), the understanding of impact structures and the processes by which they form should be of interest not only to earth scientists, but also to society in general.

GENERAL CHARACTERISTICS OF IMPACT CRATERS

As no large impact event has been observed by humans over the past several thousand years (which is, of course, not a geologically long period of time), impact experiments and the detailed study of impact craters on Earth are essential to understand these features. During an impact event, the geologic structure of the target area is changed in a characteristic way, which can be used

to help distinguish volcanic structures from meteorite impact craters. Meteorite impact craters are circular surficial features without deep roots, whereas in volcanic structures the disturbances continue to (or, rather, emerge from) great depth. Impact craters are practically always circular, with only very few exceptions that result either from highly oblique impacts (see, e.g., the Rio Cuarto structures in Argentina—Schultz and others, 1994) or from postformational distortion due to, for example, tectonism or erosion (e.g., the Sudbury structure in Canada—e.g., Stöffler and others, 1994). It is useful to distinguish between the impact crater, i.e., the feature that results from the impact, and the impact structure, which is what is observed today, long after formation and modification of the crater.

Impact craters (before erosion) occur in two distinctly different morphological forms, namely as small (≤4-km-diameter) bowl-shaped craters and large (≥4-km-diameter) complex craters with a central uplift. All craters have an outer rim and some crater infill (e.g., brecciated and/or fractured rocks, impact-melt rocks), whereas the central structural uplift in complex craters consists of a central peak or of one or more peak ring(s) and exposes rocks that are uplifted from considerable depth. The diameters of impact craters on Earth show a variation, which is, however, the result of biased processes, chiefly different effects of age and differential erosion of large and small craters. The erosional processes that obliterate small (0.5- to 10-km-diameter) craters after a few million years create a severe deficit of these craters, compared to the number that is expected from the number of larger craters and astronomical observations (Grieve and Shoemaker, 1994). Erosion also explains why most small craters are young. Older craters of larger initial diameter also suffer erosion degradation leading to the destruction of the original topographical expression or to burial of the structures under postimpact sediments. For details on crater morphology, see Grieve (1997).

RECOGNITION OF IMPACT STRUCTURES

As a consequence of the obliteration, burial, or destruction of impact craters on Earth, they can be difficult to recognize, requiring the development of diagnostic criteria for the identification and confirmation of impact structures. The most important of these characteristics are (1) evidence for shock metamorphism, (2) crater morphology, (3) geophysical anomalies, and (4) the presence of meteorites or geochemical discovery of traces of the meteoritic projectile. Of these, only the presence of diagnostic shock-metamorphic effects and, in some cases, the discovery of meteorites, or traces thereof, can provide unambiguous evidence for an impact origin.

However, morphological and geophysical observations are important in providing supplementary—but not confirming—evidence. Geophysical methods are also useful in identifying candidate sites for further studies. It should be noted that in complex craters, the central uplift usually contains severely shocked material and is often more resistant to erosion than the rest of the crater. In old eroded structures, the central uplift may be the only remnant of the crater that can be identified. Geophysical characteristics of impact craters that have been investigated include gravity, magnetic properties, reflection and refraction seismic signatures, electrical resistivity, and others (see Pilkington and Grieve, 1992, for a review). In general, simple craters have negative gravity anomalies due to the lower density of the brecciated rocks compared to the unbrecciated target rocks, whereas complex craters often have a positive gravity anomaly associated with the central uplift that is surrounded by an annular negative anomaly. Magnetic anomalies can be more varied than gravity anomalies, but seismic data show the loss of seismic coherence due to structural disturbance, slumping, and brecciation. Such geophysical surveys are important for the recognition of anomalous subsurface structural features, which may be deeply eroded craters or simply covered by postimpact sedimentary deposits (e.g., in the United States: Ames, Avak, Chesapeake Bay, Manson, Newporte, Red Wing Creek—see Koeberl and Anderson, 1996; Koeberl and Reimold, 1995a,b; Koeberl and others, 1995b,1996b,c). However, to better appreciate the other criteria for identification of impact structures, it is necessary to briefly consider some physical processes that operate during crater formation.

FORMATION OF IMPACT CRATERS

The formation of a crater by hypervelocity impact is—not only in geologic terms—a very rapid process that is usually divided into three stages: (1) contact and compression stage, (2) excavation stage, and (3) postimpact crater-modification stage. Crater-formation processes have been studied for many decades, but space limitations require that the reader be referred to the literature (see, e.g., Gault and others, 1968; Roddy and others, 1977; Melosh, 1989; and references therein) for a detailed discussion of the physical principles of impact-crater formation. Here, only a few key ideas can be mentioned.

During the impact of a large meteorite, asteroid, or comet, large amounts of kinetic energy (equal to $\frac{1}{2}\,mv^2$, m = mass, v = velocity) are released. Earlier in the century, the amount of energy was largely underestimated, because the velocities with which extraterrestrial bodies hit the Earth had not been known or assessed properly. However, any body that is not slowed down by the atmosphere will hit the Earth with a velocity be-

tween about 11 and 72 km/s. These velocities are determined by celestial mechanics. Thus, a 250-m-diameter iron or stony meteorite has a kinetic energy roughly equivalent to about 1,000 megatons of TNT, which would lead to the formation of a crater about 5 km in diameter. The relatively small Meteor (or Barringer) crater in Arizona (1.2 km diameter) was produced by an iron meteorite with a diameter of about 30 to 50 m. Many of the characteristics of an impact crater are the consequence of the enormous kinetic energy that is released almost instantaneously during the impact. This energy can be compared to that of "normal" terrestrial processes, such as volcanic eruptions or earthquakes. During small impact events, which may lead to craters of 5 to 10 km diameter, about 10^{24} to 10^{25} ergs (10^{17} to 10^{18} J) are released, whereas during formation of larger craters (50 to 200 km diameter), about 10^{28} to 10^{30} ergs (10^{21} to 10^{23} J) are liberated (e.g., French, 1968; Kring, 1993). On the other hand, about $6 \cdot 10^{23}$ ergs ($6 \cdot 10^{16}$ J) were released over several months during the 1980 eruption of Mount St. Helens, and 10^{24} ergs (10^{17} J) in the big San Francisco earthquake in 1906. It may also be surprising that the total annual energy release from the Earth (including heat flow, which is by far the largest component, as well as volcanism and earthquakes) is about $1.3 \cdot 10^{28}$ ergs ($1.3 \cdot 10^{21}$ J/yr) (French, 1968; Sclater and others, 1980; Morgan, 1989). The latter amount of energy is comparable to the energy that is released almost instantaneously during large impact events. It is also important to realize that the energy that is liberated during an impact is concentrated at almost a point on the Earth's surface, leading to an enormous local energy density.

SHOCK WAVES IN ROCKS—HUGONIOT EQUATIONS

Structural modifications and phase changes in the target rocks occur during the compression stage, and the morphology of a crater is defined in the second and third stage. For a more detailed description of crater formation, see, e.g., Grieve (1987,1991), Melosh (1989), and references therein. During the early-impact phase, the impacting body is stopped after about two projectile radii, and the kinetic energy ($\frac{1}{2} mv^2$) is transformed into heat and shock waves that penetrate into the projectile and target. The most important phenomenon, which is characteristic of impact, is the generation of a supersonic shock wave that is propagated into the target rock. The effects of shock waves on matter are well understood from decades of experimental evidence. The following discussion is based mainly on information from Melosh (1989). Matter is being accelerated very rapidly, and, as a consequence of the decrease of compressibility with increasing pressure, the resulting stress wave will become a shock wave moving initially at supersonic speed (up to about ⅔ of the impact velocity). Shock waves are inherently nonlinear and shock fronts are abrupt. They can be mathematically represented as a discontinuous jump of pressure, density, particle velocity, and internal energy. In reality, shock waves have a finite thickness, which is, however, very limited. For example, the widths of shock waves in gas are limited to about 10 μm, which is roughly equal to one molecular mean free path, but shock waves in solids are wider, up to a few meters in rocks, depending on their porosities.

The shock wave leads to compression of the target rocks at pressures far above a material property called the Hugoniot elastic limit. The Hugoniot elastic limit (HEL) can generally be described as the maximum stress that can be reached in a stress wave that a material can be subjected to without permanent deformation. Above this limit, plastic, or irreversible, distortions occur in the solid medium through which the compressive wave travels (see, e.g., compilations by Roddy and others, 1977; Melosh, 1989; and references therein). The value of the HEL is about 5 to 10 GPa for most minerals and whole rocks. For example, single crystals of quartz have HELs ranging from 4.5 to 14.5 GPa (depending on the crystal orientation); for feldspar the HEL is at 3 GPa, and for olivine it is at 9 GPa. For rocks, the HEL of dolomite is 0.3 GPa, for granite 3 GPa, and for granodiorite, 4.5 GPa. The only known process that produces shock pressures exceeding the HELs of most crustal rocks and minerals in nature is impact cratering. Volcanic processes are not known to exceed 0.5 to 1 GPa. In addition to structural changes, phase changes may occur as well.

For a thermodynamics treatment of shock fronts traveling through matter, the so-called Hugoniot equations are used (see Melosh, 1989). These equations link the pressure P, internal energy E, and density ρ in front of a shock wave (uncompressed: P_0, E_0, ρ_0) to values after the shock front (compressed: P, E, ρ). The density is also expressed as the specific volumes $V = 1/\rho$ and $V_0 = 1/\rho_0$ for the compressed and uncompressed cases, respectively. Initial pressure, energy, and density before the shock are known values, whereas the values after the shock are unknown quantities, as are the shock velocity U and particle velocity u_p behind the shock front. The Hugoniot equations are then written as

$$\rho(U - u_p) = \rho_0 U$$

$$P - P_0 = \rho_0 u_p U$$

$$E - E_0 = (P + P_0)(V_0 - V)/2.$$

These equations express the conservation of mass, momentum, and energy across the shock front to reduce the number of unknown variables from five to two. For a derivation of the Hugoniot equations, see appendix 1 in Melosh (1989) as well as Boslough and Asay (1993). In the uncompressed material, the initial particle velocity should be

zero, and the initial pressure P_0 can be neglected, yielding the approximation $E - E_0 = u_p^2/2$. In addition to the three equations mentioned above, a fourth one, the equation of state, is necessary to specify conditions on either side of the shock front. This equation links pressure, specific volume (density), and internal energy: P = (V,E). Equations of state have been determined experimentally for a large number of different materials (e.g., Marsh, 1980).

The shock-wave equation-of-state data can be plotted in pressure vs. specific-volume (Fig. 1) or shock-velocity vs. particle-velocity diagrams. The curves in these diagrams are not equivalent to conventional equilibrium in thermodynamics P,V diagrams, but represent loci of several individual shock events, i.e., each point on a curve is the result of one particular shock-wave compression event. The HEL appears as a kink in the shock curve, indicating yielding at the maximum stress of the elastic wave (Fig. 1).

After the shock wave passes, the high pressure is released by a so-called rarefaction, or release, wave, which trails the shock front. The rarefaction wave is a pressure, not shock, wave and travels at the speed of sound in the shocked material. It gradually overtakes the decaying shock front and causes a decrease in pressure with increasing distance of propagation. Although the pressure behind a rarefaction wave may drop to near zero, the residual particle velocity actually accelerates material, leading to impact-crater excavation. In addition, the rarefaction wave not only conserves mass, energy, and momentum (as the shock wave does), but also entropy. Thus, rarefaction is a thermodynamically reversible adiabatic process, whereas shock compression is thermodynamically irreversible. During shock compression, a large amount of energy is being introduced into a rock. Upon decompression, the material follows a release adiabat in a pressure vs. specific-volume diagram. The release adiabat is located close to the Hugoniot curve, but usually at generally somewhat higher P and V values, leading to excess heat appearing in the decompressed material, which may result in phase changes (e.g., melting or vaporization). The effects of the phenomena described above can be observed in various forms in shocked minerals and rocks.

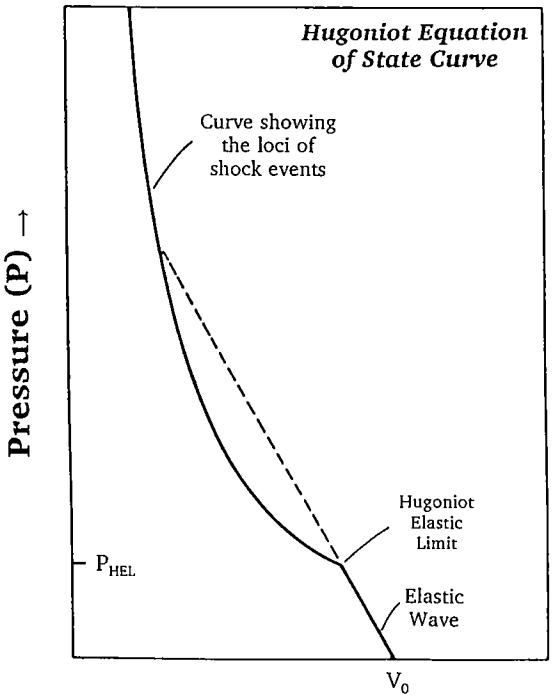

Figure 1. Idealized representation of a Hugoniot equation of state curve. The Hugoniot curve does not represent a continuum of states as in thermodynamics diagrams, but the loci of individual shock-compression events. The yielding of the material at the Hugoniot elastic limit is indicated. See text for detailed discussion.

SHOCK METAMORPHISM

A large meteorite impact will produce shock pressures of ≥100 GPa and temperatures of ≥3,000 °C in large volumes of the target rock. These conditions are in sharp contrast to conditions for endogenic metamorphism of crustal rocks, with maximum temperatures of 1,200 °C and pressures of usually <2 GPa (except static pressure affecting some deep-seated rocks, e.g., eclogites) (Fig. 2). As mentioned above, shock compression is not a thermodynamically reversible process, and most of the structural and phase changes in mineral crystals and rocks are uniquely characteristic of the high pressures (5 to >50 GPa) and extreme strain rates (106 to 108 s^{-1}) associated with impact. Also, some assemblages of high-pressure and high-temperature mineral phases are preserved together with glass in shocked rocks due to disequilibrium caused by transient high pressures followed by quenching.

As some recent literature indicates, there is still some incomplete understanding in the geological community about the precise nature of shock metamorphism (for a discussion, see, e.g., French, 1990; Sharpton and Grieve, 1990). In contrast to some assertions (e.g., Lyons and others, 1993), the existence of definite shock-metamorphic features in volcanic rocks has never been substantiated (see, e.g., de Silva and others, 1990; Gratz and others, 1992b). Static compression, as well as volcanic or tectonic processes, yields different products because of lower peak pressures and because of strain rates that are smaller by more than 11 orders of magnitude. It should be reaffirmed

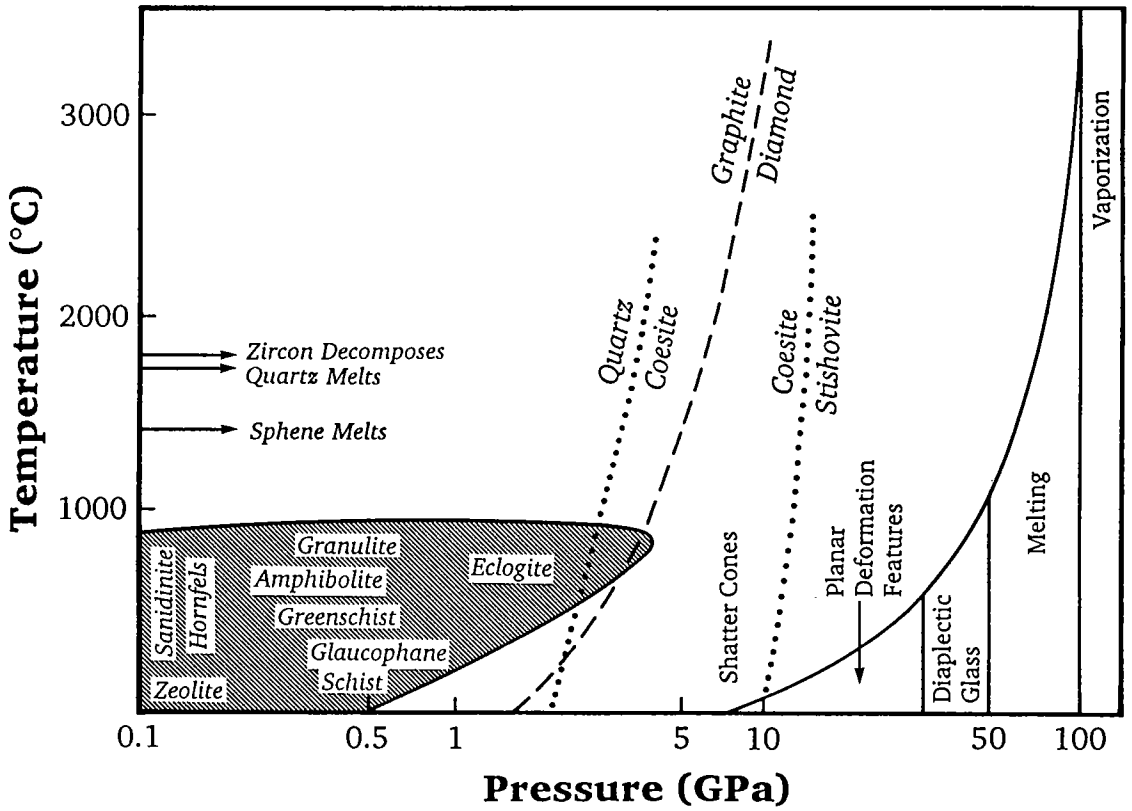

Figure 2. Comparison of pressure-temperature fields of endogenic metamorphism and shock metamorphism. Also indicated are the onset pressures of various irreversible structural changes in the rocks due to shock metamorphism. The curve on the right side of the diagram shows the relationship between pressure and postshock temperature for shock metamorphism of granitic rocks. (After Grieve, 1987, and B. M. French, personal communication, 1995.)

that the study of the response of materials to shock is not a recent development, but has been the subject of thorough investigations over several decades, in part stimulated by military research. Numerous shock-recovery experiments (i.e., controlled shock-wave experiments, which allow the collection of the shocked samples for further studies), using various techniques, have been performed in the past three to four decades. These experiments have led to a good understanding of the conditions for formation of shock-metamorphic products and a pressure-temperature calibration of the effects of shock pressures up to about 100 GPa (see, e.g., Hörz, 1968; French and Short, 1968; Stöffler, 1972,1974; Gratz and others, 1992a,b; Huffman and others, 1993; Stöffler and Langenhorst, 1994; and references therein).

Table 1 lists the most characteristic products of shock metamorphism, as well as the associated diagnostic features. The best diagnostic indicators for shock metamorphism are features that can be studied easily by using the polarizing microscope. They include planar microdeformation features; optical mosaicism; changes in refractive index, birefringence, and optical axis angle; isotropization; and phase changes.

Before discussing the various shock-metamorphic features, the type and location of impactite lithologies should be mentioned (Fig. 3). In an impact crater, shocked minerals, impact melts, and impact glasses are commonly found in various impact-derived breccias. Well-preserved ejecta at the crater rim may display a stratigraphic sequence that is inverted compared to the normal stratigraphy in the area. The impact process leads to the formation of various monomict or polymict breccias (e.g., Fig. 4), which are found within and around the resulting crater (see also Stöffler and Grieve, 1994, and Koeberl and others, 1996a). There are three main types: (1) cataclastic (fragmental) breccias, (2) suevitic (fragmental with a melt-fragment component) breccias, or (3) impact-melt (melt breccia—i.e., melt in the matrix with a clastic component) breccias. The breccias can be allochthonous or autochthonous. In addition, dikes of injected or locally formed fragmental or

TABLE 1.—CHARACTERISTICS AND FORMATION PRESSURES OF VARIOUS SHOCK DEFORMATION FEATURES

Pressure (GPa)	Features	Target characteristics	Feature characteristics
2–30	Shatter cones	Best developed in homogeneous, fine-grained, massive rocks	Conical fracture surfaces with subordinate striations radiating from a focal point
5–45	Planar fractures and planar deformation features (PDFs)	Highest abundance in crystalline rocks; found in many rock-forming minerals; e.g., quartz, feldspar, olivine, and zircon	PDFs: Sets of extremely straight, sharply defined parallel lamellae; occur often in multiple sets with specific crystallographic orientations.
30–40	Diaplectic glass	Most important in quartz and feldspar (e.g., maskelynite from plagioclase)	Isotropization through solid-state transformation under preservation crystal habit as well as primary defects and sometimes planar features. Index of refraction lower than in crystal but higher than in fusion glass
15–50	High-pressure polymorphs	Quartz polymorphs (coesite, stishovite) most common but also ringwoodite from olivine, jadeite from plagioclase, and majorite from pyroxene	Recognizable by crystal parameters, confirmed usually with XRD or NMR;[a] abundance influenced by postshock temperature and shock duration; Stishovite is temperature-labile
>35	Impact diamond	From carbon (graphite) present in target rocks; rare	Cubic and hexagonal form; usually very small but occasionally up to millimeter-size; inherit graphite crystal shape
45–>70	Mineral melts	Rock-forming minerals (e.g., lechatelierite from quartz)	Contrary to diaplectic glass, liquid-state transformation of a mineral into glass.
>60	Rock melt	Best developed in massive silicate rocks. Occur as individual melt bodies (millimeter to meter size) or as coherent melt sheets, up to >1000 km^3.	Either glassy (fusion glasses) or crystalline; of macroscopically homogeneous, but microscopically often heterogeneous composition

Data from: Alexopoulos and others (1988), French and Short (1968), Sharpton and Grieve (1990), Stöffler (1972, 1974), Koeberl and others (1995a); after Koeberl (1994).

[a]XRD = X-ray diffraction; NMR = nuclear magnetic resonance.

pseudotachylitic breccias (Reimold, 1995), which contain evidence of melting, can be found in the basement rocks. The schematic distribution of breccias, melt, and breccia dikes at a simple crater is shown in Figure 3. Whether these various breccia types are indeed present in a crater depends on factors including the size of the crater, the composition and porosity of the target area (e.g., Kieffer and Simonds, 1980), and the level of erosion (see, e.g., Roddy and others, 1977; Hörz, 1982; Hörz and others, 1983; Grieve, 1987; and references therein).

Shatter Cones

The occurrence of shatter cones has long been discussed as a good macroscopic indicator of shock effects, and a variety of structures were proposed to be of impact origin on the basis of shatter-cone occurrences (e.g., Dietz, 1968; Milton, 1977). Such cones have also been formed in (chemical) explo-

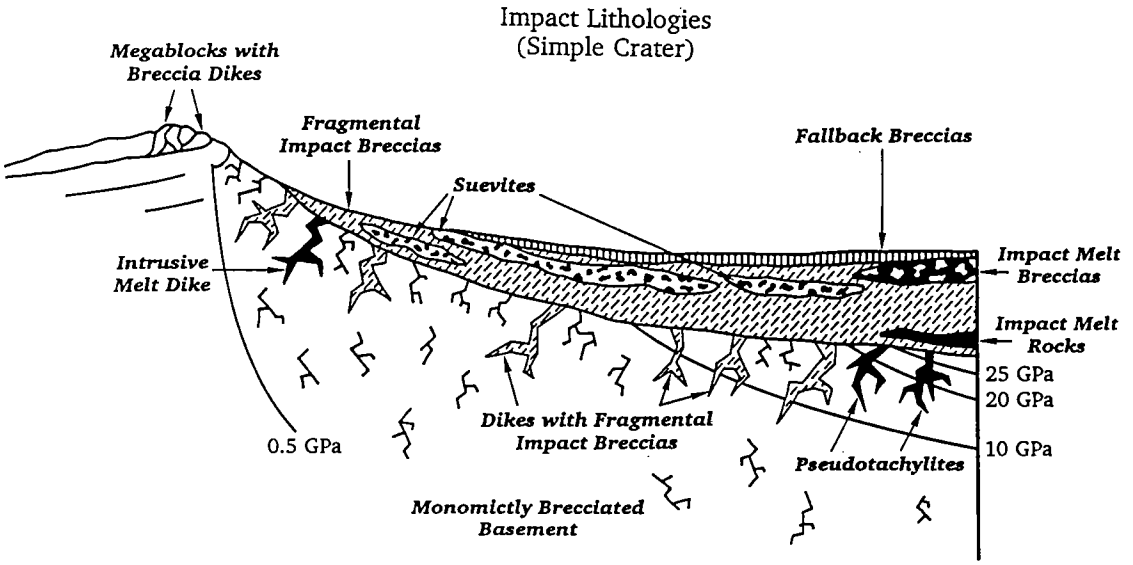

Figure 3. Schematic cross section through a simple impact crater (from the rim on the left side to the crater center on the right side). The various types and locations of occurrence of impactites (i.e., rocks affected during the impact process) are shown. (After Koeberl and Anderson, 1996.)

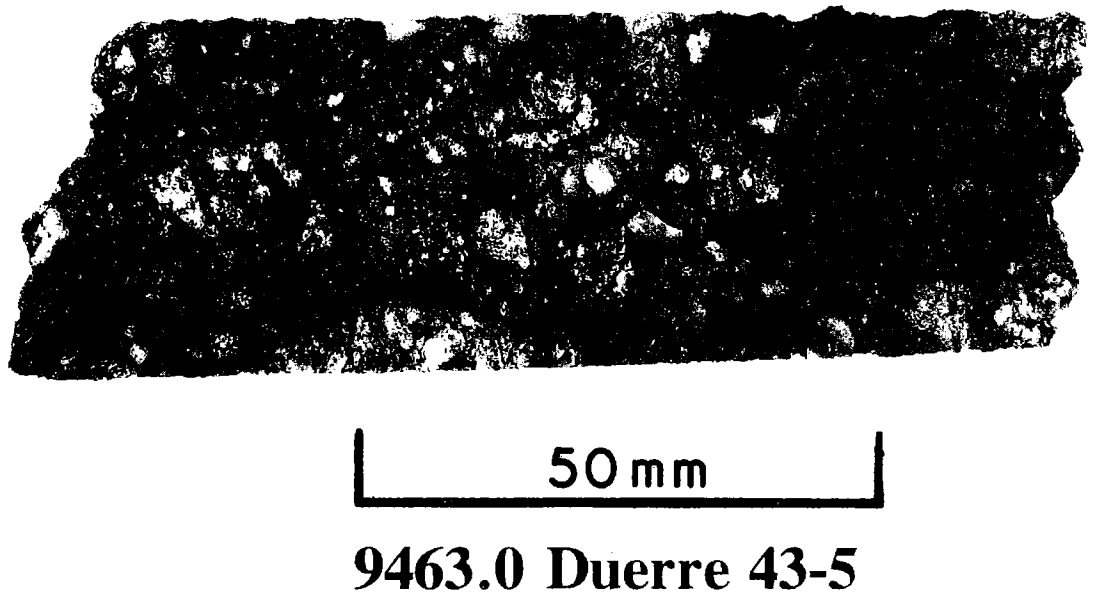

Figure 4. Macroscopic view of a granitic fragmental breccia from the Newporte impact structure, North Dakota; sample D9463.0 from the Shell no. 43-5 Duerre drill core (from 2,884 m depth), showing angular granitic fragments in a dark, fine-grained, clast-rich matrix.

sion crater experiments (see, e.g., Milton, 1977). Their formation is dependent on the type of target rock (i.e., they are better developed in certain lithologies than in others) and has been estimated to take place at pressures in the range of 2 to 30 GPa. In general, shatter cones are cones with regular thin grooves (striae) that radiate from the top (the apex) of a cone. They can range in size from <1 cm to >1 m (Fig. 5). Shatter cones occur mostly in the outer and lower parts of a crater and

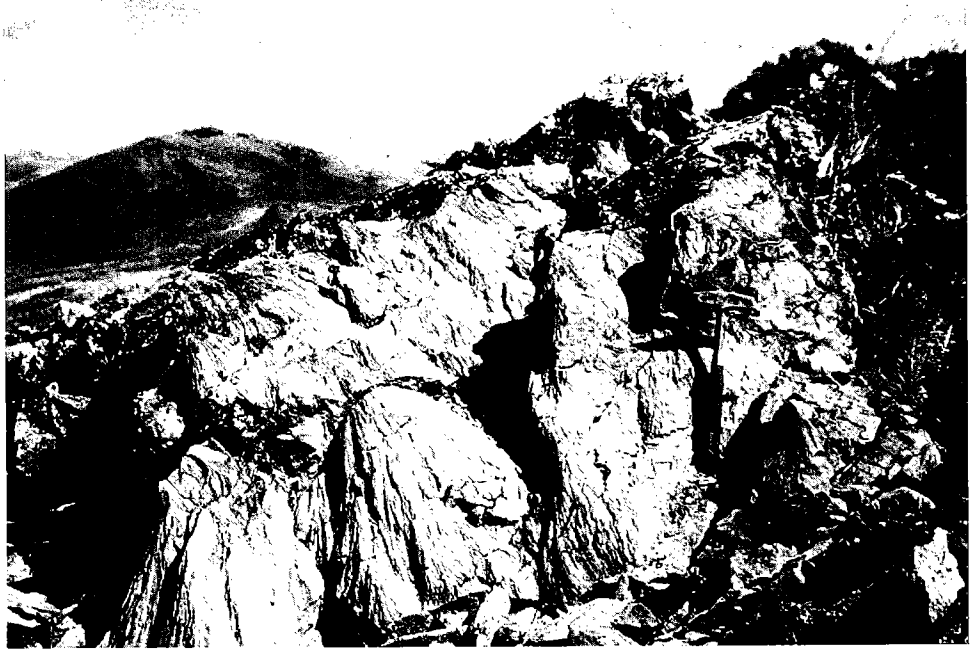

Figure 5. Assemblage of massive shatter cones, with sizes up to 1 m, at the Beaverhead impact structure, Montana (courtesy P. Fiske).

may be preserved even if a structure is deeply eroded. Unfortunately, conclusive criteria for the recognition of "true" shatter cones have not yet been defined. If they are strongly eroded, it is possible to confuse concussion features, pressure-solution features (cone-in-cone structure), or abraded or otherwise striated features with shatter cones. It would be important to arrive at some generally accepted criteria for the correct identification of shatter cones, as some impact craters have been identified almost exclusively by the occurrence of shatter cones (see, e.g., compilation by Koeberl and Anderson, 1996; cf. Koeberl and others, 1996b). However, shatter cones are important potential macroscopic shock indicators, as they are developed in large volumes of rock, and are useful as a guide for the presence of more definitive shock indicators, such as shocked minerals (see below).

Mosaicism

Mosaicism is a microscopic effect of shock metamorphism and appears as an irregular mottled optical extinction pattern (Fig. 6A), which is distinctly different from the undulatory extinction that occurs in tectonically deformed quartz. Mosaicism can be measured in the optical microscope by determining the scatter of optical axes in different regions of crystals showing mosaicism. Mosaicism can be semiquantitatively defined by X-ray diffraction studies of the asterism of single-crystal grains, where it shows up as a characteristic increase (with increasing shock) of the width of individual lattice-diffraction spots in diffraction patterns. Highly shocked quartz crystals show a diffraction pattern that becomes similar to a powder pattern, because of shock-induced polycrystallinity. Many shocked quartz grains that show planar microstructures also show mosaicism. In addition, it should be noted that the crystal lattice of shocked quartz shows lattice expansion above shock pressures of 25 GPa, leading to an expansion of the cell volume by ≤3% (Langenhorst, 1994).

Planar Microstructures

Two types of planar microstructures are apparent in shocked minerals: planar fractures (PFs) and planar deformation features (PDFs). Their characteristics are summarized in Table 2. PDFs in rock-forming minerals (e.g., quartz, feldspar, or olivine) are generally accepted to be diagnostic evidence for shock deformation (see, e.g., French and Short, 1968; Stöffler, 1972,1974; Alexopoulos and others, 1988; Sharpton and Grieve, 1990; Stöffler and Langenhorst, 1994). PFs, in contrast to irregular, nonplanar fractures (which are caused by rarefaction waves), are thin fissures, spaced about 20 μm or more apart, which are parallel to rational crystallographic planes with low

TABLE 2. —CHARACTERISTICS OF PLANAR FRACTURES AND PLANAR-DEFORMATION FEATURES IN QUARTZ

Nomenclature	1. Planar fractures (PF) 2. Planar-deformation features (PDF) 2.1. Nondecorated PDFs 2.2. Decorated PDFs
Crystallographic orientation	1. PFs: usually parallel to (0001) and {10$\bar{1}$1} 2. PDFs: usually parallel to {10$\bar{1}$3}, {10$\bar{1}$2}, {10$\bar{1}$1}, (001), {11$\bar{2}$2}, {11$\bar{2}$1}, {10$\bar{1}$0}, {11$\bar{2}$0}, {21$\bar{3}$1}, {51$\bar{6}$1}, etc.
Optical microscope properties	Multiple sets of PFs or PDFs (up to 15 orientations) per grain Thickness of PDFs: <2–3 μm Spacing: >15 μm (PFs), 2–10 μm (PDFs)
TEM properties (PDFs)	Two types of primary lamellae are observed: 1. Amorphous lamellae with a thickness of about 30 nm (at pressures of <25 GPa) and about 200 nm (at pressures of >25 GPa) 2. Brazil twin lamellae parallel to (0001)

Data after Stöffler and Langenhorst (1994).

Miller indices, such as (0001) or {10$\bar{1}$1} (e.g., Engelhardt and Bertsch, 1969). PFs form at lower pressures than PDFs and may not provide conclusive evidence of shock metamorphism, but can act as guide to other, more characteristic, shock-deformation effects.

PDFs, together with the somewhat less definitive planar fractures (PFs), are well developed in quartz (Stöffler and Langenhorst, 1994). PDFs are parallel zones with a thickness of ≤1 to 3 μm and are spaced about 2 to 10 μm apart (see examples in Fig. 6). The degree of planarity of the individual sets of PDFs is an important parameter for the correct identification of bona fide PDFs and allows their distinction from (sub-)planar features that are produced at lower strain rates, e.g., in tectonically deformed quartz. It was demonstrated in transmission electron microscopy (TEM) studies (see, e.g., Goltrant and others, 1991) that PDFs consist of amorphous silica. The structural state of the glassy lamellae is, however, slightly different from that of regular silica glass (Goltrant and others, 1991). The fact that the PDF lamellae are filled by glass allows them to be preferentially etched by, e.g., hydrofluoric acid, emphasizing the planar-deformation features (see Fig. 6C). The photomicrographs in Figure 6 show various appearances of PDFs in natural samples from impact structures in the United States.

Engelhardt and Bertsch (1969) have classified PDFs into four groups: (1) nondecorated PDFs (extremely fine lamellae, cannot be resolved in the

Figure 6 *(p. 40–41)*. Shocked quartz and feldspar. A—Quartzitic clast in impact-melt rock from the Manson crater, Iowa, showing two prominent sets of PDFs and shock mosaicism (width of field of view, 2.2 mm; crossed polarizers; see Koeberl and others, 1996a). B—Close-up of K-feldspar grain from the Ames structure, Oklahoma, Nicor no. 18-4 Chestnut core, sample 9011.0 (from 2,747 m depth), showing incipient brecciation in the feldspar grain, which contains three sets of PDFs and shows the closely spaced nature of the lamellae (width of field of view, 900 μm; crossed polarizers; courtesy W. U. Reimold, University of the Witwatersrand). C—SEM image of quartz grain from the K/T boundary layer at DSDP Site 596 (Southwest Pacific), after brief etching with HF, showing three different sets of PDFs (courtesy B. Bohor, U.S. Geological Survey). D—Shocked quartz grain from the Red Wing Creek impact structure, North Dakota, from the True Oil 11-27 Burlington Northern borehole, depth interval 2,155 to 2,201 m, within brecciated Kibbey Sandstone, with PDFs of two different orientations (width of field of view, 375 μm; crossed polarizers; see Koeberl and Reimold, 1995a; Koeberl and others, 1996b). E—Quartz grain from the Newporte crater, North Dakota (Koeberl and Reimold, 1995b), with three sets of PDFs, in granitic clast from granitic fragmental breccia D9462.2 (width of field of view, 355 μm; parallel polarizers).

Figure 6A.

Figure 6B.

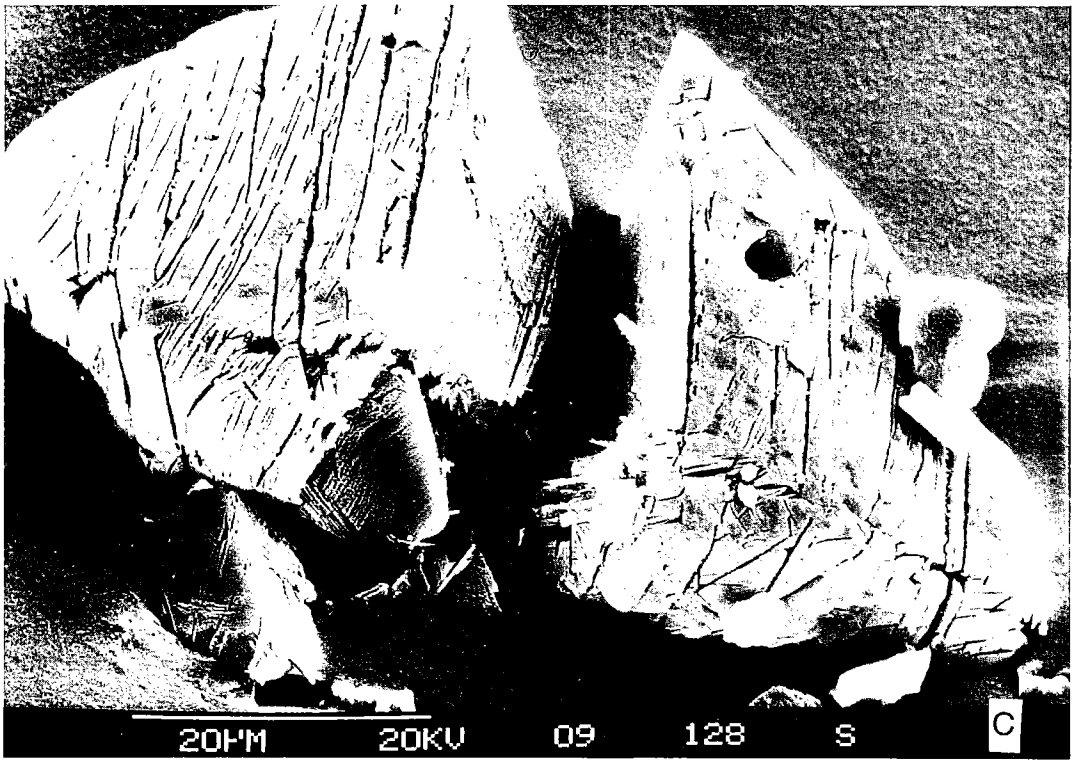

Figure 6C.

Figure 6D.

Figure 6E.

optical microscope), (2) decorated PDFs (the lamellae are lined by, or replaced with, small spherical or elliptical bubbles, often representing fluid inclusions), (3) homogeneous lamellae (thicker lamellae that can be resolved in the microscope), and (4) filled PDFs (where the lamellae are filled with very fine grained crystals). Types 1 and 2 are the most common.

In addition, TEM studies have shown that there is a second type of PDF, which consists of very thin multiple lamellae of Brazil twins. Brazil twins have been observed in hydrothermally grown quartz, but always parallel to the $\{10\bar{1}1\}$ plane, whereas the impact-derived Brazil twins form at pressures of >8 GPa, are of mechanical origin, and are exclusively parallel to the (0001) plane (Goltrant and others, 1991; Leroux and others, 1994). It was shown that such Brazil twins, from the Vredefort impact structure in South Africa, were formed by annealing of the shocked rocks (Goltrant and others, 1991; Leroux and others, 1994).

Most rock-forming minerals, as well as accessory minerals, such as zircon (Fig. 7), develop PDFs. The occurrence of diagnostic shock features is by far the most important criterion for evaluating the impact origin of a crater, particularly when several of the features that are typical of progressive shock metamorphism, as listed in Table 1, have been found. The occurrence of PDFs and PFs can be used, together with other shock effects, to determine the maximum shock pressure in impactites (Fig. 8). Most commonly, quartz is used to study these shock effects, as it is the simplest, best studied, and most widely distributed rock-forming mineral that develops PDFs.

PDFs occur in planes corresponding to specific rational crystallographic orientations. In quartz, the most abundant mineral that develops distinctive PDFs, the (0001) or c (basal), $\{10\bar{1}3\}$ or ω, and $\{10\bar{1}2\}$ or π orientations are the most common ones. In addition, PDFs often occur in more than one crystallographic orientation per grain. With increasing shock pressure, the distances between the planes decrease, and the PDFs become more closely spaced and more homogeneously distributed over the grain, until at about ≥35 GPa, complete isotropization has been achieved. Depending on the peak pressure, PDFs are observed in 2 to 10 (maximum 18) orientations per grain. To properly characterize PDFs, it is necessary to measure their crystallographic orientations by using either a universal stage (Reinhard, 1931; Emmons, 1943) or a spindle stage (Medenbach, 1985), or by using

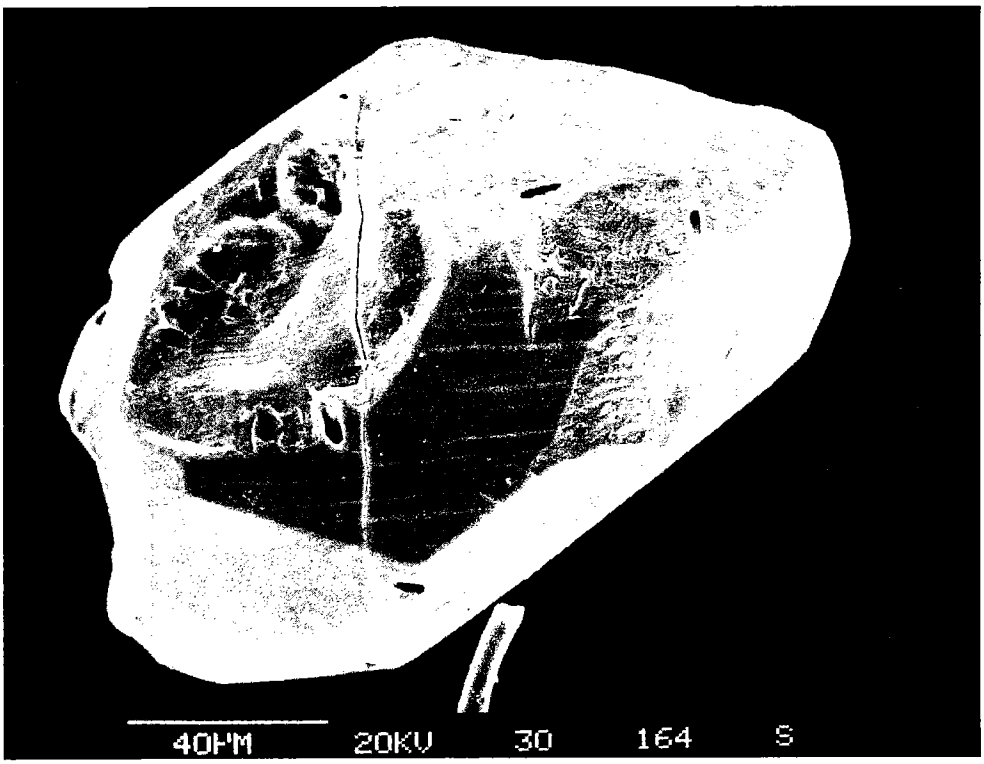

Figure 7. SEM image of an etched shocked-zircon grain from the Berwind Canyon (Raton basin, Colorado, United States) K/T boundary section; the whole grain shows the typical crystal habit of zircon and displays PDFs in two different orientations (courtesy B. Bohor, U.S. Geological Survey).

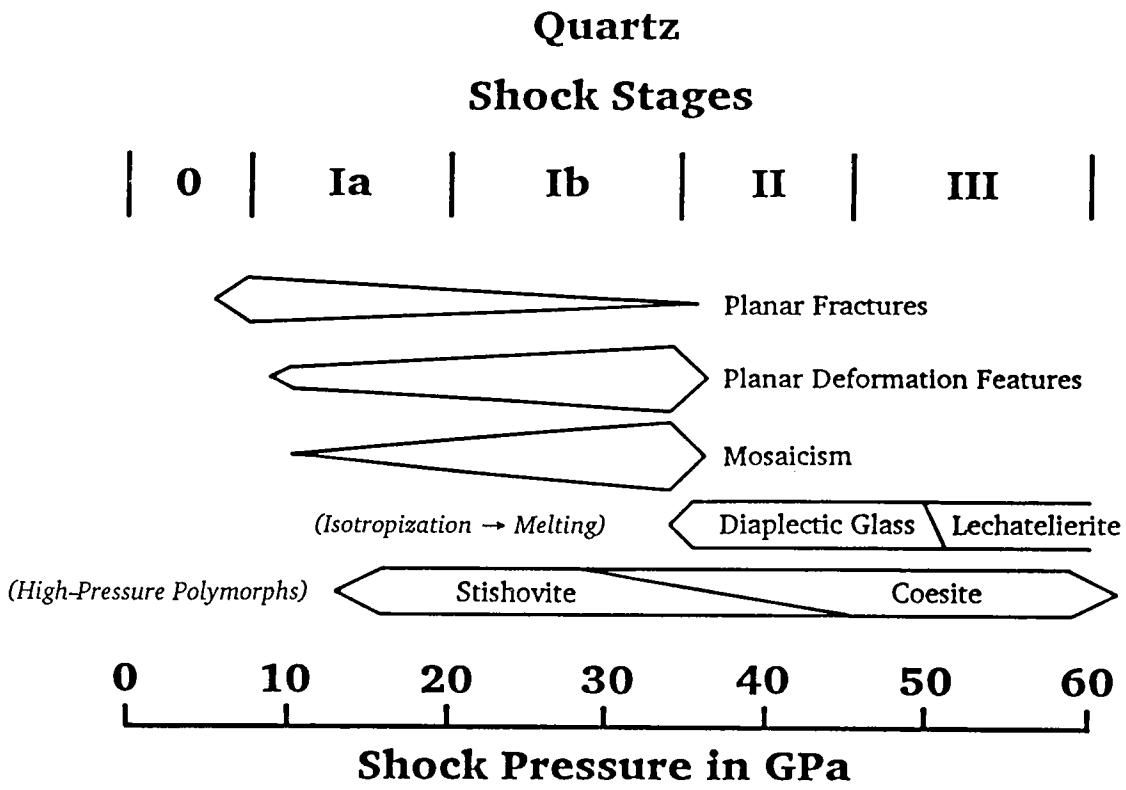

Figure 8. Pressure dependency of various characteristic shock indicators in quartz and relation to shock stages. (After Stöffler and Langenhorst, 1994.)

TEM (see, e.g., Goltrant and others, 1991; Gratz and others, 1992a; Leroux and others, 1994).

It is possible to use the relative frequencies of the crystallographic orientations of PDFs to calibrate shock pressure regimes, as given in Table 3 (see, e.g., Robertson and others, 1968; Hörz, 1968; Stöffler and Langenhorst, 1994). For example, at 5 to 10 GPa, PDFs with (0001) and {10$\bar{1}$1} orientations are formed, whereas PDFs with {10$\bar{1}$3} orientations start to form between about 10 and 12 GPa. Such studies are done by measuring the angles of the c-axis and of the PDFs in individual quartz grains with a universal stage. In a stereographic projection (Fig. 9), the optical axis (c-axis) is rotated into the center of projection, the locations of the poles of PDFs are plotted, and then those positions are compared with the stereographic projection of the rational crystallographic planes in quartz (as listed in Fig. 9). The measured angles that fall within 5° of the theoretical polar angle of the plane are considered valid and can be indexed. Figure 10 shows the results of this procedure in the form of a histographic plot of indexed PDFs. Such plots are used to identify the relative frequencies in which the various shock-characteristic crystallographic orientations occur.

The preshock temperature of a target rock also influences the formation and distribution of PDFs. Reimold (1988) and Huffman and others (1993) presented the results of shock experiments with quartzite both at room temperature (25 °C) and preheated to 450 and 750 °C. They noticed a slight difference in the relative distribution of the {10$\bar{1}$3} and {10$\bar{1}$2} orientations and a large difference in the number of PDF sets per grain (Fig. 11). Langenhorst (1993) compared PDF orientations in shocked quartz single crystals preheated to a higher temperature than Huffman and others (1993) and found a distinct change in the relative frequencies of the {10$\bar{1}$3} and {10$\bar{1}$2} orientations.

Bulk Optical and Other Properties

Recent experimental evidence shows that there is a decrease of the density of shocked quartz with increasing shock pressure (Langenhorst, 1993). At shock pressures up to about 25 GPa, only a slight decrease is noticeable, followed by a significant drop in density between 25 and 35 GPa, depending on the direction of the shock wave relative to the c-axis of the quartz crystal and the preshock temperature (Fig. 12). Optical properties, such as the birefringence of quartz and its refractive index,

TABLE 3.—RELATION BETWEEN SHOCK STAGE AND CRYSTALLOGRAPHIC ORIENTATION (INDICES) OF PLANAR MICROSTRUCTURES IN QUARTZ

Shock stage	Main orientations[a]	Additional orientations	Optical properties
1. Very weakly shocked	PFs: (0001)	PFs: rarely $\{10\bar{1}1\}$ PDFs: none	normal
2. Weakly shocked	PDFs: $\{10\bar{1}3\}$	PFs: $\{10\bar{1}1\}$, (0001) PDFs: rare	normal
3. Moderately shocked	PDFs: $\{10\bar{1}3\}$	PFs: $\{10\bar{1}1\}$, (0001) rare PDFs: $\{11\bar{2}2\}$, $\{11\bar{2}1\}$, (0001), $\{10\bar{1}0\}$+$\{11\bar{2}1\}$, $\{10\bar{1}1\}$, $\{21\bar{3}1\}$, $\{51\bar{6}1\}$	normal or slightly reduced refractive indices
4. Strongly shocked	PDFs: $\{10\bar{1}2\}$ $\{10\bar{1}3\}$	PFs: rare or absent PDFs: $\{11\bar{2}2\}$, $\{11\bar{2}1\}$, (0001), $\{10\bar{1}0\}$+$\{11\bar{2}1\}$, $\{10\bar{1}1\}$, $\{21\bar{3}1\}$, $\{51\bar{6}1\}$	reduced refractive indices (1.546–1.48)
5. Very strongly shocked	PDFs: $\{10\bar{1}2\}$ $\{10\bar{1}3\}$	none	reduced refractive indices (<1.48)

After Stöffler and Langenhorst (1994)
[a]PF = planar fractures; PDF = planar deformation features

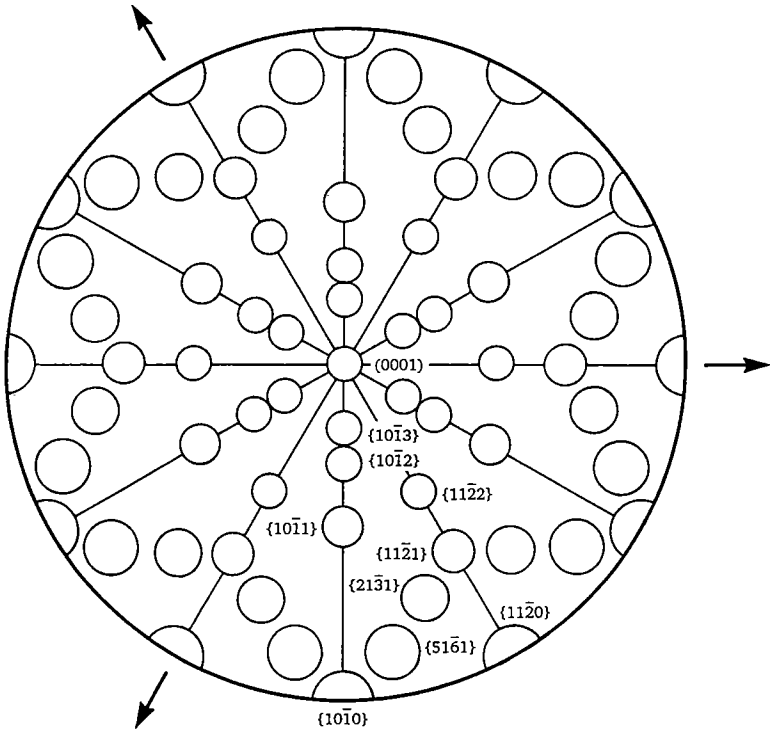

Figure 9. Standard stereographic projection (lower hemisphere) of rational crystallographic planes in α-quartz, which is used to index crystallographic planes of PDFs based on universal-stage measurements. The arrows indicate the three a-axes of quartz, and the c-axis (the (0001) plane) is in the center of the projection. Also indicated are the low Miller indices in a part of the diagram (other indices can be derived from crystal symmetry). The circles are about 5° in diameter and indicate the accuracy of the U-stage measurements (see, e.g., Engelhardt and Bertsch, 1969).

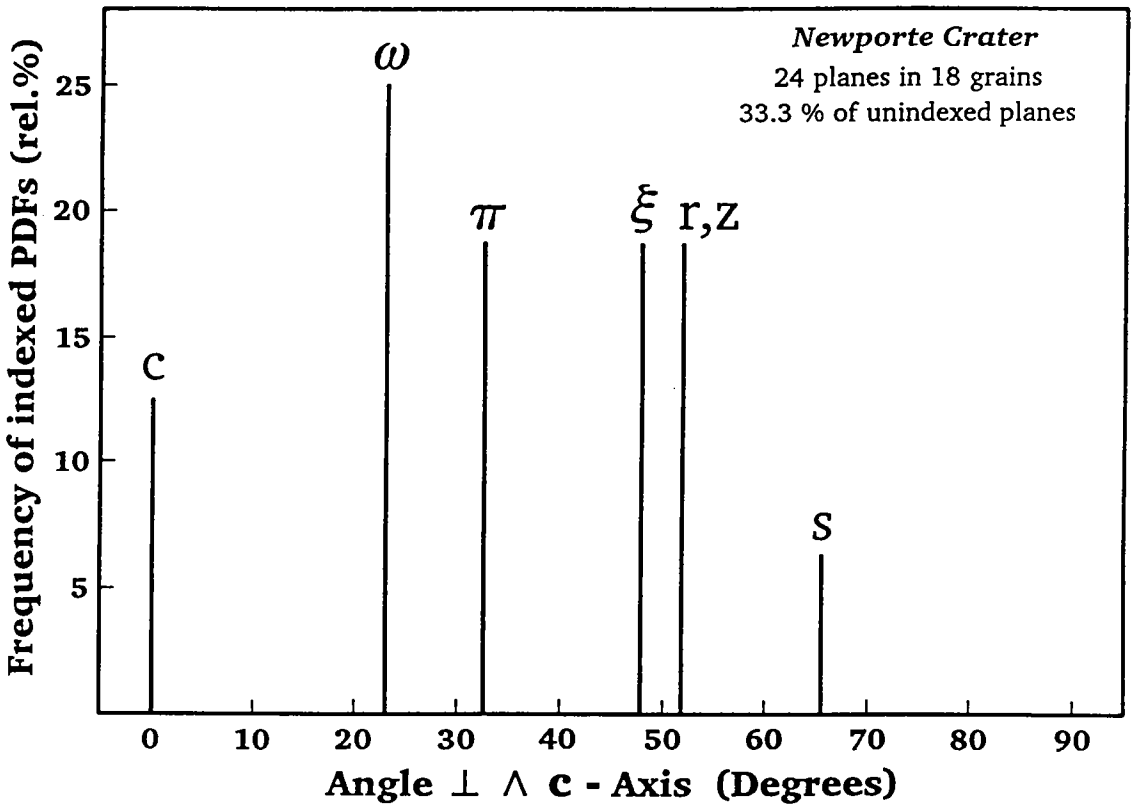

Figure 10. Crystallographic orientation of PDFs in quartz from the Newporte (North Dakota) impact structure, shown as a histogram giving the frequency of indexed PDFs vs. angle between c-axis and poles of PDFs, without plotting unindexed planes (see Grieve and Therriault, 1995); the shock-characteristic orientations (0001), $\{10\bar{1}3\}$, $\{10\bar{1}2\}$, $\{11\bar{2}2\}$, $\{10\bar{1}1\}$, $\{01\bar{1}1\}$, and $\{11\bar{2}1\}$ (*c*, ω, π, ξ, *r*,*z*, and *s*, respectively), are dominating. (After Koeberl and Reimold, 1995b.)

show also an inverse relationship with shock pressure in the 25 to 35 GPa range (Fig. 13). At about 35 GPa, isotropization (formation of diaplectic quartz glass) occurs. Figure 13 also indicates that with increasing shock pressure, the birefringence (n_ω–n_ε) decreases. Still other properties of shocked minerals can be used to either confirm a shock history or calibrate shock pressures. For example, intensity and wavelength of infrared absorption bands, the electron paramagnetic resonance, and peak width in a ^{29}Si magic-angle-spinning nuclear magnetic resonance (NMR) spectrum all depend in a quantitative way on the shock pressure (e.g., Boslough and others, 1995; references in Stöffler and Langenhorst, 1994).

Diaplectic Glass

At shock pressures in excess of about 30 GPa, diaplectic glass is formed (Table 1), which has been found at numerous impact craters. It is an isotropic phase that preserves the crystal habit, original crystal defects, and, in some cases, planar features. It forms without melting by solid-state transformation and has been described as a phase "intermediate between crystalline and normal glassy phases" (Stöffler and Hornemann, 1972). For example, maskelynite forms from feldspar. Diaplectic glass has a refractive index that is slightly lower, and a density that is slightly higher, than that of synthetic quartz glass. At pressures that exceed about 50 GPa, lechatelierite, a mineral melt, forms by fusion of quartz. Other minerals also undergo melting (fusion) at similar pressures. This complete melting is not the same process that results in the formation of diaplectic glass. The distinction between diaplectic glass and lechatelierite (both after quartz) was described by Stöffler and Hornemann (1972) and Stöffler and Langenhorst (1994).

High-Pressure Polymorphs

Another form of shock deformation is phase transitions to high-pressure polymorphs of minerals in a solid-state transformation process. Such transformation can be predicted from Hugoniot data. Many minerals form metastable high-pres-

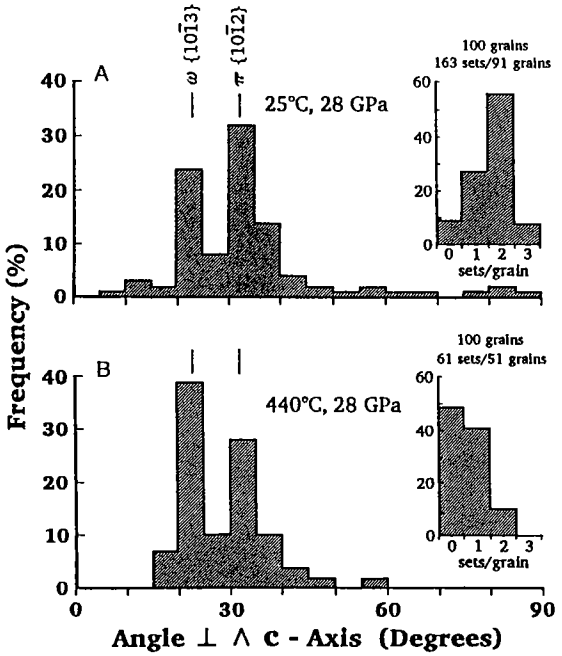

Figure 11. Histograms with crystallographic orientation of PDFs in quartz from Hospital Hill quartzite, used in shock experiments, showing the dependency of the orientations on the preshock temperature (after Huffman and others, 1993). (A) Preshock temperature 25 °C, shock pressure 28 GPa. (B) Preshock temperature 440 °C, shock pressure 28 GPa. The main difference between the data sets is that about half of the quartz grains in the high-temperature experiment remain unshocked, whereas in the low-temperature experiment, almost all quartz grains are shocked.

sure phases (Stöffler, 1972), including (density in g/cm^3 is given in parentheses) stishovite (4.23) and coesite (2.93) from quartz (2.65), jadeite (3.24) from plagioclase (2.63 to 2.76), majorite (3.67) from pyroxene (3.20 to 3.52), and ringwoodite (3.90) from olivine (3.22 to 4.34). In contrast to expectations from the equilibrium phase diagram of quartz, stishovite forms at lower pressures than coesite, probably because stishovite forms directly during shock compression, whereas coesite crystallizes during pressure release.

The formation probabilities and conditions for these phases are strongly dependent on the porosity of the target rocks. Although stishovite has never been found in any natural, non-impact-related rocks, there are rare findings of coesite in metamorphic rocks and kimberlites. However, coesite within metamorphic rocks occurs as large single crystals within, or associated with, high-pressure minerals of metamorphic or volcanic origin, but never associated with quartz. On the other hand, impact-derived coesite occurs as fine-grained, colorless to brownish, polycrystalline aggregates of up to 200 μm in size, which are usually embedded in diaplectic quartz or, rarely, in nearly isotropic shocked quartz. In addition to morphological differences, shock-produced coesite occurs in a disequilibrium assemblage of quartz + coesite + stishovite + glass (see also Grieve and others, 1996).

In addition to high-pressure phases of rock-forming minerals, impact-derived diamonds (the high-pressure polymorph of carbon) have also been found at various craters. These diamonds form from carbon in the target rocks, mainly graphite-bearing (e.g., graphitic gneiss) or less commonly coal-bearing rocks (Koeberl and others, 1995a). Impact diamonds commonly preserve the crystal habit of their precursor material, which is mostly graphite. The diamonds that formed after graphite are called "apographitic" diamonds. Many of them were found to contain up to several 10 vol% lonsdaleite, the rare hexagonal diamond polymorph.

Mineral and Rock Melts

At pressures in excess of about 60 GPa, rocks undergo complete (bulk) melting to form impact

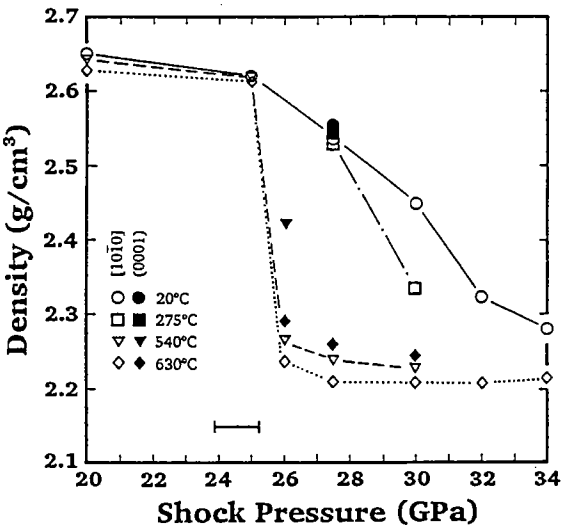

Figure 12. Densities of experimentally shocked quartz crystals at various preshock temperatures (20, 275, 540, and 630 °C), for two different directions of the shock wave relative to the c-axis of the quartz crystal (after Langenhorst, 1993). The measurement error for the shock pressure is indicated by the bar at the bottom of the diagram; the error for the density is smaller than the symbols. The starting value at the upper left of the diagram represents the density of crystalline quartz; the value marked by the diamond at the right side of the diagram marks the density of synthetic quartz glass.

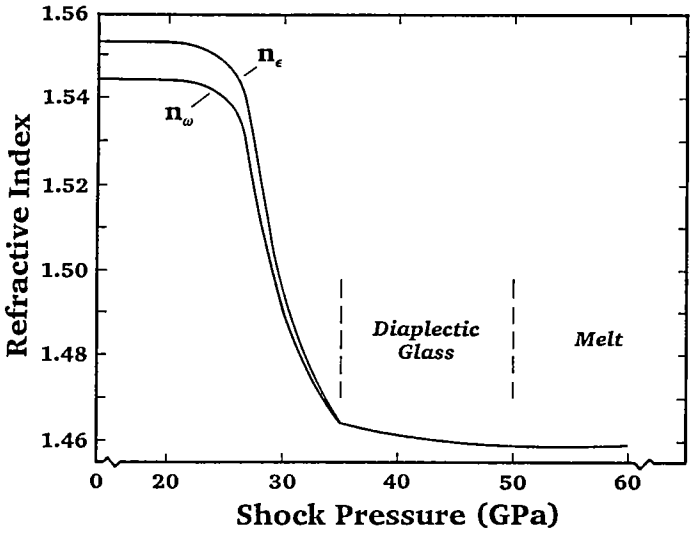

Figure 13. Relationship of refractive index to shock pressure for experimentally shocked quartz (shock front parallel to {10$\bar{1}$0}, i.e., polar angle 90° to c-axis). Preshock temperature of quartz 20 °C. The lower curve is given for the ordinary ray, and the upper curve marks the extraordinary ray in quartz. A smooth and continuous decrease in the refractive index between about 25 and 35 GPa is obvious, followed by isotropization (diaplectic glass) and melting (lechatelierite). (After Stöffler and Langenhorst, 1994.)

melts (see Table 1). The melts can reach very high temperatures because of the passage of shock waves that generate temperatures far beyond those commonly encountered in normal crustal processes or in volcanic eruptions. The very high temperatures are indicated by the presence of inclusions of high-temperature minerals, such as lechatelierite, which forms from pure quartz at temperatures of >1700 °C (see above), or baddeleyite, which is the thermal decomposition product of zircon, forming at a temperature of about 1900 °C. Impact melts may also undergo a phase of superheating (i.e., staying liquid even though the vaporization temperature has been exceeded) at temperatures of 10,000 °C or higher (e.g., Jakes and others, 1992). Depending on the initial temperature, the location within the crater, the composition of the melt, and the speed of cooling, impact melts either form impact glasses (if they cool fast enough) or, more commonly, (mostly) fine-grained impact-melt rocks (if they cool more slowly). Impact-melt rocks are also found in suevitic breccias in the form of melt clasts. Impact-melt rocks contain clasts of shocked minerals or lithic clasts (Fig. 14).

As glasses are metastable supercooled liquids, impact glasses slowly recrystallize (if dissolution is not acting faster), at a rate that depends on the composition of the glass and postimpact environmental conditions. Therefore, impact glasses are more commonly found at young impact craters than at old impact structures. Very fine grained recrystallization textures are often characteristic of devitrified impact glasses (Fig. 14A,B). Impact glasses have chemical and isotopic compositions that are very similar to those of individual target rocks or mixtures of several rock types. For example, it is possible to use the rare earth element (REE) distribution patterns or the Rb-Sr isotopic composition, which are identical to those of the (often sedimentary or metasedimentary) target rocks, to distinguish the impact-melt rocks from intrusive or volcanic rocks (e.g., Blum and Chamberlain, 1992; Blum and others, 1993). Furthermore, impact glasses have much lower water contents (about 0.001–0.05 wt%) than volcanic or other natural glasses (e.g., Koeberl, 1992b). Detailed descriptions of impact melts and glasses and their characteristics and compositions are discussed by, for example, El Goresy and others (1968), Dence (1971), Stöffler (1984), Koeberl (1986,1992a,b), and references therein.

Impact melts and glasses (or minerals that have recrystallized from the melt; e.g., Krogh and others, 1993; Izett and others, 1993) have another important use, as they often are the most suitable material for the dating of an impact structure. The methods most commonly used for dating of impact-melt rocks or glasses include the K-Ar, ^{40}Ar-^{39}Ar, fission-track, Rb-Sr, Sm-Nd, or U-Th-Pb isotope methods. However, dating impact craters is complicated and tedious and, if not done with utmost care, can easily lead to erroneous results (see, e.g., Bottomley and others, 1990, and Deutsch and Schärer, 1994, for reviews of methods of impact crater dating).

GEOCHEMISTRY AND DETECTION OF METEORITIC COMPONENTS IN IMPACTITES

No meteorites have been found at most meteorite impact craters. This fact may seem a contradiction, but it follows as a logical consequence of the physics of an impact event. A shock wave, similar to the one that penetrates through the target, also passes through the meteoritic impactor and, within fractions of a second, vaporizes most or all

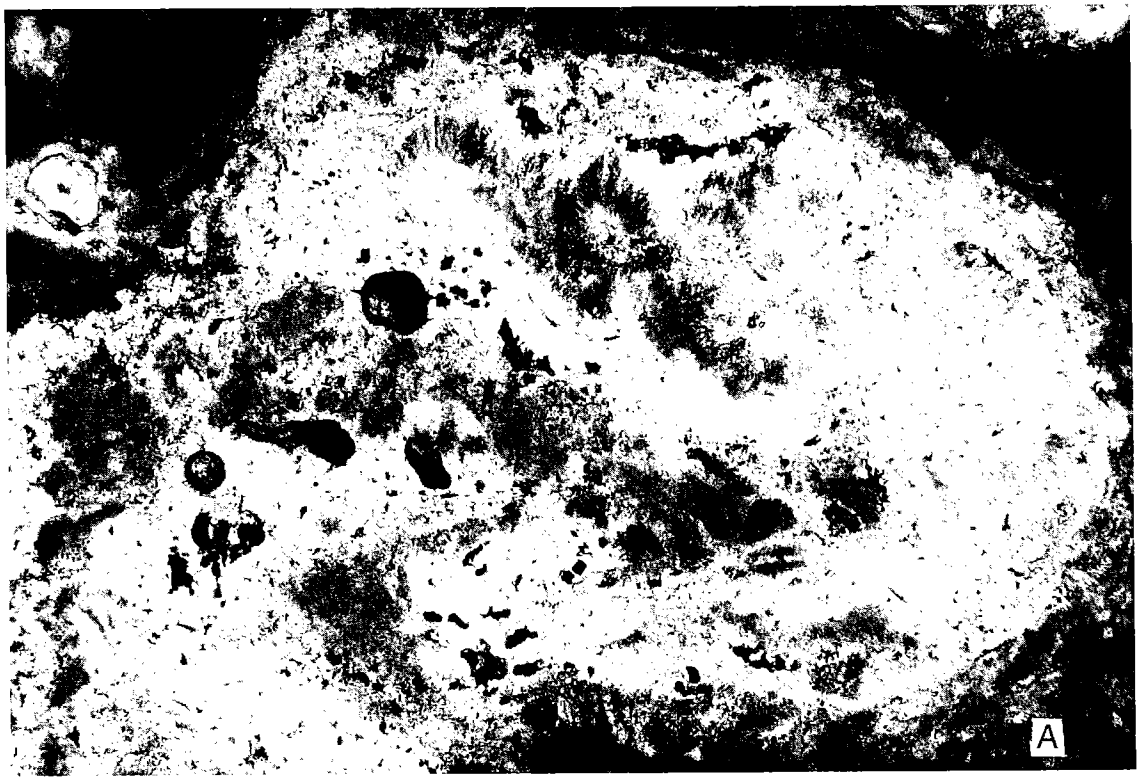

Figure 14. Photomicrographs of impact-melt rocks. A *(above)*—Largely melted quartzitic clast in flow-banded, extremely fine grained, melt matrix, in sample 277.8 from drill core M8, Manson impact structure, Iowa (see Koeberl and others, 1996a); note the fine, feathery recrystallization texture (width of field of view, 2.2 mm; parallel polarizers). B *(facing page)*—Impact-melt breccia 9018.1 from the Ames structure, Oklahoma, Nicor no. 18-4 Chestnut core, depth 2,748.7 m, with fractured and shocked mineral grains set in a finer-grained matrix, showing feathery spherulitic devitrification texture in center and upper right and a diaplectic quartz glass grain on the upper left (width of field of view, 3.4 mm; crossed polarizers; courtesy W. U. Reimold). C *(facing page)*—Aphanitic impact-melt breccia with K-feldspar clasts set in a fine-grained matrix, sample 1341.5 from the Exmore drill core, Chesapeake Bay impact structure, Virginia (see Poag and others, 1994; Koeberl and others, 1995b,1996c; width of field of view, 3.4 mm; crossed polarizers).

of the projectile. Only during the impact of small objects (less than about 40 m in diameter, depending on impact angle and velocity) may a small fraction of the initial mass of the meteorite survive, because of either spallation during entry into the atmosphere or lower impact velocity resulting from atmospheric drag. The cutoff diameter of impact craters at which some fraction of meteoritic material may be preserved is about 1 to 1.5 km. Thus, even under optimistic conditions, meteoritic fragments are preserved at only very young and small craters. The absence of meteorite fragments can, therefore, not be used as evidence against an impact origin of a crater structure.

A more generally applicable impact-diagnostic method is the detection of geochemical traces of the meteoritic projectile in target rocks. Such detection allows establishment of the impact origin for a crater structure. The meteoritic projectile undergoes vaporization in the early phases of crater formation. A small amount of the meteoritic vapor is incorporated with the much larger quantity of target-rock vapor and melt, which later forms impact-melt rocks, melt breccias, or glass. In most cases, the contribution of meteoritic matter to these impactite lithologies is very small (commonly $<<1\%$), leading to only slight chemical changes in the resulting impactites. Only elements that have high abundances in meteorites, but low abundances in terrestrial crustal rocks, can be used to detect such a meteoritic component. During the past two decades, studies of the abundances and interelement ratios of the siderophile elements, such as Cr, Co, Ni, and, especially, the platinum-group elements (PGEs) have been used for these investigations (see, e.g., Morgan and others, 1975; Palme, 1982; Evans and others, 1993; and references therein). However, the use of el-

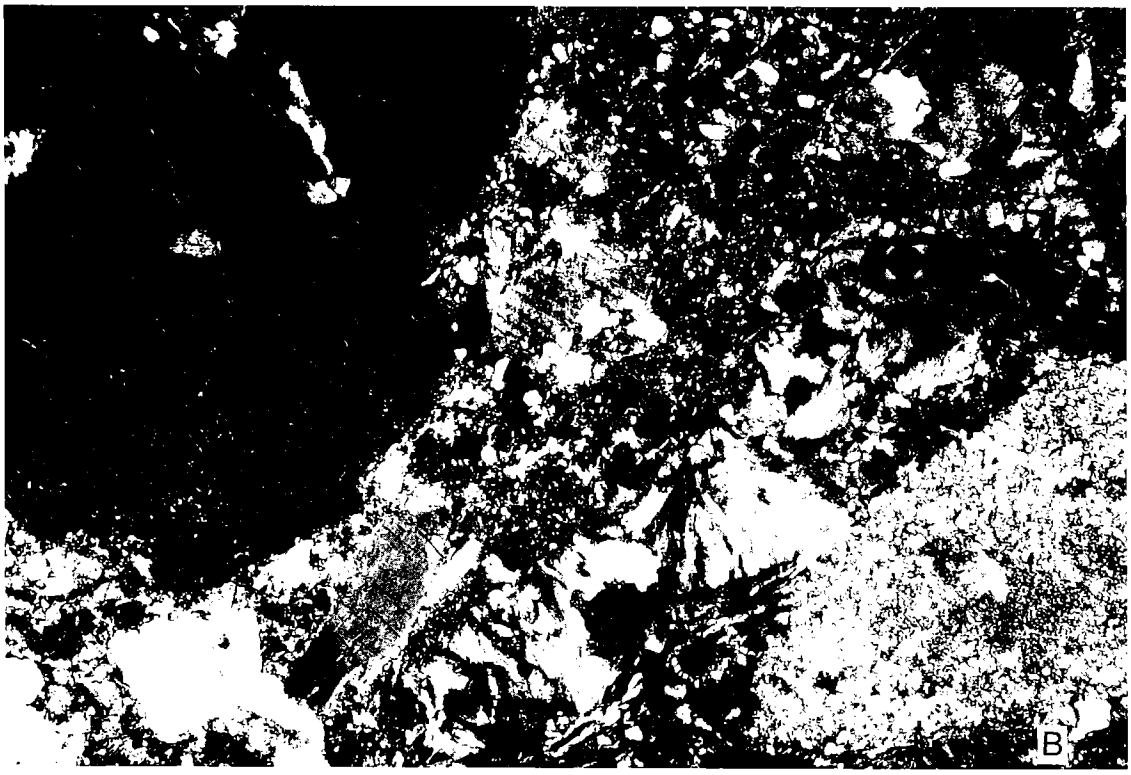

Figure 14B.

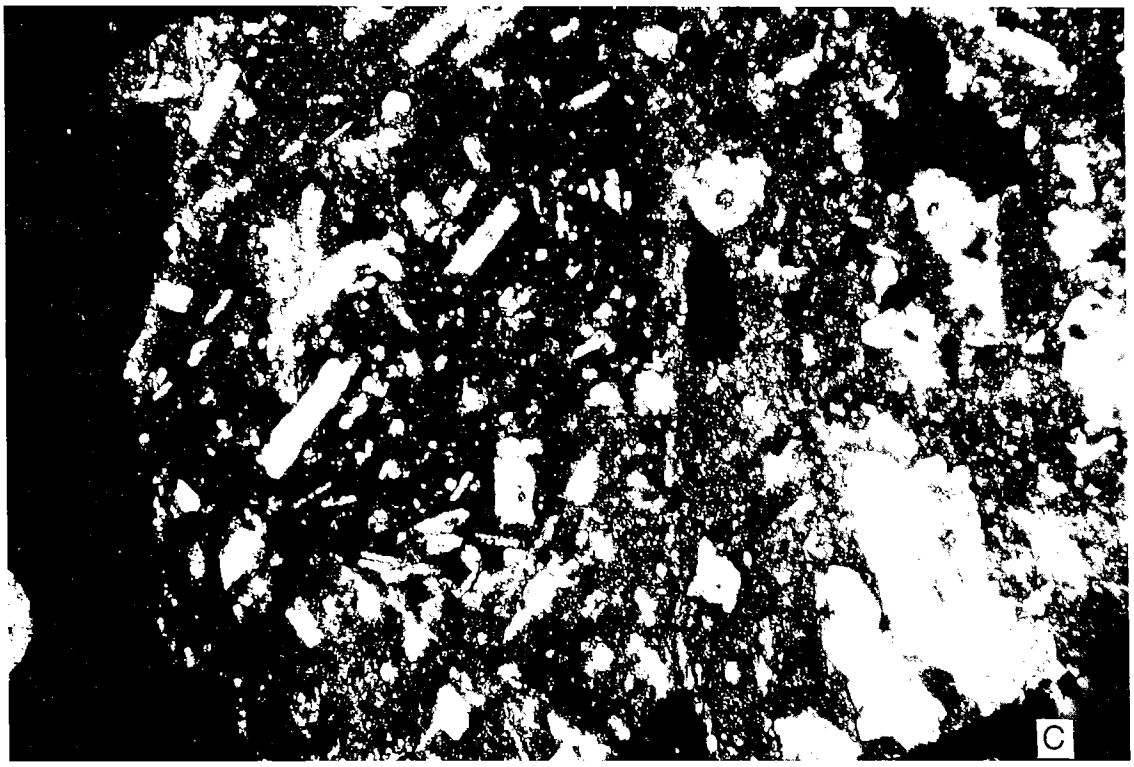

Figure 14C.

emental abundances does not necessarily lead to unambiguous results, as ultramafic rocks or ore minerals may be present among the target rocks, resulting in elevated PGE abundances. Another complication is the possible fractionation of the siderophile elements in the impact melt while it is still molten. This effect may be significant in larger craters, because there the melt can stay hot for many thousand years. Different mineral phases, such as sulfides or oxides (e.g., magnetite, chromite), may take up various proportions of the PGEs or other siderophile elements, leading to an irregular distribution of these elements and possibly fractionated interelement ratios and patterns. Such irregular distribution of siderophiles is known from, for example, the East and West Clearwater impact structures (Palme and others, 1979) and the Chicxulub impact structure (Koeberl and others, 1994c; Schuraytz and others, 1996). Hydrothermal processes associated with the hot impact melt may also change PGE abundances.

The use of the Re-Os isotope system has numerous advantages over the use of elemental abundances of the PGEs. The Re-Os isotope method is superior with respect to detection limit and selectivity, as discussed by Koeberl and Shirey (1993) and Koeberl and others (1994a,b). In principle, the abundances of Re and Os and the $^{187}Os/^{188}Os$ isotope ratios, which are measured by very sensitive mass spectrometric techniques, allow one to distinguish the isotopic signatures of meteoritic and terrestrial Os. Meteorites (and the terrestrial mantle) have much higher (by factors of 10^4 to 10^5) PGE contents than terrestrial crustal rocks. In addition, meteorites have relatively low Re and high Os abundances, resulting in Re/Os ratios less or equal to 0.1, whereas the Re/Os ratio of terrestrial crustal rocks is usually no less than 10. More important even, the $^{187}Os/^{188}Os$ isotope ratios for meteorites and terrestrial crustal rocks are significantly different.

^{187}Os is formed from the β-decay of ^{187}Re (with a half-life of 42.3 ± 1.3 b.y.). Thus, because of the high Re and low Os concentrations in old crustal rocks, their $^{187}Os/^{188}Os$ ratio increases rapidly with time. The present-day $^{187}Os/^{188}Os$ ratio of mantle rocks is about 0.13. Meteorites also have low $^{187}Os/^{188}Os$ ratios of about 0.11 to 0.18. Os is much more abundant in meteorites than Re, leading to only small changes in the meteoritic $^{187}Os/^{188}Os$ ratio with time. Because of the high Os abundances in meteorites, the addition of a minute meteoritical contribution to the crustal target rocks leads to an almost complete change of their Os isotopic signature in the resulting impact melt or breccia (see Fig. 15 for an example). For details about this method, see Koeberl and Shirey (1993, 1996,1997) and Koeberl and others (1994a,b). Like studies of shock metamorphism, Re-Os isotopic measurements of target rocks and impactites may provide good evidence for an impact origin.

CONCLUSIONS

Impact cratering still remains one of the least appreciated geologic processes, even though, over the past three decades, researchers have studied impact cratering and craters in nature, in the laboratory, and by computer modeling. Identification of further impact structures on Earth can only be achieved with diligent and careful investigations. Impact crater research is an excellent example to illustrate the necessity—and success—of interdisciplinary studies. This paper was aimed at describing how mineralogical and geochemical studies should be applied to the identification and characterization of impact craters and impact-derived rocks. As the discussions regarding the impact origin of the Ames structure (see papers in this volume) or the relationship of an impact to the K/T boundary have illustrated (see, e.g., Silver and Schultz, 1982; Sharpton and Ward, 1990; Ryder and others, 1996), there are still lots of misconceptions and a lack of understanding of the mineralogical and geochemical characteristics of shocked rocks. Thus, it is essential that the proper methods for identifying impact craters are understood and used before drawing any conclusions regarding the impact origin of a geologic structure.

ACKNOWLEDGMENTS

Many colleagues have helped with information and references or have provided various other support; I am especially grateful to B. Bohor (U.S. Geological Survey, Denver), B. M. French (Smithsonian Institution, Washington), and R. A. F. Grieve (Geological Survey of Canada, Ottawa). I am also grateful to D. Jalufka for drafting the figures, and B. M. French and W. U. Reimold for detailed comments on the manuscript. I thank K. Johnson and J. Campbell for the invitation to contribute to the symposium, for which this paper is part of the proceedings. Parts of this study were supported by the Austrian Fonds zur Förderung der wissenschaftlichen Forschung, Project P08794-GEO.

REFERENCES CITED

Alexopoulos, J. S.; Grieve, R. A. F.; and Robertson, P. B., 1988, Microscopic lamellar deformation features in quartz: discriminative characteristics of shock-generated varieties: Geology, v. 16, p. 796–799.

Alvarez, L. W.; Alvarez, W.; Asaro, F.; and Michel, H. V., 1980, Extraterrestrial cause for the Cretaceous-Tertiary extinction: Science, v. 208, p. 1095–1108.

Blum, J. D.; and Chamberlain, C. P., 1992, Oxygen isotope constraints on the origin of impact glasses from the Cretaceous-Tertiary boundary: Science, v. 257, p. 1104–1107.

Blum, J. D.; Chamberlain, C. P.; Hingston, M. P.;

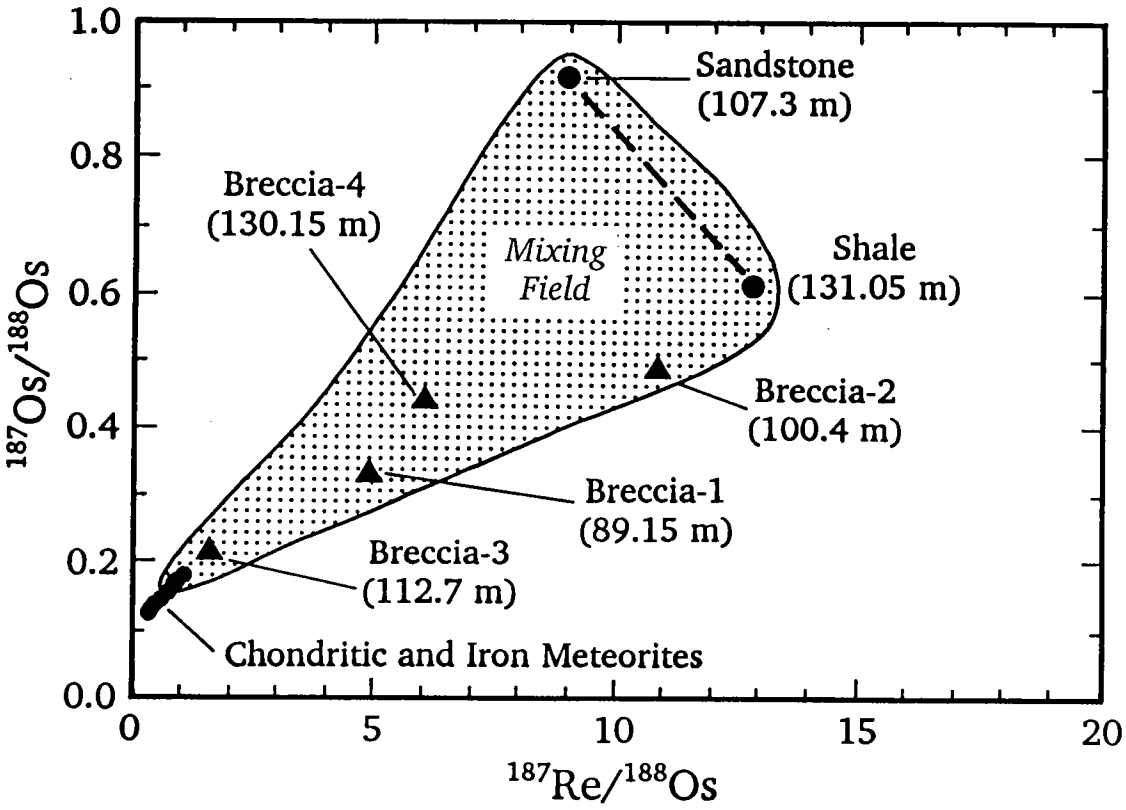

Figure 15. Ratios of $^{187}Os/^{188}Os$ vs. $^{187}Re/^{188}Os$ for target rocks (shale and sandstone) of the Kalkkop impact crater, South Africa, in comparison with data for four impact breccias (solid triangles) and the data array for chondritic and iron meteorites (small solid dots). The sample depths in the drill core are given as well (after Koeberl and others, 1994b). The dotted area marks the mixing field between target rocks and meteorites. All impact breccias fall within this mixing field; breccia-3 plots very close to the meteorite data array, indicating more meteoritic contamination than any other breccia, which is in good agreement with the high Os content of this sample (about 0.2 ppb). In addition to distinct differences in the Os isotope composition, the Os content of the target rocks, at about 0.02 ppb, is about 10 times lower than the Os content of the breccias.

Koeberl, C.; Marin, L. E.; Schuraytz, B. C.; and Sharpton, V. L., 1993, Isotopic comparison of K-T boundary impact glass with melt rock from the Chicxulub and Manson impact structures: Nature, v. 364, p. 325–327.

Bohor, B. F.; Foord, E. E.; Modreski, P. J.; and Triplehorn, D. M., 1984, Mineralogical evidence for an impact event at the Cretaceous/Tertiary boundary: Science, v. 224, p. 867–869.

Bohor, B. F.; Modreski, P. J.; and Foord, E. E., 1987, Shocked quartz in the Cretaceous/Tertiary boundary clays: evidence for global distribution: Science, v. 236, p. 705–708.

Boslough, M. B.; and Asay, J. R., 1993, Basic principles of shock compression, *in* Asay, J. R.; and Shahinpoor, M. (eds.), High-pressure shock compression of solids: Springer-Verlag, Berlin, p. 7–42.

Boslough, M. B.; Cygan, R. T.; and Izett, G. A., 1995, NMR spectroscopy of quartz from the K/T boundary: shock-induced peak broadening, dense glass, and coesite: Lunar and Planetary Science, v. 26, p. 149–150.

Bottomley, R. J.; York, D.; and Grieve, R. A. F., 1990, $^{40}Argon$-$^{39}Argon$ dating of impact craters: Proceedings of the 20th Lunar and Planetary Science Conference, p. 421–431.

Chapman, C. R.; and Morrison, D., 1994, Impacts on the Earth by asteroids and comets: assessing the hazard: Nature, v. 367, p. 33–40.

de Silva, S. L.; Wolff, J. A.; and Sharpton, V. L., 1990, Explosive volcanism and associated pressures: implications for models of endogenic shocked quartz, *in* Sharpton, V. L.; and Ward, P. D. (eds.), Global catastrophes in Earth history: Geological Society of America Special Paper 247, p. 139–145.

Dence, M. R., 1971, Impact melts: Journal of Geophysical Research, v. 76, p. 5525–5565.

Deutsch, A.; and Schärer, U., 1994, Dating terrestrial impact events: Meteoritics, v. 29, p. 301–322.

Dietz, R. S., 1968, Shatter cones in cryptoexplosion structures, *in* French, B. M.; and Short, N. M. (eds.), Shock metamorphism of natural materials: Mono Book Corp., Baltimore, p. 267–285.

El Goresy, A.; Fechtig, H.; and Ottemann, T., 1968, The opaque minerals in impactite glasses, *in* French, B. M.; and Short, N. M., (eds.), Shock metamorphism of natural materials: Mono Book Corp., Baltimore, p. 531–554.

Emmons, R. C., 1943, The universal stage (with five axes of rotation): Geological Society of America Memoir 8, 205 p.

Engelhardt, W. v.; and Bertsch, W., 1969, Shock induced planar deformation structures in quartz from the Ries crater, Germany: Contributions to Mineralogy and Petrology, v. 20, p. 203–234.

Evans, N. J.; Gregoire, D. C.; Grieve, R. A. F.; Goodfellow, W. D.; and Veizer, J., 1993, Use of platinum-group elements for impactor identification: terrestrial impact craters and Cretaceous-Tertiary boundary: Geochimica et Cosmochimica Acta, v. 57, p. 3737–3748.

French, B. M., 1968, Shock metamorphism as a geological process, *in* French, B. M.; and Short, N. M. (eds.), Shock metamorphism of natural materials: Mono Book Corp., Baltimore, p. 1–17.

_____ 1990, Absence of shock-metamorphic effects in the Bushveld complex, South Africa: results of an intensive search: Tectonophysics, v. 171, p. 287–301.

French, B. M.; and Short, N. M. (eds.), 1968, Shock metamorphism of natural materials: Mono Book Corp., Baltimore, 644 p.

Gault, D. E.; Quaide, W. L.; and Oberbeck, V. R., 1968, Impact cratering mechanics and structures, *in* French, B. M.; and Short, N. M. (eds.), Shock metamorphism of natural materials: Mono Book Corp., Baltimore, p. 87–99.

Glen, W., 1994, The mass extinction debates: Stanford University Press, Stanford, California, 370 p.

Goltrant, O.; Cordier, P.; and Doukhan, J. C., 1991, Planar deformation features in shocked quartz: a transmission electron microscopy investigation: Earth and Planetary Science Letters, v. 106, p. 103–115.

Gratz, A. J.; Nellis, W. J.; Christie, J. M.; Brocious, W.; Swegle, J.; and Cordier, P., 1992a, Shock metamorphism of quartz with initial temperatures −170 to +1000°C: Physical Chemistry of Minerals, v. 19, p. 267–288.

Gratz, A. J.; Nellis, W. J.; and Hinsey, N. A., 1992b, Laboratory simulation of explosive volcanic loading and implications for the cause of the K/T boundary: Geophysical Research Letters, v. 19, p. 1391–1394.

Grieve, R. A. F., 1987, Terrestrial impact structures: Annual Reviews of Earth and Planetary Science, v. 15, p. 245–270.

_____ 1991, Terrestrial impact: the record in the rocks: Meteoritics, v. 26, p. 175–194.

_____ 1997, Terrestrial impact structures: basic characteristics and economic significance, with emphasis on hydrocarbon production, in Johnson, K. S.; and Campbell, J. A. (eds.), Ames structure in northwest Oklahoma and similar features: origin and petroleum production (1995 symposium): Oklahoma Geological Survey Circular 100 [this volume], p. 3–16.

Grieve, R. A. F.; and Shoemaker, E. M., 1994, Terrestrial impact cratering, *in* Gehrels, T. (ed.), Hazards due to comets and asteroids: University of Arizona Press, Tucson, p. 417–462.

Grieve, R. A. F.; and Therriault, A. M., 1995, Planar deformation features in quartz: target effects: Lunar and Planetary Science, v. 26, p. 515–516.

Grieve, R. A. F.; Langenhorst, F.; and Stöffler, D., 1996, Shock metamorphism in nature and experiment; II. Significance in geoscience: Meteoritics and Planetary Science, v. 31, p. 6–35.

Hörz, F., 1968, Statistical measurements of deformation structures and refractive indices in experimentally shock loaded quartz, *in* French, B. M.; and Short, N. M. (eds.), Shock metamorphism of natural materials: Mono Book Corp., Baltimore, p. 243–253.

_____ 1982, Ejecta of the Ries crater, Germany, *in* Silver, L. T.; and Schultz, P. H. (eds.), Geological implications of impacts of large asteroids and comets on the Earth: Geological Society of America Special Paper 190, p. 39–55.

Hörz, F.; Ostertag, R.; and Rainey, D. A., 1983, Bunte breccia of the Ries: continuous deposits of large impact craters: Reviews of Geophysics and Space Physics, v. 21, p. 1667–1725.

Hoyt, W. G., 1987, Coon Mountain controversies: University of Arizona Press, Tucson, 442 p.

Huffman, A. R.; Brown, J. M.; Carter, N. L.; and Reimold, W. U., 1993, The microstructural response of quartz and feldspar under shock loading at variable temperatures: Journal of Geophysical Research, v. 98, p. 22171–22197.

Izett, G. A.; Cobban, W. A.; Obradovich, J. D.; and Kunk, M. J., 1993, The Manson impact structure: ^{40}Ar-^{39}Ar age and its distal impact ejecta in the Pierre Shale in southeastern South Dakota: Science, v. 262, p. 729–732.

Jakes, P.; Sen, S.; Matsuishi, K.; Reid, A. M.; King, E. A.; and Casanova, I., 1992, Silicate melts at super liquidus temperatures: reduction and volatilization: Lunar and Planetary Science, v. 23, p. 599–600.

Kieffer, S. W.; and Simonds, C. H., 1980, The role of volatiles and lithology in the impact cratering process: Reviews of Geophysics and Space Physics, v. 18, p. 143–181.

Koeberl, C., 1986, Geochemistry of tektites and impact glasses: Annual Reviews of Earth and Planetary Science, v. 14, p. 323–350.

_____1992a, Geochemistry and origin of Muong Nong–type tektites: Geochimica et Cosmochimica Acta, v. 56, p. 1033–1064.

_____1992b, Water content of glasses from the K/T boundary, Haiti: indicative of impact origin: Geochimica et Cosmochimica Acta, v. 56, p. 4329–4332.

Koeberl, C.; and Anderson, R. R., 1996, Manson and company: impact structures in the United States, *in* Koeberl, C.; and Anderson, R. R. (eds.), The Manson impact structure, Iowa: anatomy of an

impact crater: Geological Society of America Special Paper 302, p. 1–29.
Koeberl, C.; and Reimold, W. U., 1995a, Shock metamorphism at the Red Wing Creek structure, North Dakota: confirmation of impact origin: Lunar and Planetary Science, v. 26, p. 769–770.
_____1995b, The Newporte impact structure, North Dakota: Geochimica et Cosmochimica Acta, v. 59, p. 4747–4767.
Koeberl, C.; and Shirey, S. B., 1993, Detection of a meteoritic component in Ivory Coast tektites with rhenium-osmium isotopes: Science, v. 261, p. 595–598.
_____1996, Re-Os isotope study of rocks from the Manson impact structure, *in* Koeberl, C.; and Anderson, R. R. (eds.), The Manson impact structure, Iowa: anatomy of an impact crater: Geological Society of America Special Paper 302, p. 331–339.
_____1997, Re-Os isotope systematics as a diagnostic tool for the study of impact craters and ejecta: Palaeogeography, Palaeoclimatology, Palaeoecology, in press.
Koeberl, C.; Reimold, W. U.; and Shirey, S. B., 1994a, Saltpan impact crater, South Africa: geochemistry of target rocks, breccias, and impact glasses, and osmium isotope systematics: Geochimica et Cosmochimica Acta, v. 58, p. 2893–2910.
Koeberl, C.; Reimold, W. U.; Shirey, S. B.; and Le Roux, F. G., 1994b, Kalkkop crater, Cape Province, South Africa: confirmation of impact origin using osmium isotope systematics: Geochimica et Cosmochimica Acta, v. 58, p. 1229–1234.
Koeberl, C.; Sharpton, V. L.; Schuraytz, B. C.; Shirey, S. B.; Blum, J. D.; and Marin, L. E., 1994c, Evidence for a meteoritic component in impact melt rock from the Chicxulub structure: Geochimica et Cosmochimica Acta, v. 58, p. 1679–1684.
Koeberl, C.; Masaitis, V. L.; Langenhorst, F.; Stöffler, D.; Schrauder, M.; Lengauer, C.; Gilmour, I.; and Hough, R. M., 1995a, Diamonds from the Popigai impact structure, Russia: Lunar and Planetary Science, v. 26, p. 777–778.
Koeberl, C.; Reimold, W. U.; Brandt, D.; and Poag, C. W., 1995b, Chesapeake Bay crater, Virginia: confirmation of impact origin: Meteoritics, v. 30, p. 528–529.
Koeberl, C.; Reimold, W. U.; Kracher, A.; Träxler, B.; Vormaier, A.; and Körner, W., 1996a, Mineralogical, petrological, and geochemical studies of drill cores from the Manson impact structure, Iowa, *in* Koeberl, C.; and Anderson, R. R. (eds.), The Manson impact structure, Iowa: anatomy of an impact crater: Geological Society of America Special Paper 302, p. 145–219.
Koeberl, C.; Reimold, W. U.; and Brandt, D., 1996b, Red Wing Creek structure, North Dakota: petrographical and geochemical studies, and confirmation of impact origin: Meteoritics and Planetary Science, v. 31, 335–342.
Koeberl, C.; Poag, C. W.; Reimold, W. U.; and Brandt, D., 1996c, Impact origin of Chesapeake Bay structure and the source of North American tektites: Science, v. 271, p. 1263–1266.
Kring, D. A., 1993, The Chicxulub impact event and possible causes of K/T boundary extinctions, *in* Boaz, D.; and Dornan, M. (eds.), Proceedings of the First Annual Symposium of Fossils of Arizona: Mesa Southwest Museum and Southwest Paleontological Society, Mesa, Arizona, p. 63–79.
Krogh, T. E.; Kamo, S. L.; Sharpton, V. L.; Marin, L. E.; and Hildebrand, A. R., 1993, U-Pb ages of single shocked zircons linking distal K/T ejecta to the Chicxulub crater: Nature, v. 366, p. 731–734.
Langenhorst, F., 1993, Hochtemperatur-Stoßwellenexperimente an Quarz-Einkristallen: University of Münster, Germany, unpublished Ph.D. thesis, 126 p.
_____ 1994, Shock experiments on α- and β-quartz; II. Modelling of lattice expansion and amorphization: Earth and Planetary Science Letters, v. 128, p. 683–698.
Leroux, H.; Reimold, W. U.; and Doukhan, J. C., 1994, A T.E.M. investigation of shock metamorphism in quartz from the Vredefort dome, South Africa: Tectonophysics, v. 230, p. 223–239.
Lyons, J. B.; Officer, C. B.; Borella, P. E.; and Lahodynsky, R., 1993, Planar lamellar substructures in quartz: Earth and Planetary Science Letters, v. 119, p. 431–440.
Mark, K., 1987, Meteorite craters: University of Arizona Press, Tucson, 288 p.
Marsh, S. P., 1980, LASL shock Hugoniot data: University of California Press, Berkeley, 658 p.
Marvin, U. B., 1990, Impact and its revolutionary implications for geology, *in* Sharpton, V. L.; and Ward, P. D. (eds.), Global catastrophes in Earth history: Geological Society of America Special Paper 247, p. 147–154.
Medenbach, O., 1985, A new microrefractometer spindle stage and its application: Fortschritte der Mineralogie, v. 63, p. 111–133.
Melosh, H. J., 1989, Impact cratering: a geologic process: Oxford University Press, New York, 245 p.
Milton, D. J., 1977, Shatter cones—an outstanding problem in shock mechanics, *in* Roddy, D. J.; Pepin, R. O.; and Merrill, R. B. (eds.), Impact and explosion cratering: Pergamon Press, New York, p. 703–714.
Morgan, J. W.; Higuchi, H.; Ganapathy, R.; and Anders, E., 1975, Meteoritic material in four terrestrial meteorite craters: Proceedings of the 6th Lunar and Planetary Science Conference, p. 1609–1623.
Morgan, P., 1989, Heat flow in the Earth, *in* James, D. E. (ed.), The encyclopedia of solid earth geophysics: Van Nostrand Reinhold Co., New York, p. 634–646.
Palme, H., 1982, Identification of projectiles of large terrestrial impact craters and some implications for the interpretation of Ir-rich Cretaceous/Tertiary boundary layers, *in* Silver, L. T.; and Schultz, P. H. (eds.), Geological implications of impacts of large asteroids and comets on Earth: Geological Society of America Special Paper 190, p. 223–233.
Palme, H.; Göbel, E.; and Grieve, R. A. F., 1979, The distribution of volatile and siderophile elements in the impact melt of East Clearwater (Quebec): Pro-

ceedings of the 10th Lunar and Planetary Science Conference, p. 2465–2492.
Pilkington, M.; and Grieve, R. A. F., 1992, The geophysical signature of terrestrial impact craters: Reviews of Geophysics, v. 30, p. 161–181.
Poag, C. W.; Powars, D. S.; Poppe, L. J.; and Mixon, R. B., 1994, Meteoroid mayhem in Ole Virginny: source of the North American tektite strewn field: Geology, v. 22, p. 691–694.
Reimold, W. U., 1988, Shock experiments with preheated Witwatersrand quartzite and the Vredefort microdeformation controversy: Lunar and Planetary Science, v. 19, p. 970–971.
_____ 1995, Pseudotachylite in impact structures—generation by friction melting and shock brecciation?: a review and discussion: Earth-Science Reviews, v. 39, p. 247–265.
Reinhard, M., 1931, Universaldrehtischmethoden: Birkhäuser Verlag, Basel, 118 p.
Robertson, P. B.; Dence, M. R.; and Vos, M. A., 1968, Deformation in rock-forming minerals from Canadian craters, in French, B. M.; and Short, N. M. (eds.), Shock metamorphism of natural materials: Mono Book Corp., Baltimore, p. 433–452.
Roddy, D. J.; Pepin, R. O.; and Merrill, R. B. (eds.), 1977, Impact and explosion cratering: Pergamon Press, New York, 1301 p.
Ryder, G.; Fastovsky, D.; and Gartner, S. (eds.), 1996, The Cretaceous-Tertiary event and other catastrophes in Earth history: Geological Society of America Special Paper 307, 576 p.
Schultz, P. H.; Koeberl, C.; Bunch, T.; Grant, J.; and Collins, W., 1994, Ground truth for oblique impact processes: new insight from the Rio Cuarto, Argentina, crater field: Geology, v. 22, p. 889–892.
Schuraytz, B. C.; Lindstrom, D. J.; Marín, L. E.; Martinez, R. R.; Mittlefehldt, D. W.; Sharpton, V. L.; and Wentworth, S. J., 1996, Iridium metal in Chicxulub impact melt: forensic chemistry on the K-T smoking gun: Science, v. 271, p. 1573–1576.
Sclater, J. G.; Jaupart, C.; and Galson, D., 1980, The heat flow through oceanic and continental crust and the heat loss of the Earth: Reviews in Geophysics and Space Physics, v. 18, p. 269–311.
Sharpton, V. L.; and Grieve, R. A. F., 1990, Meteorite impact, cryptoexplosion, and shock metamorphism: a perspective on the evidence at the K/T boundary, *in* Sharpton, V. L.; and Ward, P. D. (eds.), Global catastrophes in Earth history: Geological Society of America Special Paper 247, p. 301–318.
Sharpton, V. L.; and Ward, P. D. (eds.), 1990, Global catastrophes in Earth history: Geological Society of America Special Paper 247, 631 p.
Shoemaker, E. M.; Wolfe, R. F.; and Shoemaker, C. S., 1990, Asteroid and comet flux in the neighborhood of Earth, *in* Sharpton, V. L.; and Ward, P. D. (eds.), Global catastrophes in Earth history: Geological Society of America Special Paper 247, p. 155–170.
Silver, L. T.; and Schultz, P. H. (eds.), 1982, Geological implications of impacts of large asteroids and comets on the Earth: Geological Society of America Special Paper 190, 528 p.
Stöffler, D., 1972, Deformation and transformation of rock-forming minerals by natural and experimental shock processes: 1. Behaviour of minerals under shock compression: Fortschritte der Mineralogie, v. 49, p. 50–113.
_____ 1974, Deformation and transformation of rock-forming minerals by natural and experimental processes: 2. Physical properties of shocked minerals: Fortschritte der Mineralogie, v. 51, p. 256–289.
_____ 1984, Glasses formed by hypervelocity impact: Journal of Non-crystalline Solids, v. 67, p. 465–502.
Stöffler, D.; and Grieve, R. A. F., 1994, Classification and nomenclature of impact metamorphic rocks: a proposal to the IUGS Subcommission on the Systematics of Metamorphic Rocks: Lunar and Planetary Science, v. 25, p. 1347–1348.
Stöffler, D.; and Hornemann, U., 1972, Quartz and feldspar glasses produced by natural and experimental shock: Meteoritics, v. 7, p. 371–394.
Stöffler, D.; and Langenhorst, F., 1994, Shock metamorphism of quartz in nature and experiment: I. Basic observations and theory: Meteoritics, v. 29, p. 155–181.
Stöffler, D.; Deutsch, A.; Avermann, M.; Bischoff, L.; Brockmeyer, P.; Buhl, D.; Lakomy, R.; and Müller-Mohr, V., 1994, The formation of the Sudbury structure, Canada: toward a unified impact model, *in* Dressler, B. O.; Grieve, R. A. F.; and Sharpton, V. L. (eds.), Large meteorite impacts and planetary evolution: Geological Society of America Special Paper 293, p. 303–318.
Wegener, A., 1921, Die Entstehung der Mondkrater: Friedrich Vieweg and Sohn, Braunschweig, 48 p.
Weissman, P. R., 1990, The cometary impactor flux at the Earth, *in* Sharpton, V. L.; and Ward, P. D. (eds.), Global catastrophes in Earth history: Geological Society of America Special Paper 247, p. 171–180.

Extraterrestrial Impact Craters

Paul D. Lowman, Jr.
Goddard Space Flight Center
Greenbelt, Maryland

ABSTRACT.—Craters are the most common landform in the solar system, with the notable exception of the Earth and the volcanically resurfaced satellite Io. This paper describes impact craters on the Moon, Mercury, Mars, and Venus and gives a brief account of craters on the icy satellites of the outer planets. The Moon's craters are well preserved because of the lack of tectonic reworking and Earthlike erosion and deposition. There is a complete gradation from micrometer-size impact craters to multiring basins over 2,000 km wide. The circular mare basins, essentially large impact craters, were evidently formed at about the same time—3.9 b.y. ago—and localized prolonged basaltic eruptions, thus forming the maria. Mercurian craters are morphologically similar to those of the Moon, but the higher gravity restricted distribution of impact ejecta. Mars is an intermediate planet in terms of crustal evolution and has undergone erosion and deposition; it retains considerable surface ice. Some impact craters on Mars are morphologically different from those of airless planets in that they have lobate ejecta blankets of apparently fluidized ejecta. Mars is notable for a higher than usual population of elliptical primary craters, possibly formed by infall of captured satellites. Venus has a thick and dense atmosphere and consequently a lower population of small impact craters than occurs on other extraterrestrial bodies. Venusian craters have a number of unique features, such as long fluidized ejecta outflows probably formed by entrained gas. The Venusian crater population appears to express major volcanic resurfacing, although it is not yet clear whether this was a single episode or an equilibrium process. Small bodies, notably the icy satellites of the outer planets, have abundant impact craters, but these have been altered on bodies such as Ganymede by ice flowage. On Europa, occasional releases of water may lead to resurfacing and thus erase impact craters. Early impact cratering in general appears to represent the last stages of planet or satellite accretion, although impacts have evidently also broken up small bodies.

INTRODUCTION

Impact craters are uncommon on Earth, primarily because the Earth is an active planet whose crust is continuously reworked or resurfaced, but in the solar system as a whole, they are the most abundant landform on most solid planets and satellites. Extraterrestrial craters except for those of the Moon were unknown until close-range investigation became possible with the beginning of space flight, but they have now been found on every solid body except the Jovian satellite Io, which is continually resurfaced by tide-induced volcanism. Ephemeral craters, so to speak, were observed forming in the "Great Comet Crash" of 1994, when comet Shoemaker-Levy 9 hit Jupiter in a series of spectacular impacts whose atmospheric effects were still visible a month after the last impact (Hammel and others, 1995).

Having been geologically inactive for roughly 3 b.y. (Fig. 1), and with no atmosphere or hydrosphere, the Moon provides an easily visible and accessible museum of impact craters. This review will therefore concentrate on this "museum" of abundant, varied, and often pristine examples. Emphasis will be throughout on the characteristics of craters. A number of important topics, such as age estimation from cratering rates, are beyond the scope of the review and will be mentioned only briefly (Taylor, 1992).

LUNAR IMPACT CRATERS

Although mapped and named for centuries, lunar craters were generally considered volcanoes until the late 19th century. One reason for this is that the existence of meteorites, i.e., bodies that fall from the sky, was not accepted by western sci-

Paul D. Lowman, Jr., Goddard Space Flight Center, (Code 921), Greenbelt, MD 20771.

Lowman, P. D., Jr., 1997, Extraterrestrial impact craters, *in* Johnson, K. S.; and Campbell, J. A. (eds.), Ames structure in northwest Oklahoma and similar features: origin and petroleum production (1995 symposium): Oklahoma Geological Survey Circular 100, p. 55-81.

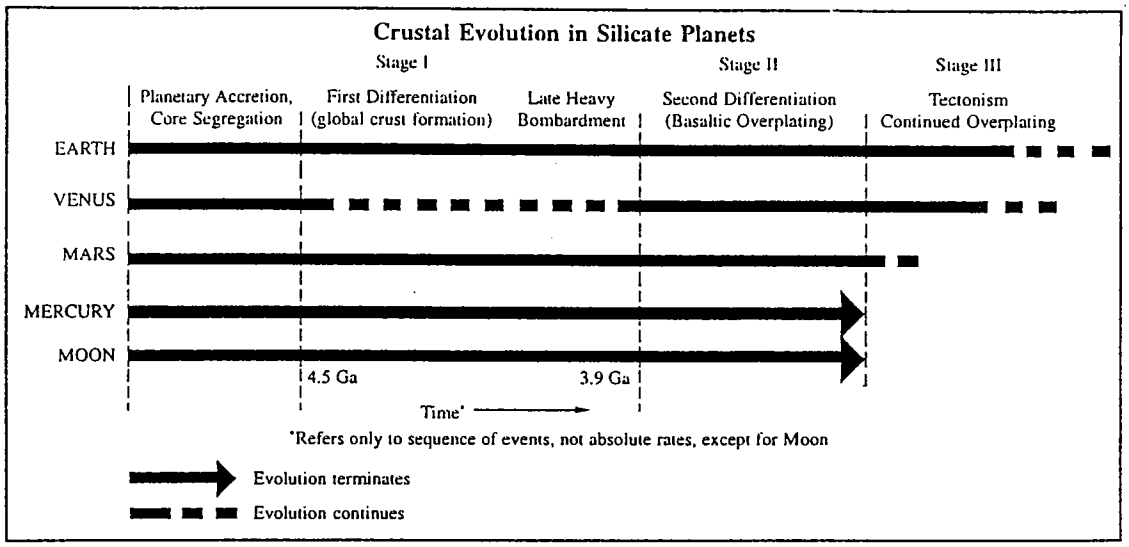

Figure 1. Comparative crustal evolution in the Moon, Mars, Venus, and Earth (from Lowman, 1989).

entific authorities until the late 18th century (Nininger, 1959). Volcanoes in contrast were well known, and it was natural to consider the Moon's craters calderas, an interpretation championed as late as 1971 (Green, 1971). The first modern authority to present a convincing case for their impact origin was G. K. Gilbert (1893), whose treatment of the Imbrium Basin is still considered valid today.

An impact origin for most lunar craters was convincingly argued by Dietz (1946), but it was the monumental study by Baldwin (1949) that convinced most scientists. Innumerable explosion craters had been produced during and after two world wars, and Baldwin showed that shell, bomb, and explosion craters fell on a smooth log-log depth vs. diameter plot (Fig. 2). Furthermore, four known terrestrial impact craters and dozens of lunar craters appeared to follow the same relationship.

The study of impact cratering was enormously stimulated by the beginning of space exploration. Assuming an impact origin for lunar craters of the Tycho-Copernicus type, and building on the work of Gilbert, the U.S. Geological Survey began systematic mapping of lunar geology under the sponsorship of NASA (the National Aeronautical and Space Administration) (Shoemaker and Hackman, 1962). The basic soundness of this work has been generally confirmed by the Apollo results and many other investigations of three decades. Lunar impact craters can be discussed in detail with considerable confidence, starting with relatively small, simple examples and working up to multiring basins covering much of the lunar surface area. The microscopic "zap pits" are well known and will not be described here.

It is important to appreciate the peculiarities of the lunar environment before comparing its craters with those of other bodies. Most important are the low gravity (one-sixth that at the Earth's surface) and absence of an atmosphere, which affect the later stages of crater excavation and distribution of ejecta. Another factor is the total absence of water in the Moon's outer layers; unlike the Earth or Mars, impacts on the Moon hit a totally anhydrous target.

Before going to examples, it will be convenient to introduce the concepts of "simple" and "complex" craters as they are applied to the Moon (Fig. 3). Small craters, a few kilometers wide, are generally "simple"; craters become "complex" at diameters of a few tens of kilometers. Figure 4 shows a large array of simple craters in a 5-km-wide area of Oceanus Procellarum, a reasonably typical mare area. The largest crater is close to the size and structure of the well-known Meteor (Barringer) Crater of Arizona. Its subdued topography suggests considerable age, very possibly several hundred million years. It is essentially a simple hole in the ground, with little structure. However, it will be noticed that a number of smaller craters nearby show concentric terraces. A closer view of such a double ring crater is shown in Figure 5. In light of what is now known about the lunar maria, this structure can be explained (Oberbeck and Quaide, 1968) as the effect of impact on a regolith (i.e., unconsolidated fragmental material) a few meters thick overlying solid rock (in this area, basalt).

The best example of a nearly pristine complex crater is 85-km-diameter Tycho (Fig. 6), whose age is estimated to be on the order of 100 m.y. despite its fresh appearance (Hörz and others, 1991). Its

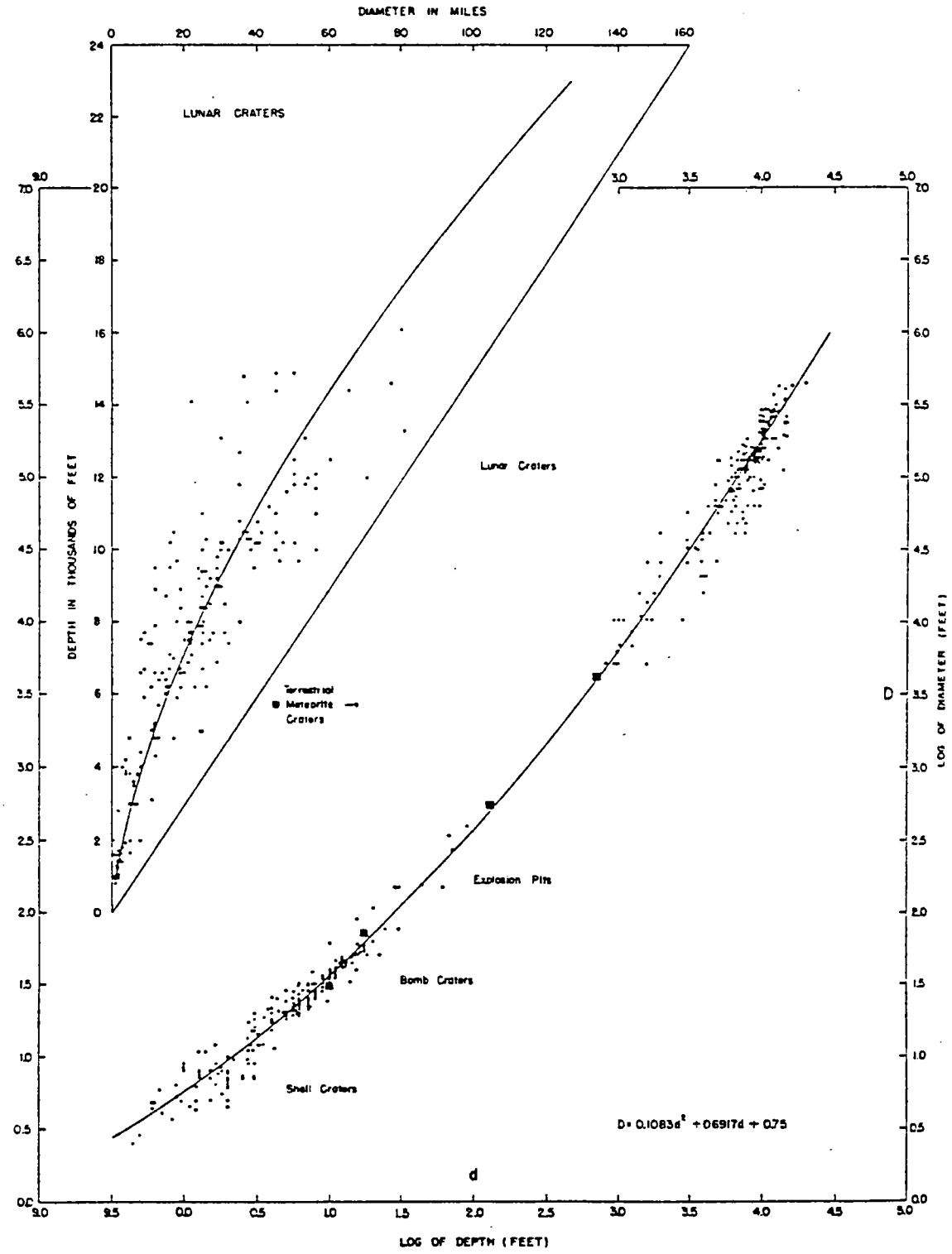

Figure 2. Relationship between diameter and depth of terrestrial explosion craters (bomb, shell, etc.) compared with lunar craters (from Baldwin, 1949).

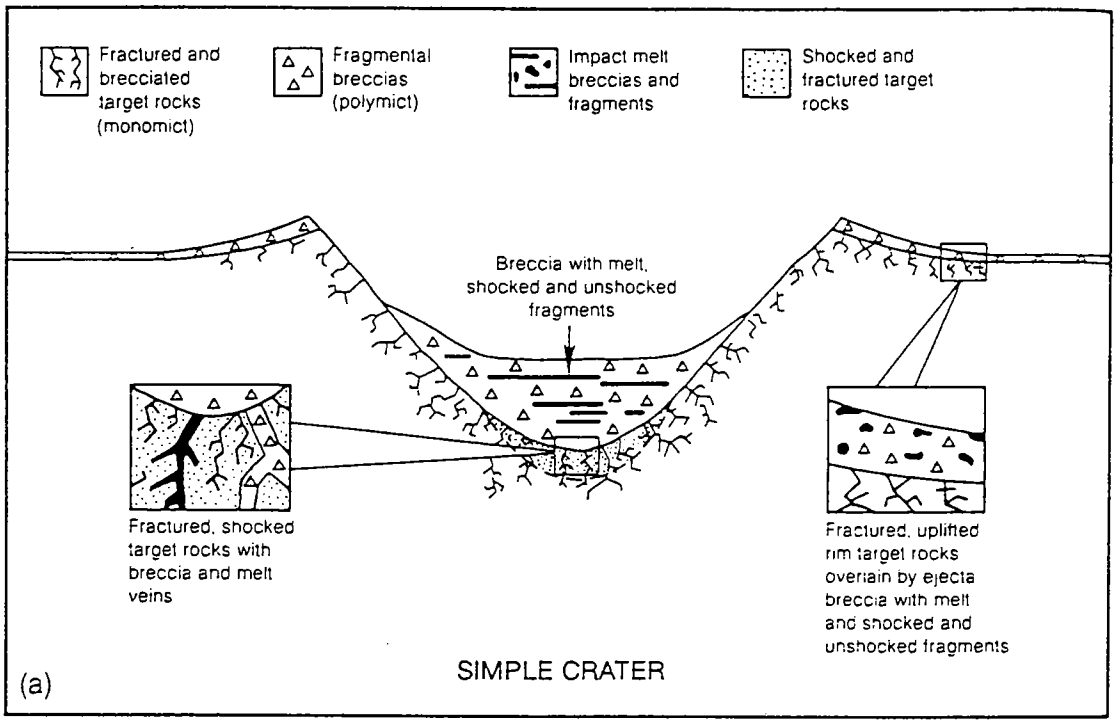

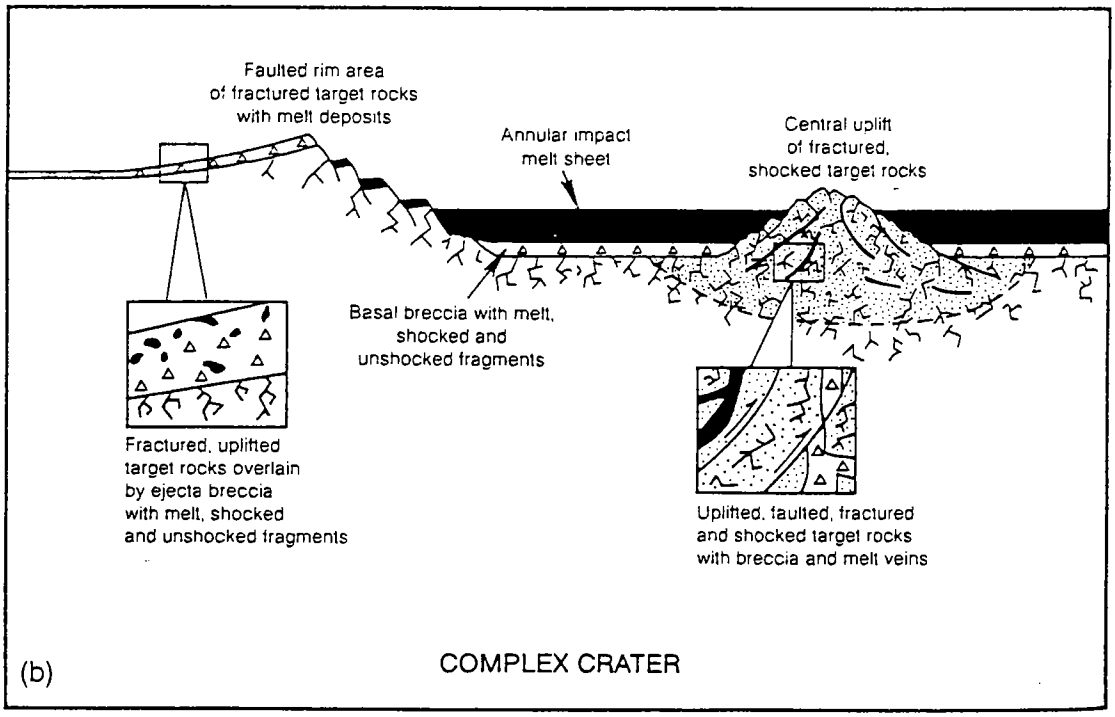

Figure 3. Schematic cross sections of simple and complex impact craters as these terms are now used (from Hörz and others, 1991).

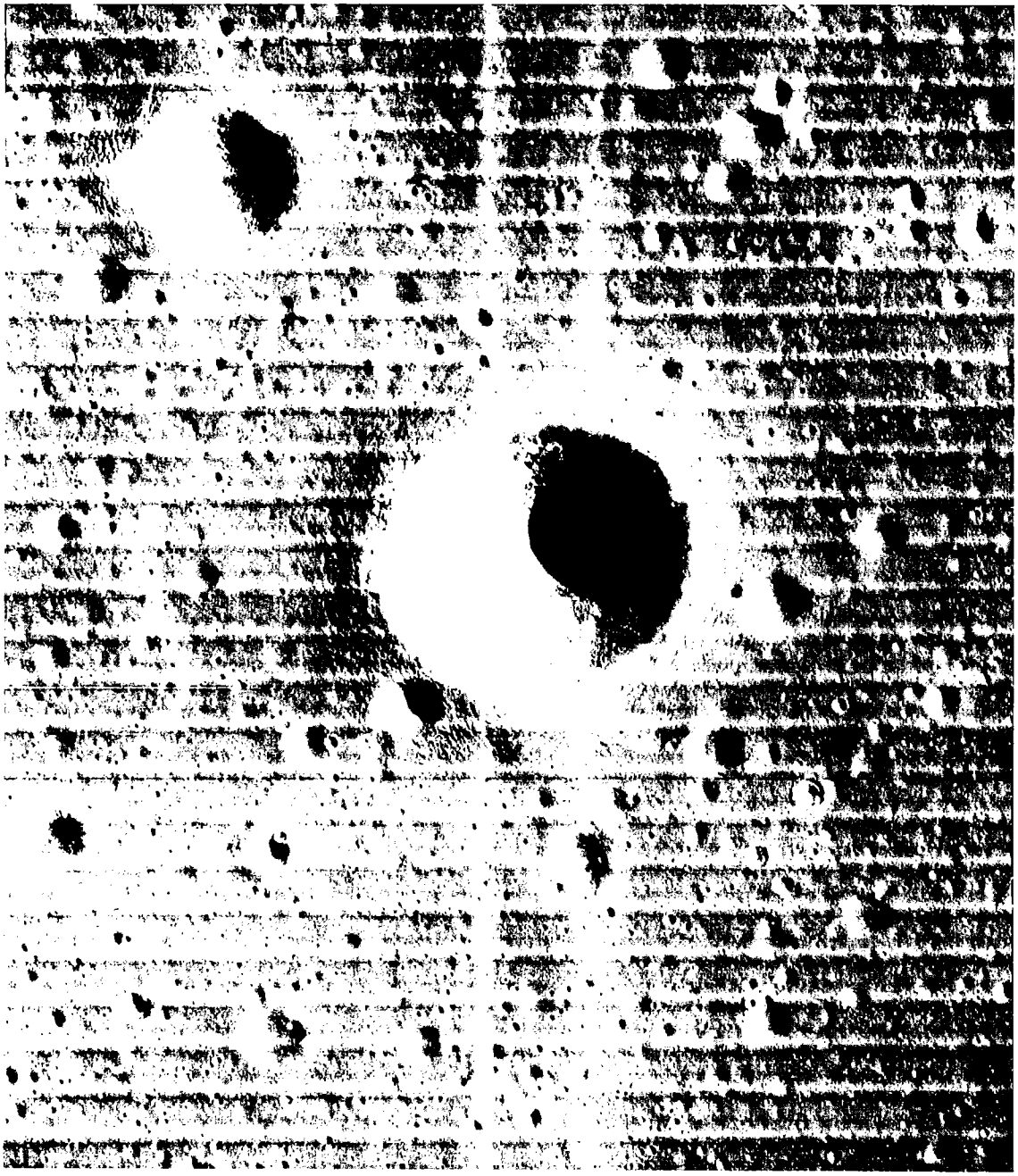

Figure 4. Lunar Orbiter picture of craters in Oceanus Procellarum, in an area about 5 km wide. Note small, double-ring craters.

relatively young age is also indicated by its optical and radar brightness, and its high thermal inertia, all indicating a thin or absent regolith. The features shown in the idealized diagram (Fig. 2) can be easily identified in Tycho: the raised rim, ejecta blanket, concentric terraces, impact-melt sheet, and central peak or uplift. The floor (Fig. 7) of Tycho is a rugged terrain with little or no regolith and very few superimposed later impact craters. This material is interpreted as impact melt and fallback breccia.

Another relatively young and fresh crater, Aristarchus, is shown in Figure 8. The general form of Aristarchus is that of a typical complex impact crater, but here the impact may have triggered some sort of internal activity. Aristarchus was

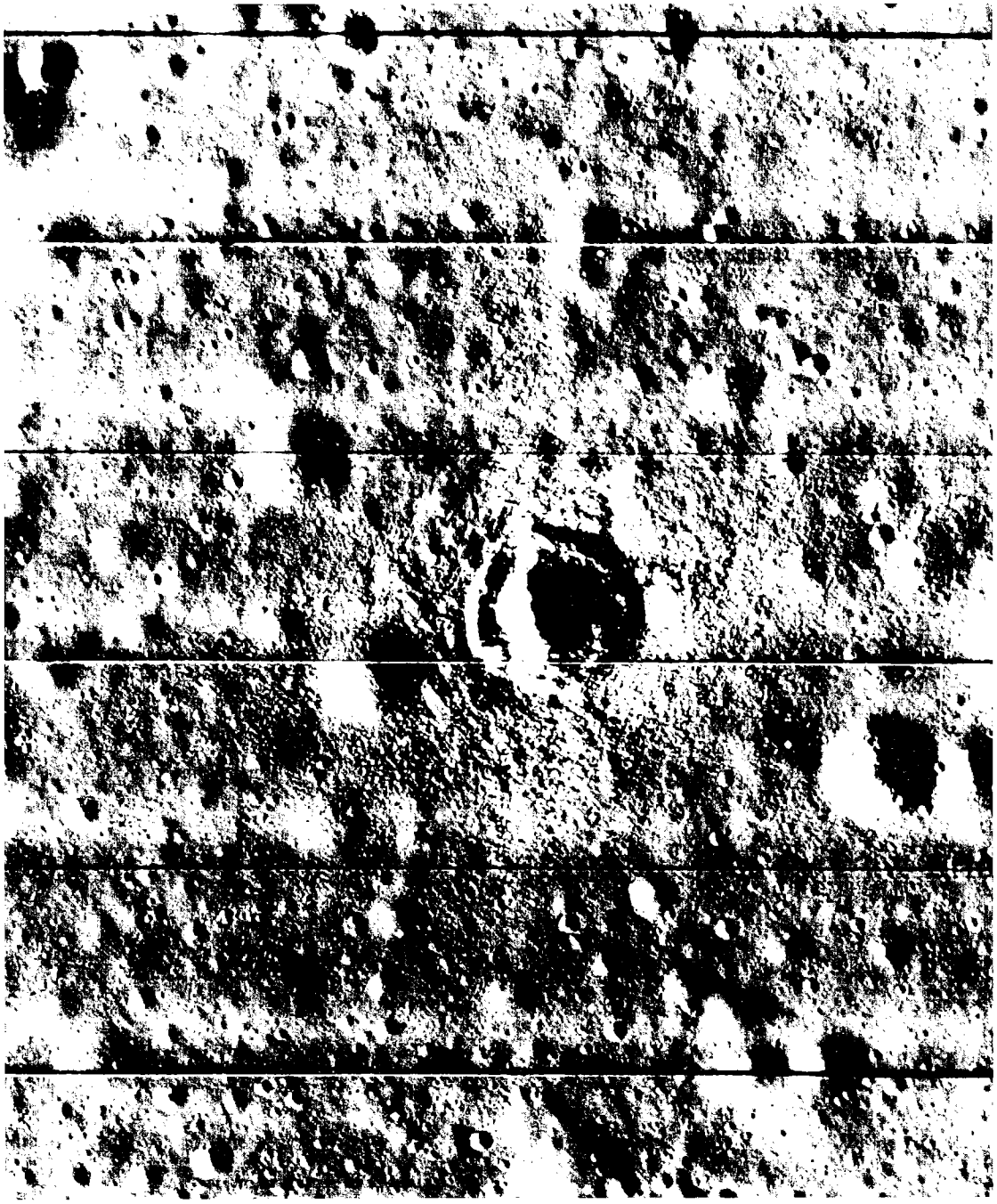

Figure 5. Lunar Orbiter high-resolution picture of fresh crater 130 m wide in Oceanus Procellarum, showing double-ring structure expressing impact effect in regolith over solid bedrock.

observed in 1963 by astronomers engaged in telescopic mapping to be emitting glowing reddish clouds of some sort, observations confirmed later by others. The Apollo 15 and 16 missions detected radon coming from the vicinity of Aristarchus, and since radon has a half-life of only a few days, its internal origin is undoubted. The actual relationship between impact and the internal activity in this area is not known. The sinuous rille shown in Figure 8 is almost certainly a volcanic feature,

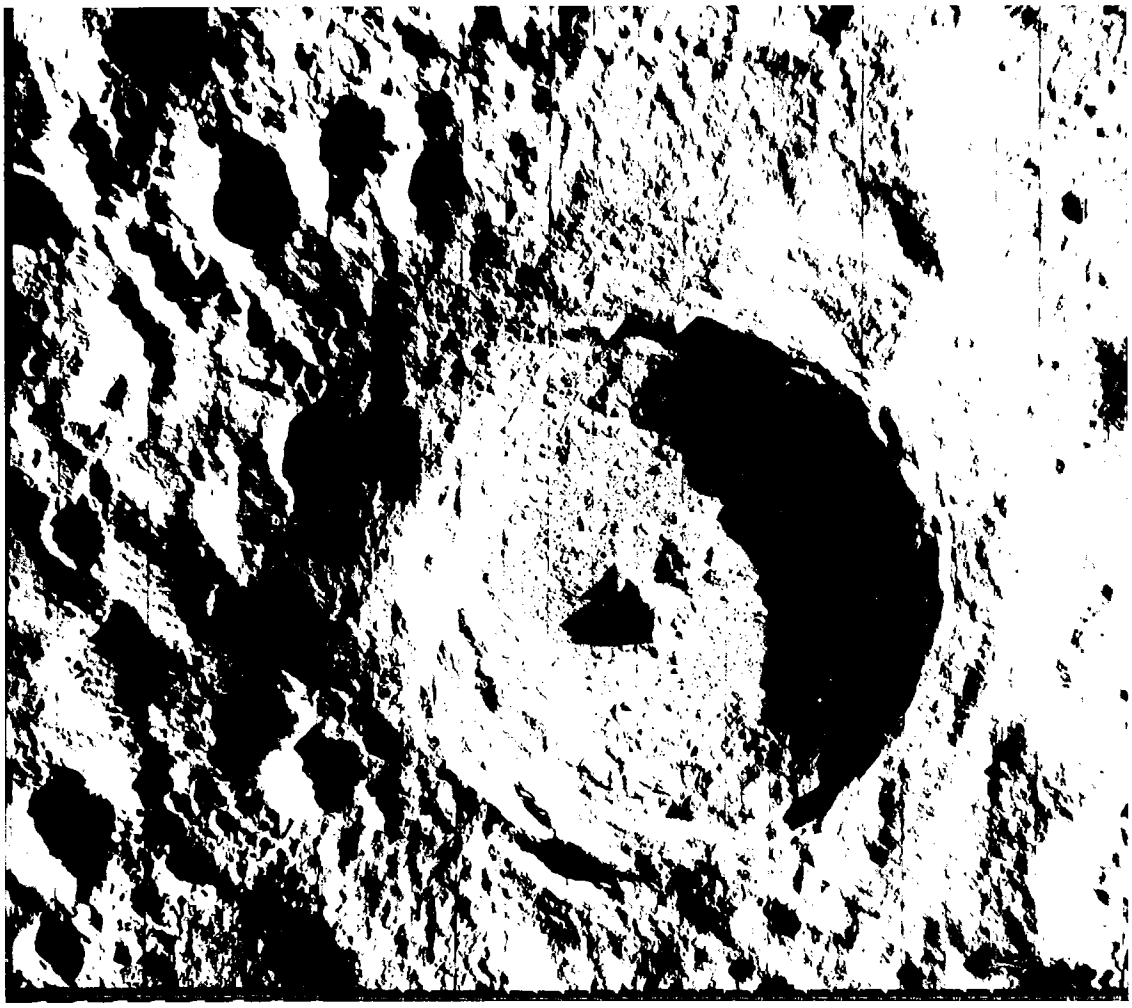

Figure 6. Lunar Orbiter picture of crater Tycho, 85 km wide; Sun from right, north at top.

probably a lava drainage channel, and it may well be that the impact simply localized gas emissions in an area inherently active to begin with. However, Aristarchus shows that major impacts on the Moon may have had more pervasive effects that crater formation alone.

Another, but older, complex crater, Copernicus, is shown in a classic telescopic view of the Moon (Fig. 9), which can be used to discuss several other crater categories. The greater age of Copernicus can be inferred from its more subdued topography and greater density of younger impact craters, well displayed in what was termed "The Picture of the Century" when transmitted from Lunar Orbiter in 1966 (Fig. 10). Figure 9 shows the Copernican ray system, as well as the chains of secondary craters formed by falling low-velocity blocks of ejecta from Copernicus. The rays overlie all features for several hundred kilometers around, superposition relationships showing that Copernicus is the youngest major feature. The similar crater Eratosthenes, to the northeast, is overlain by Copernican rays and no longer has visible rays of its own. Features of similar relative age are assigned to the Eratosthenian System (Shoemaker and Hackman, 1962).

Other types of craters are extremely well displayed in Figure 9. The largest of all is the Imbrium Basin, first interpreted as a gigantic impact crater by G. K. Gilbert (1893). This interpretation was confirmed by the Apollo missions, in particular Apollo 14, which landed on the ejecta blanket (Fra Mauro Formation) of the Imbrium Basin. The basin is actually a multiring structure, as shown by Spudis (1993), although this is not obvious because of subsequent basalt flooding. The excavation of the basin by impact of an asteroidal fragment was estimated by Spudis to have taken sev-

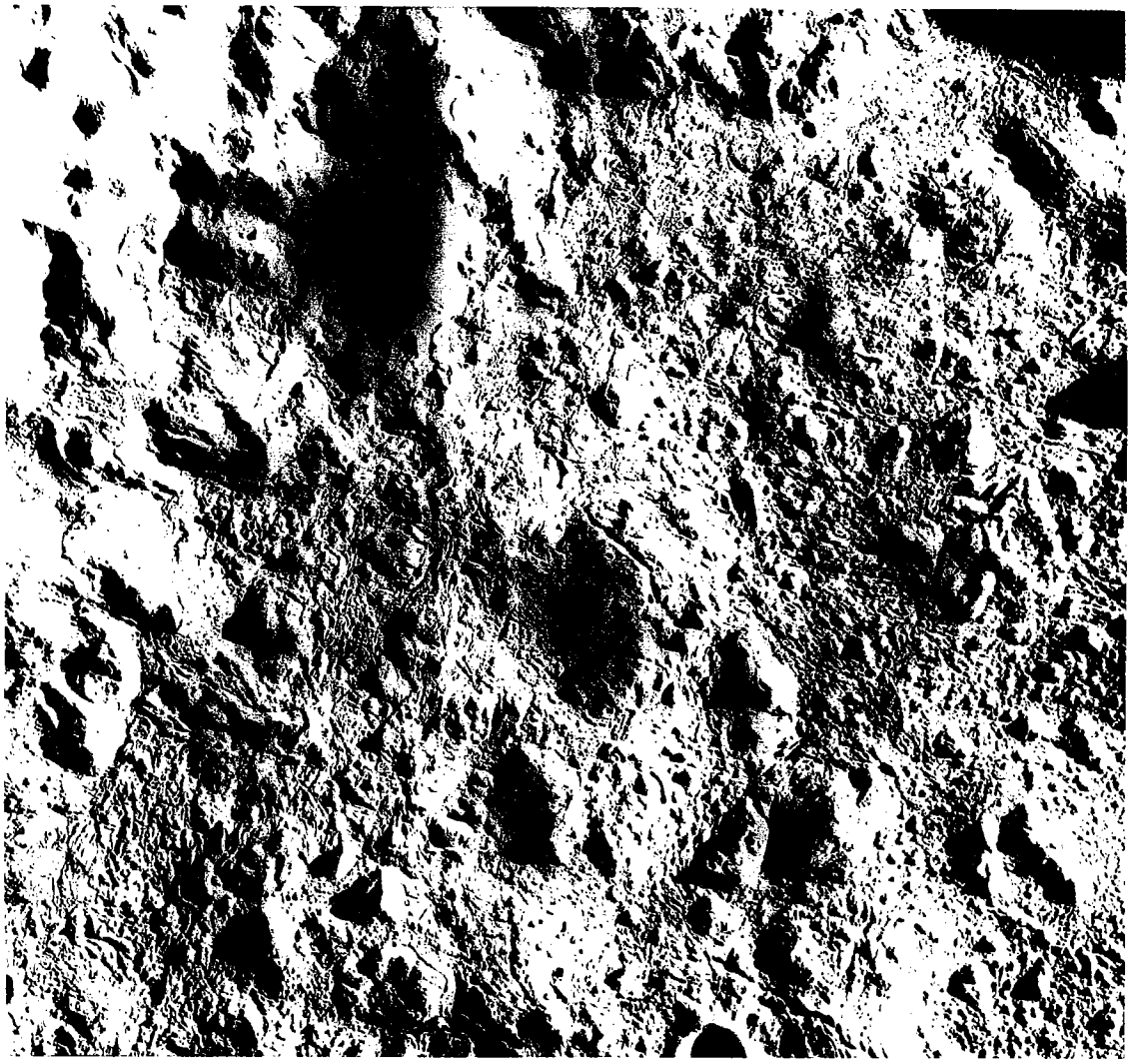

Figure 7. Lunar Orbiter picture of floor of Tycho, showing impact melt and breccia.

eral hours, an estimate since supported by the prolonged duration of the Shoemaker-Levy 9 cometary impacts on Jupiter.

Another category of impact crater has important implications for age relationships in the Imbrium Basin. Archimedes, Plato, and Sinus Iridum are essentially similar to Tycho and Copernicus, but have been filled and embayed by the basalts of Mare Imbrium. These stratigraphic relationships show that a significant time elapsed between excavation of the Imbrium Basin (which must have destroyed all preexisting topography) and the eruption of the mare basalts. Radiometric ages of these basalts, and exposures of lava flows at the Apollo 15 site, indicate that they were erupted in multiple episodes over several hundred million years. The relationship between impact and volcanism here is fairly well understood. The Imbrium impact evidently fractured the lunar crust and mantle to depths of several hundred kilometers, reaching a zone in which basaltic magma was being generated by more or less normal petrologic processes. It has been suggested by Ryder (1994) that basalts enriched in potassium, rare earth elements, and phosphorus (and therefore known as KREEP basalts) as well as other trace elements from the Imbrium Basin were impact induced.

It has been shown that the morphology of lunar craters changes with increasing size. Beyond the transition from simple to complex, there is a progression from craters to multiring basins. Departure from the complex-crater shape typified by

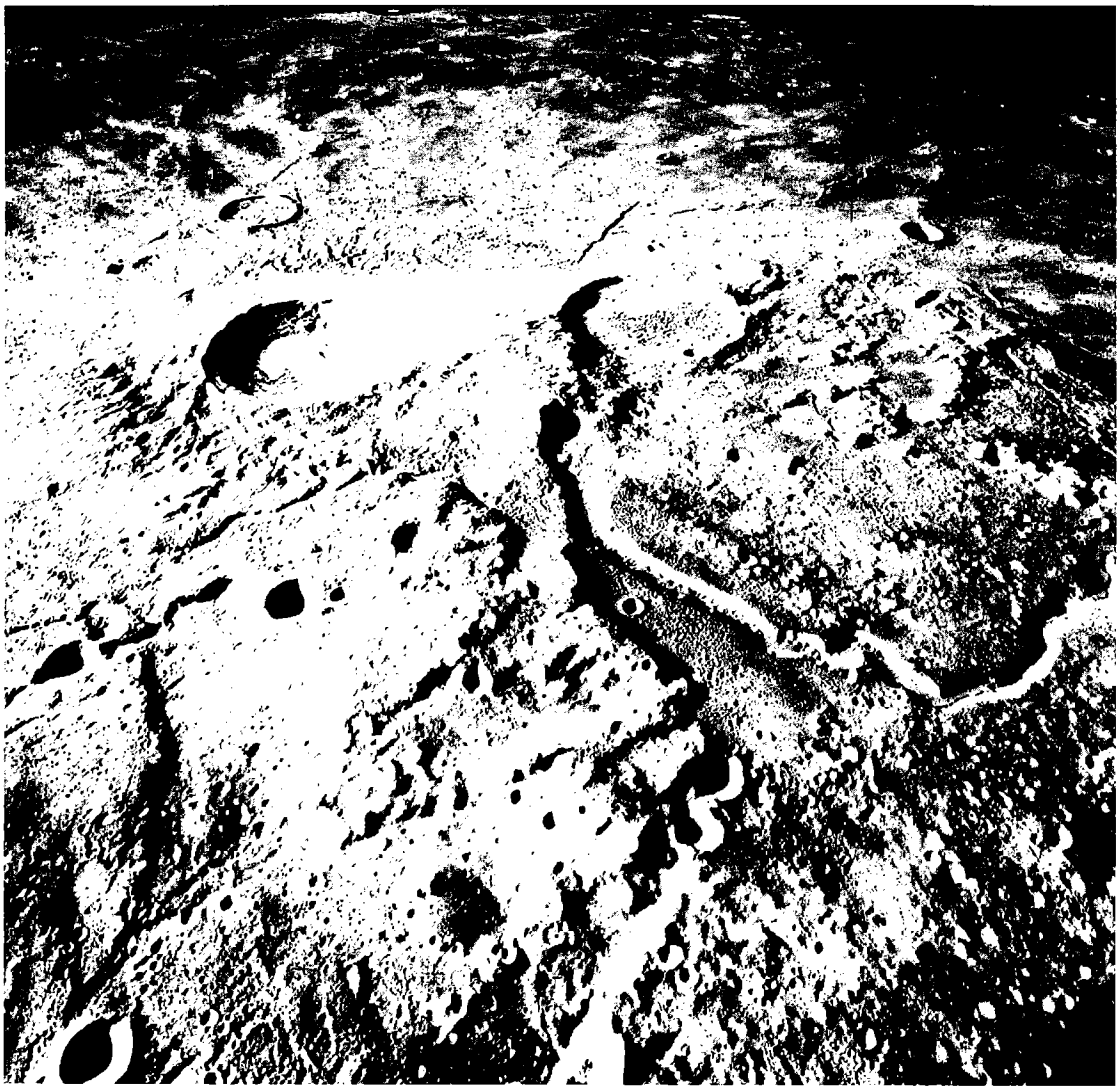

Figure 8. Apollo photograph of crater Aristarchus, 40 km wide, looking south; Schroter's Valley at lower right.

Tycho begins, on the Moon, at diameters of around 150 km, with formation of rings of isolated peaks on the crater floor. At larger diameters, well-developed inner rings appear. An excellent transition example is the 320-km-diameter two-ring crater Schrödinger (Fig. 11). As pointed out by Shoemaker and others (1994), the fractures in Schrödinger indicate continuing postimpact isostatic uplift. The dark halo crater on the floor further suggests relatively late, perhaps Copernican, volcanism in Schrödinger. Many other transitional examples are found on the Moon, but I will skip these to go directly to what Spudis (1993) calls the "archetype" basin: Orientale.

This is the multiring Orientale Basin, on the Moon's west limb (Fig. 12), nearly 1,000 km wide and never seen in its entirety until this Lunar Orbiter view was obtained. The Orientale Basin is the youngest and best-preserved multiring basin on the Moon, exhibiting structure largely concealed or destroyed in Mare Imbrium. Multiple rings begin to appear, on the Moon, when crater diameters reach a few hundred kilometers (Hörz and others, 1991). Their formation is, to say the least, not fully understood; an authoritative treatment of the subject is that of Spudis (1993). Spudis has suggested a composite mechanism for multiring basin excavation, in which the outer ring is produced by inward slumping, the next inner rings by structurally controlled slumping, and the innermost rings by acoustic fluidization (i.e., wave formation). These events are followed by

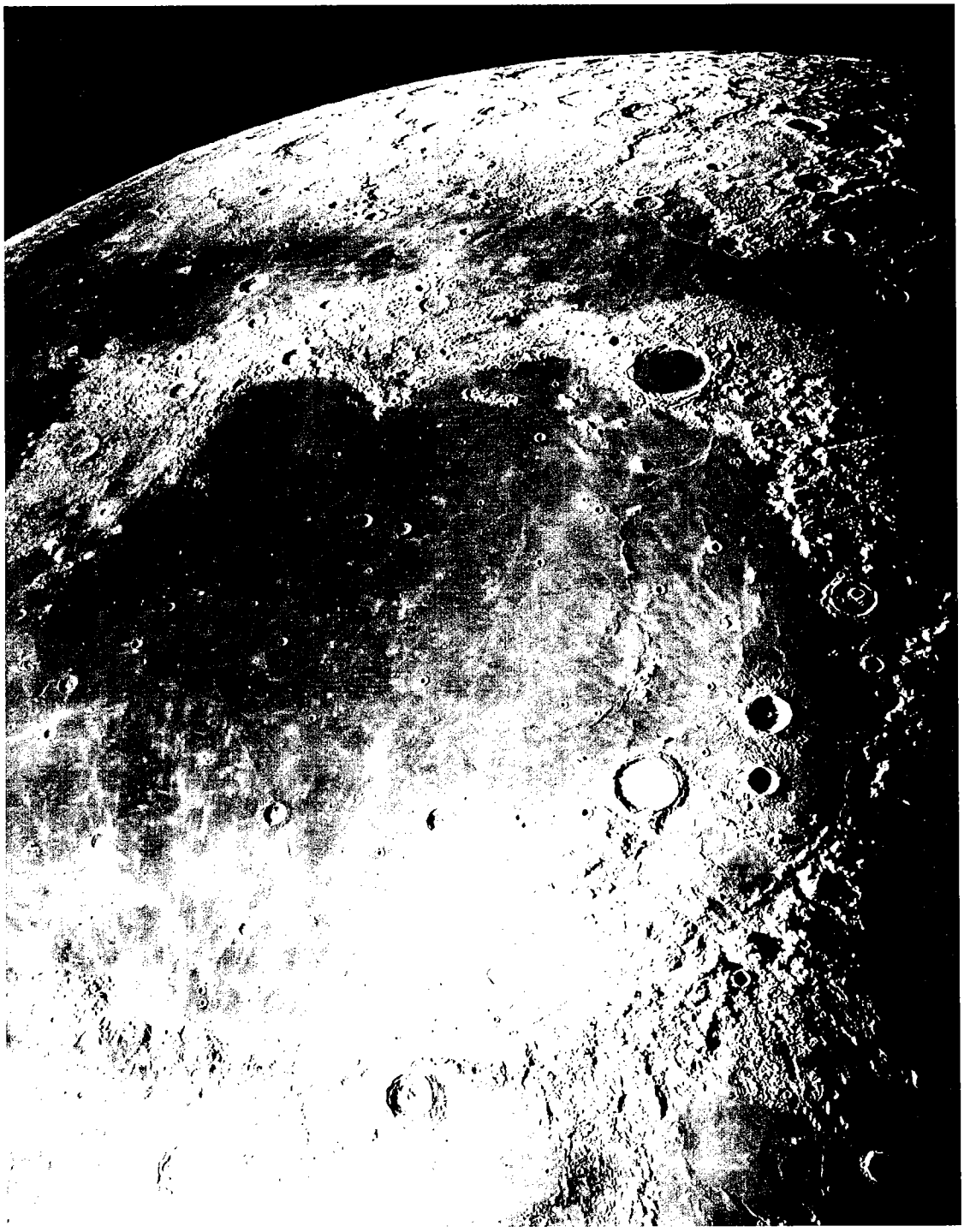

Figure 9. Mount Wilson 100-in. telescope view of Mare Imbrium, north at top. Crater Copernicus, 90 km wide, at bottom left.

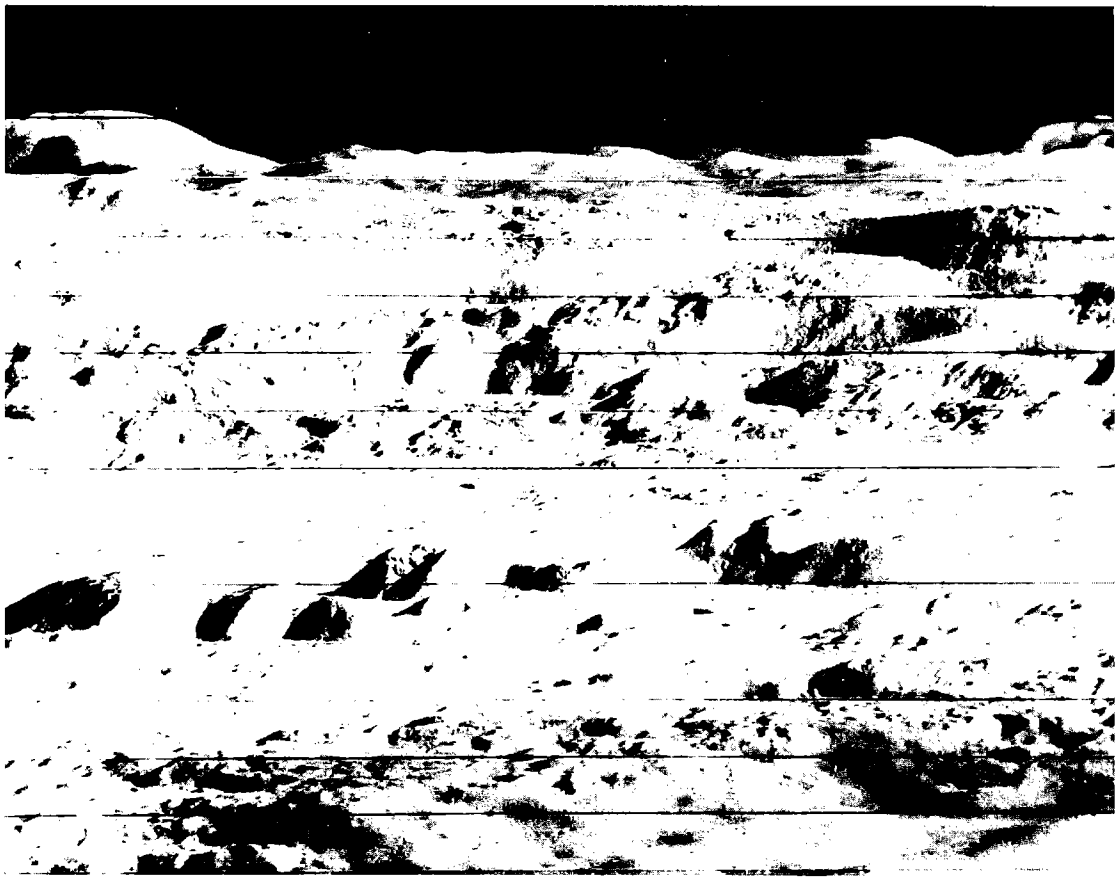

Figure 10. Lunar Orbiter oblique view to north of crater Copernicus.

isostatic uplift and repeated eruptions of mare basalts. Evidence for these events is well displayed in the Orientale Basin. The isostatic uplift is indicated by the well-known "mascons," or positive Bouguer anomalies (Muller and Sjogren, 1968).

There are many other multiring basins on the Moon, recently confirmed by laser altimetry from the Clementine mission (Spudis and others, 1994). The largest of these is the south pole Aitken Basin. It is 2,500 km wide and so old that its form has been almost completely obliterated by smaller, more recent craters, but the laser data demonstrate its reality. It is visible in a Galileo picture (Fig. 13) as a dark area southwest of Orientale. The extreme age of this basin suggests that the body that formed it was one of the planetesimals that formed the Moon, rather than an intruder from outside the Earth-Moon system. However, further investigation—in particular, surface missions that can return samples for radiometric dating—would be needed to confirm this speculation.

The review has by no means covered all the varieties in this impact-crater "museum." There are elliptical primary craters, chains of impact craters, floor-fractured craters, and others. However, having now presented the main varieties, I now turn to impact craters on other bodies, beginning with the Moon's near twin, Mercury.

MERCURIAN IMPACT CRATERS

Like the Moon, Mercury appears to be a primordial body whose internal evolution has long since stopped (Fig. 1). However, Mercury is unique in several ways, notably its high density, implying a very large iron core. Bruce Murray has in various talks aptly characterized this planet as like the Moon on the outside, but like the Earth on the inside. A Mariner 10 view (Fig. 14) illustrates this; an uninformed viewer could easily mistake Mercury for the Moon, from its marelike smooth plains and densely cratered highlands. However, there are differences in lunar and Mercurian impact craters, as discussed by Strom (1984).

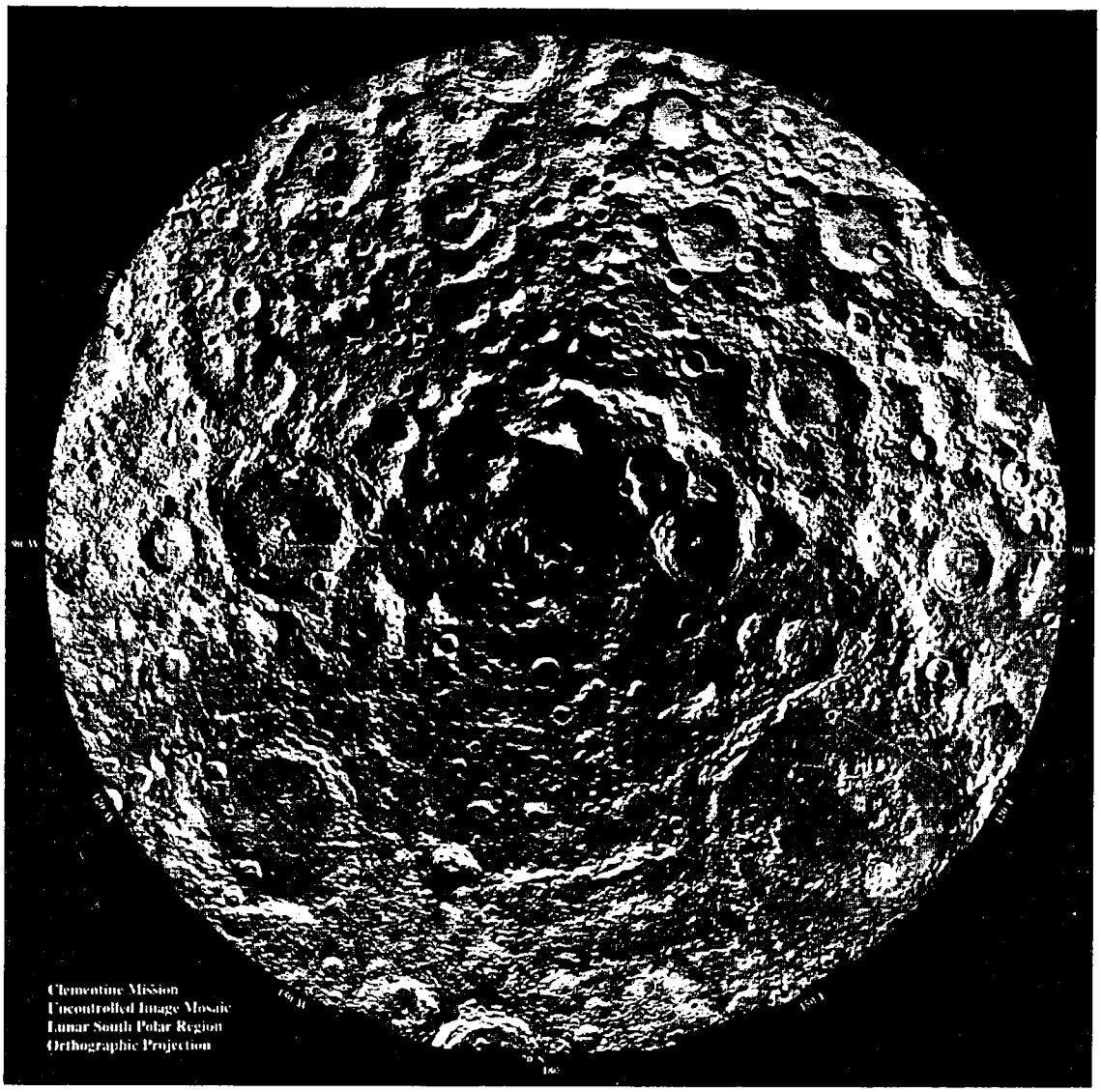

Figure 11. Clementine mosaic of about 1,500 ultraviolet and visual (750 nm band) images of the south polar region of the Moon. Crater Schrödinger, 320 km diameter, at lower right.

The main differences involve the ejecta deposits. First, for a given crater diameter, the continuous ejecta blanket on Mercury is only about one-third that for a comparable lunar crater. This is clearly the result of Mercury's stronger gravity field, about twice that of the Moon, which reduces the range of impact ejecta. Like the Moon, Mercury has no sensible atmosphere, so gravity governs ejecta range, if other factors are equal. Similarly, the secondary craters formed during Mercurian cratering events tend to be more concentrated closer to the source primary crater. Furthermore, the Mercurian secondary craters are generally deeper and better preserved than comparable lunar secondaries, also the presumed effect of the stronger gravity field.

Craters on Mercury show changes in morphology with diameter comparable to those on the Moon. The transition from simple to complex craters, defined as for lunar craters, occurs at about the same size range, suggesting that it is governed primarily by structure of the target rock rather than by gravity. However, details of crater structure on Mercury and the Moon differ. A study by Cintala and others (1977) showed that the population of features such as terraces in the lunar maria

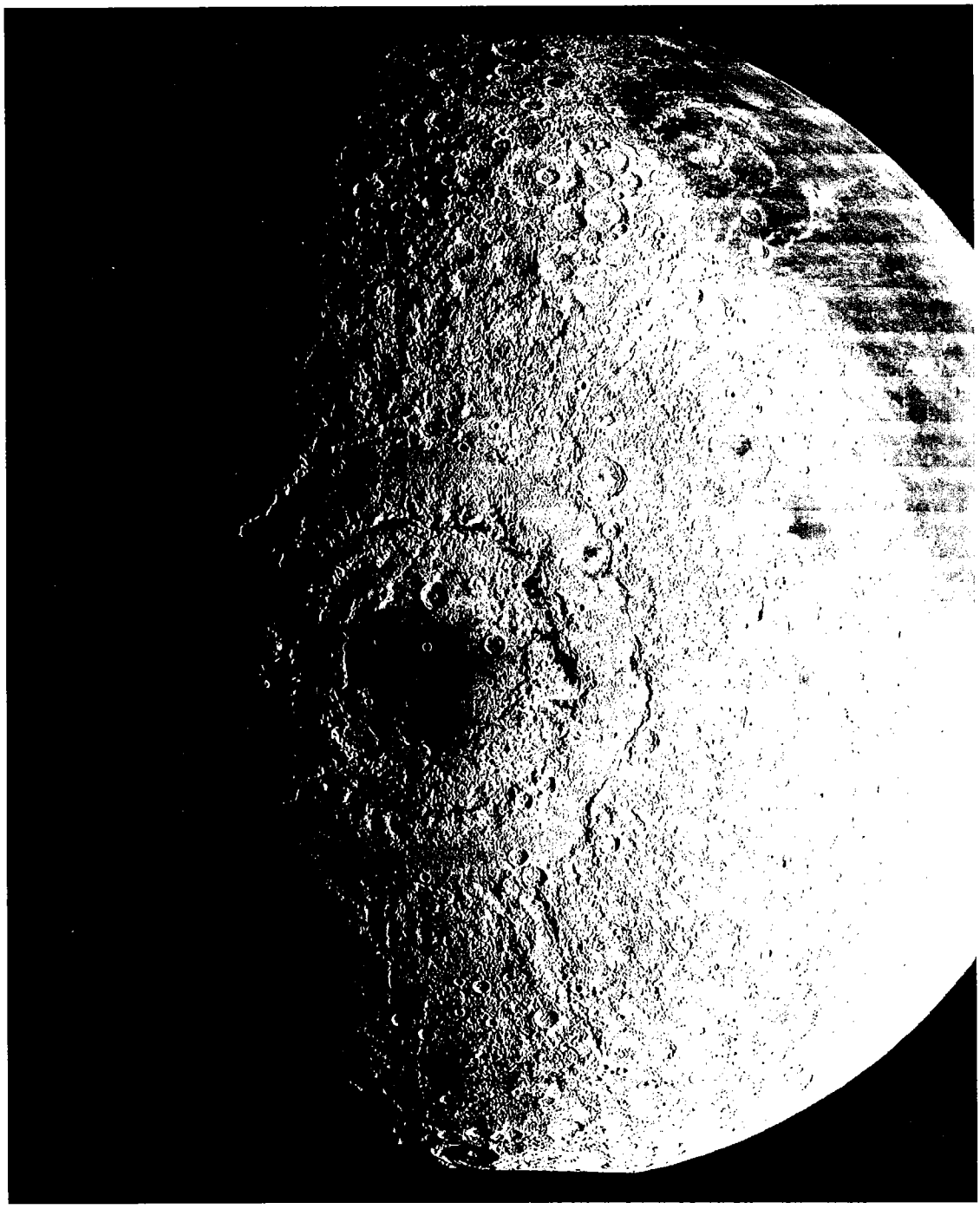

Figure 12. Lunar Orbiter picture of Orientale Basin. North at top. Earthside to right.

and the Mercurian smooth plains is similar. The maria are known to consist of layered lava flows, suggesting that the Mercurian smooth plains similarly consist of such flows.

Mercury has a population of multiring basins (Fig. 15) similar to that of the Moon. Mercury is of course an independent planet, and the existence of multiring basins on it implies that these basins are part of normal planetary accretion. This finding may have implications for the origin and early

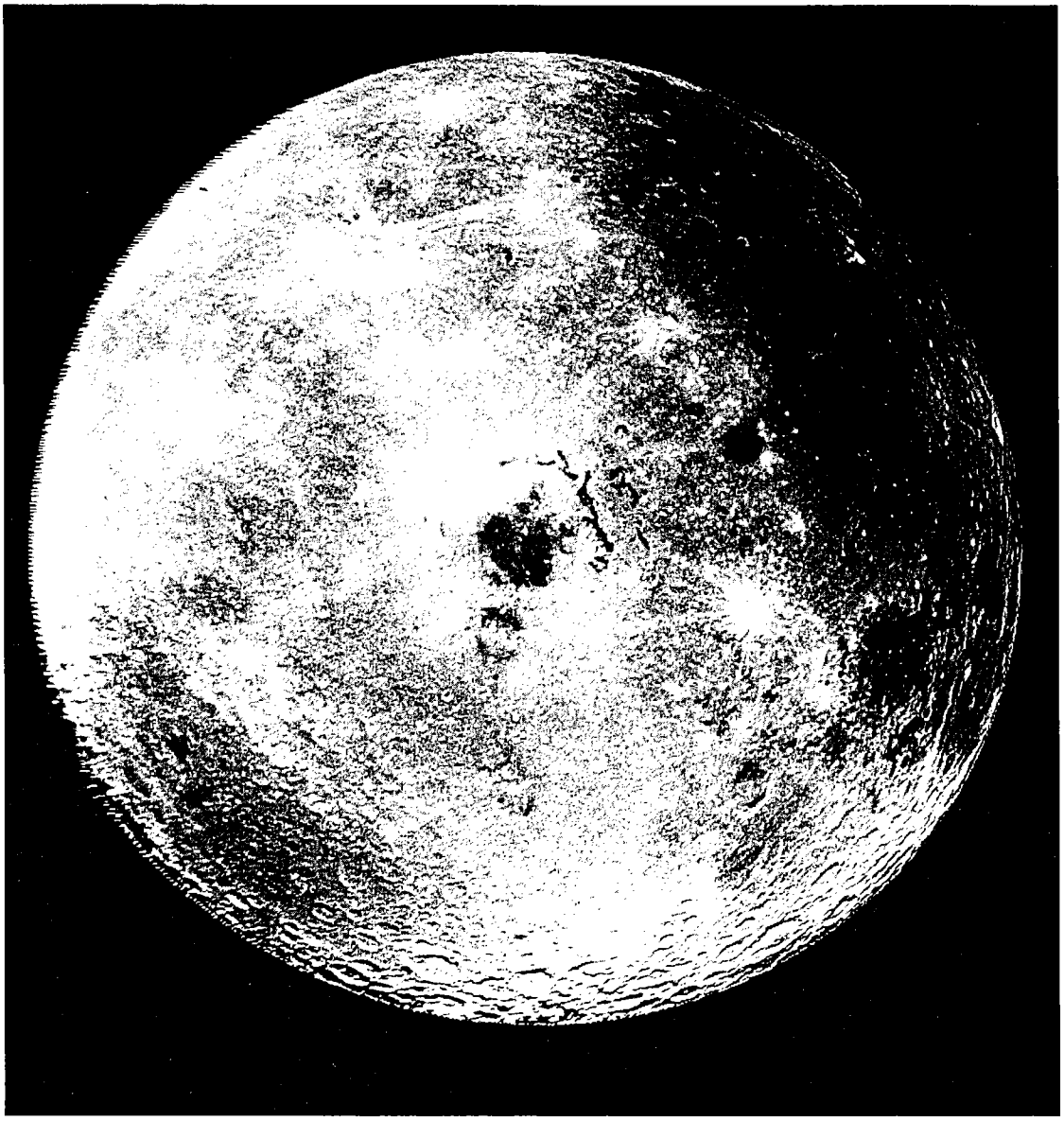

Figure 13. Galileo picture of Orientale Basin, with high Sun angle emphasizing albedo variations and mare basalts. Earthside to right.

evolution of the Moon. A unique process for the formation of the Moon, such as a giant impact in the currently favored theory (Melosh, 1992), would lead one to expect differences in the accretion process. The Mercurian highlands are not saturated with craters like those of the Moon, but the general population of craters and multiring basins is similar. Given the still-unresolved question of how the Moon was formed, this problem might be worth approaching by comparisons of the Moon with Mercury.

MARTIAN IMPACT CRATERS

Following the sequence of crustal evolution shown in Figure 1, I now examine impact craters on Mars. Mars is a transitional planet in several ways, bridging the gap between clearly primordial bodies such as the Moon and Mercury and the highly evolved Venus and Earth. Mars has a significant if unbreathable atmosphere and has clearly had a significant hydrosphere at one time. In terms of crustal evolution, it appears to have

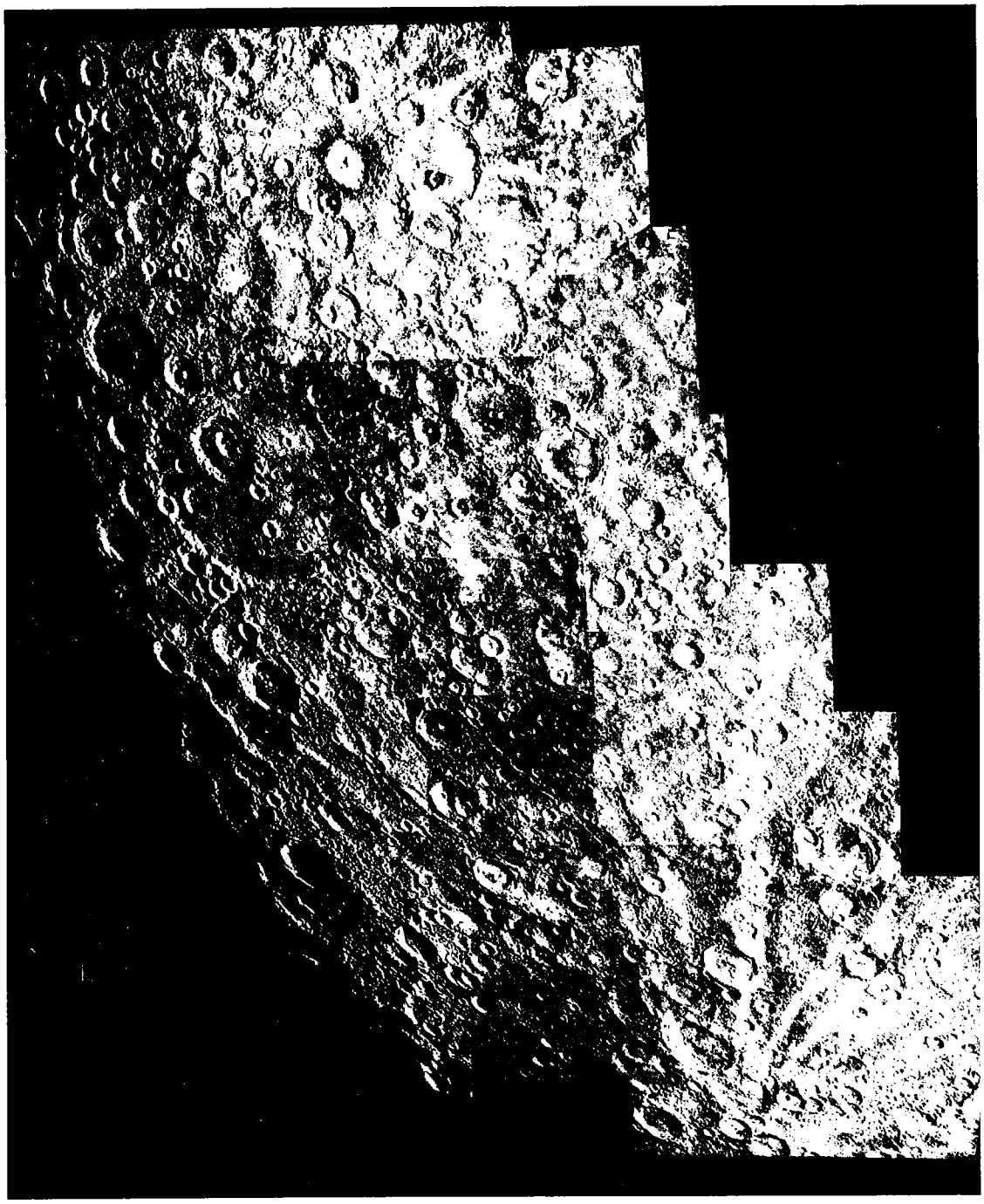

Figure 14. Mariner 10 picture of Mercury highlands, showing similarity with lunar highlands.

entered the stage of true, internally caused tectonism; features such as the Valles Marineris represent, perhaps, incipient fragmentation of a "one-plate planet" as J. Head has termed it in several presentations. Because of its processes of tectonism, volcanism, erosion, and deposition, Mars combines many geologic features of the Earth with those of the Moon.

The geomorphology of Mars is in fact extraordinarily complex (Fig. 16); the landforms are a var-

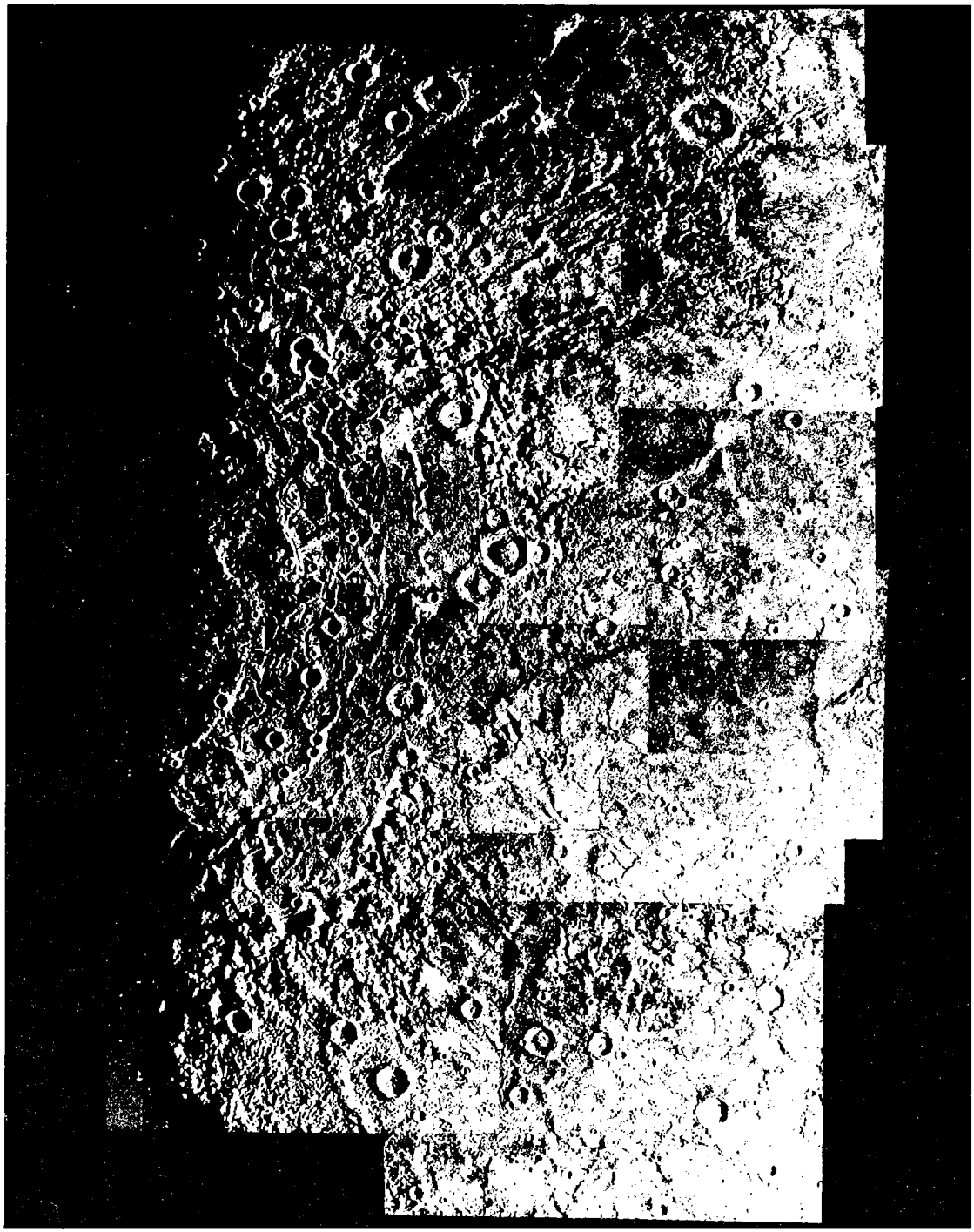

Figure 15. Mariner 10 mosaic of Caloris Basin, Mercury; 1,300 km diameter (cf. Orientale Basin, Fig. 12).

ied array of fluvial, aeolian, tectonic, volcanic, and perhaps glacial features on which are superimposed a dense array of randomly placed impact craters (Carr, 1981). These craters are in turn generally modified by erosion and deposition. Nevertheless, the pristine examples seen on the Moon and Mercury have counterparts on Mars.

The simple to complex transition in crater form takes place in the 5- to 10-km-diameter range on Mars, compared to about 20 km on the Moon (Pike

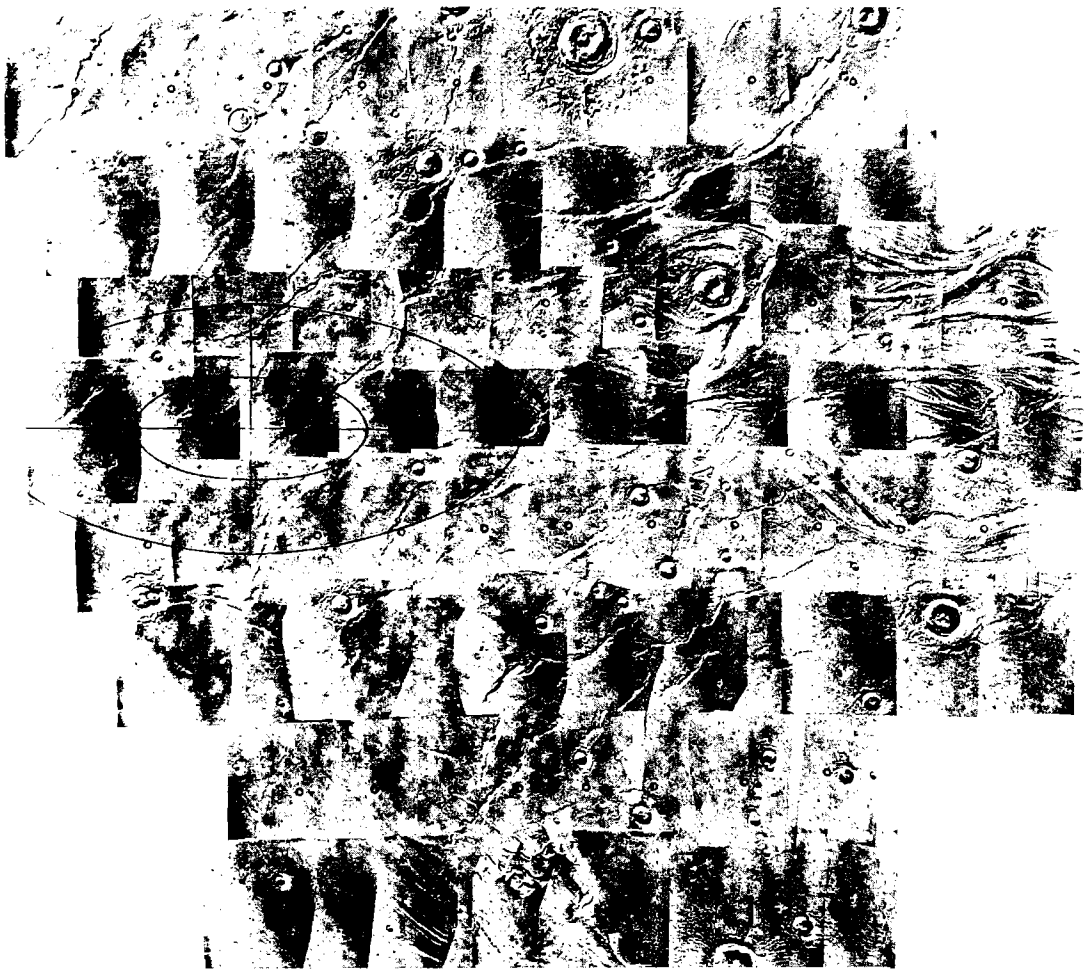

Figure 16. Viking Orbiter mosaic of Viking 1 landing-site region in Chryse Planitia on Mars. North at top; area about 240 km wide. Erosion patterns indicate flow from left to right. Note lobate ejecta around craters.

and Arthur, 1979; Carr, 1981), and Martian craters are proportionately shallower than those on the Moon. The size vs. frequency distribution curves for Mars have complex slopes (Carr, 1981), a phenomenon still not understood but evidently resulting from various erosional, depositional, and volcanic processes that obliterate craters.

The most characteristic features of Martian impact craters are shown in Figure 16, a Viking Orbiter view of the Viking 1 landing site in Chryse Planitia. Geology of this site has been described by Greeley and others (1977). In brief, it is a low-lying plains region that has been scoured by floods from the adjacent, higher, cratered terrain. Chryse Planitia is fundamentally similar to the lunar maria, as indicated by the low crater density, wrinkle ridges, and chemistry of the landing site. The role of running water is obvious, and the geomorphology resembles that of the Channeled Scablands of Washington State. The impact craters are notable for their distinctive ejecta patterns, which gave rise to the informal term "splosh craters" or "fluidized ejecta craters" (Carr, 1981). The characteristic lobate patterns imply more-fluid ejecta than corresponding lunar craters, which could result from ice or water in the ejecta or the effects of the Martian atmosphere. Such patterns occur only around large craters, perhaps reflecting the depth of ground water (Boyce, 1979). The existence of ground water on Mars is supported by the many slump features and chaotic terrain elsewhere.

Another type of crater more common though not unique to Mars is the elliptical primary impact variety (Fig. 17). There are a few such craters on the Moon, but Schultz and Lutz-Garihan (1982) have catalogued >170 elliptical craters >3 km wide

Figure 17. Viking Orbiter view of an elliptical impact crater (containing a younger volcano) and its lobate ejecta blanket on the north flank of the volcano Ceraunius Tholus.

on Mars. Their primary, high-velocity origin is indicated by the elongated central ridge and prominent ejecta blankets, quite different from the low-velocity secondary craters seen on the Moon. The example shown incidentally illustrates the complexity of Martian geology; this elliptical crater was formed on the flank of an apparently older volcano, Ceraunius Tholus, but a younger volcano

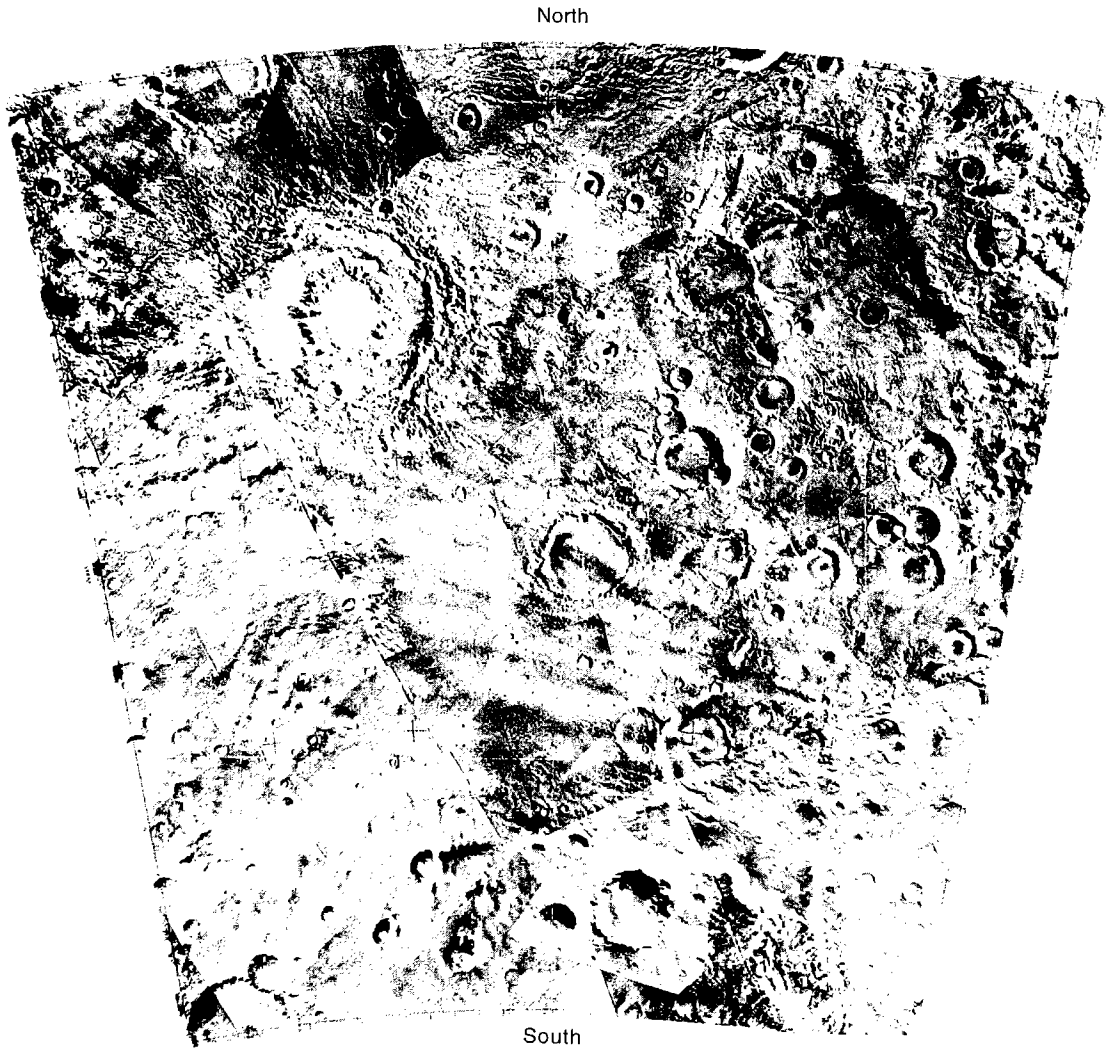

Figure 18. Viking Orbiter mosaic of area centered on lat 55°S, long 75°W, with 250-km-wide double-ring crater.

evidently erupted inside it later. The reason for the relative abundance of elliptical craters on Mars is not known, but Schultz and Lutz-Garihan (1982) suggested that they may have been formed by the infall of lost satellites.

The class of the largest impact craters, multiring basins, is now recognized on Mars. Schultz and Frey (1990) have catalogued 30 multiring basins, but this has been a difficult task in photogeology because of the pervasive effects of postimpact volcanism, erosion, and deposition. Some examples, such as the 250-km-diameter multiring crater Lowell (Fig. 18), are easily recognized. However, as shown in Figure 19, covering the northeast quadrant of the 1,850-km-diameter basin Argyre, fine structure of the rings has frequently been almost obliterated by surficial processes. There is no pristine Orientale Basin on Mars.

The geologic effects of basin-forming impacts on the Moon are fairly obvious: essentially they caused localization of later basaltic volcanism. However, Mars is demonstrably a more evolved and volatile-rich planet, and large impactors may have had correspondingly greater secondary effects. The Tharsis volcanic complex, for example, may have been localized by an early impact basin (Schultz and Frey, 1990), a more evolved magmatic process than the lava flows of the lunar maria. This interesting speculation tends to support the proposal of Grieve (1980) that the first continental nuclei on Earth were impact stimulated, although the reality of these "nuclei" is controversial (Lowman, 1989). An even more funda-

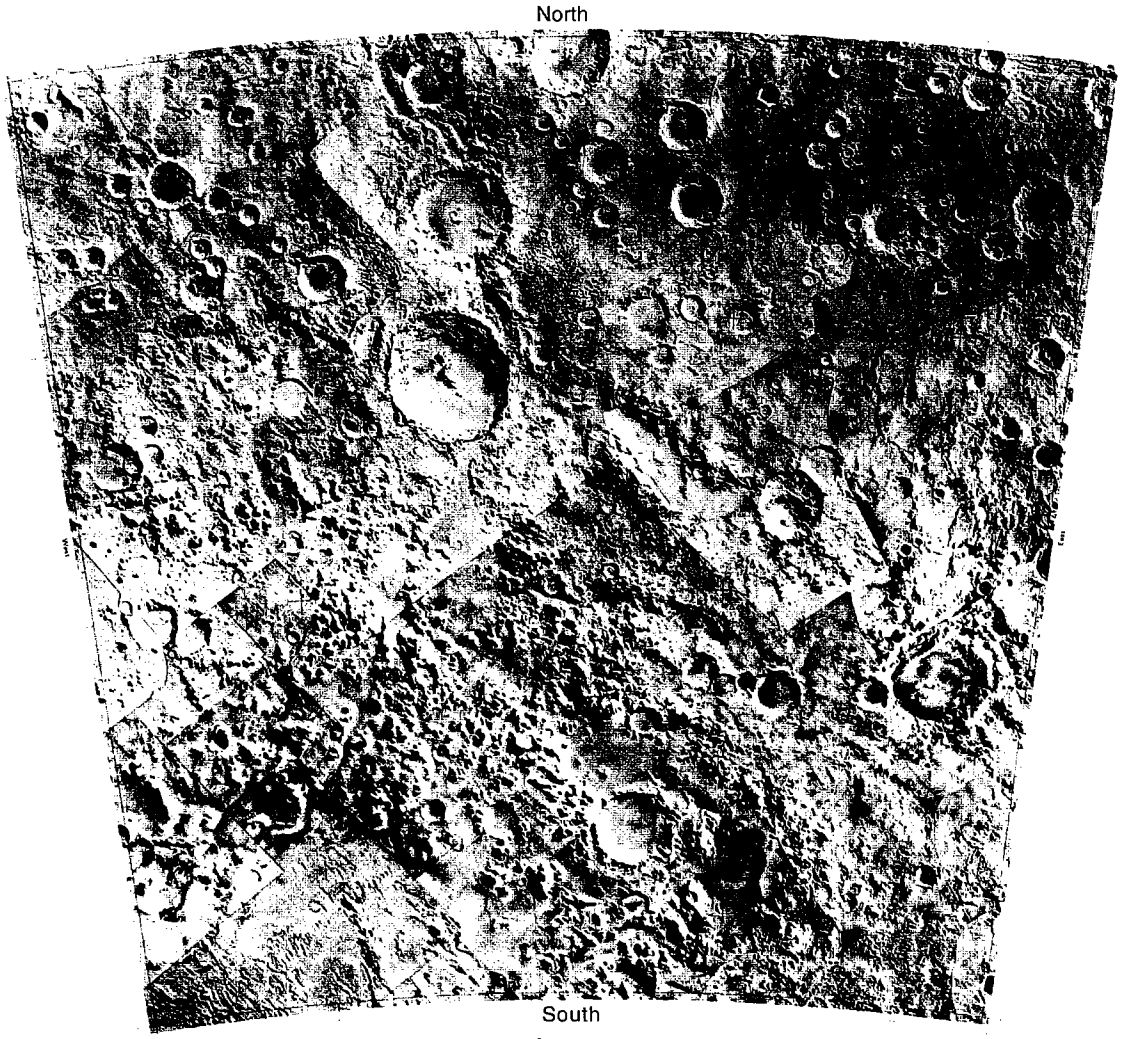

Figure 19. Viking Orbiter mosaic of area centered on lat 40°S, long 35°W, showing outer rim of Argyre Basin. Bottom of area about 900 km wide.

mental result of basin-forming impacts on Mars may have been the crustal dichotomy (Schultz and Frey, 1990) between the low-lying basaltic plains of the northern hemisphere and the higher cratered terrain to the south. This is apparently analogous to the mare vs. highlands topography of the Moon; however, the maria are relatively thin lava flows overlying highland crust, and the lunar "dichotomy" may thus be more superficial than that of Mars.

VENUSIAN IMPACT CRATERS

Venus is commonly referred to as Earth's "sister planet," being close to it in size and mass. Its geology was completely unknown until Earth-based and especially Venusian orbital radar surveys could be carried out. The most recent of these, by the Magellan spacecraft in the 1990s, covered almost the entire planet with high-resolution imagery, revealing a highly evolved and probably active planet. Despite Venus's continuing planetary evolution, well over 800 impact craters have been described on the 89% of the surface covered through the early part of the Magellan mission (Schaber and others, 1992). For comparison, roughly 130 impact structures (many no longer bearing topographic craters) are currently known on Earth (Grieve, 1991).

The surface environment of Venus must be taken into account to understand the nature of its

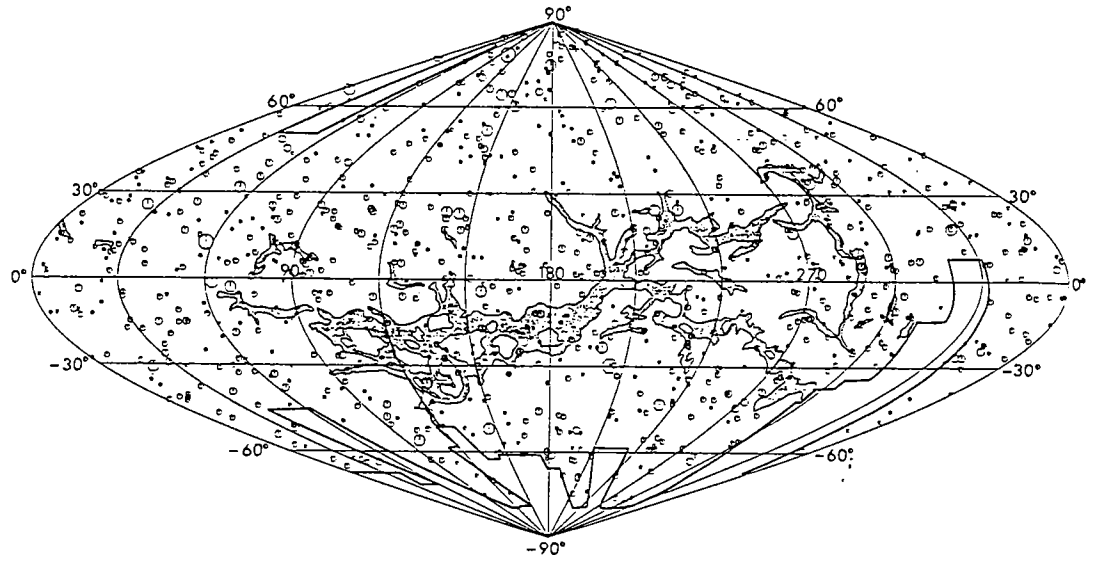

Figure 20. Map of Venus, sinusoidal equal-area projection, showing 842 impact craters, observed on 89% of surface (from Schaber and others, 1992).

impact craters. Most important is its enormously dense CO_2 atmosphere, with surface pressures of about 100 bars. The greenhouse effect of this atmosphere, coupled with the planet's closeness to the Sun, produces surface temperatures of >400 °C. The planet appears to have no significant water. There is abundant evidence of volcanism, confirmed by surface analyses made by Soviet gamma-ray spectroscopy from landed spacecraft, and comparable tectonism.

As summarized by Schaber and others (1992), the crater population appears to be uniformly distributed over the planet (Fig. 20). The size-frequency relationship for craters of >35 km diameter appears similar to that for other planets, but the abundance of craters is much lower. Craters smaller than 35 km are much less abundant than on other nonterrestrial bodies, which can be explained as the result of atmospheric filtering; small meteoroids do not penetrate the atmosphere. There are numerous diffuse "splotches," i.e., radar-visible features, thought to result from the air blast of meteoroids destroyed by the atmosphere. Large craters, >35 km in diameter, show about the same sequence of morphologies with increasing size as do those elsewhere (Fig. 21), up to multiring basins (Fig. 22). However, ejecta patterns of Venusian craters are frequently unique to that planet, in particular having radar-bright (presumably rough) outflows that in some cases extend several crater diameters (Fig. 23). These have been interpreted as impact ejecta with a great amount of gas and impact melt, forming flows resembling lava or nuees ardentes.

Some craters on Venus have clearly been partly flooded by lava or modified by tectonism, but there seem to be few transitional examples, most being pristine at the resolution of Magellan images. Schaber and others (1992) interpreted this finding as indicating major resurfacing by volcanism before about 0.5 Ga. This "catastrophic resurfacing model" has, however, been disputed by Phillips and others (1992), who have interpreted an "equilibrium resurfacing model" as more likely. The equilibrium resurfacing model implies that the resurfacing, i.e., the volcanism, is more randomly distributed in time and space.

This summary has touched on only the most conspicuous aspects of impact cratering on Venus, a topic whose study is only beginning. Interested readers are urged to consult the already-large literature on this controversial subject.

IMPACT CRATERS ON SMALL BODIES

As noted earlier, every known solid body in the solar system except the continually resurfaced Jovian satellite Io has impact craters or multiring basins. Dozens of satellites and even a few asteroids and comets have now been explored by spacecraft, so a full discussion of these bodies and their craters is impossible here. However, a few examples will be instructive.

Perhaps the most interesting craters are those on the icy satellites of the giant planets Jupiter, Saturn, Uranus, and Neptune. First revealed in detail by the decades-long Voyager missions—one

Figure 21. Magellan mosaic of Lavinia region of Venus, showing three impact craters with diameters ranging from 37 to 50 km. Bright tones indicate rough terrain, here formed by ejecta blankets.

of the great explorations of all time—these satellites have proven to be strange beyond imagining in terms of terrestrial planet geology. Almost all are essentially small planets made of water ice, rather than the familiar silicate minerals, although their mean densities indicate that some have rocky cores. Their geology is remarkably varied. Some satellites, such as Callisto (Fig. 24) are clearly inactive and essentially primitive, judging from their saturation population of impact craters. Some, such as Ganymede (Fig. 25) are transitional, with complex tectonic features in the ice but with a dense crater population. The Saturnian satellite Enceladus (Fig. 26) has a surface most of whose area has been reworked by internal ice tectonism, but with some densely cratered areas. The Uranian satellite Miranda (Fig. 26) is partly covered by large ridged ovoids, or "coronae," of unknown but presumably internal origin (Smith and others, 1986), the remaining area being heavily cratered.

Perhaps the strangest (by silicate-planet standards) impact structures are those on Ganymede (Fig. 25). In addition to more or less normal impact craters and complex ridged terrain of apparent internal origin, there are large light-colored patches. These have been interpreted (Smith and others, 1979) as the traces of former impact craters, or "palimpsests," since largely removed by solid-state flowage of the Ganymede ice. The huge, concentric structure on Callisto (Fig. 24), named Valhalla, is thought to be the trace of a former multiring basin. Thus, the satellites of the outer planets bear the ice analogues of the family of impact structures now familiar from the terrestrial planets and the "crater museum," the Moon.

Figure 22. Magellan image of Cleopatra impact crater, 105 km diameter, on Maxwell Montes, lat 65.9°N, long 7°W.

SUMMARY

Impact craters were recognized on Earth in initially a very hesitant and speculative manner; they were treated as a kind of geologic freak. But in the last half of the century, and in particular since the beginning of interplanetary flight, craters are now known to be the single most common landform in the solar system. Many of them represent the final stages of planet and satellite formation, the tail-off of creation, so to speak. Once formed, impact craters are geologically valuable as age indicators (with many caveats and assumptions) and as index marks against which tectonic deformation of a moon or planet can be gauged. They have localized true volcanism on silicate planets and possibly ice-water volcanism on ice satellites. Perhaps most important, their abundance and continuing formation reminds Earthlings that the universe is a violent place and that planets everywhere are probably subject to the bombardment seen in this solar system. One answer to the question "Where is everybody?" may be that other species and civilizations have short lifetimes in geologic terms, and that catastrophic impacts knock down communicative extraterrestrial communities before they can be contacted by their galactic neighbors.

REFERENCES CITED

Baldwin, R. B., 1949, The face of the Moon: University of Chicago Press, Chicago, 239 p.

Boyce, J. M., 1979, A method for measuring heat flow in the martian crust using impact crater morphology: U.S. National Aeronautics and Space Administration Technical Memorandum 80339, p. 114–118.

Carr, M. H., 1981, The surface of Mars: Yale University Press, New Haven, Connecticut, 232 p.

Cintala, M. J.; Wood, C. A., and Head, J. W., 1977, The effects of target characteristics on fresh crater morphology: Preliminary results for the Moon and Mercury: Proceedings of the 4th Lunar Science Conference, p. 3409–3412.

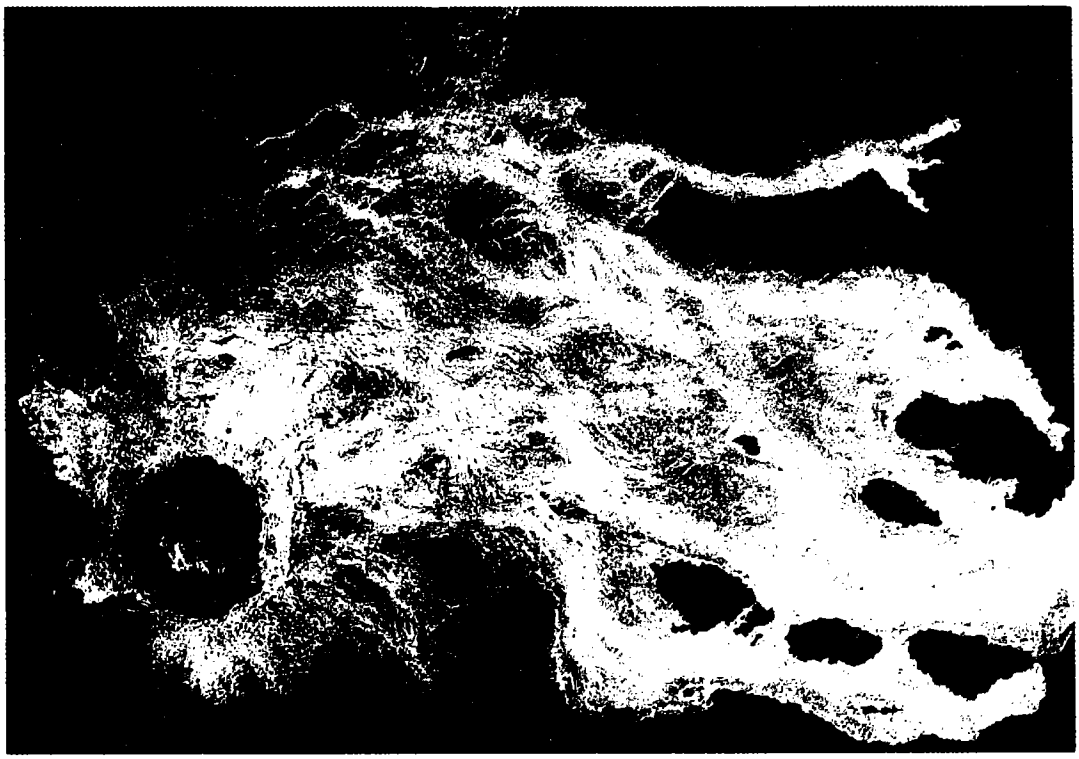

Figure 23. Magellan image of unnamed double-ring impact crater, 70 km diameter, at lat 4°S, long 156°E, with outflow deposits extending 370 km from rim (from Schaber and others, 1992).

Dietz, R. S., 1946, The meteoritic impact origin of the Moon's surface features: Journal of Geology, v. 54, p. 359–375.

Gilbert, G. K., 1893, The Moon's face, a study of the origin of its features: Philosophical Society of Washington Bulletin, v. 12, p. 241–292.

Greeley, R.; Theilig, E.; Guest, J. E.; Carr, M. H.; Masursky, H.; and Cutts, J. A., 1977, Geology of Chryse Planitia: Journal of Geophysical Research, v. 82, p. 4093–4109.

Green, J., 1971, Copernicus as a lunar caldera: Journal of Geophysical Research, v. 70, p. 5719–5732.

Grieve, R. A. F., 1980, Impact bombardment and its role in proto-continental growth on the early Earth: Precambrian Research, v. 10, p. 210–217.

_____ 1991, Terrestrial impact: The record in the rocks: Meteoritics, v. 26, p. 175–194.

Hammel, H. B., and others, 1995, HST imaging of atmospheric phenomena created by the impact of comet Shoemaker-Levy 9: Science, v. 267, p. 1288–1296.

Hörz, F.; Grieve, R. A. F.; Heiken, G.; Spudis, P.; and Binder, A., 1991, Lunar surface processes, *in* Heiken, G.; Vaniman, D.; and French, B. M. (eds.), Lunar sourcebook, a user's guide to the Moon: Cambridge University Press, Cambridge, p. 61–120.

Lowman, P. D., 1989, Comparative planetology and the origin of continental crust: Precambrian Research, v. 44, p. 171–195.

Melosh, H. J., 1992, Moon, origin and evolution, *in* Maran, S. P. (ed.), The astronomy and astrophysics encyclopedia: Van Nostrand Reinhold, New York, p. 456–458.

Muller, P. M.; and Sjogren, W. L., 1968, Mascons: lunar mass concentrations: Science, v. 161, p. 680–684.

Nininger, H. H., 1959, Out of the sky: an introduction to meteoritics: Dover Publications, New York, 336 p.

Oberbeck, V. R.; and Quaide, W. L., 1968, Estimated thickness of a fragmental surface layer of Oceanus Procellarum: Journal of Geophysical Research, v. 32, p. 4697–4715.

Phillips, R. J.; Raubertas, R. F.; Arvidson, R. E.; Sarkar, I. C.; Herrick, R. R.; Izenberg, N.; and Grimm, R. E., 1992, Impact craters and Venus resurfacing history: Journal of Geophysical Research, v. 97, p. 15,923–15,948.

Pike, R. J.; and Arthur, D. W. G., 1979, Simple to complex impact craters: The transition on Mars: National Aeronautics and Space Administration Memo 80339, p. 132–134.

Ryder, Graham, 1994, Coincidence in time of the Imbrium basin impact and Apollo 15 KREEP volcanic flows: the case for impact-induced melting,

Figure 24. Voyager image of Jovian satellite Callisto (about the size of Mercury), with multiring impact basin Valhalla.

in Dressler, B. O.; Grieve, R. A. F.; and Sharpton, V. L. (eds.), Large meteorite impacts and planetary evolution: Geological Society of America Special Paper 293, p. 11–18.

Schaber, G. G., and others, 1992, Geology and distribution of impact craters on Venus: what are they telling us?: Journal of Geophysical Research, v. 97, p. 13257–13301.

Schultz, P. H.; and Lutz-Garihan, A. B., 1982, Grazing impacts on Mars: a record of lost satellites: Journal of Geophysical Research, v. 87, supplement, p. A84–A96.

Schultz, R. A.; and Frey, H. V., 1990, A new survey of multi-ring basins on Mars: Journal of Geophysical Research, v. 95, p. 14,175–14,189.

Shoemaker, E. M.; and Hackman, R. J., 1962, Stratigraphic basis for a lunar time scale, *in* Kopal, Z.; and Mikhailov, Z. K. (eds.), The Moon; IAU Symposium 14: Academic Press, New York, p. 289–399.

Shoemaker, E. M.; Robinson, M. S.; and Eliason, E. M., 1994, The south pole region of the Moon as seen by Clementine: Science, v. 266, p. 1851–1854.

Smith, B. A., and others, 1979, The Galilean satellites and Jupiter; Voyager 2 imaging science results: Science, v. 206, p. 927–950.

_____ 1986, Voyager 2 in the Uranian system: imaging science results: Science, v. 233, p. 43–64.

Spudis, P. D., 1993, The geology of multi-ring impact basins: Cambridge University Press, New York, 263 p.

Spudis, P. D.; Reisse, R. A.; and Gillis, J. G., 1994,

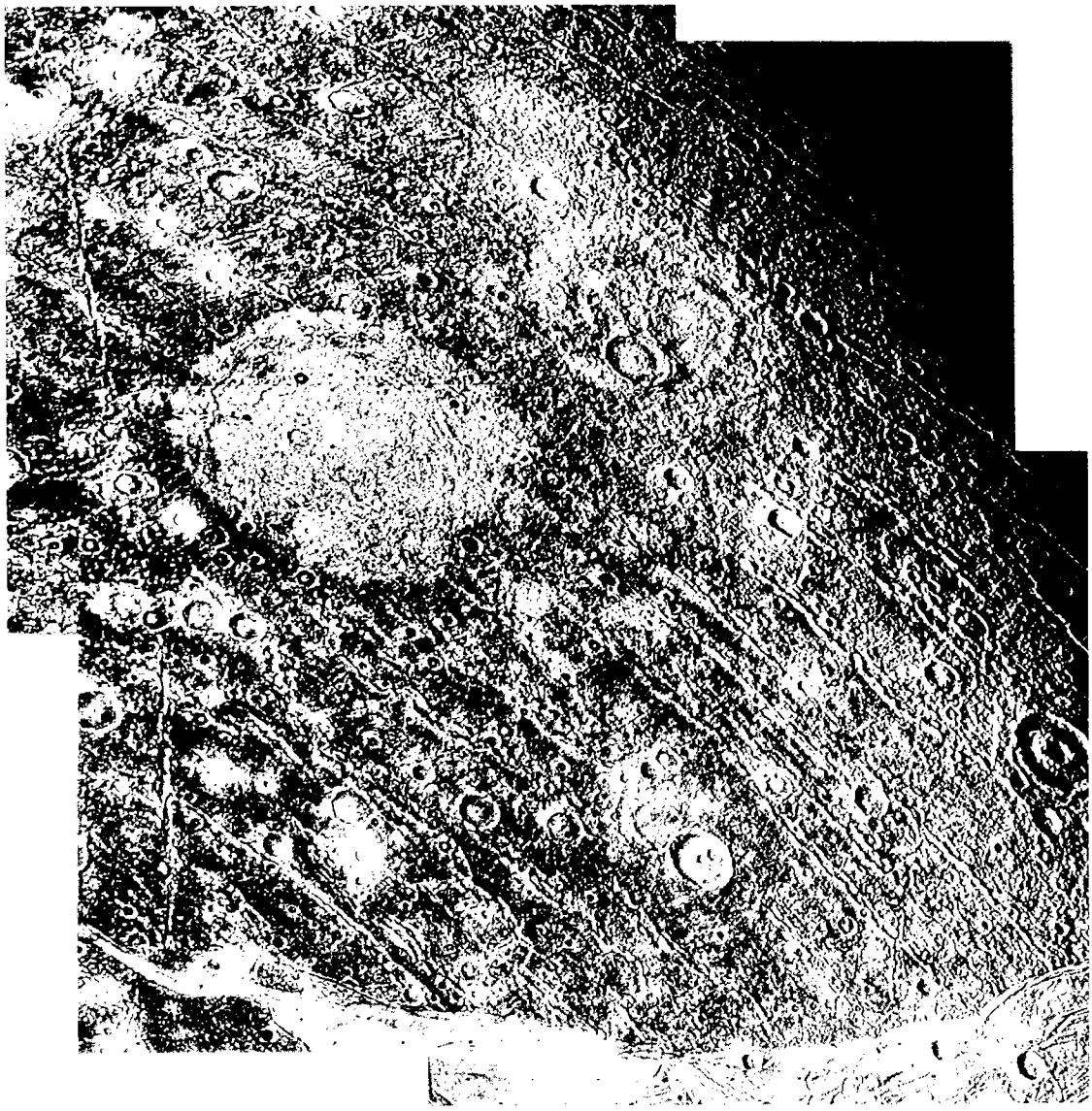

Figure 25. Voyager image of Jovian satellite Ganymede, showing reworked impact craters (palimpsest) and ridges, all in the satellite's icy outer layer.

Ancient multiring basins on the Moon revealed by Clementine laser altimetry: Science, v. 266, p. 1848–1851.

Strom, R. G., 1984, Mercury, *in* Carr, M. H.; and others (eds.), The geology of the terrestrial planets: National Aeronautics and Space Administration, Washington, D.C., NASA SP-469, p. 13–55.

Taylor, S. R., 1992, Solar system evolution: Cambridge University Press, New York, 307 p.

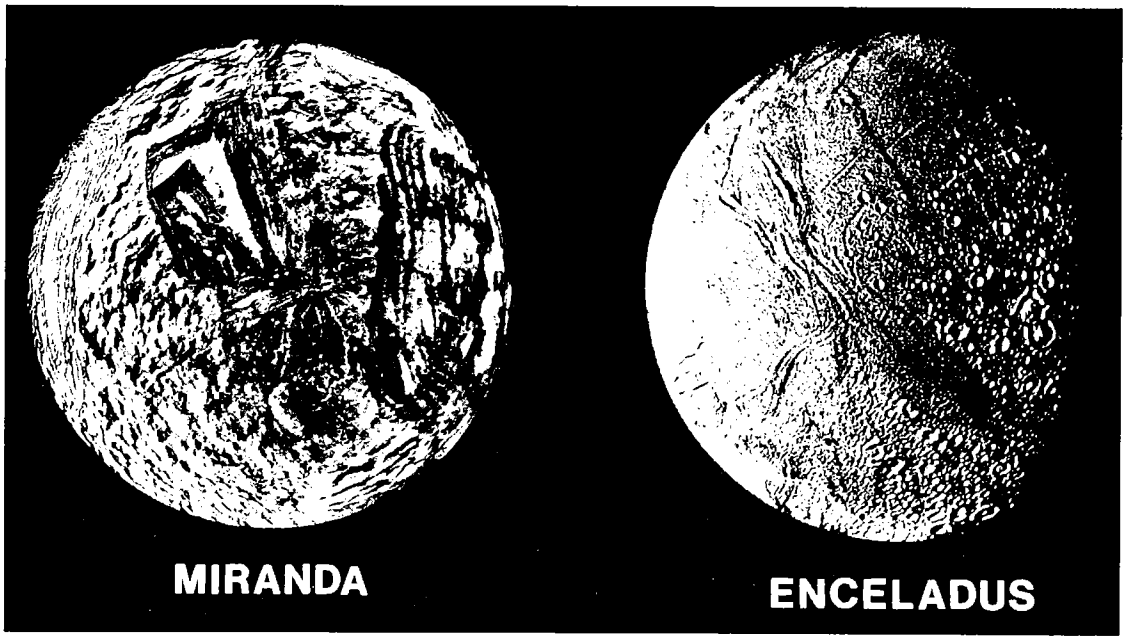

Figure 26. Voyager image of Uranian satellite Miranda and Saturnian satellite Enceladus.

Prospecting for Buried Impact Structures Using Landsat and Radar Imagery

P. Jan Cannon
Planetary Data
Tecumseh, Oklahoma

ABSTRACT.—The interpretation of remote-sensing data requires the skillful integration of the following elements: tone, texture, pattern, shape, location, relative size, and feature orientation. Often shape and tone are used without due consideration of the other elements. Shape determination should involve a consideration of the absolute geometry of the feature—not just a statement of generality, such as "round." Tone refers to intensity and chroma of the electromagnetic radiation associated with the feature. Texture is the homogeneity of tonal zones. Pattern is the spatial interface between different textures. Location provides information on regional processes. For example, areas of karst features contain numerous solution-related features. Rare is the isolated, singular volcanic feature. Most geomorphic features are restricted to a range of shapes related to the materials and processes of a certain planet. Volcanic calderas on Earth are restricted by location and size, occurring only in recognized volcanic terrains. Alignment of fractures, stream segments, sinkholes, and other features indicates asymmetry of processes. Only primary impact structures occur as random features on planetary surfaces.

Circular features are common on most planets. The above elements of interpretation can be used to identify the origins of circular features. Primary impact structures can range in size from pits a few meters across to multiring basins >800 km in diameter. Close examination of the geometry of primary impact features reveals that they often exhibit a polygonal shape related to the preexisting regional structure. The forces of impact superimpose radial and concentric fractures onto the preexisting regional structure. Associated fractures and size-related features such as central uplift zones, interior rings, and slump blocks are good diagnostic characteristics of primary impact structures.

The above physical features can be located on remote-sensing data that specifically enhance such characteristics regardless of their subtleness. The bands of Landsat imagery (both Multi-Spectral Scanner [MS] and Thematic Mapper [TM] data) acquired in the near-infrared at low angles of illumination are excellent tools to use in a search for primary impact structures. Radar imagery acquired from aircraft and space platforms specifically enhances subtle physical features. The patterns of the physical features also are propagated through the overburden by differential compaction and gravity-tide stressing of the crust. Buried primary impact craters usually show the effects of interior subsidence, which result in a topographic depression.

P. Jan Cannon, Planetary Data, 302 East Locust,
Tecumseh, OK 74873.

Cannon, P. J., 1997, Prospecting for buried impact structures using Landsat and radar imagery, *in* Johnson, K. S.; and Campbell, J. A. (eds.), Ames structure in northwest Oklahoma and similar features: origin and petroleum production (1995 symposium): Oklahoma Geological Survey Circular 100, p. 82.

Global Hydrocarbon Potential of Impact Structures

David B. Buthman
Unocal
Sugar Land, Texas

ABSTRACT.—Astroblemes, or ancient weathered impact craters, have produced hydrocarbons in North America at Red Wing Creek field, North Dakota; Viewfield field, Saskatchewan; Barrow gas field in the Avak structure, Alaska, Calvin-28 field, Michigan; and, discovered in 1991, the Ames astrobleme, Oklahoma, with estimated recoverable reserves approaching 50 million barrels of oil (MMBO) plus gas. Numerous oil and gas fields throughout North America produce from reservoirs and traps of astrobleme origin, and it is hypothesized that dozens more, if not hundreds, of already productive structures have yet to be recognized as having an astrobleme origin. Cumulative production from astroblemes is estimated to have already exceeded 1 billion barrels of oil.

Impact craters in the universe range from planet- or moon-annihilating monsters, to Copernican-scale basins, to craters a few miles to several dozen miles in diameter that may be prospected for hydrocarbons. Copernican-scale craters comprise the basins filled with flood basalt on the Moon, whereas on the Earth, such craters are filled with sedimentary deposits and evolve into what are recognized as sedimentary basins—features that may contain oil and gas deposits.

A contrarian theory is presented that challenges the prevailing paradigm that meteorite impacts are random, unpredictable events in time and space. A plot of the ages and locations of the meteorite-impact craters in North America shows that the majority of those discovered thus far lie within a northeast-trending belt extending from west Texas to Quebec. Plotting these impact craters and contouring their ages result in an isotime contour map that illustrates this trend. This impact-crater trend started forming in the Ordovician, about 450 Ma, and culminated about 300 Ma ago, during the Early Pennsylvanian. The plate-tectonics reconstruction of the contour map illustrates how the Pennsylvanian paleoequator once paralleled this meteorite-impact belt. One possible explanation for the existence of this meteorite-impact belt is that between the Ordovician and the Pennsylvanian Periods, a loosely indurated asteroid, comet, or primordial moon, in a decaying orbital trajectory around Earth, lofted fragmented masses toward the Earth over a time span of 150 m.y., leaving a swath of impact craters below. Hundreds, perhaps thousands, of significant impact craters will be found within this belt. A modern analogue to this Pennsylvanian meteorite-impact belt was the 1994 breakup of the Shoemaker-Levy 9 comet and the subsequent impact belt that formed across the face of the planet Jupiter.

It is hypothesized that other meteorite-impact belts, in addition to the Pennsylvanian trend, occur along different orbital trajectories during different ages of geologic history. For example, during the Cretaceous, a comet with an orbit antithetic to the galaxy's ecliptic lofted fragments toward the Earth in an orbit extending from the Gulf of Mexico to Barrow, Alaska, to offshore Japan. Undoubtedly, more meteorite belts will be found on Earth, many of which will have economic potential for their discoverers.

INTRODUCTION

The most common geologic structures in the solar system are craters formed by the hypervelocity impact of meteorites. The Moon, Mercury, Venus, Mars, the millions of asteroids, Encelades, Phobos, Deimos, Ariel, Uranus, Neptune, even Pluto—all exhibit abundant impact cratering. Through binoculars or a telescope one could, with enough perseverance, count 10,000 impact craters. After the landing on the Moon in 1969, it became evident that the Moon hosts hundreds of millions, perhaps billions, of impact craters.

David B. Buthman, Spirit Energy 76, 14141 SW Freeway, Sugar Land, TX 77478.

Buthman, D. B., 1997, Global hydrocarbon potential of impact structures, *in* Johnson, K. S.; and Campbell, J. A. (eds.), Ames structure in northwest Oklahoma and similar features: origin and petroleum production (1995 symposium): Oklahoma Geological Survey Circular 100, p. 83–99.

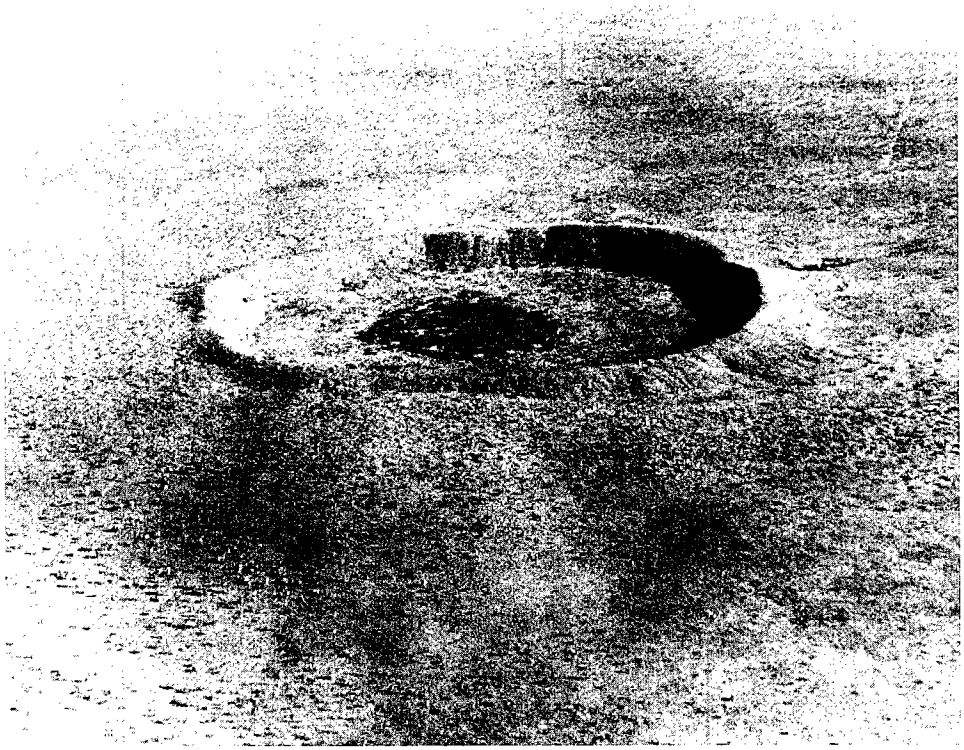

Figure 1. The 0.53-mi-diameter Wolf Creek Crater, Western Australia. South-looking, oblique aerial photograph of a well-preserved, 300,000-yr-old impact crater. (Courtesy of V. L. Sharpton, in "Terrestrial Impact Craters," Lunar and Planetary Institute slide set "S-IMPACT.")

On Earth, fresh terrestrial impact craters (Fig. 1) are relatively rare, numbering about two dozen. Moderately weathered impact craters—those that are still exposed at the surface—number in the hundreds. And weathered impact craters, or astroblemes, buried beneath hundreds and thousands of feet of sedimentary rock strata, undoubtedly number in the tens of thousands. These elusive, weathered, not-so-obvious craters have been relatively invisible until the resolution of studies of the Earth's crust was increased. With data from orbiting thematic mapping (TM) satellites, orbiting wide-beam radar, tens of millions of miles of reflection seismic data, billions of delicate gravity and magnetics measurements, a dataset of millions of boreholes probing the Earth's subsurface—these and many more technologies have provided a short list of tools with which to recognize the abundance (and simplicity) of astroblemes.

RECOGNITION OF IMPACT CRATERS

Mankind's greatest advances in the study of the formation of impact craters were born from the necessity of waging war. Bombs, like meteorites, leave craters; as the tools of war advanced, when bombs were placed in the noses of supersonic missiles, the bomb payloads traveled at speeds rivaling meteoritic hypervelocity just before they impacted their targets.

The U.S. Geological Survey studied more than 50 craters produced by the impact of missiles at the White Sands Missile Range, New Mexico, between 1964 and 1973 (Moore, 1976). Missiles traveling along oblique trajectories and having kinetic energies of 2.1×10^{14} to 81×10^{14} ergs resulted in the formation of impact craters measuring 6.6 to 33 ft across. Because the masses, velocities, and trajectories of the missiles was known (once unclassified by the Command at White Sands), important scaling factors could be deduced that could then be applied to the study of larger, extraterrestrial impact events.

The conclusions arrived at in Moore's (1976) study are (1) even when the missiles impacted at an oblique trajectory, the resulting craters were bilaterally symmetrical with respect to the plane of the missile trajectory, (2) ejecta were deposited downtrajectory and were absent uptrajectory, (3) secondary-impact craters were often produced by the primary-impact event, the nearest secondary craters containing blocks almost the size of the

primary craters themselves, whereas farther away, the fragments become progressively smaller. When the crater floors were excavated, mixed breccias, sheared and compressed target materials, overturned synclines beneath the downtrajectory rims, and, depending upon the velocity at impact, fragmented, powdered, even partly fused missile fragments were found.

In short, results of the White Sands missile experiments indicate that bilaterally symmetrical craters result from hypervelocity impact; simply put: Craters are circular.

THE MOST COMMON GEOLOGIC PHENOMENON IN THE UNIVERSE

The most common crustal structures on the terrestrial planets, asteroids, moons, and outer planets are impact craters. With the bare eye, one can see thousands of craters on the Moon. With binoculars or telescopes, one can see tens of thousands.

Impact craters are more common than plate tectonics, more common than volcanoes, more common than faults and salt diapirs and cratons and deserts and water. The Moon and Mercury are covered (Gault and others, 1975). Mars is covered. Millions of asteroids, Venus, and Pluto—the most striking, simple, and abundant geologic features on all their surfaces are impact craters.

This observation is so simple and obvious that it is perplexing that it was not obvious before.

Because human beings are not currently commuting to Mars or Pluto, it cannot be proved with utmost scientific rigor whether the circular, craterlike features observed on these planets are truly meteorite-impact craters. Elusive are the "smoking gun" evidences that define, irrefutably, an impact origin, such as the characteristic metamorphic minerals coesite and stishovite, diaplectic glass, fused feldspars, kinked micas, Widmanstätten and Neumann bands (herringbone and twinning structures, respectively, in iron meteorites), or cataclysmically disrupted strata. Breccias. Tektites. Concussion axes. Shatter cones. These things cannot be sampled on Pluto or Mars (not yet).

Today, it seems obvious that the craters on the Moon were formed by meteoritic impact. This is accepted as scientific truth. However, not long ago, eminent scientists and scholars argued with great vehemence about the origin of the craters on the Moon. One school argued that the craters were the result of lava extruding from continuously subsiding volcanic fissures in the lunar crust. The lava subsequently ponded and formed the maria of the Moon.

When the Apollo astronauts landed on the Moon in the late 1960s, the data they collected proved to everyone's satisfaction that indeed the craters, even the large Copernican-scale ones, were the result of hypervelocity impact events. Simply put, small meteorite impacts formed small craters, and big meteorite impacts formed very large craters.

On Earth, most impact craters on the continents and their shelves will eventually be buried under thousands of feet of sedimentary rock. Finding a shatter cone, a glass shard, or coesite or stishovite thousands of feet underground will, in most cases, prove prohibitively expensive. Drilling into a suspected astrobleme for economic reasons, however, in the search for oil and gas for example, is tolerable, even encouraged. Millions of barrels of crude oil and gas have been produced from deeply buried astroblemes. But drilling wells to prove irrefutably the origin of a circular structure, to spend millions of dollars to locate mineralogical and kinematic smoking-gun evidence, is in most cases, impractical unless economically rewarded.

For purposes of this study—specifically impact craters on Earth but also including analogue impact craters within the solar system—Pareto's 80/20 rule will be employed. Pareto's 80/20 rule states that roughly 20% of tasks account for 80% of the desired results. Pareto's rule suggests that most time is spent on low-payout projects, and very little is spent on big payout projects. It is typical to become bogged down in details, distracted by noise, and crippled in the processes of criticism and then to forget what it is that truly needs to be accomplished.

If a geologic structure is bilaterally symmetrical, with morphologic elements that mimic those of all other meteorite-impact craters, then for this study, unless other conflicting data exists, it has been considered an impact crater. Evidence such as impact metamorphism may be lacking. Petrophysical evidence may be lacking. In fact, the sole evidence in many cases for such a structure's being an impact crater has been its geometry: It looks like an impact crater, therefore it is an impact crater. Pareto's rule says that 20% of the time it may not be an impact crater, but why waste the remaining 80% of the time bogged down on the details that might yield only 20% of the desired results?

IMPACT-CRATER SIZE DISTRIBUTIONS

The largest impact "craters" in the universe result from impacts that catastrophically rifted or annihilated the target object (Fig. 2). The next generation of sizes are Copernican-scale craters—those measuring hundreds of miles in diameter (Fig. 3). On the Moon, these Copernican-scale craters have been filled with flood basalts, whereas on Earth, as well as on Mars, similar-scale impact craters have imposed the architecture for subsequent development of the major, and minor, basins of deposition.

The last size class of impact craters are those with the most economic potential. They range in size from tens of feet to tens of miles in diameter.

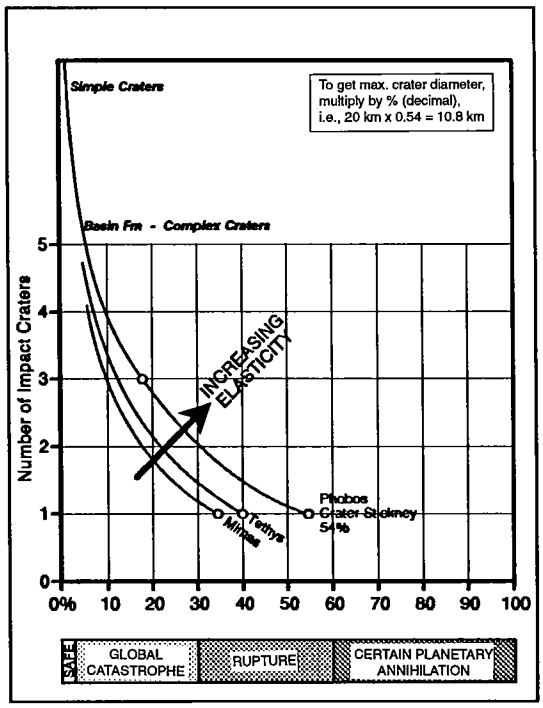

Figure 2. Planetary annihilation curves: the largest impactors annihilate planets and moons. X-axis is crater size relative to host diameter, in percent.

On the Moon, the median size of this class of craters is 8 mi in diameter, and on the Earth it is 6.2 mi (Fig. 4).

THE ABUNDANCE OF IMPACT CRATERS

Reported Astroblemes on Earth

It is peculiar that humans can gaze pie-eyed at the Moon, then turn around and deny the possibility that impact craters exist on the Earth. In 1936, scientific literature reported 6 craters on Earth (Bucher, 1936); in 1982, 103 impact craters were reported on Earth (Grieve, 1982). Today, including Unocal's proprietary inventory of an additional 200 possible terrestrial impact craters, predominantly in North America, as well as 50 probable hydroblemes—impact crater forms on the ocean floors—throughout the world, the crater count on Earth now exceeds 300 (Table 1). But even 300 impact craters is too few. Even though fewer than 300 probable impact sites have been identified on Earth, data from the solar system suggests that there are thousands of terrestrial astroblemes and hydroblemes left to be found.

In the equatorial region of Mars, in an area the size of the state of Texas (about 360,000 mi^2), there are between 25 and 200 impact craters measuring 2.4 to 6.0 mi in diameter (Condit, 1977).

In Fennoscandia (Sweden, Norway, Finland, Baltic Russia), researchers have recently reported 62 significant impact-crater forms, all in an area measuring 926,489 mi^2 (Henkel and Pesonen, 1992). Because 50% of the area is under water, the 62 crater-form structures should be distributed over 50% of the total area, or 926,489 × 50%, or 67 crater-form structures over 463,245 mi^2: that represents one significant impact crater per 7,472 mi^2.

In Oklahoma, 37 crater-form structures with associated Ordovician Arbuckle or Viola oil production have been identified in an area measuring 26,000 mi^2, for an average crater density of one significant crater per 703 mi^2 (Table 2).

Prior to 1962, before the manned missions to the Moon, over 30,000 large craters had been catalogued on the 57% of the Moon that was visible to Earth-based observers (Tocquet, 1962). The 30,000 craters are distributed over a visible surface area of 8,354,726 mi^2, which translates to one significant crater per 278 mi^2.

The crater densities on Mars have been reported to range from 1 crater per 1,000 mi^2 (for craters larger than 1 mi in diameter) to as low as 1 crater per 340,000 mi^2 (for craters larger than 100 mi in diameter) (Morrison and Owen, 1988). Overall, for craters larger than 1 mi in diameter, the planet Mars exhibits crater densities ranging from 1 crater per 1,800 mi^2 to 1 crater per 14,400 mi^2 (minimum).

Other bodies in the solar system that have very high crater densities, similar to the Moon's, include the planet Mercury, the planetary satellites Enceladus (Saturn), Ariel and Oberon (Uranus), Phobos and Deimos (Mars), and dozens of others, as well as the tens of thousands of asteroids (Table 3). As it turns out, determining an average crater density for the heavily cratered planets and moons proves to be a difficult task. Many craters have diameters of several hundred miles, and inside these large Copernican-scale craters are hundreds, if not thousands, of smaller craters. Furthermore, there are wind-swept deserts on Mars where craters have for the most part been buried and are thus hidden from detection. And Venus is so tectonically active that craters, though apparent, have been deformed, reoriented, chemically weathered, and buried beneath broad deltas of hot, sulfuric acid sediment, and there are peculiar circular structures that, although they may be deformed impact craters, appear to be venting molten materials and gases from the planet's mantle.

Earth has a total surface area of 197,751,000 mi^2. About two-thirds of the surface area is water, i.e., 139,781,000 mi^2 of water and 57,970,000 mi^2 of land. The data from Earth and the solar system indicate that 90% of the time at least one significant crater can be expected per 10,000 mi^2 and 10% of the time one significant crater can be expected per 120 mi^2. The mean value of the set distribution is one significant crater per 3,840 mi^2.

Figure 3. Copernican-scale craters, such as the 600-mi-wide Orientale Basin on the near side of the Moon, have been infilled with mare basalts and exhibit secondary-crater trains (arrows). On Earth, similar size classes of impact craters probably initiated the formation of large sedimentary basins. (Photograph L-67-4825, courtesy of NASA, 1967.)

On the Earth, then, there should be 5,797 to 144,925 impact craters, with 15,096 impact craters as the mean expected number (Table 4). But since two-thirds of the Earth is water, the majority of the impacts would have occurred in water, resulting in hydrobleme formation on the sea floor. The land surface of the Earth, then, is expected to have suffered between 5,797 and 144,925 crater-forming events, with 15,096 as the mean expected number. Conversely, the sea would have suffered

TABLE 1.—CRATER COUNT ON EARTH

No. reported	Reference
6	Bucher (1936)
59	Pike (1980)
103	Grieve (1982)
160	Henkel (1993)
300	Unocal proprietary data (1994)

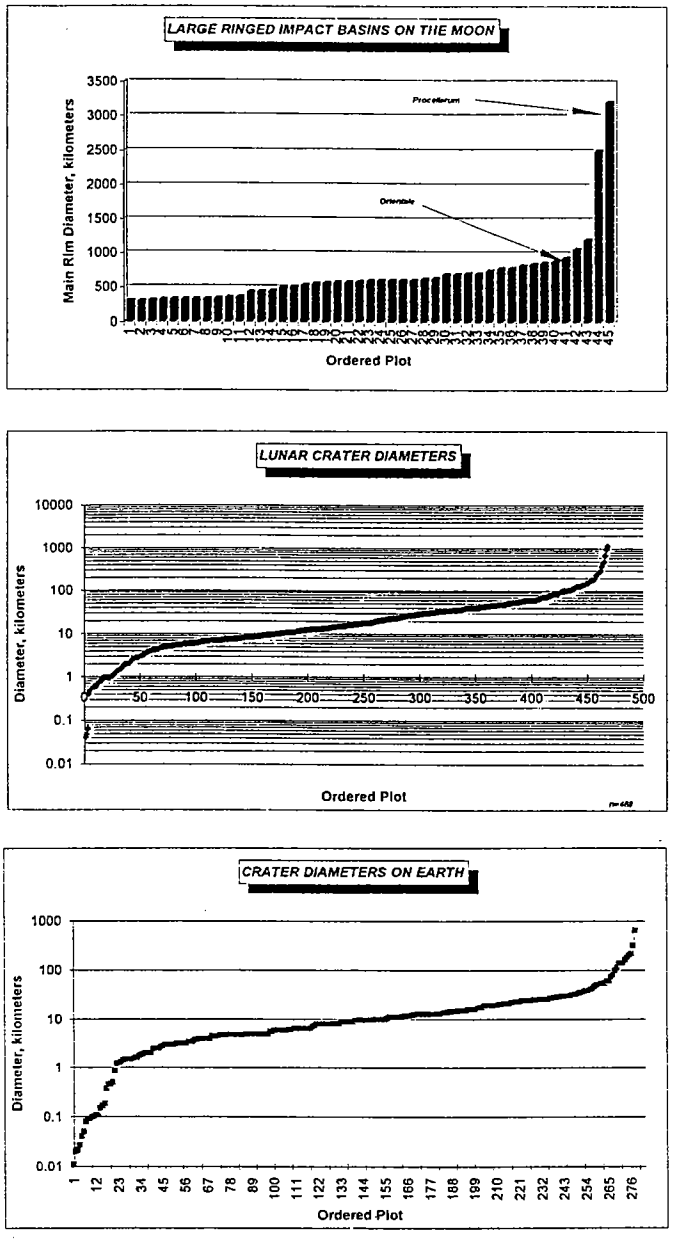

Figure 4. Comparison of the size distributions of (top) Copernican-scale craters on the Moon and (middle and bottom) mid-size crater distributions on the Moon and Earth.

between 13,978 and 349,378 impacts, or a mean of 36,401 potential hydrobleme-forming events.

The data above suggest that there are 15,096 impact craters on the Earth's continents. To date, only 300 have been identified. Where are the others? How can they be located? And what might motivate people to search for astroblemes on the Earth? Additionally, there are no positively identified hydroblemes reported in the literature. None. And the data suggest that there should be 36,401 of them. So where are these elusive hydroblemes? How can they be located, and how might people be motivated to seek them out?

HYDROBLEMES

Grieve and Dence (1979) have estimated that approximately five Copernican-scale craters, with diameters in excess of 60 mi, have formed in the present ocean floor. The mass of the objects that are capable of producing such crater dimensions would have little trouble penetrating the water of the oceans. However, the ocean water column could effectively shield the seabed from the effects of smaller incoming bolides.

Laboratory simulations (Schmidt, 1980) have shown that, once the threshold mass has been exceeded and the incoming projectile does indeed penetrate the water column, the resultant crater, or hydrobleme, on the seabed will have an average depth to diameter ratio on the order of 1:2, as compared to the average depth to diameter ratio on land of 1:0.2 (McKinnon, 1982). In short, hydroblemes are wide, shallow basinlike depressions hidden on the dark seabed.

The penetration of bolides about 6 mi in diameter is not expected to be significantly impeded by the oceans, whose mean depth is 2.2 mi (O'Keefe and Ahrens, 1982). Although there are a number of interdependent conditions to satisfy in order to determine threshold diameters (including kinetic energy, mass, velocity, and trajectory), Gault and Sonett (1982) have determined empirically that, for normal benthic ocean depths of 2.4 mi and impact velocities on the order of 15.5 mi/s, projectiles of >1,312 ft in diameter are likely to form sea-bottom

TABLE 2.—AVERAGE DENSITY OF LARGE CRATERS

Location	Large crater density
Oklahoma	1 crater per 703 mi^2
Fennoscandia	1 crater per 7,472 mi^2
Mars (max.)	1 crater per 1,800 mi^2
Mars (min.)	1 crater per 14,400 mi^2
Mars (mean)	1 crater per 4,000 mi^2
Moon	1 crater per 278 mi^2

TABLE 3.—AREA PER SIGNIFICANT CRATER

In our solar system probability*	Area per significant crater
P10	400 mi^2
P90	10,000 mi^2
Mean	3,840 mi^2

*Probability is expressed thus: P90 means 90% of the data is smaller than or equal to the value (area per significant crater); P10 means 10% of the data is smaller or equal to the given value.

TABLE 4.—EXPECTED NUMBER OF CRATERS

Probability*	Expected no. of craters
Earth Total	
P10	494,378
P90	19,775
Mean	51,498
Earth/Land	
P10	144,925
P90	5,797
Mean	15,096
Earth Hydroblemes	
P10	349,378
P90	13,978
Mean	36,401

*See Table 3 for explanation.

hydroblemes with minimum diameters of 5 to 6 mi.

At the White Sands Missile Range, missiles that impacted water-saturated sediments resulted in craters that were five to ten times wider than the craters formed when missiles with equivalent energies impacted dry sediments (Moore, 1976). Thus, in order to identify true hydroblemes on the ocean floor, the search must look for subdued, low-relief, and unusually wide, shallow crater-form structures. Hydroblemes will not mimic the morphology of their continental counterparts.

What would the formation of a hydrobleme look like from the surface? Don't get too close. But the sequence of events would involve an initial high-velocity central spout formation. The spout would persist, and a bubblelike lid would extend from the rim wave over the cavity. On the sea surface, the encircling rim of water bubbles, a gauntlet of steam spouts into the atmosphere, the central rebound peak eventually collapses, and then a series of globe-threatening tsunamis—horrible tidal waves rolls toward land.

Foremost evidence for past impacts of meteorites in the oceans are chondritic ablation debris, extinction of planktonic foraminifera (little sea critters), the enrichment of sea-floor clays with the rare element iridium, and the widespread microtektite layers called strewnfields. Microtektites are small, melted shards of black glass shaped like drops, twisted projectiles, or bullets. Presumably when the meteorite struck, the intense heat generated melted part of the Earth's crust, and the force of the impact lofted the melt as fused glass particles and deposited them thousands of miles away. The largest tektite strewnfields are the North American strewnfield, which extends westward into the Pacific Ocean from Cuba and the northern coast of South America, the Ivory Coast strewnfield, linked irrefutably to the Bosumtwi crater in Ghana, the Czechoslovakian strewnfield, and the largest on Earth, the Australasian strewnfield, which encompasses all of Australia, Southeast Asia, and parts of India, Madagascar, and southeast Africa (Alvarez and others, 1982). Some have even postulated that the Australasian strewnfield (Schneider and others, 1992) may be the scar from which the Moon was born.

Circular sea-floor features that are likely candidates for being hydroblemes include the Tagus Abyssal Plain, west of Portugal, and near Bombay, India, a paleohydrobleme is thought responsible for the origin of the Deccan basalts (Alvarez and others, 1982). Other candidates include the Massachusetts Bay—an arc along the eastern seaboard between Providence, Rhode Island, and Portland, Maine; the Lesser Antilles, Caribbean Sea; the Southern Ocean late Pliocene asteroid impact (off the southwest tip of South America); the circular area associated with the Australasian strewnfield (related to the Brunhes-Matuyama geomagnetic polarity reversal and coeval climate change); the Sea of Japan—a circular sea-floor anomaly surrounded by North Korea, South Korea, Japan, and Vladivostok; the Wrangel Abyssal Plain in the Arctic Ocean; the Sohm Abyssal Plain in the Atlantic Ocean; and the Pernambuco Abyssal Plain in the Atlantic Ocean off Brazil.

TABLE 5.—OIL AND GAS FIELDS CONTROLLED BY METEORITE IMPACT CRATERS, EARTH

Country	Location	Name	Diameter (km)	Age (Ma)	Morphology*	Source**	Rim height (ft)	Central peak height (ft)	Production	Estimated reserves†
U.S.A.	Colorado	Haswell Hole	35	1400		unpub.			Morrow	
U.S.A.	North Dakota	Red Wing Creek	9	190	C	B-78	800	800	Oil field	10 MMBO
U.S.A.	North Dakota	Newporte			S				Oil and gas field	
U.S.A.	Oklahoma	Ames	12.8	430	C	H-92	250	1600	Oil and gas field	50 MMBO
U.S.A.	Alaska	Avak	12.8	K/T		K-91		1640	Gas field	37 BCFG
U.S.A.	Michigan	Cass County	13.6	395	C	M-97		1363	Oil field	600 MBO
U.S.A.	Texas	Ochiltree	32.2	390	C	unpub.			Gas field	120 BCFG
U.S.A.	Michigan	Warren	38.6	395	C	unpub.			Prospect	60 MMBO
U.S.A.	Indiana	Lima	112.6			unpub.			Oil and gas field	700 MMBO
Canada	Saskatchewan	Viewfield	1.24	190		S-75			Oil	20 MMBO
Canada	Manitoba	Hartney	11.2	190		S-75			Oil	
Canada	Alberta	Steen Field	12.8	Mid-Devonian		unpub.			Oil	50 MBO
U.S.A.	Oklahoma	Central Oklahoma	‡	Ordovician	S-C	unpub.			Oil and gas	130 MMBO

*C = complex, s = simple.
**B-78 = Bridges, 1978; H-92 = Hammand Olsen, 1992; K-91 = Kirschner and others, 1991; M-97 = Milstein, 1997; S-75 = Sawatzky, 1975; unpub. = unpublished data.
†MMBO = million barrels of oil, BCFG = billion cubic feet of gas, MBO = thousand barrels of oil, MMBOE = million barrels of oil equivalent.
‡Numerous.

HYDROCARBON POTENTIAL OF ASTROBLEMES

Existing Oil and Gas Fields

On Earth, numerous buried impact craters have proven to be productive for oil and gas. Typically, oil and gas is trapped within and above the encircling rim anticlines and on the central rebound peaks. In a relatively stable geologic environment, with rapid burial of the crater, the full circumference of the rim anticlines and the central peak may contain hydrocarbons. More commonly, the impact crater was formed tens or hundreds of millions of years ago and has eroded substantially, leaving monadnocklike remnants of structure. If, however, the crater lay within a larger sedimentary basin that continued to subside, the resulting tilting and reorienting of the original crater form will have caused any oil and gas rise to the highest point in the subsurface reservoir environment. Because the downbasin side of the crater rims commonly loses structural closure, oil and gas pools associated with astroblemes are most common on the upbasin side.

Astroblemes, or ancient weathered impact craters, have produced hydrocarbons in North America at the Red Wing Creek field, North Dakota (130 MMBO in place; cumulative production, >10 MMBO); the Viewfield field, Saskatchewan (100 MMBO in place; 20 MMBO recoverable); the Avak structure and Barrow gas fields, Alaska (37 BCFG recoverable gas), the Calvin-28 field, Michigan (600 MBO recoverable reserves at 763 ft depth); and discovered in 1991, the Ames astrobleme, Oklahoma, with estimated recoverable reserves approaching 50 MMBO plus gas (Kirschner and others, 1991; Bridges, 1978; Grieve, 1982; Hamm and Olsen, 1992; Sawatzky, 1975; Milstein, 1997). In all, dozens of fields have proven productive, with cumulative reserves of nearly 1 billion barrels of oil (Table 5). The list in Table 5 is not all-inclusive. There is the Rif of Morocco (Michard, 1976), dozens of Arbuckle oil-productive astroblemes bordering the Anadarko basin of Oklahoma, Kansas, North Texas, and the Texas Panhandle, and countless prospects in Australia, Russia, Antarctica, and the rest of the world.

If, on the basis of good maps of an oil field that exhibits the required morphology, relief, and so

forth, the operator of the field suspects that a given reservoir is related to an astrobleme, then the first step to fully develop the production potential is to determine how the oil wells are situated on the astrobleme. If they are all on the encircling rim anticline, either on the upbasin or downbasin side, then the field may be extended along that structure. If the rim anticline has been developed satisfactorily, then the risks of there being a prospective central peak must be considered.

On Mercury, Venus, and the Moon, nearly all the impact craters larger than 2.5 to 3.1 mi have rim anticlines, some completely encircling, some broken into arcuate segments. On Mars, whose impact craters are thought to have formed under conditions very similar to those on the Earth, only about 50% of the impact craters larger than 2.5 to 3.1 mi have measurable encircling rim anticlines.

Throughout the solar system, central peaks associated with impact craters are much less common than encircling rim anticlines. Of the impact craters on Mercury, 62% have central peaks; 57% of the impact craters on the Moon have central peaks; 25% on Venus have peaks; and on Mars, only 11% of the impact craters exhibit measurable central rebound peaks. Earth's conditions place it between those of Venus and Mars.

The operator of a Midcontinent astrobleme-related oil field would predict the risk of drilling the center of the astrobleme thus: an astrobleme on Earth has an 11 to 25% chance of having a central peak. The worldwide odds of a wildcat well striking oil or gas, however, are no better than 10%. Of that 10%, only 1 or 2% of the strikes turn out to be a significant discovery. Compared to these odds, drilling the suspected central peak of any already oil-productive astrobleme seems like pretty good odds.

Warren Astrobleme

During the late 1920s to the late 1940s, Mt. Pleasant, Michigan, and surrounding towns, endured a major oil boom. Wells flowed as much as 10,000 barrels of oil per day from the Devonian Dundee Limestone above depths of 4,000 ft. Thousands of people flooded the area, thousands of wells were sunk, millions of barrels of oil were produced. The development of the Mt. Pleasant and Porter oil fields was not without problems. At first, geologists thought the Mt. Pleasant and Porter fields were one large connected anticlinal trap. Subsequent drilling proved this not to be the case. Near Oil City and eastward, drillers then found a surprise: the east flank of the Mt. Pleasant oil field was not structurally controlled; it was stratigraphically controlled. And because the rocks, not the subsurface structure, controlled production beyond Oil City, the field expanded.

As the years rolled by, the Mt. Pleasant field mapped out as an arcuate, part structure, part stratigraphic, oil pool. Then, in the early 1980s, the Rosebush field was discovered to the northwest (Fig. 5). This field proved to be a north-trending structure—very unlike the surrounding structural grain.

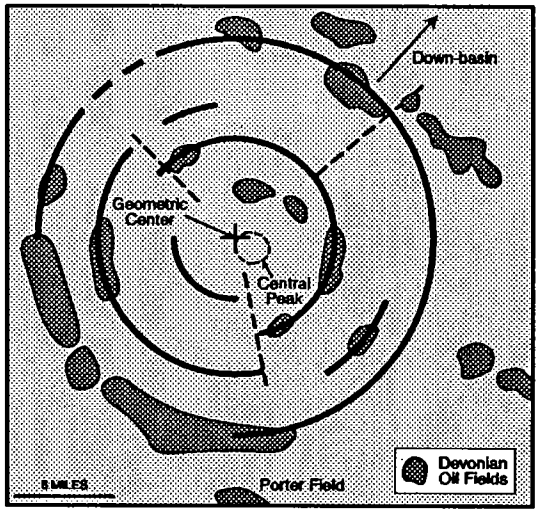

Figure 5. Proposed Warren astrobleme, central Michigan basin. Arcuate oil field to the northwest of Porter field is the Mt. Pleasant–Greendale field complex, and northwest of Mt. Pleasant is the north-trending Rosebush field.

In the middle 1980s, Union Oil Company mapped a dome, based on seismic and well data, located 14 mi to the northeast of the town of Mt. Pleasant. The dome covered approximately 2½ mi², had 80 ft of structural closure on top of the Ordovician, had a seismic velocity anomaly associated with it, and shallow wells with oil shows had already been drilled on top.

Today, though there is no longer any evidence of the oil fields between Oil City and Mt. Pleasant, nor any evidence of the once prosperous boom days and associated excesses, about 14 mi northeast of Mt. Pleasant there does still exist an oil and gas prospect, one that in all likelihood represents the central rebound peak of a 395 Ma astrobleme. The Warren astrobleme measures 24 mi in diameter, is a complex, highly eroded astrobleme, and its location in the center of an unusually circular Michigan basin begs the correlation to be made: did the Warren impact somehow effect the subsidence and subsequent deposition of sediments within the Michigan basin? Is the formation of the Michigan basin the result of asteroidal impact?

In today's dollars, it will take $3 million to find out, for that is what it will cost to drill to the depth of a possible central uplift.

Lima Field, Indiana and Ohio

The largest oil field east of the Mississippi River and north of Dixie is the Lima field, Indiana

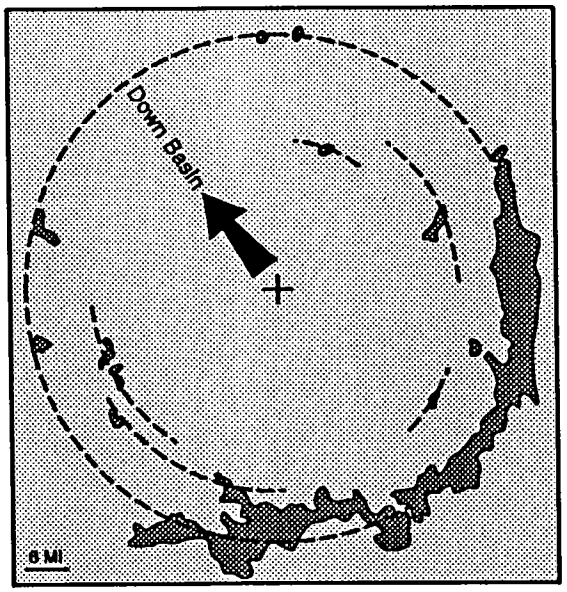

Figure 6. The only giant oil field in the northeast United States (Ohio and Indiana) is Lima-Indiana field, discovered in 1886, which has produced over 500 million barrels of oil. The concentration of curvilinear oil pools opposite the downbasin direction suggests an astrobleme origin for this giant oil field.

and Ohio. Discovered in 1886 at depths ranging from 800 to 3,000 ft, the Lima field soon sprawled across two states and ultimately produced between 500 million and 1 billion barrels of crude oil.

Today, the Lima field produces only a trickle of oil. Many won their fortunes there; many lost them. Even though thousands of wells were drilled in the Lima field, very little geologic data are available. Very little was even gathered in the first place.

Geologically, the Lima field is a stratigraphic trap. Downdip tight limestones grade updip into porous, nearly cavernous, Trenton dolomites that are soaking with oil. The oil pool has an arcuate, semicircular, shape, with the concave side facing downbasin (Fig. 6). Huge radial faults emanate from the center of the arc of oil production. The Bowling Green fault, the Albion-Scipio fault, and many other fault lineaments in the region exhibit a torque screw pattern that suggests that the suspected impactor—the creator of the crater—was spinning when it struck as rifle bullets do.

Anadarko Basin

The Anadarko basin is a fascinating basin for astroblemes. It is heavily drilled, with good geologic and geophysical data available for study. In any given area, when the main pay zone was

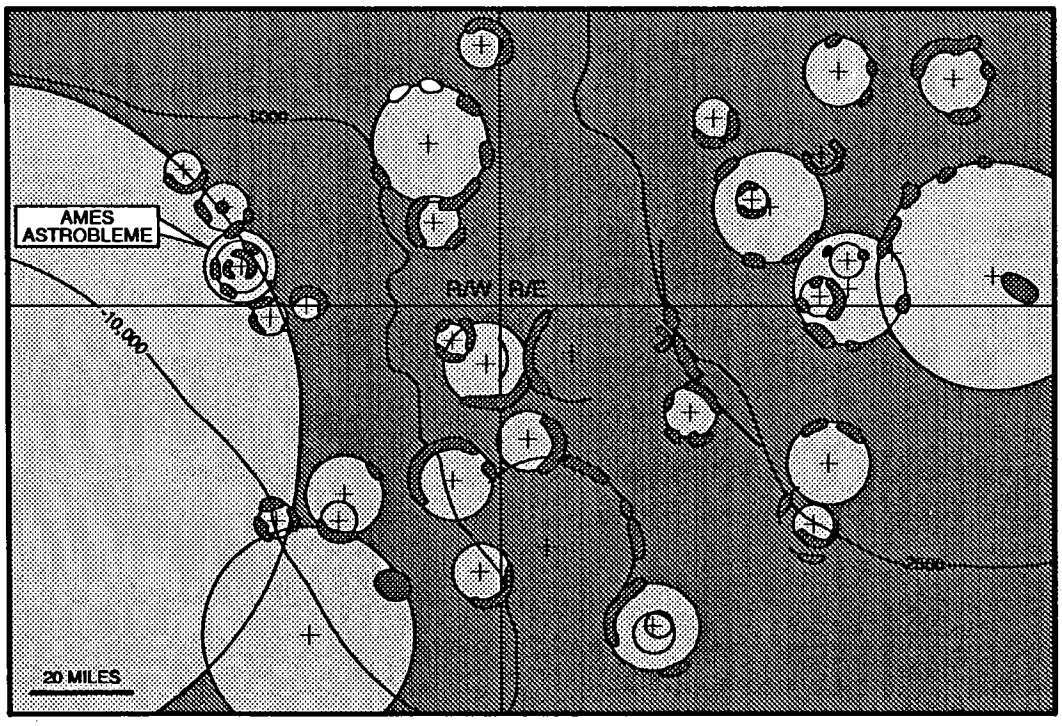

Figure 7. Viola Limestone structure map, central Oklahoma, showing Ordovician Arbuckle Group and Viola Formation oil and gas fields situated atop encircling rim, probably of astrobleme origin. Crosses represent ground zeros. Mapped density is one crater per 703 mi^2.

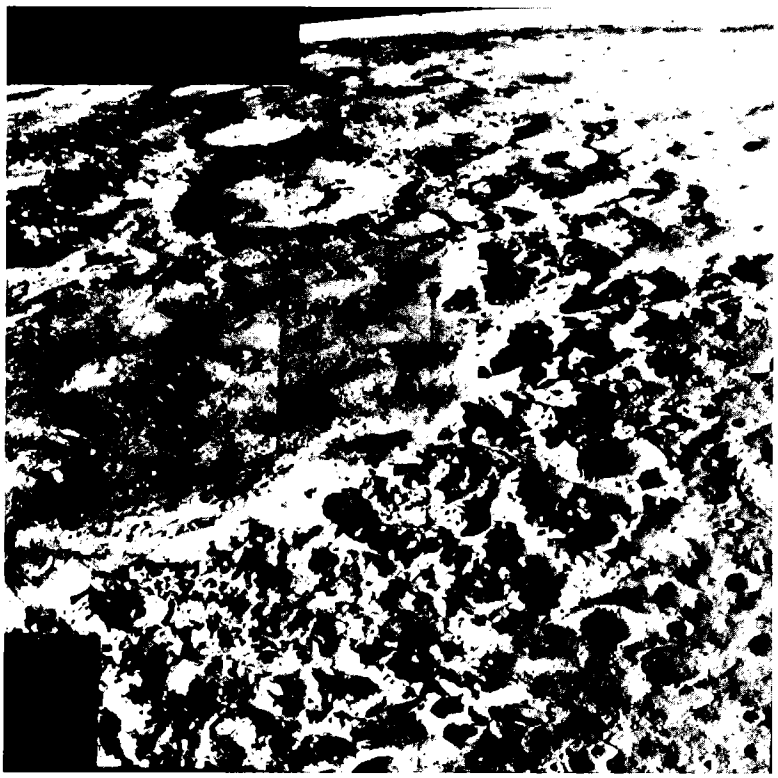

Figure 8. Oblique view of the 560-mi-diameter Argyre Basin on Mars—analogue for the Anadarko basin, Oklahoma. (Courtesy of NASA, Viking mosaic P17022.)

drilled, the drillers stopped drilling. As a consequence, >90% of all wells stop short of the Ordovician. Now data from these "shallow" wells are pointing drillers at other, deeper-target formations. Many fields in the Anadarko basin already produce from the Ordovician Viola and/or Arbuckle limestones. Most of these fields have semicircular geometry, and their production is concentrated on the upbasin side of the interpreted astrobleme. Many fields also produce from a central peak (Fig. 7).

The amount of oil and gas produced, or enhanced, by astrobleme structure in the Anadarko basin measures in the hundreds of millions of barrels. The problem is that a large number of oil fields that have been produced for decades may be producing from astrobleme-enhanced reservoirs and the operators do not even realize it. Furthermore, the complex erosional history probably sculpted the paleolandscape into a terrain like the Martian Argyre Basin (Fig. 8).

Ames, Oklahoma

Only one astrobleme-related oil field in Oklahoma has been so identified in publication: the Ames astrobleme in Major County, Oklahoma. A crater in the subsurface measuring 8 mi in diameter was first discovered during oil and gas drilling. The Ames astrobleme has two annular, concentric mountain ranges, annular valleys, and a 1,600-ft-tall central rebound peak. The high-velocity meteor impact blasted away nearly a 2,000 ft thickness of carbonate sediment in a nearshore-shelf setting; the 1,600 ft thickness of granite basement rock, 2 mi across at the center, rebounded; then the sea overran the structure and charged subsequently deposited sedimentary infill with hydrocarbons. During the summer of 1991, DLB Oil Company discovered oil above the circular rim mountain ranges, at a well called the DLB Oil #1-20 Gregory, which averaged 425 barrels of oil per day, flowing, during its first four months of production. Since then, dozens more successful producers have been added to the area, many of them as good or better than the Gregory well.

Calvin-28 Impact Crater, Cass County, Michigan

The Calvin-28 structure lies in Cass County, Michigan, in T. 7 S., R. 14 W. The village of Calvin Center lies within the annular depression surrounding the central uplift (Fig. 9). The crater is 4.5 mi in diameter, with an encircling depression and an encircling anticlinal ring. Over 100 wells have been drilled into this structure since 1982, when oil and gas were discovered in the central peak and also along the anticlinal rims. The original new field discovery and several subsequent associated oil fields have, or will ultimately, produce 600,000 barrels of oil from an average reservoir depth of 763 ft.

The age of the meteorite-impact event is thought to be Early Silurian, when the Michigan basin hosted warm shallow seas and, on the north and southern perimeters, contained hundreds of carbonate islands protecting the back-reef areas from primordial waves. The meteorite struck a shallow carbonate ramp in southwest Michigan. The massive heat generated, and the horrendous tsunamis radiated from the point of impact would have pounded any carbonate islands standing at the time, crushing many of them, destroying others.

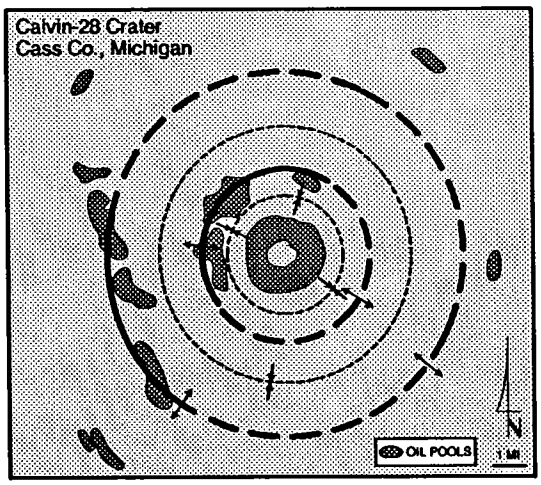

Figure 9. Oil-productive Calvin-28 impact structure, southwest Michigan (after Milstein, 1997).

The energy released by the meteorite that formed the Calvin-28 structure was on the order of 1×10^{26} ergs (Milstein, 1997). The result was a point-focused, nearly instantaneous penetration of an otherwise flat-lying terrain.

EXPLORING FOR ASTROBLEMES

Tools and Techniques

Imperative to the study of impact craters on the Earth is the evaluation of analogues. There is a whole universe of analogues to choose from: the Moon, Mars, Mercury, Venus, their moons and asteroids, and the planets outboard from Jupiter. Dozens of rigorous studies of crater morphologies on the Moon preceded the first landing on the Moon. Today, scientists are studying the craters on Mars, and on other terrestrial planets, in anticipation of manned and unmanned missions thereto.

Most of what has been published on the topic of impact craters has been incorporated into this study. However, more emphasis is placed on the structural geology, sedimentology, potential reservoir development, and potential economic geology of impact craters as these topics apply to the exploration and development of Earth's natural resources.

A host of methods are employed to locate impact craters both on the Earth's surface and in its subsurface, including satellite thematic mapper and multispectral mapper data, radar imagery, and optical photography. Potential-fields methods allow precise gravity and magnetics delineations of possible impact sites. The reflection seismic studies, subsurface geology utilizing borehole data, the making of hundreds and thousands of maps—structure maps, isopach maps, third-order vertical-derivative structure maps—the integration of many different disciplines and methods, along with the power to reorder and enhance and play multivariate gymnastics with the data using computers, all assists in the delineation of impact craters on and within the Earth's crust. The tools at explorationists' disposal are limited only by their imaginations.

The Model: A Contrarian View

Secondary-impact craters radiate from the primary-impact site as either concentric or radial crater trains (Fig. 10). Their distributions and ages are *dependent* upon the primary impactor. Secondary craters are aligned in discrete, age-related trends and have less rugged rims than those of primary craters. Secondary craters have a 50% greater depth to width ratio than do primary-impact craters. Other than these differences, the geometric characteristics are the same for both primary and secondary craters.

Many people assume that meteorite impacts are random, unpredictable events—"acts of God." However, secondary impacts are not random, unpredictable events. Secondary-impact craters are dependent upon the primary impactor. If the primary impactor strikes, then secondary-impact craters *will form* within a short span of time, and they *will be aligned* in belts related to the ejecta's trajectories. Numerous secondary-crater trains emanate from the Moon's Crater Orientale (Fig. 3). The Jovian satellites Ganymede and Callisto have 15 linear crater chains thought to be the result of tidally split comets such as occurred on Jupiter with the breakup of the Shoemaker-Levy comet (Schenk, 1993). The solar system is full of examples of secondary-meteorite crater trains, or belts, that resulted from larger primary-meteorite impact.

But what about the primary-impact craters? Is the assumption that they, also, are random, unpredictable events valid?

Contrary to popular opinion, primary-impact craters may not be randomly distributed on planetary or satellite surfaces of a given age. True, there is an inverse size vs. frequency distribution for impact craters on the Earth and the terrestrial planets and the Moon that may or may not match the mass distribution of cosmic projectiles. But that does not mean that the cosmic meteorite flux has been homogeneous throughout time; there have been anomalies—large, poorly indurated planetesimals or asteroids or swarms of cosmic materials being captured by planetary gravitational forces (for example, Jupiter's capture of the Shoemaker-Levy comet in 1993–1994; Schenk, 1993)—and, over time, one by one, projectiles have dropped and impacted the target surface along an orbital ecliptic, sometimes coincident with the paleoequatorial plane, sometimes antithetic to it.

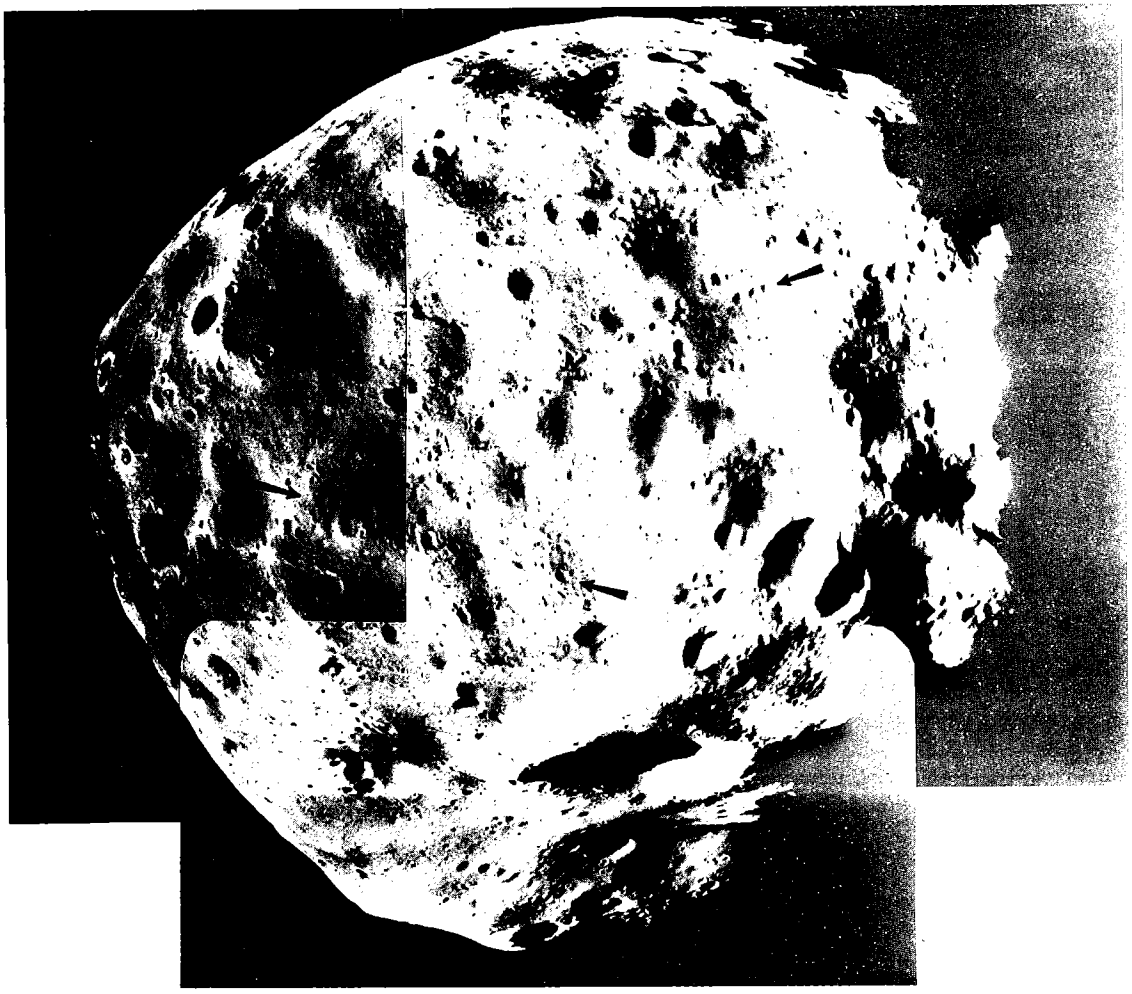

Figure 10. Viking Orbiter 300-mi-altitude flyby of Phobos, the inner satellite of Mars, showing chains of secondary-impact craters. In this image, Phobos measures approximately 13 mi × 11.8 mi. (Photograph 77-H-97, courtesy of NASA, released February 22, 1977.)

Five Cretaceous/Tertiary impact sites have been reported in recent literature. These are the Manson crater, Iowa (74 Ma); the Avak crater, Alaska (estimated to date at 65 Ma); the Marquez crater (58 Ma, Wong and others, 1997), the Chicxulub crater, Yucatan Peninsula, Mexico (65 Ma), and offshore Japan (Stein, 1993). These sites define an orbital trajectory antithetic to the Earth's equator, similar to what occurred on Jupiter in 1993–1994 (Figs. 11,12). If, over a period of 16 m.y., this orbit were to decay, craters would form beneath the orbital trajectory. Just such a case may have occurred during the Late Cretaceous—a dangerous time for any creatures of Earth that were not able to burrow safely into the ground and hide from the Armageddon.

I plotted meteorite-impact sites on a map of North America, coded the approximate ages of the impact events, and then reconfigured the continents into their relative plate-tectonic positions during various time slices. Then I constructed an impact isotime contour map that revealed a peculiar trend within the 300 Ma contour: The vast majority of the impact craters in North America (as well as those in Fennoscandia, i.e., the Siljan Ring region) lie within a northeast-trending belt. This Early Pennsylvanian meteorite belt is coincident with the Early Pennsylvanian paleoequator as determined from paleomagnetic data (Fig. 13).

Model Involving Two Moons During the Paleozoic

Starting during the Ordovician, 450 m.y. ago, and ending in the Early Pennsylvanian, 300 m.y. ago, the orbit around Earth of a large, loosely in-

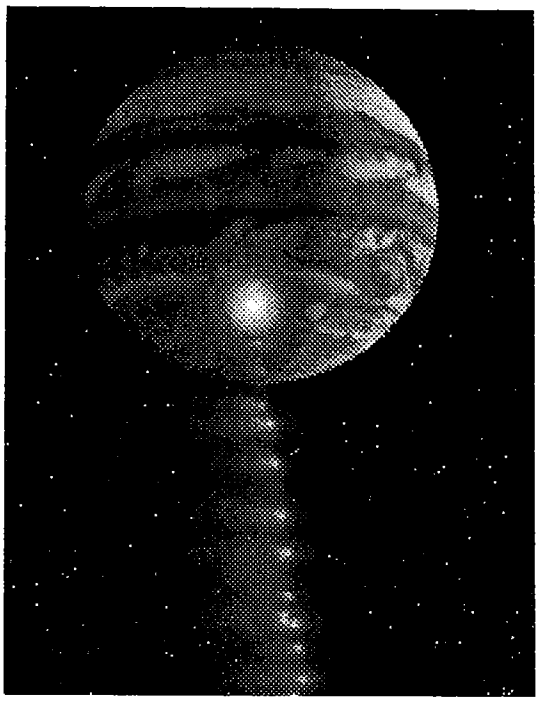

Figure 11. Hubble Telescope image of the breakup of comet Shoemaker-Levy. Numerous comet fragments impacted the Jovian surface in a belt antithetic to the Jovian equator. (Image acquired via on-line computer service).

durated, mass started decaying. For a time the orbiting bolide would have resembled Earth's second moon: two moons sharing the same sky, two Paleozoic moons working together to create the most dramatic tidal forces in all of Earth's history (Fig. 14). During the Middle Ordovician, the normal high-tide mark extended hundreds of miles inland (Rex Cole, personal communication, 1991). Huge seas of agitated sand were deposited in broad flats and basins. As time passed, the orbit of the second moon decayed, and ultimately it fell to Earth in pieces. A twenty-ton meteorite would crash to Earth in Michigan, twenty-five m.y. later another would crash down in Kansas, ten million years later a mile-wide bolide would crash into Oklahoma. Once the moon cluster disappeared, the tides would diminish, and the remaining Moon, with diminished gravitational effects imposed upon it, would commence its 1½-in./yr outward drift away from Earth.

Hypothetical Approach to Locating Meteorite Impact Belts

If the orbital trajectory of the Paleozoic second moon determined the crater-belt orientation on the Earth's crust (which, naturally, it should), then such belts should be predictable. I hypothesize that other meteorite-impact belts, in addition to the Pennsylvanian and Cretaceous/Tertiary trends, occur along different orbits during different ages of geologic history. Undoubtedly more meteorite belts will be discovered on Earth, many of which will have economic potential to their discoverers.

SUMMARY

1. The most common, abundant, and simple crustal structures on the terrestrial planets, moons, asteroids, and the outer planets are impact craters.
2. Earth has not been immune to impact.
3. On Earth, oil and gas discoveries have been made above or within astrobleme structures.
4. Secondary-impact craters are not random in space in time—they are dependent variables. Similarly, primary-impact craters may also not be random in time and space, particularly if the time is long enough and the space is large enough. If trends of primary-impact craters can be mapped, then trends of astroblemes that may yield oil and gas can be predicted.
5. Oil explorationists ever-on-the-lookout for new trends will undoubtedly agree: Astroblemes are a definite high-impact possibility.

ACKNOWLEDGMENTS

I thank Unocal for continued support of this project and Dave Courtis, Tom Shaw, Scott Schapper, Bob Meyer, John Forbes, Ned Butler, Andrew Fawthrop, and others, whose interest, discussions, and criticisms strengthened this paper. A special thanks to "Leen Astrobleme" for her patience and encouragement.

REFERENCES CITED

Alvarez, W.; Alvarez, L. W.; Asaro, F.; and Michel, H. V., 1982, Current status of the impact theory for the terminal Cretaceous extinction, *in* Silver, L. T.; and Schultz, P. H. (eds.), Geological implications of impacts of large asteroids and comets on the Earth: Geological Society of America Special Paper 190, p. 305–315.

Bridges, L. W. D., 1978, Red Wing Creek field, North Dakota: a concentricline of structural origin: Montana Geological Society 24th Annual Conference, 1978 Williston Basin Symposium, Billings, p. 315–326.

Bucher, W. H., 1936, Cryptovolcanic structures in the United States: 16th International Geological Congress, United States, 1933, Reports, v. 2, p. 1055–1084.

Condit, C. D., 1977, Distribution and relationships of 4–10 kilometer diameter craters to global geologic units on Mars: Icarus, v. 34, p. 465–478.

Gault, D. E.; and Sonett, C. P., 1982, Laboratory simulation of pelagic asteroidal impact: atmo-

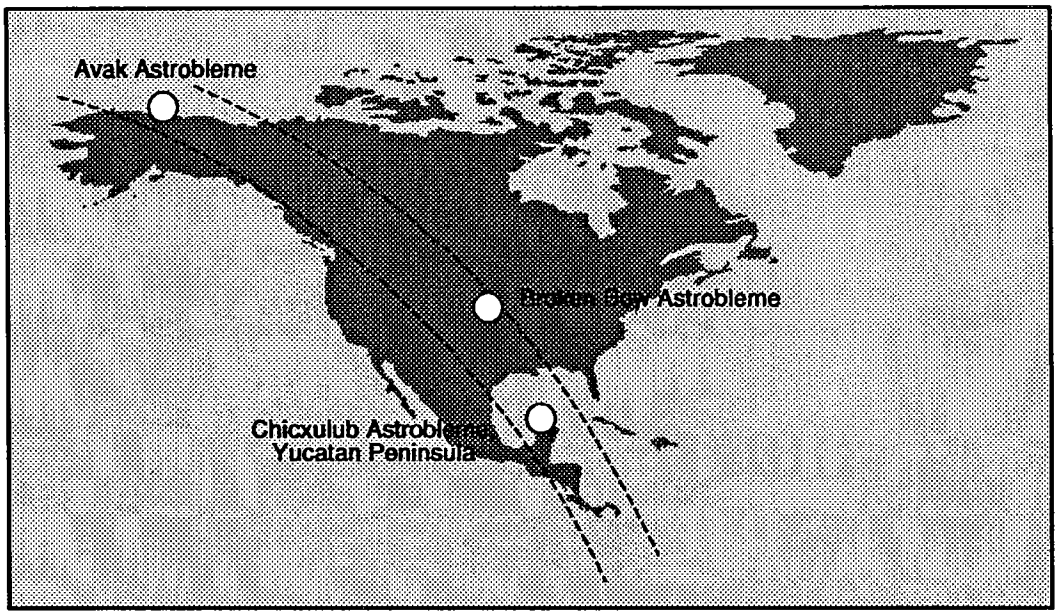

Figure 12. Cretaceous/Tertiary impact craters in North America. Random geographically? Or within a belt?

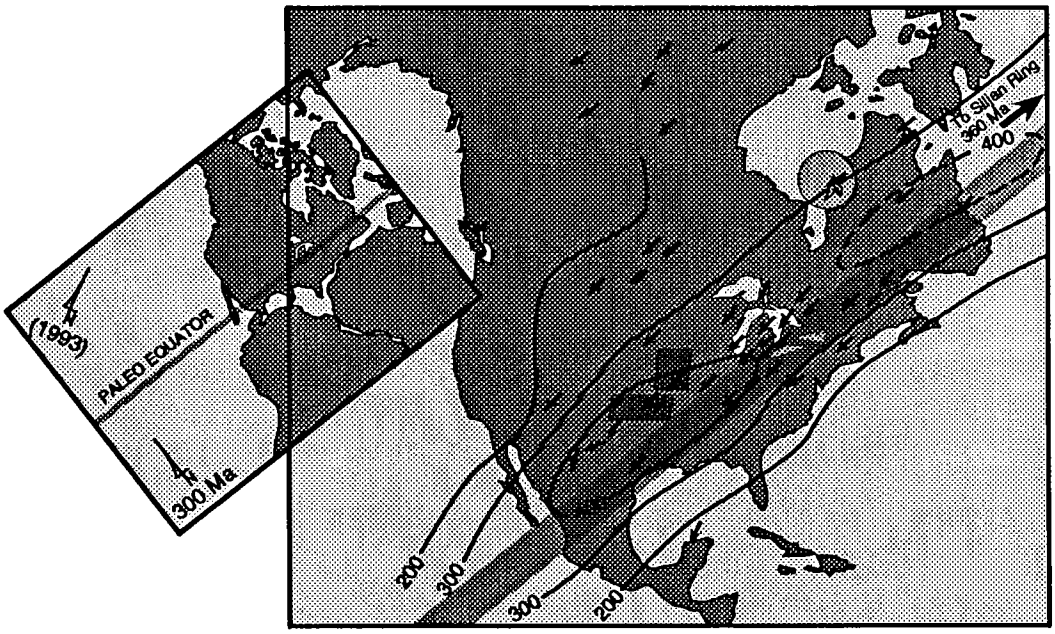

Figure 13. Impact isotime contour map of North America and plate-tectonic reconstruction at 300 Ma (left inset). Does the equatorial impact belt track the orbit of Earth's primordial second moon?

spheric injection, benthic topography, and the surface wave radiation field, *in* Silver, L. T.; and Schultz, P. H. (eds.), Geological implications of impacts of large asteroids and comets on the Earth: Geological Society of America Special Paper 190, p. 69–92.

Gault, D. E.; Guest, G. E.; Murray, D. D.; and Malin, M. C., 1975, Some comparisons of impact craters on Mercury and the Moon: Journal of Geophysical Research, v. 80, p. 2444.

Grieve, R. A. F., 1982, The record of impact on Earth: implications for a major Cretaceous/Tertiary im-

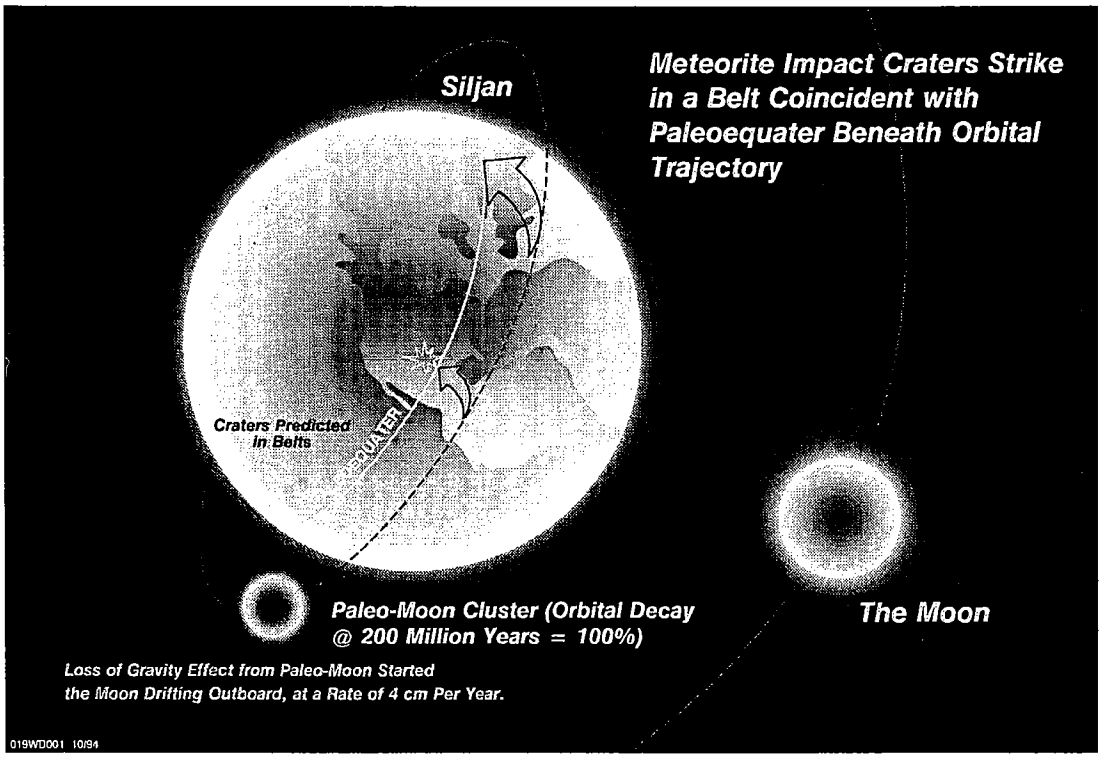

Figure 14. Rendition of the formation of meteorite primary-impact belts due to the landward fall of fragments from Earth's prehistoric second moon.

pact event, *in* Silver, L. T.; and Schultz, P. H. (eds.), Geological implications of impacts of large asteroids and comets on the Earth: Geological Society of America Special Paper 190, p. 25–37.

Grieve, R. A. F.; and Dence, M. R., 1979, The terrestrial cratering record; II. The crater production rate: Icarus, v. 38, p. 230–242.

Hamm, Harold; and Olsen, R. E., 1992, Oklahoma Arbuckle lime exploration centered on buried astrobleme structure: Oil and Gas Journal, April, p. 113–116.

Henkel, H.; and Pesonen, L. J., 1992, Impact craters and craterform structures in Fennoscandia: Tectonophysics, v. 216, no. 1/2, p. 31–40.

Kirschner, C. E.; Grantz, Arthur; and Mullen, M. W., 1991, Impact origin of the Avak structure, Arctic Alaska, and genesis of the Barrow gas fields: American Association of Petroleum Geologists Bulletin, v. 76, p. 651–679.

McKinnon, W. B., 1982, Impact into the Earth's ocean floor: preliminary experiments, a planetary model, and possibilities for detection, *in* Silver, L. T.; and Schultz, P. H. (eds.), Geological implications of impacts of large asteroids and comets on the Earth: Geological Society of America Special Paper 190, p. 129–142.

Michard, A., 1976, Eléments de géologie morocaine: Notes et Memoires du Service Géologique, Royaume du Maroc, Ministère du Commerce, Division de la Géologie, Rabat.

Milstein, R. L., 1997, The Calvin impact structure, Cass County, Michigan: identification and analysis of a subsurface Ordovician astrobleme, *in* Johnson, K. S.; and Campbell, J. A. (eds.), Ames structure in northwest Oklahoma and similar features: origin and petroleum production (1995 symposium): Oklahoma Geological Survey Circular 100 [this volume], p. 391–393.

Moore, H. J., 1976, Missile impact craters (White Sands Missile Range, New Mexico) and applications to lunar research, *in* Contributions to astrogeology: U.S. Geological Survey Professional Paper 812-B, 47 p.

Morrison, D.; and Owen, T., 1988, The planetary system: Addison-Wesley Publishing Co., Reading, Massachusetts, 519 p.

O'Keefe, J. D.; and Ahrens, T. J., 1982, The interaction of the Cretaceous/Tertiary extinction bolide with the atmosphere, oean, and solid Earth, *in* Silver, L. T.; and Schultz, P. H. (eds.), Geological implications of impacts of large asteroids and comets on the Earth: Geological Society of America Special Paper 190, 528 p. Pike, R. J., 1980, Geometric interpretation of lunar craters, *in* Apollo 15–17 orbital investigations: U.S. Geological Survey Professional Paper 1046-C, 77 p.

Sawatzky, H. B., 1975, Astroblemes in Williston basin: American Association of Petroleum Geologists Bulletin, v. 59, p. 694–710.

Schenk, P. M., 1993, Comet to hit Jupiter: Jovians doomed!: Lunar and Planetary Institute, Lunar and Planetary Information Bulletin, no. 69, p. 2–3.

Schmidt, R. M., 1980, Meteor crater: energy of formation—implications of centrifuge scaling, *in* Proceedings of the 11th Lunar and Planetary Science Conference, Houston: Pergamon Press, New York, p. 2099–2128.

Schneider, D. A.; Kent, D. V.; and Mello, G. A., 1992, A detailed chronology of the Australasian impact event, the Brunhes-Matuyama geomagnetic polarity reversal, and global climate change: Earth and Planetary Science Letters, v. 3, p. 395–405.

Stein, M. A., 1993, Shower of meteorites may have killed dinosaurs: Houston Chronicle, June 21, p. 8B.

Tocquet, R., 1962, Life on the planets: N. V. Grafische Industrie, Haarlem, Netherlands.

Wong, A. C.; Sadow, J. C.; Reid, A. M.; Hall, S. A.; and Sharpton, V. L., 1997, The Marquez crater in Leon County, Texas, *in* Johnson, K. S.; and Campbell, J. A. (eds.), Ames structure in northwest Oklahoma and similar features: origin and petroleum production (1995 symposium): Oklahoma Geological Survey Circular 100 [this volume], p. 278.

Source-Rock Potential of Impact Craters

John R. Castaño*
DGSI
The Woodlands, Texas

James H. Clement*
Consultant
Houston, Texas

Michael D. Kuykendall
Solid Rock Resources
Tulsa, Oklahoma

Virgil L. Sharpton
Lunar and Planetary Institute
Houston, Texas

ABSTRACT.—A meteorite impact can create a local closed lacustrine or marine depression favorable for the deposition of source rocks for oil and gas. These organic-rich rocks act both as hydrocarbon source and seal for entrapment. Reservoir lithologies include sandstones, carbonates, and igneous rocks; typically porosity has been enhanced by the impact event. Several impact craters have associated hydrocarbon production; in this paper we show how the impacts have controlled source-rock distribution at productive areas such as the Ames structure in Oklahoma and at the Newporte field in North Dakota. Nonproductive examples—such as Bosumtwi, Ries, and Flynn Creek—are also illustrative of the process of source-rock deposition in impact craters. The presence of hydrocarbon source rocks greatly enhances the value of an impact crater as an oil prospect.

INTRODUCTION

Several impact craters have associated hydrocarbon production (e.g., Red Wing and Newporte fields in North Dakota and the Ames structure in Oklahoma). Thus, interest has been raised concerning the source of oil and gas in these areas.

Our thesis is that meteorite impacts can create a local, closed lacustrine or marine depression in which anoxic conditions prevail, favoring deposition of hydrocarbon source rocks. In effect, a local petroleum system is formed. The organic-rich rocks act both as a seal and a source for hydrocarbons, whereas the rocks affected by the impact are the reservoirs. The trap for oil or gas is also related to the deformation caused by the impact. Most workers studying craters have concentrated their efforts on the rocks directly affected by an impact and have largely ignored the superjacent sedimentary units. In addition, we have found that in the past, many scientists have been reluctant to seriously consider meteorite craters as a basis for trap formation.

There is another possible way for oil to come to exist in an impact structure: the great, impact-caused heat operating over a period of several thousand years would be sufficient to mature a preexisting source rock, and oil entrapment would be afforded by the deformation created by the impact. Hydrocarbon seeps in Ordovician limestones on the east side of the Siljan structure in Sweden originated in this manner (Vleirboom and others,

Michael D. Kuykendall, Solid Rock Resources, 1408 S. Delaware Place, Tulsa, OK 74104; Virgil L. Sharpton, Lunar & Planetary Institute, 3600 Bay Area Blvd, Houston, TX 77058.

*Deceased.

Castaño, J. R.; Clement, J. H.; Kuykendall, M. D.; and Sharpton, V. L., 1997, Source-rock potential of impact craters, *in* Johnson, K. S.; and Campbell, J. A. (eds.), Ames structure in northwest Oklahoma and similar features: origin and petroleum production (1995 symposium): Oklahoma Geological Survey Circular 100, p. 100–103.

1986; Castaño, 1993). At the Siljan impact structure, the sources of oil are the organic-rich beds that are interbedded with the limestones.

Maar-type volcanic craters can be filled with lacustrine, organic-rich sediments (Hetényi and Bruckner-Wein, 1993) that provide the petroleum source. However, these features lack both the trap and reservoir needed for hydrocarbon accumulation.

BOSUMTWI CRATER, GHANA

The Bosumtwi crater in Ghana is a modern analogue to the older examples cited in this paper; the crater is 10–11 km in diameter and is occupied by a lake 7–8 km wide. The impact occurred during the Pleistocene; it penetrated Precambrian graywackes and phyllites (Jones, 1983). As described by Jones (1983), the deep lake contains 200–500 m of organic-rich sediments with an average total organic carbon (TOC) content of 12.5%. The lake is permanently anoxic at depths greater than 40 m. Methane seeps are abundant; because of the shallow burial, the gas must be biogenic. The seal and source for gas are the finely laminated, organic-rich lacustrine shales; the principal reservoir at Bosumtwi is the fallback breccia, which has an estimated porosity of 15–20%. The potential gas volume is estimated at 250 BCF (billion cubic feet).

RIES CRATER, GERMANY

The Ries crater in Germany is an extremely well studied crater. It is 24 km in width; the crater was filled with Miocene lacustrine sediments more than 300 m thick (Füchtbauer and others, 1977). The Nördlingen 1973 borehole continuously cored the sedimentary section into the underlying suevite. Toward the base of the sedimentary sequence in the Nördlingen 1973 core are laminated, organic-rich marls between the depths of 146 and 256 m. These marls range from 4 to 16% TOC. They are algal rich and were deposited in an anerobic, highly saline environment. When the cores were recovered, some seeped "liquid bitumen" when fresh. Unfortunately, this material was not recovered or investigated. The section is immature, with a vitrinite reflectance of less than 0.50% (Wolf, 1977). The critical element to note is that the impact at Ries created a depositional setting where more than 100 m of highly oil prone, very organic rich source-rock shales were deposited.

FLYNN CREEK STRUCTURE, TENNESSEE

The Devonian Flynn Creek structure in eastern Tennessee formed at about 360 Ma (Roddy, 1968). The crater is 3.6 km in diameter and 120 m deep. A study of outcrop and drill-hole information showed that Ordovician limestones are mixed and brecciated to a depth of 200 m and the degree of deformation decreases downward. The depression caused by the impact was filled with the Chattanooga Shale, a well-recognized organic-rich marine shale of Late Devonian age. The lower unit of the Chattanooga Shale is 2 m thick outside the crater, but it is 48 m thick within the crater. The Flynn Creek crater is a case in which the depression caused by the impact greatly increased the thickness of the source rock for hydrocarbons. If this crater were buried to a sufficient depth to mature the hydrocarbons in the source rock, the Chattanooga Shale would act as the source and seal, and the limestone breccias in the central uplift would be the reservoir.

NEWPORTE STRUCTURE, NORTH DAKOTA

We interpret the structure at the Newporte field in North Dakota as an astrobleme. Production from this small, circular structure (2.4 km wide) is obtained from the Cambrian Deadwood Sandstone plus brecciated, weathered Precambrian granite. In an early study, Clement and Mayhew (1979) referred to the feature as a localized, early Paleozoic differential vertical uplift, although the possibility that the structure was caused by an impact was raised because the structure is totally out of context in the Williston basin. Recent studies have documented the occurrence of shock features in the Deadwood Sandstone and in the granite basement, conclusively confirming the origin of the structure (Forsman and others, 1995; Koeberl and Reimold, 1995). The locally developed lower Winnipeg Shale is identified as the source rock; it was deposited in a small enclosed basin with an anoxic depositional environment. The lower Winnipeg Shale is not present in the high part of the structure, whereas the upper Winnipeg Shale is present throughout the entire basin. However, only the lower Winnipeg Shale is organic rich, and the vast majority of the Ordovician oil found elsewhere in the Williston basin is derived from very thin organic-rich intervals in the overlying Red River Formation. Compared with Red River oil, Newporte oil has a much higher isoparaffin content; it has a higher C_{20}+ content; it is waxy (18–32 (C pour point); and it lacks the marked odd predominance characteristic of the Red River oil. Red River source rocks are dominated by the alga *Gleocapsamorpha prisca*, whereas the lower Winnipeg Shale contains primarily amorphous kerogen. Geochemical analyses run on extracts from the lower Winnipeg Shale verify the oil–source-rock correlation.

AMES STRUCTURE, OKLAHOMA

The Ames structure produces from brecciated granite and brecciated and fractured dolomite of the Ordovician Arbuckle Group. Ordovician shale

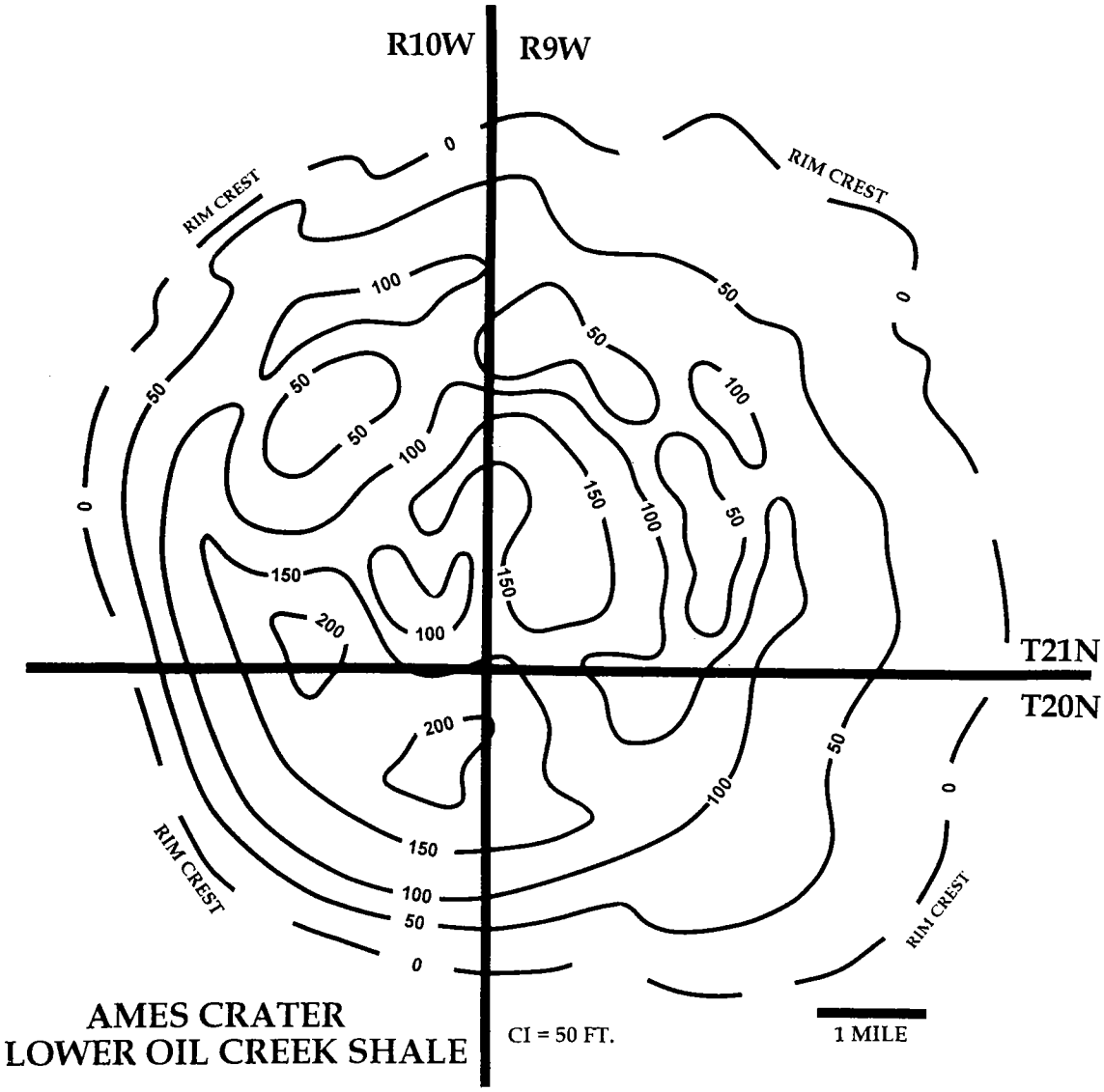

Figure 1. Isopach map of the lower Oil Creek Shale, Ames Structure, Oklahoma

of the Oil Creek Formation in the Simpson Group provides the seal. (This shale has been ascribed to the Oil Creek Formation [early Middle Ordovician], but conodont evidence indicates that a bettter correlation would be to the McLish Formation [middle Middle Ordovician; see Repetski, 1997].) The lower part of the crater-filling shale is the likely source; this unit ranges in thickness from 8 to 225 ft and is restricted to the crater floor (Fig. 1). The upper part of the crater-filling shale is too lean in organic matter (less than 0.5% TOC) to be considered as an oil source. In the D. & J. no. 1-20 James well, TOC averaged 1.56% from the lower crater-filling shale. The Nicor no. 18-4 Chestnut cored the basal segment of the lower crater-filling shale; at this location, TOC averaged 0.82%. Source-rock identification is based on TOC analysis, but the mapping was done on log character tied to the TOC data.

The crater-filling shale is thermally mature for hydrocarbon generation based on reflectance measurements made on solid bitumen. In the D. & J. no. 1-20 James well, solid bitumen reflectance is 0.63%, which has a vitrinite reflectance equivalent (VRE) of 0.90% according to the calibration of solid bitumen to vitrinite reflectance (Landis and Castaño, 1994). Solid bitumen in the Nicor no. 18-4 Chestnut well has a VRE of 0.86%.

Oil produced from the Ordovician sedimentary rocks and the granite at Ames is not like the classic Ordovician oils; instead it is more like the oil produced at Newporte, except that the Ames oil is more mature. The oil at Ames has an API gravity of 36°–37°, and it is waxy with a pour point of 18°–27°C. The oil does not have a strong *n*-alkane predominance; it has a high content of heavier *n*-alkanes and a significant isoprenoid content. Biomarker analysis demonstrates that the oil is fully isomerized. Maturity evaluation based on C_7 hydrocarbon parameters indicates that the oil has a VRE of 0.85%, coinciding very well with source-rock maturity measurements. Source-rock extract analyses agree with the oil data, confirming that the lower crater-filling shale is the hydrocarbon source.

CONCLUSIONS

Meteorite impacts can create depressions into which locally thick, organic-rich sediments can be deposited. The source rocks can be lacustrine or marine and are usually very thin or absent outside the crater. These beds act as seals to adjacent reservoirs, either those created by the impact or conventional ones. Source-rock maturation is not related to impact heating. However, preexisting source rocks can be matured by heat related to an impact, as observed in the Siljan structure. The presence of source rocks greatly enhances the value of an impact crater for hydrocarbon exploration, because a local petroleum system is formed.

REFERENCES CITED

Castaño, J. R., 1993, Prospects for commercial abiogenic gas production: implications from the Siljan Ring area, Sweden, *in* Howell, D. G.; Wiese, K.; Fanelli, M.; Zink, L.; and Cole, F. (eds.), The future of energy gases: U.S. Geological Survey Professional Paper 1570, p. 133–154.

Clement, J. H.; and Mayhew, T. E., 1979, Newporte discovery opens new pay: Oil and Gas Journal, v. 77, June 25, p. 165–172.

Forsman, Nels; Gerlach, T. R.; and Anderson, N. L., 1966, Impact origin of the Newporte structure, Williston basin, North Dakota: American Association of Petroleum Geologists Bulletin, v. 80, p. 721–730.

Füchtbauer, H.; Von Der Breile, G.; Dehm, R.; Förstner, U.; Gall, H.; Höfling, R.; Hoefs, J.; Hollerbach, A.; Hufnagel, H.; Jankowski, B.; Jung, W.; Malz, H.; Mertes, H.; Rothe, P.; Salger, M.; Wehner, H.; and Wolf, M., 1977, Tertiary lake sediments of the Ries research borehole Nördlingen 1973—a summary: Geologica Bavarica, v. 75, p. 13–19.

Hetényi, M.; and Bruckner-Wein, A., 1993, Effect of the micropaleoenvironment to the organic geochemical features of kerogens formed in volcanic crater lakes, *in* Øygard, K. (ed.), Geochemistry poster sessions from the 16th International Meeting on Organic Geochemistry, Stavanger 1993, Falch Hurtigtrykk, Oslo, p. 331–334.

Jones, W. B., 1983, A proposed gas pool in the Pleistocene Bosumtwi impact crater, Ghana: Journal of Petroleum Geology, v. 5, p. 315–318.

Koeberl, C.; and Reimold, W. E., 1995, The Newporte impact structure, North Dakota, USA: Geochimica et Cosmochimica Acta, v. 59, p. 4747–4767.

Landis, C. R.; and Castaño, J. R., 1994, Maturation and bulk chemical properties of a suite of solid hydrocarbons: Organic Geochemistry, v. 22, p. 137–149.

Repetski, J. E., 1997, Conodont age constraints on the Middle Ordovician black shale within the Ames structure, Major County, Oklahoma, *in* Johnson, K. S.; and Campbell, J. A. (eds.), Ames structure in northwest Oklahoma and similar features: origin and petroleum production (1995 symposium): Oklahoma Geological Survey Circular 100 [this volume], p. 363–369.

Roddy, D. J., 1968, The Flynn Creek crater, Tennessee, *in* French, B. M.; and Short, N. M. (eds.), Shock metamorphism of natural materials: Mono Book Corp., Baltimore, p. 292–322.

Vleirboom, F. W.; Collini, B.; and Zumberge, J. E., 1986, The occurrence of petroleum in sedimentary rocks of the meteor impact crater at Lake Siljan, Sweden: Organic Geochemistry, v. 10, p. 153–161.

Wolf, M., 1977, Kohlenpetrographische Untersuchung der See-Sedimente der Forschungsbohrung Nördlingen 1973 und Vergleich mit anderen Untersuchungergbnissen aus dem Ries: Geologica Bavarica, v. 75, p. 127–138.

The Ames Meteorite-Impact Crater

Bruce N. Carpenter
Log Experts
Edmond, Oklahoma

Rick Carlson
DLB Oil and Gas, Inc.
Oklahoma City, Oklahoma

INTRODUCTION

Since the first recognition of an anomalous structural low near the town of Ames, in the southeastern part of Major County, Oklahoma, the origin of this and possibly related subsurface structural features in the area of T. 20–21 N., R. 9–10 W., has been the subject of much speculation. Detailed maps on subsurface horizons from the Devonian up to the Upper Pennsylvanian show an intriguing circular-shaped closure around a low that occupies ≈20 mi^2, approximately centered near the town of Ames. Because drilling in secs. 1 and 2 of T. 20 N., R. 10 W., had revealed an unusually thick and low Hunton (Silurian-Devonian) section, an early characterization of this part of the larger multipay Ringwood field was as the "Hunton graben." Recent deeper drilling has established oil and gas production from the Arbuckle dolomite on a circular rim around this low, leading to its later characterization as the "Ames hole." It was then speculated that this "hole" was an impact or volcanic crater. The presence of the Oil Creek shale (Middle Ordovician)—which seals the structure and directly overlies the Arbuckle Group—indicates that the age of the crater is late Early Ordovician. Figure 1 contains a stratigraphic column for the Anadarko basin. The lower part of the right-hand column has a sketch showing the effect of the crater.

Subsequent drilling and mapping have provided enough new data to confirm that the deep structure is a meteorite-impact crater or astrobleme. Initial Arbuckle wells drilled by J. L. Thomas Engineering, Inc., and DLB Oil and Gas, Inc. (DLB)—now known to be located on the rim of the impact crater—were significant Arbuckle dolomite discoveries; however, the discovery of prolific oil production from brecciated granite, granite wash, and dolomite in wells located on the crater floor has proved to be even more significant.

The first crater-floor well, the D. & J. Oil Co. (D. & J.) no. 1-20 Gregory, sec. 20, T. 21 N., R. 9 W., may be the most productive oil well from a single pay zone in Oklahoma. The pay zone is in an essentially continuous section of brecciated granite that formed as a central rebound structure, a common feature in impact craters larger than a few miles in diameter. More than 200 ft of very effective porosity and very low water saturation combine to provide a conservatively estimated primary recovery of >4 million BO (barrels of oil). The well has produced at state allowable since November 1991. Production from three D. & J. wells (the Gregory, James, and Wayne wells) that share the small structure has totaled 2,101,300 BO and 0.732 BCFG (billion cubic feet of gas) through March 1996. These three wells averaged 1,666 BOPD (barrels of oil per day) during 1995.

Other crater-floor wells have established production from granite overlying brecciated dolomite and from outstanding solution-enhanced porosity and fracture systems that are developed in intact, but not in-place, blocks of Arbuckle dolomite. Oil and gas production from both the rim and the crater-floor features, all sealed by shales within the Oil Creek Formation, will probably make the Ames impact feature the most productive known astrobleme.

BACKGROUND

A structural feature near the southeast corner of Major County, Oklahoma, has been known for years as the "Hunton graben" to geologists who study the subsurface geology of the northern Ana-

Bruce N. Carpenter, Log Experts, 300 N. Broadway, Suite D, Edmond, OK 73034; Rick Carlson, DLB Oil and Gas, Inc., 1601 NW Expressway, Suite 700, Oklahoma City, OK 73118.

Carpenter, B. N., and Carlson, Rick, 1997, The Ames meteorite-impact crater, *in* Johnson, K. S.; and Campbell, J. A. (eds.), Ames structure in northwest Oklahoma and similar features: origin and petroleum production (1995 symposium): Oklahoma Geological Survey Circular 100, p. 104–119.

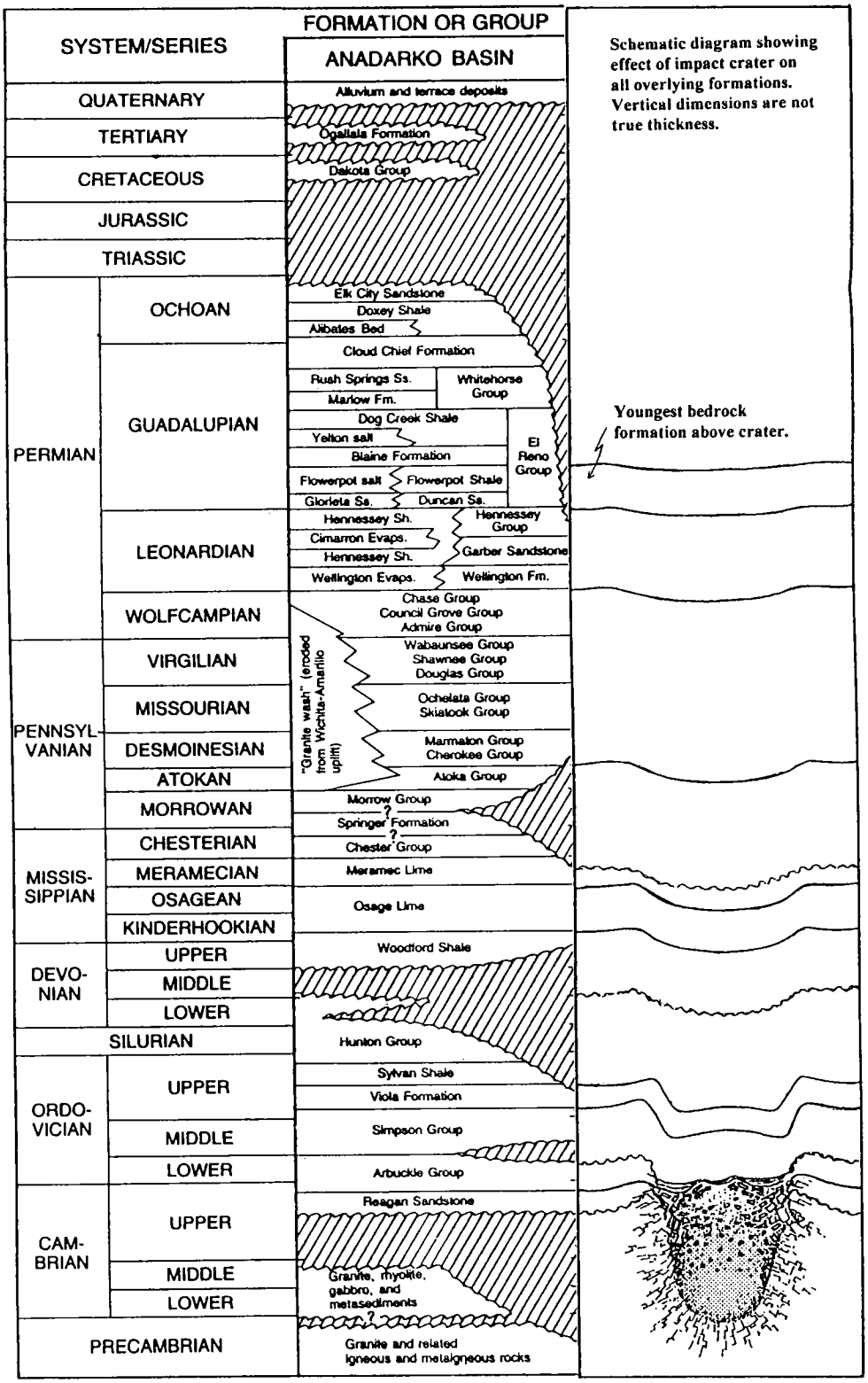

Figure 1. Stratigraphic column for the Anadarko basin. The Oil Creek Formation (Middle Ordovician) is in the lower part of the Simpson Group. The graphic portion has been modified (from Johnson, 1989) to show the formations affected by the impact crater.

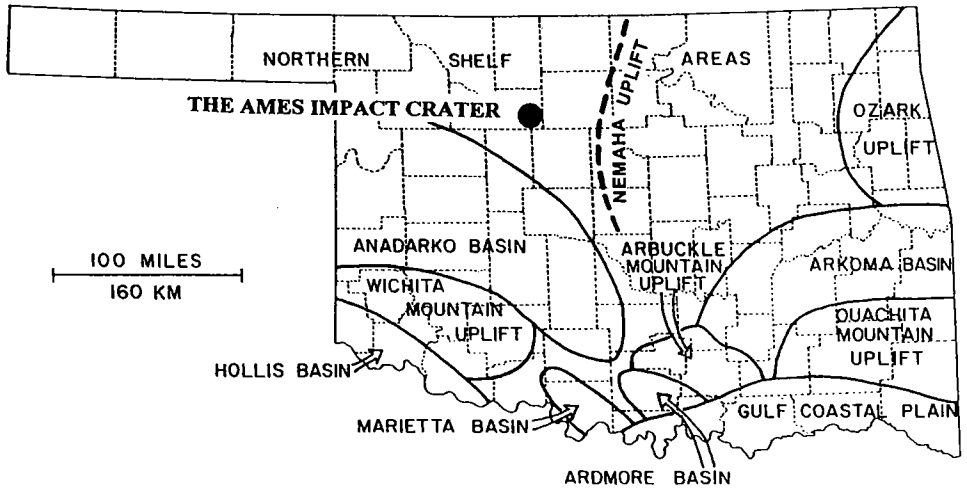

Figure 2. Major geologic provinces of Oklahoma and the location of the Ames structure in the southeast corner of Major County, Oklahoma. (From Carpenter and Carlson, 1992.)

darko shelf area (Smith, 1985). The feature is centered ≈2 mi southwest of the town of Ames. In the local area, the Hunton thickens from 225 ft to as much as 475 ft, and the base of the Hunton is locally as much as 200 ft lower than the regional base. This local preservation of thick and structurally low Hunton carbonates suggests a graben.

It is now recognized that the Hunton graben is a small part of a much larger feature that has become known as the "Ames hole" or Ames structure. This unusual feature has no relationship to known major faults or uplifts, as shown on a current map of major geologic provinces (Fig. 2). The location of an impact structure is random and not determined by the presence of other tectonic features.

A three-dimensional map of the Ames structure (Fig. 3) illustrates features common to impact craters: an outer rim with local closed highs and an interior low, including an irregular central high area that is also characterized by local closed highs (Sawatsky, 1975; Cannon, 1977; Roddy, 1977; Donofrio, 1981; Hartung and others, 1990; Anderson and Hartung, 1992; Kirschner and others, 1992). Although the local structural closures on the outer rim had been recognized on a structure-contour map on the Sylvan Shale (Upper Ordovician), the rim itself was not recognized, nor was its relationship to the deepest part of the structure to the southwest, prior to the construction of the computer-generated model (Fig. 3).

Several Arbuckle tests had been conducted in the area before the actual origin of the feature was identified. J. L. Thomas drilled the Ott no. 1 and no. 2 wells in the SW¼ and SE¼, respectively, sec. 4, T. 21 N., R. 9 W., on mapped north dip. When DLB Oil and Gas, Inc., drilled their no. 27-4 Cecil well in the NW¼ sec. 27, T. 21 N., R. 10 W., these Ott wells were recognized by DLB as being positioned, like the Cecil well, on small structural closures on a common rim surrounding a central low. The realization that a substantial gas and oil column was present in Arbuckle dolomite with significantly enhanced reservoir properties led to early speculation about the origin of the structurally high Arbuckle feature and its possible association with the Hunton graben. A program to lease the Arbuckle rim was conducted essentially by using maps corresponding to the three-dimensional structure (Fig. 3). Later discovery of brecciated granite in the first well drilled to the crater floor provided additional evidence that the crater had been created by the impact and explosion of a meteorite. This interpretation suggested that the rim had been uplifted and fractured by crater-forming processes associated with the impact and that the granite breccia was part of a central rebound feature. A second leasing program targeted the inner ring on the central rebound feature (Fig. 3).

ORIGIN OF THE AMES STRUCTURE

An interpretation for this structural anomaly is as follows. Sometime shortly before or soon after the end of the Arbuckle deposition, a meteorite exploded low over the surface of what is now the southeast corner of Major County, Oklahoma, creating a bowl-shaped crater centered near the present town of Ames. It is apparent that a thickness of ≈2,000 ft of Cambrian–Ordovician carbonate and some basement rock was excavated by the explosion. Basement granite under the bottom of the crater was subjected to sudden and enormous compressive stress; the granite fractured as the result of the exploding meteorite. The granite basement subsequently rebounded, particularly in the central part of the crater (Figs. 3,4). Brecciated granite is the major component of the

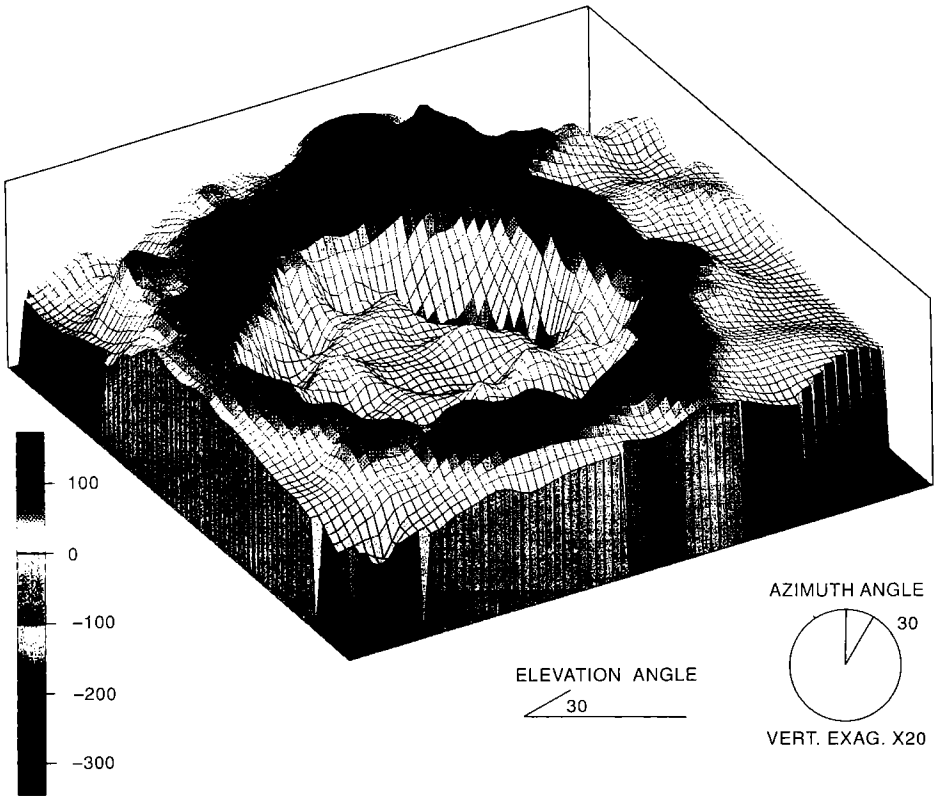

Figure 3. Computer-generated three-dimensional structure map on the top of the Sylvan Shale (Upper Ordovician) showing the effect of the underlying Ames impact structure. View is elevated 30° above the surface and toward the south-southwest with regional dip removed so that the residual surface more clearly shows the nearly circular shape, a distinct outer rim, and the central low that bears an inner ring of local highs. Vertical exaggeration, 20×. Map control is provided by approximately four penetrations of the Sylvan Shale per square mile.

ridges that form the inner ring. Some of the ridges are as much as 1 mi across, 2 mi long, and 1,600 ft thick.

Part of the crater was filled with breccia that had become airborne and fell back after the explosion. That breccia is a mix of basement granite and Arbuckle dolomite rocks. The outer ring, composed mostly of fractured blocks of Arbuckle dolomite, was formed when the inside part of the crater rim collapsed into the central low along arcuate normal faults.

There is evidence that fragments of Arbuckle rock and granite excavated by the explosive event were heated sufficiently to resemble pyroclastic rock (Coughlon and Denney, 1993). Because of such occurrences, it is not uncommon for impact structures to be interpreted as having a volcanic origin (Donofrio, 1981, discussion of fig. 17 on p. 296). Several feet of such pseudopyroclastic rock (Ambers and others, 1997; Fischer, 1997) occurs locally on the crater floor, overlying the more abundant granite and carbonate breccia (Fig. 5). At least two wells several miles outside the rim appear to have penetrated the ejecta blanket. Homogeneous intervals, as much as 90 ft thick, on top of the Arbuckle have log characteristics corresponding to a mix of about 75–85% dolomite and 25–15% granite. There is evidence of an even more widespread occurrence of the ejecta blanket (Mescher and Schultz, 1997).

The rim and breccia highs were exposed to subaerial weathering and erosion. Most of the local ejecta blanket was eroded, and much of it was subsequently deposited on the crater floor. The rim, composed mostly of Arbuckle Group rocks, developed karst features. The highs eroded and were redeposited as carbonate and arkosic clastic layers that occur on the crater floor, lying on top of and infiltrating into the brecciated rock that had previously fallen back into, and partially filled, the crater. A stratified cap of tight dolomite overlies the crater-floor breccia. It may have been some time after the impact before the beginning of deposition of the very fine sediments that would form the overlying Oil Creek Formation. The impact-related strata grade upward into the Oil Creek For-

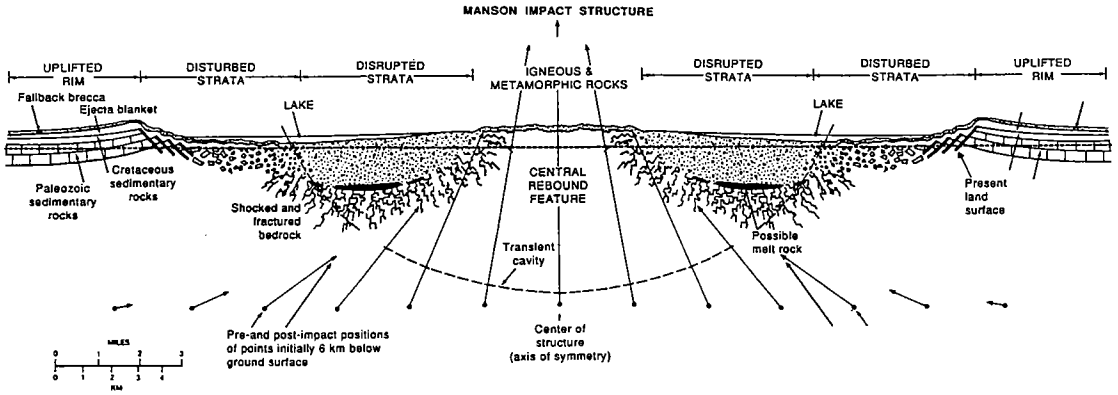

Figure 4. Interpretive cross section of a larger and younger, analogous impact crater near Manson, Iowa. The position of the transient cavity present during formation of the structure is indicated by the curved dashed line. Rough estimates of the movement of material required to fill the transient cavity and produce the central peak are indicated by the arrows. Arrows extending above the ground surface suggest that some material in the rising central peak may have been airborne for a short time before crashing back to Earth and producing an impact breccia. (Modified from Hartung and others, 1990.)

mation. The entire feature is overlain and sealed by Oil Creek shales, forming structural traps that may have held hydrocarbon columns of several hundred feet. The fortuitous presence of a source and sealing shale is critical for the formation of productive astroblemes.

The Ames structure continued to fill during Paleozoic and Mesozoic deposition, and the sedimentary units and underlying breccia continued to compact. Strata from the Oil Creek Formation (Middle Ordovician) through the Flowerpot Shale (Upper Permian) are preserved within and beyond the structural low (Johnson and Smith, 1996, 1997). The closed low is clearly shown in structure maps drawn on the top of the Sylvan Shale (Upper Ordovician) (Fig. 6), on the base of the Woodford Shale (Upper Devonian) (Fig. 7), and on the top of the Checkerboard Limestone Member (Upper Pennsylvanian) of the Coffeyville Formation in the Skiatook Group (Fig. 8). These maps document the continuing subsidence caused by differential compaction and collapse of crater-floor breccia and the progressive filling of the structure by sedimentation.

Astrogeologists Roddy (1977; personal communication, 1992) and P. J. Cannon (personal communication, 1992) have concurred that the feature is an astrobleme on the evidence of its circular shape, the central high composed of fractured crustal rock, the outward-dipping rim, and the presence of shock-metamorphosed quartz (Fig. 9). The documentation of abundant shock lamellae in quartz in cores and samples from crater-floor wells removed all doubt as to the impact origin of the crater, as such lamellae can only be produced by high-strain-rate shock during impact (Sharpton and Grieve, 1990; Sharpton and others, 1990).

EXPLORATION AND DEVELOPMENT

Arbuckle discoveries at Cottonwood Creek (Read and Richmond, 1993), Wilburton (Carpenter and Evans, 1991), and in the subject area have caused renewed interest in drilling exploration wells into the Arbuckle. The Arbuckle dolomite does not normally have significant matrix porosity or permeability, and reservoir size and quality are commonly limited. However, in April 1991, DLB completed the no. 27-4 Cecil well (N¼ NW¼ sec. 27, T. 21 N., R. 10 W.) and discovered excellent flow rates on separate tests for both gas and oil (Fig. 10).

The upper Arbuckle produced gas at a rate of 3,440 MCFGPD (million cubic feet of gas per day), as determined by a drill-stem test in DLB's discovery well. The well was initially completed without stimulation, flowing 300 BOPD from a lower Arbuckle dolomite zone, which was then commingled with a portion of the gas zone. Seismic data indicated closure on the Arbuckle at this location, but the indicated hydrocarbon column exceeded the trap mapped as a local closure. This original closure is now recognized to be a small feature on a much larger structure, the northwestern rim of the crater.

Continental Resources, Inc. (CRI), offset the no. 27-4 Cecil well with their no. 1-22 Mary Ellen well (SE¼ SW¼ SW¼ sec. 22, T. 21 N., R. 10 W.), just across the section line to the north, but the oil-bearing portion of the Arbuckle was less fractured and porous than in the Cecil. A whole core from this interval exhibits many collapsed karst features. The well was finally completed as a gas producer from an interval (ejecta?) near the top of the Arbuckle dolomite.

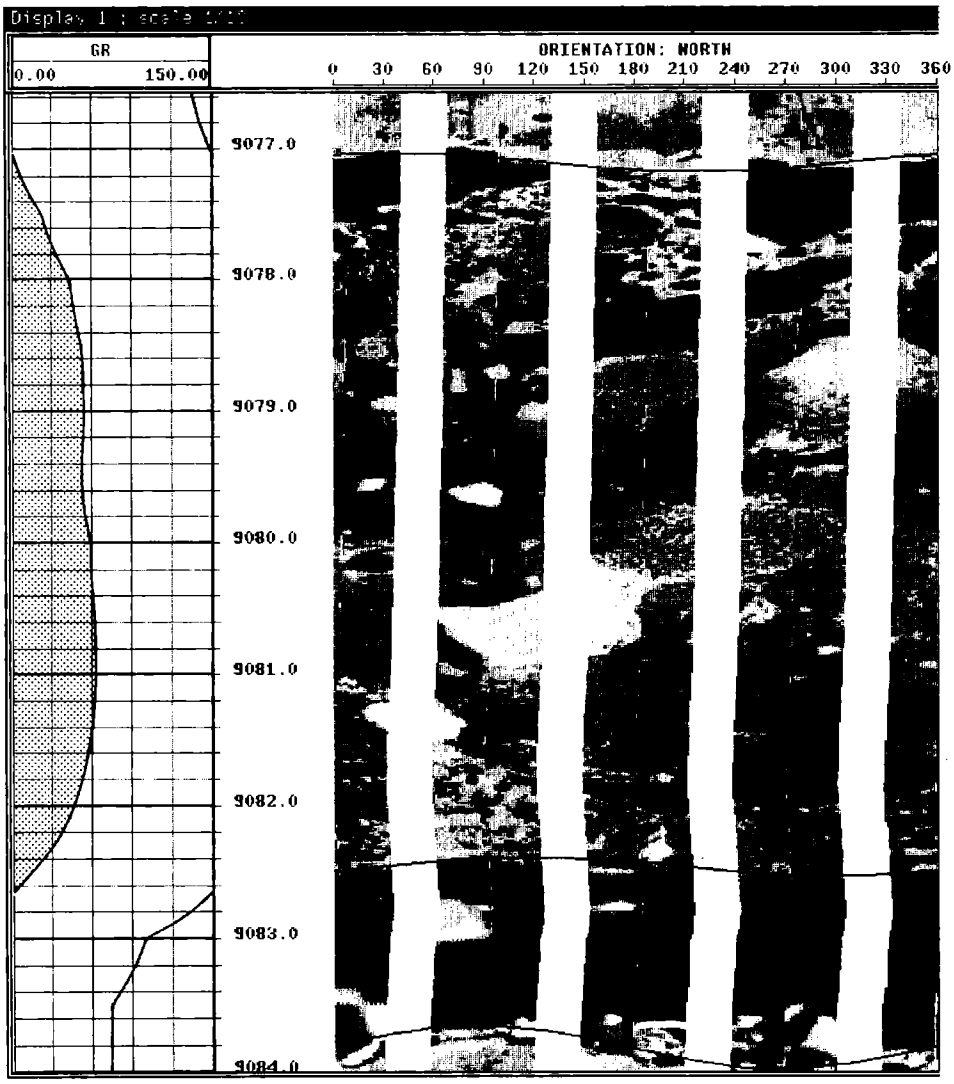

Figure 5. Black and white reproduction of false-color print of one of many FMI logs (Formation Microscanner Image, a trademark of Schlumberger, Inc.) taken in an unidentified crater-floor well in the Ames structure. Sine-wave–shaped lines are oriented dip planes and/or geologic contacts projected onto the image of the bore-hole wall. Units: brecciated Arbuckle dolomite below 9,083.75 ft; cave-fill material (probably from collapse) below 9,082.5 ft (fill consists of dust and microbreccia carried down from above); pseudopyroclastic breccia-to-microbreccia below 9,077 ft; and finely stratified dolomite dust above 9,077 ft. These deposits are overlain, in turn, by Oil Creek shale (not shown). Image has been reduced 50% vertically at the workstation; objects, therefore, appear flattened. Dark areas are the most conductive; white areas are the most resistive. Gamma-ray response at left illustrates very high radioactivity associated with pseudopyroclastic material. Abundant shocked quartz was found in the pseudopyroclastic material.

During this period, DLB completed their no. 28-9 Bierig (NE¼ SE¼ sec. 28, T. 21 N., R. 10 W.), an excellent Arbuckle gas well southwest of their Cecil well. These Arbuckle successes on the crater rim encouraged DLB and CRI to join with D. & J. to drill the first test on a small feature within the crater. This test, completed in November 1991, was the very successful Gregory well (NE¼ NW¼ sec. 20, T. 21 N., R. 9 W.) (Shirley, 1992).

The Arbuckle was expected in the Gregory at a depth of ≈8,800 ft, on the basis of seismic data. At 8,838 ft, below an unusually thick Oil Creek shale, a drilling break occurred with drilling rates reaching <1 min/ft. This very fast drilling was accompa-

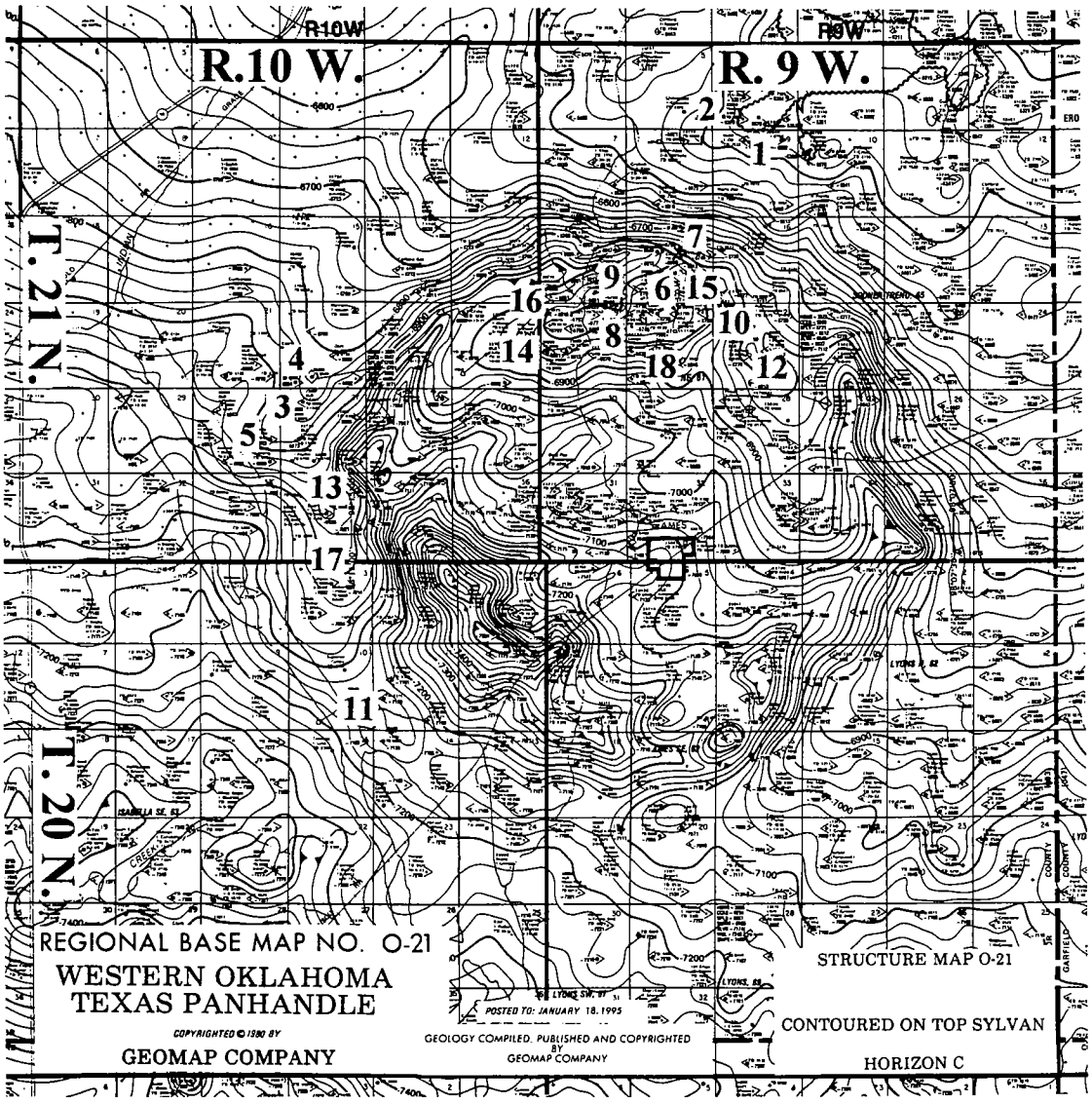

Figure 6. Geologic structure at the top of the Sylvan Shale (Upper Ordovician). (Courtesy of GEOMAP Company.) Contour interval is 25 ft; datum is sea level. The –7,300-ft contour identifies the approximate location of the "Hunton graben." Small, closed circles identify well control for this map. Larger, numbered symbols identify drilling discussed in text. (Also see Smith, 1989, fig. 3.) (1) J. L. Thomas no. 1 Ott. (2) J. L. Thomas no. 2 Ott. (3) DLB no. 27-4 Cecil (discovery). (4) CRI no. 1-22 Mary Ellen (offset to discovery). (5) DLB no. 28-9 Bierig (gas well). (6) D. & J. no. 1-20 Gregory (first well within the crater). (7) D. & J. no. 1-17 Lloyd. (8) CRI no. 1-19 Dorothy. (9) D. & J. no. 1-18 Peggy. (10) CRI no. 1-21 Stansberry. (11) DLB no. 13-11 Allen. (12) DLB no. 21-11 DeHaas. (13) CRI no. 1-34 Terry. (14) CRI no. 1-19 Chet (horizontal extension). (15) D. & J. no. 1-20 James. (16) CRI no. 1-19 Heinrich. (17) CRI no. 6-3 Fisher (plugged and abandoned). (18) D. & J. no. 1-20 Herman (plugged and abandoned).

nied by cuttings of brecciated granite with excellent shows. These cuttings contained abundant shattered quartz and feldspar with cleavage faces, causing the rock to be prematurely characterized as "glass rock" (Hamm and Olsen, 1992). A drill-stem test over the upper 60 ft of the zone flowed 40.4° API gravity oil to the surface at a rate in excess of 50 BOPH (barrels of oil per hour) (Fig. 11). Final flowing tubing pressure (FTP) was 4,025 psi, as compared to a final shut-in pressure (SIP)

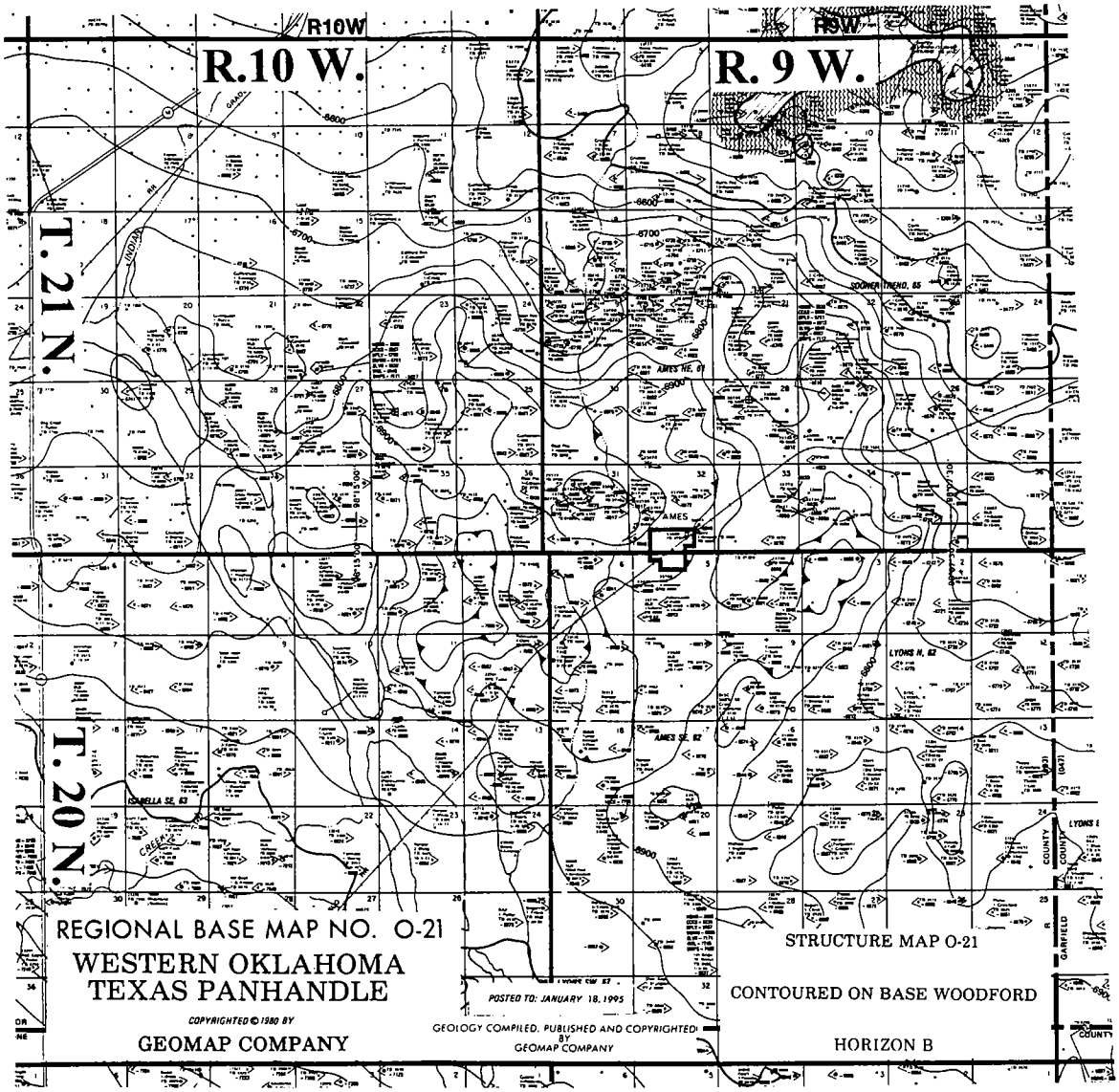

Figure 7. Geologic structure on the base of the Woodford Shale (Upper Devonian). (Courtesy of GEOMAP Company.) Contour interval is 50 ft; datum is sea level. The Hunton graben is shown by two closed contour lines located mostly in secs. 1, 2, 11, and 12 of T. 20 N., R. 10 W., about 2 mi southwest of the town of Ames. Continued compaction and collapse of the brecciated crater fill over long periods of geologic time is typical of impact craters.

of 4,045 psi, a bottom-hole pressure (BHP) of 4,055 psi, and a hydrostatic pressure of 4,181 psi. Surface flowing pressure was 1,200 psi through a 16/64-in. choke. A thickness of more than 320 ft of brecciated basement rock was penetrated without encountering carbonates of the Arbuckle Group. This well produces from only 30 ft of perforations without stimulation. The top perforation is located ≈110 ft below the top of the breccia and well above any indications of water. Initial flow was 713 BO in 14 hours, at a flowing tubing pressure of 1,080 psi with a 18/64-in. choke. No water was produced on any test. A conservative estimate of reserves from the Gregory well is >4 million barrels by primary recovery. Subsequent drilling has established a deeper water level in the granite breccia and suggests a strong water drive. The well has flowed its allowable since completion in November 1991 and produced >113,000 BO and 3,700 MCFG in less than one year without water production or significant loss of pressure. Production is currently reported with two other wells in

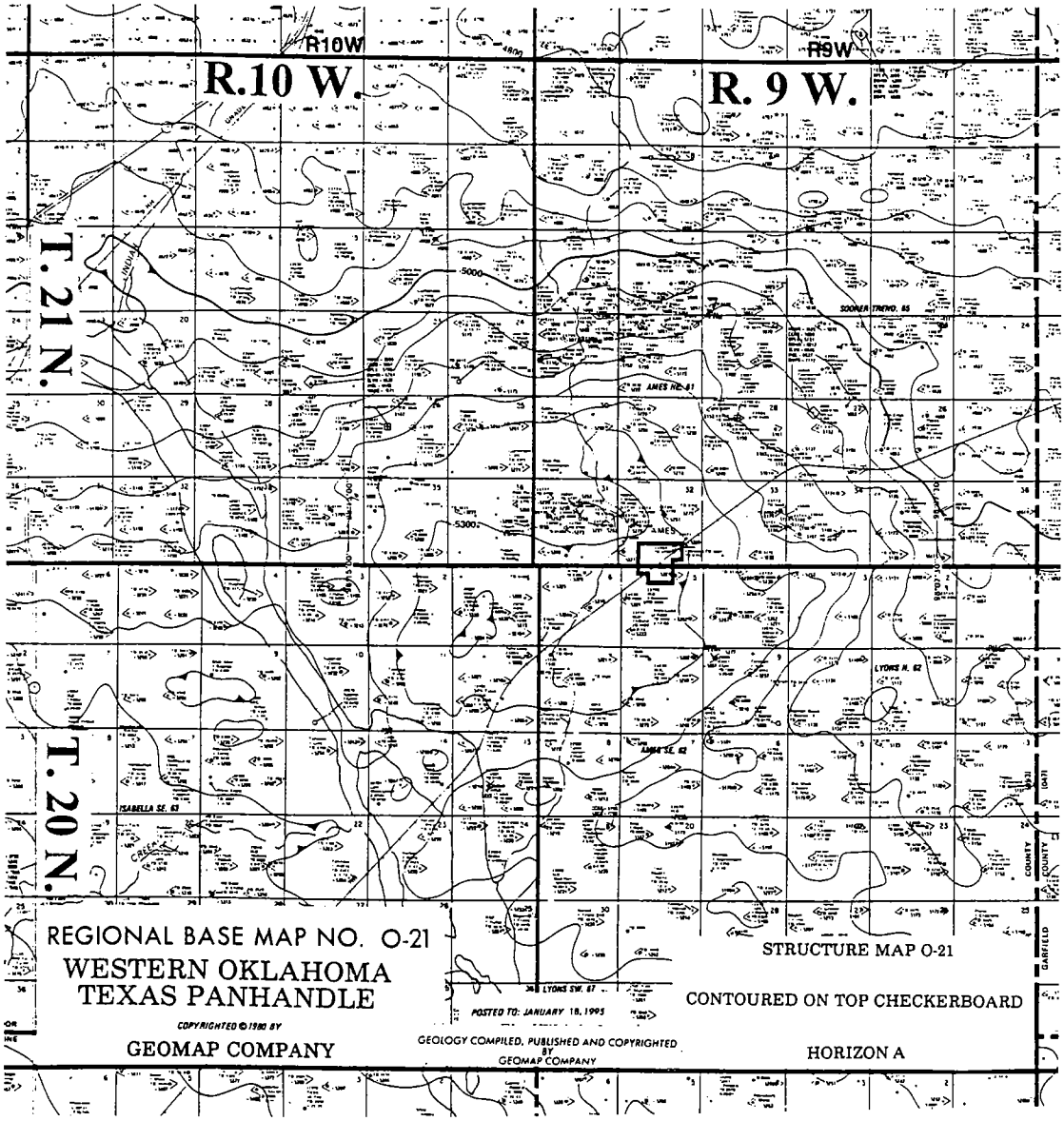

Figure 8. Geologic structure on the top of the Checkerboard Limestone Member (Upper Pennsylvanian) of the Coffeyville Formation in the Skiatook Group. (Courtesy of GEOMAP Company.) Contour interval is 50 ft; datum is sea level. Note that the Cimarron River is deflected to a more southerly course at the western crater rim. A similar deflection from the northeast of Red Fork sandstone (Pennsylvanian) channel deposits can be mapped around the northern rim. Wind-blown sands from the Cimarron River cover most of the southwest part of the crater, but surface indications of the crater have been observed over the north and northeast part of the rim.

the same reservoir. The three wells average 1,666 BOPD.

Cuttings and thin sections of the basement rock were examined, by using scanning electron microscope and X-ray diffraction techniques, to identify the mineral composition. The analysis indicated that the rock is granitic, composed of 31% quartz, 11% potassic feldspar, and 52% sodic feldspar. This analysis was reconfirmed by later examination of rotary sidewall cores from the D. & J. no. 1-17 Lloyd (SW¼ SE¼ sec. 17, T. 21 N., R. 9 W.) drilled to the northeast of the Gregory. The age of the granite is 1,690 Ma, according to Rb-Sr isotopic analysis. This is similar to other basement rock

Figure 9. Shock lamellae in quartz, as seen in a photomicrograph of a thin section of granite from a drilled sidewall core, at about 8,990 ft in the DLB no. 21-11 DeHaas well (sec. 21, T. 21 N., R. 9 W.), in the northeast part of the crater floor of the Ames impact crater (see Fig. 6, no. 12). The large quartz grain exhibits two sets of deformation (strain) lamellae, resulting from high-pressure shock metamorphism. Scale bar is 100 mm. Rock sample provided by DLB Oil and Gas, Inc. (Photograph by Bruce Carpenter.)

dates in the area when adjusted for strontium enrichment from the Arbuckle dolomite (Roberts and Sandridge, 1992).

Several confirmation wells have been drilled. The D. & J. Herman (NE¼ SW¼ sec. 20) to the south also penetrated brecciated granite but was low and encountered water. Two wells to the west, the CRI Dorothy (NE¼ NE¼ sec. 19) and D. & J.

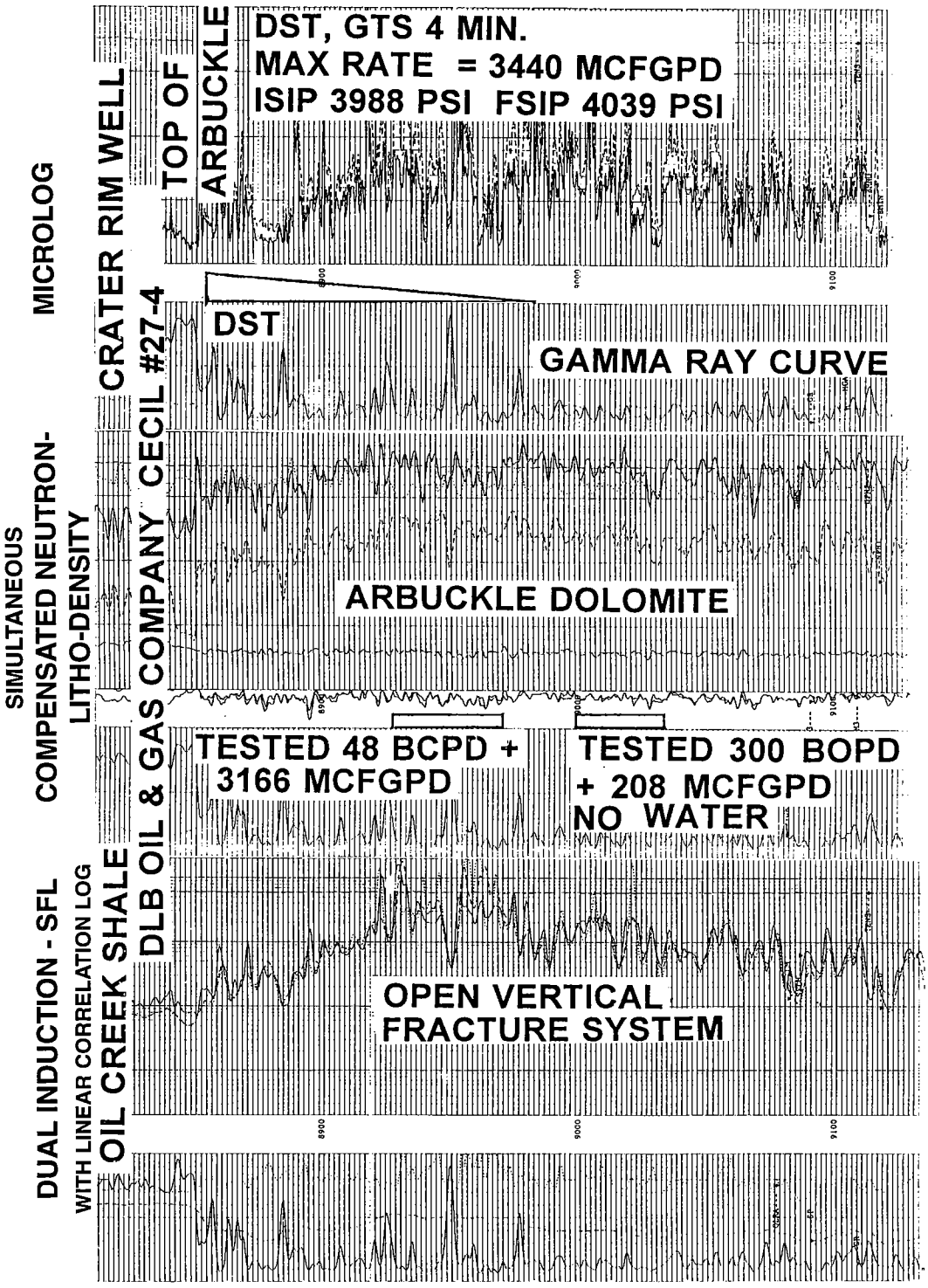

Figure 10. Resistivity log, porosity log, and microlog of two Arbuckle dolomite intervals, tested separately by drill-stem test (DST) and through perforated intervals shown without major stimulation in the DLB no. 27-4 Cecil well, on the western rim of the structure in sec. 27, T. 21 N., R. 10 W.

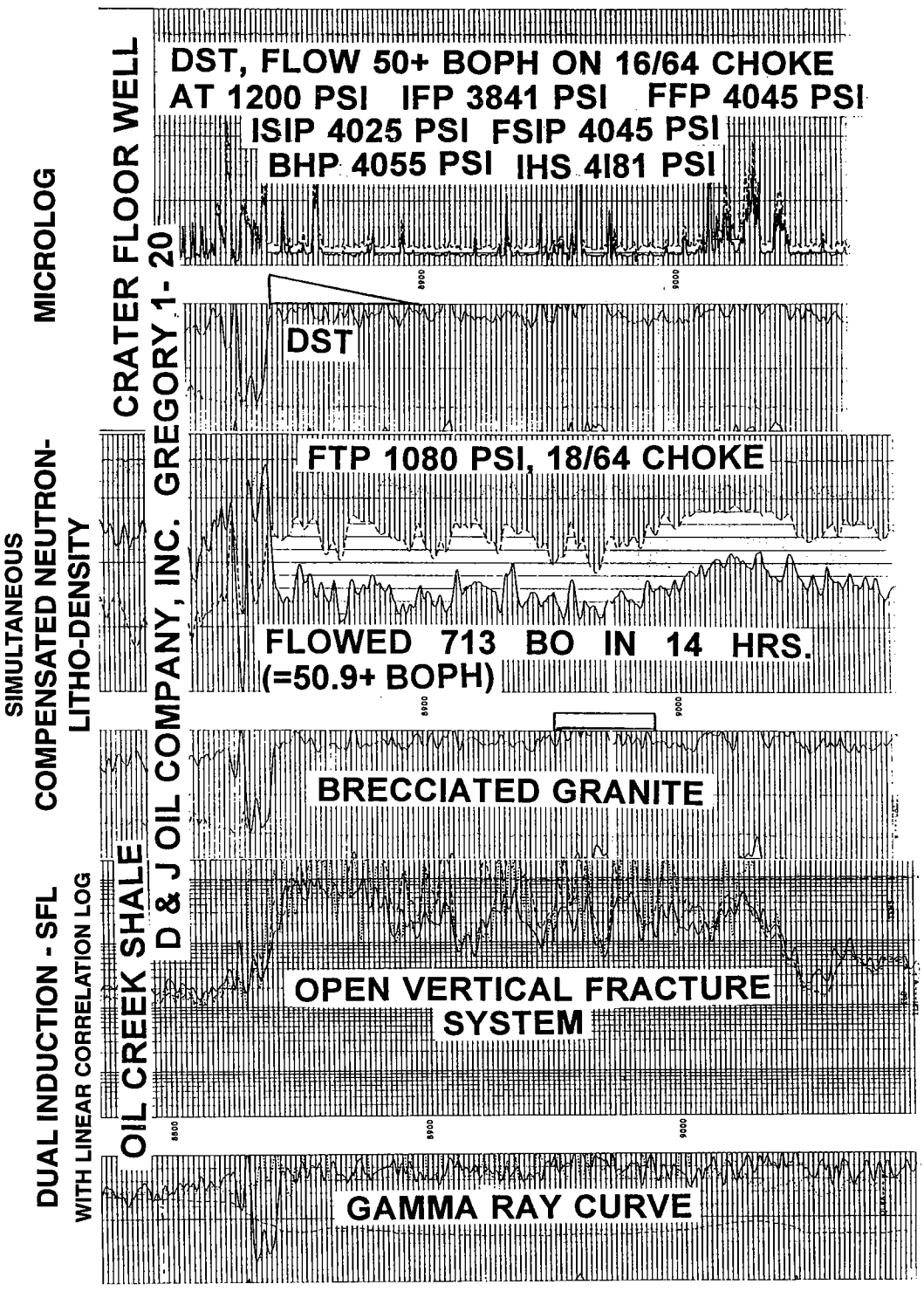

Figure 11. Resistivity log, porosity log, and microlog of two brecciated granite intervals tested separately by DST and through perforated intervals shown without stimulation in the D. & J. no. 1-20 Gregory well, on the crater floor in sec. 20, T. 21 N., R. 9 W.

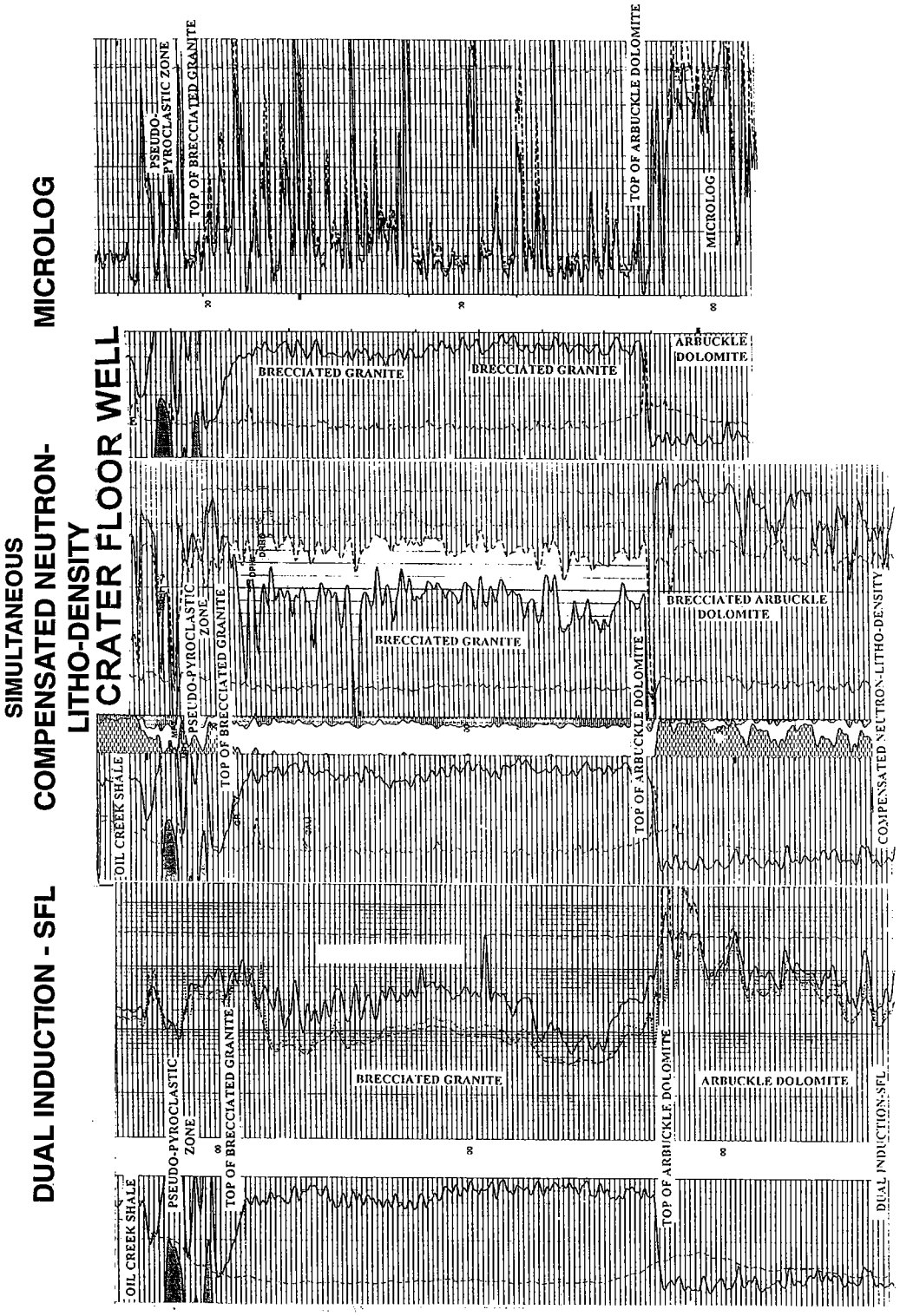

Figure 12. Resistivity log, porosity log, and microlog of part of an unidentified crater-floor well in the Ames structure. Logs support drill-cuttings examination indicating the presence of brecciated granite underlying the Oil Creek Formation and overlying brecciated dolomite of the Arbuckle Group. Brecciation was determined in part from FMI imagery (see Fig. 5).

Peggy (SE¼ SE¼ sec. 18), as well as the D. & J. Lloyd (SW¼ SE¼ sec. 17) to the northeast, are oil productive, although apparently none of the three is producing from the same reservoir as the Gregory well. The Dorothy and Peggy wells are completed in granite wash and in the underlying brecciated Arbuckle dolomite. One well penetrated an abnormally thick section of Oil Creek shale, followed by granite breccia, overlying Arbuckle breccia (Fig. 12). It is apparent that the granite breccia was deposited in this position as the result of mass movement. FMI (Formation Microscanner Image; a trademark of Schlumberger, Inc.) analysis in one well indicated granite talus slides resting at the angle of repose.

The Gregory well continues to flow with little difference between shut-in and flowing tubing pressures. Its direct offset is the D. & J. James, which flowed 492 BOPD from granite breccia. CRI, testing seismic closures, drilled successful offsets of the Gregory well to the east at the Stansberry (SE¼ NW¼ sec. 21) and to the west at the Heinrich (S½ NW¼ sec. 19). However, both of these wells produce from Arbuckle dolomite; each well tested at an initial rate of 50 BOPH. DLB also found Arbuckle production in their Allen no. 13-11 rim well (NE¼ SW¼ sec. 13, T. 20 N., R. 10 W.) on the south side of the structure. They were also successful in establishing production from Arbuckle dolomite breccia in their DeHaas well (NE¼ SE¼ sec. 21, T. 21 N., R. 10 W.). CRI drilled two rim wells on the west side. The Terry (SW¼ NE¼ sec. 34, T. 21 N., R. 10 W.) is an Arbuckle gas well, and the Fisher (SW¼ NE¼ sec. 3, T. 20 N., R. 10 W.) was not commercial.

CURRENT ACTIVITY

As of October 1992, 38 wells had been completed on the Ames feature. Of these, 31 were producing or waiting for production facilities. One of these was a horizontal extension of a vertical hole. Seven have been plugged or temporarily plugged, but some of these may be recompleted in shallower reservoirs or as horizontal extensions. Approximately eight wells were drilling as of November 1992. Locations or spacing and increased density applications are pending with the State Corporation Commission for an additional 90 wells. One company (DLB) accounts for most of these wells and locations. CRI and D. & J. each have 19. A total of 21 companies make up the balance of about 40 additional wells and locations, for a total of 121 potential wells. Many locations await the results of three-dimensional seismic surveys, currently being processed. Others await better completion and stimulation techniques to overcome problems related to high-paraffin crude, early water coning, and possible migration of fines, which may have infiltrated into the open fractures on the rim and breccia on the crater floor. The 1995 well count found that only about 100 wells were actually drilled. Many locations were condemned by poor results from offset wells. Many later wells were drilled where data indicated marginal prospects. These wells diluted the overall economics (Evans, 1997). Many of the early wells are very profitable.

A significant precedent was set with the redrilling of CRI's Chet well (NW¼ NW¼ SW¼ sec. 19, T. 21 N., R. 9 W.). The original crater-floor well was drilled vertically and intersected a hydrocarbon-saturated reservoir in the breccia. CRI made the decision to recomplete the well as a horizontal extension, which intersected the tops of several Arbuckle and granite breccia highs on the crater floor. The well tested >700 BOPD before being shut in to apply for a special allowable. This technique promises to increase production rates and to salvage wells that are structurally low and close to water or that lack sufficient fracturing and dissolution porosity in the hydrocarbon column to produce at commercial rates.

DLB and others acquired three-dimensional seismic data over a structurally complex part of the inner ring near the Gregory well. This approach was intended to reduce the risk of drilling off-structure wells and to provide producing locations that will not be drained by conventional well patterns. The results were complicated by difficulty in tracking the contact between the base of the Oil Creek and the top of the breccia.

The discovery of attractive production in the Ames structure generated considerable renewed interest in these features. Regional and international meetings of the American Association of Petroleum Geologists (AAPG), the Geological Society of America (GSA), and the Society of Independent Professional Earth Scientists (SIPES) formed special sessions to consider these unconventional reservoirs. The March 28–29, 1995, Oklahoma Geological Survey and U.S. Department of Energy workshop on the Ames structure and similar features resulted in the presentation of over one dozen papers and poster sessions. A majority of those attending seemed to firmly accept the impact theories (Petzet, 1995).

ACKNOWLEDGMENTS

We acknowledge the cooperation of DLB Oil and Gas, Inc., and Continental Resources, Inc., for providing well logs and other well data that make the publication of this study possible. We thank Jock A. Campbell for his critical review and helpful suggestions. This paper was first published in the *Oklahoma Geology Notes* (Carpenter and Carlson, 1992).

REFERENCES CITED

Ambers, C. P.; Brändlein, Peter; and Gilbert, M. C., 1997, Petrology of enigmatic rocks from 2.75 km depth in the Ames structural anomaly, Major County, Oklahoma, and their relationship to suevite from the Ries crater, Nördlingen, Bavaria, *in* Johnson, K. S.; and Campbell, J. A. (eds.), Ames structure in northwest Oklahoma and similar features: origin and petroleum production (1995 symposium): Oklahoma Geological Survey Circular 100 [this volume], p. 302–309.

Anderson, R.; and Hartung, J. B., 1992, The Manson impact structure: its contribution to impact material observed at the Cretaceous/Tertiary boundary: Proceedings of Lunar and Planetary Science, v. 22, p. 101–110.

Cannon, P. J., 1977, Meteorite impact crater discovered in central Alaska with Landsat imagery: Science, v. 196, p. 1322–1324.

Carpenter, B. N.; and Carlson, Rick, 1992, The Ames impact crater: Oklahoma Geology Notes, v. 52, p. 208–223.

Carpenter, B. N.; and Evans, M. C., 1991, Comparison of the Arbuckle Group at Wilburton field, Latimer County, with N.E. Alden field, Caddo County, Oklahoma, *in* Johnson, K. S. (ed.), Arbuckle Group core workshop and field trip: Oklahoma Geological Survey Special Publication 91-3, p. 111–132.

Coughlon, John; and Denney, Paul, 1993, The Ames structural depression: an endogenic cryptoexplosion feature along a transverse shear: Shale Shaker, v. 43, no. 4, p. 44–58.

Donofrio, R. R., 1981, Impact craters: implications for basement hydrocarbon production: Journal of Petroleum Geology, v. 3, p. 279–302.

Evans, Jim, 1997, Historical development and production of the Arbuckle and exotic lithologies in the Ames structure, Oklahoma, *in* Johnson, K. S.; and Campbell, J. A. (eds.), Ames structure in northwest Oklahoma and similar features: origin and petroleum production (1995 symposium): Oklahoma Geological Survey Circular 100 [this volume], p. 207–213.

Fischer, J. F., 1997, The Nicor no. 18-4 Chestnut core, Ames structure, Oklahoma: description and petrography, *in* Johnson, K. S.; and Campbell, J. A. (eds.), Ames structure in northwest Oklahoma and similar features: origin and petroleum production (1995 symposium): Oklahoma Geological Survey Circular 100 [this volume], p. 223–239.

Hamm, Harold; and Olsen, R. E., 1992, Oklahoma Arbuckle lime exploration centered on buried astrobleme structure: Oil and Gas Journal, v. 90, no. 16, p. 113–116.

Hartung, J. B.; Kunk, M. J.; and Anderson, R. R., 1990, Geology, geophysics and geochronology of the Manson impact structure, *in* Sharpton, V. L.; and Ward, P. D. (eds.), Global catastrophes in Earth history: Geological Society of America Special Paper 247, p. 207–221.

Johnson, K. S., 1989, Geologic evolution of the Anadarko basin, *in* Johnson, K. S. (ed.), Anadarko basin symposium, 1988: Oklahoma Geological Survey Circular 90, p. 3–12.

Johnson, K. S.; and Smith, Dorothy, 1996, Ames structure reflected in overlying Permian strata: Shale Shaker, v. 46, no. 6, p. 120–123.

_____ 1997, Ames structure of northwestern Oklahoma is reflected in overlying Permian strata, *in* Johnson, K. S.; and Campbell, J. A. (eds.), Ames structure in northwest Oklahoma and similar features: origin and petroleum production (1995 symposium): Oklahoma Geological Survey Circular 100 [this volume], p. 357–362.

Kirschner, C. E.; Grantz, A.; and Mullen, M. W., 1992, Impact origin of Avak structure, arctic Alaska, and genesis of Barrow gas fields: American Association of Petroleum Geologists Bulletin, v. 76, p. 651–679.

Mescher, P. K.; and Schultz, D. J., 1997, Gamma-ray marker in Arbuckle dolomite, Wilburton field, Oklahoma—a widespread event associated with the Ames impact structure, *in* Johnson, K. S.; and Campbell, J. A. (eds.), Ames structure in northwest Oklahoma and similar features: origin and petroleum production (1995 symposium): Oklahoma Geological Survey Circular 100 [this volume], p. 379–384.

Northcutt, R. A.; and Campbell, J. A., 1995, Geologic provinces of Oklahoma: Shale Shaker, v. 46, no. 5, p. 100–103.

Petzet, G. A., 1995, Postulated impact craters yield oil and gas, lively debate: Oil and Gas Journal, v. 93, no. 15, p. 110–111.

Read, D. L.; and Richmond, G. L., 1993, Geology and reservoir characteristics of the Arbuckle Brown zone in the Cottonwood Creek field, Carter County, Oklahoma, *in* Johnson, K. S.; and Campbell, J. A. (eds.), Petroleum reservoir geology in the southern Midcontinent, 1991 symposium: Oklahoma Geological Survey Circular 95, p. 113–125.

Roberts, Craig; and Sandridge, Bob, 1992, The Ames hole: Shale Shaker, v. 42, no. 5, p. 118–121.

Roddy, D. J., 1977, Large-scale impact and explosion craters, comparisons of morphological and structural analogs, *in* Roddy, D. J.; Pepin, R. O.; and Merrill, R. B. (eds.), Impact and explosion cratering, planetary and terrestrial implications: Pergamon Press, New York, p. 185–246.

Sawatsky, H. B., 1975, Astroblemes in Williston basin: American Association of Petroleum Geologists Bulletin, v. 59, p. 694–710.

Sharpton, V. L.; and Grieve, R. A. F., 1990, Meteorite impact, cryptoexplosion and shock metamorphosis; a perspective on evidence at the K/T boundary, *in* Sharpton, V. L.; and Ward, P. D. (eds.), Global catastrophes in Earth history: Geological Society of America Special Paper 247, p. 301–318.

Sharpton, V. L.; Schuraytz, B. C.; Burke, K.; Murali, A. V.; and Ryder, G., 1990, Detritus in K/T boundary clays of western North America; evidence against a single oceanic impact, *in* Sharpton, V. L.; and Ward, P. D. (eds.), Global catastrophes in Earth history: Geological Society of America Special Paper 247, p. 349–357.

Shirley, Kathy, 1992, Overlooked "hole" found: American Association of Petroleum Geologists Explorer, v. 13, no. 5, p. 1, 12–13.

Smith, D. J., 1985, Subsurface geology of the northern shelf of the Anadarko basin, Woods, Woodward, Alfalfa, and Major Counties, Oklahoma: Oklahoma Geological Survey unpublished report.

_____ 1989, Subsurface geology of the northern shelf of the Anadarko basin, *in* Johnson, K. S. (ed.), Anadarko basin symposium, 1988: Oklahoma Geological Survey Circular 90, p. 245–251.

The Ames Structure Reservoirs and Three-Dimensional Seismic Development

Robert Sandridge and Kenneth Ainsworth
Continental Resources, Inc.
Enid, Oklahoma

ABSTRACT.—The Ames structure of Major County, Oklahoma, has been one of the most exciting projects to emerge in the Midcontinent area in this decade. Its impact crater vs. caldera controversy has provided scientific excitement, and its prolific oil and gas wells have provided economic excitement. The Ames structure reservoirs are those oil and gas accumulations trapped in granite breccia and sedimentary rocks in structures generated by the impact of a cosmic body into the Arbuckle Group dolomite surface of the Earth very near where the small Oklahoma town of Ames resides today.

As of January 1, 1995, there were 17 reservoirs that had been tapped by the drill bit: 11 in lithified granodiorite and dolomite breccias, 5 in the Arbuckle dolomite of the crater rim, and 1 substantial accumulation in recrystallized dolomite ejecta on the west rim. Most if not all of the producing Ames structure reservoirs were initiated as subsurface closures, and most were qualified for drilling by two-dimensional seismic studies. In several cases, three-dimensional seismic data have been used in the development of these reservoirs.

Although Continental Resources, Inc. (CRI), has drilled only three wells for stratigraphic traps, in reality nearly all of the reservoirs discovered to date at the Ames structure are stratigraphically trapped. Production is from dolomite and granodiorite breccia rocks; these are clastic units that once stood in topographic relief and now are deeply buried. There is one notable structural-trap reservoir: the Cecil oil reservoir below the terrace fronting the western rim of the crater. This reservoir was discovered by the DLB no. 13-27 Cecil well and appears to be trapped by the closure of a porous bed in the Arbuckle dolomite.

This is the discovery that set off the leasing and drilling frenzy which gave us the subsurface data to define the Ames structure and provide evidence that it is an impact feature. Let us point out the following: at that time, we had only a Sylvan Shale structure map with sufficient well-log control to illustrate the "Ames hole."

The Sylvan Shale is of Late Ordovician age, and in the Ames area, it is 600–1,500 ft above the Arbuckle. That 900-ft range in thickness is the difference between the Ames hole and the Ames structure. These two features are illustrated by computer-generated three-dimensional plots and are used to show the reservoirs' distribution.

To deal with the structural complexities of the crater, CRI, in partnership with DLB and others, acquired four separate sets of three-dimensional seismic data for various exploratory and development projects across the inner crater. Integrated three-dimensional seismic and subsurface control indicated the presence of three separate domed features, called South Meno, Box Canyon, and West Drummond, within the northern part of the crater floor; these have yielded oil and gas in commercially viable quantities from the "Arbuckle/siliceous" unit. In a qualitative way, the data helped suggest which of the two principal reservoir types would be encountered. These data also help to define the crater-rim syncline and to illuminate the relationship between the downward movement of this feature and Silurian–Devonian hydrocarbon traps. Another integrated three-dimensional seismic and subsurface project defined the extent of an additional commercial accumulation within the central rebound area of the crater and directed the development of the Hoyle Creek field.

Although the general level of success using the three-dimensional tool amply justified the expenditures, some drilling failures occurred. Some of these resulted from velocity variations, and others, from event-correlation misinterpretations.

Robert Sandridge, Continental Resources, Inc., Box 122, Marmarth, ND 58643; Kenneth Ainsworth, Continental Resources, Inc., 302 N. Independence, Suite 300, Enid, OK 73701.

Sandridge, Robert; and Ainsworth, Kenneth, 1997, The Ames structure reservoirs and three-dimensional seismic development, *in* Johnson, K. S.; and Campbell, J. A. (eds.), Ames structure in northwest Oklahoma and similar features: origin and petroleum production (1995 symposium): Oklahoma Geological Survey Circular 100, p. 120–132.

INTRODUCTION

Brecciated basement granite is the reservoir rock in the discovery well of crater-floor production in the Ames structure. The D. & J. Oil Company (with Continental Resources, DLB, and others) no. 1-20 Gregory (location shown in Fig. 1) flowed 50 BOPH (barrels of oil per hour) during a drill-stem test of its Arbuckle objective. The interval later proved to be a breccia of basement granite. The Arbuckle rock interval, some 1,600 ft thick in the Ames area, had been replaced by basement granite in the central portion of the Ames structure.

The Ames structure is a horseshoe-shaped structural feature mapped in the subsurface around the town of Ames, Oklahoma. The feature proved to be a meteorite-impact crater, as determined from oil-well drilling data gathered during exploration of the Arbuckle Group across the area.

The Arbuckle Group is of Cambrian–Ordovician age and is the lowest major producing horizon in the state, although locally there is some production from the Reagan Sandstone, which occurs between the Arbuckle and the Precambrian basement. The Reagan is not recognized as such in the Ames area, but probably will be someday and probably will be described as an argillite. Until then, the Arbuckle will be regarded as resting on basement rocks. There are some basement-rock shows (if not production) and Arbuckle production related to basement-rock highs in northeastern Oklahoma (Reeder, 1974; Roundtree, 1991).

The discovery of the absence of Arbuckle rocks—and, in their place, Precambrian granite breccia—in the no. 1-20 Gregory laid the foundation for an impact-crater model for the Ames feature. The breccia, having been formed near the end of or after Arbuckle deposition, rests on the basement granite. Rock types, their distribution, and the reconstructed topographic shape of the feature (similar to an impact-crater model put forth by Roddy and others in 1977) were used to support the interpretation that the Ames structure originated as an impact crater.

Drill cuttings from the no. 1-20 Gregory (Fig. 1) enabled dating of the basement rocks of the Ames structure (Rb-Sr age of 1.692 Ma, by Krueger Enterprises, Inc.) and showed the presence of shocked quartz (recognized by David Roddy, U.S. Geological Survey, and Kevin Nick, Stim-Lab, Inc.) in offset cores. Additional cores and well cuttings have found no volcanic rocks in the area; thus, there is no support to a volcanic origin for the crater. For conclusions that the Ames structure is a "cryptoexplosion" or some other kind of non-impact feature, the reader is referred to other papers (e.g., Coughlon and Denney, 1997) from this workshop, but as for a working model, the impact-crater model works best for us.

Since the oil and gas accumulations have been predominantly localized in the structurally most updip locations, seismic exploration has been one of the main tools used in the selection of drill sites by most of the leading operators drilling in the crater. As three-dimensional seismic technology became a viable and affordable tool, it replaced two-dimensional seismic exploration as the method of choice of active drillers.

AMES STRUCTURE RESERVOIRS

Ames structure reservoirs are those oil and gas accumulations trapped in sedimentary rocks and structures that were created by impact of a cosmic body into the Arbuckle dolomite at the surface of Earth, very near where the small town of Ames is located today. As of January 1, 1995, 17 of these reservoirs had been tapped by the drill bit: 11 in lithified granodiorite and dolomite breccia, 5 in Arbuckle dolomite of the crater rim, and at least 1 substantial accumulation of recrystallized dolomite breccia on the dip slope of the western rim of the crater.

To our knowledge, most, if not all, of the producing Ames structure reservoirs were identified as subsurface closures and were proven by two-dimensional seismic methods. The use of seismic is discussed below.

The no. 1-20 Gregory well was completed in November 1990, flowing from the granite breccia interval, at an allowable of 250 BOPD (barrels of oil per day) (increased later to 500 BOPD), and the quarter section with this well had produced 2.1 million barrels of oil by the end of 1994. Subsequent offsets to this well have logged and cored the producing zone as leached and vuggy Precambrian granodiorite and granite breccia.

Flanking this reservoir are wells that logged and cored leached and vuggy dolomite breccia at an equivalent level. Some of these wells have produced over 250,000 barrels of oil to date (Evans, 1997). There are a number of similar reservoirs in the crater floor, but none so prolific as the Gregory reservoir.

The crater walls and rim rocks also house oil reservoirs, but are logged and cored as Arbuckle dolomite. A prolific gas reservoir (the DLB no. 28-9 Bierig well has produced over 3 BCFG [billion cubic feet of gas]) also was discovered on the rim in a dolomite breccia fallout deposit. For whatever reason, the other oil and limited gas accumulations around the crater rim appear to be in sucrosic dolomite beds.

The Ames structure-floor reservoirs appear to have formed by gravity segregation within huge mounds of brecciated Arbuckle dolomite and basement granite. The bottom waters in the crater-floor deposits were interconnected by various avenues. The crater-rim reservoirs are housed in both brecciated Arbuckle dolomite (possible fallout accumulations) and normal Arbuckle intercrystalline dolomite beds in normal structural closures or rim topographic scarps; all are found in a

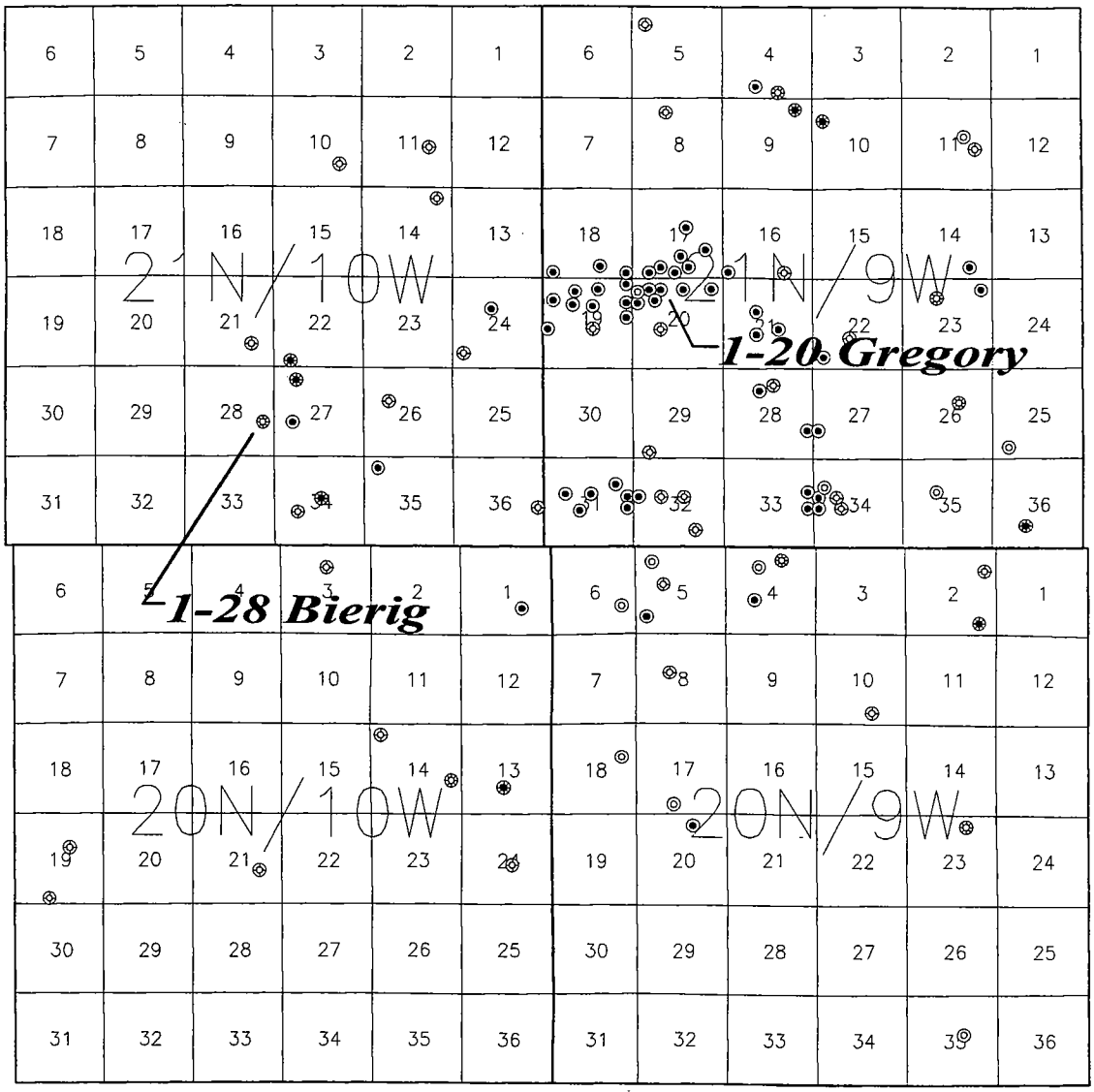

Figure 1. Index map illustrating the location of the Ames structure, with Arbuckle penetrations designated. The map embraces Tps. 20–21 N., Rs. 9–10 W., in Major County, northwest Oklahoma.

position above and outside the crater floor and not connected to the crater-floor water-drive system.

All of the impact-affected sedimentary rocks were modified by the accompanying high temperatures and pressure that created rock melt and hydrothermal fluids. During diagenesis, abundant secondary dolomite (saddle and rhombohedral) and quartz (chalcedony and rock crystal) formed in the fractures and crevasses (especially across the crater floor) between the blocks and grains as hypothermal solutions circulated through the masses of fallback material. Erosion and dissolution by these solutions further modified the void spaces into a permeable network that in some places acts like wide-open fractures and commonly as limited reservoirs. It also appears the hydrocarbons were generated, and even in part destroyed, by the high temperatures and pressures (vesicles within the impact tuff clasts are partly filled with degraded hydrocarbon material). Later, and through time, hydrocarbons were generated and migrated into and through these permeable networks, always seeking the highest level for accumulation.

Because of this unique environment and the erratic distribution of porosity and permeability, the migrating oil-bearing fluids were not able to generate a normal or typical regional oil-water contact and structural relationship, but were dis-

tributed into oil and water pockets, especially in the "blind" cavities. With the restricted delivery of the regional water drive and the dissolved gas in these waters, water would be produced with the oil when these reservoirs were tapped by a well bore. The Gregory reservoir appears to be unique as a classic example of a water-drive reservoir, but the rest of the Ames structure reservoirs appear to be complex for the reasons described above.

Continental Resources, Inc. (CRI), drilled only three wells for stratigraphic traps in the crater area, but in reality nearly all of the reservoirs discovered in the Ames structure area, including the noncrater reservoirs in the Hunton Group and the Mississippi limestones, are in stratigraphic traps. Most of the production comes from dolomite and granite breccias that are clastic units that once stood as low-relief, topographic features on the crater floor.

There is one structural closure of a porous bed in the Arbuckle dolomite below the rim terrace between the crater wall and the rim crest on the west side of the crater. This reservoir is in a fine sucrosic dolomite, with fair intercrystalline porosity and permeability, and has a distinct oil-water contact and solution-gas drive. The reservoir is typical and, indeed, the primary Arbuckle reservoir objective of Oklahoma, and it was found in the typical and primary way: subsurface mapping, seismic studies, and drilling. The discovery well for this reservoir is the DLB no. 13-27 Cecil, which kicked off the leasing and drilling frenzy in 1990 and 1991 in the Ames area. The drilling of these subsequent leases provided the subsurface data to define the Ames structure and provide evidence that it is an impact feature.

The primary and typical Ames structure reservoir is in altered and leached brecciated rock and has an expanding water-drive mechanism. The effectiveness of the expansion depends on the volume of water under pressure and any dissolved gas (Jeff Hume, CRI, personal communication). As in all reservoirs, the effectiveness of the permeability is the controlling factor, and, at Ames, the extreme recovery estimates of these reservoirs vary from 10% to 60%. The high end applies where there is a uniform homogeneous network of pore throats, such as intergranular porosity. At the low end, heterogeneity, where favored directions of flow are dominant, and perched waters and limited reservoir conditions have been encountered.

BASIC PARAMETERS

Subsurface Rocks

The subsurface rocks associated with the Ames structure are identified from borehole drill cuttings and cores. The first rocks were of the Arbuckle Group, which is approximately 1,600 ft thick just outside the crater area. Normal Arbuckle dolomite is primarily light brown, often mottled and laminated gray-brown and black with organic and clay material. In the upper half, it is typically dull and drab and microcrystalline to cryptocrystalline, but some beds are very sandy. In the lower half, it is caramel or chocolate colored, rich in rhombohedral dolomite crystals, and cherty with occasional oolitic chert rock fragments. Some intercrystalline sucrosic porosity is recognized, but not in abundance. Any well-developed porosity, especially at the top of the formation, would call for further investigation. This definitely is the case at Ames.

The brecciated Arbuckle rocks created by the meteor impact at Ames are almost always rich in rhombohedral dolomite and bright in appearance. Much recrystallization is suggested, with scattered saddle dolomite in evidence. It is difficult to differentiate between normal lower Arbuckle dolomite and brecciation dolomite. In some cases, the breccia is "bleached" white, and commonly there is an abundance of secondary quartz in the form of rock crystal or white and translucent chalcedony. Banded and botryoidal chert is a common associate, as well as pyrite, and traces of sphalerite and sulfur have been recognized. An abundance of brown oil staining with "fluorescence and cut" is the indicator of a reservoir.

Some karst breccia of Arbuckle dolomite is suggested in a rim-terrace core, but is not yet thought to be an important rock in the scheme of the Ames structure. This core, from the CRI no. 1-22 Mary Ellen well, is complex in that we recognize normal Arbuckle beds overlain by a karst breccia, which in turn is overlain by a recrystallized fallout breccia or outwash. There appears to be Simpson sandstone and shale as matrix for some of the middle breccia. These findings would indicate karst development, but how could this occur under impact sediments? The "fallout breccia" is gas productive in this well, and the "karst breccia" carries a little oil.

The magic of the Ames structure to the rockhounds is the granite breccia in the well cuttings. When I (R. Sandridge) walked up onto the rig floor of the no. 1-20 Gregory, the "pusher" handed me a handful of cuttings and said "they look like glass." They did, but, under microscopic investigation, the cuttings were over 50% clear quartz with some light gray and white silicates. On the basis of the observance of perthite, these gray silicates were interpreted as plagioclase feldspar, and the rock type was identified as "granite." The cuttings were examined by Kevin Nick at Stim-Lab, Inc., in Duncan, Oklahoma, and the rock was classified as a granodiorite (AGI Data Sheet 48.1).

Continental Resources drilled their no. 1-30 Fred on a deep knob on the crater floor and found oil-saturated, "pink granite" breccia of basement origin. We do not know the significance, but there always seems to be some smashed or leaflike pyrite on the faces of many of the granite breccia grains. There is an abundance of quartz over-

growths on the quartz grains from every core. These granite breccia reservoir rocks were thought to be the best objectives because the dolomite breccia could heal more easily and thus reduce the available pore space, but quartz can heal a granite breccia just as easily, apparently.

Continental Resources drilled their no. 1-19 Dorothy offsetting the no. 1-20 Gregory and found a unique rock type in a sidewall core. Its fabric was that of a welded tuff; most of its clasts were brecciated granodiorite and dolomite, and it had a limited amount of glass and devitrified glass. It contained a lot of light-green bentonite or montmorillonite and chalcedony and chert, some being tripolitic. A spectacular core of this interval was taken at the Nicor no. 1-18 Chestnut.

The no. 1-19 Dorothy core also contained a three-foot-thick bed of dolomitic quartzite overlying the "impact tuff" (a better term than the earlier, unfortunate use of the term "granite wash"). This quartzite bed (which may be a dense siliceous dolomite) caps most of the crater-floor pre-Simpson rocks, and we refer to it as the "cap rock." It also contains numerous shocked quartz grains, the first recognized in the crater.

Another unique rock was cored in the D. & J. no. 1-20 James. This unit lies just above the cap rock discussed above and is a Woodford Shale–like, brown-black greasy shale. It is the oldest Simpson unit within the crater and thickens into the deepest part of the crater. We refer to this interval as the "crater shale" (correlated to the Oil Creek shale in this paper, but see also Repetski, 1997), and we think that it could, in part, be a source bed for the hydrocarbons at Ames. A strange pyritized and carbonized fossil was observed in this shale; it has been examined, but no conclusive identification was arrived at. It could be a graptolite.

Continental Resources has given all their cuttings, and those we kept from the D. & J. wells and several cores, to the Oklahoma Geological Survey. The Survey has made these samples available to the public in Norman, Oklahoma.

Reservoir Rock

Thus, from the foregoing descriptions, there are three reservoir rock types: intercrystalline porosity–bearing Arbuckle dolomite, intergranular and leached porosity–bearing dolomite, and granite breccia. Karst features developed in the exposed Arbuckle beds around the rim of the crater, but karst is not yet recognized as a significant reservoir rock type in the Ames area. The void spaces in the three reservoir rock types appear to be interclastic and range in size from minute to enormous. Avenues of permeability were originally enormous within the unconsolidated breccia of explosion material, but were filled and altered by fluid-flow friction and dissolution, deposition, and cementation to form its present-day complexity.

Hydrocarbon Source

There are two distinct possibilities for the source of the oil: (1) the Arbuckle sediments or rocks, as they were exposed to the "cracking" environment of a meteor impact, and (2) the overlying sediments of the "crater shale" that accumulated within the crater during its early stage of burial by Simpson sediments. Later Simpson sediments are believed to be the source for the gas reservoirs housed in Arbuckle rocks in the Ames area, primarily those in the rim rocks.

Seal or Cap

The seals for the Ames structure reservoirs are obviously the overlying Simpson shales, with the "crater shale" on the floor of the crater being the oldest. There is also the cap rock, described above, that overlies several of the producing reservoirs; it not only sealed the reservoirs below, but would have hindered fluid migration down from above.

Produced Water

Produced waters may have been a travel companion with the oil, coming from perched water, from edge breakthrough, from the oil-water contact, or coning. For the most part, bottom water replaces the produced fluids. Water breakthrough is possible through fracturelike avenues between very coarse to huge blocks of disoriented target rock. Water analysis indicates that chloride concentrations average 157,000 ppm; the water resistivities are 0.022 Ω at 165 °F. There are no major production problems reported in the area.

THREE-DIMENSIONAL SEISMIC EXPLORATION

Continental Resources, Inc., began a program of two-dimensional seismic acquisition in 1990. These data were used in the selection of the earlier drill sites; the locations of the seismic lines are shown in Figure 2. After the drilling of the Gregory discovery well, a flurry of drilling activity took place, with the purpose of duplicating the discovery well's success. This drilling was driven by a combination of Sylvan Shale structural control and two-dimensional seismic data, with resulting mixed success. Late in 1992, after a series of dry holes and marginally commercial wells, leading operators in the play, principally CRI and DLB, concluded that the Ames feature was an appropriate site at which to try three-dimensional seismic technology. It was hoped that through the application of this tool, some determinations could be made about the varying lithology of the granodiorite and Arbuckle dolomite breccias. At the least, it was hoped that a better structural interpretation would enable operators to avoid the seismically obvious low-structural positions that almost guarantee nonproduction.

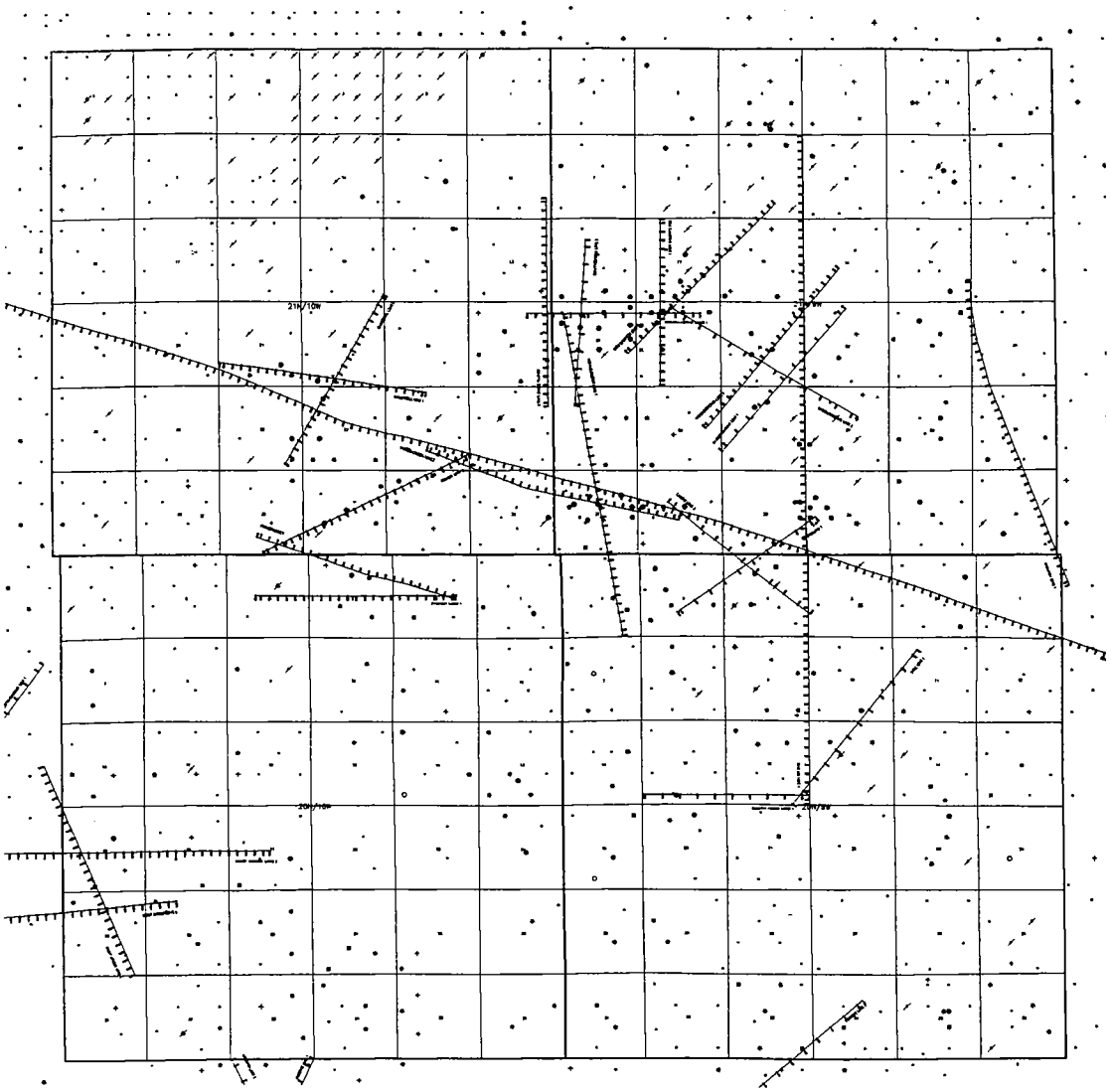

Figure 2. Index map illustrating two-dimensional seismic data acquired by Continental Resources, Inc., principally before the drilling of the Gregory discovery well.

Fairly generic and consistent parameters were used in all of the surveys made within the crater. Deep-shothole dynamite charges were used by all the surveys as an energy source. Standard brick patterns with 110 × 110 ft bins and 12-fold nominal multiplicity were established as appropriate acquisition-geometry templates for all projects prior to actual recording. Although the Ames feature is situated in a rural area, many of the water-supply wells for the city of Enid are located in and around the town of Ames. Consequently, substantial rearrangement of both source and receiver stations became necessary. That the data quality remained high, despite the nonideal field layouts, demonstrates the dynamic nature of the three-dimensional seismic tool.

Data processing primarily involved standard procedures. Static corrections included both refraction-based and surface-consistent methods. Two passes of velocity analyses handled dynamic corrections. Very weak spatial filtering eliminated much of the random noise associated with the acquisition process. Single-pass migration methods were used to help collapse all diffractions and Fresnel zones.

Four separate surveys were recorded in which CRI was either the operator or a participant. The locations of these surveys are shown in Figure 3.

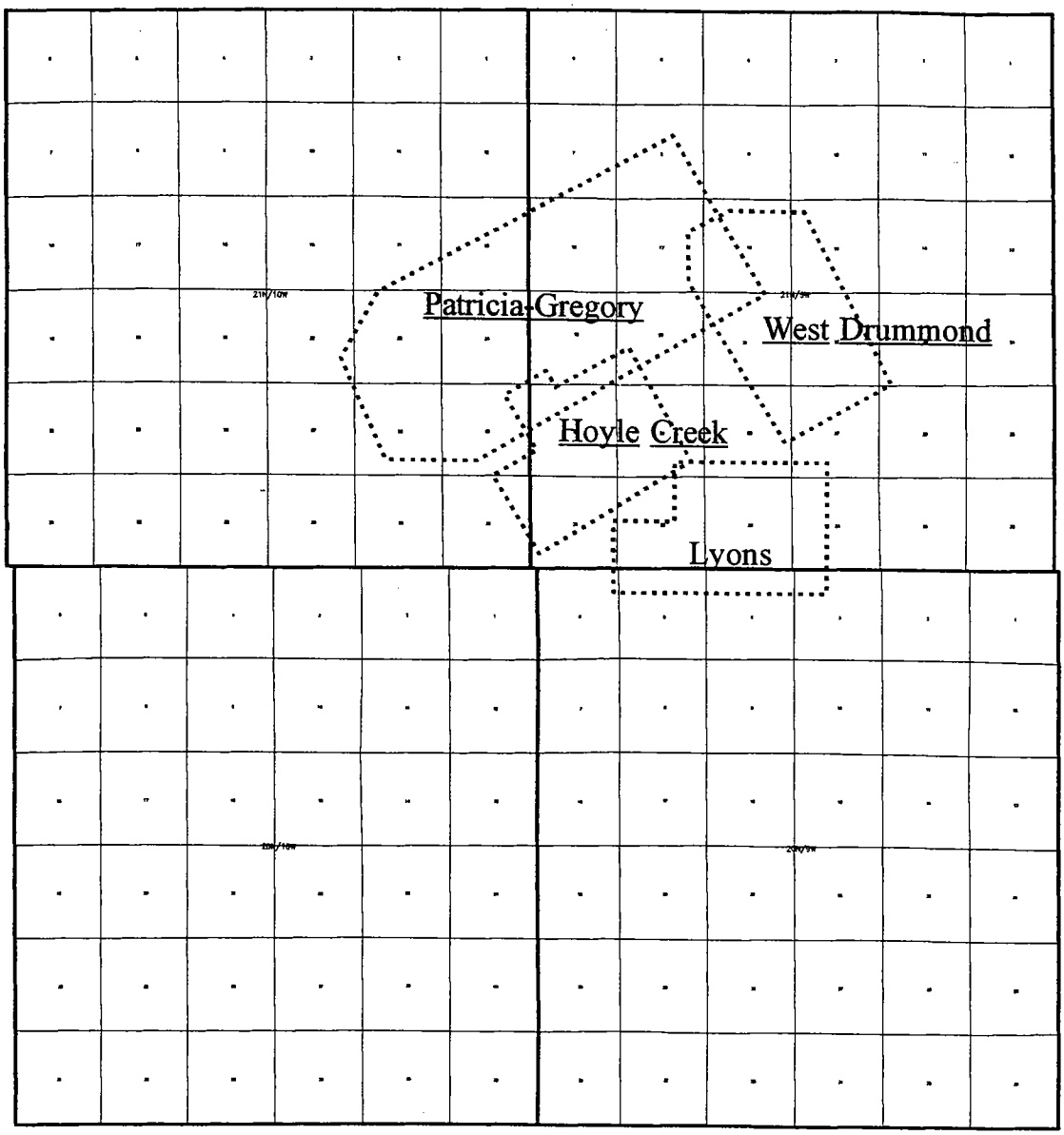

Figure 3. Index map illustrating the areal extents of the four separate three-dimensional seismic surveys in which Continental Resources, Inc., was involved.

Hoyle Creek, the first survey, was situated over the central-rebound area, in which oil production comes from fractured Precambrian granite. Later surveys were shot over the West Drummond area, along the northeastern rim syncline, the Lyons area, and finally the Patricia-Gregory project, which covers the largest and most prolific Arbuckle oil production in the Ames area. Each of these surveys aided in further unraveling the structural complexities of the crater. The Patricia-Gregory and West Drummond surveys were merged in processing, and thus are treated as a single project. The Lyons survey was tested only once, with a resulting dry hole. Further work was never done. Hence it is not treated in this discussion.

Figure 4 shows an arbitrary line out of the Patricia-Gregory and West Drummond project that illustrates most of the various components of the Ames structure rather nicely. This line illustrates most of the key features of the complex crater, from the western crater rim on the left, to the rim syncline, to the crater floor, to the northeast-

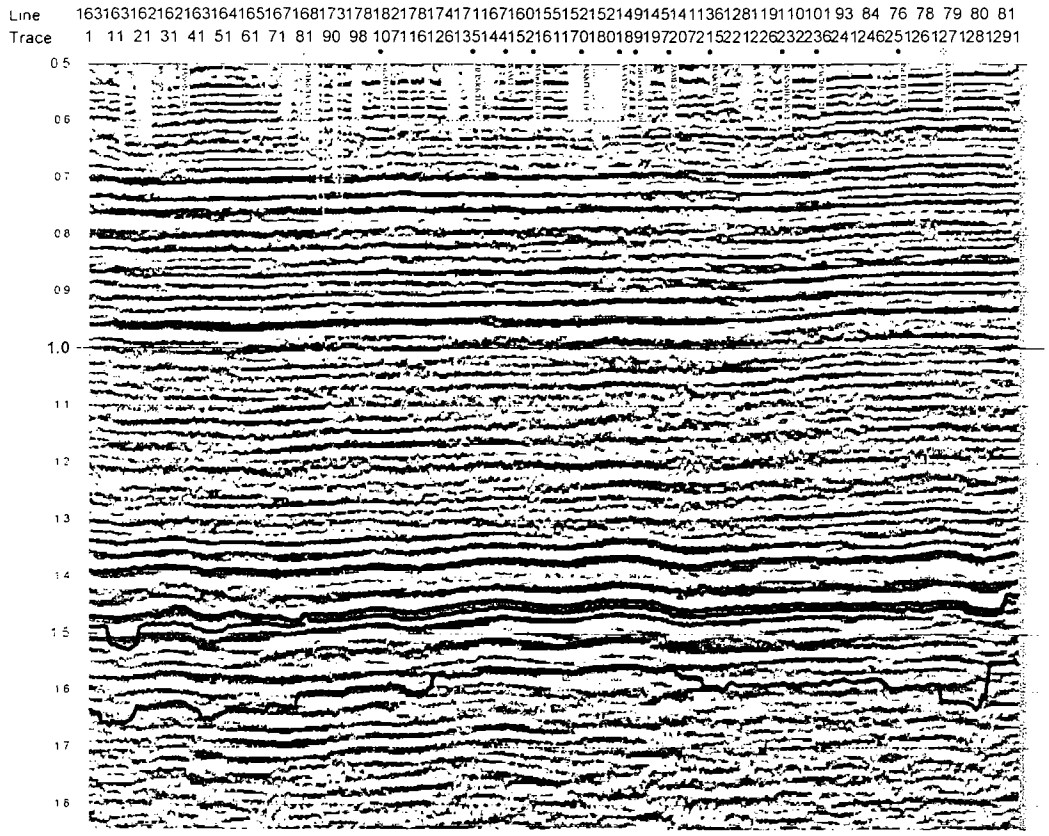

Figure 4. East-west–oriented arbitrary vertical line out of the Patricia-Gregory survey showing the primary components of the crater, including west rim, west-rim syncline, crater floor, east rim syncline, and east rim.

ern rim syncline, and then to the eastern rim on the right.

Figure 5 is a larger-scale display of the northwestern section of the crater, showing a localized structural high within the rim syncline. A deep test drilled by Continental Resources, the no. 2-26 Mason, encountered oil shows in the Arbuckle dolomite section, but no reservoir rock; the well was subsequently plugged and abandoned. To the east of the rim syncline, the seismic line shows the easternmost of four relatively high structural areas within the northern crater floor. Drilling by DLB at their Patricia location resulted in saltwater recovery in the Arbuckle dolomite. At the apex of the feature, CRI's Gladys well encountered oil production, although the dolomite reservoir was incapable of delivering at high rates.

Figure 6, an expanded version of the central section of Figure 4, illustrates the two principal producing features of the Ames structure. To the west, the so-called South Meno feature produces from Arbuckle dolomite, with some of the best producing rates out of the carbonate facies in northern Oklahoma. At the CRI Marita location, the granodiorite breccia facies begins to be developed atop the dolomite and thickens eastward through the D. & J. Wayne and Gregory tests, then thins until it is gone at the D. & J. Marvin location. Although some geophysicists have claimed to be able to identify a distinguishing "granite" signature on seismic records, we have not seen indications of a reliable, consistent seismic character. A number of both compressional and shear-wave sonic logs have been run in drill holes across the crater which suggest that, unfortunately, the lithologies' acoustic characteristics are too similar to expect a dependable change in the key reflectors.

The dip components of the crater morphology are represented in Figure 7. This seismic section shows the key trapping fault between the D. & J. Herman and J. D. locations. To the north, the reversal into the rim syncline is clear, as is the climb into the northern rim. It is of note that the Hunton thickening in the rim syncline can be easily seen in this display. This graben-type syncline resulted in preserved porous Hunton dolomite that provided for commercial oil and gas accumulations. Although data quality is generally good, the reflector offset at faults between the basal Oil Creek reflector and that of new reflections in the Oil

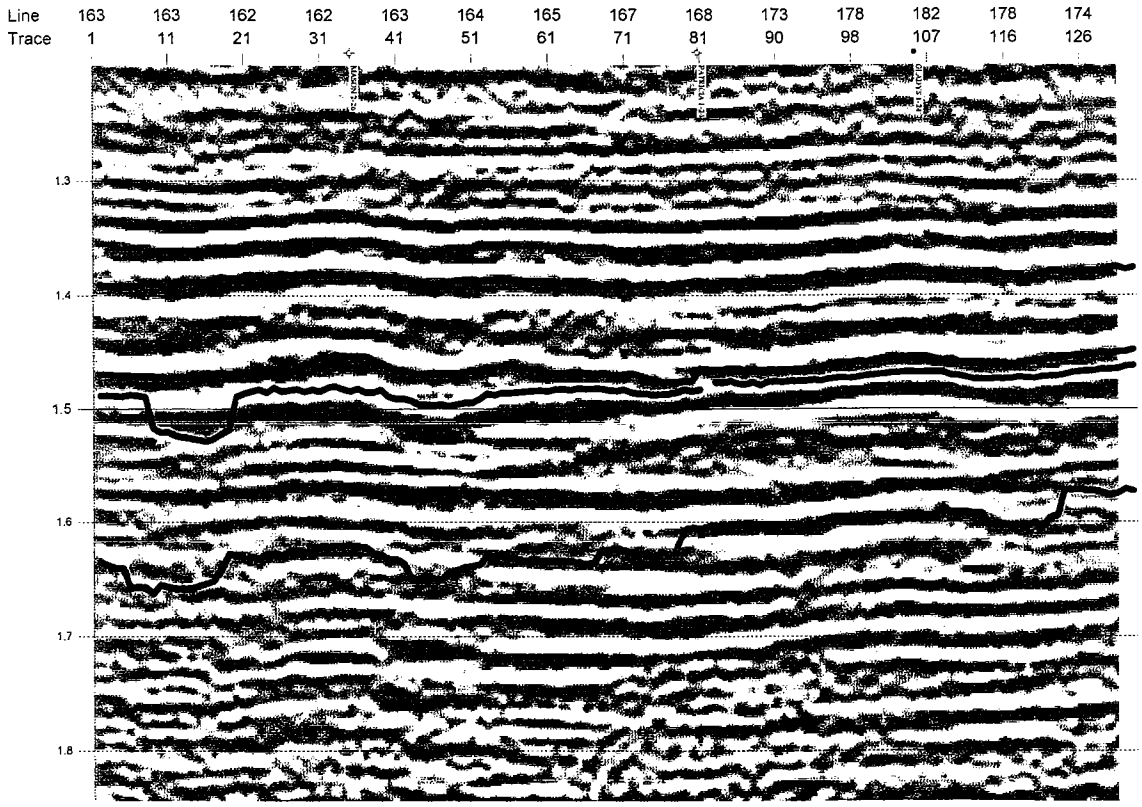

Figure 5. Eastern segment of arbitrary line in Figure 4, more clearly showing the east rim, rim syncline, and eastern crater-floor morphology.

Creek section adjacent to and across the faults is often extremely subtle to detect even on the three-dimensional data sets and virtually impossible on some two-dimensional data sets. Consequently, the change in the reflector character of the interface between the Sylvan Shale and Viola Formation is often a much more reliable indicator of those faults. This change can be seen at SP 140/184 at a time of 1.475 s in Figure 7. The Herman and Gregory wells were both drilled with reliance on the two-dimensional data, and the separating fault was not anticipated. What was expected to be a loss of perhaps 50 ft of structure at the Herman location proved to be a greater loss.

The time slice illustrated in Figure 8 cuts the data volume at the pay horizon in the Gregory, Wayne, and Sam well bores. The general configuration of the crater structural features is evident, with the succession of relatively high structural features displayed. The basal Oil Creek time structure shown in Figure 9 further demonstrates the key features of the crater floor itself. With the rim syncline girding the south-dipping crater floor to the north, it is easy to envision why the very large area of continuous production exists from the Gladys to the Stansberry areas. The rim syncline provided an ideal trapping mechanism for Arbuckle oil locally migrating out of the basin.

Some of the key objectives to using three-dimensional seismic data are reasonably straightforward to examine. Does it provide the interpreter with a better mental image of the feature being surveyed? Does it enable better drilling decisions? Are the results of those decisions cost effective? Although a host of statistics could be presented by which to analyze the appropriateness of the tool within the Ames structure, one simple statistic probably is most useful in evaluating its effectiveness. With about the same number of CRI-operated wells drilled before and after the implementation of a three-dimensional seismic data acquisition program in the Ames structure, the company's daily production nearly tripled after use of that seismic data. The reserves added by the no. 1-19 Sam alone more than paid for any seismic costs incurred in the Ames area. Furthermore, within the limits of those surveys where it has data, the company feels it understands quite well what its future opportunities are and what the risks associated with those opportunities are. By almost anyone's standards, the use of three-

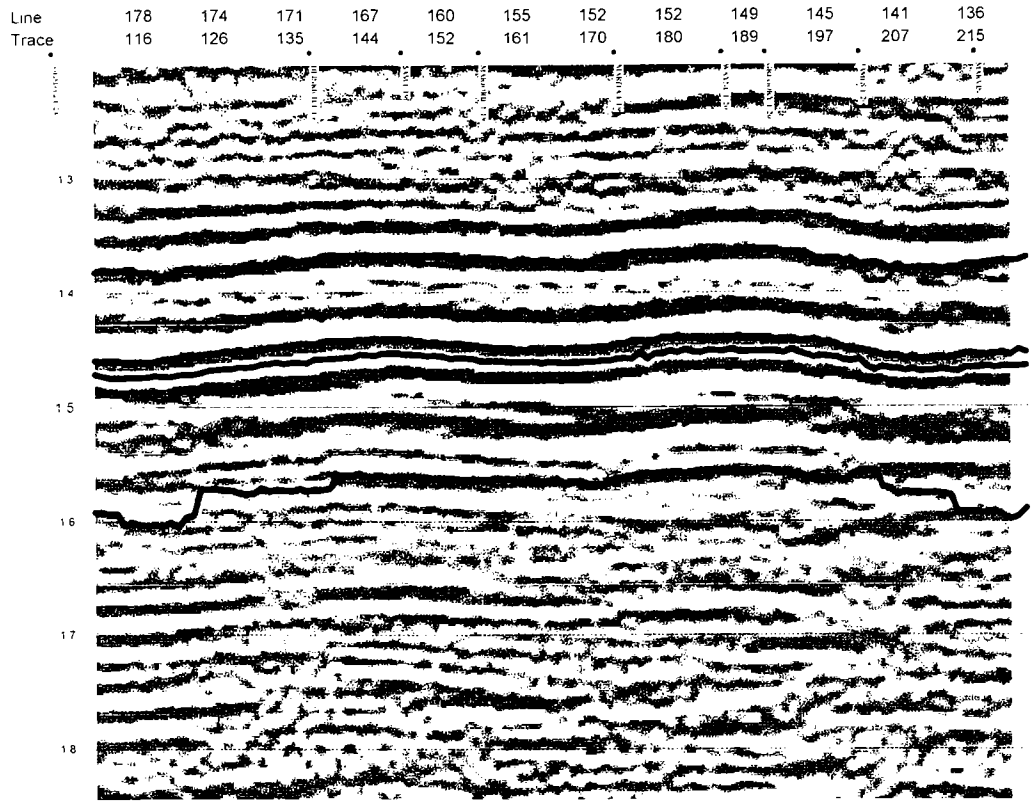

Figure 6. Central segment of arbitrary line in Figure 4, showing the morphology of the crater floor in the area of densest drilling to date, including a crossing of the Gregory at line 148/trace 190.

dimensional seismic data in the Ames area has been a successful venture.

PRODUCTION CHARACTERISTICS

Producing from a water-drive reservoir, such as the no. 1-20 Gregory, is simple, but concern must be given to the placement of the original perforations and setting production rate to restrict water coning. D. & J. chose to perforate just above the oil-water contact and produce the reservoir by "floors." Like an elevator, you stop at each floor and shop, working your way to the top. Working with the state commission for the most efficient rate (MER) of production is a good policy.

Producing a "hindered" water-drive reservoir (from a trickle up to open floodgate performances) gives the engineers something to do. Sometimes the more water you make, the more oil you make; other times trying to shut the water off is more effective. Shutting off water from the Ames structure wells has proved most difficult. Select perforating has not proved too effective, either. It appears that the difficulty lies in trying to figure out a completely heterogeneous reservoir rock. The first thing you need is a disposal well and reasonable offset operators. There are tight breccias also, which are worse. Porosity and permeability values as such are not so important, but determining their effectiveness and distribution is.

CONCLUSIONS

1. The basic procedure for searching for impact craters involves subsurface mapping for rings and basins, modeling porosity and permeability distribution, and seismic definition. This basic procedure has not changed in 35 years.

2. On the basis of examination of cuttings and cores from 50 wells in the Ames area, the subsurface feature on structure maps of the Ames area having the appearance of a crater is the result of a meteorite impact of the Arbuckle dolomite, leaving mounds of brecciated Arbuckle and basement rock for the accumulation of migrating hydrocarbons. Most of the reservoirs at Ames are the result of this impact crater.

3. The impact cratering process results in unique structures and extensive fracturing and brecciation of the target rock that can be conducive to hydrocarbon accumulations.

4. The use of three-dimensional seismic data

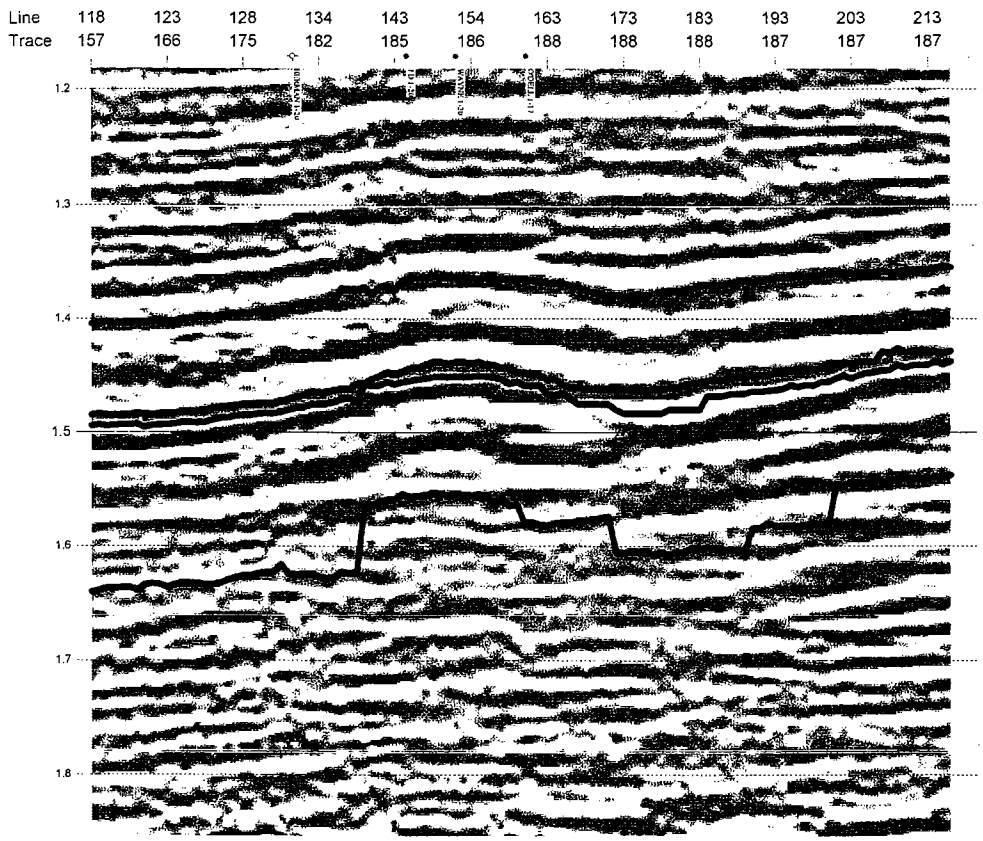

Figure 7. Arbitrary north-south vertical section showing crater morphology from near the central rebound structure, north across the crater floor, into the north-rim syncline, then onto the north rim.

within the Ames structure provided a more comprehensive visualization of the morphology of those parts of the crater that were surveyed.

5. The use of three-dimensional seismic data within the Ames structure enabled those operators employing the tool to make more informed drilling decisions. Consequently, their commercial success exceeded their success levels before they obtained the three dimensional data.

ACKNOWLEDGMENTS

Although we disagree with the interpretation of John P. Coughlon and P. Paul Denney (1997) on the origin of the remarkable rock type in the core from the Nicor no. 1-18 Chestnut, we thank them for graciously allowing us access to the core for study.

SELECTED REFERENCES

Coughlon, J. P.; and Denney, P. P., 1997, The Ames structure and other North American cryptoexplosion features: evidence for endogenic emplacement, *in* Johnson, K. S.; and Campbell, J. A. (eds.), Ames structure in northwest Oklahoma and similar features: origin and petroleum production (1995 symposium): Oklahoma Geological Survey Circular 100 [this volume], p. 133–152.

Donofrio, R. R., 1981, Impact craters: implications for basement hydrocarbon production: Journal of Petroleum Geology, v. 3, p. 279–302.

Evans, Jim, 1997, Historical development and production of the Arbuckle and exotic lithologies in the Ames structure, Oklahoma, *in* Johnson, K. S.; and Campbell, J. A. (eds.), Ames structure in northwest Oklahoma and similar features: origin and petroleum production (1995 symposium): Oklahoma Geological Survey Circular 100 [this volume], p. 207–213.

Fischer, J. F., 1997, The Nicor no. 18-4 Chestnut core, Ames structure, Oklahoma: description and petrography, *in* Johnson, K. S.; and Campbell, J. A. (eds.), Ames structure in northwest Oklahoma and similar features: origin and petroleum production (1995 symposium): Oklahoma Geological Survey Circular 100 [this volume], p. 223–239.

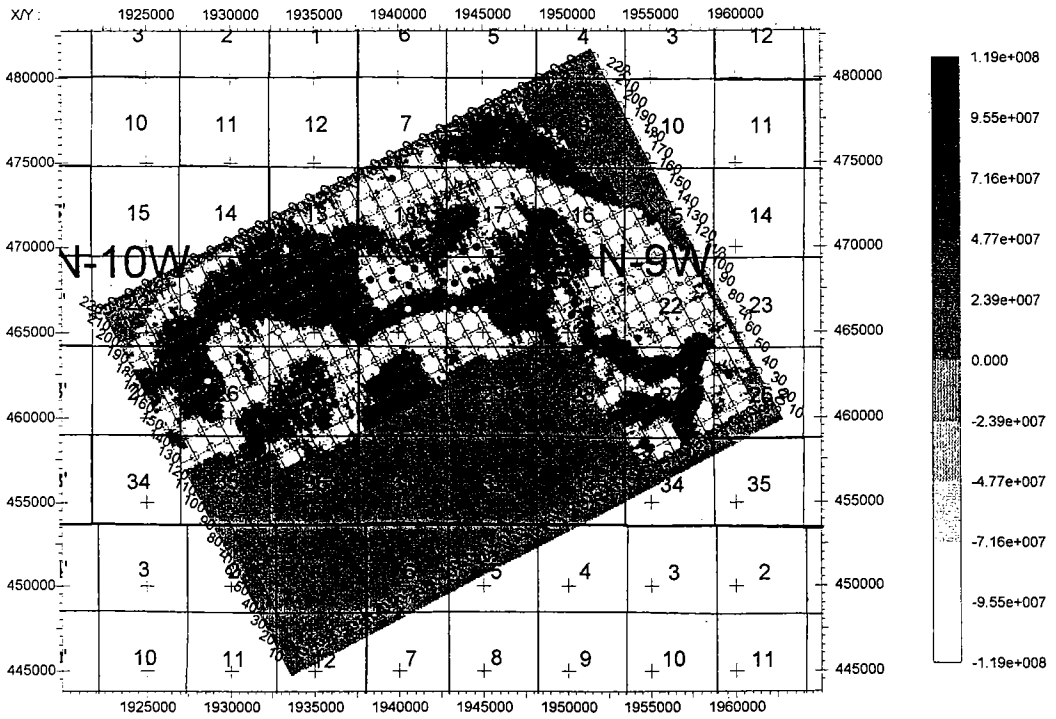

Figure 8. Time slice across Patricia-Gregory/West Drummond projects, showing general crater morphology.

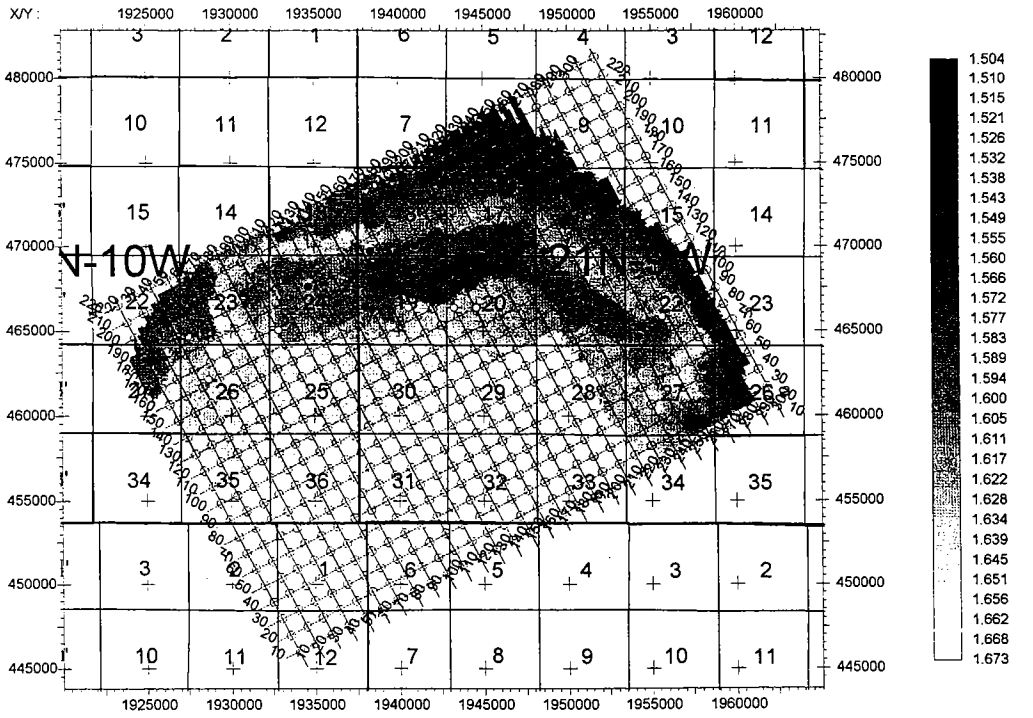

Figure 9. Time structure map across Patricia-Gregory and West Drummond projects, with datum being the base of the Oil Creek shale (but see Repetski, 1997, for another view of the stratigraphic correlation of this shale). Lighter shades represent structurally higher areas, and darker shades show deeper parts.

Grieves, R. A. F.; and Masaitis, V. L., 1994, The economic potential of terrestrial impact craters: International Geology Review, v. 36, p. 105–151.

Reeder, L. R., 1974, The control of potential Arbuckle hydrocarbon traps in northeastern Oklahoma by Precambrian topography: Shale Shaker, v. 24, p. 84–93, 96.

Repetski, J. E., 1997, Conodont age constraints on the Middle Ordovician black shale within the Ames structure, Major County, Oklahoma, *in* Johnson, K. S.; and Campbell, J. A. (eds.), Ames structure in northwest Oklahoma and similar features: origin and petroleum production (1995 symposium): Oklahoma Geological Survey Circular 100 [this volume], p. 363–369.

Roddy, D. J.; Pepin, R. O.; and Merrill, R. B. (eds.), 1977, Impact and explosion cratering; planetary and terrestrial implications: Pergamon Press, New York, 1301 p.

Roundtree, J. H., 1991, Petroleum geology of the Arbuckle Group, southern Osage and eastern Pawnee Counties, Oklahoma: Shale Shaker, v. 42, p. 2–16, 28–36.

The Ames Structure and Other North American Cryptoexplosion Features: Evidence for Endogenic Emplacement

John P. Coughlon
AMOCO Production Company
Denver, Colorado

P. Paul Denney
Global Exploration Consulting, Inc.
Delta, Colorado

ABSTRACT.—A long history of tectonic activity is documented for the development of the Ames structure. Subsidence in the Lower Ordovician section is demonstrated prior to uplift, erosion, and igneous activity that occurred in earliest Middle Ordovician time. This circular, highly faulted structure, cored by an igneous breccia, is typical of a cryptoexplosion structure as defined by W. H. Bucher in 1963. Regional geologic mapping documents the Ames structure as one of many endogenic cryptoexplosion features in North America. The origin of such features can be attributed to the ascent of alkalic and alkalic ultramafic magmas along deep-seated faults within Precambrian rifts, grabens, transform-fault systems, or uplifted shield areas. Most cryptoexplosion features are of Paleozoic age in the east-central United States and southern Canada and of either Paleozoic or Mesozoic age throughout the rest of Canada. Many circular, brecciated features distributed worldwide appear to be tectonically attributable phenomena rather than exotic structures resulting from random bolides.

INTRODUCTION

The Ames structure is located along the northwest shelf of the Anadarko basin in T. 20–21 N., R. 9–10 W., Major County, Oklahoma (Fig. 1). Detailed subsurface mapping from the Lower Ordovician rocks up through the Silurian–Devonian Hunton Group indicates an anomalous circular depression of ≈36 mi^2 (58 km^2), centered near the town of Ames.

The origin of the Ames structure has been the topic of debate between those espousing an exogenic origin (Hamm and Olsen, 1992; Roberts and Sandridge, 1992; Shirley, 1992; Carpenter and Carlson, 1992,1997; Koeberl and others, 1997; Fischer, 1997; Kuykendall and others, 1997; Huffman, 1997) and those favoring an endogenic origin (Roemer and others, 1992; Coughlon and Denney, 1993; Bridges, 1997). The impact theory suggests that a meteor of low-angle trajectory exploded near the surface of what is now the southeast corner of Major County, Oklahoma (Carpenter and Carlson, 1992). This event presumably occurred shortly before or soon after the end of Arbuckle Group deposition, excavating a bowl-shaped depression centered near the present town of Ames.

The most compelling evidence cited for an impact origin is the presence of shock-deformation features in various cores within the brecciated central uplift of the Ames feature. These include suevite, breccias, and shock microstructures in quartz, including planar deformation features and shock mosaicism. These features have been described in detail by Coughlon and Denney (1993), Fischer (1997), Ambers and others (1997), Huffman (1997), and Koeberl (1997). Those favoring an exogenic origin for the Ames feature consider these phe-

John P. Coughlon, AMOCO Production Co., 1670 Broadway, Denver, CO 80202; P. Paul Denney, Global Exploration Consulting, Inc., P.O. Box 171, Delta, CO 81416.

Coughlon, J. P.; and Denney, P. P., 1997, The Ames structure and other North American cryptoexplosion features: evidence for endogenic emplacement, *in* Johnson, K. S.; and Campbell, J. A. (eds.), Ames structure in northwest Oklahoma and similar features: origin and petroleum production (1995 symposium): Oklahoma Geological Survey Circular 100, p. 133–152.

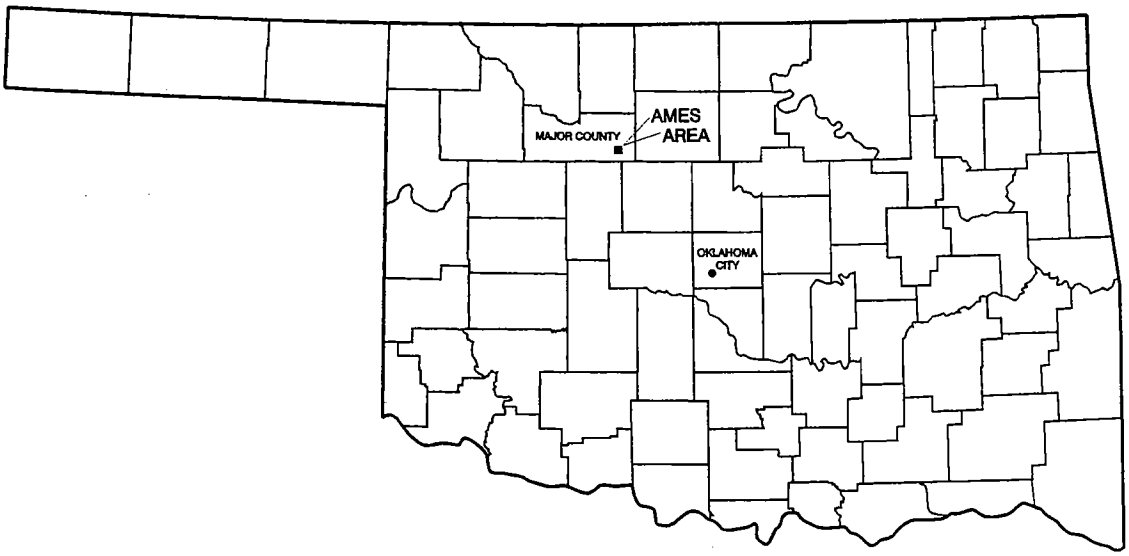

Figure 1. Index map of Oklahoma showing Ames area location.

nomena to be conclusive evidence of hypervelocity impact (e.g., Koeberl, 1997; Ambers and others, 1997; Fischer, 1997; Huffman, 1997). They have stated that such features form only at extremely high pressures and strain rates on the order of 15–30 GPa and 10^6 to 10^8 s^{-1}, respectively (A. R. Huffman, personal communication, 1995), and are currently believed to be unique to hypervelocity impact.

The geologic evidence presented herein shows that an impact origin of the Ames depression cannot be supported. Detailed subsurface correlations of the Kindblade and West Spring Creek Formations of the Arbuckle Group show conclusively that the Ames depression was in existence in Early Ordovician time, and that these intervals were subsequently domed, eroded, and brecciated in response to stretching and thinning of the crust over a rising magma body. The emplacement of the magma body resulted in intrusion of igneous breccia pipes and dikes and extrusion of highly brecciated, partially melted felsic tuffs and felsic tuff breccias that were deposited within paleo–topographic lows on the Arbuckle surface. Isopach data of postextrusion rocks show resumed subsidence through the Silurian–Devonian Hunton Group. Recent data presented by Johnson and Smith (1997) show evidence of post-Permian subsidence within the crater as well.

We propose that the Ames structure is one of many cryptoexplosion features in North America whose origin can be attributed to alkalic magmas rising along preexisting zones of weakness (i.e., faults) in the continental crust. Most of these features are associated with upper-mantle–derived kimberlites, lamprophyres, ultramafic lamprophyres, lamproites, carbonatites, and other alkalic ultramafic magmas. We support a cogenetic relationship between kimberlitic processes and North American cryptoexplosion structures, as discussed by Bucher (1963), Snyder and Gerdemann (1965), Currie (1965), Amstutz (1965), Nicolaysen (1972), Nicolaysen and Ferguson (1990), and Kopecký (1974).

SUBSURFACE STRATIGRAPHY

Because of the abundant well control available, the Ames feature is an excellent candidate for the study of the debate over exogenic vs. endogenic causes of craters. This well control has provided significant subsurface data for interpreting the origin and timing of events affecting this unusual structure.

The more-or-less west-to-east cross section shown in Figure 2 (location on map in Fig. 6) is hung on the top of the West Spring Creek 1 (WSC1) datum, an easily recognized regional marker that corresponds to a basal member of the West Spring Creek Formation of the Arbuckle Group, as published by Gatewood (1968) and Derby and others (1991). The low-resistivity couplet (see Fig. 2) separating the overlying WSC2 from the underlying WSC1 is consistent throughout the shelf area of the Anadarko basin. This couplet gradually increases in resistivity upward and is terminated by another low-resistivity couplet, WSC3.

A similar resistivity profile can be seen within the underlying Kindblade Formation. Here, the uppermost member of the Kindblade consists of a low-resistivity interval that gradually increases

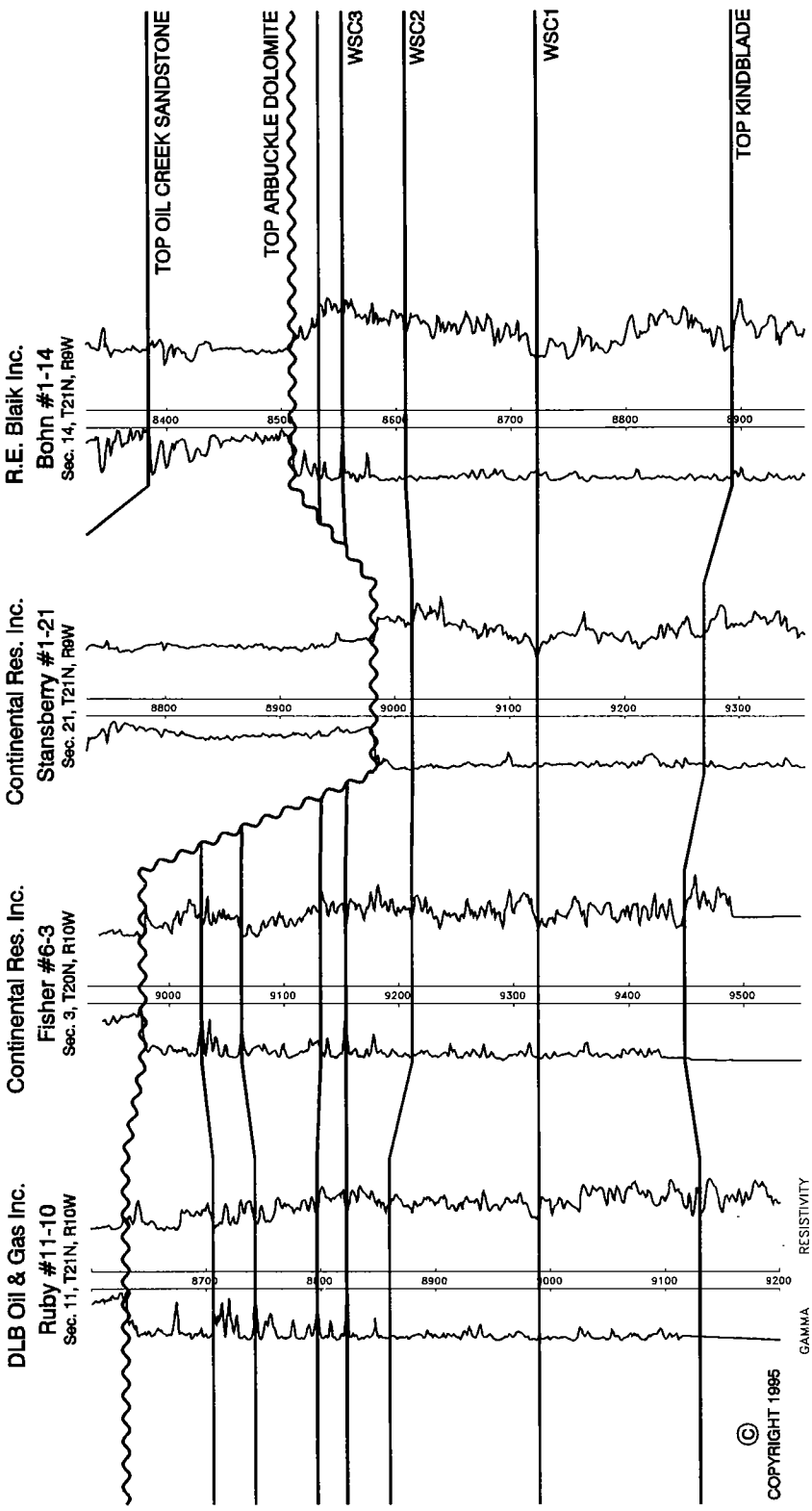

Figure 2. More-or-less west-to-east stratigraphic cross section through the Ames structure, showing continuity of Arbuckle strata: from left to right, (1) regional Arbuckle along the northwest shelf of the Anadarko basin, (2) immediately west of the Ames structure along the ring anticline, (3) within the "central rebound high" in the core of the Ames structure, and (4) immediately east of the Ames structure. Section is hung on member 1 of the West Spring Creek Formation (WSC1) of the upper Arbuckle Group. Line of cross section is shown in Figure 6.

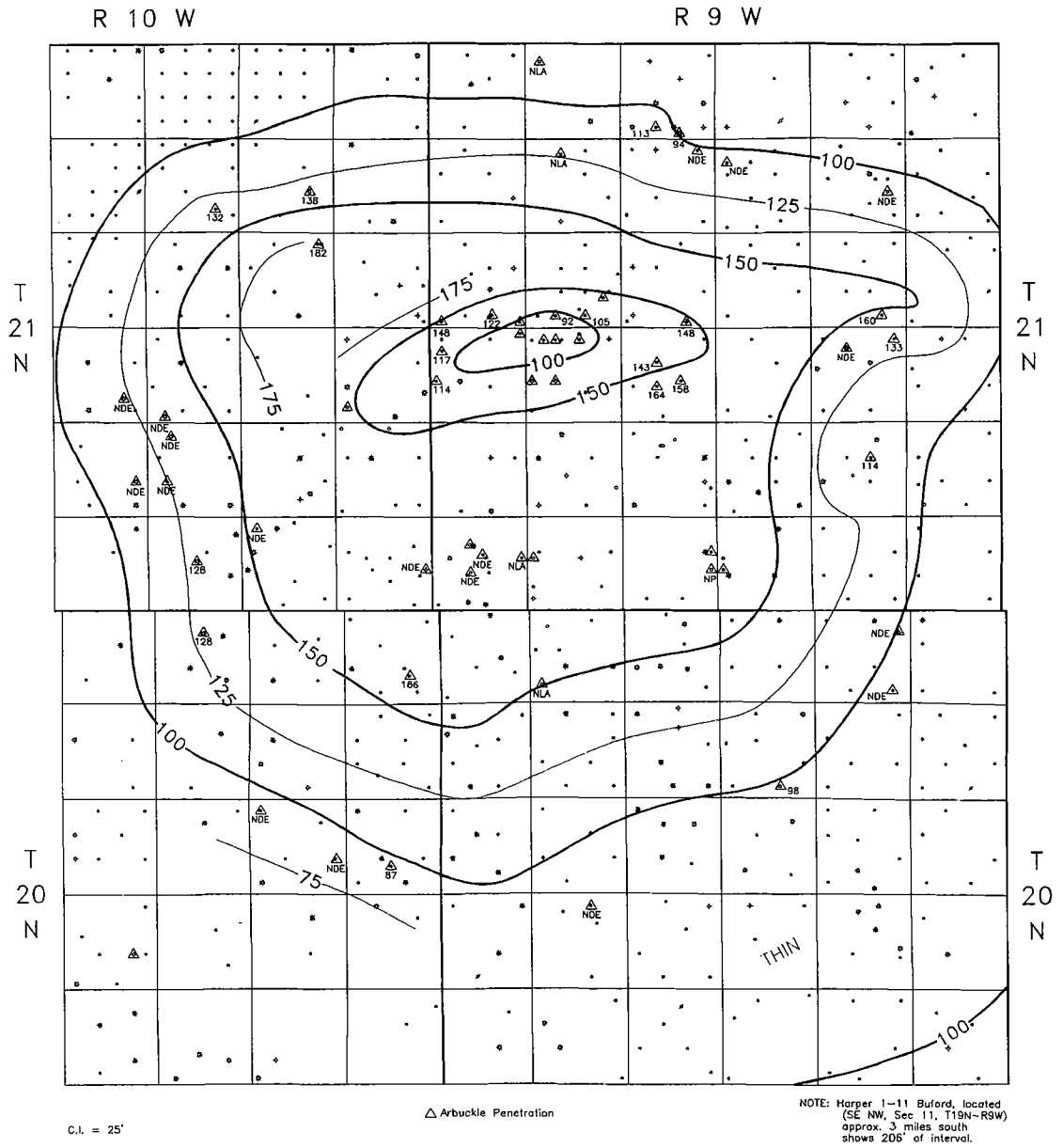

Figure 3. Isopach map of the lower West Spring Creek Formation interval—top of Kindblade Formation to WSC1. Map shows early subsidence of Ames structure, i.e., early development of thin intervals within depression.

upward and is abruptly terminated by a sharp resistivity break at the top.

Detailed correlations of these stratigraphic intervals unquestionably confirm the presence of continuous in situ Arbuckle strata both internal and external to the Ames structure. This stratigraphic continuity is inconsistent with interpreted suevite deposits resulting from a bolide impact. Our evidence suggests that brecciation of Arbuckle strata internal to the Ames structure is confined to small areas in and around faults associated with subsequent emplacement of post-Arbuckle igneous pipes and breccias. Postintrusive collapse breccias are present near radial faults on the periphery of the structure. The continuous, conformable nature of the Kindblade and West Spring Creek Formations both within the crater and regionally along the northwest shelf of the Anadarko basin is dem-

onstrated further by a series of cross sections published by Coughlon and Denney (1993).

GEOLOGIC EVOLUTION OF THE AMES STRUCTURE

A series of isopach maps has been constructed to explore the timing of movements within the Ames anomaly. Without exception, these isopach maps—from the Hunton Formation downward to the top of the Kindblade Formation of the Arbuckle Group—show a pronounced circular depression defined by thick intervals surrounding a group of small structures revealed as thin intervals. Correlations within the West Spring Creek Formation of the Arbuckle Group have permitted the construction of two isopach maps (Figs. 3,4) and a subcrop map (Fig. 5). The isopach map (Fig. 3) of member 1 of the West Spring Creek Formation (WSC1 in the figures) is a series of rocks 85–200 ft in thickness directly overlying the Kindblade Formation of the Arbuckle Group. Member 2 of the West Spring Creek Formation (WSC2 in the figures) is a 121–168-ft-thick rock interval directly overlying member 1 and is shown in the companion isopach map (Fig. 4). Both isopachs reveal a concentric feature that happens to underlie the much shallower, younger (Silurian-Devonian age) structure in the Sylvan Shale (Fig. 6). Thickening of both members 1 and 2 occurs toward the southwest quadrant of T. 21 N., R. 9 W., although, as previously discussed, within the center of each isopach map, thin intervals (i.e., paleostructures) are present. These isopach thins directly overlie highs shown by drilling to consist of igneous (alkalic) breccia pipes.

Although the two isopach maps discussed above reveal a small basin with central thin intervals, the subcrop map (Fig. 5) on the pre–Oil Creek and preigneous surface (i.e., the Arbuckle unconformity) shows just the opposite. Arbuckle units form a concentric pattern in the subcrop: oldest Arbuckle rocks are in the center, and progressively younger rocks form the perimeter. The older interior rocks are structurally as high today as those younger fringing rocks (Fig. 7), thus indicating a structural dome that was uplifted at the end of Arbuckle deposition and partially eroded prior to the subsequent extrusion of the igneous breccias and tuffs, intrusion of the igneous pipes, or deposition of the overlying Oil Creek shale. The domal structure of these preigneous deposits is suggestive of a point source from below and is inconsistent with a bolide-impact origin for the Ames feature.

As discussed above, interval isopachs of the West Spring Creek Formation members 1 and 2 show a depression in the Kindblade Formation–lower West Spring Creek (WSC1) interval. Within this depression are areas with an exceptionally thin WSC1 interval that, when drilled, were found to contain extrusive igneous breccias and/or intrusive, vertically continuous yet laterally discontinuous, brecciated pipes extending to Precambrian basement, as proven by the presence of Precambrian granite xenoliths within the Nicor no. 18-4 Chestnut core (Coughlon and Denny, 1993). The pipes were the conduits for the surrounding coeval extrusive felsic tuffs and the likely cause of localized thinning in the Kindblade and lower West Spring Creek Formations of the Arbuckle.

DISTRIBUTION OF PHANEROZOIC IGNEOUS BRECCIAS AND TUFFS

Within the Ames area, the Phanerozoic igneous rocks are currently found and appear to be limited to the southwest quadrant of T. 21 N., R. 9 W. Four areas occur within that region where wells drilled in excess of 250 ft of igneous rock without encountering Arbuckle sedimentary rocks. These areas (patterned in Figs. 8 and 9) are hereafter referred to as igneous pipes.

Regional mapping of the igneous breccias and tuffs within the Ames structure is revealing. Figures 8 and 9 show the distribution of these rocks to be restricted to small areas around the suspected igneous pipes. When compared to Figure 7, the relationship between paleo–topographic lows and thick intervals of extrusive rocks becomes obvious. For example, the Nicor no. 18-4 Chestnut well (SW¼ SE¼ sec. 18, T. 21 N., R. 9 W.) encountered the Arbuckle unconformity 108 ft low compared to the offsetting D. & J. no. 1-18 Peggy well (SE¼ SE¼ SE¼ sec. 18, T. 21 N., R. 9 W.). The Chestnut well encountered 122 ft of igneous rocks whereas the Peggy well encountered only 46 ft. This relationship of thick intervals of extrusive igneous rocks within paleo–topographic lows proximal to intrusive igneous pipes is consistent within the core of the Ames structure.

The limited areal extent of these rocks, their abrupt transition into undeformed, unbrecciated, in situ Arbuckle, and the restriction of extrusive igneous material to paleo–topographic lows proximal to intrusive pipes suggest to us an endogenic origin. Had these been suevite deposits from a meteorite impact, then much of the core of the Ames structure should be composed of laterally discontinuous blocks of chaotic igneous rocks and Arbuckle breccias. Our evidence does not show this prediction to be true.

As already discussed, the Phanerozoic igneous rocks in the Ames structure contain abundant planar deformation features that many think form conclusive evidence of hypervelocity impact (e.g., Koeberl, 1997; Huffman, 1997; Fischer, 1997). In view of the geologic evidence presented herein, this association of shock deformation with impact events is suspect and must be addressed in future instances where stratigraphic and field evidence suggests that igneous and tectonic activity preceded the shock deformation event!

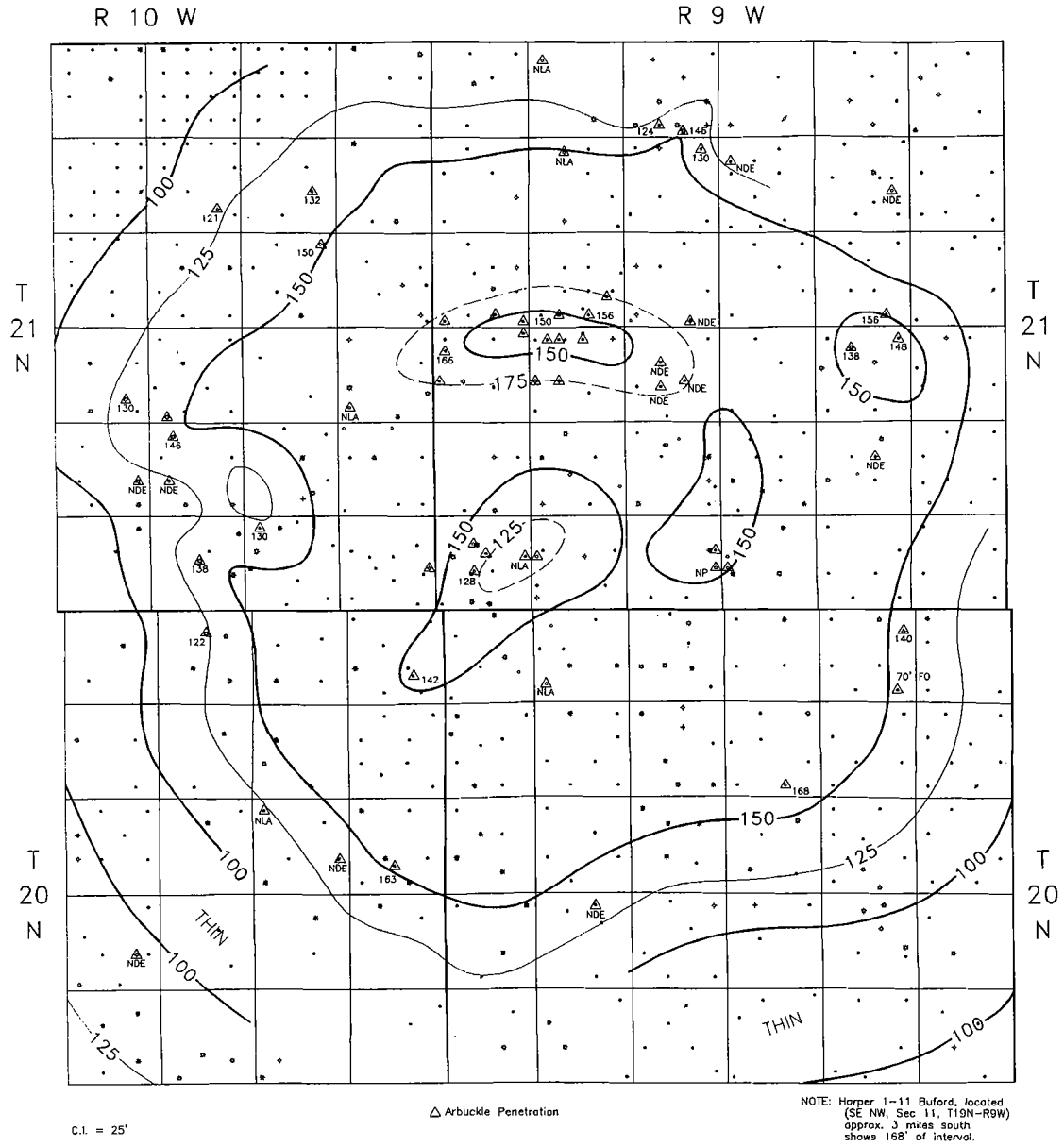

Figure 4. Isopach map of the middle interval of the West Spring Creek Formation (WSC1 to WSC2). Map shows continued subsidence of Ames depression and further development of intradepression thin intervals.

Isopach mapping of post-Arbuckle rocks shows continued subsidence and movement of the Ames feature. Following extrusion of the Phanerozoic igneous breccias and tuffs, the Ames depression continued to subside. Figures 10, 11, and 12 show thickening of units in the depression from the early deposition of the Oil Creek Formation (Ordovician) through the end of Hunton Group deposition (Silurian–Devonian). In fact, the post-Arbuckle through Hunton rocks mappable within the "Hunton graben" (extending from west to east across secs. 34–36, T. 21 N., R. 10 W.) show a total stratigraphic thickening that exceeds by 125 ft the maximum structural relief existing on the post-Arbuckle surface at its deepest point of excavation. An additional 70 ft of thickening from the base of the Woodford Shale through the top of the Oswego limestone of the Marmaton

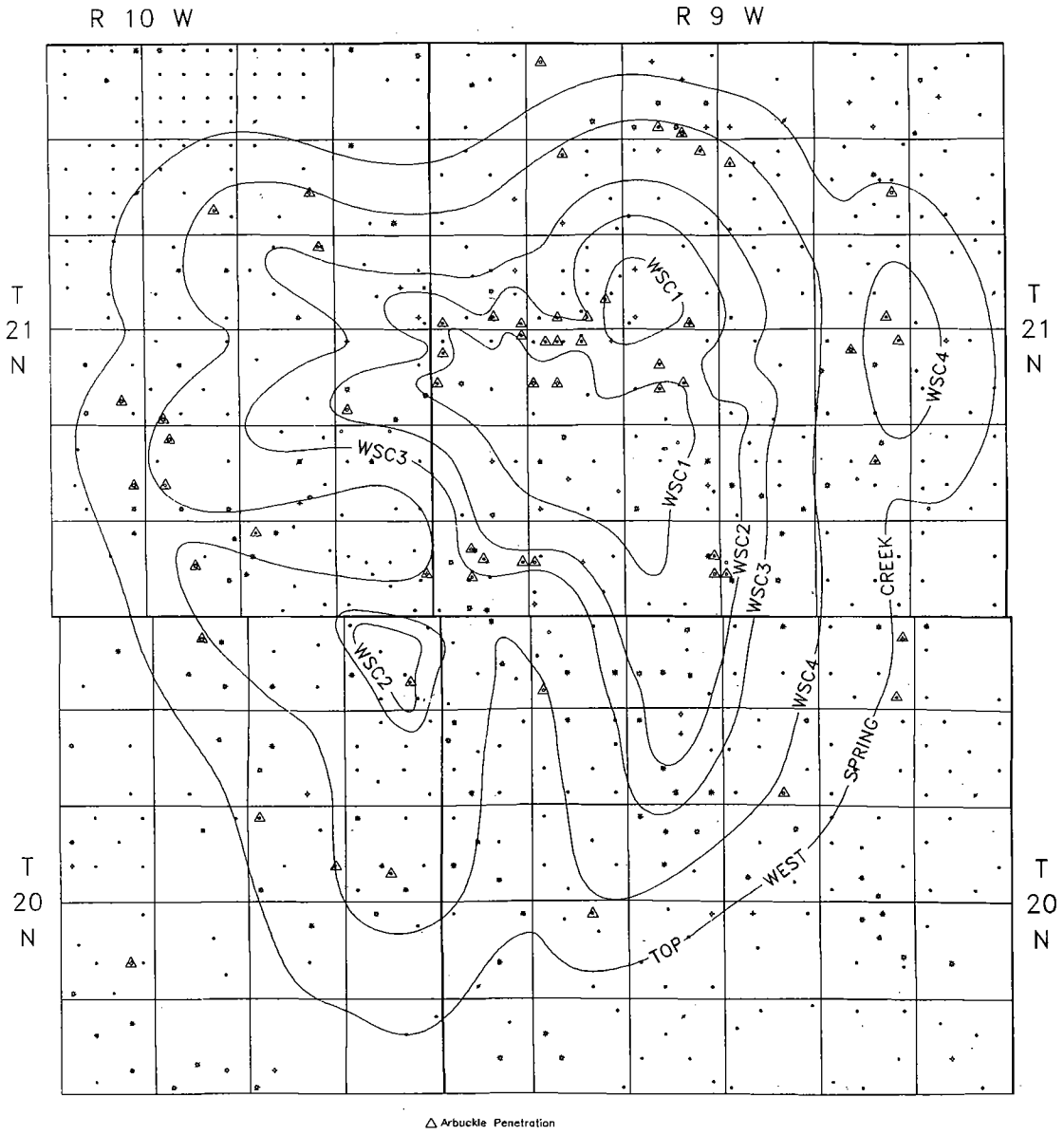

Figure 5. Subcrop map, prior to intrusion of igneous pipes and dikes and concomitant extrusion of felsic tuffs and felsic tuff breccias. Stratigraphic sequence WSC1 is older than the interval WSC2 through top of the West Spring Creek Formation. This map reveals the presence of a broad structural dome following post-Arbuckle erosion.

Group can be documented in the "Hunton graben." Finally, 75–150 ft of post-Permian subsidence within the Ames structure has been documented by Johnson and Smith (1997). Recent earthquake activity beneath the Ames structure suggests continued movement even today.

These post-Arbuckle isopachs, showing continued subsidence and movement, do not necessarily refute the presumption of a bolide cause of the Ames feature. Subsidence of impact craters with time has been documented (A. R. Huffman, personal communication, 1995). However, the dynamic nature of the Ames structure from an early Middle Ordovician (pre-event) basin that was uplifted and subsequently subsided throughout Paleozoic time is consistent with an endogenic origin.

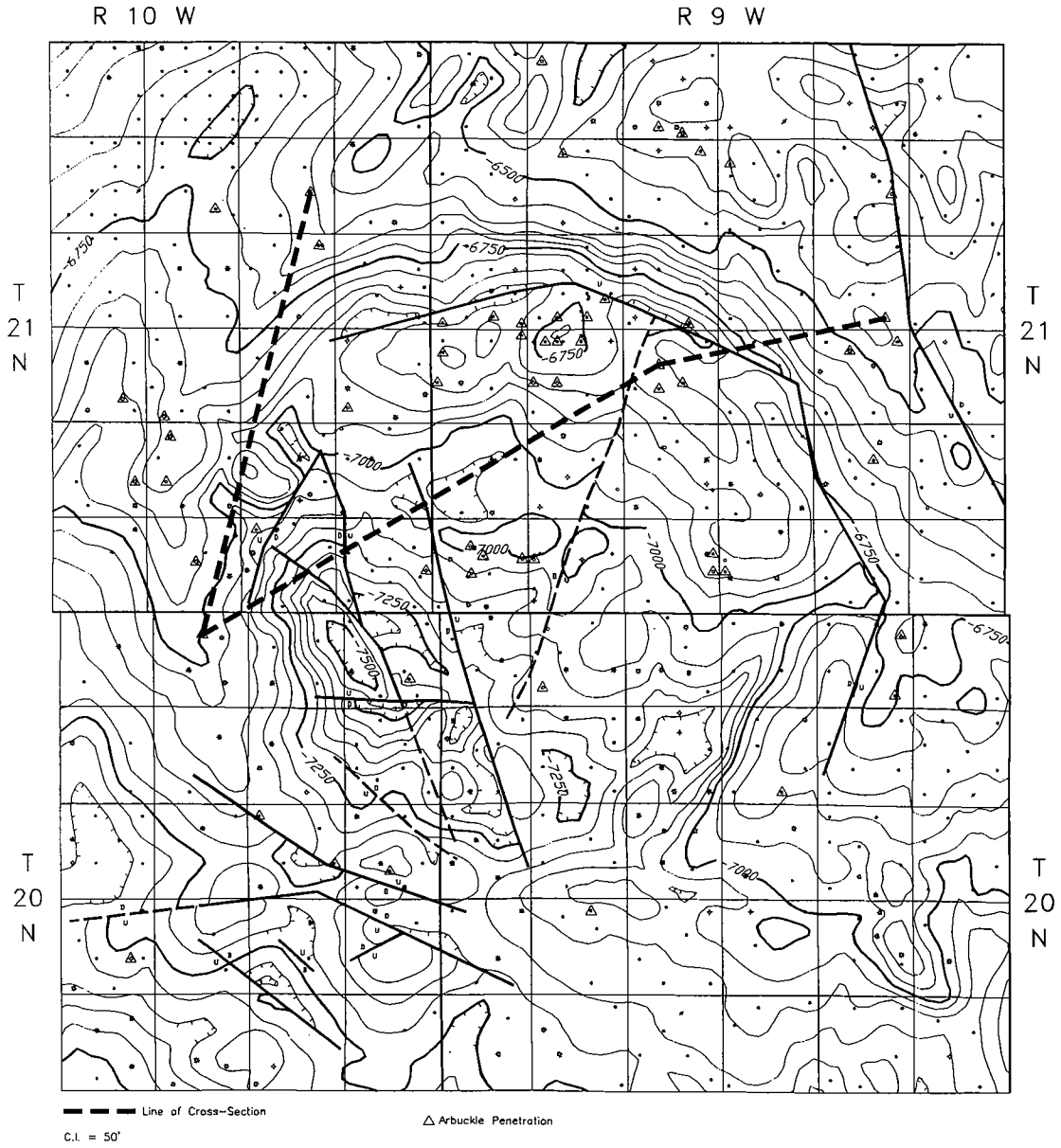

Figure 6. Structure map contoured on the top of the Sylvan Shale. Heavy dashed line is line of cross section shown in Figure 2. Lighter lines and dashed lines are faults with relative movement shown.

REGIONAL STRUCTURAL AND TECTONIC SETTING OF THE AMES FEATURE

The Ames feature is 1 of 14 known circular, brecciated anomalies present within or peripheral to either the Midcontinent rift or Reelfoot rift of the eastern-central part of the United States (Fig. 13). The locations of these anomalies are Ames, Oklahoma; Manson, Iowa; Rock Elm, Wisconsin; the Slate Islands, Canada; Lake County, Cass County, and Kent County, Michigan; Serpent Mound, Ohio; Jeptha Knob and Versailles, Kentucky; Middlesboro, Flynn Creek, and Wells Creek, Tennessee; and Hicks dome, Illinois.

In addition, another seven circular, brecciated anomalies (cryptoexplosion features) are present along a major northwest-trending Precambrian transform fault system connecting the Midcontinent rift to the Reelfoot rift. Their locations are Avon, Furnace Creek, Crooked Creek, Bee Fork, Decaturville, and Weaubleau, Missouri; and Rose

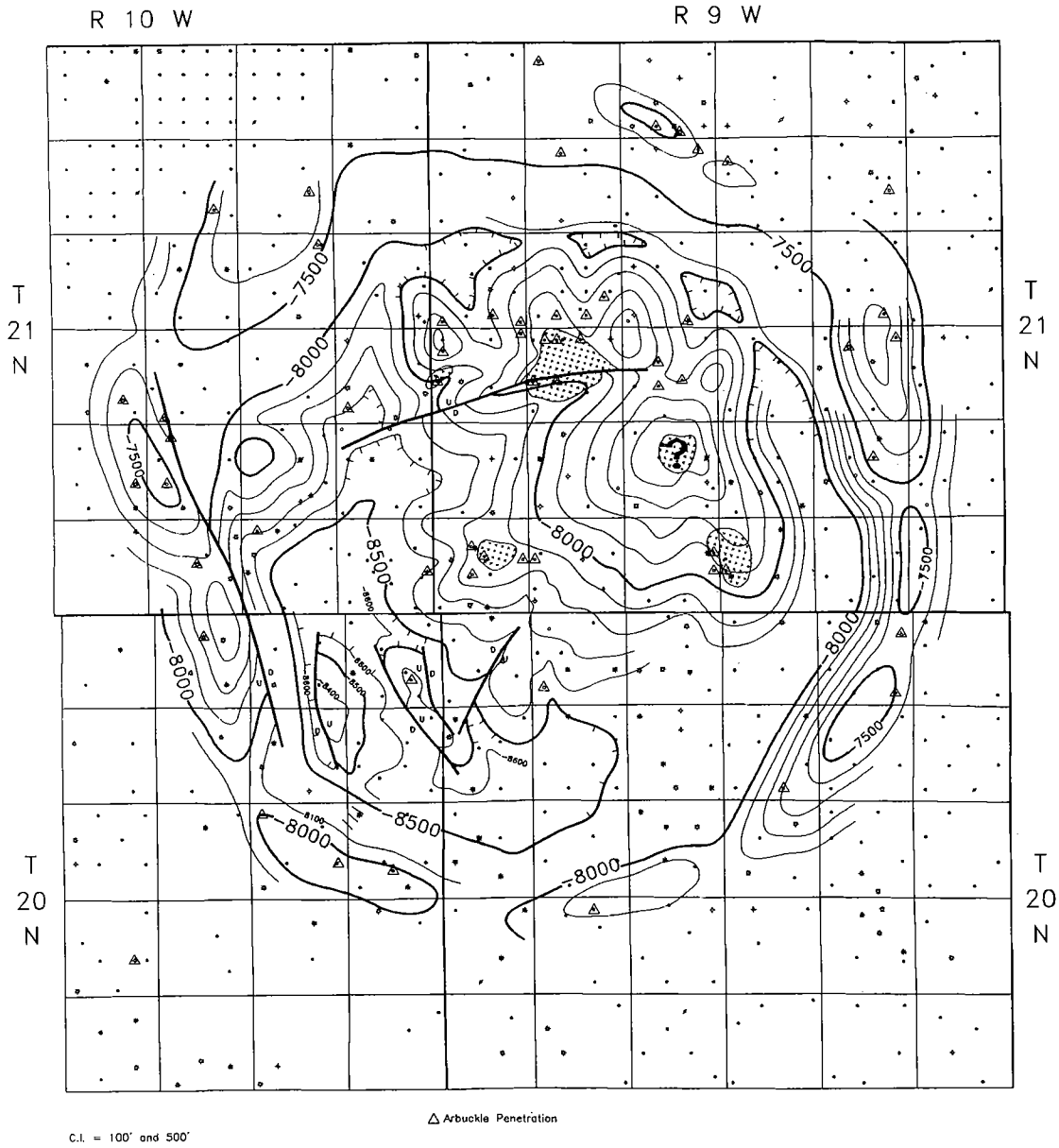

Figure 7. Structure map contoured on the top of the Arbuckle unconformity. The map indicates a post–West Spring Creek Formation structural dome with WSC1 and WSC2 occupying the highest structural positions within the core of the feature. The map also demonstrates that topographic valleys are proximal to igneous pipes (shown by patterned areas). Lines and dashed lines are faults with relative movement shown.

dome, Kansas. Two other features at Kentland, Indiana, and Des Plaines, Illinois, are present along a parallel northwest trend. Also, a feature at Glassford, Illinois, may be associated with a previously unrecognized parallel, northwest-trending fault as well.

Finally, adjacent to the Midcontinent rift in southern Canada, within the Ottawa-Bonnechère graben, are another eight features (Fig. 14). They are located at Sudbury, Lake Wanapitei, Burritt Island, Iron Island, Manitou Island, Callander Bay, Powassan, and Bancroft.

All of the above features are of Paleozoic age except Manson, Rose dome, Kentland, and Lake Wanapitei, which are Mesozoic, and Sudbury, which is Precambrian. The exact dates of emplacement of many of the Paleozoic features have yet to be determined isotopically; however, relative ages

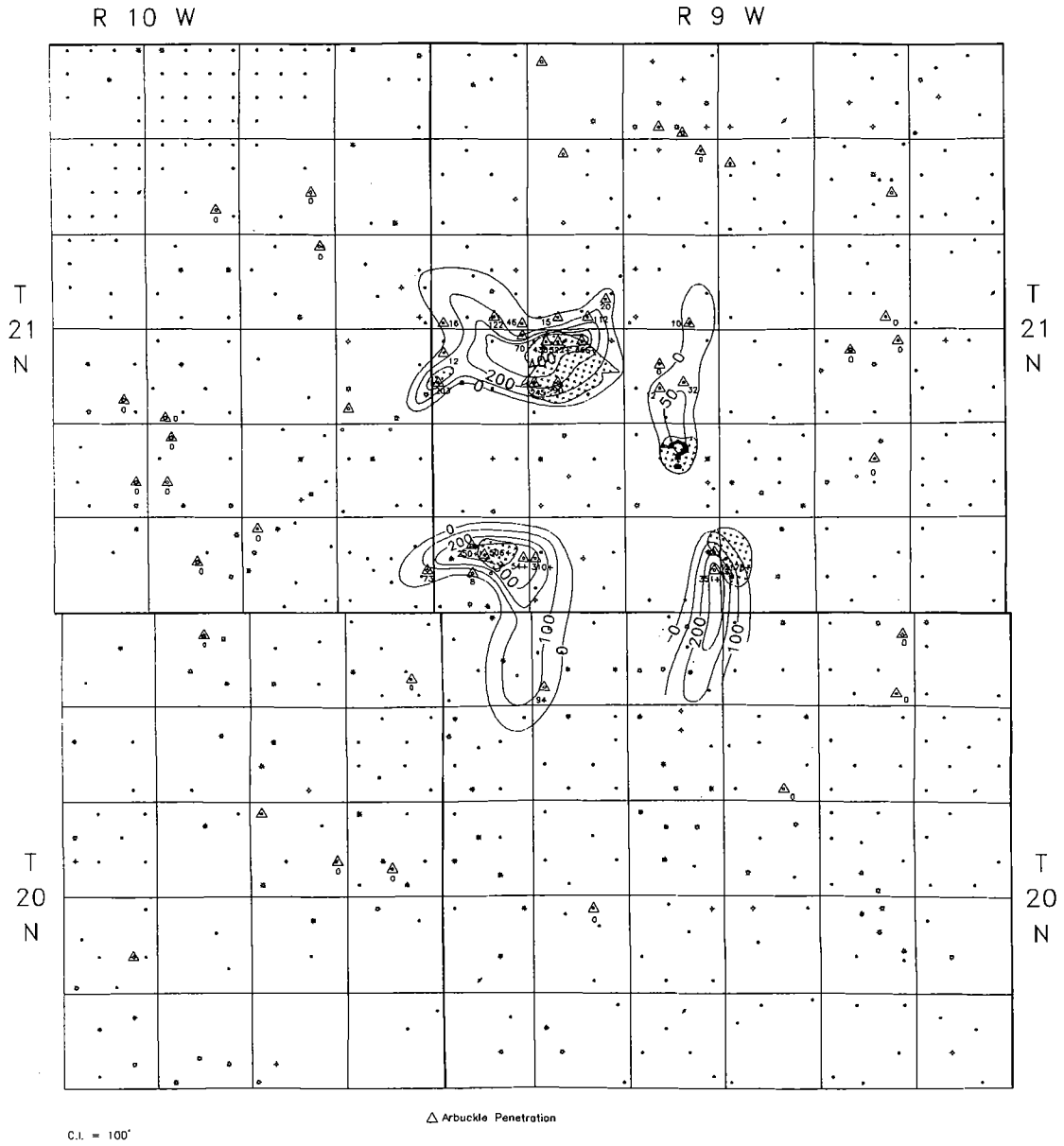

Figure 8. Gross isopach map of extrusive igneous rocks (both felsic tuffs and felsic tuff breccias; shown by contours) within the Ames structure. Proximity of the extrusive rocks to the igneous pipes (patterned areas) is evident. Extrusive rocks thicken into topographic valleys outward from the igneous pipes.

range from Late Cambrian through Permian. Many of these features are considered, or have been considered, to be meteorite impacts (e.g., Sharpton and Grieve, 1991; Grieve and others, 1995). Like Ames, many contain shocked quartz with multiple sets of planar deformation features and/or shatter cones.

The common structural setting of all of these features (with the possible exceptions of Kentland, Indiana; and Glassford and Des Plaines, Illinois) is within a Precambrian graben, rift, and/or transform-fault system, which has undergone Paleozoic reactivation and/or deformation. Most features that crop out are associated with upper-mantle–derived kimberlites, ultramafic lamprophyres, or lamproites and with hydrothermal mineralization or hydrocarbons. In addition, each is within a seismically active structural setting.

In outcrop, many of these features show field relationships contradictory to a genesis by a single

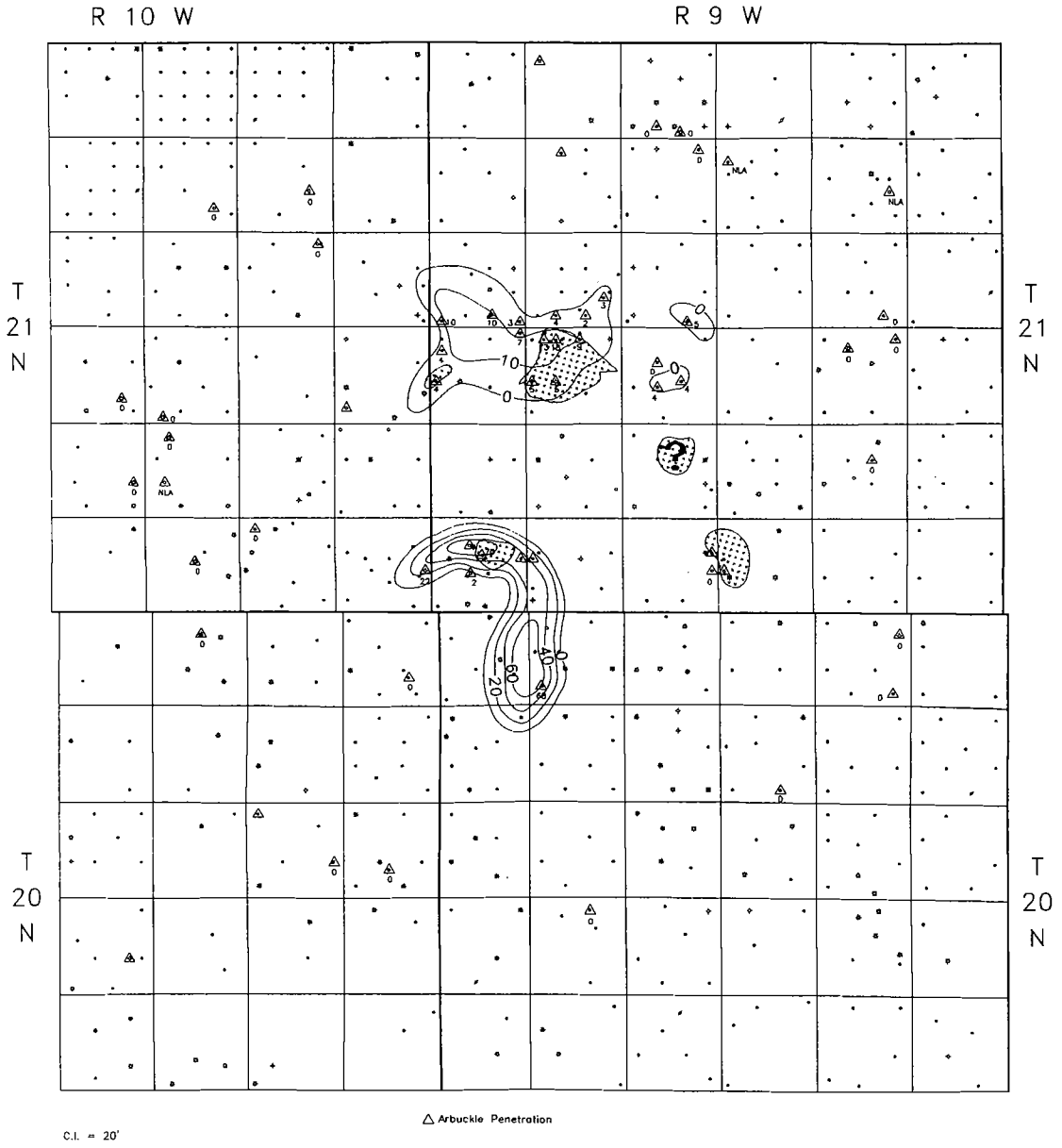

Figure 9. Isopach map of the felsic tuffs. (See Coughlon and Denney, 1993, for detailed petrographic description.)

bolide impact. Snyder and Gerdemann (1965) demonstrated that Avon, Furnace Creek, Crooked Creek, Bee Fork, Decaturville, Weaubleau (Fig. 15), and Rose dome all showed field relationships inconsistent with a meteorite-impact origin. Structurally, however, all are affiliated with magnetic mineralization and/or mafic plutons associated with the transform-fault system joining the Midcontinent rift to the Reelfoot rift. Also, all are affiliated with mafic igneous dikes composed of lamprophyres, peridotites, and alnoites (i.e., kimberlites). Grieve and others (1995) indicated that Crooked Creek and Decaturville are recognized terrestrial impact structures. Their conclusion presumably was based on the presence of shock deformation features at these locations. However, they failed to address the identical composition (alkalic mafic and alkalic ultramafic rocks) and tectonic coincidences common to all of these features. Since these intrusions have ages spread over a substantial period of time, yet all are aligned in a linear fashion, the most plausible ex-

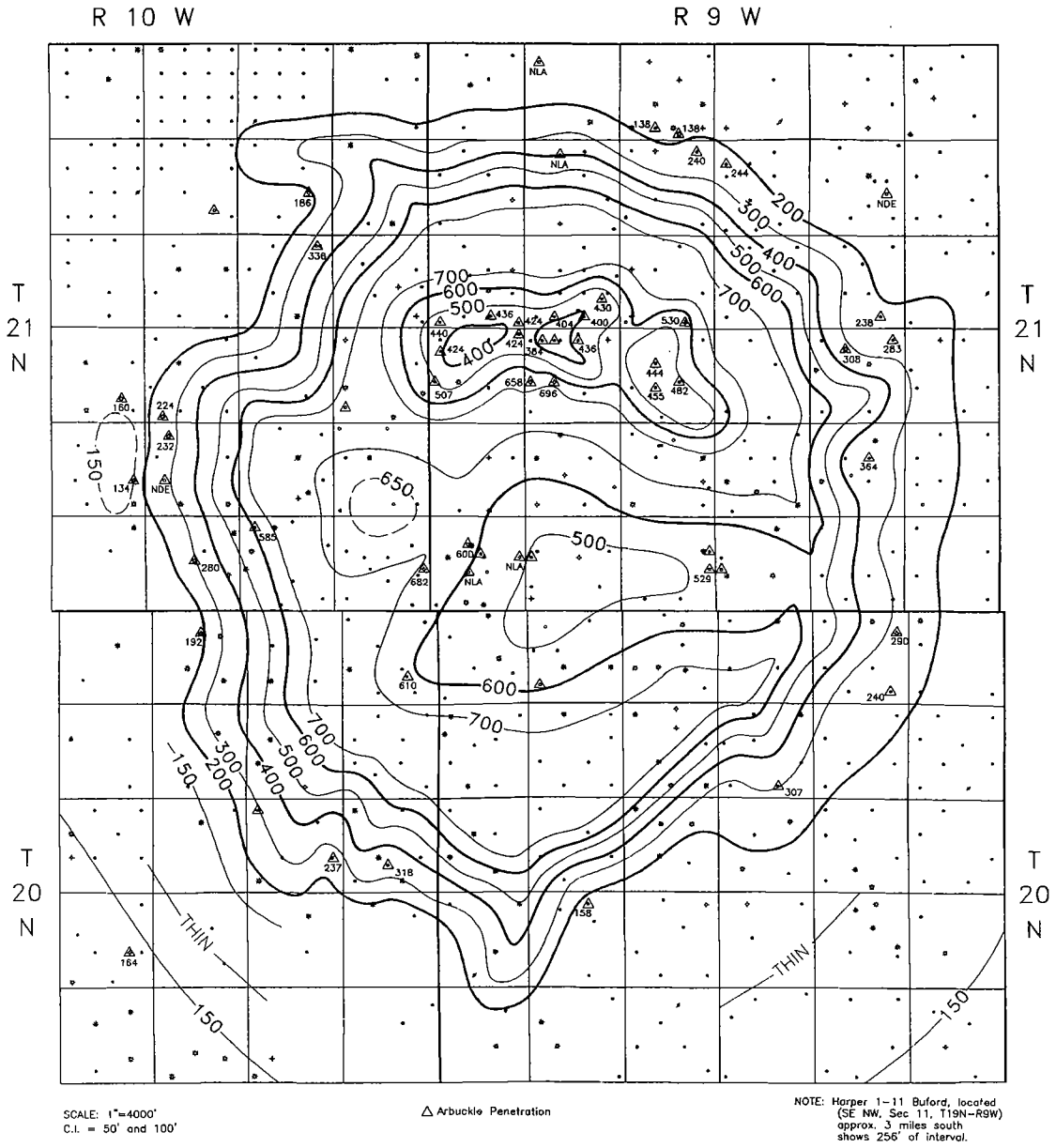

Figure 10. Isopach map for the interval from the top of the Tyner shale (Simpson Group) to the top of the Arbuckle unconformity or to top of the igneous unconformity.

planation of origin would appear to be a deep-seated fault zone or crustal discontinuity that has been reactivated periodically throughout Paleozoic time. This interpretation has been described in great detail by Bucher (1963), Snyder and Gerdemann (1965), Zartman and others (1967), Nicolaysen (1972), Nicolaysen and Ferguson (1990), Lidiak and Zietz (1976), and many others.

Brown and others (1954) showed that Hicks dome, Illinois, has field relationships inconsistent with a meteorite-impact hypothesis. They also showed that this feature is affiliated with the igneous lamprophyric or peridotitic intrusions that abound in the Kentucky-Illinois fluorspar field.

Reidel and Koucky (1981) and Reidel and others (1982) showed that Serpent Mound, Ohio, is situated on a northwest-trending fault zone that predates the structure and is coincident with Precambrian basement. They further showed evidence suggestive of at least two deformation

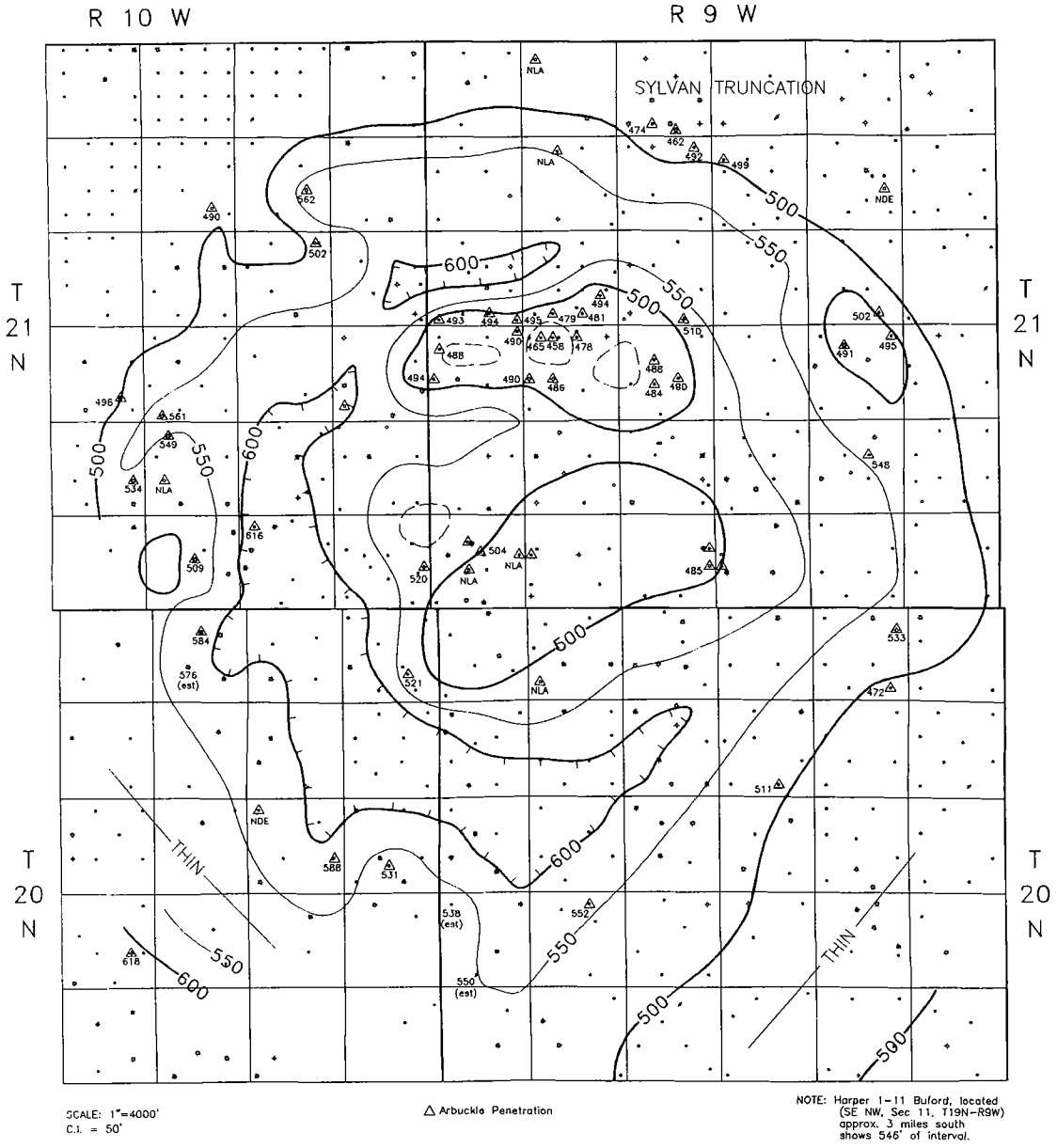

Figure 11. Isopach map for the interval from the top of the Sylvan Shale to the top of the Oil Creek shale (Tyner Formation).

events and a complex geologic history. Finally, they documented the presence of shatter cones and coesite, both of which have been suggested to form only via hypervelocity impact.

Shrock and Malott (1933) showed that Kentland dome, Indiana, had a complex structural history involving a mosaic of fault blocks acting vertically and originating at considerable depth. This feature is located on the south side of a pronounced magnetic high bounded by magnetic lows to the north, southeast, and south. Abundant shatter cones are present here as well.

Nicolaysen and Ferguson (1990) showed eight circular complexes with fenitization in the Nipissing branch of the Ottawa-Bonnechère graben system (Fig. 14). These complexes constitute the 560 Ma Nipissing alkalic province (Nicolaysen and Ferguson, 1990, p. 307). Craters are present at four of these locations; yet, analogous to the Missouri cryptoexplosion trend, Grieve and others

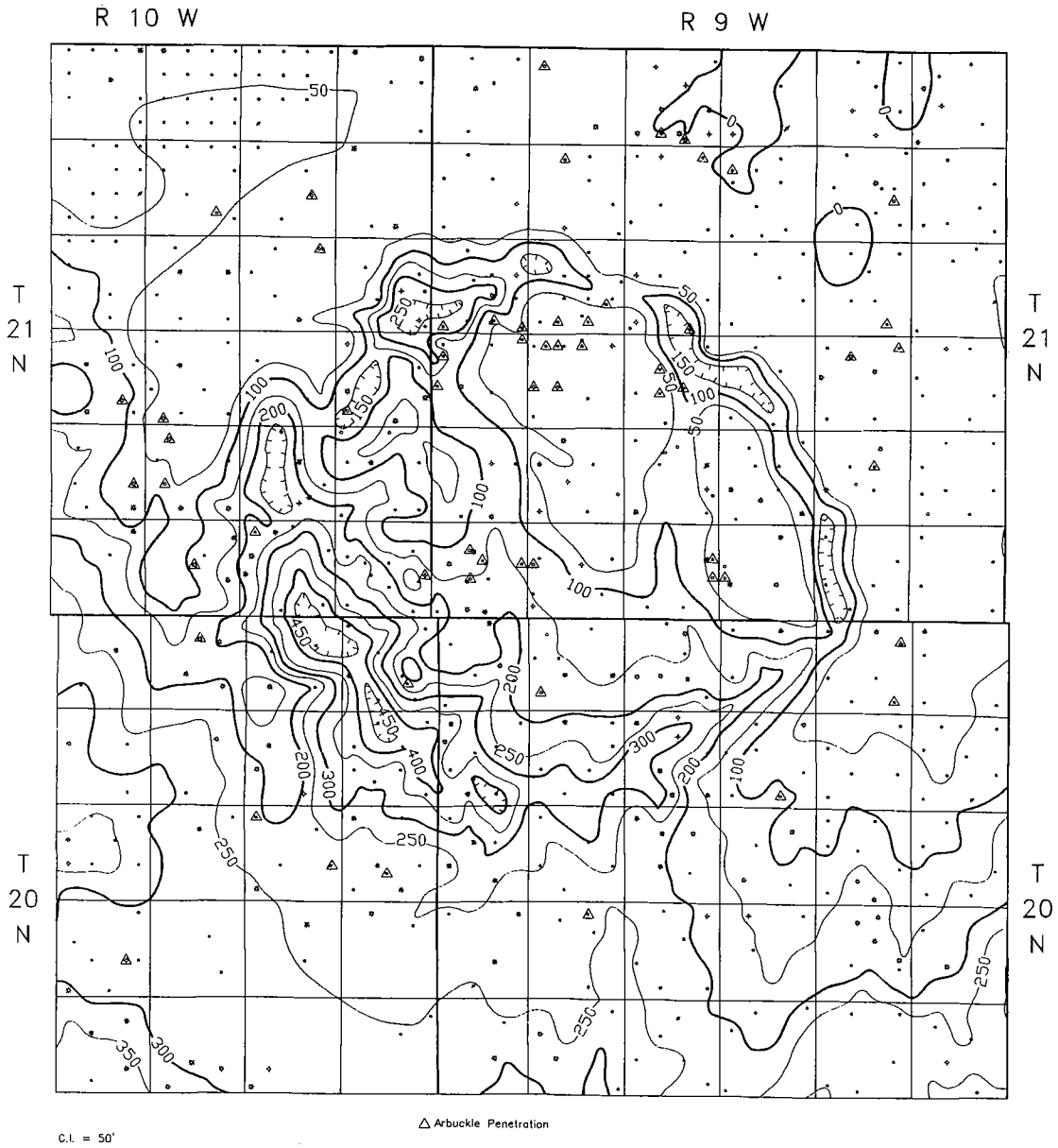

Figure 12. Isopach map of the Hunton Group.

(1995) accounted for three of these (Sudbury, Lake Wanapitei, and Brent) as recognized terrestrial impact structures without mention of the five other accompanying structures. The compositional and tectonic coincidences and age variations (Precambrian–Mesozoic) again suggest periodic reactivation of a deep-seated fault system rather than an extraterrestrial impact origin. Currie (1971) related both the fenite development and cratering to explosive alkalic volcanism.

GLOBAL SETTING AND EMPLACEMENT OF CRYPTOEXPLOSION STRUCTURES

Figure 16 shows the distribution of recognized terrestrial impact sites worldwide as interpreted by Sharpton and Grieve (1991), with Precambrian shield areas added. Significantly, a majority of such recognized impact sites occur on areas of uplifted Precambrian shields and/or reactivated Precambrian rifts, transform-fault systems, or gra-

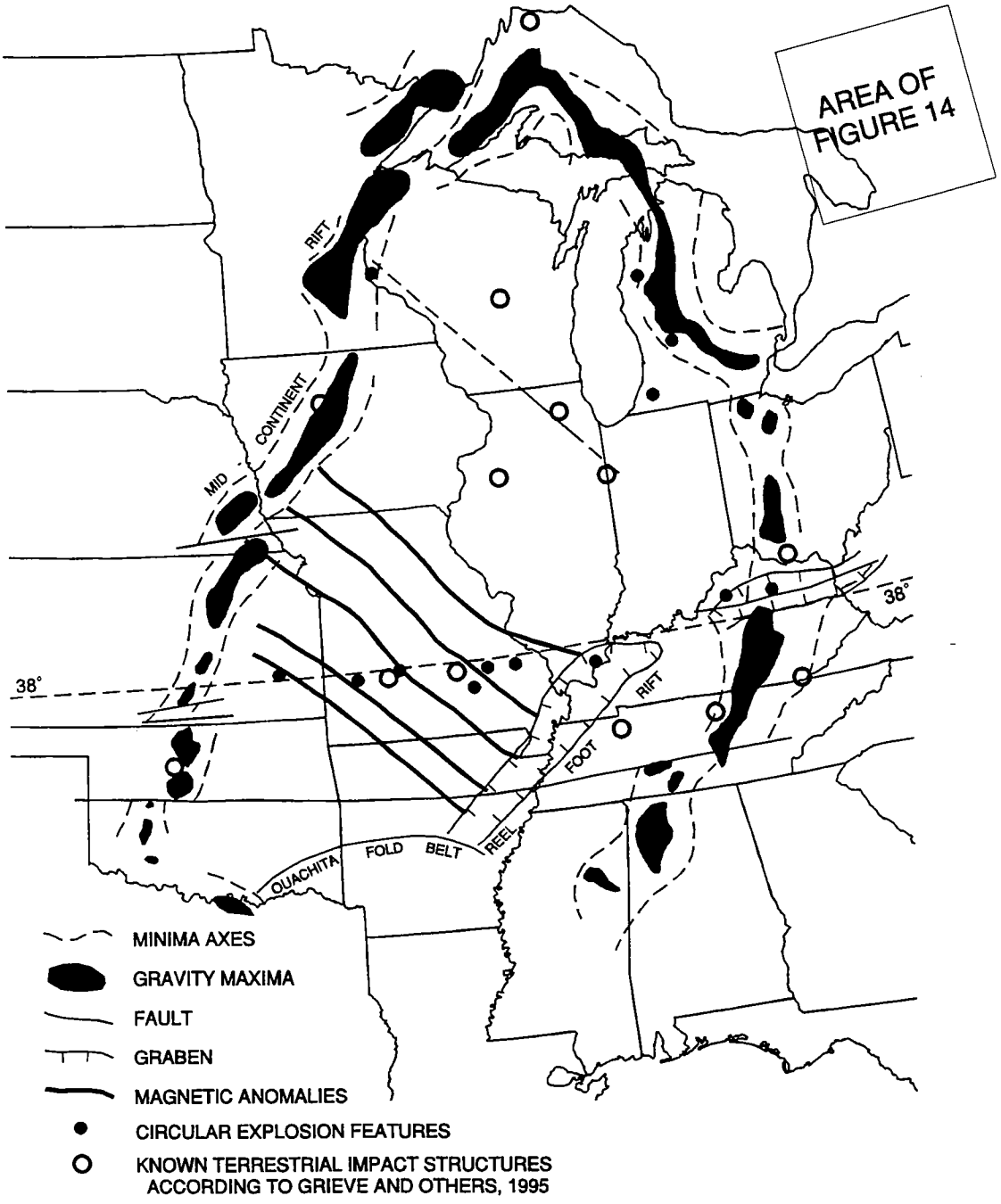

Figure 13. Geographic distribution of circular, brecciated explosion features in the east-central United States. Latitude line denotes the 38th Parallel lineament trend of Lidiak and Zietz (1976). The coincidence of Precambrian rifts, grabens, and transform-fault systems with these circular, anomalous features appears to be anything but random. Delineation of Midcontinent rift is from Lyons (1987).

bens of North America. Figure 17 includes known alkalic ultramafic rocks, kimberlites, lamproites, ultramafic lamprophyres, and komatiites proximal to these features. These maps demonstrate an interesting coincidence between recognized terrestrial impact sites and exposed and/or uplifted Precambrian shield areas and known upper-mantle–derived alkalic rocks. Unfortunately, most of these

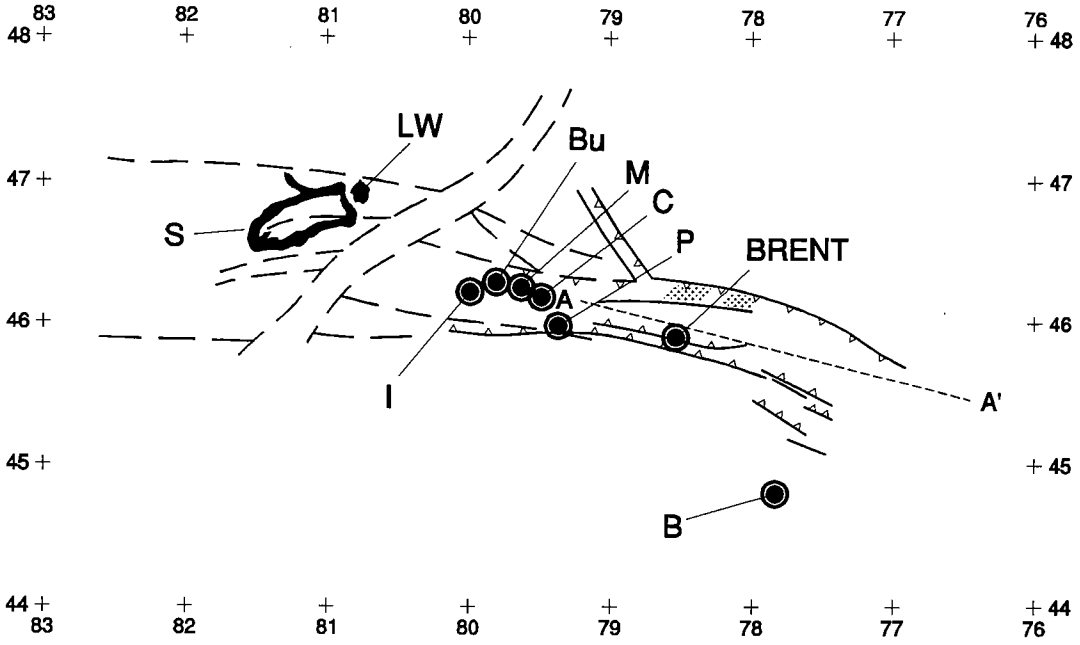

Figure 14. Geographic distribution of circular explosion features in the Ottawa-Bonnechère graben system. Grieve and others (1995) have classified Sudbury (S), Lake Wanapitei (LW), and Brent as impact structures. Nicolaysen (1990) has interpreted these three structures and Burritt Island (Bu), Iron Island (I), Manitou Island (M), Callander Bay (C), Powassan (P), and Bancroft (B) all to be examples of volatile-driven alkalic volcanism within a graben that formed because of a discontinuity in crustal structure. (Modified from Nicolaysen, 1990.) Patterned areas show dike concentrations; circles with solid dots indicate alkalic complexes with zones of fenitization.

sites do not have the subsurface stratigraphic control present at Ames and therefore have been subject to interpretation based solely on petrographic examination. The presence of shocked quartz, shatter cones, stishovite, and/or coesite has often been used as conclusive evidence of an exogenic petrogenesis at the expense of evaluations of critical field relationships suggesting otherwise.

ENDOGENIC MECHANISM

As previously discussed, known cryptoexplosion sites within the east-central United States and southern Canada are confined to Precambrian rifts, transform faults, and grabens. It is interesting that all but 5 are of Paleozoic age. However, north of the southern Canada trend, 14 out of 25 craters are Mesozoic or younger whereas 10 are Paleozoic and 1 is Precambrian. The Mesozoic Canadian craters are confined to a belt of Cretaceous or younger uplifts that occur along a great welt, situated east, south, and west of Hudson Bay (see line of deduced maximum epeirogenic uplift in Figs. 16,17). Nearly all Canadian craters fall within 100 mi of the line of deduced maximum epeirogenic uplift, although only 15% of the Canadian Shield does. Currie (1965, p. 935) stated that the close association of Canadian craters with epeirogenic movement is "damning evidence against a random exogenic origin, entirely apart from detailed structural and petrographic evidence."

Currie (1965) also noted that Quebec and Labrador have the most continuous uplifted terrain, including the Torngat and Manicouagan areas, both of which are of Mesozoic or younger age. Twelve of the known craters and basins on the Canadian Shield occur in Quebec and Labrador. The Northwest Territories, which occupy roughly the same area, are noticeably flat and lacking in uplifted area. Significantly, only three craters are known there. Thus, the tectonically quiet areas, where impacts should be preserved, are lacking those very structures.

Analogous to the Paleozoic craters in the United States and southern Canada, the Mesozoic Canadian craters are coincident with local structural features, usually faults, older than or contemporaneous with the crater. Like Ames, these craters were arched from below, followed by extrusion and in some cases collapse. Hydrothermal activity is always prominent during formation of the crater, and true volcanic activity has occurred

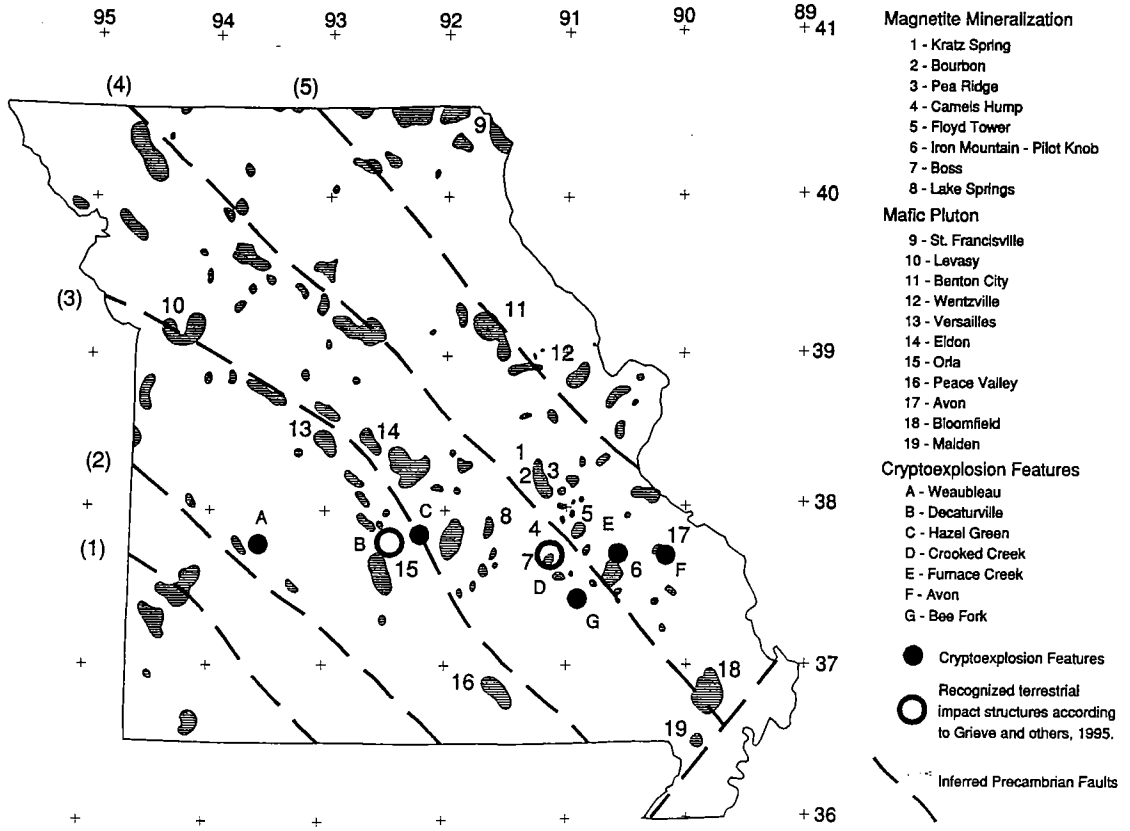

Figure 15. Geographic distribution of circular, brecciated explosion features and their relationship to Precambrian basement magnetic features in Missouri. Linear, northwest-trending aeromagnetic anomalies numbered 1 to 5 represent an inferred Precambrian transform-fault complex joining the Midcontinent and Reelfoot rift systems. Snyder and Gerdemann (1965) have approximated the ages of emplacement of these features as follows, from east to west: Avon—post-Devonian, Furnace Creek—Cambrian, Crooked Creek—Early Ordovician–Middle Ordovician, Hazel Green—Cambrian, Decaturville—post-Silurian, Weaubleau—Mississippian. They further documented field relationships for all of these features that were inconsistent with an impact genesis. All are affiliated with mafic igneous dikes including lamprophyres, peridotites, and alnoites. Grieve and others (1995) have classified Crooked Creek and Decaturville as impact structures. (Modified from Kisvarsanyi, 1984.)

in the largest craters. The continental distribution of these craters and their lithologic assemblage of alkalic ultramafic rocks suggest that their root cause must be deep-seated and connected presumably to conduits in the upper mantle.

The similarities between Paleozoic craters in the east-central United States and southern Canada and the Mesozoic craters of Canada are suggestive of a common tectonic origin. All appear to be related to reactivation of structures in the Precambrian shield or stable cratonic areas. Paleozoic compressional events (i.e., arc-continent and/or continent-continent collisions) and Mesozoic extensional events (i.e., Pangean breakup) appear to be the mechanisms by which these reactivations occurred.

CONCLUSIONS

The establishment of regionally continuous, in situ Arbuckle stratigraphy within the core of the Ames structure has permitted us to reconstruct the growth history of this feature. Without exception, these data show a dynamic circular depression that was in existence by Early Ordovician time (as shown in the Kindblade and West Spring Creek Formations) and domed prior to emplacement of igneous breccias and tuffs in early Middle Ordovician (pre–Oil Creek) time. This feature continued to subside throughout the Paleozoic and is still seismically active today.

Regional geologic evidence documents the Ames structure as one of many cryptoexplosion

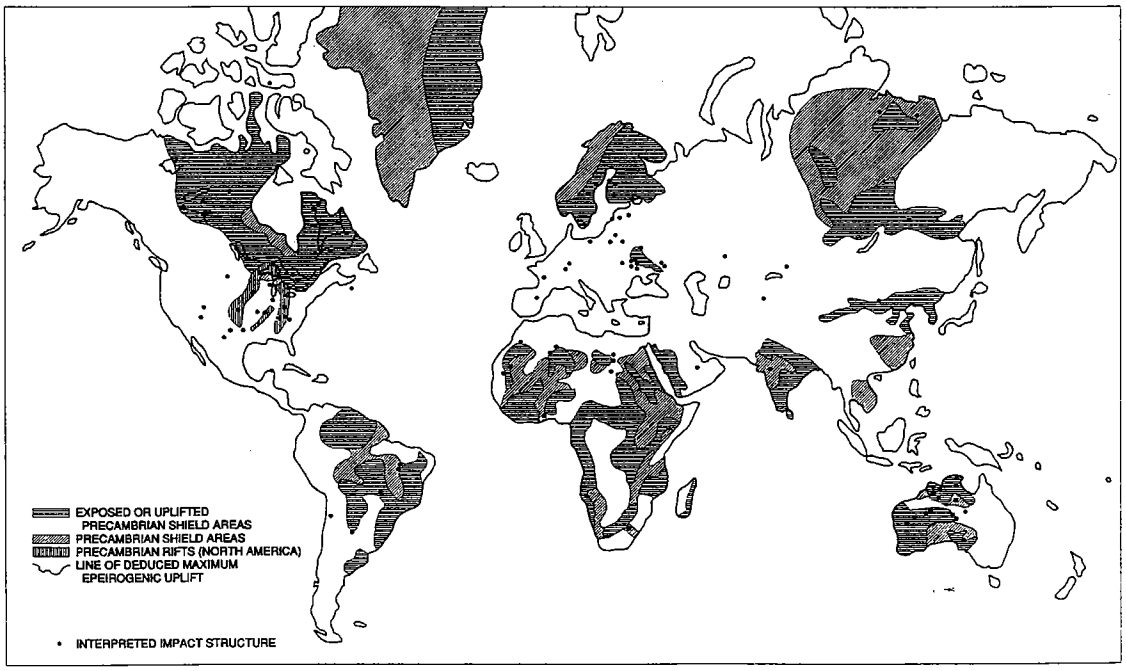

Figure 16. "Recognized terrestrial impact sites" and their distribution relative to exposed and/or uplifted Precambrian shields, rifts, transforms, and grabens. Note the coincidence between these areas and the impact sites. (Modified from Sharpton and Grieve, 1991; data included from Kopecký and others, 1970.)

features in North America whose origin can be attributed to alkalic magmas that ascended deep-seated faults and/or crustal discontinuities within Precambrian rifts, grabens, transform-fault systems, and uplifted shield areas.

The data presented suggest that Ames and other cryptoexplosion features are not the result of random bolide impacts, but rather are predictable phenomena attributable to endogenic processes. Meteorite impacts do occur and have occurred in the past. We do not propose that all circular features with brecciated cores, shock metamorphism, etc., are cryptoexplosion features. Each feature must be examined in detail and must be dealt with in terms of its regional tectonic setting, growth history, and petrographic characteristics. The generation of shock-metamorphic features (including planar deformation features and shock mosaicism in quartz) needs to be addressed vis-à-vis endogenic processes (e.g., Nicolaysen, 1972; Nicolaysen and Ferguson, 1990) and cannot be ignored. We recognize that studies to date have been unable to recreate these types of deformations in the laboratory and that this lack of results will cast some doubt on our interpretations. However, categorizing individual features as endogenic or exogenic without reviewing all available data will always lead to questionable interpretations.

ACKNOWLEDGMENTS

We extend our sincerest gratitude to Ken Johnson of the Oklahoma Geological Survey for his relentless encouragement of us to bring this paper to fruition. In addition, Alan Huffman was extremely helpful in explaining and simplifying to us the complexities relating to shock deformation and *P-T* conditions in the upper mantle. Alan also was invaluable in critiquing the manuscript and giving us focus and direction. Although we may not agree with him on the origin of the Ames feature, we have learned much in our discussions with Alan.

We give special thanks to John Ladd for lending us his reference material on cryptoexplosion structures and for critiquing and improving the manuscript.

We are also indebted to Jill Mally and Julie Smallin for assisting with research and John Schaffer for drafting and reproduction of the figures.

Finally, we thank Tom Patton, Rich Bottjer, Lynn Peyton, and Meri Taliaferro for reviewing and editing the manuscript.

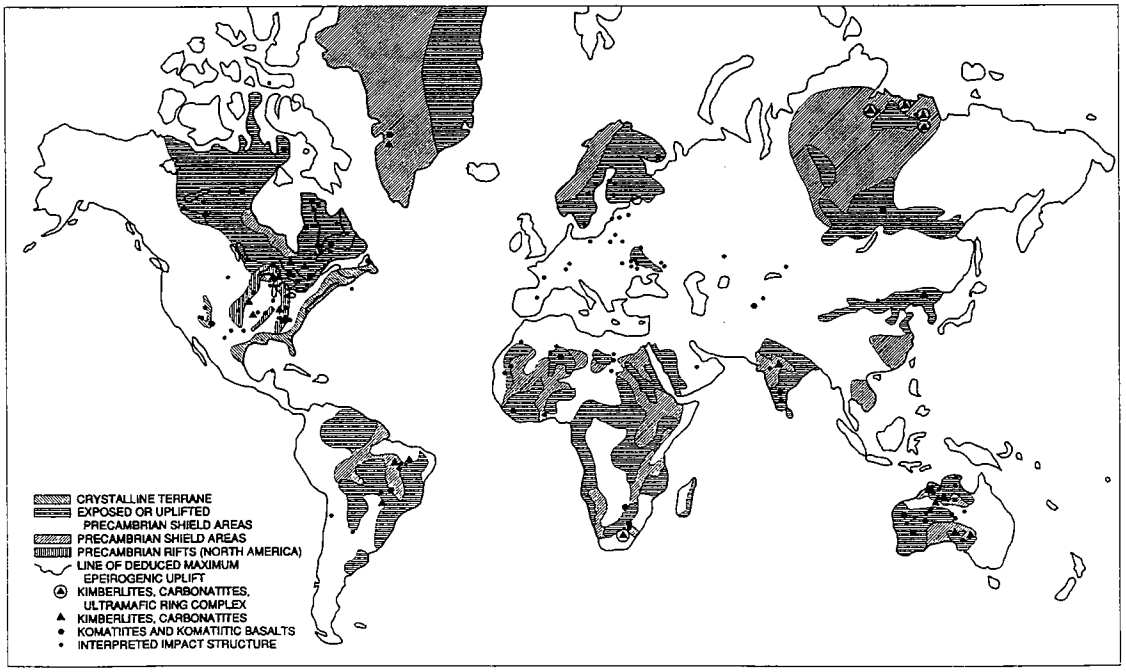

Figure 17. "Recognized terrestrial impact sites" and their distribution relative to exposed and/or uplifted Precambrian shields, rifts, transforms, and grabens and their association with known kimberlites, carbonatites, komatiites, and other alkalic ultramafic rocks. In many areas the relationship appears more than coincidental. (Modified from Sharpton and Grieve, 1991; data included from Kopecký and others, 1970.)

REFERENCES CITED

Ambers, C. P.; Brändlein, Peter; and Gilbert, M. C., 1997, Petrology of enigmatic rocks from 2.75 km depth in the Ames structural anomaly, Major County, Oklahoma, and their relationship to suevite from the Ries crater, Nördlingen, Bavaria, *in* Johnson, K. S.; and Campbell, J. A. (eds.), Ames structure in northwest Oklahoma and similar features: origin and petroleum production (1995 symposium): Oklahoma Geological Survey Circular 100 [this volume], p. 302–309.

Amstutz, G. C., 1965, Tectonic and petrographic observations on regional polygonal structures in Missouri: Annals of the New York Academy of Science, v. 123, p. 876–894.

Bridges, L. W. D., 1996, Ames depression, Oklahoma: domal collapse and later subsurface solution, *in* Johnson, K. S.; and Campbell, J. A. (eds.), Ames structure in northwest Oklahoma and similar features: origin and petroleum production (1995 symposium): Oklahoma Geological Survey Circular 100 [this volume], p. 153–168.

Brown, J. S.; Emery, J. A.; and Meyer, P. A., Jr., 1954, Explosion pipe in test well on Hicks dome, Hardin County, Illinois: Economic Geology, v. 49, p. 891–902.

Bucher, W. H., 1963, Cryptoexplosion structures caused from without or within the earth ("astroblemes or geoblemes")?: American Journal of Science, v. 261, p. 597–649.

Carpenter, B. N.; and Carlson, Rick, 1992, The Ames impact crater: Oklahoma Geology Notes, v. 52, p. 208–223.

_____ 1997, The Ames meteorite-impact crater, *in* Johnson, K. S.; and Campbell, J. A. (eds.), Ames structure in northwest Oklahoma and similar features: origin and petroleum production (1995 symposium): Oklahoma Geological Survey Circular 100 [this volume], p. 104–119.

Coughlon, J. P.; and Denney, P. P., 1993, The Ames structural depression: an endogenic cryptoexplosion feature along a transverse shear: Shale Shaker, v. 43, no. 4, p. 44–58.

Currie, K. L., 1965, Analogues of lunar craters on the Canadian Shield: Annals of the New York Academy of Sciences, v. 123, p. 915–940.

_____1971, A study of potash fenitization around the Brent crater Ontario—a Paleozoic alkaline complex: Canadian Journal of Earth Sciences, v. 8, p. 481–497.

Derby, J. R.; Hinch, H. H.; and Repetski, J. R., 1991, Lithology, stratigraphy, and age of the Arbuckle Group in the Amoco SHADS no. 4: a continuous core from grassroots into basement, Rogers County, Oklahoma, *in* Johnson, K. S. (ed.), Arbuckle Group core workshop and field trip: Oklahoma Geological Survey Special Publication 91-3, p. 69–82.

Fischer, J. F., 1997, The Nicor no. 18-4 Chestnut core, Ames structure, Oklahoma: description and petrography, *in* Johnson, K. S.; and Campbell, J. A.

(eds.), Ames structure in northwest Oklahoma and similar features: origin and petroleum production (1995 symposium): Oklahoma Geological Survey Circular 100 [this volume], p. 223–239.

Gatewood, L. E., 1968, Arbuckle handbook: Privately published, p. 37.

Grieve, R. A. F.; Rupert, J. S.; and Therrialt, A., 1995, The record of terrestrial impact cratering: Geological Society of America GSA Today, v. 5, p. 189–196.

Hamm, H.; and Olsen, R. E., 1992, Oklahoma Arbuckle lime exploration centered on buried astrobleme structure: Oil and Gas Journal, April 20, p. 113–116.

Huffman, A. R., 1997, Shock-induced microstructures and experimental constraints on the formation of the Ames impact structure, *in* Johnson, K. S.; and Campbell, J. A. (eds.), Ames structure in northwest Oklahoma and similar features: origin and petroleum production (1995 symposium): Oklahoma Geological Survey Circular 100 [this volume], p. 310–325.

Johnson, K. S.; and Smith, Dorothy, 1997, Ames structure of northwestern Oklahoma is reflected in overlying Permian strata, *in* Johnson, K. S.; and Campbell, J. A. (eds.), Ames structure in northwest Oklahoma and similar features: origin and petroleum production (1995 symposium): Oklahoma Geological Survey Circular 100 [this volume], p. 357–362.

Kisvarsanyi, E. B., 1984, The Precambrian tectonic framework of Missouri as interpreted from the magnetic anomaly map: Missouri Department of Natural Resources, Contribution to Precambrian Geology, no. 14, part B, 19 p.

Koeberl, Christian, 1997, Impact cratering: the mineralogical and geochemical evidence, *in* Johnson, K. S.; and Campbell, J. A. (eds.), Ames structure in northwest Oklahoma and similar features: origin and petroleum production (1995 symposium): Oklahoma Geological Survey Circular 100 [this volume], p. 30–54.

Koeberl, Christian; Reimold, W. U.; Brandt, Dion; Dallmeyer, R. D.; and Powell, R. A., 1997, Target rocks and breccias from the Ames impact structure, Oklahoma: petrology, mineralogy, geochemistry, and age, *in* Johnson, K. S.; and Campbell, J. A. (eds.), Ames structure in northwest Oklahoma and similar features: origin and petroleum production (1995 symposium): Oklahoma Geological Survey Circular 100 [this volume], p. 169–198.

Kopecký, L., 1974, Detection of faults and determination of their order in regions of platform volcanism: [Czechoslovakia] Sborník Geologickych Ved, v. 26, p. 197–220.

Kopecký, L.; Dobeš, M.; Fiala, J.; and Štovíčková, N., 1970, Fenites of the Bohemian massif and the relations between fenitization, alkaline volcanism and deep fault tectonics: [Czechoslovakia] Sborník Geologických Věd, v. 16, p. 51–107.

Kuykendall, M. D.; Johnson, C. L.; and Carlson, R. A., 1997, Reservoir characterization of a complex impact structure: Ames impact structure, northern shelf, Anadarko basin, *in* Johnson, K. S.; and Campbell, J. A. (eds.), Ames structure in northwest Oklahoma and similar features: origin and petroleum production (1995 symposium): Oklahoma Geological Survey Circular 100 [this volume], p. 199–206.

Lidiak, E. G.; and Zietz, I., 1976, Interpretation of aeromagnetic anomalies between latitude 37°N and 38°N in the eastern and central United States: Geological Society of America Special Paper 167, 37 p.

Lyons, P. L., 1987, Gravity and magnetic expression of the tectonic framework of the Mid-Continent, *in* Rascoe, Bailey, Jr.; and Hyne, N. J. (eds.), Petroleum geology of the Mid-Continent: Tulsa Geological Society Special Publication 3, p. 15–18.

Nicolaysen, L. O., 1972, North American cryptoexplosion structures: interpreted as diapirs which obtain relief from strong lateral confinement, in Shagam, R., and others (eds.), Studies in earth and space sciences: Geological Society of America Memoir 132, p. 605–620.

Nicolaysen, L. O.; and Ferguson, J., 1990, Cryptoexplosion structures, shock deformation, and siderophile concentration related to explosive venting of fluids associated with alkaline ultramafic magmas: Tectonophysics, v. 171, p. 303–335.

Reidel, S. P.; and Koucky, F. L., 1981, The Serpent Mound cryptoexplosion structure, southwestern Ohio: Geological Society of America Field Trip no. 6/16 Guidebook, p. 391–403.

Reidel, S. P.; Koucky, F. L.; and Stryker, J. R., 1982, The Serpent Mound disturbance, southwestern Ohio: American Journal of Science, v. 42, p. 1343–1377.

Roberts, C.; and Sandridge, B., 1992, The Ames hole: Shale Shaker, v. 42, p. 118–120.

Roemer, C. D.; Roemer, C.; and Williams, K., 1992, Gravity, magnetics points to volcanic origin for Oklahoma's Ames anomaly: Oil and Gas Journal, June 29, p. 75–80.

Sharpton, V. L.; and Grieve, R. A. F., 1991, Meteorite impact, cryptoexplosion, and shock metamorphism; a perspective on the evidence at the K/T boundary, *in* Sharpton, V. L.; and Ward, P. D. (eds.), Global catastrophes in Earth history: Geological Society of America Special Paper 247, p. 301–318.

Shirley, K., 1992, Overlooked "hole" found: American Association of Petroleum Geologists Explorer, v. 13, p. 3.

Shrock, R. R.; and Malott, C. A., 1933, The Kentland area of disturbed Ordovician rocks in northwestern Indiana: Journal of Geology, v. 41, p. 337–370.

Snyder, F. G.; and Gerdemann, P. E., 1965, Explosive igneous activity along an Illinois-Missouri-Kansas axis: American Journal of Science, v. 263, p. 465–493.

Zartman, R. E.; Brock, M. R.; Heyl, A. V.; and Thomas, H. H., 1967, K-Ar and Rb-Sr ages from some alkalic intrusive rocks from central and eastern United States: American Journal of Science, v. 265, p. 848–870.

Ames Depression, Oklahoma: Domal Collapse and Later Subsurface Solution

L. W. Dan Bridges
Independent Petroleum Geologist
Aurora, Colorado

ABSTRACT.—Three bold new proposals are made. Most shocked quartz and nearly all shatter cones are caused by intense faulting, not meteorite impact. Central peaks in impact craters are caused by carved topography, not rebound; and ring depressions are caused by concentric collapse into depleted magma chambers or cavities created by faulting, not by shock waves. Thus, most of the circular features on Earth attributed to meteorite impact were caused by varying combinations of long-term structural growth, magmatic activity, and subsurface solution.

The Ames depression in northwestern Oklahoma has a long and complicated history. Doming of the Arbuckle Group in Early Ordovician time was apparently caused by magmatic intrusion at depth. Withdrawal of this magma led to progressive, long-term, domal collapse into this former magma chamber; the collapse has created a circular depression 6 mi in diameter and 400 ft deep at the Arbuckle level. The depth of the depression decreases gradually upsection to and including the Permian outcrop. A small earthquake on the southeastern rim of the depression in April 1994 further documents continuous, long-term, domal collapse.

In post-Ordovician time, a high-pressured hydrothermal slurry created vertical solution pipes, possibly along reactivated Precambrian faults, and caused lateral subsurface solution both above and below the Arbuckle unconformity within the Ames depression. These solution cavities were filled with clasts and breccias of reworked Precambrian granite with a reprecipitated carbonate matrix that is highly porous in many places. A small component of igneous material became quenched to form glass, since devitrified; and there are some small Reagan Sandstone clasts and some chert from reprecipitated silica. Radiometric dating suggests that the late Paleozoic Wichita orogeny was the time of formation of the solution cavities containing Precambrian granite clasts that were carried 1,000 to 1,400 ft upsection by the high-pressured slurry.

Earlier interpretations that the Ames depression was created by meteorite impact relied, in part, on the presence of shock-metamorphosed quartz. I think that this deformation of quartz took place in Precambrian time, possibly along Precambrian faults. Furthermore, the structurally high rim around the southwestern, downdip edge of the Ames depression was caused by regional southwest dip and domal collapse, not by impact.

INTRODUCTION

Contrary to most current geologic thinking, I do not accept meteorite impact as the cause for the circular features originally called "cryptovolcanic" structures, then "cryptoexplosion" structures, and more recently "astroblemes." My conclusion stems primarily from my research on the subsurface Red Wing Creek structure in North Dakota (Bridges, 1978, 1987b). Long-term structural growth over hundreds of millions of years with no explosion is still my conclusion for the origin of the Red Wing Creek structure. However, the master fault may flatten out into the Mississippian carbonate section. If this is the case, an expanding Earth may be largely responsible for the Red Wing Creek structure.

L. W. Dan Bridges, 1925 S. Vaughn Way, #207, Aurora, CO 80014.

Shocked Quartz

Shocked quartz and shatter cones are usually attributed to meteorite impact because laboratory experiments indicate that extremely high pres-

Bridges, L.W. D., 1997, Ames depression, Oklahoma: domal collapse and later subsurface solution, *in* Johnson, K. S.; and Campbell, J. A. (eds.), Ames structure in northwest Oklahoma and similar features: origin and petroleum production (1995 symposium): Oklahoma Geological Survey Circular 100, p. 153–168.

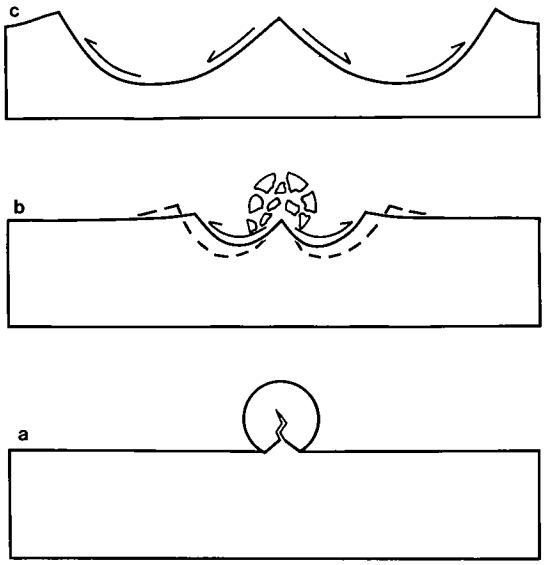

Figure 1. Central peak development in meteorite-impact craters by carved topography, an alternative explanation to the rebound theory: (a) impact, which breaks meteorite into fragments, (b) erosion by meteorite fragments around center area, and (c) resulting topography. From Bridges (1987b, Fig. 7), reprinted by permission.

sures are needed to create them. Some geologists still insist that shocked quartz is proof of meteorite impact; but "shocked" quartz has been created in the laboratory under constant strain, and quartz with planar deformation features is found in quartzites in metamorphic terrane (Lyons and others, 1993).

Wegener's theory of continental drift was not accepted for a long time because no one could believe that there was sufficient power within the Earth to produce this movement. I think that most shocked quartz and nearly all shatter cones are caused by intense faulting. The jolt, wrenching, and/or torque caused by fault displacement under high pressures, which cannot be adequately duplicated in the laboratory, create shocked quartz and shatter cones at much lower pressures than is believed, in my opinion. Hargraves (1993) reported shocked quartz and shatter cones in a large thrust-faulted area in southwestern Montana without any evidence of impact.

Meteor Crater, Arizona

There is no question that Meteor (or Barringer) Crater in Arizona is a meteorite crater. Fragments of the meteorite and the high-pressure silica minerals coesite and stishovite have been found in and around the crater (Chao and others, 1960, 1962). To the best of my knowledge, no meteoritic material has been found in other so-called astroblemes. Those who believe in impact claim that all of the meteoritic material was vaporized during the impact process. Many, if not most, of the so-called astroblemes do not contain coesite or stishovite.

Rebound

Rebound after impact is invoked to explain the central uplifts in the circular features on Earth. I maintain that the central peaks in impact craters on the Moon and planets are caused by carved topography (Fig. 1), not rebound. In my opinion, central uplifts on Earth are caused by long-term structural growth. An impact crater on Mars called Yuty (Fig. 2) has a prominent central peak with large lobes of slide material (possibly including permafrost) around it. How could soft material like this rebound into a sharp peak? A large comet or asteroid exploded over the Siberian taiga and knocked down cows hundreds of miles away. Tunguska (Fig. 3) has always been called strange because trees in the central area had their limbs and bark peeled off but remained standing. The standing trees support the carved topography concept, not the rebound concept.

Manicouagan Structure, Canada

According to the impact theory, the ring depressions around many circular features both on Earth and on the planets are caused by shock waves. I fail to understand how shock waves emanating from an impact site could cause the concentric faulting that forms ring depressions. Manicouagan (Currie, 1972; Grieve and Floran, 1979) in Quebec, Canada (Fig. 4), has two ring depressions (Warner and others, 1977) that I think were caused by concentric collapse into depleted magma chambers (Fig. 5). In my opinion, Chicxulub, on the Yucatán Peninsula of Mexico, and other ringed, circular planetary features were caused by volcanic activity, not impact. However, I think the ring depression around the Red Wing Creek structure was caused by concentric collapse into a void created by faulting. No magmatic activity or subsurface solution affected the Red Wing Creek long-term structural growth.

Serpent Mound Disturbance, Ohio

In contrast to Manicouagan, the Serpent Mound disturbance, in Ohio (Fig. 6), is quite small (4 km diameter) and has no continuous ring depression. It is smaller than the Ames depression, but the central uplift of 1,000 ft (Reidel and others, 1982) is about twice the domal uplift at Ames. Unlike Ames, which has domal uplift extending 2 mi outside of the central collapse, there is only regional northeasterly dip outside the feature.

Paragon Geophysical, Inc., shot a southwest–northeast seismic line across Serpent Mound (Fig. 7) (Hansen, 1994). It revealed a deformation pattern typical of vertical block faulting and totally unlike the high-angle reverse faulting in the Red

Figure 2. Photograph of Yuty, an impact crater on Mars (courtesy of the National Aeronautics and Space Administration).

Wing Creek structure (see Fig. 13). My interpretation of Serpent Mound is that pressure from an expanding Earth pushed up the central uplift over a period of hundreds of millions of years. This process created a cavity or void, and the feature irregularly collapsed into the void.

AMES GEOLOGIC HISTORY

Because my concept for the Ames structure is so different from the impact model, I think it is best to summarize my interpretation of the geologic history with a generalized southwest–northeast schematic cross section across the Ames depression (Fig. 8). There is no proof that the shocked quartz at Ames formed in Paleozoic time. Instead, I think the shocked quartz was formed in Precambrian time, possibly by regional Precambrian faulting. In Early Ordovician time, magma at depth created a domal uplift of the Arbuckle Group. Subsequent erosion peneplained the dome and formed a local angular unconformity. As the

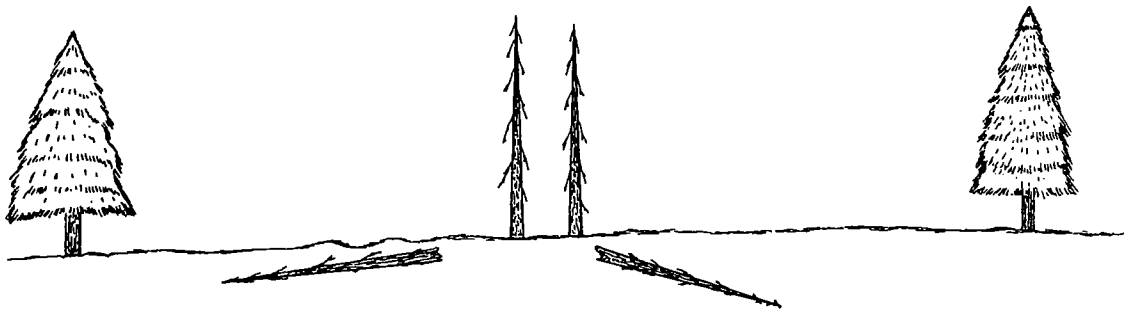

Figure 3. Cross section showing the results of a comet that exploded over Tunguska, Siberia, on June 30, 1908. The explosion left a circular area, 60 km in diameter, of mostly downed trees. The trees in the center of the circle remained standing although they had their limbs and bark peeled off.

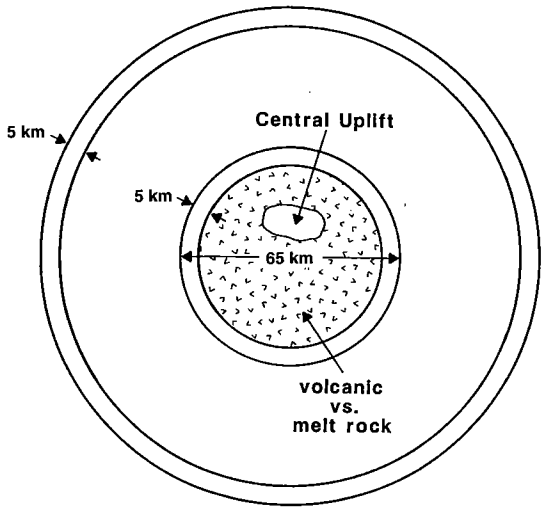

Figure 4. Map of the Manicouagan, Quebec, circular structure that is 150 km in diameter.

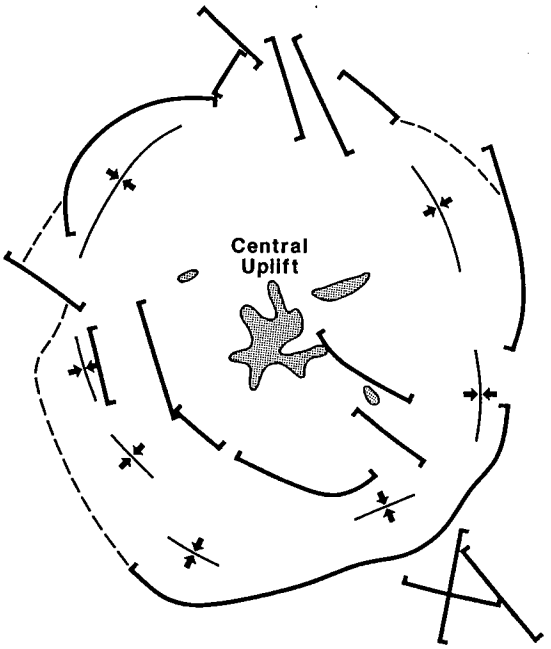

Figure 6. Map of Serpent Mound disturbance, south-central Ohio. Modified from Reidel and others (1982), reprinted by permission.

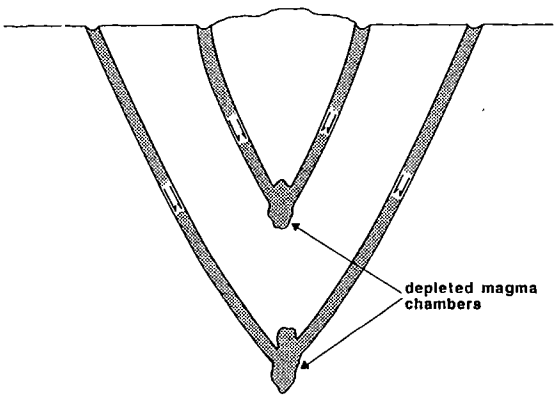

Figure 5. Cross section of Manicouagan, Quebec, showing an interpretation of concentric collapse into depleted magma chambers.

magma withdrew and/or a solution cavity developed, slumping into this cavity created a circular depression in the center of the dome much like caldera collapse in a volcano. Instead of compaction, which is invoked by those who conclude that this feature was caused by impact, collapse into the former magma and/or solution chamber has continued to the present, causing a small earthquake on the southeastern rim of the depression in April 1994. Could compaction create an earth-

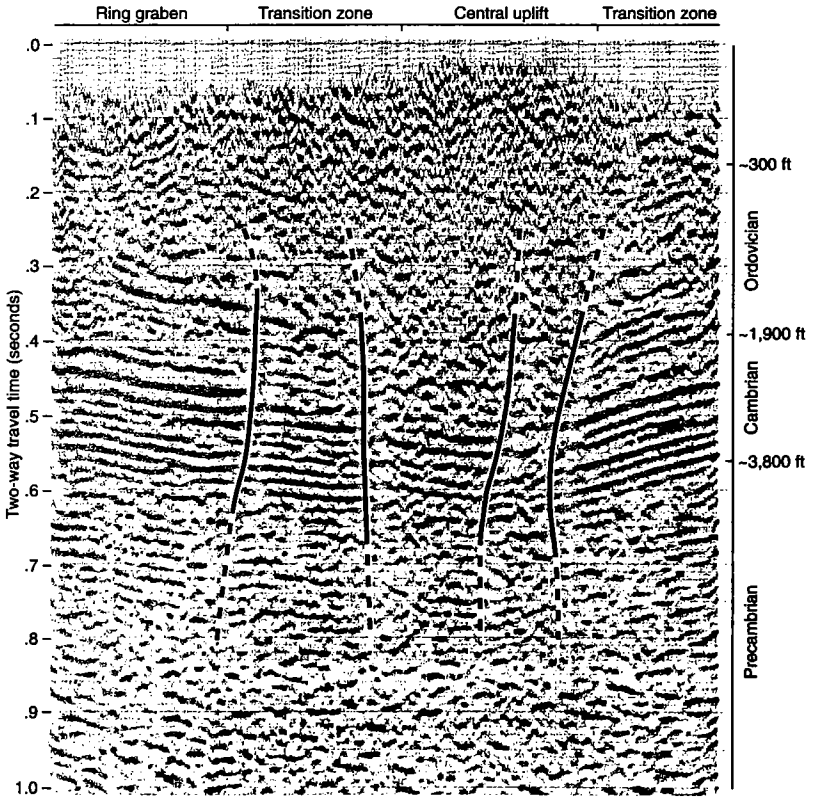

Figure 7. Compressed and migrated southwest–northeast seismic section through the Serpent Mound cryptoexplosion structure. The section crosses the outer ring graben, the central uplift, and the transition zone. Prominent reflectors, which are faulted, show the boundary between crystalline basement and Cambrian sedimentary rocks at a depth of about 3,800 ft. The seismic line was donated to the Ohio Department of Natural Resources, Division of Geological Survey, by Perry Dean, Paragon Geophysical, Inc.; its processing was courtesy of Lauren Geophysical, Inc. Interpretation is by Mark Baranoski of the Division of Geological Survey. Faults dashed where inferred. (Reprinted with permission from the Ohio Department of Natural Resources, Division of Geological Survey.)

quake? High-pressured subsurface hydrothermal solutions created vertical solution pipes that carried clasts and fragments of Precambrian granite containing shocked quartz upward to the Arbuckle unconformity. Radiometric dating by Koeberl and others (1997) suggests that this event occurred during the late Paleozoic Wichita orogeny, rather than impact in Ordovician time.

Using the stepwise-heating method for ^{40}Ar-^{39}Ar age determination, Koeberl and others (1997) obtained three radiometric dates of 282.7, 285.4, and 312 Ma from granitic rocks in cores from the CRI (Continental Resources, Inc.) no. 1-19 Dorothy well in the Ames depression. They concluded that whatever caused these ages occurred at about 285 Ma. Through the use of K-Ar radiometric dating, Teledyne obtained whole-rock dates of 245 ± 12 Ma from a granite clast from a depth of 9,026 ft and 405 ± 20 Ma from 9,005 ft from "tuffaceous" carbonate in the Nicor no. 18-4 Chestnut core (J. P. Coughlon and P. P. Denney, personal communication, 1995). From unaltered granite in the Bland well, R. J. Stern and R. E. Denison (R. E. Denison, personal communication, 1995) obtained an $^{87}Rb/^{86}Sr$ radiometric date of 1,194 Ma on whole-rock and feldspar samples. "But high initial $^{87}Sr/^{86}Sr$ indicates that this is a reset or partially reset age. Assuming an initial $^{87}Sr/^{86}Sr = 0.703$, an age of 1,320 Ma is calculated. This is probably a better estimate of the crystallization age of the granite" (R. E. Denison, personal communication, 1995). If the radiometric date was partially reset, it could have been reset during the Wichita orogeny. If impact occurred in Ordovician time, why aren't some of these radiometric age determinations Ordovician?

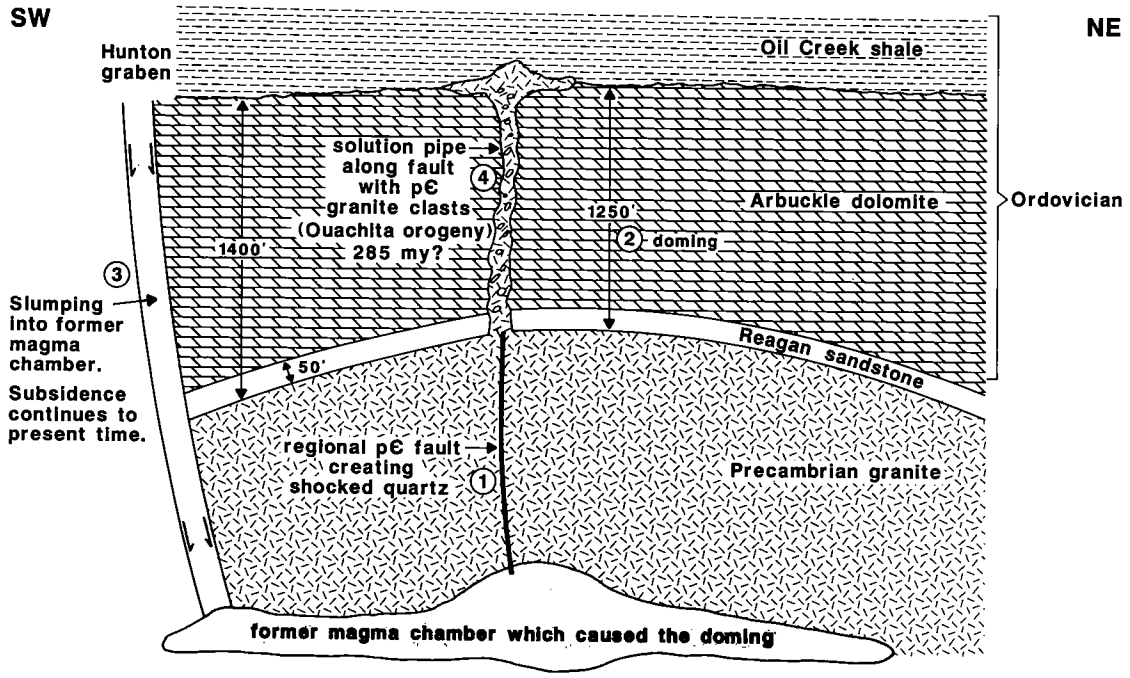

Figure 8. Schematic southwest-northeast cross section of Ames structure with an interpretation of its geologic history.

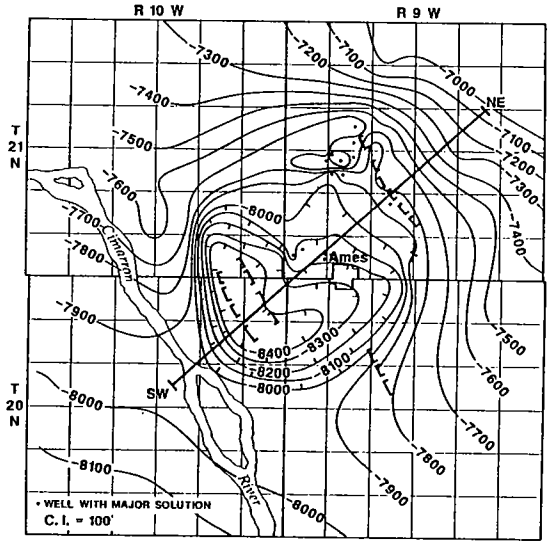

Figure 9. Arbuckle unconformity (Early Ordovician) structure map of Ames depression.

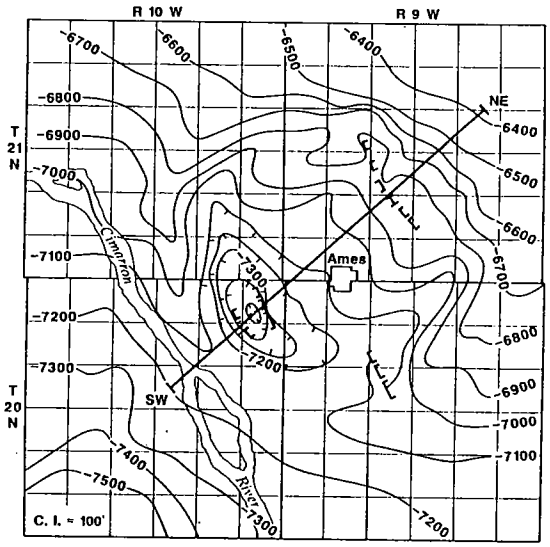

Figure 10. Sylvan Shale (Late Ordovician) structure map of Ames depression.

STRUCTURE MAPS

The three structure maps document progressively less relief in the Ames depression higher in the section. At the unconformity at the top of the Lower Ordovician Arbuckle Group (Fig. 9), the depression is 400 ft deep. At the top of the Upper Ordovician Sylvan Shale (Fig. 10), it is 200 ft deep; and on the Pennsylvanian Oswego limestone (of the Marmaton Group; Fig. 11), it is only 50 ft deep. Johnson and Smith (1997) demonstrated some thickening in the Permian. The fact that this de-

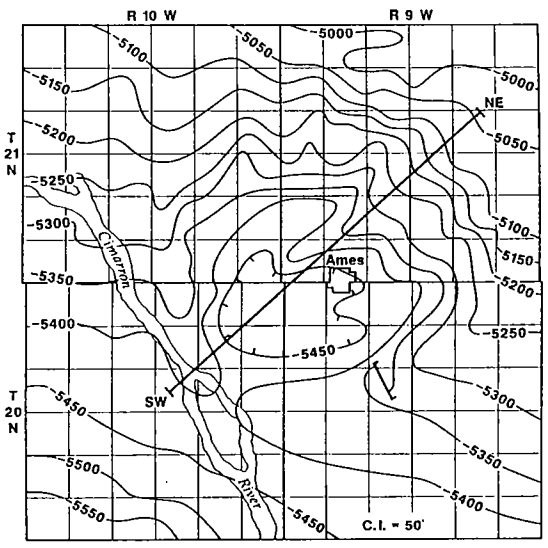

Figure 11. Oswego limestone (of the Pennsylvanian Marmaton Group) structure map of Ames depression.

pression persisted from Ordovician to Permian time implies long-term structural growth. If the depression had been created by an Early Ordovician impact, it should have been filled before Sylvan deposition.

TRUE-SCALE CROSS SECTIONS

A true-scale cross section (Fig. 12) emphasizes the lack of structural relief in the Ames depression. The location of this cross section is shown in Figures 9, 10, 11, and 14. In contrast, the Red Wing Creek structure (Fig. 13) has 2,200 ft of structural relief (Bridges, 1987b). According to David Roddy and Paul Lowman (presentation at the 1995 Ames workshop), there is a 98% probability that an impacting bolide will strike the target approximately at a 45° angle. So how can the Ames and Red Wing Creek structures, which are about the same size, yet are so different, both be explained by impact at a 45° angle?

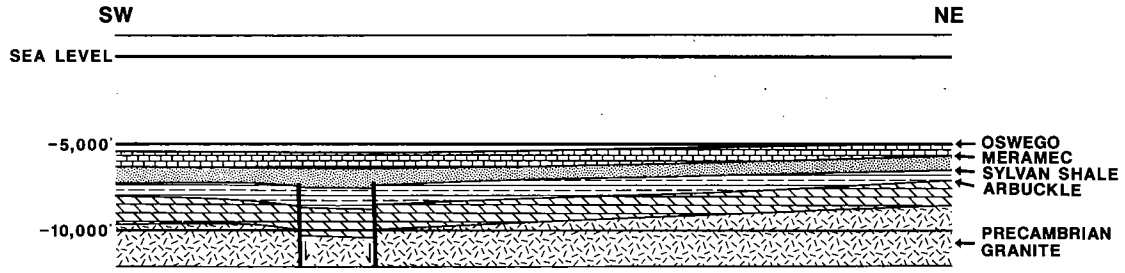

Figure 12. True-scale southwest-northeast cross section at Ames.

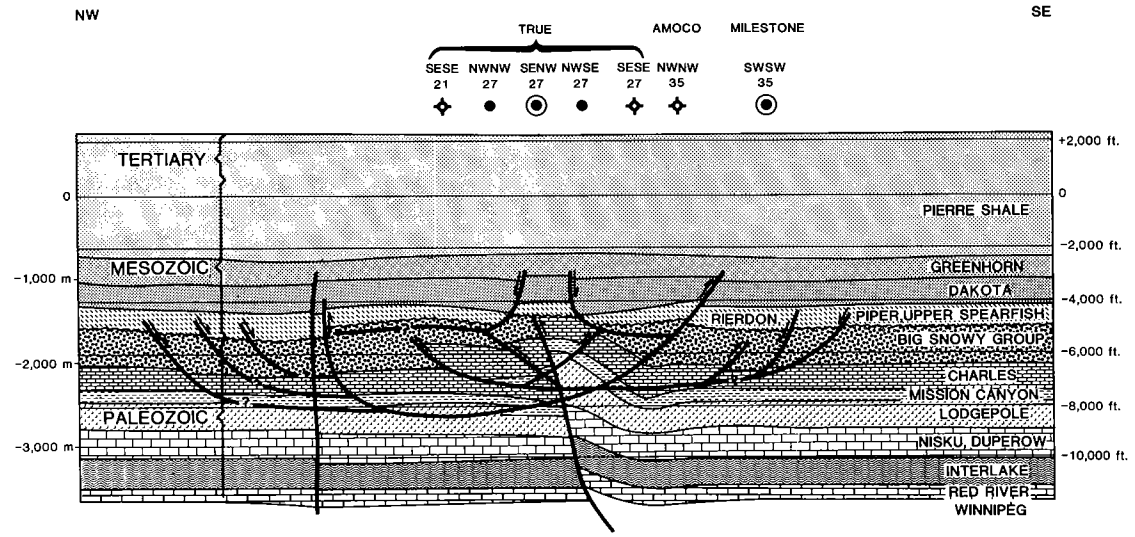

Figure 13. True-scale northwest-southeast cross section of Red Wing Creek structure, North Dakota (Bridges, 1987b, Fig. 2).

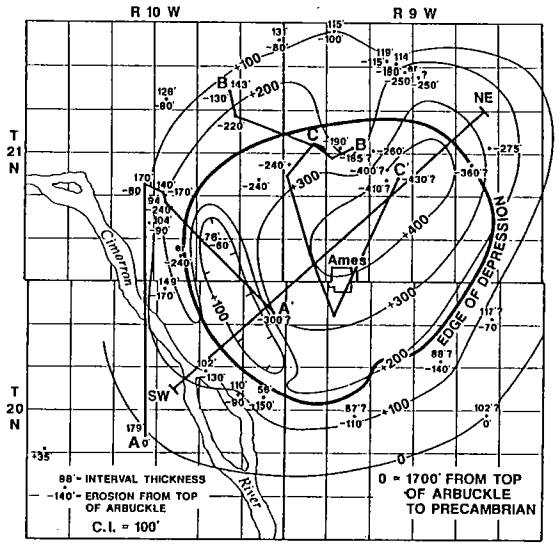

Figure 14. Domal uplift at Ames. The uplift preceded the depression.

DOMAL UPLIFT

Coughlon and Denney (1993,1997) first recognized the Early Ordovician doming of the Arbuckle Group in the Ames structure. The lower numbers in each pair posted by the wells in Figure 14 represents an attempt to quantify the amount of doming. Two wells on the south side of the structure (DLB no. 21-10 Henry NW¼SE¼ sec. 21, T. 20 N., R. 10 W., and BRG no. 2-23 Gregory NW¼NE¼ sec. 23, T. 20 N., R. 9 W.) were arbitrarily assigned a zero value of missing Arbuckle section, meaning that these wells had a full section of Arbuckle. There is progressively more section missing toward the center of the depression. Thus, –110 ft in the NW¼NE¼ sec. 20, T. 20 N., R. 9 W., means that 110 ft of section was eroded from the top of the Arbuckle Group. Outside the depression, Arbuckle correlations are easy; but inside the depression, alteration of massive carbonate in the Arbuckle makes correlations very difficult or impossible. I correlated into the depression from the north side and concluded that there is about 450 ft of doming of the Arbuckle Group. To contour the dome, I simply changed the minus values (amount of missing section) to positive values.

The upper numbers in each pair posted by the wells in Figure 14 indicates the thickness of an interval within what is locally called the West Spring Creek Formation in the upper part of the Arbuckle Group. These correlations are debatable, but the interval generally thins toward the center of the dome. In some wells, each group of beds is thinner. In other wells, the thinning is caused by missing section at the top of the interval. These two types of thinning indicate irregular structural growth. If this feature had been caused by instantaneous impact, there should not be any structural growth.

The edge of the depression is shown as a heavy circle superimposed over the domal contour lines in Figure 14. Certainly, one cannot accept the idea that the bolide scored a direct hit on the center of the dome. If, as the geologists supporting impact propose, the bolide caused uplift around the impact site, why is there no such uplift around the Red Wing Creek and Serpent Mound structures? It seems far more logical to conclude that none of these features was caused by impact, but that each had its own unique structural development.

ELECTRIC LOGS

Cross Section A–A′

The location of cross section A–A′ (Fig. 15) is shown in Figure 14. The section is hung on the Arbuckle angular unconformity to visually demonstrate the doming and interval thinning. The Bogo no. 3-35 Campbell well (NW¼NW¼ sec. 35., T. 21 N., R. 10 W.) in the Hunton graben is the only well in the depression in which the West Spring Creek Formation is preserved. In all other wells in the depression, it has been removed by deeper erosion prior to domal collapse. The Bogo well indicates that domal collapse into the Hunton graben began before domal uplift was complete. This complicated geologic history does not support the instantaneous impact hypothesis.

Cross Sections B1–B1′ and B2–B2′

Three different versions of cross section B–B′ are presented. The Nicor no. 18-4 Chestnut well is placed next to the D. & J. no. 1-20 Wayne well for visual contrast. B1–B1′ (Fig. 16) is hung on the base of the Ordovician Wilcox Sandstone to demonstrate thickening of the underlying Oil Creek shale into the depression. B2–B2′ (Fig. 17) represents an attempt to hang the section on the Arbuckle unconformity on the assumption that the event that brought the clasts of Precambrian granite upsection had occurred before deposition of the Oil Creek shale. This hypothesis creates considerable topographic relief that should be compensated by thinning of the Oil Creek over highs and thickening of the Oil Creek into lows. There is no thickening or thinning of the Oil Creek shale, so I conclude that this hypothesis cannot be correct. Therefore, the event did not precede deposition of the Oil Creek shale.

Cross Section B3–B3′

Cross section B3–B3′ (Fig. 18) is hung on the Arbuckle unconformity with the assumption that the clasts of Precambrian granite were injected upward into the section later, like an igneous sill,

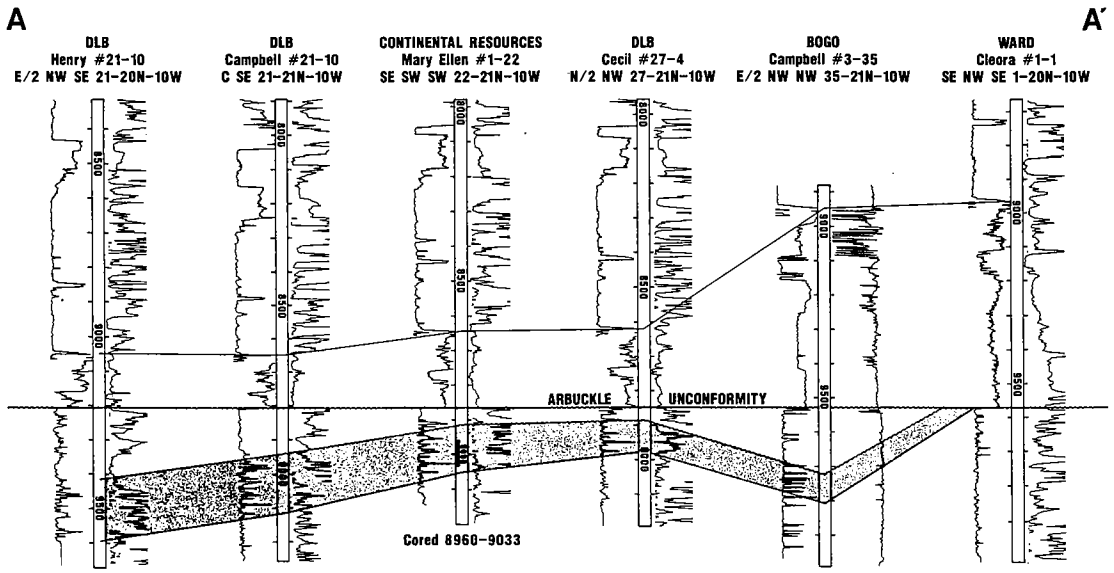

Figure 15. Cross section A–A′ showing Arbuckle doming and interval thinning.

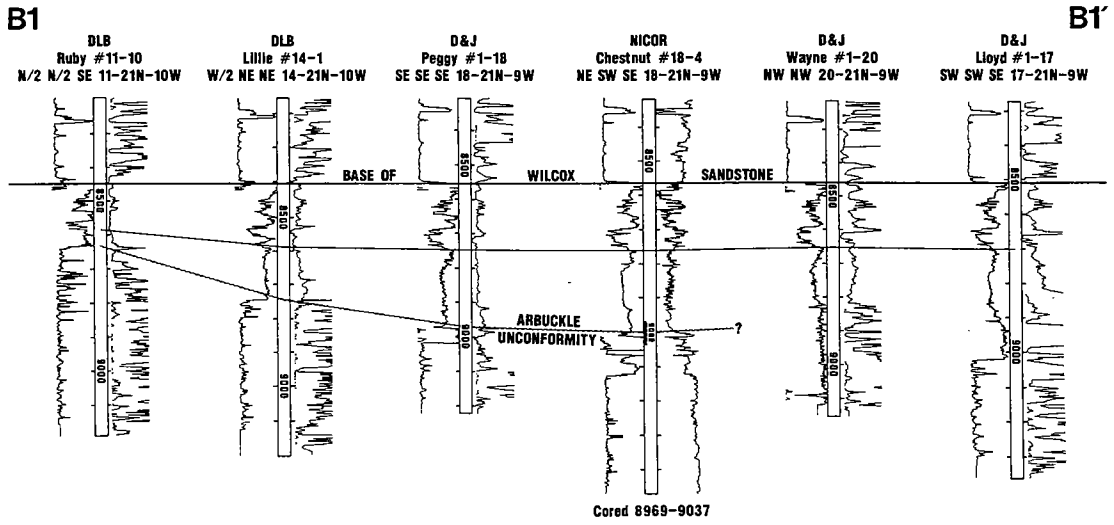

Figure 16. Cross section B1–B1′ showing thickening of the Oil Creek shale into the depression.

by high-pressured hydrothermal subsurface solution (see Fig. 8). I think that this is the correct interpretation. Therefore, above the solution pipes where subsurface solution was most active, the lower part of the Oil Creek shale was removed by solution and replaced by sand- to pebble-sized fragments of Precambrian granite as shown in the patterned interval of the D. & J. no. 1-20 Wayne well. As the power and temperature of this high-pressured aqueous slurry waned, the water level dropped so that reprecipitation of carbonate cement took place below the patterned interval in the Wayne well. This left the patterned interval relatively uncemented with extremely high porosity and permeability. Thus the Wayne well and nearby Gregory well, which are perforated in the patterned interval, are two of the most prolific single-zone oil wells in Oklahoma.

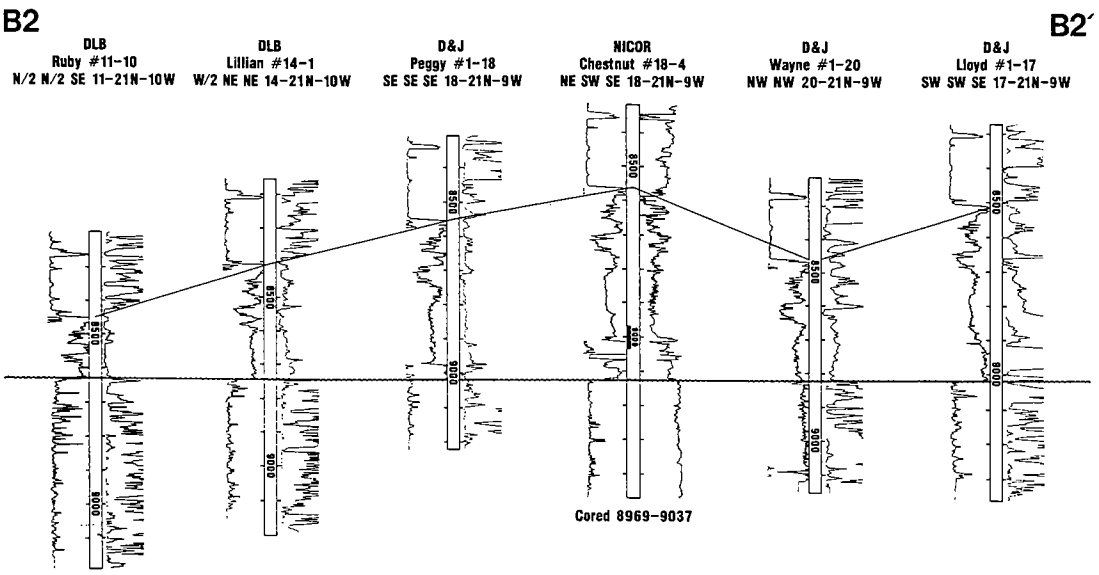

Figure 17. Cross section B2–B2′ interpreting the introduction of the clasts of Precambrian granite as a pre–Oil Creek shale event.

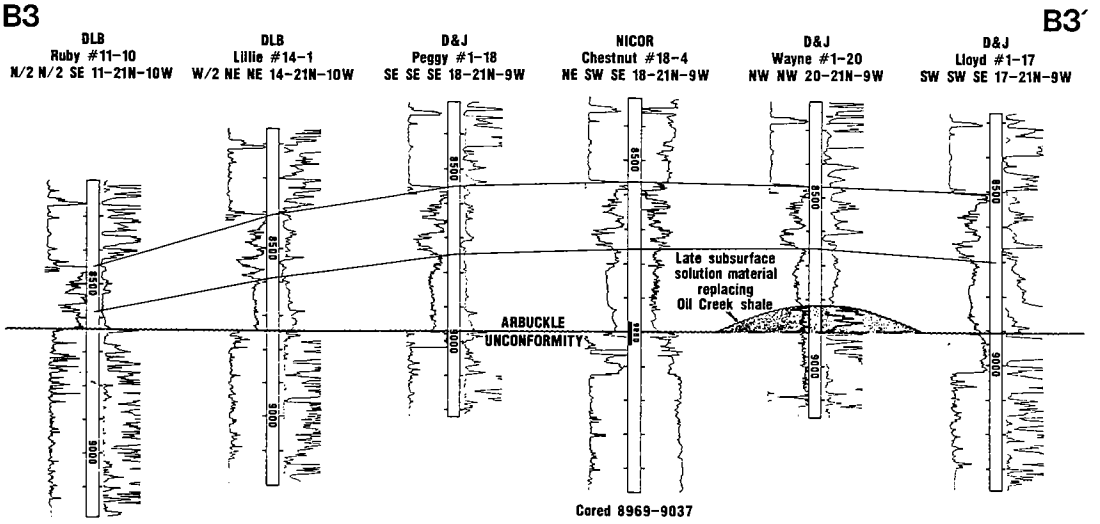

Figure 18. Cross section B3–B3′ interpreting the introduction of the clasts of Precambrian granite as a post–Oil Creek shale event.

Cross Section C–C′

Cross section C–C′ (Fig. 19) is presented to explain the subsurface solution concept in the Ames structure (see Bridges, 1982, 1987a, 1991). In Colorado, I maintain that what is usually called karst on top of the Mississippian Leadville Limestone actually represents Tertiary subsurface solution (see Bridges and McCarthy, 1990). Typically, the hydrothermal solutions come up until they meet an impermeable formation, like shale. Then they move laterally along the interface between permeable and impermeable rocks, as appears to have happened in the Continental Resources no. 1-21 Pacific well. Sometimes, when the top of the

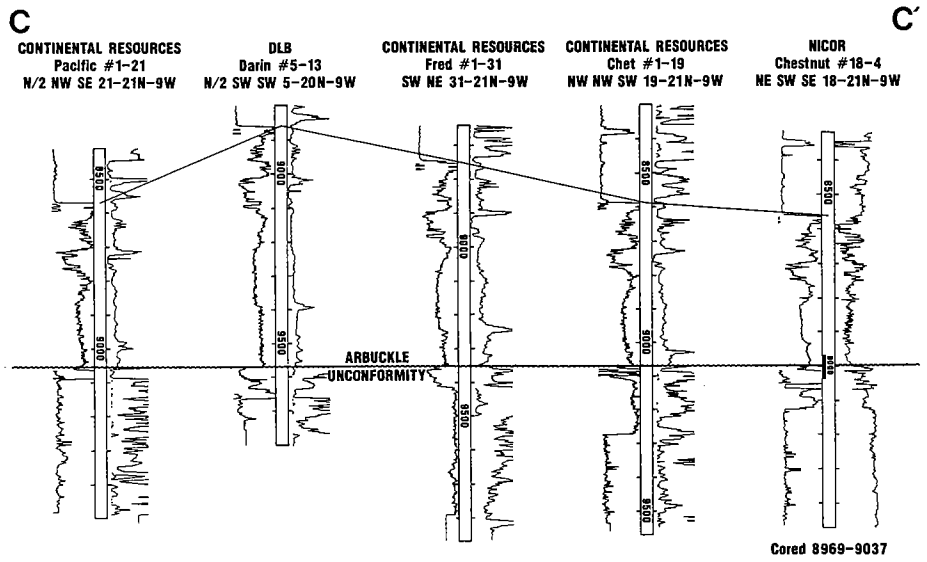

Figure 19. Cross section C–C′ showing subsurface solution at Ames.

carbonate is less permeable, the solutions move laterally, leaving a cap of carbonate, as is seen in the DLB no. 5-13 Darin and Continental Resources no. 1-31 Fred and no. 1-19 Chet wells. The greater thickness of replacement material in the Fred well indicates that it is near a solution pipe that brought up clasts of Precambrian granite. In the Nicor no. 18-4 Chestnut well, I interpret the 20-ft-thick interval from 9,050 to 9,070 ft as a bridge of Arbuckle dolomite that escaped solution. The high gamma-ray interval at 9,030 ft is documented in the core to be caused by clasts of Precambrian granite. Lower gamma-ray readings in the solution intervals indicate less granitic material and more reprecipitated carbonate.

SUBSURFACE SOLUTION

To facilitate a better understanding of the subsurface-solution concept, some discussion seems warranted.

Rose Dome

Rose dome, in Woodson County, southeastern Kansas (Merriam, 1963), is 180 mi northeast of the Ames structure. It lies along the 38th Parallel transverse shear (Coughlon and Denney, 1993) (see Snyder and Gerdemann, 1965). The small outcrop (Fig. 20) is composed of highly weathered, rounded boulders 2–4 ft in diameter of Precambrian granite weathering out of a peridotitic (Bickford and others, 1981) dike intruded into Pennsylvanian sedimentary rocks (Merriam, 1963). Cole's 1962 basement map of Kansas indicates that these granite boulders came up through 2,500 ft of Paleozoic rocks. The dike was intruded in Cretaceous time (Bickford and others, 1981).

Garnet Ridge, Arizona, and Avon, Missouri

At Garnet Ridge in northeastern Arizona (Malde and Thaden, 1963) there are three dikes, pipes, and sills. Some of the inclusions are Precambrian boulders that have come up more than 5,000 ft. One boulder is 10 ft in diameter. So there are subsurface mechanisms capable of moving Precambrian clasts upsection without invoking impact or volcanism. At Avon in Missouri (Kidwell, 1947), small inclusions of Precambrian granite occur in dikes that have been called diatremes, implying explosive volcanism. Shocked quartz has not been found at Avon. I interpreted these dikes to be caused by subsurface solution (Bridges, 1991).

Ames Depression

In the Ames depression, the largest granite clasts in the Nicor no. 18-4 Chestnut core are about 8 in. in diameter. Most of the clasts are angular, but a few show some rounding. They have come up through 1,000–1,400 ft of Arbuckle section. The largest solution area covers more than two sections, but I think it may neck downward into much smaller pipes. Much of the rock in these solution pipes and cavities is reprecipitated carbonate, but there is a small component of intrusive igneous material that became quenched to form glass (now devitrified), a few small clasts of Reagan Sandstone, and some chert from reprecipitated silica (thin section work by Rodger E. Denison). I think the Ames solution was caused

Figure 20. Outcrop of boulders of Precambrian granite weathering out of a Cretaceous peridotitic dike in Pennsylvanian rocks. Rose dome, Woodson County, Kansas.

by high-pressured, high-temperature hydrothermal activity related to the Wichita and/or Ouachita orogenies. In my opinion, the best analogue for this material is the dike at Rose dome in Kansas.

Geothermal gradients in the wells at Ames are uniformly low, averaging 0.8° F/100 ft. It has been my experience in the Rocky Mountains that areas affected by Cretaceous–Tertiary tectonism still have latent heat effects, and the geothermal gradients are variable—some high, some low. The fact that everything at Ames has cooled down convinces me that the solution at Ames must be older than Cretaceous. John Castaño (personal communication), using vitrinite reflectance, determined that the maximum temperature for the Oil Creek shale in the Ames depression was 125 °C. Even with considerable Cretaceous overburden, which I doubt existed, these low geothermal gradients cannot account for more than 90 °C. So the heating event that affected the Oil Creek shale took place after Oil Creek deposition, at ca. 285 Ma and not during the Ordovician.

Guernsey, Wyoming

At Guernsey State Park in southeastern Wyoming there are some excellent subsurface solution outcrops (Bridges, 1982, 1987a). Most geologists consider them to be the result of Mississippian karst solution, but Figure 21 clearly shows Pennsylvanian sandstone to have collapsed into a solution cavity in the underlying Mississippian carbonate. Regional geologic history implies that the subsurface solution took place in Tertiary time. Just upstream from the solution cavity (Fig. 22), one can see that the upper solution surface is very irregular and marked by solution arches and tunnels. The lower solution surface is on top of the Mississippian limestone, and redeposited sandstone and limestone with some chert breccia form a unit about 30 ft thick between the two solution surfaces. "Floating clasts" are common in the Guernsey solution material.

Nicor Chestnut Core, Ames Structure

Two thin shale intervals in the upper part of the solution material in the Nicor no. 18-4 Chestnut core resemble the soft shale at the top of the solution arches at Guernsey. As at Guernsey, clasts 1–2 in. in diameter are scattered in a reprecipitated carbonate matrix in the middle of the solution interval in the core. Fischer (1997) discovered three graded beds at the top of the solution interval in the Nicor Chestnut core and suggested that the graded beds might be caused by tsunami activity. My subsurface-solution explanation would appeal to waning pulses of a high-pressured solution slurry that brought the clasts of Precam-

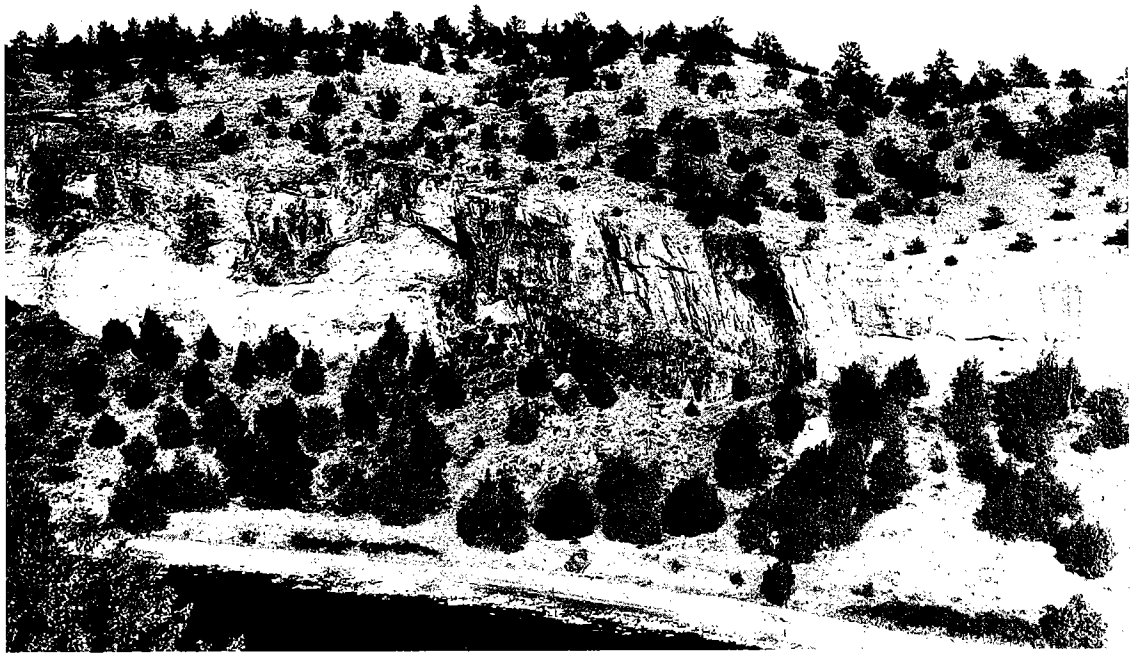

Figure 21. Pennsylvanian sandstone faulted down into a solution cavity in Mississippian limestone. Guernsey, Wyoming.

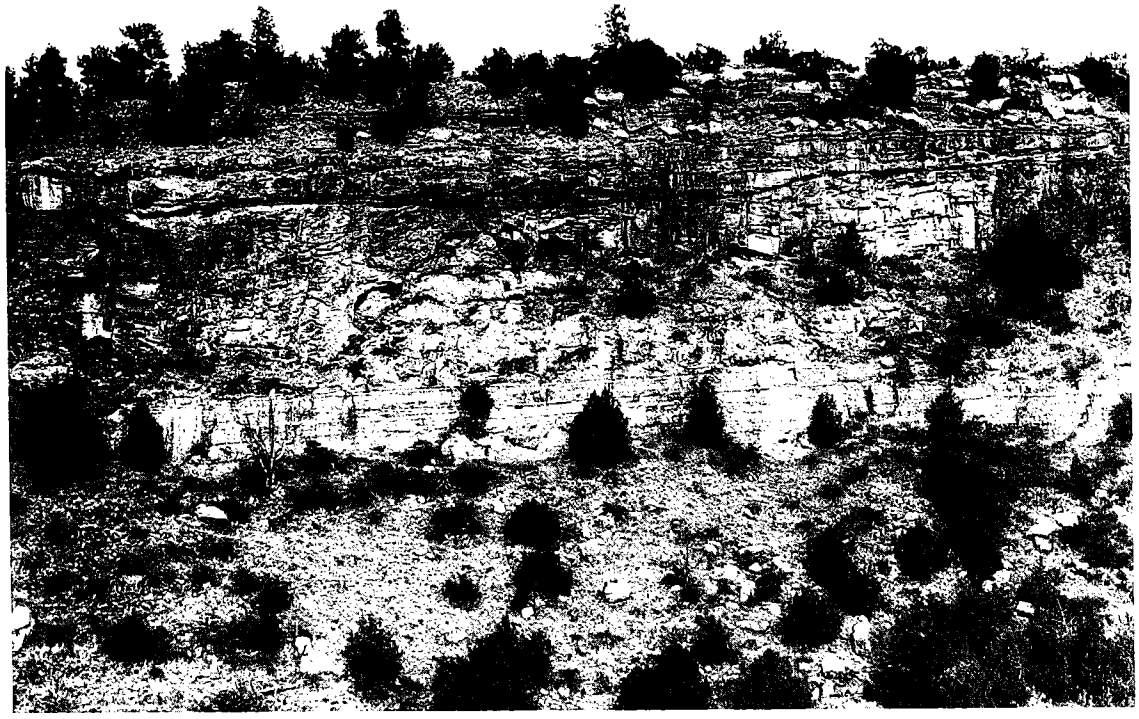

Figure 22. Solution arches caused by subsurface solution. Guernsey, Wyoming.

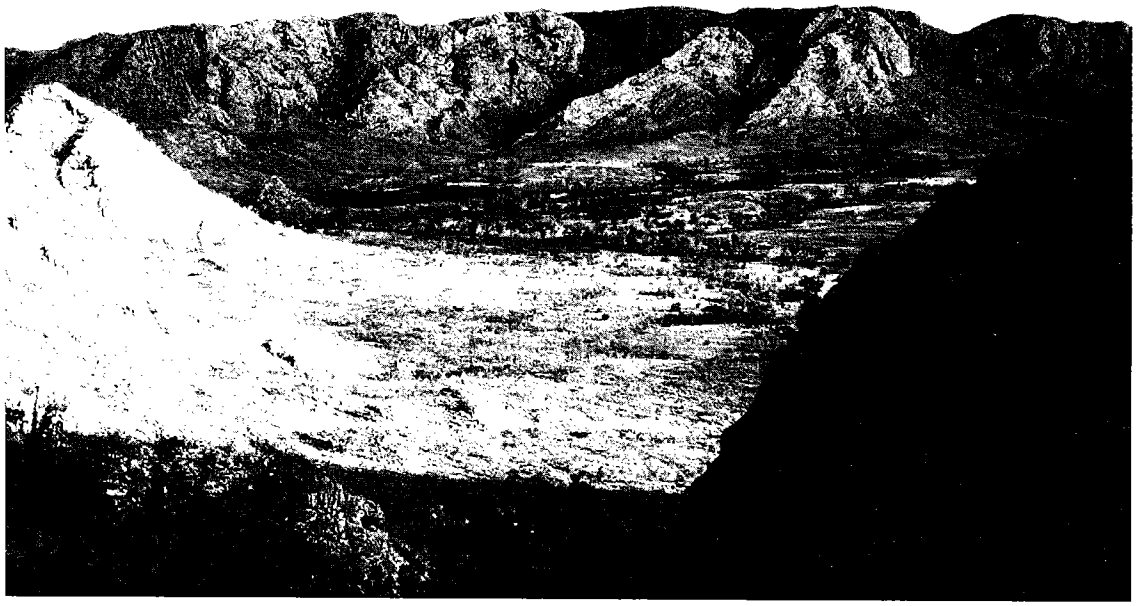

Figure 23. Central topographic low created by differential erosion. Gosse Bluff, Australia.

Figure 24. Was this breccia on Mt. Pyroclast, Australia, caused by impact or solution?

brian granite upsection. When the fluidized mixture of finer material was forced into the solution cavity like a turbidity current, the largest fraction settled first.

Gosse Bluff, Australia

Looking down into the central part of Gosse Bluff (Fig. 23), one can see that older, less-resistant rocks in the central area have been eroded lower than the rim of resistant Devonian sandstone. Note the continuous bedding on the left. If this feature had been caused by impact, the bedding should be more chaotic. I think Gosse Bluff was caused by long-term structural growth. One kilometer south of Gosse Bluff is a little hill called Mt. Pyroclast (Fig. 24), which is composed of breccia. According to Milton and others (1972), this rock is impact breccia. I think it is solution breccia caused by hydrothermal fluids coming up the master fault. Unlike at Ames, there is no mixing of rock types in this in situ breccia. If this unit had been caused by impact, why is there no mixing of rock types?

CONCLUSIONS

The primary reasons against impact at Ames are as follows: (1) A bolide striking the top of a dome is highly improbable. Domal uplift extending 2 mi outside the rim of the crater is unknown in other so-called astroblemes. (2) In the Ames depression, 400 ft of compaction is unrealistic. Domal collapse makes better sense. (3) There are no ejecta on the rim, no meteorite fragments, nor any coesite or stishovite at Ames.

The primary reasons favoring domal collapse and later subsurface solution at Ames are as follows: (1) Domal uplift proceeded gradually rather than instantaneously, creating irregular stratigraphic thinning of the Arbuckle Group toward the center of the dome and preserving a thicker section of Arbuckle in the Hunton graben. (2) At Ames, 450 ft of domal uplift is about equal to 400 ft of domal collapse. (3) Log correlations indicate replacement of the lower part of the Oil Creek shale with small fragments of Precambrian granite. Thus the solution took place after deposition of the Oil Creek. (4) Only about 5–10% of the Arbuckle Group in the depression is disturbed. (5) There is no proof that the shocked quartz was formed in Paleozoic time. I think it formed during the Precambrian by regional faulting.

ACKNOWLEDGMENTS

I gratefully acknowledge an exchange of ideas and a review by Rudolph Kopf, although he disagrees with some opinions expressed herein because he favors a hydrotectonic interpretation (see Kopf, 1979a, 1979b, 1982). Very useful discussions were held with Robert Sandridge and John Castaño. I thank Rodger E. Denison for thin-section work and radiometric dating.

SELECTED REFERENCES

Bickford, M. E.; Harrower, K. L.; Hoppe, W. J.; Nelson, B. K.; Nusbaum, R. L.; and Thomas, J. J., 1981, Rb-Sr and U-Pb geochronology and distribution of rock types in the Precambrian basement of Missouri and Kansas: Geological Society of America Bulletin, v. 92, p. 323–341.

Brenan, R .L.; Peterson, B. L.; and Smith, H. J., 1975, The origin of Red Wing Creek structure: McKenzie County, North Dakota: Wyoming Geological Association of Earth Science Bulletin, v. 8, no. 3, 41 p.

Bridges, L. W. D., 1978, Red Wing Creek field, North Dakota: a concentricline of structural origin: Montana Geological Society Williston Basin Symposium, p. 315–326.

_____ 1982, Rocky Mountain Laramide-Tertiary subsurface solution vs. Paleozoic karst in Mississippian carbonates, *in* Geology of Yellowstone Park area: Wyoming Geologic Association Guidebook, p. 251–264.

_____ 1987a, Tertiary subsurface solution versus Paleozoic karst solution, Guernsey, Wyoming: Geological Society of America Centennial Field Guide, v. 2, p. 205–208.

_____ 1987b, Red Wing Creek field, North Dakota: a growth faulted or meteorite impact structure?, *in* Longman, M. W. (ed.), Williston basin anatomy of a cratonic oil province: Rocky Mountain Association of Geologists, p. 433–440.

_____ 1991, A hydrothermal reinterpretation of southeast Missouri's Avon diatremes and Dent Branch lapilli tuffs: Geological Society of America Abstracts with Programs, v. 23, no. 3, p. 5.

Bridges, L. W. D.; and McCarthy, K., 1990, Tertiary subsurface solution in the Mississippian Leadville Limestone geothermal aquifer of Colorado: Mountain Geologist, v. 27, p. 57–67.

Carpenter, B. N.; and Carlson, Rick, 1992, The Ames impact crater: Oklahoma Geology Notes, v. 52, p. 208–223.

Chao, E. C. T.; Shoemaker, E. M.; and Madsen, B. M., 1960, First natural occurrence of coesite: Science, v. 132, p. 220–222.

Chao, E. C. T.; Fahey, J. J.; Littler, J.; and Milton, D. J., 1962, Stishovite, SiO_2, a very high pressure new mineral from Meteor Crater, Arizona: Journal of Geophysical Research, v. 67, p. 419–421.

Cole, V. B., 1962, Configuration of top of Precambrian basement rocks in Kansas: Kansas Geological Survey Oil and Gas Investigation Map no. 26.

Coughlon, J. P.; and Denney, P. P., 1993, The Ames structural depression: an endogenic cryptoexplosion feature along a transverse shear: Shale Shaker, v. 43, no. 4, p. 44–58.

_____ 1997, The Ames structure and other North American cryptoexplosion features: evidence for endogenic emplacement, *in* Johnson, K. S.; and Campbell, J. A. (eds.), Ames structure in north-

west Oklahoma and similar features: origin and petroleum production (1995 symposium): Oklahoma Geological Survey Circular 100 [this volume], p. 133–152.

Currie, K. L., 1972, Geology and petrology of the Manicouagan resurgent caldera, Quebec: Geological Survey of Canada Bulletin 198, 153 p.

Fischer, J. F., 1997, The Nicor no. 18-4 Chestnut core, Ames structure, Oklahoma: description and petrography, *in* Johnson, K. S.; and Campbell, J. A. (eds.), Ames structure in northwest Oklahoma and similar features: origin and petroleum production (1995 symposium): Oklahoma Geological Survey Circular 100 [this volume], p. 223–239.

Grieve, R. A. F.; and Floran, R. J., 1979, Manicouagan impact melt, Quebec; chemical interrelations with basement and formational processes: Journal of Geophysical Research, v. 83, p. 2761–2771.

Hansen, M. C., 1994, Return to sunken mountain: the Serpent Mound cryptoexplosion structure: Ohio Geology, Ohio Division of Geological Survey, p. 1–7.

Hargraves, R. B., 1993, Where's the Beaverhead beef?: Lunar and Planetary Institute Contribution 790, p. 35–36.

Johnson, K. S.; and Smith, Dorothy, 1997, Ames structure of northwestern Oklahoma is reflected in overlying Permian strata, *in* Johnson, K. S.; and Campbell, J. A. (eds.), Ames structure in northwest Oklahoma and similar features: origin and petroleum production (1995 symposium): Oklahoma Geological Survey Circular 100 [this volume], p. 357–362.

Kidwell, A. L., 1947, Post-Devonian igneous activity in southeastern Missouri: Missouri Geological Survey and Water Resources, Report of Investigations no. 4, 83 p.

Koeberl, Christian; Reimold, W. U.; Brandt, Dion; Dallmeyer, R. D.; and Powell, R. A., 1997, Target rocks and breccias from the Ames impact structure, Oklahoma: petrology, mineralogy, geochemistry, and age, *in* Johnson, K. S.; and Campbell, J. A. (eds.), Ames structure in northwest Oklahoma and similar features: origin and petroleum production (1995 symposium): Oklahoma Geological Survey Circular 100 [this volume], p.169–198.

Kopf, R. W., 1979a, Fault slurry, the self generating lubricant of thrust faults: Geological Society of America Abstracts with Programs, v. 11, no. 7, p. 460.

_____ 1979b, Tectonic model for the development of breccia pipes: Geological Society of America Abstracts with Programs, v. 12, p. 277.

_____ 1982, Hydrotectonics: principles and relevance: U.S. Geological Survey Open-File Report 82-307, 29 p.

Lyons, J. B.; Officer, C. B.; Borella, P. E.; and Lahodynsky, R., 1993, Planar lamellar substructures in quartz: Earth and Planetary Science Letters, v. 119, p. 431–440.

Malde, H. E.; and Thaden, R. E., 1963, Serpentine at Garnet Ridge: U.S. Geological Survey Bulletin 1103, p. 54–61.

Merriam, D. F., 1963, The geologic history of Kansas: Kansas State Geological Survey Bulletin 162, 317 p.

Milton, D. J.; Barlow, B. C.; Brett, R.; Brown, A. R.; Glikson, A. Y.; Manwaring, E. A.; Moss, F. J.; Sedmik, E. C. E.; Van Son, J.; and Young, G. A., 1972, Gosses Bluff impact structure, Australia: Science, v. 175, p. 1199–1207.

Reidel, S. P.; Koucky, F. L.; and Stryker, J. R., 1982, The Serpent Mound disturbance, southwestern Ohio: American Journal of Science, v. 282, p. 1343–1377.

Snyder, F. G.; and Gerdemann, P. E., 1965, Explosive igneous activity along an Illinois-Missouri-Kansas axis: American Journal of Science, v. 263, p. 465–493.

Warner, J. L.; Floran, R. J.; Simonds, C. H.; Phinney, W. C.; and McGee, P. E., 1977, The Manicouagan impact crater, Quebec: New England Intercollegiate Geological Conference Guidebook A5, 12 p.

Target Rocks and Breccias from the Ames Impact Structure, Oklahoma: Petrology, Mineralogy, Geochemistry, and Age

Christian Koeberl
Institute of Geochemistry
University of Vienna, Austria

Wolf Uwe Reimold and Dion Brandt
University of the Witwatersrand
Johannesburg, South Africa

R. David Dallmeyer
University of Georgia
Athens, Georgia

Robert A. Powell
Universal Resources Corporation
Oklahoma City, Oklahoma

ABSTRACT.—The 15-km-diameter Ames structure is a circular structural anomaly, buried beneath almost 3,000 m of sedimentary rock, at 36°15′N, 98°12′W, in northwestern Oklahoma near the town of Ames in southeastern Major County. Structural disturbances in several overlying horizons drew attention to the existence of an unusual feature. Stratigraphic information indicates that the Ames structure is set in Cambrian–Ordovician Arbuckle dolomite.

Structural studies showed the presence of two concentric structures, an outer rim, which is about 1.5 to 3 km wide, and an inner "ring." The rocks of the outer rim consist mainly of fractured and brecciated Arbuckle dolomite. The rocks of the inner ring, which is about 5 km in diameter and seems to be the remnant of a structural uplift within a central depression, are composed of brecciated Precambrian granite and Arbuckle dolomite. The structure is covered by shale of reportedly Middle Ordovician age, which overlies the Arbuckle dolomite. Boreholes into both the crater rim and the central uplift are oil- and gas-producing, making Ames one of the economically important impact structures.

On the basis of geophysical measurements and the presence of possibly shocked quartz grains, an impact origin was earlier suggested by several authors. To confirm this origin, we have performed a detailed mineralogical, petrographical, and geochemical study of a variety of samples from nine drill cores from the Ames structure. The results of the petrographical study show that lithic breccias and impact-melt breccias from the Universal Resources Corporation (URC) no. 1-34 Gammon, URC no. 2-18 Dixon, Continental Resources, Inc. (CRI), no. 1-19 Dorothy, URC no. 1-33 Bland, and Nicor no. 18-4 Chestnut drill cores contain numerous

Christian Koeberl, Institute of Geochemistry, University of Vienna, Althanstrasse 14, A-1090 Vienna, Austria; Wolf Uwe Reimold and Dion Brandt, Department of Geology, University of the Witwatersrand, Johannesburg, 2050, South Africa; R. David Dallmeyer, Department of Geology, University of Georgia, Athens, GA 30602; Robert A. Powell, Universal Resources Corp., Oil Center East, 2601 Northwest Expressway, Oklahoma City, OK 73112.

Koeberl, Christian; Reimold, W. U.; Brandt, Dion; Dallmeyer, R. D.; and Powell, R. A., 1997, Target rocks and breccias from the Ames impact structure, Oklahoma: petrology, mineralogy, geochemistry, and age, *in* Johnson, K. S.; and Campbell, J. A. (eds.), Ames structure in northwest Oklahoma and similar features: origin and petroleum production (1995 symposium): Oklahoma Geological Survey Circular 100, p. 169–198.

shocked quartz and feldspar grains, with up to three sets of shock-characteristic planar deformation features (PDFs), and some rare impact-glass fragments. These findings confirm the features previously reported by B. N. Carpenter and R. Carlson and provide unambiguous evidence of an impact origin for this structure. In addition, samples from 2,951-, 2,954-, and 2,964-m depths in the CRI no. 1-19 Dorothy drill core were found to represent fine-grained subophitic and aphanitic impact-melt rocks. The chemical composition of the impact-melt rocks is very similar to that of the target granite, with some minor carbonate admixture for some of the melt-rock samples.

On the basis of stratigraphic arguments, an age of 470 Ma has been estimated for the crater. To better constrain that age, ^{40}Ar-^{39}Ar incremental-release age analyses of three whole-rock impact-melt samples from the CRI no. 1-19 Dorothy core were carried out. Plateau ages of about 285 Ma were obtained for the three impact-melt rocks. We are uncertain of the geologic significance of the discrepancy between the stratigraphic and isotopic ages. A more detailed geochronological study of this economically important impact crater is needed.

INTRODUCTION AND GEOLOGIC SETTING

The Ames structure is a relatively circular, concentric, structural anomaly, which is situated at 36°15′N, 98°12′W, in northwestern Oklahoma near the town of Ames, in the southeastern corner of Major County, in the area of Townships 20 and 21 N., Ranges 9 and 10 W. Major County is located on the northwest shelf of the Anadarko basin just west of the Nemaha uplift.

Structural disturbances that are obvious in maps of subsurface horizons in Devonian to Upper Pennsylvanian strata drew attention to the existence of an unusual circular feature (Carpenter and Carlson, 1992). For example, mapping of the top of the Upper Ordovician Sylvan Shale showed the presence of a relatively circular, concentric, structural depression with a minimum diameter of about 15 km (9 mi; Fig. 1). The Ames structure is unrelated to any major faults, uplifts, or other tectonic features in the area. However, the so-called Hunton graben, a feature that had been recognized earlier in the area, actually is related to the Ames structure; in the "graben," rocks of the Hunton Group occur stratigraphically about 60 m lower and can be up to >100 m thicker than their regional development (Carpenter and Carlson, 1992). Arbuckle test boreholes were sunk in the area, and oil and gas production was established from the Arbuckle dolomite on a circular ring around the low of the Hunton "graben." The discovery well (DLB no. 27-4 Cecil), which was completed in April 1991, indicated abundant oil and gas flow.

This discovery caused some interest, as Arbuckle dolomite does not normally have significant porosity or permeability, and reservoir size and quality are often limited (Carpenter and Carlson, 1992). Several other holes, including the D. & J. no. 1-20 Gregory well (Fig. 1), which was noted subsequently as probably the most prolific oil well from a single pay in Oklahoma (Carpenter and Carlson, 1992), were drilled to the floor of the structure and there established even more prolific oil production from brecciated granite (previously called "granite wash," i.e., an unconsolidated granite breccia) and dolomite than from the "Hunton graben" (which really is the central part of the Ames structure).

Carpenter and Carlson (1992), on the basis of stratigraphic arguments, noted that the whole Ames structure is set in Arbuckle dolomite and is supposedly overlain directly by Middle Ordovician Oil Creek shale, which is thicker in parts of the structure than is common in the region. This observation would provide an upper limit for the age of the structure. It should be noted, though, that Repetski (1997) has concluded from paleontological studies that the shale in the Ames structure is more likely correlated to the middle Middle Ordovician McLish Formation instead of the lower Middle Ordovician Oil Creek Formation. This change would lower the age of the structure slightly. The Cambrian-Ordovician Arbuckle dolomite is dominated by ramp-type peritidal carbonates with thicknesses of about 450 to 600 m (Wilson and others, 1991), which were deposited upon the Cambrian Reagan Sandstone and Precambrian granite. Figure 2 shows the stratigraphic column of these and related rocks from the Anadarko basin. Above the (thicker than regional) Oil Creek shale, a normal rock section is present (Fig. 2). The top of the Arbuckle unconformity (granite breccia) at Ames is about 2,750 m below the surface.

Structural studies to define the limits and outline of the Ames structure were mainly performed by mapping the surface of the Sylvan Shale, as many older drill cores in the area have penetrated this unit, which is shallower than the Arbuckle dolomite. The mapping showed the presence of two concentric structures (Fig. 3), an outer rim zone, which is about 1.5–3 km wide and has been tilted upward to the north by later tectonic movements, and an inner ring. The rocks of the outer rim, which is currently buried about 2,600 to 2,750 m below the surface, consist mainly of fractured and

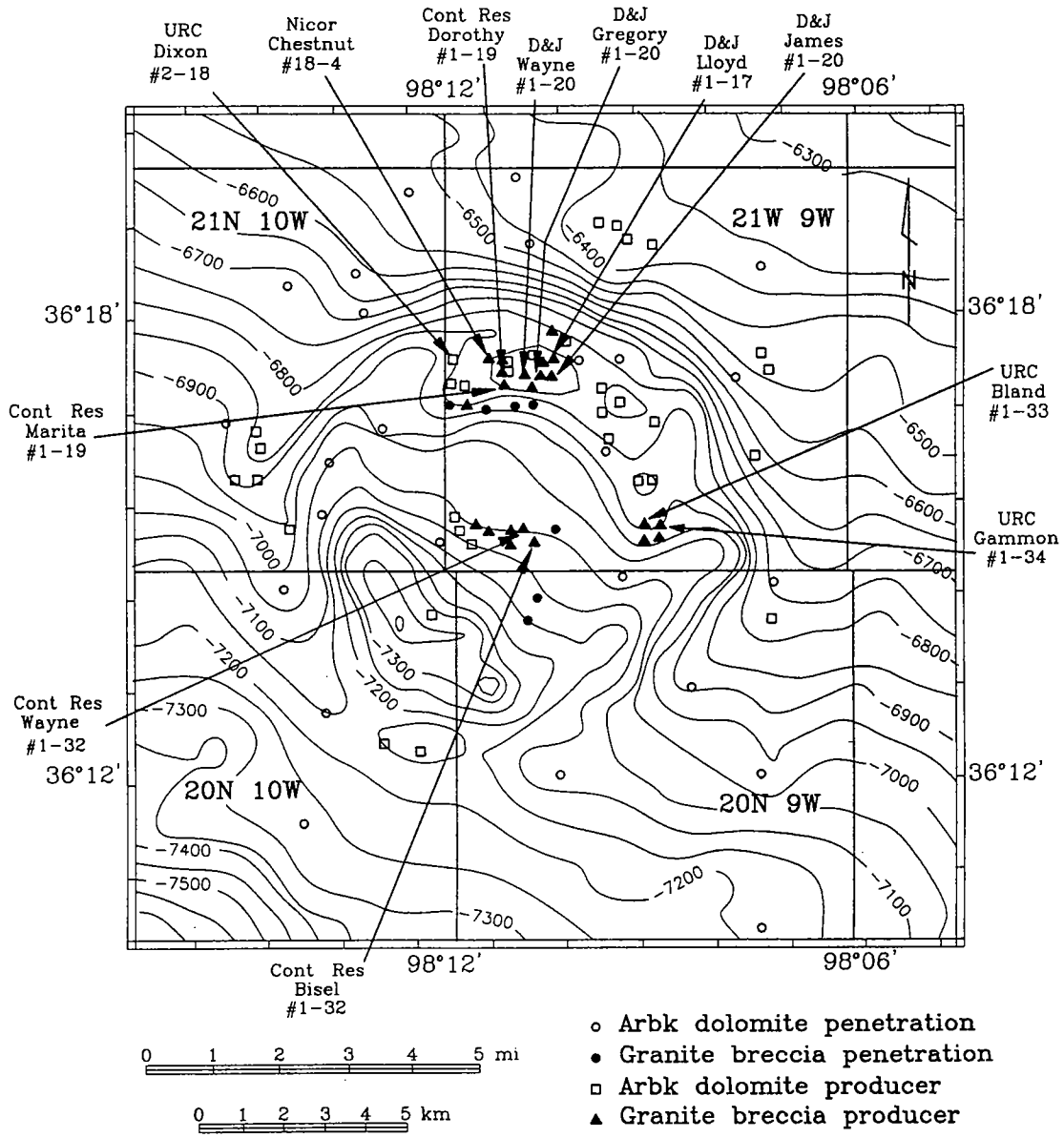

Figure 1. Structural map on the top of the Upper Ordovician Sylvan Shale, showing the deformation evident above the Ames impact structure and the locations of most of the boreholes that are discussed in the present paper. Arbk = Arbuckle.

brecciated Arbuckle dolomite. There is some evidence of karst development in the upper 60 m of the section. A highly porous and permeable zone found at the very top of some of the outer rim boreholes may be a remnant of an ejecta blanket.

A 1.5-km-wide moat or depression separates the outer rim from the inner ring; most of the stratigraphic section between the Arbuckle and the Woodford Shale (Fig. 2) is thicker in this area than is common in the region. Porous Hunton limestone, which is a prolific oil and gas producer, fills the lower part of the moat. Within this central depression, the rocks of the 5-km-diameter inner ring structure are composed of brecciated Precambrian granite and Arbuckle dolomite (Fig. 3). The inner ring structure may represent the remnant of a central structural uplift whose core has either collapsed or has been eroded. There is about 60 m of relief between the moat floor and the top of the inner ring, and there is another 60 m between the

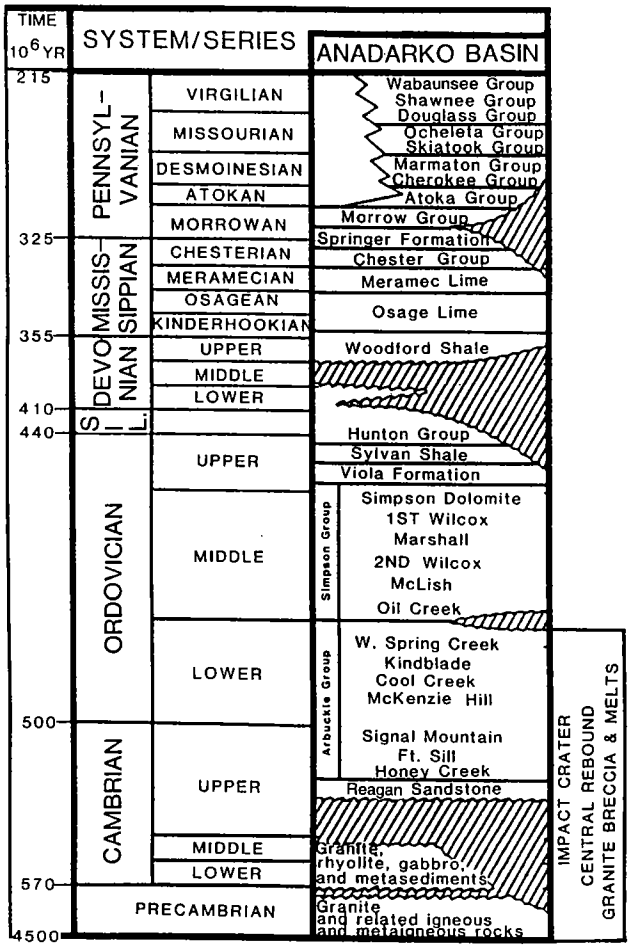

Figure 2. Stratigraphic cross section of the Anadarko basin, close to the Ames area, after data of Johnson (1989) and Wilson and others (1991).

inner ring crest and the floor of the collapsed inner part of the central uplift. Many of the boreholes in the outer rim and on or within the inner ring have a layer of brecciated granite on top of the granite breccia or Arbuckle dolomite, and most of the inner ring boreholes are covered by fine-grained, pulverized granite and dolomite on top of the contact with the Arbuckle. This cover rock has very low permeability. The whole feature is buried beneath almost 3,000 m of sedimentary cover, making exploration difficult.

ORIGIN OF THE AMES STRUCTURE

Since the discovery of the structural anomaly at Ames, there has been a vigorous debate regarding its origin. Geophysical studies and drill-core analyses led to the suggestion that this structure could be a buried impact crater (e.g., Roberts and Sandridge, 1992; Hamm and Olsen, 1992; Carpenter and Carlson, 1992). The Ames structure has morphological characteristics, such as a central uplift (now partly eroded or collapsed) surrounded by a circular depression and an outer ring (Fig. 3), that are typical of complex impact craters (e.g., Grieve, 1987; Koeberl, 1994). The morphology and geologic setting of Ames is not unlike that of other buried impact structures, such as Red Wing Creek, North Dakota (Brenan and others, 1975; Koeberl and Reimold, 1995a; Koeberl and others, 1996b), Avak, Alaska (Kirschner and others, 1992), and Newporte, North Dakota (Koeberl and others, 1995; Koeberl and Reimold, 1995b). Some rocks recovered from the Ames central uplift contain quartz grains with shock-diagnostic planar deformation features, as reported by Carpenter and Carlson (1992), indicating an impact origin for the structure. Although the interpretation of the Ames "hole" as an impact structure has been challenged in favor of a volcanic origin (e.g., Roemer and others, 1992; Coughlon and Denney, 1993), the discovery of shocked quartz (confirmed by our orientation measurements discussed below) is strong evidence in favor of an impact origin. The 50 or so oil- and gas-producing wells have so far yielded about 5.9 million barrels of crude oil and 10 billion cubic feet of gas. These wells are currently (December 1996) making a total of 2,362 barrels of oil per day and about 3 million cubic feet of gas per day. Therefore, Ames is one of the more economically important impact structures, and more detailed studies of the rocks from this area are certainly warranted.

We have begun detailed studies of samples from several drill cores (Koeberl and others, 1994a,b), in the hope of confirming the presence of shock-diagnostic mineralogical features. In this paper we provide a thorough geochemical and mineralogical description of the crater units, and we present the results of our dating of some melt rocks by radiometric methods.

SAMPLES

For this study, samples from nine boreholes were available: Universal Resources Corporation (URC) no. 1-33 Bland, Harper Oil Company no. 1-11 Buford, URC no. 1-34 Gammon, URC no. 2-18 Dixon, D. & J. no. 1-20 James, D. & J. no. 1-17 Lloyd, Continental Resources, Inc. (CRI), no. 1-32 Wayne, CRI no. 1-19 Dorothy, and Nicor no. 18-4 Chestnut. The locations of these boreholes are shown in Figure 1 (except for the no. 1-11 Buford, which is located outside the Ames area).

The URC no. 1-33 Bland and URC no.

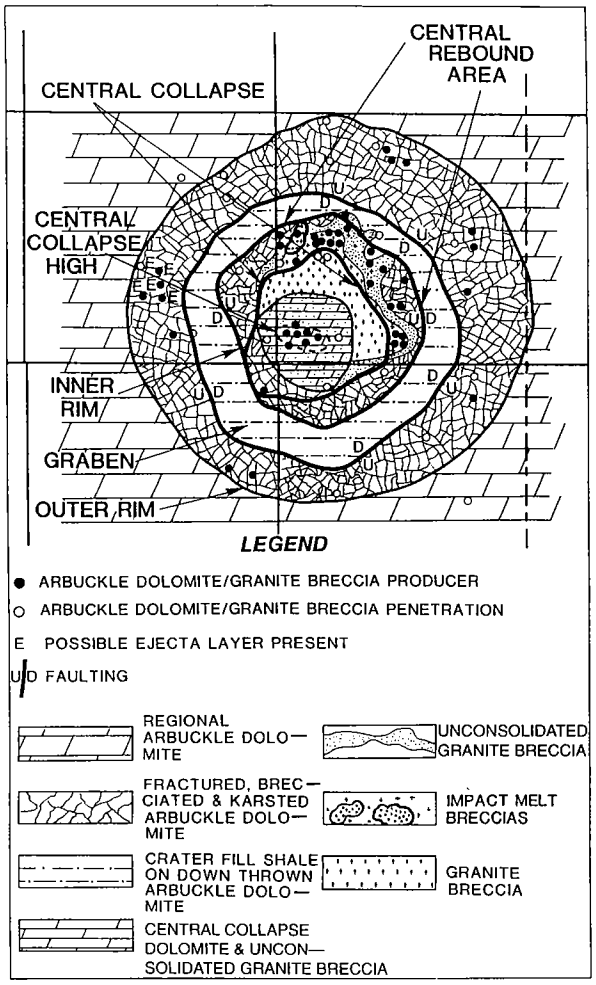

Figure 3. Interpretation of the geology of the Ames structure, based on drill-core and geophysical data.

1-34 Gammon boreholes are in the eastern part of the structure, whereas the other boreholes are in the northern part. Samples for the first eight cores were obtained from a variety of sources, mostly through the courtesy of drillers and oil companies. Decimeter-sized sections of the Nicor no. 18-4 Chestnut drill core were taken for the present study directly at the Oklahoma Geological Survey in Norman.

The URC no. 1-33 Bland well, which was drilled to a total depth of 2,885 m (9,465 ft), produces more than 300 barrels of oil per day. A drill core was taken only from 2,801 to 2,803 m (9,190 to 9,196 ft) depth, but drill cuttings are available from 2,743 to 2,885 m (8,999 to 9,465 ft) depth. The top of the granite was intercepted in the Bland borehole at 2,797 m (9,177 ft) depth. The granite breccia in the Bland core was saturated with hydrocarbons. The granite in the drill-core section (9,190 to 9,196 ft) is brecciated throughout; above that, no core is available, but gamma-ray logs indicate a higher porosity than normal for granite. Large pores and vugs up to 2 cm in size are present throughout the core. Apparently missing pieces of core could be interpreted to represent even larger interclastic pores and fractures. This possibility is supported by calculated porosities from the drill log and gamma-ray log data that are much higher than those measured for the core. The high production rate of the Bland well is another good indicator of high porosity and permeability.

The Universal Resources URC no. 2-18 Dixon borehole is located on the northwest side of the inner ring and is about 0.8 km (0.5 mi) west of the Nicor no. 18-4 Chestnut borehole (Fig. 1). There are about 5 m of fine-grained, pulverized granite and dolomite cover on top of the Arbuckle dolomite in the Dixon borehole that could be similar to the rock cored in the Chestnut borehole. These rocks are found from 2,757 to 2,761.5 m (9,045 to 9,060 ft) depth in the Dixon borehole and from 2,744 to 2,760 m (9,002 to 9,054 ft) in the Chestnut borehole. The Arbuckle dolomite is found at 2,761.5 m (9,060 ft) depth in the Dixon drill core.

Sidewall cores and drill cuttings from the D. & J. no. 1-20 James and no. 1-17 Lloyd were available for this study as well. These wells are on the northern side of the inner ring and are both producing oil from the granite breccia. The no. 1-20 James borehole is a deflection of the D. & J. no. 1-20 Gregory well (which was the discovery borehole). The James is very similar to the Gregory, but is structurally about 27 m lower. The James borehole also has a thicker layer of fine-grained, pulverized granite and dolomite cover on top of the Arbuckle and unconsolidated granite breccia. In the James borehole, the top of the pulverized granite and dolomite cover is at 2,721 m (8,926 ft), and the granite breccia begins at 2,734 m (8,970 ft) and was found to continue all the way to the final depth at 2,839 m (9,315 ft). A core was taken from 2,721 to 2,723 m (8,928 to 8,934 ft), containing shale and pulverized granite and dolomite. The Lloyd no. 1-17 borehole is a northerly deflection of the Gregory and James boreholes. In this borehole, the granite breccia begins at 2,716 m (8,912 ft), and the dolomite begins at 2,750 m (9,022 ft), with a sharp contact between the granite and the dolomite.

The Harper Oil Company Buford no. 1-11 borehole (sec. 11, T. 19 N., R. 9 W.; Major County) was drilled almost 10 km from the outer rim of the structure and was drilled to a total depth of 3,502 m (11,490 ft). It is the closest granite-penetrating borehole near the Ames structure and was chosen for study because it represented the normal stratigraphic sequence of the target area (cf. Fig. 2). The Arbuckle dolomite has a thickness of about 539 m (1,770 ft) and is in its normal stratigraphic position be-

low the Oil Creek shale at 2,811 m (9,222 ft). Below the dolomite are 11 m of Reagan Sandstone. The Precambrian granite and metasedimentary rocks begin at 3,360 m (11,025 ft).

EXPERIMENTAL METHODS

From the total of about 50 particulate, drill-cuttings, and drill-core samples, 55 subsamples were selected and studied petrographically. Polished thin sections were prepared from representative particulate and all coherent samples. Optical microscopic studies were carried out on all 55 thin sections. Figures 4–7 are typical microphotographs taken from these thin sections and show a variety of deformation and other features. Shock petrographic studies were made with a four-axis universal stage. A total of 20 samples (most of them larger drill cuttings or parts of coherent drill-core samples) were selected for chemical analysis. Table 1 gives short petrographical summaries of the samples that were selected for geochemical analysis. The sample numbers used in Table 1 and below in the text are equal to the sample depths in feet; however, owing to the nature of collecting drill cuttings, the exact sample depth may be off by 3–4 m.

Major element analyses were done on powdered samples by standard X-ray fluorescence (XRF) procedures (see Reimold and others, 1994, for details on procedures, precision, and accuracy). The concentrations of V, Cu, Y, and Nb were also determined by XRF analysis. All other trace elements were analyzed by instrumental neutron activation analysis (INAA), following procedures described by Koeberl and others (1987) and Koeberl (1993). For most samples, Sr and Zr concentrations were determined by both XRF and INAA, and for some of the low-abundance samples, Ni data were also obtained by XRF. Age dating was done with ^{40}Ar-^{39}Ar incremental-release dating methods. Samples were incrementally heated until fusion in a double-vacuum, resistance-heated furnace with temperature control to ±1 °C. Details of the analytical method are listed in Dallmeyer and Gil-Ibaruchi (1990).

PETROGRAPHIC OBSERVATIONS

URC No. 1-33 Bland Borehole

Both drill-core and particulate samples were available from the URC no. 1-33 Bland borehole. Figure 4 shows some examples of microphotographs of samples. Particulate samples were obtained from the depth interval between 2,743 and 2,883 m, and drill-core and drill-cuttings samples covered the depth interval from 2,798 to 2,803 m (9,180 to 9,196 ft) (sample numbers used in the following text consist of the depth in feet). Sample 9188.53 comprises a very fine grained carbonate with silt-sized quartz and carbonate clasts. At other depths in this core, similar material was encountered in the form of veins or fracture fillings in granite and lithic breccia (i.e., polymict impact breccia with clastic matrix containing shocked and unshocked mineral and lithic clasts but lacking cogenetic melt particles; cf. below) and, therefore, appears to have been formed at a late stage. Sample 9188.7 consists of coherent, coarse-grained granite with hardly any irregular fracturing. However, in contrast to other samples of this type (9188, 9189.4, 9189.54, 9190, 9192, 9193), 9188.7 also contains a few <1-mm-wide veinlets of clastic breccia, which obviously represent local brecciation zones. These pieces of coherent granite probably represent clasts within a wider package of monomict lithic breccia, which itself was sampled in specimens 9189, 9191, 9191.4, and 9193.7.

Sample 9189.0 (2,800.8 m depth) is a lithic breccia with carbonate-rich matrix and with mainly granite-derived feldspar, quartz, and related clasts, but also containing <5 vol% of schist and carbonate clasts. This sample was taken at the contact between the breccia and a >2-cm-wide zone (vein or layer?) of the fine-grained carbonate phase described above. A second section cut from this sample contains a vein of lithic breccia with lots of clasts of a medium-grained carbonate. This breccia cuts across coherent granite, which again is barely fractured. Generally, no annealing was observed in these granite pieces either. Samples 9191 and 9191.4 represent lithic granitic breccia, as described before, with abundant carbonate clasts. Sample 9193.7 (2,802.2 m depth) is similar to these samples but has a finer-grained matrix

Figure 4 *(p. 175–177).* Photomicrographs of deformation in samples from the URC no. 1-33 Bland and URC no. 1-34 Gammon cores. Each explanation that follows lists the borehole, depth interval, width of the field of view, and type of illumination in parentheses. A—Cataclastic granite fragment, sample 9400 (Bland borehole, 2,865–2,868 m [9,400–9,410 ft], 2.2 mm, crossed polarizers). B—Another example of clastic granitic breccia (Bland borehole, 2,850–2,853 m [9,350–9,360 ft], 1.75 mm, crossed polarizers). C—Quartz grain that is partially isotropic (upper half) and has local breccia zones; at higher magnification, relicts of PDFs were seen (Bland borehole, 2,880–2,883 m [9,450–9,460 ft], 1.1 mm, crossed polarizers). D—Alkali feldspar displaying local isotropization and brecciation (Gammon borehole, 2,804–2,807 m [9,200–9,210 ft], 1.1 mm, crossed polarizers). E—Fragment of mylonitic shale intercalated with quartzite (Bland borehole, 2,877.5 m [9,440.8 ft], 2.2 mm, parallel polarizers). F—Pyrite-carbonate aggregate (center) flanked by fine-grained carbonate fragment (lower left) and partially oxidized siltstone fragment (upper right) (Bland borehole, 2,800 m [9,190 ft], 2.2 mm, crossed polarizers).

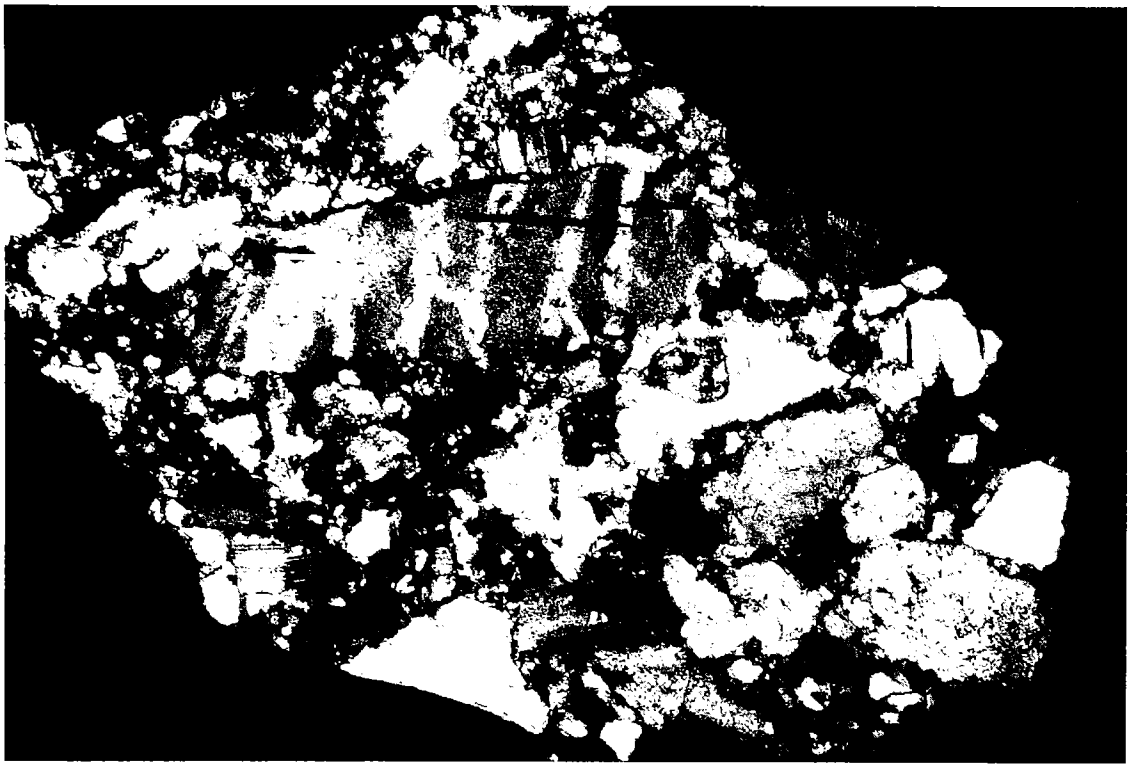

Figure 4A.

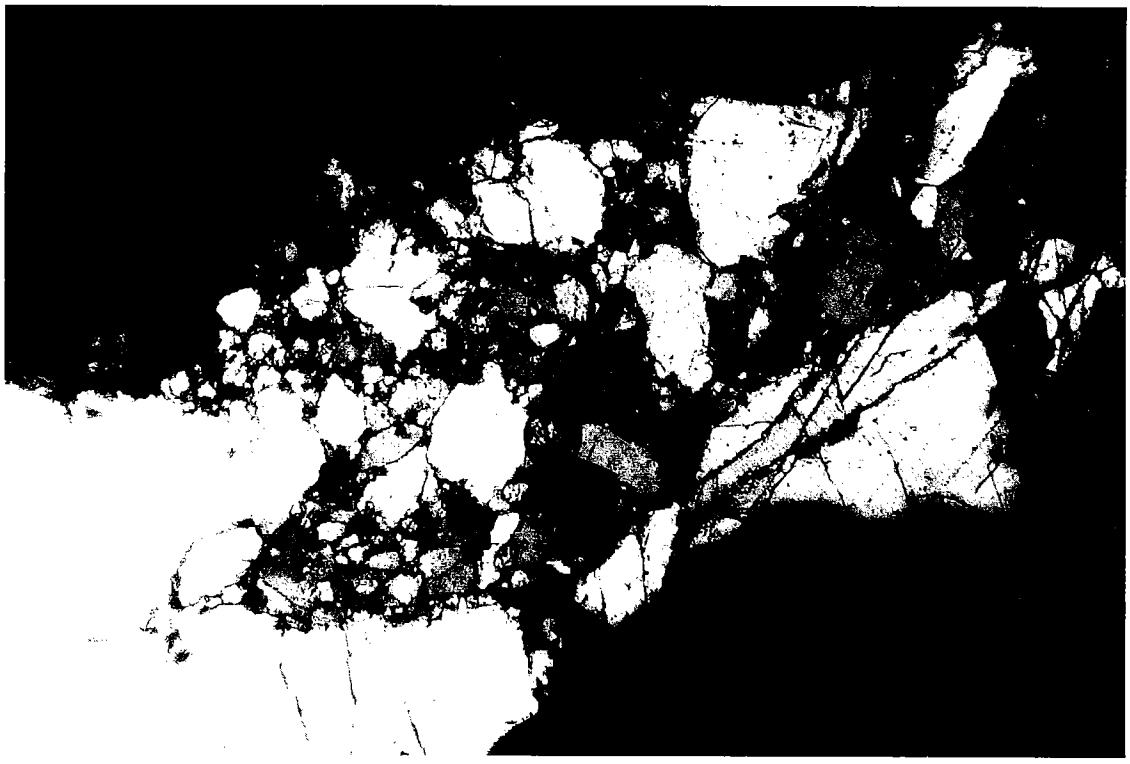

Figure 4B.

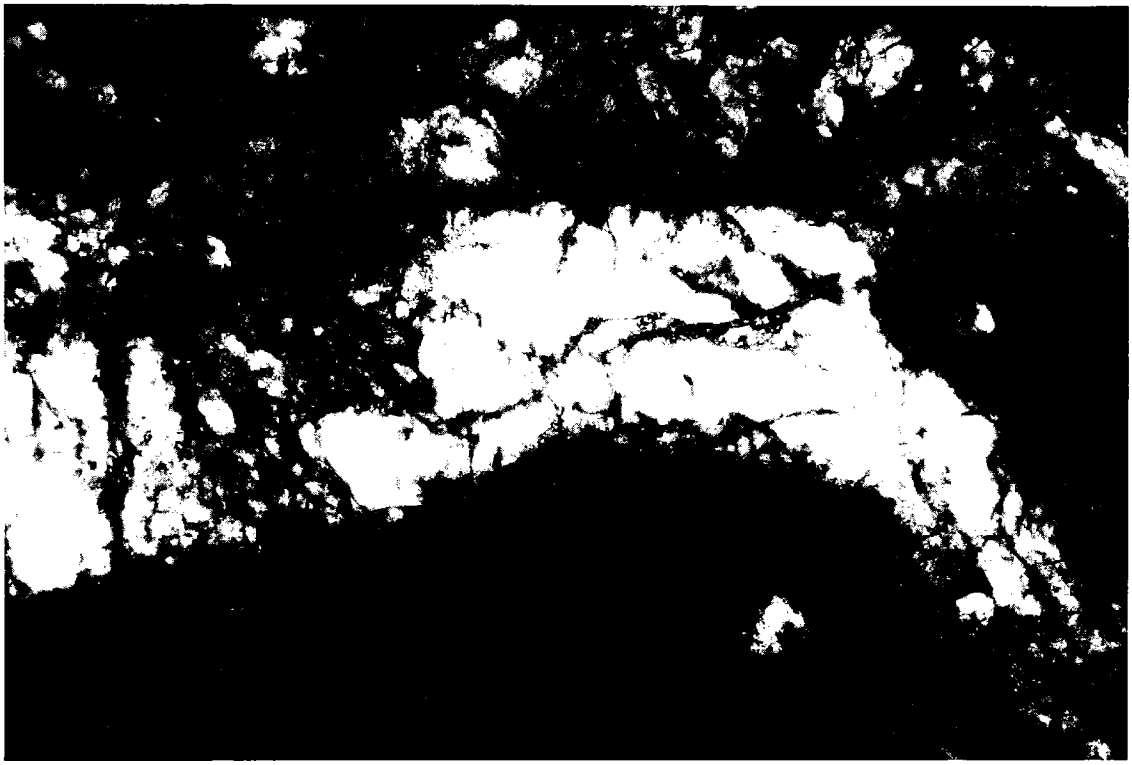

Figure 4C.

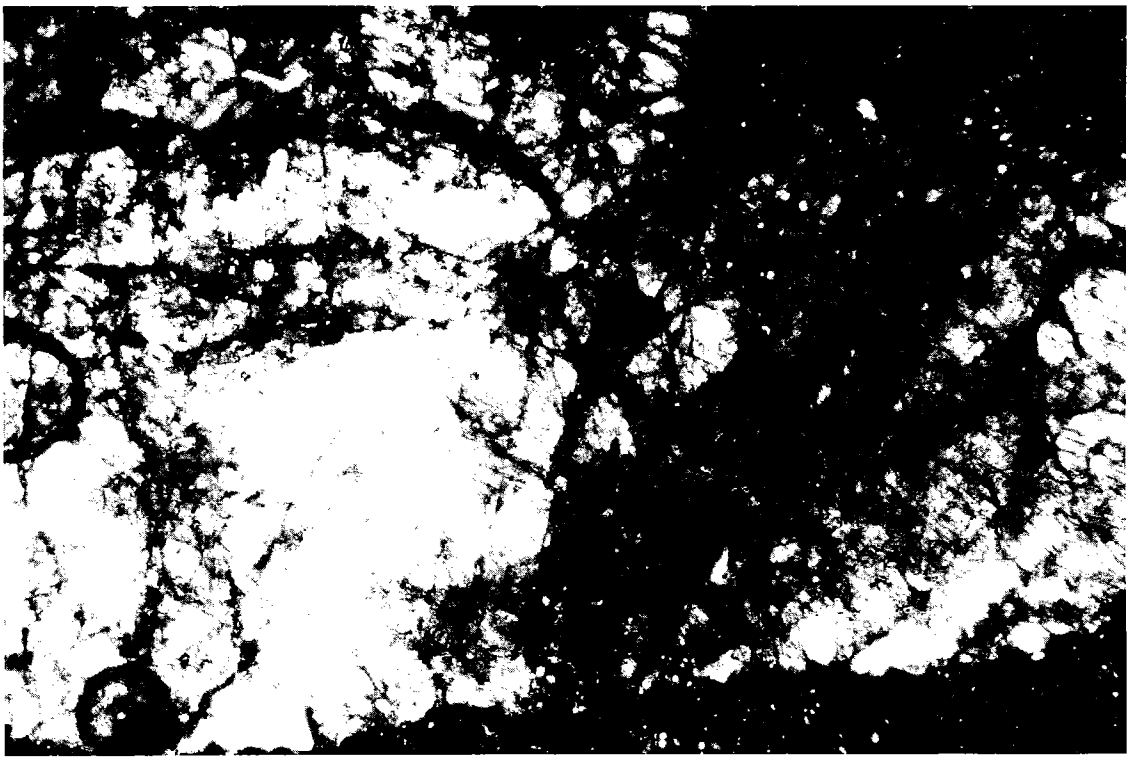

Figure 4D.

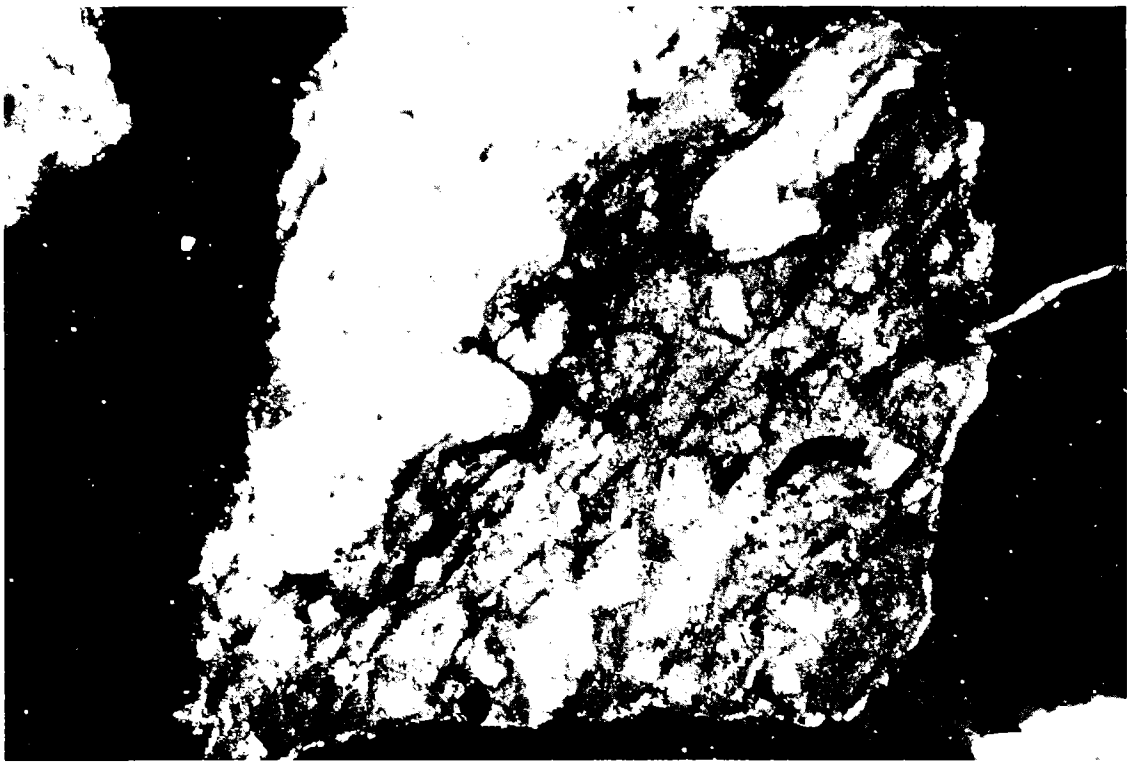

Figure 4E.

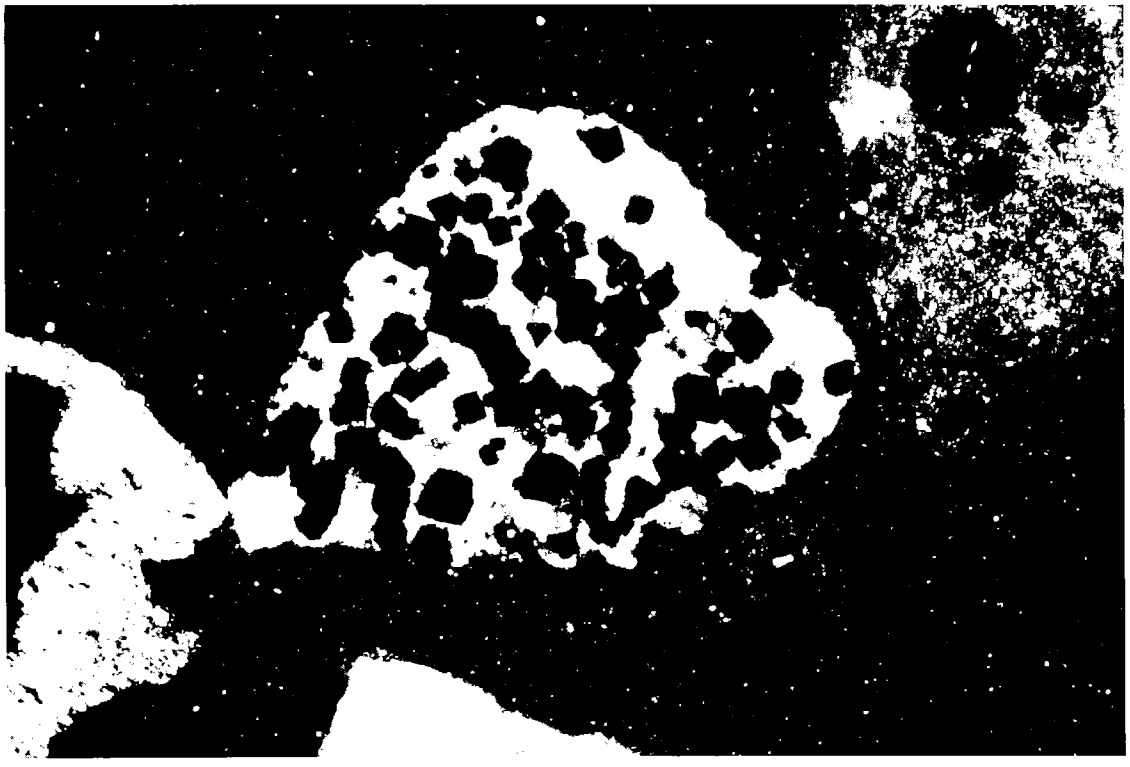

Figure 4F.

that closely resembles the fine-grained, late-stage carbonate phase. Another section of sample 9189.1 contains a large clast of lithic breccia in a matrix of fine-grained carbonate, thus supporting the idea that the fine-grained carbonate phase could perhaps be the result of reworking of older lithic breccia.

No definitive evidence of shock metamorphism was found in these samples (see below). However, within local, cataclastic breccia zones in otherwise intact granite, fracturing of the felsic minerals is enhanced and some shear fracturing and intragranular brecciation are observed as well (Fig. 4).

A suite of particulate specimens—i.e., samples composed of angular to subrounded chips and grains <7 mm in size—was also available from the Bland drill cuttings from the depth interval between 2,774 and 2,883 m. Splits of representative samples from various depths in this interval were taken for the preparation of grain mounts. Sample 9100 from 2,774 m depth contains fragments of carbonate and carbonate + chert and of a fine-grained sandstone with carbonate cement in roughly equal proportions. Near depths of 2,804 m (9,200 ft), relative abundances of carbonate > siltstone + shale > granite > quartzite + sandstone > pyrite fragments were observed. At 2,819 m (9,250 ft), granite and sandstone occur at 50 vol% each, but at 2,835 m (9,300 ft), only granite fragments could be identified. At 2,850 m (9,350 ft), granite > sandstone > carbonate was the relative abundance found, whereas from 2,865 m (9,400 ft) downward, granite dominates and is accompanied by only a small percentage of calcite and chert fragments.

Evidence of shock metamorphism in the form of a few quartz grains with single sets of planar deformation features (PDFs; Fig. 5) was found in samples 9240–9250 and 9450–9460 (2,816–2,819 and 2,880–2,883 m depths, respectively). These shock features are discussed in more detail in the section on Shock Petrography.

Harper Oil Company No. 1-11 Buford Borehole

Particulate samples were also studied from the 2,865–2,957 and 3,383–3,501 m (9,400–9,700 and 11,100–11,490 ft) intervals of drill core from the Harper Oil Company Buford no. 1-11 borehole, from outside the Ames structure area. Sample 9440.8 has carbonate > shale > sandstone, whereas in sample 9480, granite fragments make up 95 vol% and carbonate fragments only 5 vol%. Below 2,923 m (9,590 ft), the situation is changed to carbonate > chert > quartzite + sandstone, with granite being absent. In sample 11100, carbonate >> chert > granite fragments. Sample 11240 contains granite > quartz > carbonate fragments, but in sample 11350, granite and carbonate fragments are estimated at 50 vol% each. It is obvious, as observed in the Bland core, that the relative proportions of sedimentary and granitic fragments vary throughout these depth intervals. Sample 11100 yielded a fragment of devitrified glass (Fig. 6A,B), and sample 11240 revealed a quartz fragment with a single set of planar deformation features. It is possible that the very limited amount of shocked material in the Buford core represents ejecta from the Ames impact event, but a more detailed study (preferably involving other boreholes and, if available, continuous cores) would be necessary to confidently detect and map any possible Ames ejecta.

URC No. 1-34 Gammon Borehole

A rather regular variation is observed among particulate samples 9070 to 9350 from drill core URC no. 1-34 Gammon, covering the depth interval from 2,764 to 2,850 m.

Sample 9070 (2,765 m depth) consists of 100 vol% sedimentary fragments, including pyrite, shale, carbonate, and sandstone clasts. Sample 9100 (2,774 m depth), carbonate > carbonate-cemented quartzite + sandstone > chert > granite was observed (granite only accounts for about 10 vol% of these fragments). Sedimentary clasts make up 70 vol% of sample 9120 (2,780 m depth), and granite clasts make up 30 vol%; these proportions are shifted in sample 9140 (2,786 m depth) to 60 and 40 vol%, respectively, and in sample 9150 (2,789 m depth), to 70 and 30 vol%, respectively. Besides minor carbonate and carbonate-bearing sandstone, sample 9200 (2,804 m depth) contains about 95 vol% granite fragments. In sample 9250 (2,819 m depth), about 70 vol% granite and 30 vol% carbonate and chert fragments were registered; and in sample 9300 (2,835 m depth), about 80 vol% was granite, and the rest consisted of sandstone, carbonate, and chert. Sample 9340 (2,847 m depth) yielded only granite fragments.

Many of these specimens contain shock-metamorphosed quartz, either as individual quartz grains or as quartz grains in sandstone or granite fragments. Shocked quartz was observed in sample 9100 (2,774 m depth) in sandstone. Samples 9120 and 9150 (2,780 and 2,789 m depths, respectively) both contain one granite

Figure 5 *(p. 179–180).* Photomicrographs of typical shock deformation. A—K-feldspar grain with multiple sets of PDFs (URC no. 2-18 Dixon core, 2,774–2,775 m [9,100–9,105 ft], 3.4 mm, crossed polarizers). B—Enlarged area of K-feldspar grain in Figure 5A; note the high density of PDFs parallel to different crystallographic orientations (220 μm, crossed polarizers). C—Another enlarged area of Figure 5A (355 μm, crossed polarizers). D—Quartz grain with PDFs (URC no. 1-33 Bland core, 2,818–2,819 m [9,240–9,250 ft], 1.1 mm, parallel polarizers).

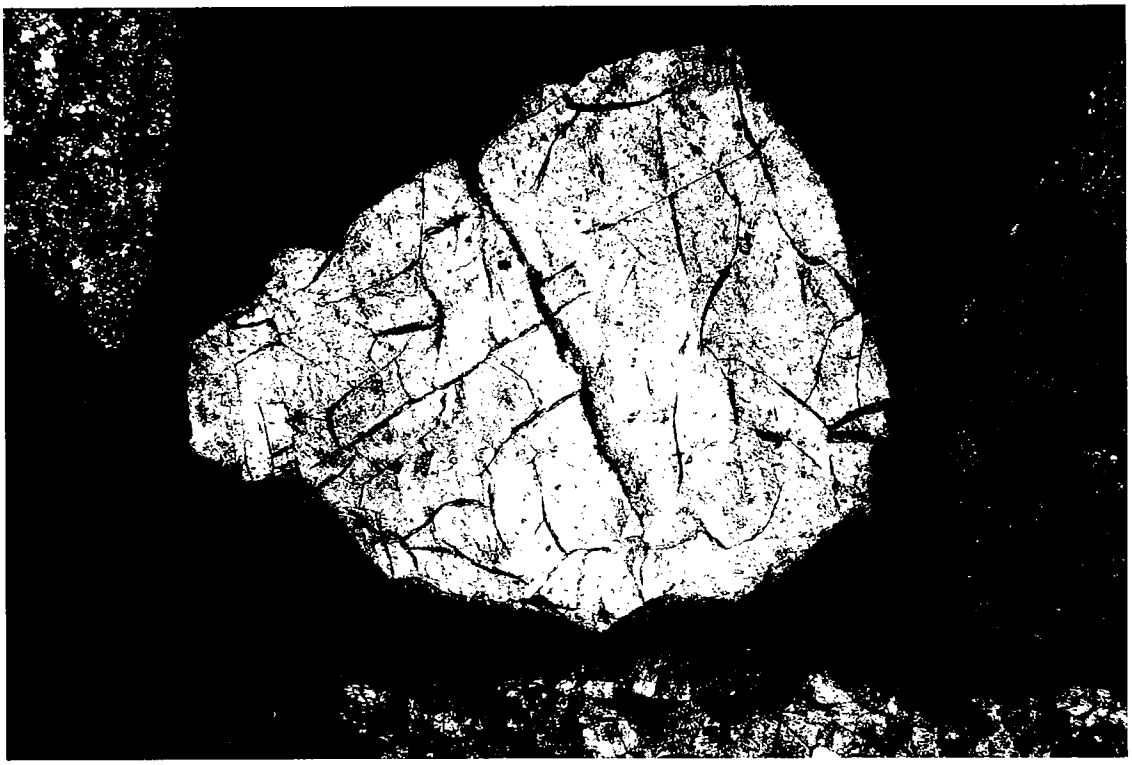

Figure 5A.

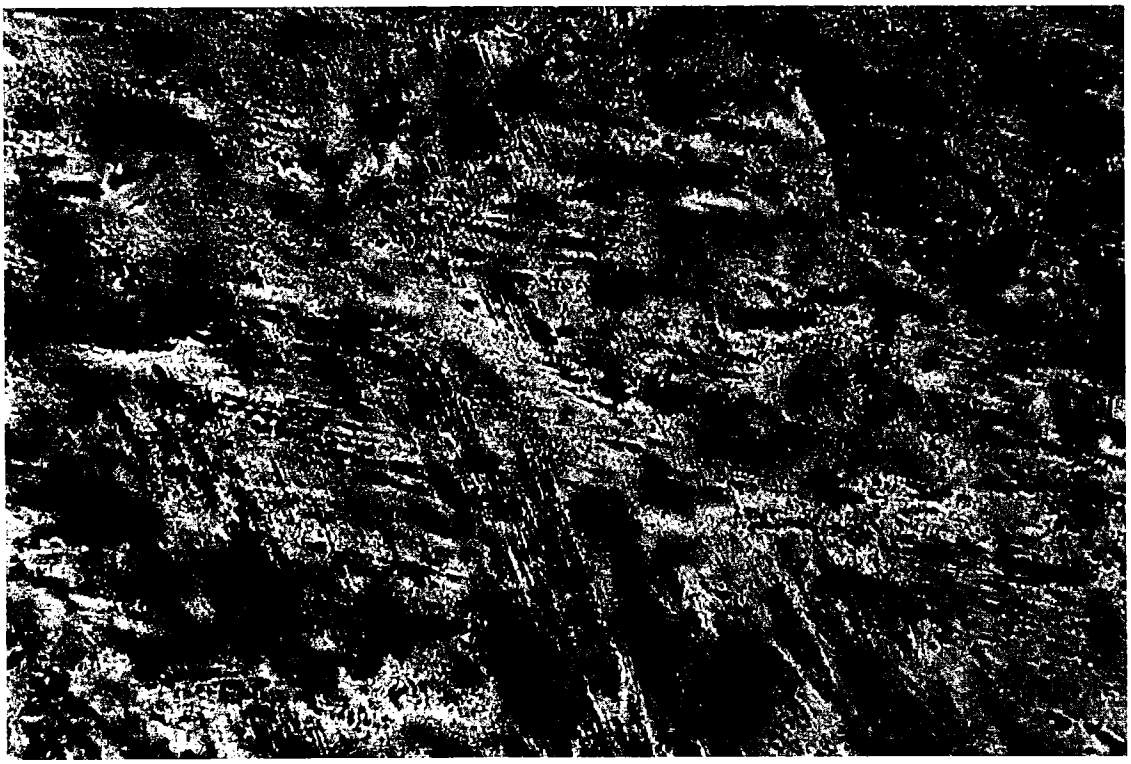

Figure 5B.

Figure 5C.

Figure 5D.

fragment each with shocked quartz, and samples 9200 and 9250 (2,804 and 2,819 m depths, respectively) contain several granitic fragments with shocked quartz. In sample 9340 (2,847 m depth), no quartz with PDFs was observed, but this sample contains some cataclasite particles.

URC No. 2-18 Dixon Borehole

Particulate samples from the URC no. 2-18 Dixon borehole were studied from the depth interval 2,749 to 2,874 m (9,020–9,310 ft). The following observations were made: sample 9020 (2,749 m depth) contains carbonate > sandstone > fine-grained quartzite; sample 9060 (2.761 m depth) contains carbonate > quartzite > chert; sample 9100 (2,774 m depth) contains carbonate > carbonate + chert > sandstone with carbonate cement > carbonate + vein quartz > shale >> granitic fragments; sample 9200 (2,804 m depth) has carbonate (chert > chert; and sample 9300 (2,835 m depth) has carbonate > carbonate + chert > sandstone + carbonate cement >> quartzite. In the samples from this drill core, one strongly shock-metamorphosed K-feldspar fragment with PDFs in three or more sets of different crystallographic orientations was noted (Fig. 5A–C).

D. & J. No. 1-20 James Borehole

Only two particulate samples were available from the D. & J. no. 1-20 James borehole. Sample 9315 (2,839 m depth) consists of 95 vol% granitic and 5 vol% carbonate fragments, including several cataclasite fragments. The other specimen from 2,722 m depth (sample 8930) contained only granitic fragments, all of which are basically undeformed (just minor intra- and intergranular fracturing).

D. & J. No. 1-17 Lloyd and CRI No. 1-32 Wayne Boreholes

A single sample from the D. & J. no. 1-17 Lloyd borehole consists only of carbonate. Two drill-core samples from the CRI no. 1-32 Wayne borehole were studied: a particulate specimen from 2,877 to 2,926 m (9,440 to 9,600 ft) depth, which consists of 95 vol% granitic and 5 vol% of sandstone fragments, with a lot of cataclastic granite, but no shock-metamorphosed mineral grains, and a completely undeformed and unshocked granite specimen from 2,694.8 m (8,841.3 ft) depth.

CRI No. 1-19 Dorothy Borehole

Two particulate and six coherent drill-core samples from the CRI no. 1-19 Dorothy borehole were studied. The particulates originate from 2,737 and 2,774 m (8,980 and 9,100 ft) depths and consist of 85 vol% brecciated granite and 15 vol% carbonate and shale and 50 vol% carbonate (chert and 50 vol% granitic fragments, respectively. Sample 8980 (2,737 m depth) did not display any evidence of shock metamorphism, whereas sample 9100 (2,774 m depth) contained several granite fragments with PDFs in quartz.

Of the six coherent Dorothy borehole samples, sample 9137 (2,785 m depth) consists of medium-grained dolomite, which, locally along fractures, contains narrow, <1-mm-wide, brecciation zones. Sample 8978.5 (2,737 m depth) consists of sandstone with a carbonate cement, which contains a number of shocked quartz, microcline, and plagioclase grains (Fig. 7A–C). Dorothy sample 8984 (2,738 m depth) is a sandstone fragment, also with carbonate cement, that contains some quartz grains with one or multiple sets of PDFs (Fig. 7D). Other quartz grains appear as if they were melted and then annealed.

The remaining four samples of Dorothy material represent melt rocks. Samples 9003.5 and 9033.5 (2,744.3 and 2753.4 m depth, respectively) are very similar and consist of a melt breccia, the matrix of which locally shows fine-grained subophitic texture (Fig. 6C). Other areas of this matrix are devitrified, originally glassy melt. Clasts are mainly quartz or quartzitic (either of sedimentary or of granitic origin) and are often partially or completely annealed. Some quartz clasts contain planar deformation features (Figs. 7E,F). Local clast melting is indicated by corroded clast margins and the presence of devitrification features along such grain boundaries. Small patches rich in dark oxides probably represent the relicts of melting of mafic minerals (biotite, amphibole) of the precursor rock. Contrary to these two samples, specimen 8994.5 (2,741.5 m depth), an aphanitic melt rock with quartz and carbonate clasts that were partially melted and partially fluidized, contains a number of carbonate-filled vesicles. Some coarse-grained carbonate clasts are still well preserved. Many quartz clasts are annealed. No shocked particles could be identified in our thin section. Because of the presence of shocked clasts in samples from this interval in the Dorothy drill core, however, we conclude that these melt rocks represent impact-melt rock. Sample 9038 (2,755 m depth) represents a partially isotropic melt breccia with a number of weakly shocked quartz clasts and large carbonate-filled vesicles.

Nicor No. 18-4 Chestnut Borehole

In 1995, 17 large samples from the Nicor no. 18-4 Chestnut core became available for petrographic and chemical analysis. Our preliminary petrographic identification of these samples is as follows:

2,744 m (9,002.6 ft). Fine-grained carbonate, cut by two quartz veinlets each less than 1 mm wide.

2,744.3 m (9,003.7 ft). Alternating layers of fine-grained carbonate and lithic breccia composed of carbonate and granite clasts in a fine-grained

Figure 6B.

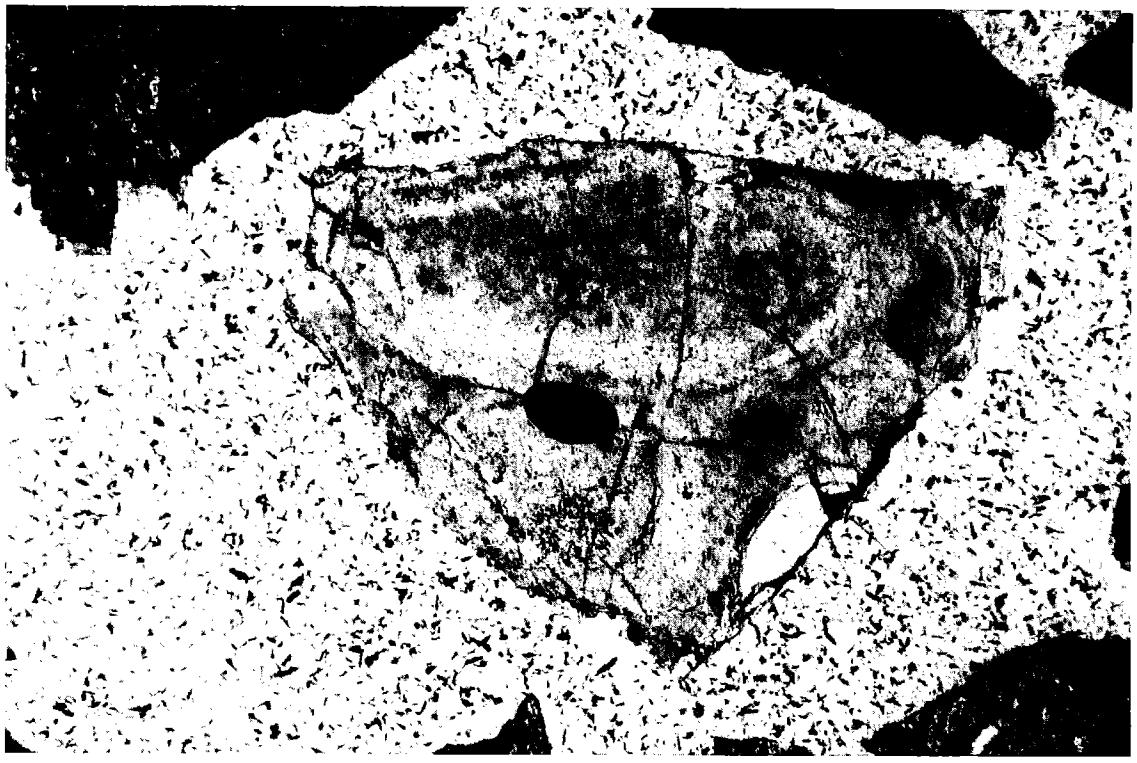

Figure 6A.

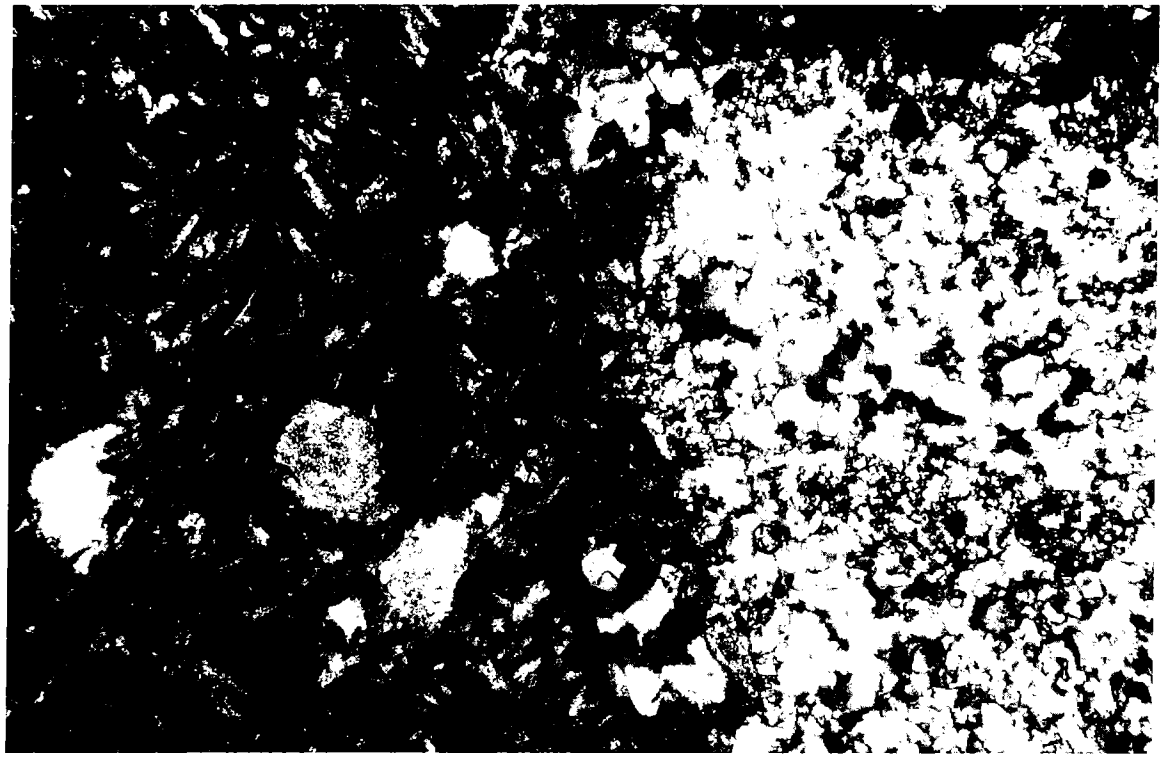

Figure 6C.

Figure 6. Photomicrographs of devitrified glass and impact-melt rock. A *(top left)*—Fragment of devitrified glass (no. 1-11 Buford core, 3,383–3,386 m [11,100–11,110 ft], 1.75 mm, parallel polarizers). B *(top right)*—Same as Figure 6A, but with crossed polarizers; the devitrified matrix is clearly visible and surrounds two finer-grained, fully annealed fragments, as well as a small quartz fragment without shock deformation. C *(bottom)*—Very fine grained, subophitic impact-melt rock with an annealed quartzitic clast and several carbonate-filled vesicles (CRI no. 1-19 Dorothy core, 2,744 m [9,003.5 ft], 2.2 mm, crossed polarizers).

matrix of clay minerals and carbonate; sample is cut by a quartz vein; shocked quartz and K-feldspar are present.

2,744.4 m (9,004 ft). Same as sample 9003.7; shocked quartz is abundant.

2,744.8 m (9,005.2 ft). Lithic breccia of granite-derived and carbonate clasts; sample is cut by a 6-mm-wide carbonate-filled veinlet; sample contains a single plagioclase clast with alternating shocked and unshocked twin lamellae.

2,745.6 m (9,008 ft). Same as sample 9005.2; contains a perthitic alkali feldspar clast with three sets of PDFs.

2,746.6 m (9,011 ft). Same as sample 9005.2, but somewhat more clay minerals in matrix; a K-feldspar clast displays PDFs and incipient brecciation.

2,747.9 m (9,015.5 ft). Clast-rich, originally aphanitic impact-melt breccia with devitrified matrix; sample contains large granitic clasts and other clasts of schist and carbonate; some secondary carbonate is present; many quartz grains in granitic clasts contain PDFs, often in more than three sets per host grain.

2,748.6 m (9,017.6 ft). Aphanitic impact-melt breccia with matrix that, in places, is still glassy; most clasts are fully annealed; several K-feldspar clasts contain relicts of PDFs.

2,748.7 m (9,018.1 ft). Clast-rich, originally aphanitic, now devitrified impact-melt breccia; some clasts consist of diaplectic quartz glass.

2,749.5 m (9,020.7 ft). Devitrified, originally glassy, impact-melt breccia, with quartz clasts showing multiple sets of PDFs.

2,750.5 m (9,024.1 ft). Similar to sample 9020.7, but in patches has a glassy matrix; contains some carbonate, which, at least partially, is primary; this sample is vesicular.

2,750.9 m (9,025.1 ft). Devitrified aphanitic, highly vesicular impact-melt rock; many clasts are completely annealed, but others are full of quartz with multiple sets of PDFs.

2,751.2 m (9,026.3 ft). Part of a largely annealed, locally melted granite clast in devitrified aphanitic melt breccia.

2,751.6 m (9,027.6 ft). Aphanitic, now largely devitrified, vesicular impact-melt breccia.

2,752.2 m (9,029.5 ft). Same as sample 9027.6.

2,753.6 and 2,754.2 m (9,034.1 and 9,036 ft). Same as sample 9,027.6, but contains more carbonate.

The above sample descriptions show that there is clear evidence for the existence of shocked minerals and impact-melt rocks in the samples from the Chestnut 18-4 core, in agreement with observations by Fischer (1997). A more detailed petrography and a geochemical study of the Chestnut samples will be the subject of another paper.

SHOCK PETROGRAPHY

The presence of rocks and minerals exhibiting shock-metamorphic features provides an unambiguous indication for the high pressures uniquely associated with impact cratering (see, e.g., papers in French and Short, 1968; Stöffler and Langenhorst, 1994). Shock pressures and temperatures during hypervelocity impact reach many 100s of gigapascals (GPa) and several 1000s of degrees Celsius. Such values are far above the conditions reached during endogenic metamorphism of crustal rocks, with maximum temperatures of 1200 °C and maximum pressures of 2 GPa (e.g., Gratz and others, 1992a; Huffman and others, 1993; Huffman and Reimold, 1996). Most of the structural and phase changes in minerals are uniquely characteristic of the high pressures (5 to >50 GPa) and extreme strain rates (10^6 to 10^8 s^{-1}) associated with impact. Static compression and volcanic or tectonic processes yield different products because their peak pressures and strain rates are lower by more than 11 orders of magnitude. Observations of naturally and experimentally shocked rocks have enabled calibration of shock pressures up to about 100 GPa (see, e.g., Hörz, 1968; French and Short, 1968; Stöffler, 1972,1974; Gratz and others, 1992a,b; Huffman and others, 1993; Stöffler and Langenhorst, 1994; Huffman and Reimold, 1996; and references therein).

Various macroscopic and microscopic shock-metamorphic effects have been recognized, depending upon the peak shock pressure experienced. The best and most generally accepted indicators for shock metamorphism are features that can be studied by using the polarizing optical microscope, such as planar microstructures, optical

Figure 7 *(p. 185–187).* Microphotographs of shock-characteristic deformation in samples from CRI no. 1-19 Dorothy borehole. A—Two quartz grains with PDFs in a sandstone fragment (2,737 m [8,978.5 ft], 220 μm, crossed polarizers). B—Another quartz grain with a well-developed set of PDFs from the same sample as that in Figure 7A (220 μm, crossed polarizers). C—Another quartz grain with two sets of PDFs, from a sandstone fragment in the same sample as that in Figure 7A (220 μm, crossed polarizers). D—Quartz grain with multiple sets of PDFs in a carbonate-rich sandstone fragment (2,738 m [8,984.0 ft], 220 μm, crossed polarizers). E—Quartz clast with two sets of PDFs (2,744 m [9,003.5 ft], 220 μm, crossed polarizers). F—Another quartz clast with two sets of PDFs from the same sample as in Figure 7E (220 μm, crossed polarizers).

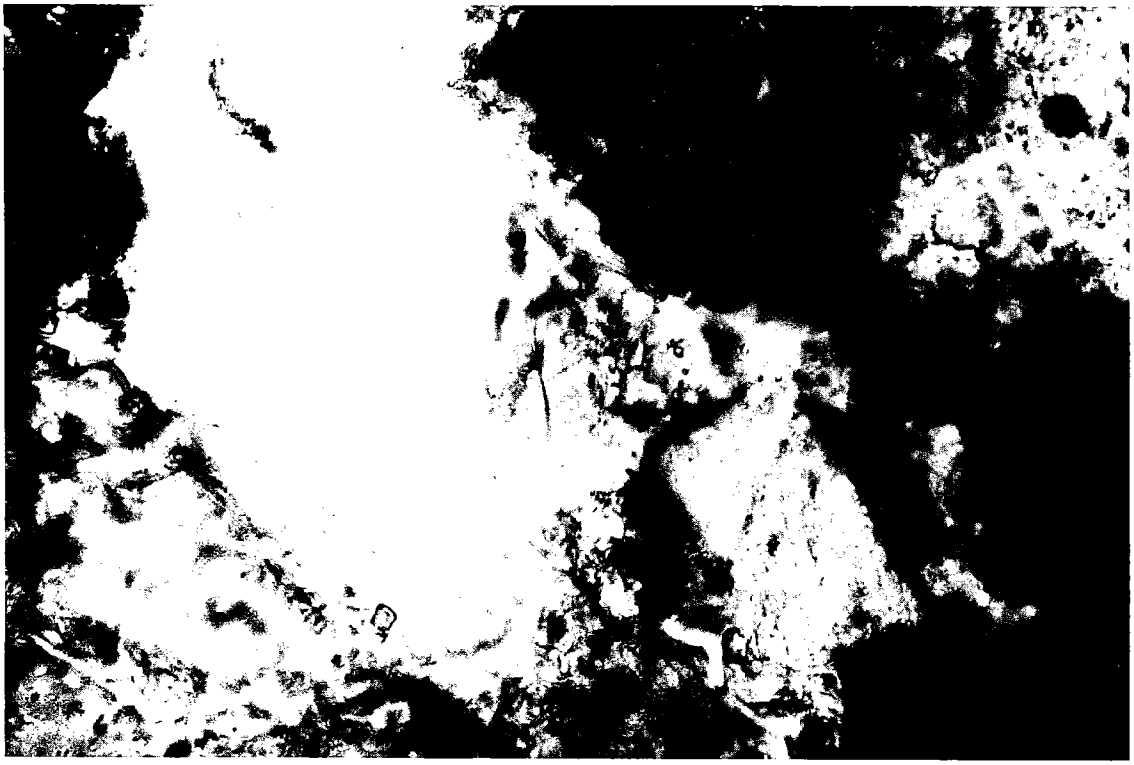

Figure 7A.

Figure 7B.

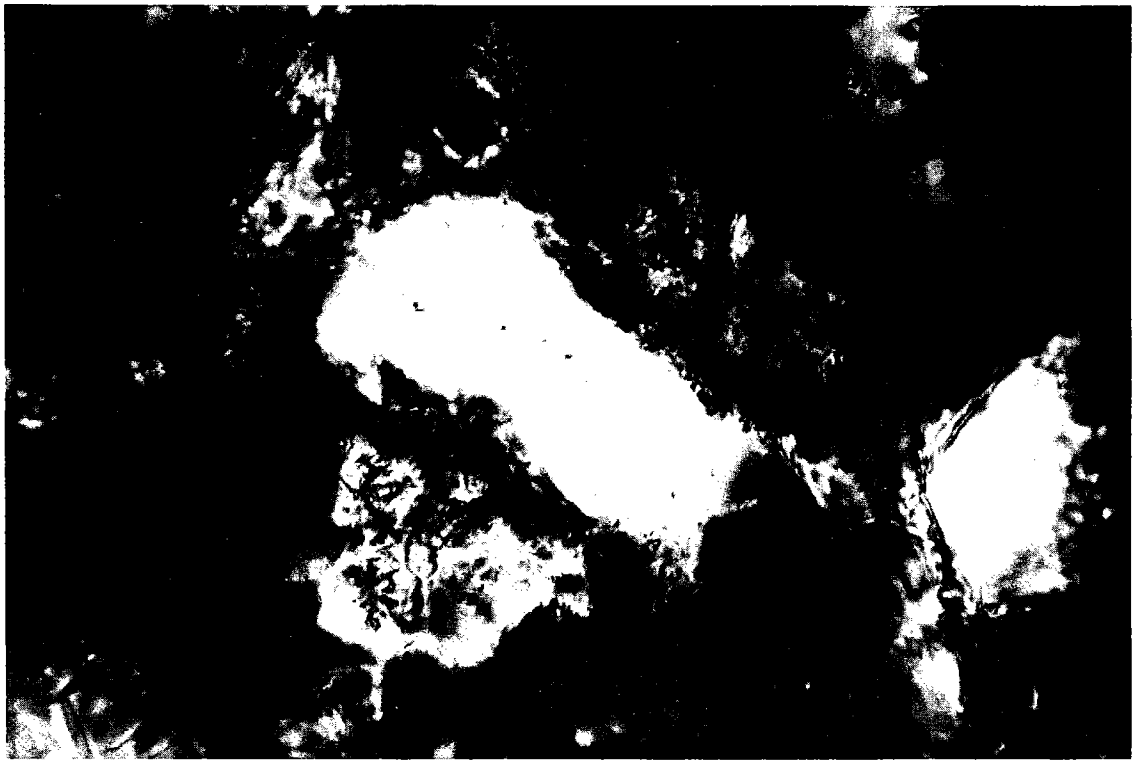

Figure 7C.

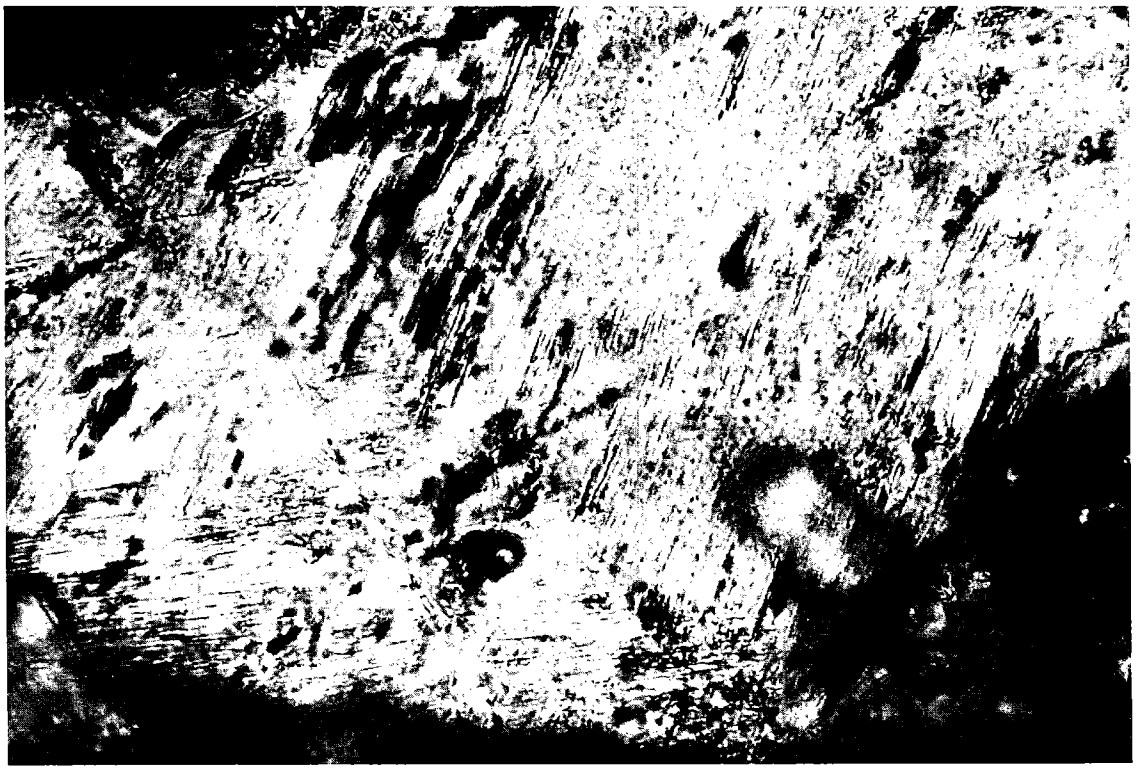

Figure 7D.

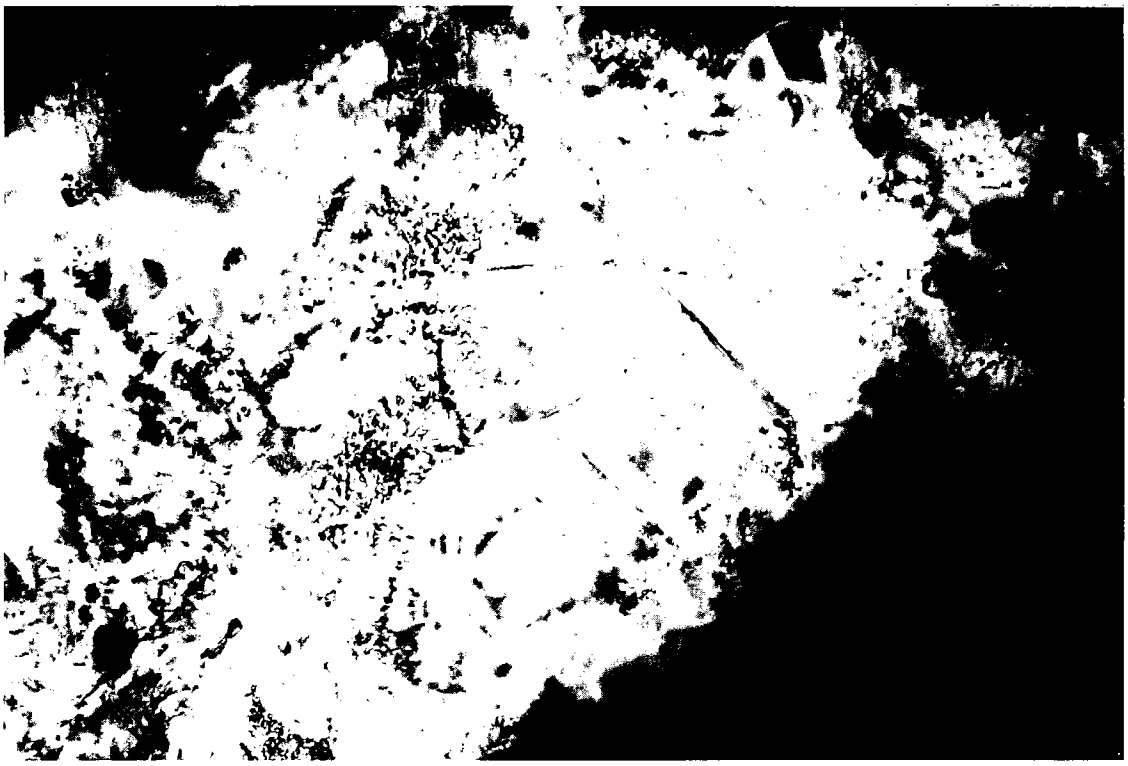

Figure 7E.

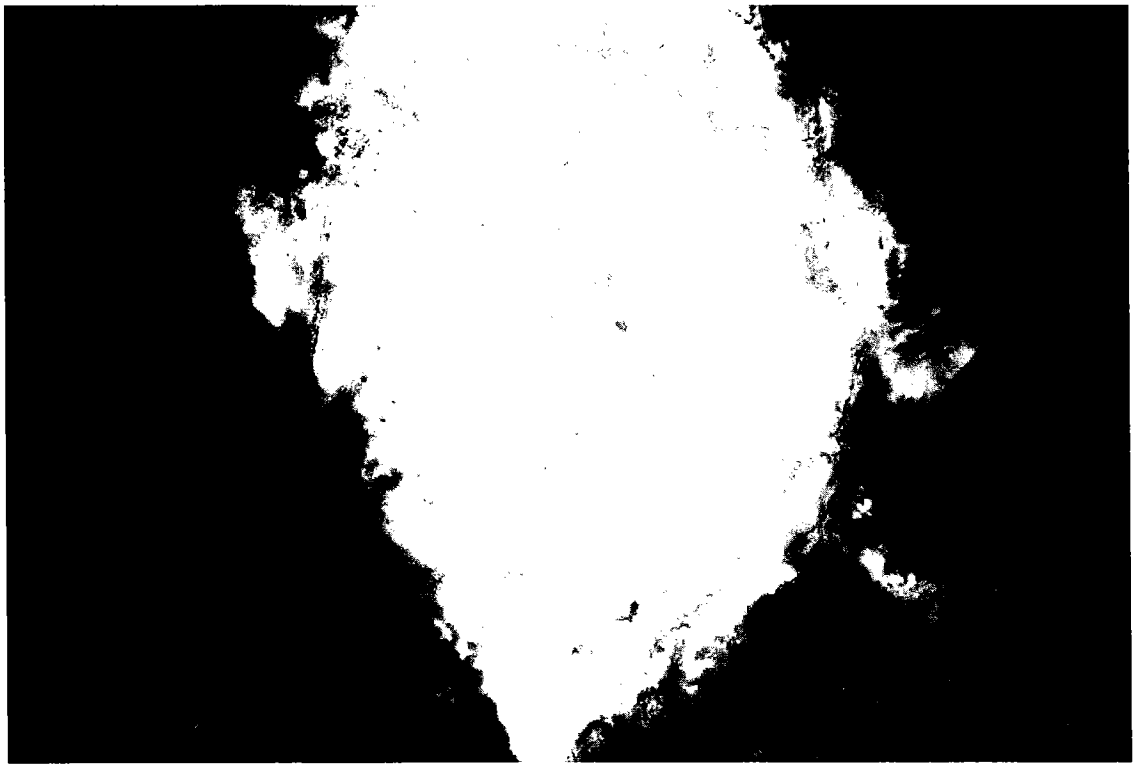

Figure 7F.

TABLE 1.—CLASSIFICATION OF CHEMICALLY ANALYZED SAMPLES

Sample number	Sample depth (m)	Classification; petrologic observations
Bland 1-33		
9189.0br	2,800.8	Dolomitic breccia; granite fragments set into dolomite cement; altered sample
9189.0jnk	2,800.8	Breccia of granite fragments set into dolomite cement; contains some pyrite
9189.1dol	2,800.8	Matrix to dolomitic breccia (secondary carbonates)
9189.1gr	2,800.8	Granite fragment; not brecciated
9191.0br	2,801.4	Monomict fragmental breccia; granitic cataclasite
9191.4br	2,801.5	Monomict fragmental breccia; granitic cataclasite
9193.4br	2,802.1	Monomict fragmental breccia with dolomite infilling of interstices; granitic cataclasite
9193.4su	2,802.1	Subsample of 9193.4br with pyrite coating
9193.7br	2,802.2	Monomict fragmental breccia with dolomite infilling of interstices; granitic cataclasite
9193.8gr	2,802.3	Granite fragment; not brecciated
9194.0br	2,802.3	Granitic fragmental breccia with secondary dolomite cement
9194.0gr	2,802.3	Granite fragment; not brecciated
Wayne 1-32		
8841.3	2,694.8	Unshocked coherent granite
Dorothy 1-19		
8978.5	2,736.6	Carbonaceous sandstone with several vol% of microcline and plagioclase; contains shocked quartz grains and microcline
8984.0	2,738.3	Carbonaceous sandstone; a number of quartz grains with multiple sets of PDFs and several annealed quartz and feldspar grains observed
8994.5	2,741.5	Aphanitic melt rock with partially melted or annealed quartz clasts; no PDFs observed; contains some carbonate clasts
9003.5	2,744.3	Fine-grained, subophitic melt rock with quartz, quartzitic, and feldspar clasts; contains several quartz clasts with PDFs
9033.5	2,753.4	Fine-grained crystalline melt rock similar to 9003.5
9038.5	2,754.9	Aphanitic melt rock with several weakly shocked (one set of PDFs) quartz clasts; contains a carbonate-filled vesicle
9137.0	2,785.0	Dolomite; not brecciated

mosaicism, changes in refractive index, isotropization, and phase changes. Planar deformation features (PDFs) in rock-forming minerals (e.g., quartz, feldspar, or olivine) have been shown to be diagnostic evidence for shock pressures that are in nature only reached during impact (see, e.g., French and Short, 1968; Stöffler, 1972,1974; Alexopoulos and others, 1988; Sharpton and Grieve, 1990; Stöffler and Langenhorst, 1994; Koeberl and Anderson, 1996). Despite some claims to the contrary, no such features have ever been documented in volcanic or tectonic environments (see, e.g., de Silva and others, 1990; Gratz and others, 1992a,b; Huffman and others, 1993; Huffman and Reimold, 1996). The experienced observer cannot confuse PDFs with tectonically produced Böhm lamellae, as PDFs are extremely straight, parallel zones consisting of amorphous silica with a thickness of about <1–3 μm that are spaced about 2–10 μm apart. They occur in planes corresponding to specific crystallographic orientations, with the (0001) or *c* (basal), $\{10\bar{1}3\}$ or ω, and $\{10\bar{1}2\}$ or π orientations being common (see, e.g., Engelhardt and Bertsch; 1969; Stöffler and Langenhorst, 1994), but, depending on the target material (particularly its porosity) and the shock pressure, orientations such as $\{11\bar{2}1\}$ and $\{51\bar{6}1\}$ can be common as well (Robertson and others, 1968).

We have found abundant evidence of shock metamorphism in a variety of samples from the URC no. 1-33 Bland, URC no. 2-18 Dixon, URC no. 1-34 Gammon, CRI no. 1-19 Dorothy, and Nicor no. 18-4 Chestnut boreholes. Shocked quartz and K-feldspar grains with three or more sets of PDFs

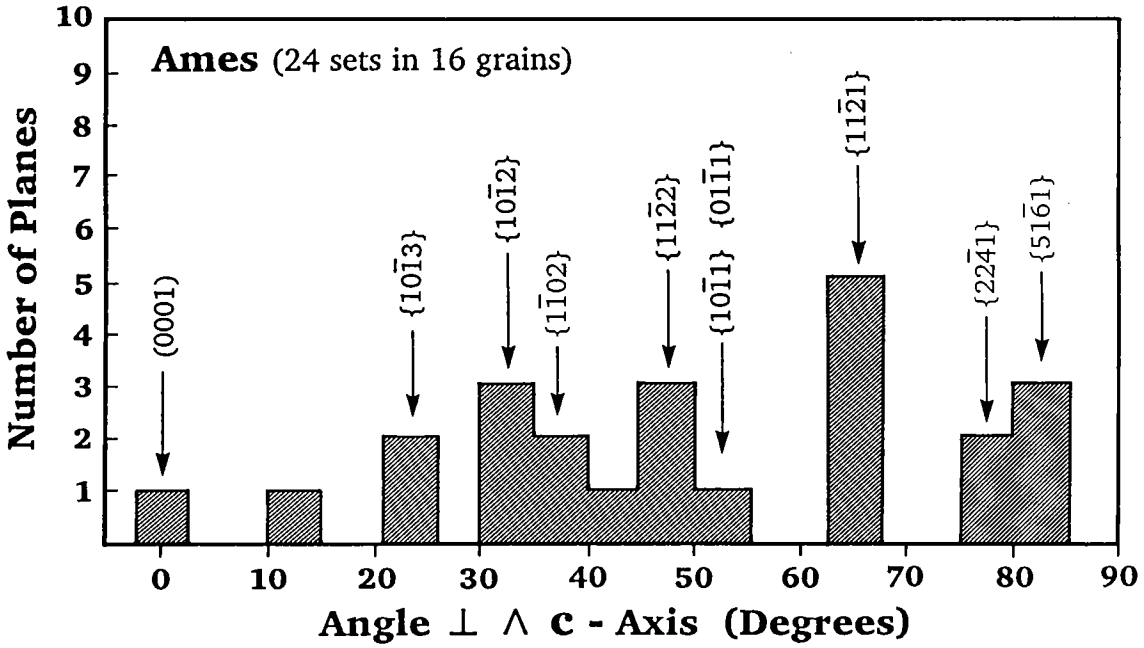

Figure 8. Crystallographic orientation of 24 PDFs from Ames samples as shown by a histogram with frequency (number of PDF planes) vs. angle between the c-axis and the PDF plane. All measurements are plotted, following the commonly used method of Engelhardt and Bertsch (1969) and Robertson and others (1968). The shock-characteristic orientations (0001), {10$\bar{1}$3}, {10$\bar{1}$2}, {11$\bar{2}$2}, {10$\bar{1}$1}, {01$\bar{1}$1}, {11$\bar{2}$1}, and {51$\bar{6}$1} (*c*, ω, π, ξ, *r*,*z*, and *s*, respectively) dominate.

in characteristic crystallographic orientations were found. To provide more detailed evidence for the shock pressures involved, we measured the crystallographic orientations of the PDFs on the optical microscope by using a universal stage with four axes (Reinhard, 1931; Emmons, 1943). A histogram of the orientations of the poles of the PDF planes relative to the c-axes of the quartz grains, using the conventional plotting method (e.g., papers in French and Short, 1968; Engelhardt and Bertsch, 1969), is shown in Figure 8. Out of 24 measured planes, 22 could be indexed according to crystallographic planes (Engelhardt and Bertsch, 1969; Stöffler and Langenhorst, 1994). The relative frequencies of the {11$\bar{2}$1} and {51$\bar{6}$1} orientations are high, similar to those that have been observed by Robertson and others (1968) for some Canadian impact craters. Our results confirm the impact origin of the Ames structure, in agreement with recent observations by Fischer (1997).

GEOCHEMISTRY OF AMES ROCKS

Twenty samples from three Ames drill cores (from URC no. 1-33 Bland, D. & J. no. 1-32 Wayne, and CRI no. 1-19 Dorothy boreholes) were analyzed for their major and trace element composition. The analyzed samples are summarized, together with a short petrographic description, in Table 1. The results of our geochemical analyses of the various rock types encountered in the URC no. 1-33 Bland drill core are given in Table 2. Samples include Arbuckle dolomite, Precambrian granite, and breccias with various proportions of mainly dolomite and granite. The composition of the granitic rocks found in the Bland borehole does not show significant variation. The standard deviation calculated from the composition of the coherent granite clasts is usually between about 5 and 10 rel% (Table 2). The dolomites from the Bland core are of typical dolomitic composition. Various amounts of carbonate are included in the different breccias from the Bland core, as is obvious from the higher Mg, Ca, and L.O.I. data compared to the granitic values.

Table 3 gives the results of the major and trace element analyses for target rocks and melt breccias from the CRI no. 1-32 Wayne borehole. The Wayne sample is a granite from 2,695 m (8,842 ft) depth, with a composition that is very similar to the average granitic composition obtained from the URC no. 1-33 Bland samples. Sample 9137 (2,785 m depth) from the CRI no. 1-19 Dorothy borehole is an almost pure dolomite. Two sandstones (samples 8978.5 and 8984 [2,736.6 and 2,738.3 m depth]) from the Dorothy borehole have compositions that are very similar to each other, and both contain shocked clasts (see above). The

TABLE 2.—MAJOR AND TRACE ELEMENT COMPOSITION OF ROCK CLASTS

	9189.0br Breccia	9189.0-jnk Breccia	9189.1dol Dolomite	9189.1gr Granite	9191.0br Breccia	9191.4br Breccia	9193.4br Breccia
SiO_2	7.60	33.65	9.59	73.30	66.11	73.57	52.83
TiO_2	0.07	0.10	0.09	0.22	0.17	0.21	0.17
Al_2O_3	1.65	6.69	1.67	11.20	10.38	10.91	8.33
Fe_2O_3	1.99	10.54	4.41	1.43	1.33	1.82	2.32
MnO	0.418	0.243	0.427	0.051	0.108	0.065	0.197
MgO	18.60	8.34	17.23	0.85	2.57	0.99	5.78
CaO	27.27	12.54	25.16	1.75	4.32	2.11	9.13
Na_2O	0.34	1.98	0.48	3.41	3.36	3.38	2.62
K_2O	0.75	2.21	0.86	4.77	4.74	4.76	4.04
P_2O_5	0.001	0.023	0.015	0.024	0.013	0.029	0.014
L.O.I.	41.15	23.41	37.37	2.93	6.93	2.07	14.56
Total	99.84	99.72	97.30	99.94	100.02	99.90	99.99
Sc	11.7	26.7	37.2	4.49	6.32	3.05	20.7
V	38.4	32.6	68.5	17.3	28.6	17.4	34.3
Cr	50.3	28.6	49.8	21.9	24.5	33.4	41.1
Co	3.97	6.53	4.83	3.71	3.75	3.61	4.75
Ni	20	44	20	22	14	4	15
Zn	46	73	86	32	30	25	62
Ga	12	20	12	15	17	41	32
As	4.12	29.8	9.04	4.06	3.21	3.05	4.54
Se	1.68	0.99	1.19	2.79	1.59	2.41	1.79
Br	2.44	0.66	0.65	0.56	0.48	0.52	0.18
Rb	18.4	105	20.6	181	155	173	126
Sr	82	50	75	35	39	31	52
Y	182	105	186	47	59	49	83
Zr	33	106	52	221	165	244	156
Nb	8.6	9.8	11.2	19.4	17.2	20.8	19.2
Ag	0.02	0.19	0.13	0.05	0.03	0.02	0.11
Sb	0.37	1.33	0.57	0.57	0.39	0.48	0.44
Cs	0.17	1.19	0.43	2.22	1.89	2.09	1.53
Ba	76	116	64	234	174	167	180
La	18.2	32.5	26.8	26.2	20.8	18.2	38.9
Ce	70.5	78.8	93.1	59.5	53.1	45.7	99.8
Nd	33.7	37.7	43.7	30.3	26.3	21.6	50.6
Sm	10.7	9.88	12.7	6.28	5.75	4.47	10.2
Eu	0.91	0.74	1.07	0.54	0.51	0.41	0.79
Gd	14.5	12.5	17.1	5.8	6.1	5.2	10.9
Tb	3.96	3.86	4.38	1.22	1.29	1.05	2.27
Dy	31.6	24.7	32.7	8.7	9.5	7.6	16.1
Tm	4.11	2.26	4.36	0.89	0.98	0.84	1.67
Yb	34.5	19.4	34.9	6.41	8.29	6.59	14.7
Lu	5.01	2.71	5.03	0.89	1.21	0.98	2.17
Hf	0.59	3.27	1.26	6.97	4.58	7.55	5.19
Ta	0.19	0.56	0.56	1.73	1.21	1.68	1.37
W	1.08	5.54	0.27	0.66	0.37	0.68	13.1
Ir (ppb)	<1	<0.5	<0.5	<0.2	0.4	<0.3	<1
Au (ppb)	0.7	0.8	0.8	0.4	0.2	0.4	1.1
Hg	<1	0.08	1.8	0.03	<0.5	<0.1	<1
Th	1.43	4.04	3.52	11.1	5.55	10.6	8.15
U	17.7	8.45	5.8	7.84	9.45	7.21	11.2
K/U	159	1,943	686	3,606	2,950	3,886	1,939
Th/U	0.08	0.48	0.61	1.42	0.59	1.47	0.73
La/Th	12.73	8.04	7.61	2.36	3.75	1.72	4.77
Zr/Hf	55.93	32.42	41.27	31.71	36.03	32.32	30.06
Hf/Ta	26.37	4.84	8.98	0.51	1.00	0.58	1.58
La_N/Yb_N	0.36	1.13	0.52	2.76	1.70	1.87	1.79
Eu/Eu*	0.223	0.203	0.222	0.273	0.263	0.260	0.229

All Fe as Fe_2O_3; major element data in wt%, trace element data in ppm (except as noted).
Sample number includes depth in feet.

AND BRECCIAS FROM THE BLAND 1-33 BOREHOLE, AMES CRATER

9193.4su Breccia	9193.7br Breccia	9193.8gr Granite	9194.0br Breccia	9194.0gr Granite	Granite Average	Std. dev.
	55.41	75.92	63.63	75.40	74.87	1.13
	0.15	0.20	0.22	0.23	0.22	0.02
	8.07	12.91	9.71	12.26	12.12	0.71
26.10	2.48	0.76	1.86	1.71	1.30	0.40
	0.194	0.017	0.119	0.020	0.029	0.015
	5.43	0.01	3.19	0.01	0.29	0.40
	8.55	0.27	5.23	0.41	0.81	0.67
1.91	2.69	4.16	3.18	3.94	3.84	0.31
3.97	3.26	5.09	4.28	4.88	4.91	0.13
	0.023	0.031	0.028	0.011	0.022	0.008
	13.64	0.54	8.55	1.17	1.55	1.01
	99.90	99.89	99.99	100.03	99.95	
10.9	20.3	1.94	11.9	2.33	2.92	1.12
	33.9	9.5	27.3	11.8	12.9	3.27
8.3	40.8	15.4	39.6	29	22.1	5.55
5.41	4.93	2.87	4.57	4.47	3.68	0.65
8	21	9	25	18	16	5
19	69	22	48	30	28	4
30	139	30	21	73	39	25
13.9	4.98	2.03	3.59	3.99	3.36	0.94
0.61	1.81	2.01	2.03	2.57	2.46	0.33
0.17	0.41	0.36	0.49	0.53	0.48	0.09
126	127	204	141	208	198	12
18	35	35	38	33	34	1
	72	49	72	57	51	4
108	125	217	270	253	230	16
	15.1	18.6	22.2	19.5	19.17	0.40
0.12	0.02	0.04	0.03	0.06	0.05	0.01
0.74	0.55	0.36	0.43	0.55	0.49	0.09
1.14	1.58	2.51	1.86	2.51	2.41	0.14
107	165	206	165	250	230	18
5.21	35.8	26.9	28.6	16.7	23.3	4.65
14.1	87.5	58.8	73.2	41.8	53.4	8.18
7.8	42.8	28.2	35.9	19.1	25.9	4.86
2.27	9.44	5.38	7.06	4.35	5.34	0.79
0.24	0.76	0.52	0.63	0.47	0.51	0.03
3.1	11.3	4.6	7.3	6.2	5.53	0.68
0.83	2.28	0.96	1.63	1.18	1.12	0.11
6.4	15.6	6.4	11.3	8.2	7.77	0.99
0.82	1.58	0.66	1.22	0.89	0.81	0.11
7.52	14.7	5.02	10.9	6.95	6.13	0.81
1.15	2.14	0.71	1.71	0.95	0.85	0.10
4.01	4.72	7.39	7.01	8.23	7.53	0.52
0.29	1.22	1.36	1.48	1.63	1.57	0.16
0.1	0.91	0.15	14.3	15.1	5.30	6.93
<1	<0.5	<0.4	0.8	0.1	0.03	0.05
0.2	0.9	0.8	1.1	0.9	0.70	0.22
0.04	0.11	0.18	0.29	0.15	0.12	0.06
1.97	9.71	12.1	25.1	12.6	11.9	0.6
2.47	9.17	5.19	10.1	6.66	6.56	1.08
6,410	2,432	6,637	2,610	4,909	4,846	
0.80	1.06	2.33	2.49	1.89	1.82	
2.64	3.69	2.22	1.14	1.33	1.95	
26.93	26.48	29.36	38.52	30.74	30.59	
3.97	1.75	0.52	1.16	0.58	0.54	
0.47	1.65	3.62	1.77	1.62	2.57	
0.276	0.225	0.319	0.268	0.277	1.700	

TABLE 3.—MAJOR AND TRACE ELEMENT COMPOSITION OF TARGET ROCKS AND IMPACT MELT BRECCIAS FROM THE WAYNE 1-32 AND DOROTHY 1-19 BOREHOLES, AMES CRATER

	Wayne	Dorothy					
	8841.3 Granite	8978.5 Sandstone	8984 Sandstone	8994.5 Impact melt	9003.5 Impact melt	9033.5 Impact melt	9038.5 Impact melt	9137 Dolomite
SiO_2	77.76		52.81	57.73	75.98			2.61
TiO_2	0.08		0.20	0.31	0.30			0.02
Al_2O_3	11.85		6.19	11.32	10.64			0.30
Fe_2O_3	0.52	2.13	1.79	1.10	0.54	0.93	0.81	0.28
MnO	0.032		0.106	0.045	0.016			0.062
MgO	0.10		6.64	3.67	0.40			20.67
CaO	0.21		10.68	5.59	0.59			29.75
Na_2O	3.77	2.79	1.84	0.93	0.23	1.14	1.32	0.20
K_2O	5.18	1.59	2.65	9.08	9.72	8.78	8.71	0.08
P_2O_5	0.012		0.036	0.036	0.033			0.160
L.O.I.	0.58		16.60	9.49	1.51			44.75
Total	100.08		99.54	99.31	99.96			98.88
Sc		3.19	3.85	2.09	2.76	10.6	8.61	0.35
Cr		9.7	12.9	18.2	17.6	20.4	53.5	2.9
Co		2.19	3.71	3.31	4.97	5.17	2.53	1.51
Ni		18	55	31	22	20	21	18
Zn		18	32	51	17	28	75	4.5
Ga		4	6	17.6	9.4	9.2	68.3	1.1
As		2.49	1.86	0.64	0.79	0.79	0.51	7.45
Se		0.21	0.28	0.39	0.09	0.36	0.13	0.02
Br		0.47	0.59	0.49	0.52	0.48	2.74	0.64
Rb		38.6	42.9	59.9	62.1	55.8	162	4.7
Sr		79	65	25	8	12	145	95
Zr		160	180	220	260	250	267	400
Ag		0.05	0.09	0.05	0.02	0.03	0.09	0.03
Sb		0.13	0.071	0.075	0.11	0.077	0.47	0.25
Cs		0.41	0.47	0.54	0.09	0.11	7.47	0.13
Ba		61	89	156	200	167	85	8.5
La		20.8	30.1	19.1	56.4	26.3	31.6	1.21
Ce		46.5	68.6	41.5	123	56.4	53.2	2.29
Nd		24.1	33.4	20.5	54.7	32.3	26.3	1.2
Sm		5.18	6.41	3.87	9.72	7.31	5.21	0.24
Eu		0.49	0.64	0.57	0.86	0.79	0.47	0.039
Gd		5.2	5.9	4	9.3	9.3	4.3	0.19
Tb		0.85	0.98	0.75	1.51	1.62	0.84	0.033
Dy		5.4	6.1	5.3	9.5	10.2	6.1	0.18
Tm		0.47	0.51	0.54	0.89	0.79	0.67	0.014
Yb		3.32	3.44	3.82	6.21	6.25	5.91	0.07
Lu		0.44	0.52	0.57	0.81	0.94	0.83	0.011
Hf		4.81	5.29	7.32	7.53	7.05	8.64	0.074
Ta		0.87	1.21	1.31	1.91	1.51	2.34	0.014
W		0.27	0.46	0.12	0.08	0.16	0.28	0.05
Ir		<1	<1	<1	<1	<1	<1	<1
Au		1.1	0.9	0.9	0.6	0.7	0.9	0.4
Hg		0.08	0.06	0.09	0.02	0.03	0.03	0.04
Th		3.61	6.18	6.61	11.7	14.1	14.9	0.28
U		1.51	2.31	9.89	3.96	3.85	5.03	0.94
K/U		15,317	6,603	780	479	2,455	2,176	1,764
Th/U		2.39	2.68	0.67	2.95	3.66	2.96	0.30
La/Th		5.76	4.87	2.89	4.82	1.87	2.12	4.32
Zr/Hf		33.26	34.03	30.05	34.53	35.46	30.90	5,405.41
Hf/Ta		0.51	0.43	0.44	0.42	0.62	0.35	0.79
La_N/Yb_N		4.23	5.91	3.38	6.14	2.84	3.61	11.68
Eu/Eu*		0.289	0.318	0.443	0.276	0.293	0.303	0.558

All Fe as Fe_2O_3; major element data in wt%, trace element data in ppm (except as noted); sample No. = depth in feet.

other four samples from the Dorothy borehole, 8944.4, 9003.5, 9033.5, and 9038.5 (2,726.3, 2,744.3, 2,753.4, and 2,759.7 m), are impact-melt rocks (which include shocked clasts). Their composition is, in general, similar to that of average granite, with some dolomite admixture. Figure 9 is a comparison between the composition of the impact-melt rocks and the average granite. Samples 8994.5 and 9003.5 have similar patterns, with prominent Na depletions and Mg enrichments. Changes in the Na/K ratio between target rocks and impact-melt rocks have been commonly observed in other craters (e.g., Koeberl and others, 1996a; Korotev and others, 1996; McCarville and Crossey, 1996; and references therein).

The similarity in composition between the granites and the impact-melt rocks is also obvious in a chondrite-normalized rare earth element (REE) plot (Fig. 10A). The granites and the impact-melt rocks show almost identical REE patterns. A wider variety of REE abundances and patterns is seen in Figure 10B, showing average granitic composition in comparison with two sandstones and a dolomite from the CRI no. 1-19 Dorothy core. The siderophile element abundances in the impact-melt rocks do not allow the unambiguous identification of a meteoritic contribution, requiring more detailed studies of the concentrations of Ir and other platinum-group elements, with better sensitivities than available for the present study.

AGE OF IMPACT-MELT ROCKS

To evaluate the age of the Ames structure, three whole-rock impact-melt rock samples were dated from the CRI no. 1-19 Dorothy core by using ^{40}Ar-^{39}Ar incremental-release methods. The ^{40}Ar-

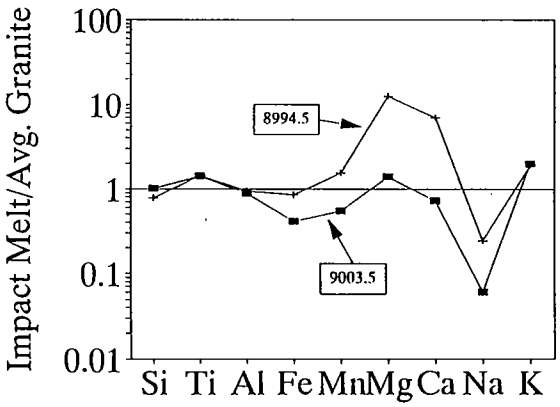

Figure 9. Comparison of the major element compositions of two impact-melt samples 8994.5 (2,741.5 m) and 9003.5 (2,744.3 m) from the CRI no. 1-19 Dorothy borehole with average granitic target rock composition. For data, see Tables 2 and 3.

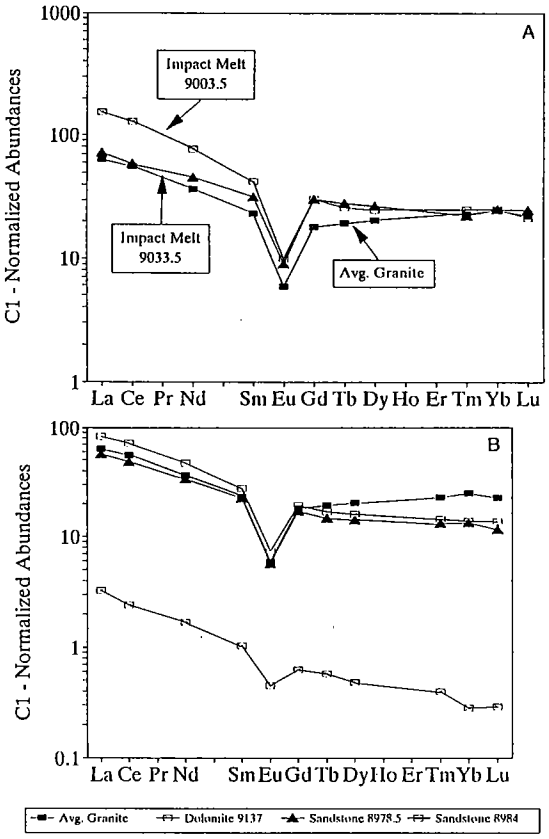

Figure 10. Chondrite-normalized rare earth element (REE) abundance patterns for Ames rocks in the CRI no. 1-19 Dorothy borehole; normalization factors from Taylor and McLennan (1985). A—Average composition of granites (Table 2) compared with composition of two impact-melt rocks from depths of 2,744.3 and 2753.4 m (9,003.5 and 9,033.5 ft). The patterns are very similar. B—Average granite, typical dolomite from 2,785 m (9,137 ft) depth, and two sandstones from 2,737 and 2,738 m (8,978.5 and 8,984 ft) depths. The patterns are almost identical.

^{39}Ar whole-rock analytical data are listed in Table 4. The data are portrayed as incremental-release spectra in Figure 11A–C. Each of the whole-rock samples displays internally discordant apparent ages and apparent K/Ca ratios. Total-gas ages of the Ames samples range between about 303 Ma (sample 8994.5 [2,741.5 m depth]) and about 267 Ma (sample 9033.5 [2,753.4 m depth]). Apparent ages and K/Ca ratios recorded at low experimental temperatures are markedly variable and low (see Fig. 11A–C). Subsequent intermediate-temperature increments are characterized by generally similar intrasample apparent ages and mutually less discordant and generally higher K/Ca ratios. The intermediate-temperature increments yielded plateau ages of 312.0 ± 0.2 Ma (sample 8994.5; Fig.

TABLE 4.—^{40}Ar-^{39}Ar ANALYTICAL DATA FOR INCREMENTAL-HEATING EXPERIMENTS ON WHOLE-ROCK IMPACT MELT SAMPLES FROM THE AMES STRUCTURE, DOROTHY 1-19 WELL

Release temp (°C)	$(^{40}Ar/^{39}Ar)^*$	$(^{36}Ar/^{39}Ar)^a$	$(^{37}Ar/^{39}Ar)^b$	^{39}Ar % of total	% ^{40}Ar nonatmos.[c]	$^{36}Ar_{Ca}$ %	Apparent age (Ma)[d]
Sample 1 (8994.5 ft): J = 0.009673							
500	17.05	0.00858	0.069	6.25	85.13	0.22	236.9 ± 0.2
550	19.58	0.00358	0.319	14.89	94.69	2.43	297.5 ± 0.1
600	20.54	0.00353	0.773	12.21	95.19	5.95	312.5 ± 0.2
650	20.20	0.00161	0.048	13.37	97.63	0.81	314.9 ± 0.2
700	20.29	0.00247	0.023	7.87	96.39	0.25	312.5 ± 0.1
750	20.19	0.00194	0.019	7.34	97.14	0.26	313.3 ± 0.3
800	20.04	0.00246	0.010	10.16	96.34	0.11	308.8 ± 0.1
850	19.89	0.00189	0.017	8.54	97.16	0.24	309.1 ± 0.2
900	19.23	0.00102	0.047	3.49	98.42	1.24	303.2 ± 0.2
950	19.54	0.00310	0.010	8.13	95.29	0.09	298.7 ± 0.2
Fusion	19.49	0.00297	0.043	7.73	94.48	0.40	298.6 ± 0.2
Total	19.77	0.00298	0.164	100.00	95.48	1.36	302.7 ± 0.2
Total without 500–550°C, 900°C - fusion				59.50			312.0 ± 0.2
Sample 2 (9003.5 ft): J = 0.009662							
450	31.56	0.07392	0.026	2.11	30.78	0.01	161.9 ± 0.5
500	15.93	0.00716	0.097	8.46	86.73	0.37	226.0 ± 0.1
550	18.31	0.00313	0.231	4.28	95.02	2.01	280.3 ± 0.2
600	18.09	0.00105	0.133	4.36	98.31	3.46	286.0 ± 0.1
650	17.93	0.00027	0.014	4.64	99.53	1.43	286.9 ± 0.1
700	17.90	0.00046	0.009	4.25	99.20	0.54	285.7 ± 0.2
750	17.95	0.00069	0.007	5.06	98.83	0.29	285.3 ± 0.2
800	17.98	0.00103	0.011	6.31	98.27	0.28	284.3 ± 0.2
850	17.82	0.00074	0.014	7.10	98.75	0.50	283.2 ± 0.2
900	17.71	0.00081	0.006	7.44	98.62	0.21	281.3 ± 0.1
950	17.61	0.00056	0.016	11.26	99.03	0.79	280.8 ± 0.1
1000	17.63	0.00061	0.014	11.01	98.96	0.64	281.0 ± 0.0
1050	17.76	0.00127	0.008	11.06	97.86	0.17	280.0 ± 0.1
1100	17.80	0.00069	0.008	7.93	98.82	0.32	283.1 ± 0.2
Fusion	18.15	0.00112	0.025	4.73	98.16	0.62	286.5 ± 0.2
Total	17.96	0.00297	0.034	100.00	96.07	0.67	275.4 ± 0.1
Total without 450–500°C				89.42			282.7 ± 0.1
Sample 3 (9033.5 ft); J = 0.009672							
450	29.90	0.8236	0.162	3.86	18.64	0.05	94.7 ± 0.3
500	13.84	0.00485	0.159	10.02	89.68	0.89	204.5 ± 0.1
550	18.74	0.00388	1.009	10.60	94.28	7.07	284.7 ± 0.2
600	19.07	0.00758	9.579	11.34	92.27	34.39	285.1 ± 0.2
650	18.40	0.00262	1.218	5.39	96.30	12.66	285.6 ± 0.2
700	17.62	0.00029	0.146	10.32	99.55	13.68	282.7 ± 0.1
750	17.85	0.00016	0.048	5.82	99.73	8.22	286.5 ± 0.1
800	18.34	0.00115	0.043	8.90	98.13	1.02	289.4 ± 0.1
850	18.22	0.00183	0.054	4.70	97.02	0.80	284.6 ± 0.4
900	17.72	0.00317	0.036	3.77	94.70	0.31	271.3 ± 0.3
950	17.83	0.00286	0.060	6.52	95.25	0.57	274.3 ± 0.2
1000	17.82	0.00231	0.039	4.89	96.15	0.45	276.6 ± 0.3
1050	18.25	0.00406	0.063	6.82	93.42	0.42	275.3 ± 0.2
Fusion	18.21	0.00421	0.076	7.04	93.18	0.49	274.1 ± 0.2
Total	18.26	0.00630	1.322	100.00	92.15	7.58	266.8 ± 0.2
Total without 450–500°C, and 900°C - fusion				57.07			285.4 ± 0.2

[a]Measured.
[b]Corrected for post-irradiation decay of ^{37}Ar (35.1-day half-life).
[c]$[^{40}Ar_{tot.} - (^{36}Ar_{atmos.})\ (295.5)]/^{40}Ar_{tot.}$
[d]Calculated using correction factors of Dalrymple and others (1981); 2σ, intralaboratory errors.

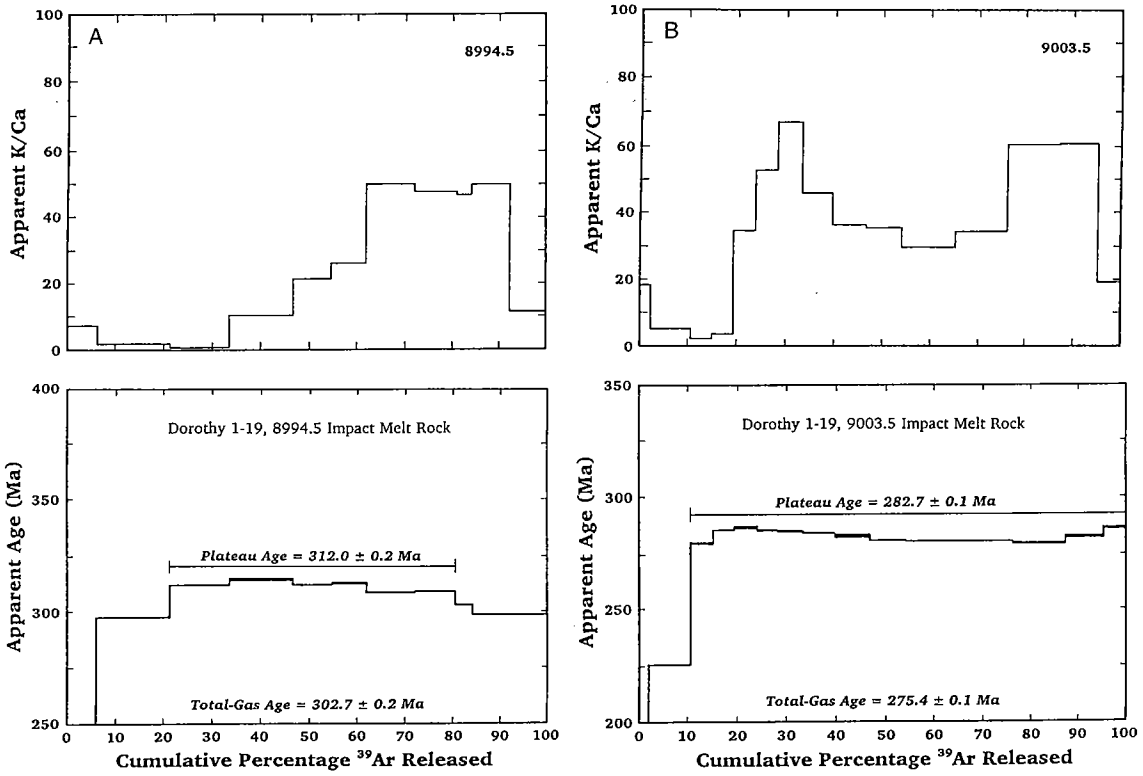

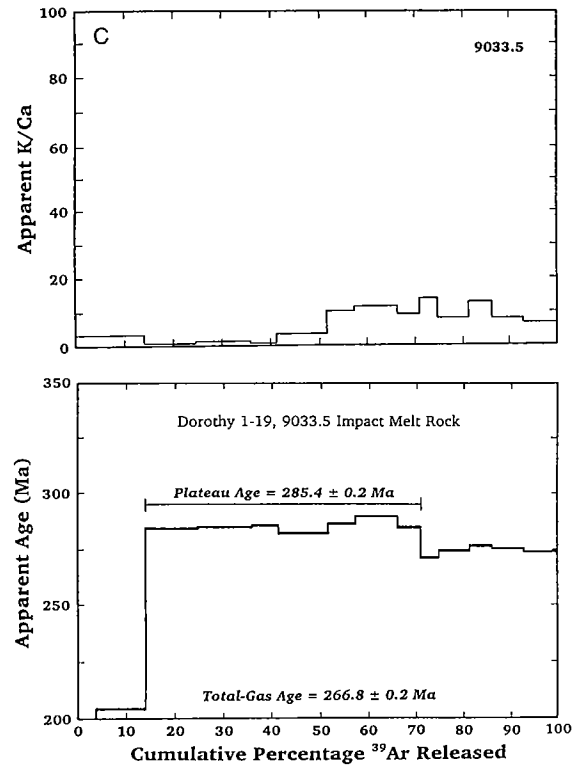

Figure 11. ^{40}Ar-^{39}Ar apparent age and apparent K/Ca spectra of three whole-rock impact-melt samples from the CRI no. 1-19 Dorothy borehole: A—2,741.5 m (8,994.5 ft), B—2,744.3 m (9,003.5 ft), and C—2,753.4 m (9,033.5 ft). Analytical uncertainties are represented by vertical width of bars. Experimental temperatures increase from left to right. Total gas and plateau ages are listed on each spectrum. For discussion, see text. Data presented in Table 4.

11A), 282.7 ± 0.1 Ma (sample 9003.5 [2,744.3 m depth]; Fig. 11B), and 285.4 ± 0.2 Ma (sample 9033.5; Fig. 11C). Apparent ages and apparent K/Ca ratios systematically decrease in highest-temperature segments of each analysis. Of the samples used for dating, samples 9003.5 and 9033.5 are very fresh and unaltered fine-grained impact-melt rocks (Fig. 6C). Their chemical compositions (Table 3; measured on aliquots of the samples that were used for dating) are very similar to the composition of the granitic target rock (see Table 2), from which they were derived by melting. Because the impact origin of these samples is confirmed by the presence of shocked minerals (with PDFs) as clasts in the melt rocks (Fig. 7E,F), the hypothesis that these samples represent volcanic or other melt samples that originated from elsewhere in the stratigraphic column can, thus, be excluded.

Contamination or incomplete degassing has been reported to be a problem for dating some impact craters by the ^{40}Ar-^{39}Ar method (e.g., Bottomley and others, 1990; Deutsch and Schärer, 1994). The variably discordant ^{40}Ar-^{39}Ar age spectra displayed by the three Ames whole-rock samples are difficult to interpret directly. Systematic intrasample variations in apparent K/Ca ratios suggest that several phases contributed gas at various stages of the analyses. The consistency of apparent K/Ca ratios recorded by intermediate-temperature increments liberated from each sample suggests that experimental evolution of gas occurred from compositionally uniform intracrystalline sites. Therefore, the 312 and 283 Ma plateau ages are considered geologically significant and are interpreted to date the last cooling through temperatures required for intracrystalline retention of radiogenic ^{40}Ar.

Several interpretations of these ages are possible. They could date formation of the impact-melt rocks at about 285 Ma, which is in contrast to the stratigraphic age of about 470 Ma. However, the stratigraphic correlation of the supposedly postimpact shale that covers the Ames structure as being from the Oil Creek Formation has recently been revised somewhat (Repetski, 1997). Incomplete digestion of older target materials is unlikely, because such a phenomenon would likely be recognizable by high-temperature increases in apparent ages and would result in higher, not lower, total ages. An alternative interpretation is that the ages could be related to a later alteration event. It is important to note that primary carbonate and shale clasts (not alteration products; possibly from higher in the section) occur within the impact breccias. Their presence could indicate that the crater may not be as old as indicated by stratigraphic data available so far. On the other hand, there is some evidence for Late Carboniferous–Early Permian (ca. 300 Ma) mobilization of brines in the eastern and central United States (Hearn and Sutter, 1985; Hearn and others, 1987). It is conceivable that the Ames area also experienced some elevated temperatures during the Wichita orogeny. Clearly, more detailed Ar-Ar dating on melt rocks from the Nicor no. 18-4 Chestnut core and a thorough re-examination of the stratigraphic evidence are required to more completely constrain the age of the Ames event.

SUMMARY AND CONCLUSIONS

The Ames structure is a circular structural anomaly at 36°15′N, 98°12′W, in northwestern Oklahoma near the town of Ames in southeastern Major County. The feature has a diameter of about 15 km. Attention was drawn to the Ames area when in 1991 several wells drilled into the structure turned out to be prolific oil and gas producers. Geophysical and drilling studies indicate the presence of two concentric structures: (1) an outer rim, which is about 1.5 to 3 km wide and which consists mainly of fractured and brecciated Arbuckle dolomite, and (2) within a central depression, an inner ring structure, which is about 5 km in diameter and seems to be the remnant of a structural uplift of mostly brecciated Precambrian granite and Arbuckle dolomite. The whole feature is buried beneath almost 3,000 m (9,843 ft) of sedimentary rock. On the basis of geophysical measurements and the presence of possibly shocked quartz grains, an impact origin was interpreted earlier by, e.g., Roberts and Sandridge (1992), Hamm and Olsen (1992), and Carpenter and Carlson (1992). The morphology and geologic setting of Ames are similar to those of other complex impact structures. Although a volcanic and/or tectonic origin has been suggested for Ames (e.g., Roemer and others, 1992; Coughlon and Denney, 1993), the discovery of some shocked quartz is evidence in favor of an impact origin.

We have performed a detailed mineralogical, petrographical, and geochemical study of a variety of samples from nine drill cores from the Ames structure. The results of the petrographical study show that lithic and melt breccias from the URC no. 1-33 Bland, URC no. 1-34 Gammon, URC no. 2-18 Dixon, CRI no. 1-19 Dorothy, and Nicor no. 18-4 Chestnut drill cores contain numerous shocked quartz and feldspar grains, with up to three sets of shock-characteristic planar deformation features (PDFs), and some rare impact-glass fragments. These findings confirm the features previously reported by Carpenter and Carlson (1992) and Fischer (1997) and provide unambiguous evidence of an impact origin for this structure. None of the proponents of a volcanic origin of the Ames structure has been able to explain these features in any way, preferring to simply ignore over 30 years of impact research and abundant evidence in the Ames rocks. Samples from 2,951, 2,954, and 2,964 m (9,682, 9,692, and 9,724 ft) depths from the CRI no. 1-19 Dorothy drill core were identified as fine-grained subophitic and aphanitic impact-melt rocks with shocked clasts; the chemical composition of these melt rocks is very similar to that of the target granite, although there is minor carbonate admixture in some of the samples.

The age of the impact event is not well constrained. The structure is covered by Oil Creek shale of reportedly Middle Ordovician age, which overlies the Arbuckle dolomite. On the basis of these stratigraphic arguments, the age of the crater was estimated at about 470 Ma. We have performed ^{40}Ar-^{39}Ar age determinations of whole-rock impact-melt rock samples. Plateau ages of about 285 Ma were obtained for two of the impact-melt rocks, which is in contrast to the stratigraphic age. The finding of shale and carbonate clasts within the impact breccias may indicate an age that is

younger than the stratigraphic age accepted so far. Alternatively, later overprinting (of so far unknown origin) may have reset the Ar isotopic system. However, as Ames is one of the more economically important impact structures, more detailed petrographical, geochemical, and dating studies are warranted.

ACKNOWLEDGMENTS

We thank Universal Resources Corporation, D. & J. Oil Company, Continental Resources, Inc., the Shawnee Sample Library, and individual colleagues for samples and data. We also appreciate the help of F. Fischer (Fischer Petrologic, Denver) and K. Johnson (Oklahoma Geological Survey) in obtaining samples of the Nicor no. 18-4 Chestnut core. We are grateful to D. Jalufka, L. Whitfield, D. du Toit, and G. Stropus for drafting of figures. The present research was supported by the Austrian Fonds zur Förderung der wissenschaftlichen Forschung (FWF), Project P08794-GEO (to Koeberl) and by the Foundation for Research Development, South Africa (to Reimold).

REFERENCES CITED

Alexopoulos, J. S.; Grieve, R. A. F.; and Robertson, P. B., 1988, Microscopic lamellar deformation features in quartz: discriminative characteristics of shock-generated varieties: Geology, v. 16, p. 796–799.

Bottomley, R. J.; York, D.; and Grieve, R. A. F., 1990, ^{40}Ar-^{39}Ar dating of impact craters, *in* Sharpton, V. L.; and Ryder, G. (eds.), Proceedings of the Twentieth Lunar and Planetary Science Conference: Houston, Texas, Lunar and Planetary Institute, p. 421–431.

Brenan, R. L.; Peterson, B. L.; and Smith, H. J., 1975, The origin of Red Wing Creek structure, McKenzie County, North Dakota: Wyoming Geological Association Earth Science Bulletin, v. 8, p. 11–41.

Carpenter, B. N.; and Carlson, Rick, 1992, The Ames impact crater: Oklahoma Geology Notes, v. 52, p. 208–223.

Coughlon, J.; and Denney, P., 1993, The Ames structural depression: an endogenic cryptoexplosion feature along a transverse shear: Shale Shaker, v. 43, no. 4, p. 44–58.

Dallmeyer, R. D.; and Gil-Ibaruchi, J. I., 1990, Age of ophiolitic metamorphism in the ophiolitic unit of the Morais allochthon (Portugal): implications for "Early" Hercynian orogenesis in the Iberian massif: Geological Society [London] Journal, v. 147, p. 873–878.

Dalrymple, G. B.; Alexander, E. C.; Lanphere, M. A.; and Kraker, G. P., 1981, Irradiation of samples for $^{40}Ar/^{39}Ar$ dating using the Geological Survey TRIGA reactor: U.S. Geological Survey Professional Paper 1176.

de Silva, S. L.; Wolff, J. A.; and Sharpton, V. L., 1990, Explosive volcanism and associated pressures: implications for models of endogenic shocked quartz, *in* Sharpton, V. L.; and Ward, P. D. (eds.), Global catastrophes in Earth history: Geological Society of America Special Paper 247, p. 139–145.

Deutsch, A.; and Schärer, U., 1994, Dating terrestrial impact events: Meteoritics, v. 29, p. 301–322.

Emmons, R. C., 1943, The universal stage (with five axes of rotation): Geological Society of America Memoir 8, 205 p.

Engelhardt, W. v.; and Bertsch, W., 1969, Shock induced planar deformation structures in quartz from the Ries crater, Germany: Contributions to Mineralogy and Petrology, v. 20, p. 203–234.

Fischer, J. F., 1997, The Nicor Chestnut 18-4 core: description and petrography, *in* Johnson, K. S.; and Campbell, J. A. (eds.), Ames structure in northwest Oklahoma and similar features: origin and petroleum production (1995 symposium): Oklahoma Geological Survey Circular 100 [this volume], p. 223–239.

French, B. M.; and Short, N. M. (eds.), 1968, Shock metamorphism of natural materials: Mono Book Corp., Baltimore, 644 p.

Gratz, A. J.; Nellis, W. J.; Christie, J. M.; Brocious, W.; Swegle, J.; and Cordier, P., 1992a, Shock metamorphism of quartz with initial temperatures –170 to +1000°C: Physics and Chemistry of Minerals, v. 19, p. 267–288.

Gratz, A. J.; Nellis, W. J.; and Hinsey, N. A., 1992b, Laboratory simulation of explosive volcanic loading and implications for the cause of the K/T boundary: Geophysical Research Letters, v. 19, p. 1391–1394.

Grieve, R. A. F., 1987, Terrestrial impact structures: Annual Reviews of Earth and Planetary Science, v. 15, p. 245–270.

Hamm, H.; and Olsen, R. E., 1992, Oklahoma Arbuckle lime exploration centered on buried astrobleme structure: Oil and Gas Journal, v. 90, p. 113–116.

Hearn, P. P., Jr.; and Sutter, J. F., 1985, Authigenic potassium feldspar in Cambrian carbonates: evidence of Alleghanian brine migration: Science, v. 228, p. 1529–1531.

Hearn, P. P., Jr.; Sutter, J. F.; and Belkin, H. E., 1987, Evidence for Late-Paleozoic brine migration in Cambrian carbonate rocks of the central and southern Appalachians: implications for Mississippi Valley–type sulfide mineralization: Geochimica et Cosmochimica Acta, v. 51, p. 1323–1334.

Hörz, F., 1968, Statistical measurements of deformation structures and refractive indices in experimentally shock loaded quartz, *in* French, B. M.; and Short, N. M. (eds.), Shock metamorphism of natural materials: Mono Book Corp., Baltimore, p. 243–253.

Huffman, A. R., and Reimold, W. U., 1996, Experimental constraints on shock-induced microstructures in naturally deformed silicates: Tectonophysics, v. 256, p. 165–217.

Huffman, A. R.; Brown, J. M.; Carter, N. L.; and Reimold, W. U., 1993, The microstructural response of quartz and feldspar under shock loading

at variable temperatures: Journal of Geophysical Research, v. 98, p. 22171–22197.

Johnson, K. S., 1989, Geologic evolution of the Anadarko basin, *in* Johnson, K. S. (ed.), Anadarko basin symposium, 1988: Oklahoma Geological Survey Circular 90, p. 3–12.

Kirschner, C. E.; Grantz, A.; and Mullen, M. W., 1992, Impact origin of the Avak structure, Arctic Alaska, and genesis of the Barrow gas fields: American Association of Petroleum Geologists Bulletin, v. 76, p. 651–679.

Koeberl, Christian, 1993, Instrumental neutron activation analysis of geochemical and cosmochemical samples: a fast and proven method for small sample analysis: Journal of Radioanalytical and Nuclear Chemistry, v. 168, p. 47–60.

_____ 1994, African meteorite impact craters: characteristics and geological importance: Journal of African Earth Sciences, v. 18, p. 263-295.

Koeberl, Christian; and Anderson, R. R., 1996, Manson and company: impact structures in the United States, *in* Koeberl, C.; and Anderson, R. R. (eds.), The Manson impact structure, Iowa: anatomy of an impact crater: Geological Society of America Special Paper 302, p. 1–29.

Koeberl, Christian; and Reimold, W. U., 1995a, Shock metamorphism at the Red Wing Creek structure, North Dakota: confirmation of impact origin: Lunar and Planetary Science, v. 26, p. 769–770.

_____ 1995b, The Newporte impact crater, North Dakota: Geochimica et Cosmochimica Acta, v. 59, p. 4747–4767.

Koeberl, Christian; Kluger, F.; and Kiesl, W., 1987, Rare earth element determinations at ultratrace abundance levels in geologic materials: Journal of Radioanalytical and Nuclear Chemistry, v. 112, p. 481–487.

Koeberl, Christian; Reimold, W. U.; and Powell, R. A., 1994a, Ames structure, Oklahoma: an economically important impact crater: Lunar and Planetary Science, v. 25, p. 721–722.

_____ 1994b, Shocked quartz and impact melt rock at the Ames structure, Oklahoma: Meteoritics, v. 29, p. 483.

Koeberl, Christian; Reimold, W. U.; and Brandt, D., 1995, The Newporte impact structure, North Dakota: shock metamorphism in breccias: Lunar and Planetary Science, v. 26, p. 773–774.

Koeberl, Christian; Reimold, W. U.; Kracher, A.; Träxler, B.; Vormaier, A.; and Körner, W., 1996a, Mineralogical, petrographical, and geochemical studies of drill core samples from the Manson impact structure, Iowa, *in* Koeberl, C.; and Anderson, R. R. (eds.), The Manson impact structure, Iowa: anatomy of an impact crater: Geological Society of America Special Paper 302, 145–219.

Koeberl, Christian; Reimold, W. U.; and Brandt, D., 1996b, Red Wing Creek structure, North Dakota: Petrographical and geochemical studies, and confirmation of impact origin: Meteoritics and Planetary Science, v. 31, p. 335–342.

Korotev, R. L.; Rockow, K. M.; Jolliff, B. L.; Haskin, L. A.; McCarville, P.; and Crossey, L. J., 1996, Geochemical comparison of four cores from the Manson impact structure, *in* Koeberl, C.; and Anderson, R. R. (eds.), The Manson impact structure, Iowa: anatomy of an impact crater: Geological Society of America Special Paper 302, p. 275–315.

McCarville, P.; and Crossey, L. J., 1996, Post-impact hydrothermal alteration of the Manson impact structure, *in* Koeberl, C.; and Anderson, R. R. (eds.), The Manson impact structure, Iowa: anatomy of an impact crater: Geological Society of America Special Paper 302, p. 347–376.

Reimold, W. U.; Koeberl, Christian; and Bishop, J., 1994, Roter Kamm impact crater, Namibia: geochemistry of basement rocks and breccias: Geochimica et Cosmochimica Acta, v. 58, p. 2689–2710.

Reinhard, M., 1931, Universaldrehtischmethoden: Birkhäuser Verlag, Basel, 118 p.

Repetski, J. E., 1997, Conodont age constraints on the Middle Ordovician black shale within the Ames structure, *in* Johnson, K. S.; and Campbell, J. A. (eds.), Ames structure in northwest Oklahoma and similar features: origin and petroleum production (1995 symposium): Oklahoma Geological Survey Circular 100 [this volume], p. 363–369.

Roberts, C.; and Sandridge, B., 1992, The Ames hole: Shale Shaker, v. 42, no. 5, p. 118–121.

Robertson, P. B.; Dence, M. R.; and Vos, M. A., 1968, Deformation in rock-forming minerals from Canadian craters, *in* French, B. M.; and Short, N. M. (eds.), Shock metamorphism of natural materials: Mono Book Corp., Baltimore, p. 433–452.

Roemer, C. D.; Romer, C.; and Williams, K., 1992, Gravity, magnetics point to volcanic origin for Oklahoma's Ames anomaly: Oil and Gas Journal, v. 90, no. 26, p. 75–80.

Sharpton, V. L.; and Grieve, R. A. F., 1990, Meteorite impact, cryptoexplosion, and shock metamorphism: a perspective on the evidence at the K/T boundary, *in* Sharpton, V. L.; and Ward, P. D. (eds.), Global catastrophes in Earth history: Geological Society of America Special Paper 247, p. 301–318.

Stöffler, D., 1972, Deformation and transformation of rock-forming minerals by natural and experimental shock processes: 1. Behaviour of minerals under shock compression: Fortschritte der Mineralogie, v. 49, p. 50–113.

_____ 1974, Deformation and transformation of rock-forming minerals by natural and experimental processes: 2. Physical properties of shocked minerals: Fortschritte der Mineralogie, v. 51, p. 256–289.

Stöffler, D.; and Langenhorst, F., 1994, Shock metamorphism of quartz in nature and experiment; I. Basic observations and theory: Meteoritics, v. 29, 155–181.

Taylor, S. R.; and McLennan, S. M., 1985, The continental crust: its composition and evolution: Blackwell Scientific Publications, Oxford, 312 p.

Wilson, J. L.; Fritz, R. D.; and Medlock, P. L., 1991, The Arbuckle Group—relationship of core and outcrop analysis to cyclic stratigraphy and correlation, *in* Johnson, K. S. (ed.), Arbuckle Group core workshop and field trip: Oklahoma Geological Survey Special Publication 91-3, p. 133–143.

Reservoir Characterization of a Complex Impact Structure: Ames Impact Structure, Northern Shelf, Anadarko Basin

Michael D. Kuykendall
Solid Rock Resources, Inc.

Christopher L. Johnson
Petra Technologies

Rick A. Carlson
DLB Oil & Gas, Inc.

The concentric structural feature known as the Ames structure or Ames impact structure, on the northern shelf of the Anadarko basin, was discovered in the spring of 1991 (Fig. 1). A detailed, proprietary, reservoir-characterization field study of the structure was conducted; the study utilized extensive subsurface data including information from horizontal wells, formation-imaging logs, and three-dimensional seismic results (Masera, 1993). Petrophysical evaluation included digital log analysis, petrographic and standard core analyses of whole cores and rotary sidewall core-plugs, and examination of drill cuttings. Correlation and calibration of log and rock characteristics of distinct Arbuckle plus basement granite reservoir lithofacies from key wells provided the basis for field-wide inferences about rock and pore types, porosity and permeability, fluid saturations and fluid contacts, and related production characteristics.

The buried impact feature contains several heterogeneous and uniquely associated hydrocarbon reservoirs within extremely brecciated, fractured, and faulted Cambrian–Ordovician Arbuckle Group dolomites, Precambrian granodiorites, and devitrified pseudopyroclastic (i.e., impact-melt) rocks (Table 1 and Fig. 2). The crater is 8–10 mi in diameter (rim crest to rim crest) and is buried at 8,500–9,500 ft. The original crater depth is estimated to have been 300 to 400 ft. There has been significant postimpact modification of the crater by karst processes and subsequent compaction (Fig. 3). Crater morphology, critical diagnostic structural features, and petrographic evidence from cores and cuttings strongly support an impact origin for the structure.

Morphologically distinct areas, based on analogy with well-documented complex-type impact craters, include (1) a central rebound feature composed of a concentric ring-type horst-and-graben structure enclosing a central peak and bounded by concentric normal faults, (2) a relatively steep crater wall containing concentric growth faults, (3) an uplifted inner rim, and (4) a hummocky outer rim (Table 2 and Fig. 4). An associated collapse zone in the southwestern part of the crater is believed to be the result of the collapse and continued compaction of a network of solution cavities (paleocaverns) (Fig. 4). An April 1994 earthquake (2.8 magnitude) was centered along the southeastern rim of the crater, suggesting continued structural adjustments possibly related to compaction and/or regional tectonics.

Numerous trapping mechanisms have operated within the distinctive and unique reservoir lithofacies in and around the Ames impact structure, which is estimated to contain ultimate recoverable reserves of 50 MMBO (million barrels of oil) and 20 BCFG (billion cubic feet of gas). In addition, both locally and regionally with respect to the Ames structure, stratigraphic trapping of hydrocarbons may occur in reservoir-quality ejecta lithologies unconformably present in the upper part of the Arbuckle Group and in reworked, arkosic and dolomitic, impact-related lithofacies

Michael D. Kuykendall, Solid Rock Resources, 1408 So. Delaware Place, Tulsa, OK 74104; Christopher L. Johnson, Petra Technologies, 2201 S. Florence Place, Tulsa, OK 74114; Rick A. Carlson, DLB Oil and Gas, Inc., 1601 NW Expressway, Suite 700, Oklahoma City, OK 73118.

Kuykendall, M. D.; Johnson, C. L.; and Carlson, R. A., 1997, Reservoir characterization of a complex impact structure: Ames impact structure, northern shelf, Anadarko basin , *in* Johnson, K. S.; and Campbell, J. A. (eds.), Ames structure in northwest Oklahoma and similar features: origin and petroleum production (1995 symposium): Oklahoma Geological Survey Circular 100, p. 199–206.

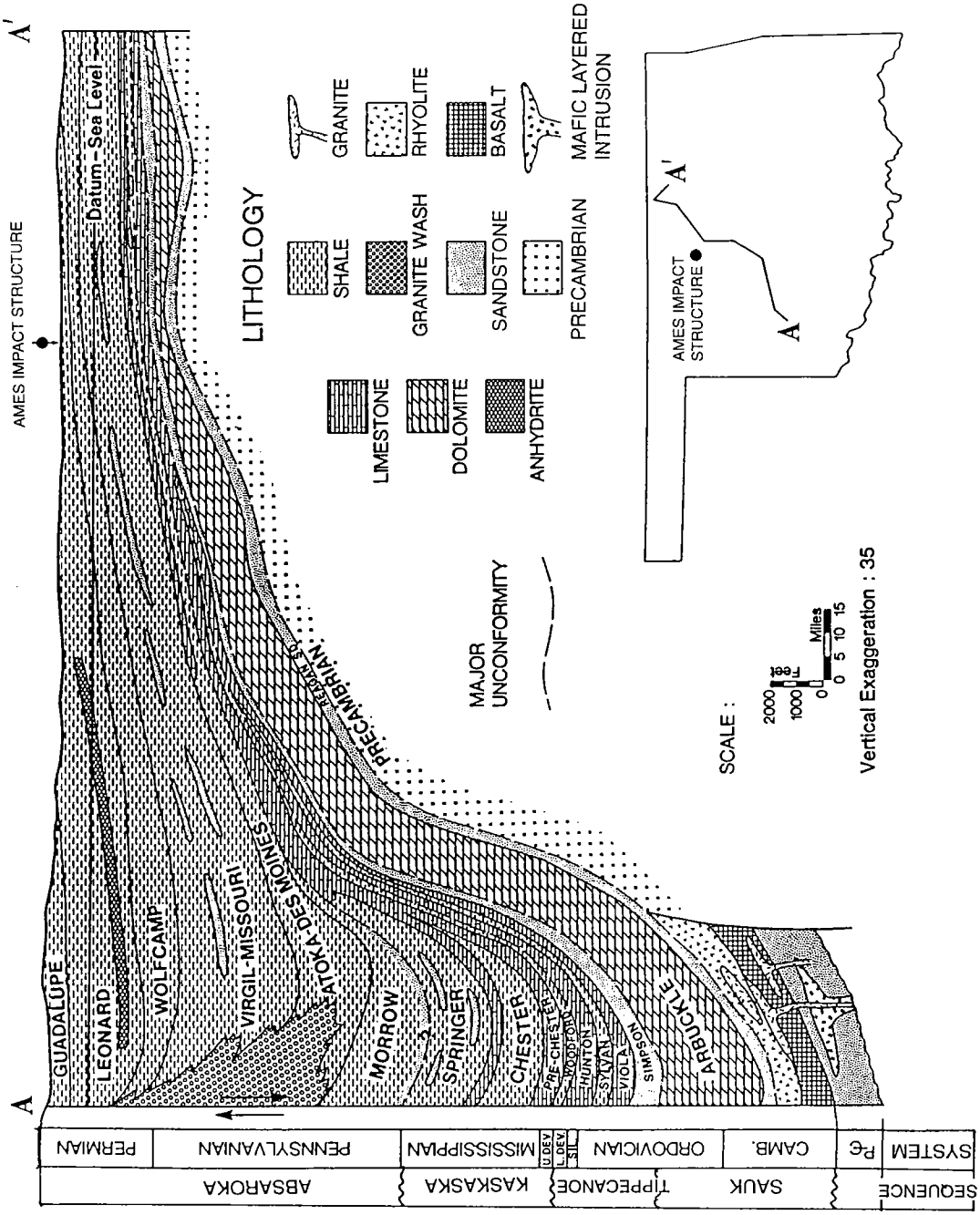

Figure 1. Diagrammatic stratigraphic cross section of the Anadarko basin, showing the approximate location of the Ames impact structure. (Modified after Adler and others, 1971.)

TABLE 1.—RESERVOIR LITHOFACIES IN THE AMES IMPACT STRUCTURE

Zone or formation	Lithologic and reservoir characteristics
Ejecta and/or fallout (crater rim and flank)	Heterolithic dolomite microbreccia and conglomerate containing abundant sand-sized clasts of dolomite, chert, quartz, feldspar, glass droplets (microtektites), and sand grains, showing moderate to sparse shock-metamorphism textures; clayey; homogeneous in part but may contain dolomite megablocks and impact melt; vuggy intercrystalline porosity, some fracturing; paleokarstic overprint.
West Spring Creek Fm. (possible occurrences on rim, flank, and wall)	Homogeneous fine-crystalline dolomite with thin interbeds of sandstones, shales, and sandy shales; may be heavily karsted and contain sand-filled cavities; intercrystalline porosity and minor vugs enhanced by fractures in some areas along the crater rim. Good local (crater rim and flank) and regional well-log correlations.
Kindblade Fm. (possible occurrences on rim, flank, and wall)	Homogeneous, fine- to coarse-crystalline dolomite with good intercrystalline and vuggy porosity in correlatable zones; thin intertidal shales and massively bedded, subtidally dominated peritidal dolomites. The Arbuckle Group Cool Creek Formation below is similar and contains abundant thin sandstones and silicified oolites.
Caprock (crater floor)	Dolomitic (partly silicified) microbreccia and conglomerate containing a variety of poorly sorted angular clasts (dolomite, chert, silica, feldspar) with moderate shock-metamorphism features; tight, minor vuggy porosity with fractures in some areas; not currently considered reservoir quality; in sharp contact with crater-filling shales.
Impact melt (crater floor and in breccia)	Siliceous, pseudopyroclastic breccia containing an abundance of shocked clasts (quartz, feldspar, and dolomite) and glassy matrix that is partially devitrified; shows abundant recrystallization (dolomitization, pyritization, illitization) and iron dolomite cementation. Excellent vuggy porosity, but lacks permeability unless fractured.
Crater dolomite (crater floor and in breccia megablocks)	Heterolithic to homogeneous dolomite breccia and conglomerate containing an extreme range in clast size (sand to megablock); clayey, moderate shock features, and glassy matrix; interbeds (lenses) of impact melt; tight (in part); good vuggy and intercrystalline porosity, extensively fractured, solution-enhanced cavernous porosity as observed in FMI and FMS logs; extreme heterogeneity and suspected reservoir compartmentalization; complex association with megablocks of granite breccia.
Granite breccia (crater floor and in breccia megablocks)	Homogeneous (compositionally) granite to granodiorite breccia and conglomerate containing an extreme range in clast size (sand to megablock); irregular vuggy and fracture porosity around granite clasts within a fine- to medium-crystalline dolomitic matrix; intramoldic porosity within granite clasts; extensively fractured with high reservoir heterogeneity and suspected reservoir compartmentalization; complex association with crater dolomite; the best reservoir.

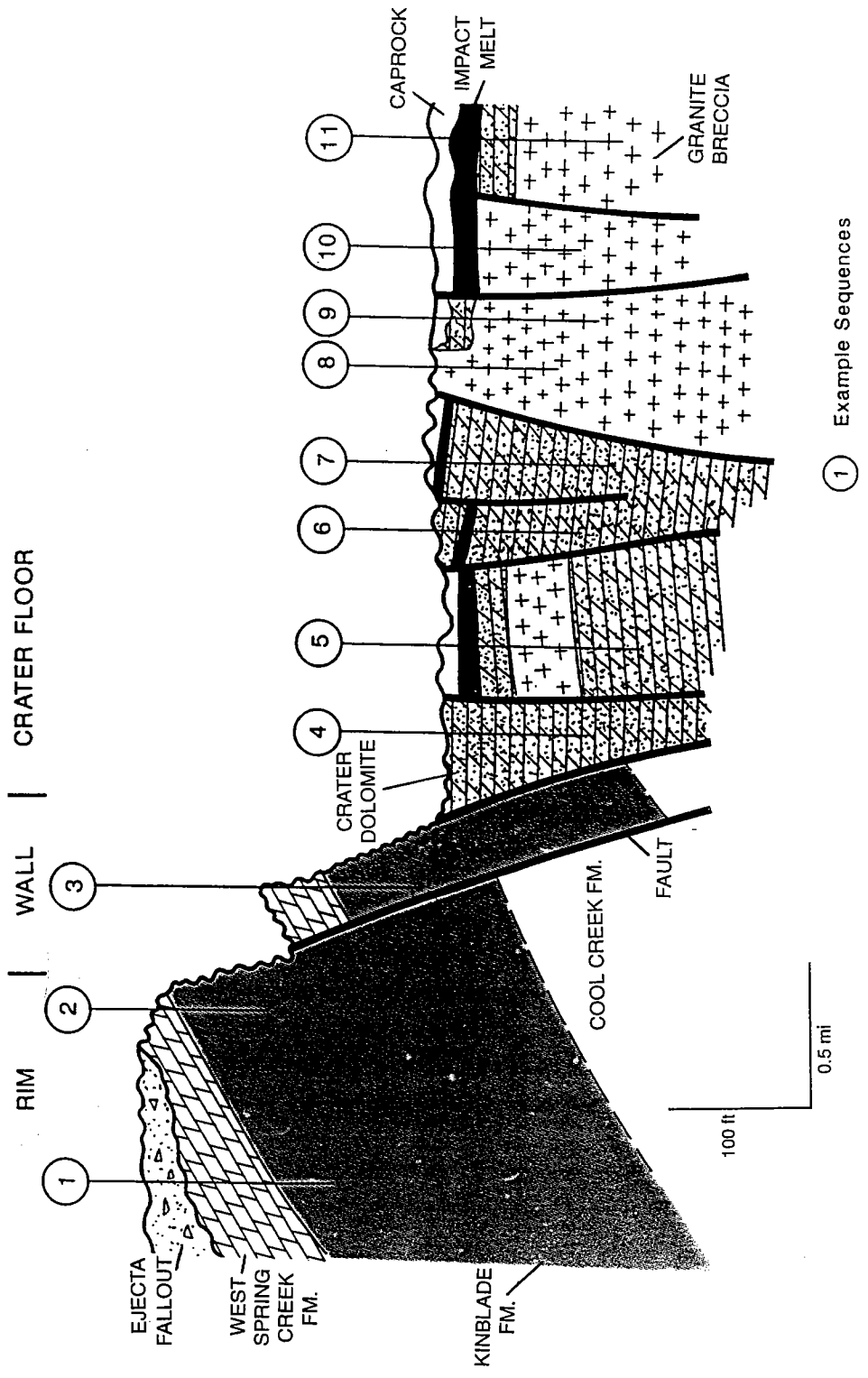

Figure 2. Diagrammatic preburial stratigraphic cross section of the Ames impact structure from crater rim to crater floor, showing the generalized subcrop relationships among the various reservoir lithofacies and major faults (heavy, black, near-vertical lines). Position of numbers (1–11) indicates example vertical sequences from representative well data in those areas shown in Figure 4.

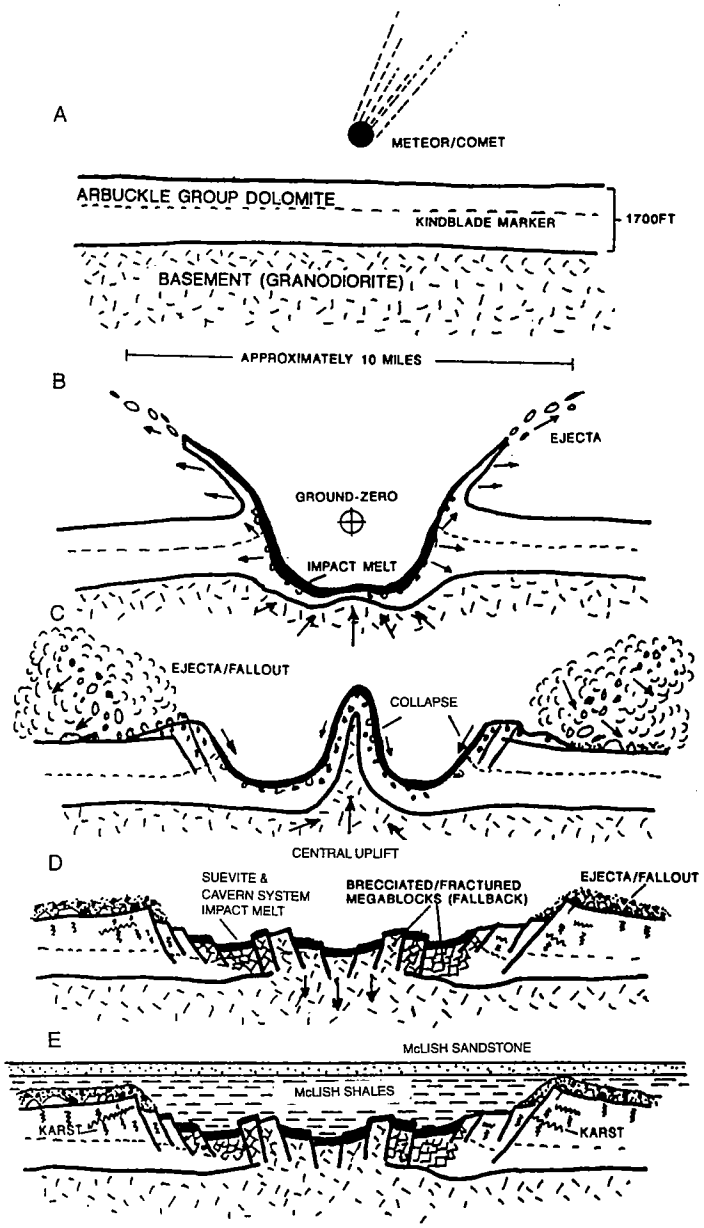

Figure 3. Generalized model for the development of the Ames impact structure, showing the relative sequence of events in the formation, karstification, and initial burial of the impact crater. *A*—Preimpact setting at 480 Ma (Sauk-Tippecanoe sequence boundary) with about 1,700 ft of peritidal platform-carbonate deposits (now the Arbuckle Group) overlying the basement granodiorite. *B*—Impact of meteor or comet caused crater excavation, rim uplift and possible overturning, shock metamorphism (impact melt and shocked quartz), ballistic trajectory of ejecta material, and the beginning of formation of the central uplift (sometimes referred to as the central rebound structure) by release of the initial shock-wave compression. *C*—Central uplift overshoots stable height and collapses; crater wall also collapses, and ejecta and fallout are deposited (megablocks of crater fallback breccia are not shown). *D*—Development of "complex peak-ring crater" with concentric crater-floor horst-and-graben structural morphology; exposure followed and karstification formed an extensive cavern system in parts of the crater floor, i.e., the present "collapse zone." *E*—Crater filling and burial with black, organic-rich, marine shales and a relatively thin, shallow-marine sandstone of the McLish Formation (initial transgression of Tippecanoe sequence). Between event E and the present, the cavern system continued to collapse; the impact site was buried by approximately 10,000 ft of Paleozoic sedimentary deposits, and continued compaction led to structural adjustments at crater level and in the overlying rocks.

TABLE 2.—STRUCTURAL, MORPHOLOGICAL, AND RESERVOIR CHARACTERISTICS OF THE AMES IMPACT STRUCTURE

1. Broad, hummocky, structurally complex crater floor
2. Concentric ring structure (horst/graben) on crater floor
3. Central basin or depression ("pit") and locally terraced crater walls (circumferential listric normal faults)
4. Moderately steep crater walls and talus-covered lower crater walls with blocky terrain
5. Locally high, sharp, rim crest with uplifted and depressed rim segments
6. Smooth to hummocky terrain on outer-rim ejecta blanket
7. Karstification and collapse features (cavernous porosity and filled caves) (southwestern part of crater)
8. Central uplift "peak-ring" cored with (fractured and/or brecciated) basement granodiorite and dolomite megablocks
9. Crater filled by marine black shale (upper, middle, lower) (possible source rocks)
10. Shallow-marine (shoreface?) sandstone (McLish Formation) along rim in upper crater-filling shale
11. Fallout and fallback breccias (polymictic and monomictic); ejecta-blanket deposits on rim
12. Dolomitized "suevite" caprock; impact-melt breccia (pseudopyroclastic breccia)
13. Crater-breccia lens and disrupted zone of uplifted material (granodiorite and dolomite megablocks)
14. Faulted (normal, reverse, thrust), folded, brecciated, and fractured rim strata
15. Concentric and radial fault, fold, and fracture (extensional and shear) systems along rim
16. Inverted strata in ejecta on rim (overturned flap?)
17. Injection breccia dikes and veins (fines)
18. Shock-metamorphism features:
    a. Multiple sets of planar features (shock lamellae) in quartz, feldspar, dolomite
    b. Vitrification (glasses) (e.g., maskelynite—glass pseudomorph of plagioclase)
    c. Microbending and microfracturing of feldspar, dolomite, and quartz grains
    d. Structural disordering of feldspars (i.e., orthoclase to sanidine)
    e. Microtektites
    f. Shatter cones? (none documented so far, because of lack of whole core)
19. Lithologies:
    a. Granodiorite basement (fractured and brecciated)
    b. Crater-floor dolomite (megablocks and fallback breccia)
    c. Crater-rim dolomite (ejecta blanket and fallout breccia)
    d. Autochthonous dolomite (rim and flanks)
    e. Karst and collapse dolomite (crater and rim)
    f. Pseudopyroclastic breccia (impact melt and suevite) (crater)
20. Reservoir complexities:
    a. Complex porosity distribution and prediction
    b Complex pore geometries and inherent log analysis problems
    c. High reservoir heterogeneity, vertical communication, reservoir compartmentalization
    d. High-paraffin (13–14 wt%), low-asphaltene (0.673 wt%) oil (pour point = 65–70 °F).
    e. Apparent extreme variations in R
21. Geophysical anomalies due to density and magnetic contrasts of lithologies

within the overlying basal Simpson Group. Reservoir porosities and permeabilities are quite variable, but can be rather exceptional as shown by the tremendous production and reserve potential of some wells. For example, individual granite breccia wells may contain up to 285 ft of net pay with initial potentials of several thousand barrels of oil per day and estimated oil reserves of up to 10 million barrels.

Lithologic and geochemical data suggest that the principal source rock (and seal) consists of the organic-rich black shales and calcisiltites within

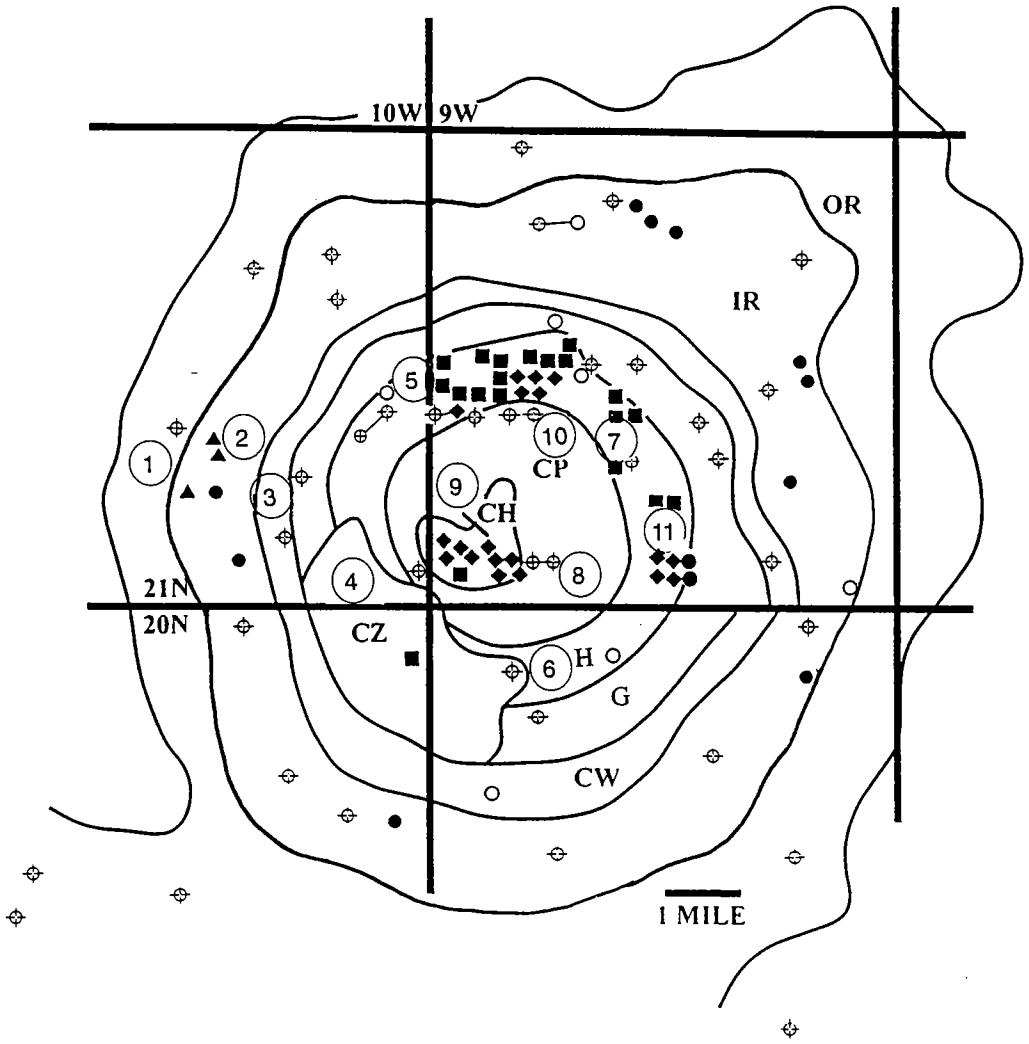

Figure 4. Distribution of production and well tests (as of January 1995) and morphological boundaries of the Ames impact structure as defined by the concentric solid lines. Well symbols: Open circle with cross—dry hole. Straight line from well symbols—horizontal well. Open circle—drilling or testing hole. Solid circle—production from West Spring Creek Formation and/or Kindblade Formation. Solid triangle—production from ejecta and/or fallout. Solid square—production from dolomite in crater. Solid diamond—production from granite breccia. Crater morphology abbreviations: IR—inner rim, OR—outer rim, CW—crater wall, G—graben, H—horst, CZ—collapse zone, CP—central pit, CH—central high. Note the apparent right-lateral offset of the eastern part of the crater wall along the township line between T. 20 N. and T. 21 N. Circled numbers (1–11) represent example vertical sequences as shown in the crater subcrop model (Fig. 2).

the lower parts of the overlying (crater-filling) Middle Ordovician Simpson Group (presumably the McLish Formation and not the generally accepted Oil Creek Formation). Several lines of evidence support the time of the crater-filling episode to have been during deposition of the McLish Formation: (1) detailed regional and local stratigraphic correlations of middle to lower Simpson and Arbuckle Group rocks on the northern shelf of Oklahoma (Masera, 1993; Kuykendall, 1995), (2) biostratigraphic recognition of a major regional unconformity in southern Oklahoma between the Oil Creek and McLish Formations interpreted by Derby and others (1991) to be the Sauk-Tippecanoe sequence boundary, and (3) conodont age constraints (middle Simpson Group; McLish For-

mation–Bromide Formation) on the crater-filling shales by Repetski (1997). Integration of this information indicates that the Ames impact crater formed in Sauk sequence rocks (upper Arbuckle Group; West Spring Creek Formation) and was subsequently filled by the initial marine transgression (McLish Formation) of the Tippecanoe sequence. Outside of the Ames area and as far away as the southern part of the Anadarko basin, the McLish Formation contains sandstones with 1–2% (rarely, up to 15%) feldspar and is the only Simpson Group sandstone with any appreciable feldspar and/or lithic content. Detailed petrographic analysis of rocks from the Ames impact structure has shown that the sandstone (correlative with the McLish) immediately above the crater-filling shale (originally believed to be correlative with the Oil Creek Formation) contains feldspars, chert (devitrified glass?) fragments, and dolomite fragments (Kuykendall, 1995). Thus, prior to complete burial during Middle Ordovician time, the crater was probably a point source for most of the feldspars and lithic fragments present within the McLish Formation, and locally no sediments correlative with the Oil Creek Formation were either deposited or preserved.

The Ames feature contains unique structural components, complex heterolithic reservoirs, and an apparently local (crater-filling) source rock and seal. Future development and exploration success in the Ames feature, and similar structures, must be based on a thorough understanding of the genesis, distribution, and petrophysical properties of the various crater lithofacies, as well as an awareness of the associated structural complexities. The Ames impact structure may prove to be one of the most extensively explored and most hydrocarbon-productive impact craters in the world, with over 100 wells drilled and cumulative production from approximately 50 wells of over 6 MMBO and 10 BCFG, as of mid-1996. It is truly one of the Midcontinent's most significant oil and gas discoveries and is certain to become a future exploration and development analogue for similar impact structures worldwide.

ACKNOWLEDGMENTS

We thank DLB Oil & Gas, Inc. (Oklahoma City, Oklahoma) and Masera Corporation (Tulsa, Oklahoma) for allowing presentation and publication of this work.

REFERENCES CITED

Adler, F. J.; Caplan, W. M.; Carlson, M. F.; Goebel, E. D.; Henslee, H. T.; Hicks, I. C.; Larson, T. G.; McCracken, M. H.; Parker, M. C.; Rascoe, Jr., B.; Schramm, M. W.; and Wells, J. S., 1971, Future petroleum provinces of the Mid-Continent, *in* Cram, I. H. (ed.), Future petroleum provinces of the United States—their geology and potential: American Association of Petroleum Geologists Memoir 15, v. 2, p. 985–1120.

Derby, J. R.; Bauer, J. A.; Creath, W. B.; Dresbach, R. I.; Ethington, R. L.; Loch, J. D.; Stitt, J. H.; McHargue, T. R.; Miller, J. F.; Miller, M. A.; Repetski, J. E.; Sweet, W. C.; Taylor, J. F.; and Williams, Mark, 1991, Biostratigraphy of the Timbered Hills, Arbuckle, and Simpson Groups, Cambrian and Ordovician, Oklahoma: a review of correlation tools and techniques available to the explorationist, *in* Johnson, K. S. (ed.), Late Cambrian–Ordovician geology of the southern Midcontinent, 1989 symposium: Oklahoma Geological Survey Circular 92, p. 15-41.

Kuykendall, M. D., 1995, Recognition and regional correlation of impact-related "Ames crater" Arbuckle and Simpson reservoir lithofacies [abstract]: American Association of Petroleum Geologists Bulletin, v. 79, p. 1404.

Masera Corp., 1993, Proprietary study of the Arbuckle reservoir in the "Ames crater"—Ringwood field, Major County, Oklahoma: Prepared exclusively for DLB Oil & Gas, Inc., by Masera Corp., Tulsa, Oklahoma.

Repetski, J. E., 1997, Conodont age constraints on the Middle Ordovician black shale within the Ames structure, Major County, Oklahoma, *in* Johnson, K. S.; and Campbell, J. A. (eds.), Ames structure in northwest Oklahoma and similar features: origin and petroleum production (1995 symposium): Oklahoma Geological Survey Circular 100 [this volume], p. 363–369.

Historical Development and Production of the Arbuckle and Exotic Lithologies in the Ames Structure, Oklahoma

Jim Evans
Ward Petroleum Corp.
Enid, Oklahoma

The Ames feature has been recognized as a structural anomaly since the early 1970s when Hunton wells were drilled and structure maps were made on the underlying Sylvan Shale approximately 1,000 ft above the Arbuckle. The structure contours shown in Figures 1–3 are a very generalized representation of this Sylvan map. Initially, there were no Arbuckle penetrations of any significance in the area, but the feature was developed in the numerous shallower horizons as part of the Sooner trend.

Arbuckle production was discovered in late 1990 by J. L. Thomas Engineering on the far north flank of the feature (Fig. 1). One producer and one dry hole were drilled, but viable commercial production was not established. In late 1991, the D. & J. no. 1-20 Gregory well was drilled in sec. 20, T. 21 N., R. 9 W. (Fig. 2); it became the discovery well for the "exotic" reservoir rock and the beginning of the discussions that led to the 1995 Ames seminar jointly sponsored by the Oklahoma Geological Survey and the Bartlesville Project Office, U.S. Department of Energy. Other papers in this volume will deal with the exotic lithologies and their proposed origins. In this discussion, only the term "exotics" will be used to refer to the noncarbonate lithologies beneath the Simpson shale that are found in the Ames feature. The noncarbonate lithologies are exotic because the regional Arbuckle facies consists of limestone and dolomite, with dolomite being the most prevalent.

In the same year, the no. 1-20 Gregory was offset by a dry hole and three other completions. The famous no. 1-20 Gregory started a drilling boom in 1992. This well appears to be a 5–10 million barrel well and is by far the best oil well in the field. The wide range of the estimate is due to the numerous unknowns about this reservoir. Interestingly enough, the best gas well by far, the DLB no. 28-9 Bierig in sec. 28, T. 21 N., R. 10 W. (Fig. 2), was also drilled during the last half of 1991. Therefore, the best two wells in the field were drilled early, and all the other seismic and drilling activity did not discover any other production of their magnitudes.

The first half of 1992 saw 14 completions and only four dry holes, giving the industry a tremendous sense of confidence. The second half of 1992 realized only a 50% success rate, which was an indication of a more reasonable future expectation. Several flank wildcats were disappointments.

The first half of 1993 experienced a similar activity level and a similar success rate. The second half of 1993 saw an increase in the success rate because of a higher level of development work. This period concluded the major activity for the Arbuckle at the Ames feature. During 1994, similar success rates were experienced but at a decreased level of activity. During the 3½-year span from late 1991 through 1994, 92 wells were drilled with 53 completions and 39 dry holes (Fig. 3). In addition, four horizontal wells were drilled, of which three were dry and one was noncommercial.

It is now possible to evaluate the play statistically on the basis of the completions through 1994. During this period, there were 54 completions and 42 dry holes for a success rate of 56%. Considering the amount of close-in development drilling and extensive three-dimensional seismic work, this percentage is not impressive.

A further breakdown of the economics of the completed wells has been attempted. This is subject to interpretation because some wells are new enough not to have significant production histories, and data on some wells are limited at the operator's discretion. In the attempt to classify the completed wells, some general categories are defined as follows:

Jim Evans, Ward Petroleum Corp., Box 1187, Enid, OK 73702.

Evans, Jim, 1997, Historical development and production of the Arbuckle and exotic lithologies in the Ames structure, Oklahoma, *in* Johnson, K. S.; and Campbell, J. A. (eds.), Ames structure in northwest Oklahoma and similar features: origin and petroleum production (1995 symposium): Oklahoma Geological Survey Circular 100, p. 207–213.

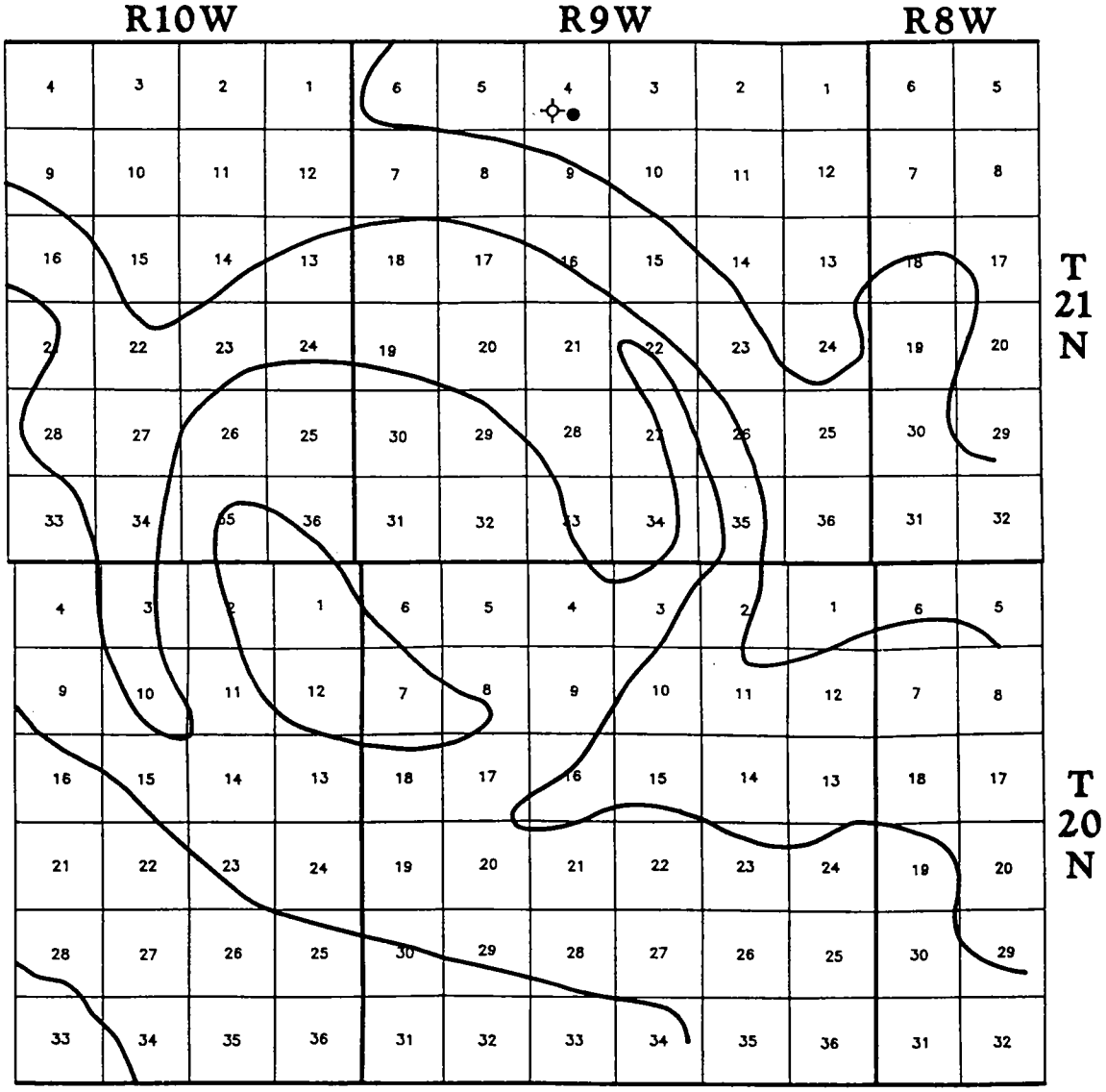

Figure 1. Map of the Ames area, showing generalized structure contours on Sylvan Shale established in the 1970s and location of the two wells (one producer and one dry hole) drilled to the Arbuckle in 1990.

Poor. A well that will probably not payout.

Fair. A well that will payout but likely will not produce a 2:1 ROI (return on investment), undiscounted.

Good. A well that will payout in less than three years and yield an ROI of at least 3:1, undiscounted.

Excellent. Those wells that are clearly superior to all other wells in the field with rates of return in excess of 10:1.

The number of wells drilled at Ames in each of the above rankings is as follows, according to the information available to me (see Table 1): excellent, 6; good, 13; fair, 10; poor, 22; dry hole, 42; unknown, 4.

For the purpose of this discussion, an average dry-hole cost of $260,000 and a completed-well cost of $460,000 were used. The four horizontal wells cost about $1 million each. An average net price of $15 per barrel, unescalated, was used and considered sufficient to account for royalties, operating costs, and taxes. A similar average net price of $1.35 per thousand cubic feet was used for gas. Because of the extensive development of the shal-

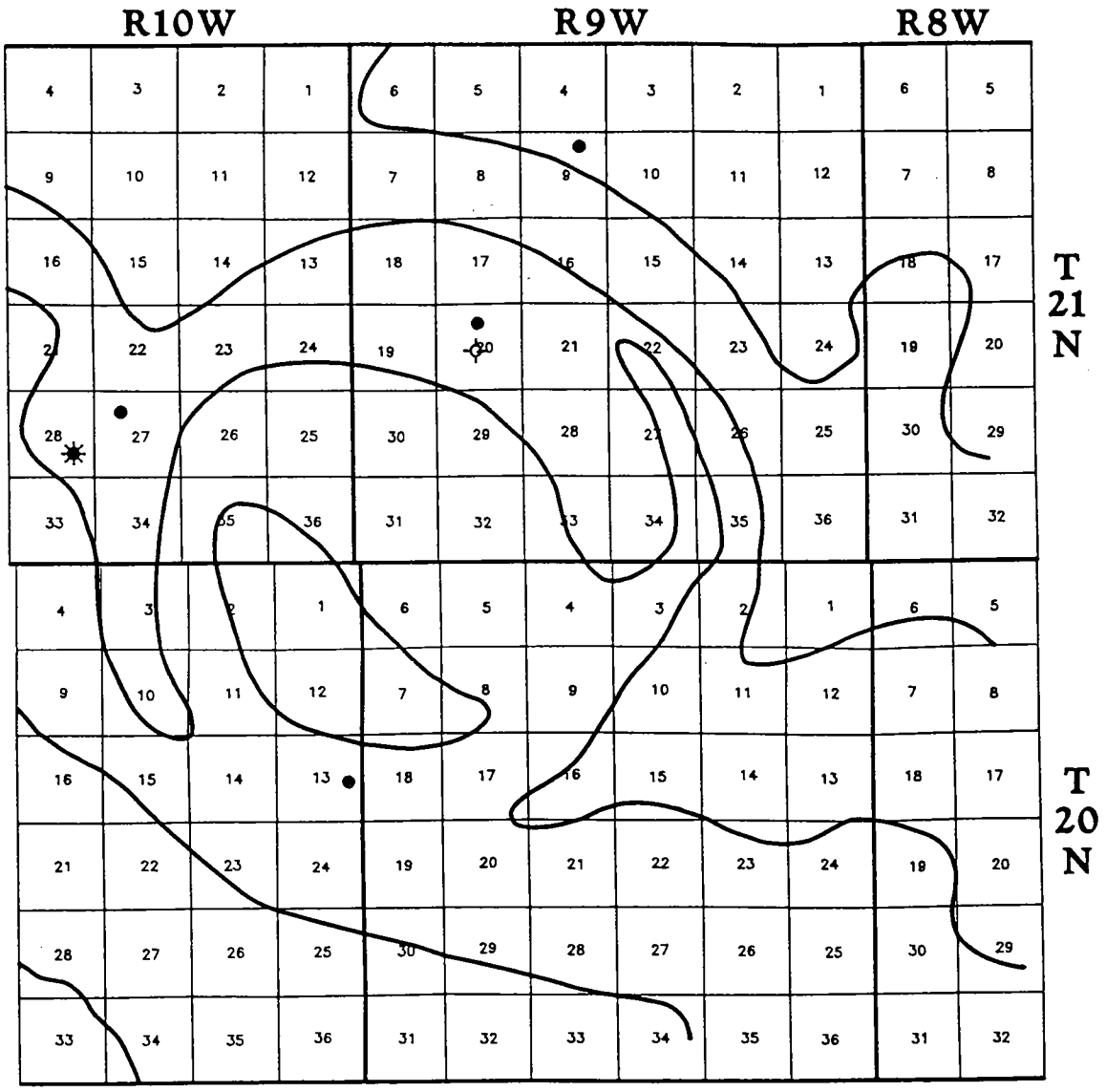

Figure 2. Map of the Ames area, showing location of five producers and one dry hole drilled to the Arbuckle in the last half of 1991. Structure contours on Sylvan Shale.

low production, product markets were readily available.

Using these numbers, the expense of completing 54 wells and drilling an additional 42 dry holes is estimated to be $34.5 million, plus an additional $4 million for the horizontal wells, to yield a total of $38.5 million. For an ROI of 3:1 on only the drilling and completion dollars, 7.7 million BOE (barrels of oil equivalent) is required.

The cost of acreage and of two-dimensional and three-dimensional seismic studies was in addition to the drilling cost. The acreage dollars are impossible to estimate because most of the feature was covered with shallower production and HBP (held by production). Therefore, the complexity of the land deals precludes any meaningful estimate. The seismic costs, however, can be estimated, although the estimate could be in error by as much as $100,000.

It would appear that at least 50 mi of new 2-D seismic lines were shot at a cost of about $4,000 per mile, and approximately 100 mi of 3-D seismic lines were shot at a cost of $30,000 per square mile. This work represents a total seismic cost of

TABLE 1.—WELLS DRILLED TO THE ARBUCKLE IN THE AMES AREA THROUGH 1994

Location	Well name	Initial potential	Cumulative prod.	Well quality	Date first prod.
Township 21N-9W					
S/2 SW SE Sec. 4	Ott	1.1 MM + 48 BC	0.3 B + 40 M	Poor	7/90
SE SW Sec. 4	Ott #2		Dry hole		12/90
W/2 NE NE Sec. 9	Munkres	850 MCF + 182 BO	0.13 B + 19 M	Poor	6/91
W/2 NE NW Sec. 20	Gregory	155 MCF + 402 BO	0.4 B + 1 MM	Excellent	12/91
NW NE SW Sec. 20	Herman		Dry hole		12/91
SW SE Sec. 17	Lloyd	166 MCF + 480 BO	0.1 B + 182 M	Excellent	1/92
SE SE SE Sec. 18	Peggy	81 NCF + 405 BO	29 M	Poor	1/92
W/2 NW Sec. 18	Heinrich	275 MCF + 584 BO	111 M	Good	1/92
NE NE NE Sec. 19	Dorothy	435 MCF + 218 BO	38 M	Fair	1/92
W/2 SE SW Sec. 17	Shelby	140 MCF + 390 BO	107 M	Good	4/92
N/2 NE SW Sec. 19	Chet		83 M	Fair	4/92
N/2 NW SE Sec. 21	Pacific	82 MCF + 160 BO	24 M	Poor	5/92
SE NW Sec. 21	Stransberry	31 MCF + 71 BO	34 M	Poor	5/92
NE SW Sec. 21	DeHaas	141 MCF + 432 BO	123 M	Good	5/92
S/2 NE NE Sec. 23	Buckles	60 MCF + 45 BO	14 M	Poor	5/92
SW SW NE Sec. 31	Fred	76 MCF + 172 BO	91 M	Good	5/92
SW NE Sec. 26	#7 Jim	68 MCF + 264 BO	1 M	Poor	6/92
S/2 NE NW Sec. 23	#6 Elsie		Dry hole		8/92
NE NE SW Sec. 31	#11 Jimmy	45 MCF + 23 BO	4 M	Poor	8/92
S/2 SE Sec. 14	Bohn	300 MCF + 275 BO	20 M	Poor	8/92
SE SW SE Sec. 16	#2 Pyfee		Dry hole		8/92
SW NE SE Sec. 17	Mary Helen	72 MCF + 180 BO		Fair	8/92
S/2 NE NW Sec. 8	#3 Delores		Dry hole		10/92
W/2 NW Sec. 10	Farber	450 MCF + 265 BO	0.13 B + 15 M	Poor	10/92
S/2 SW SW Sec. 18	#2 Dixon	95 BO	10 M	Poor	11/92
W/2 NW NE Sec. 20	James	166 MCF + 492 BO		Fair	11/92
E/2 NW NE Sec. 20	Wayne	171 MCF + 510 BO	See Gregory	Good	12/92
NE SW SE Sec. 18	#4 Chestnut	60 MCF + 107 BO	30 M	Good	1/93
SE NW NW Sec. 5	#2 Sherman		Dry hole		3/93
NW NE SE Sec. 11	Mears		Dry hole		3/93
NW NW SW Sec. 20	Dorothy		Dry hole		4/93
E/2 E/2 NW Sec. 28	#6 Della		Dry hole		4/93
SE SW NW Sec. 31	Donna	159 MCF + 477 BO	0.1 B + 260 M	Excellent	4/93
SE SE NE Sec. 31	Gerald	101 MCF + 230 BO	See Donna	Excellent	4/93
SW SW NW Sec. 32	Wayne	95 MCF + 215 BO	28 M	Poor	4/93
NE NE SE Sec. 33	#9 Marilyn	80 MCF + 247 BO	58 M	Good	5/93
E/2 E/2 NW Sec. 28	#6 Della	50 MCF + 115 BO		Poor	6/93
SW NW SE Sec. 31	#9 Turner	50 MCF + 167 BO	28 M	Fair	6/93
NE NE SE Sec. 31	Bowles	45 MCF + 180 BO	28 M	Fair	6/93
SW SW SW Secl 16	#3 Chestnut		Dry hole		7/93
SE NW NW Sec. 31	Christina	44 MCF + 54 BO	4 M	Poor	7/93
E/2 SE NE Sec. 33	Bland	230 MCF + 335 BO	44 M	Good	7/93
SW SW NE Sec. 32	Charles		Dry hole		8/93
NE SE NW Sec. 31	Dean Earl	34 MCF + 138 BO	38 M	Poor	9/93
NE SE NE Sec. 19	Manita	141 MCF + 408 BO	72 M	Fair	10/93
NW NW SE Sec. 19	Detrick		Dry hole		10/93
NW SE NW Sec. 19	Sam	140 MCF + 391 BO	80 M	Good	10/93
NE NW SW Sec. 32	Bisel	95 MCF + 222 BO	11 M	Poor	10/93
SW SW Sec. 22	Nellie	68 MCF + 174 BO	12 M	Poor	10/93
NW NW SW Sec. 34	Carl	165 MCF + 462 BO	54 M	Good	12/93
NW Sec. 20	JD	211 MCF + 528 BO	4 B 117 M	Good	12/93

(continued on next page)

TABLE 1. *CONTINUED*

Location	Well name	Initial potential	Cumulative prod.	Well quality	Date first prod.
Township 21N-9W ***(continued)***					
SW SE NW Sec. 32	Viola		Dry hole		12/93
SW SW NW Sec. 34	Gammon	251 MCF + 600 BO	54 M	Good	12/93
NW SE NE Sec. 19	Marjorie	147 MCF + 315 BO	37 M	Good	12/93
SW NW SW Sec. 27	Mackie	70 MCF + 173 BO	16 M	Poor	1/94
SW SW NE Sec. 17	Uvah	20 BO		Poor	3/94
SE NW Sec. 35	Little		Dry hole		3/94
NW NE SW Sec. 34	Linda		Dry hole		4/94
E/2 SW Sec. 36	Emma	200 MCF + 203 BO		Fair	5/94
NE NE Sec. 20	Maruin		12 M	Poor	5/94
SE SE SW Sec. 17	E-1-17		57 M	Fair	6/94
SW SE NW Sec. 34	Jennifer		Dry hole		6/94
N/2 SW NW Sec. 34	Roger #5	54 MCF + 100 BO		Poor	7/94
NE SW SE Sec. 32	Townsite		Dry hole		8/94
NE NW Sec. 18	Munkres		Dry hole		11/94
Township 20N-9W					
NW NE Sec. 20	Bullis		Dry hole		6/92
E/2 NW NE Sec. 23	Gregory		Dry hole		10/92
SW SE Sec. 10	Carolyn Sue		Dry hole		11/92
E/2 NE Sec. 2	Scott		Dry hole		1/93
W/2 SE SE Sec. 2	Edwards #2	23 BO + 357 MCF	0.2 B + 10 M	Poor	2/93
N/2 SW SW Sec. 5	Darin		Dry hole		3/93
S/2 NW NE Sec. 4	Orin		Dry hole		5/93
S/2 SE NW Sec. 5	Sturgeon		Dru hole		7/93
SW SE NW Sec. 5	Hammer		Dry hole		10/93
W/2 NE SW Sec. 4	Laubhans #2		Dry hole		7/94
Township 21N-10W					
S/2 N/2 NW Sec. 27	Cecil #4	170 BO + 3.3 MM	0.8 B + 150 M	Good	8/91
NE SE Sec. 28	Beirig		3.5 B + 24 M	Excellent	11/91
S/2 N/2 NW Sec. 27	Cecil #4 (Owwo)	227 BO + 1.1 MM		Fair	1/92
SE SW SW Sec. 22	Mary Ellen	8 BC + 1.4 MM	0.5 B + 4 M	Fair	1/92
SW SW NE Sec. 34	Terry	64 BO + 3.2 MM	0.2 B + 11 M	Fair	4/92
SE Sec. 21	Campbell		Dry hole		6.92
NE NE Sec. 14	Lillie		Dry hole		7/92
N/2 N/2 SE Sec. 11	Ruby		Dry hole		9/92
NE NE SE Sec. 36	Monsees		Dry hole		9/92
E/2 NW NW Sec. 35	Campbell		Dry hole		9/92
SW SW NE Sec. 34	Terry (Owwo)	1110 BO + 23 MCF		Poor	11/92
SE Sec. 10	Kennedy		Dry hole		2/93
E/2 NW SW Sec. 27	Jesse #12	320 BO + 250 MCF	25 M	Fair	3/93
SE NE Sec. 1	Dillman		Dry hole		7/93
W/2 SE NW Sec, 26	Mason #2		Dry hole		1/94
NW NE SW Sec. 34	Tina		Dry hole		3.94
NE SE NW Sec. 24	Gladys	15 BO	4 M	Poor	5/94
Township 20N-10W					
SE NE SW Sec. 13	Allen #11	90 BO + 1.0 MM	0.2 B + 39 M	Fair	12/91
W/2 W/2 NE Sec. 3	Fisher		Dry hole		6/92
SE NE SE Sec. 14	Federal	440 MCF	.03 B	Poor	10/92
SE NW SE Sec. 1	Cleora	441 BO + 500 MCF	23 M	Poor	1/93
NW NW Sec. 14	Lydia		Dry hole		3/93

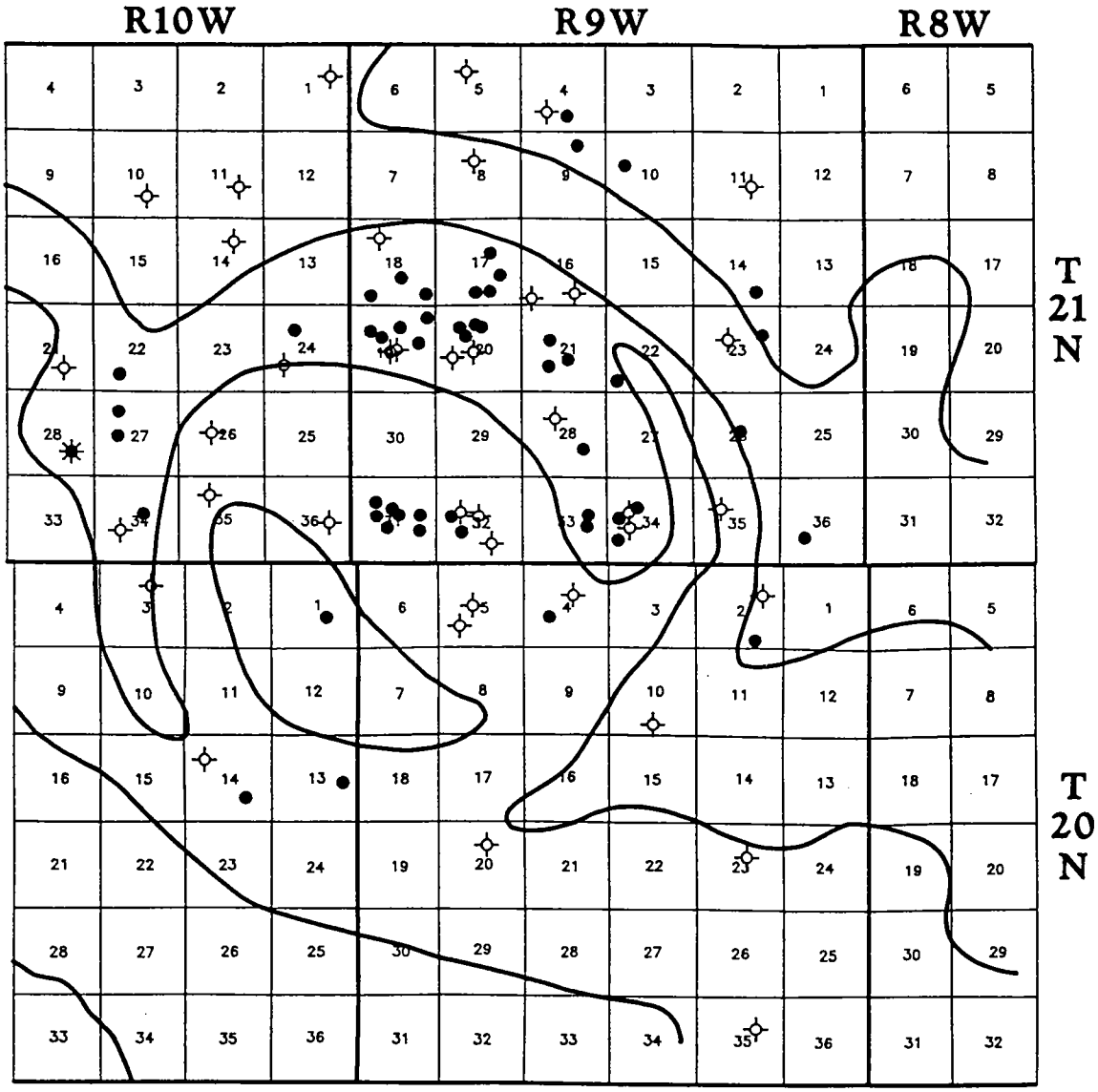

Figure 3. Map of Ames area, showing all wells drilled to the Arbuckle through 1994. Structure contours on Sylvan Shale.

at least $3.2 million. This amount would require an additional 640,000 BOE for a 3:1 R.O.I., for a total of 8.34 MMBO (million barrels of oil).

As of year end, 1994, the Arbuckle at Ames had produced just over 3 MMBO plus 7 BCFG (billion cubic feet of gas). Again, at $15 per barrel net for oil and $1.35 per thousand cubic feet net for gas, this total represents a return to the investors of $54.45 million against at total investment to date for drilling and seismic data collection estimated at $41.72 million, or 130% of payout in the first three years (Table 2). It should be noted that the $41.72 million is a most conservative number for two reasons. First, a simple multiplier of $260,000 per dry hole does not take into account the dry holes in which pipe was set and full completion costs were expended before the well was abandoned. Second, the cost of some of the acreage was very significant and exceeded $500 per acre when the play was most active. Nevertheless, because of the few good wells, the Arbuckle production at the Ames feature is projected to be a commercial venture and should achieve a 3:1 ROI in 8 to 10 years.

TABLE 2.—SUMMARY OF SEISMIC AND DRILLING COSTS AND PRODUCTION INCOME FOR ALL WELLS DRILLED TO THE ARBUCKLE IN THE AMES AREA THROUGH 1994

Costs		Income	
Item	**$MM**	**Item**	**$MM**
Seismic	3.20	3 MMBO @ $15	45.00
53 completions	24.38	7 BCF @ $1.35	9.45
39 dry holes	10.14		
4 horizontal	4.00		
Total	41.72	Total	54.45

The economics are skewed tremendously, however, by two wells. This field is not a case of similar porosities draped over a simple structure where all wells approach the same economics. Of the 3 MMBO produced, the D. & J. no. 1-20 Gregory lease has produced 1 MMBO, or one-third of the total oil. Of the 7 BCFG produced, the DLB no. 1 Bierig has produced 3.5 BCFG or one-half of the total gas. Removing just these two wells from the total would render the entire project noncommercial. As previously mentioned, both of these wells were drilled during the first six months and predated the exploration concept of an impact crater and the extensive three-dimensional seismic acquisitions.

Of the top 10 wells in the field, only 3 produce from the carbonate or dolomite facies. The others produce from the "exotics" or noncarbonate facies, leading to the obvious conclusion that without the exotic facies present at Ames, the Arbuckle would not be commercial. Therefore, using three-dimensional seismic data to identify other Arbuckle structures along the shelf of the Anadarko basin is not enough to locate and discover commercial quantities of hydrocarbons.

If the Ames feature is cryptoexplosive and related to specific structural events and trends, then exploration could locate other features with similar exotic rock types and prolific producing characteristics. If, on the other hand, the Ames feature is an impact structure, then the location of other impact features would be random in both time and space. An older or younger crater would not similarly affect Arbuckle and basement rocks and therefore would be difficult to explore for with any extensional logic.

Trapping Mechanisms in Arbuckle Strata, Major County, Oklahoma

Jeffrey F. Heyer
Cross Timbers Oil Company
Fort Worth, Texas

ABSTRACT.—Located on the northern shelf of the Anadarko basin, Major County is uniquely situated for hydrocarbon accumulation. To the south into the basin, Ordovician–Pennsylvanian strata thicken. In a northeasterly direction, these strata thin, creating stratigraphic traps. The monoclinal dip to the southwest on the shallow horizons gives only subtle indications of the more complex deeper structures. The Ames structure is anomalous because it is a reversal to all of the established regional trends. Sedimentary layers dip in a southwesterly direction into the Ames structure, but then abruptly reverse dip on the southern edge. Strata of the Hunton Group, which are generally thin in the surrounding area, are completely preserved along the axis of the Ames structural low. A perceived circular shape to the Ames structure has caused many geologists to conclude it is the result of an asteroid impact.

Arbuckle Group lithotypes are typically dolomitic grainstones and mudstones. Matrix-supported chaotic-breccia and collapse-breccia facies seen in cores imply a karst overprint to the carbonate facies. Unique to the Ames play is an additional lithotype—an aphanitic rhyolite. Production of oil and gas can be from either the carbonate or rhyolite.

Arbuckle carbonate grainstones usually have 17% porosity, and their permeability is typically 1.5 md (millidarcies). The mudstone facies has a micropore system that generally must be naturally fractured to be productive. No matrix porosity was observed in the rhyolite, and so natural fractures must be present for there to be production.

Currently, five individual fields produce in the Ames area. The most mature field in terms of drilling density and production history is a horst block. A normal fault within the structure acts as a permeability barrier, segmenting the structure into a north and south block. Of the remaining fields, two produce from rhyolite and two produce from carbonate sedimentary units.

INTRODUCTION

Exploration for hydrocarbons from Arbuckle Group strata in Major County, Oklahoma, was initiated in 1952 with the drilling of the Continental Oil Company no. 1 Kimball, sec. 34, T. 20 N., R. 16 W. Core descriptions from the well indicate the Arbuckle Group to be a very finely crystalline sucrosic dolomite that had dead oil stain. The cored interval was drill-stem tested, recovering 100 ft of gas-cut mud. Sinclair Oil drilled the second Arbuckle test in the county in sec. 33, T. 23 N., R. 16 W. Neither well was completed in Arbuckle Group strata. In 1990, Thomas Engineering drilled the first commercially successful Arbuckle test in sec. 4, T. 21 N., R. 9 W. DLB Energy Company extended the play to T. 21 N., R. 10 W., in 1991. D. & J. Oil Company drilled the no. 1-20 Gregory well in sec. 20, T. 21 N., R. 9 W., and completed the well for 624 BOPD (barrels of oil per day).

Jeffrey F. Heyer, Cross Timbers Oil Co., 810 Houston Street, #2000, Fort Worth, TX 76102.

LITHOLOGY

Dolomite is the primary lithotype of the Arbuckle Group. It can be cream, brown, or light gray. Lithofacies observed in cores and samples range from mudstones (Fig. 1A) to bioclastic grainstones (Fig. 1B). The bioclastic grainstones consist of medium crystalline dolomite with foraminifer, echinoderm, and bryozoan allochems. A uniform size to the bioclasts suggests that the grainstone is well sorted. The original bioclasts have been

Heyer, J. F., 1997, Trapping mechanisms in Arbuckle strata, Major County, Oklahoma, *in* Johnson, K. S.; and Campbell, J. A. (eds.), Ames structure in northwest Oklahoma and similar features: origin and petroleum production (1995 symposium): Oklahoma Geological Survey Circular 100, p. 214–222.

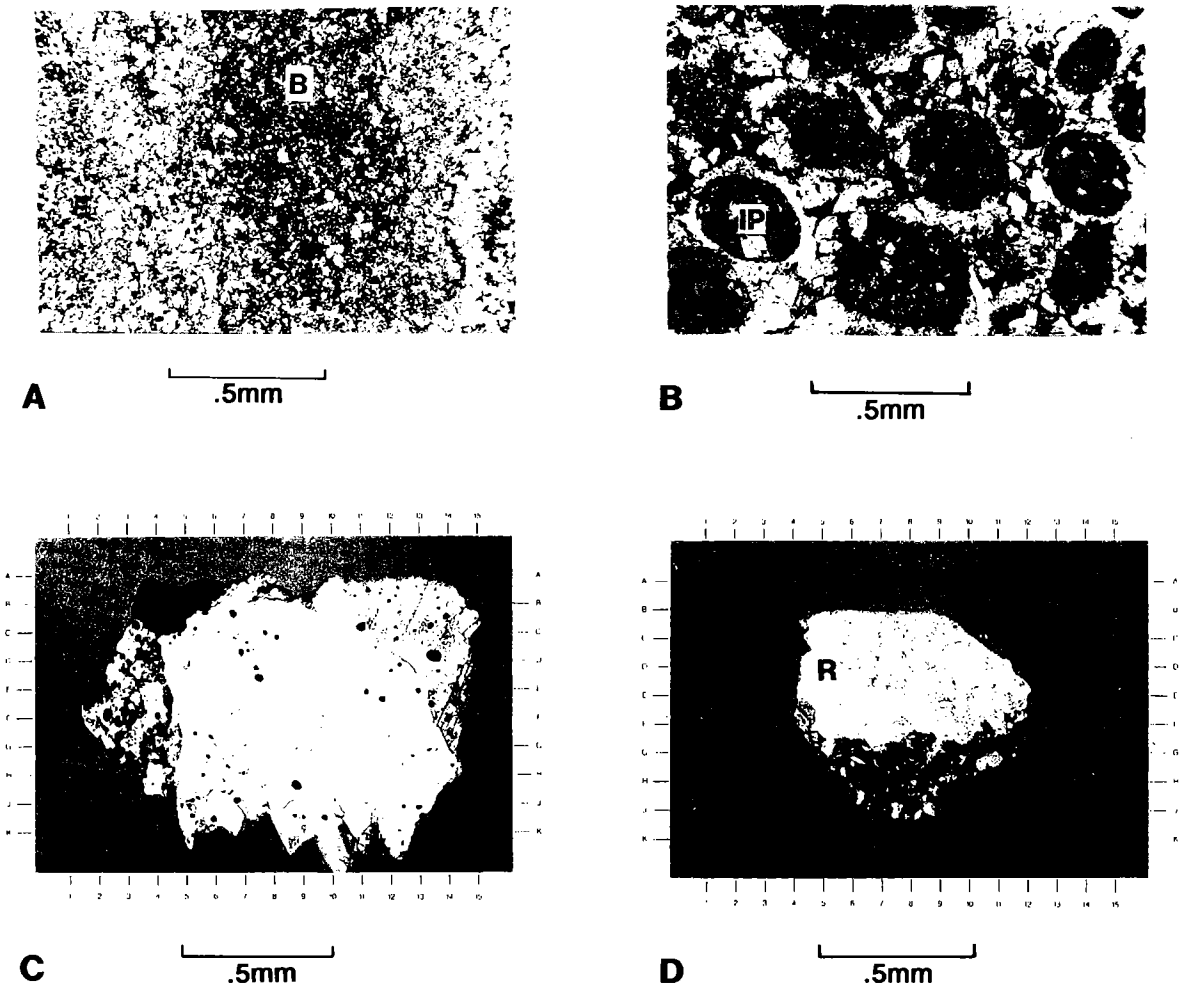

Figure 1. *A*—Microcrystalline mudstone with less than 5% porosity. The shaded area (B) is a burrow, discolored by pyrite. Plane-polarized light. *B*—Bioclastic grainstone facies. Intraparticle porosity (IP) and intergranular porosity represent 17% of the sample. Natural fractures connecting both pore systems must be present for this to be a productive reservoir. Plane-polarized light. *C*—Rhyolite. Viewed under cross-polarized light, this sample consists of quartz, plagioclase, and potassium feldspar. The lack of granular texture or associated matrix porosity suggests that this lithotype must be naturally fractured for it to be a reservoir. *D*—Rhyolite (R) in contact with Arbuckle dolomite. The pore-filling nature of the rhyolite suggests that dolomite sedimentation and lithification occurred prior to rhyolite extrusion. Cross-polarized light.

leached, creating intraparticle porosity. Intercrystalline porosity between leached bioclasts is also present, giving this lithofacies a dual porosity system. Porosities as high as 17% with permeabilities of 1.82 md (millidarcies) have been measured (Fig. 1B).

Horizontally laminated and mottled textured mudstones are the primary lithofacies recognized in cores. Generally, these lithofacies are very finely crystalline dolomites that have no porosity. All of the lithofacies observed in core samples resemble various outcrop descriptions, substantiating the shallow carbonate-platform sedimentation model (Ragland and Donovan, 1991).

Saddle dolomite occurs as a pore, vug, and fracture-filling material. Bioclastic grainstones with pores occluded by saddle dolomite were observed in the Shenandoah Oil Company no. 2 Miesner core. Nodular-shaped chert can also be interbedded with the dolomite. Minor amounts of

authigenic pyrite are disseminated along the laminae of the mudstone facies. Shale lenses 1 to 3 ft thick separate the dolomite beds, giving an interbedded dolomite-shale pattern in gamma-ray logs. The shales are gray and fissile bedded, and they have a substantial quantity of disseminated pyrite.

Probably the most unusual lithotype encountered is an aphanitic rhyolite that has been previously described as "glass rock" (Fig. 1C). This lithotype consists of 15% quartz, 15% plagioclase, and 64% potassium feldspar. Minor amounts of biotite and pyrite are also present. The fine-grained nature of the rock texture suggests rapid cooling. Undulatory extinction of the quartz grains and deformed feldspar twins indicates that the rhyolite has been cataclastically deformed. The deformed rhyolite has a rock-flour texture, making it easily identifiable in the drill cuttings. Cataclastically deformed rhyolite is caused by the crushing action associated with movement along fault planes. No visible porosity is present, but secondary quartz overgrowths are present along with hydrocarbon staining, implying the presence of a pore structure consisting of natural fractures (Fig. 1). Thickness of the rhyolite ranges from 0 to >310 ft, the latter as seen in the D. & J. no. 1-20 Gregory well. In at least two wells in the Gregory field, the rhyolite forms two layers separated by Arbuckle dolomite (Fig. 2). Drill-cutting samples from the no. 1-20 Gregory well illustrate that the rhyolite intrudes the pore space of the dolomite (Fig. 1D), but there is no evidence of chilling or baking.

Associated with the carbonate lithofacies is a paleokarst overprint. Whole core samples from the CRI no. 1-22 Mary Ellen recovered 66 ft of matrix-supported chaotic breccia, followed by 2 ft of shale and then 25 ft of horizontally laminated mudstones. The matrix-supported chaotic-breccia facies is characterized by large clasts of dolomite surrounded by progressively smaller clasts of dolomite (Fig. 3). Maximum porosity is 4% with less than 1 md of permeability. Electric logs typically have a suppressed gamma-ray and resistivity response through the chaotic-breccia facies. I interpret this particular whole core as representing cave fill associated with postdepositional subaerial exposure.

Whole core samples from the Shenandoah Oil Company no. 2 Miesner recovered clasts of Arbuckle dolomite within horizontally laminated mudstones. Erosion of Arbuckle deposits across paleostructures created source rocks for carbonate sedimentation in adjacent areas. The relict texture resulting from this syndepositional erosion is a sedimentary breccia.

TRAPPING MECHANISMS

Hydrocarbons are trapped in the Arbuckle Group sedimentary rocks as a result of structural relief caused by normal faults. The field-defining faults have 100 to 425 ft of displacement, giving the play a horst-and-graben structural fabric. Production has yet to be established from wells drilled into the grabens. Normal faults with minor amounts of displacement act as seals to hydrocarbon migration; low-relief structures on horst blocks can trap hydrocarbons.

Traps associated with stratigraphic and facies changes will also accumulate hydrocarbons. Bioclastic grainstones with 17% porosity and 1.82 md permeability grade laterally into nonporous grainstones and mudstones. Impermeable cave-fill chaotic breccia acts as a seal to hydrocarbon migration when juxtaposed to a porous collapse-breccia facies. Porous Arbuckle dolomite that subcrops against nonporous impermeable Oil Creek shale also traps hydrocarbons.

Gregory Field

Since the Gregory structure was discovered first and has been developed more extensively, it best illustrates the faulting pattern and reservoir segmentation. The D. & J. no. 1-20 Gregory encountered Arbuckle rhyolite at –7,571 ft and has an oil column of 204 ft. Subsequent development drilling has defined a structure that is approximately 640 acres in areal extent. South of the field, a development well encountered Arbuckle rhyolite 413 ft low to the no. 1-20 Gregory. To the east and west, wells drilled in the grabens were 240 ft low to the no. 1-20 Gregory. The north bounding fault on this structure has yet to be defined (Fig. 4).

Areal extent of the rhyolite in the Gregory field is limited to 16 wells. Only 6 wells had 100% rhyolite; all other wells were in interbedded rhyolite and dolomite.

Production data and well histories suggest that the Gregory field can be subdivided into two separate fault blocks and that well performance is highly dependent upon the lithology of the reservoir. The no. 1-20 Gregory is the highest structural well in the field and produces from a rhyolite reservoir. Subsea elevations of perforations range from –7,693 to –7,723 ft. This well and subsequent development wells on the lease have exhibited no decline in production since inception. The D. & J. no. 1-17 Lloyd, an offset well to the east, encountered the Arbuckle Group 168 ft low to the no. 1-20 Gregory. A 3-ft-thick interval of dolomite was drilled, followed by 110 ft of rhyolite and then back into dolomite, which was the lithology at total depth. A completion attempt was made in the dolomite from –7,815 to –7,865 ft. This attempt recovered formation water. A completion attempt from –7,695 to –7,715 ft in the rhyolite resulted in a well initially producing 480 BOPD with a decline rate of 50% (Fig. 5).

A westerly offset to the no. 1-20 Gregory, the D. & J. no. 1-29 Dorothy (Fig. 5), encountered the

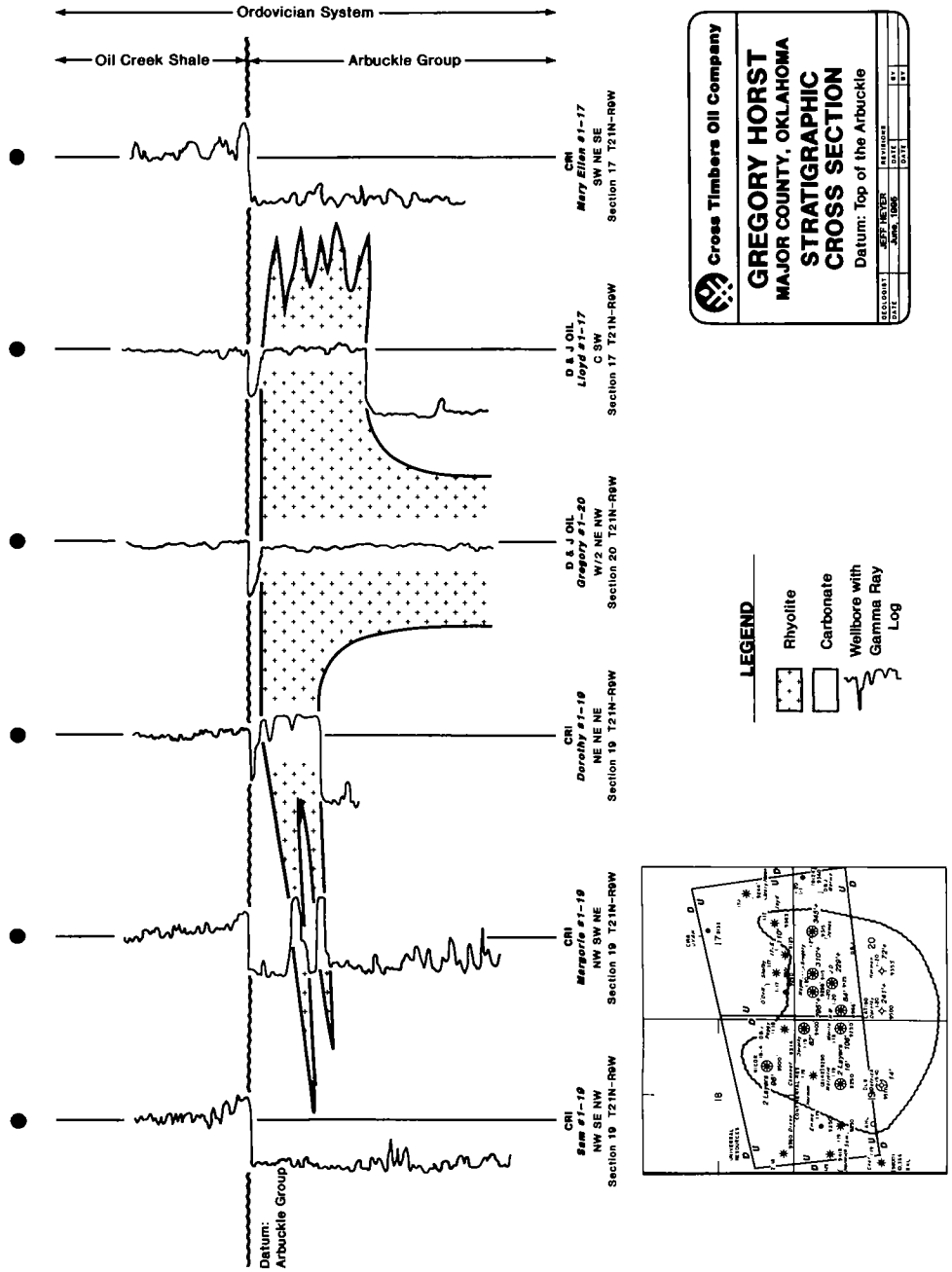

Figure 2. Stratigraphic cross section and areal distribution map illustrating the geometry of the rhyolite. The D. & J. no. 1-20 Gregory penetrated a thin dolomite and then went into rhyolite. Two adjacent wells penetrated rhyolite and dolomite. Farther away from the no. 1-20 Gregory, the gamma-ray log illustrates an interbedded profile with multiple layers of rhyolite separated by dolomite.

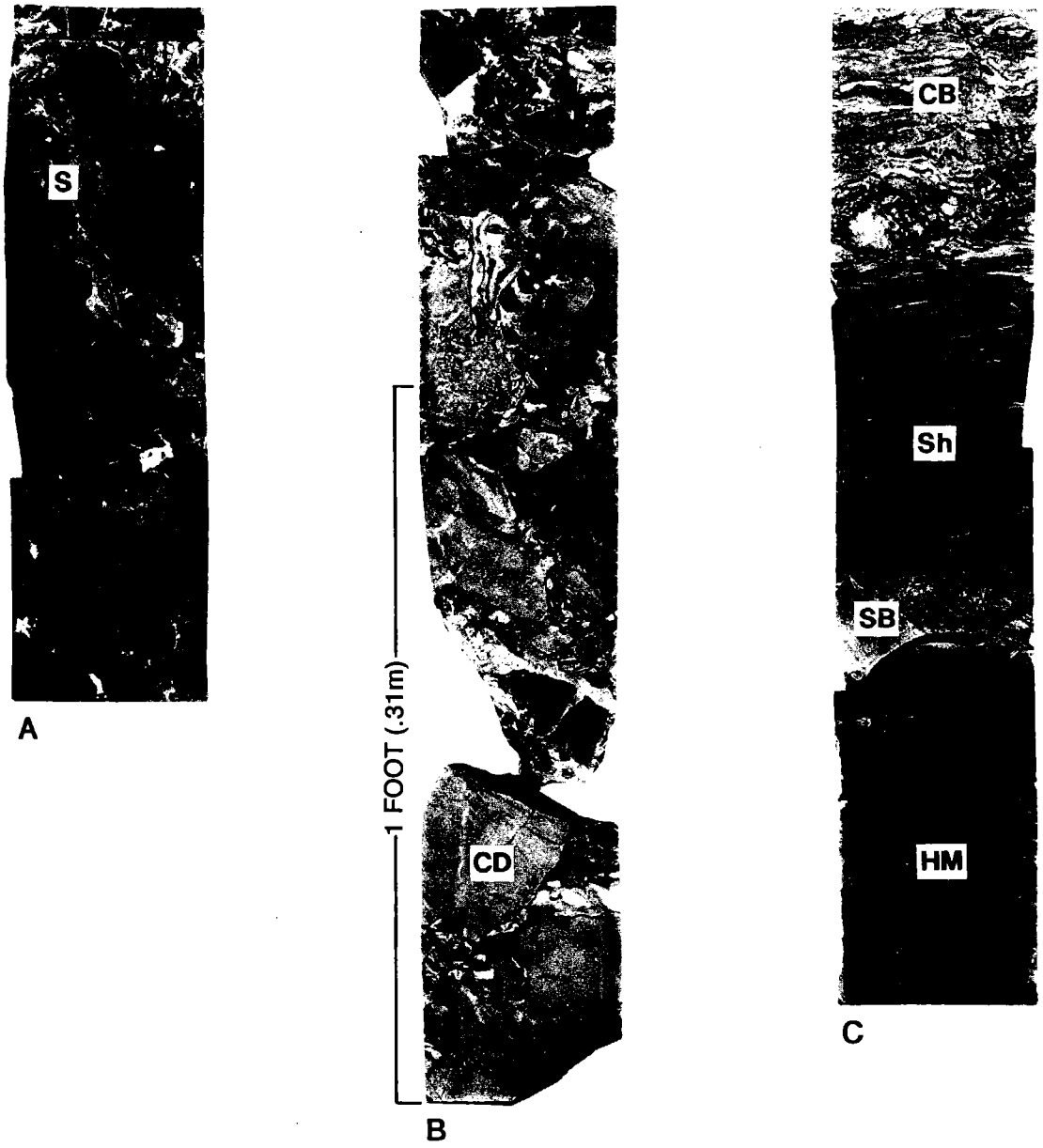

Figure 3. Whole core from the D. & J. no. 1-22 Mary Ellen, illustrating the paleokarst overprint to the carbonate lithofacies. *A*—Solution pipe (S) begins at the top of the core and exits through the right side of the core. *B*—Large clasts of dolomite (CD) are surrounded by progressively smaller clasts of dolomite, typical of a matrix-supported chaotic breccia. *C*—The transition from paleokarst lithofacies (CB [chaotic breccia]) to horizontally laminated mudstones (HM). A shale (Sh) acts as an aquiclude to the karstification process. Sedimentary breccias (SB) mark the contact between the shale and the horizontally laminated mudstones.

Arbuckle Group strata at –7,719 ft. An 8-ft-thick interval of dolomite was encountered, followed by 62 ft of rhyolite and then back into dolomite. A completion attempt in the lower dolomite from –7,838 to –7,846 ft permitted production of 218 BOPD. This well declined at a rate of 78% upon initial completion. The structurally low position of the no. 1-19 Dorothy and the presence of oil production from that well—which is 120 ft below the oil/water contact in the no. 1-20 Gregory and the no. 1-17 Lloyd—imply the presence of a normal fault separating the Gregory from the Dorothy. This fault acts as a seal to hydrocarbon migration.

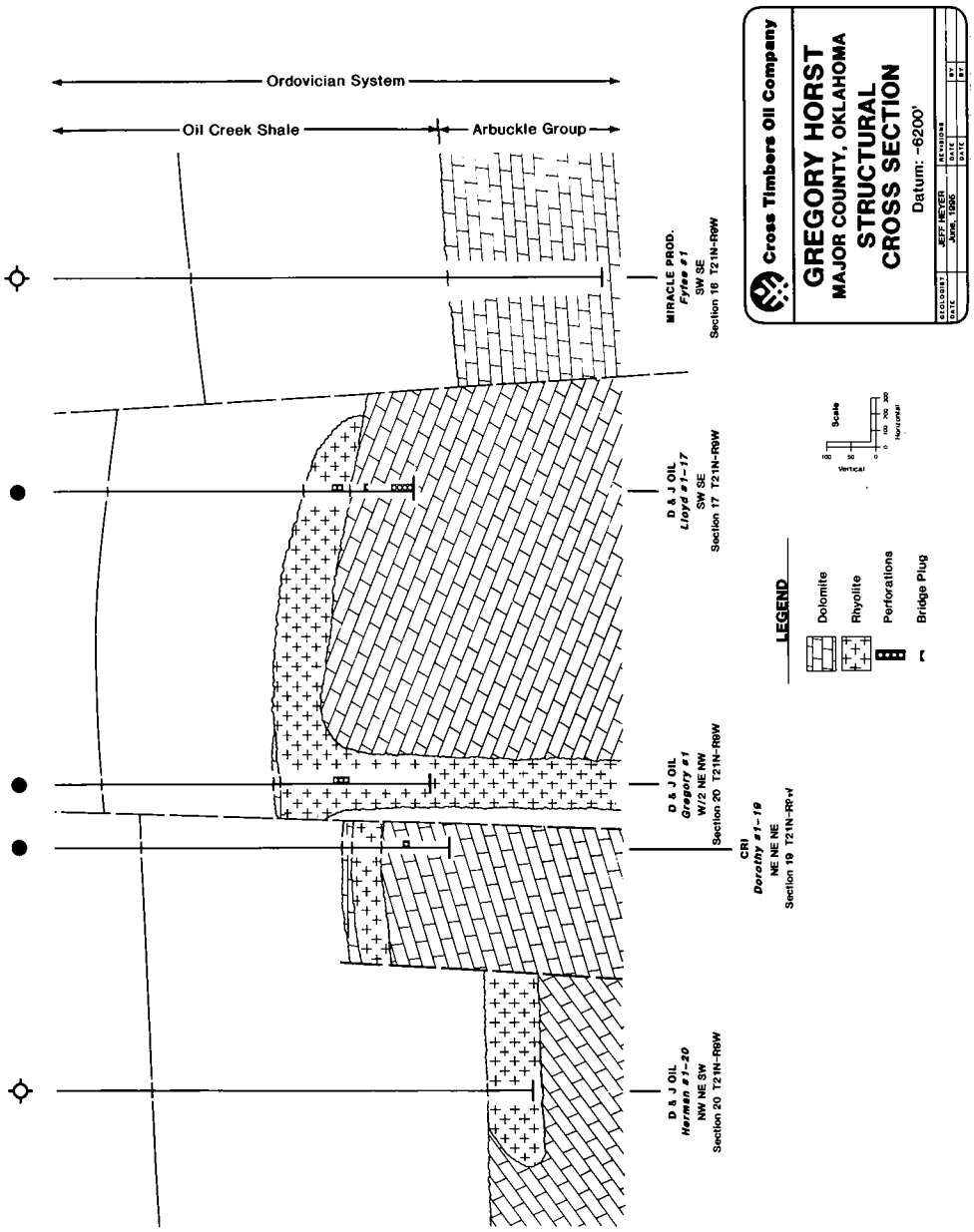

Figure 4. Structural cross section illustrating that structural displacement is the primary trapping mechanism in the play. Rhyolite is found on horst blocks and in the grabens, but is productive only on horst blocks.

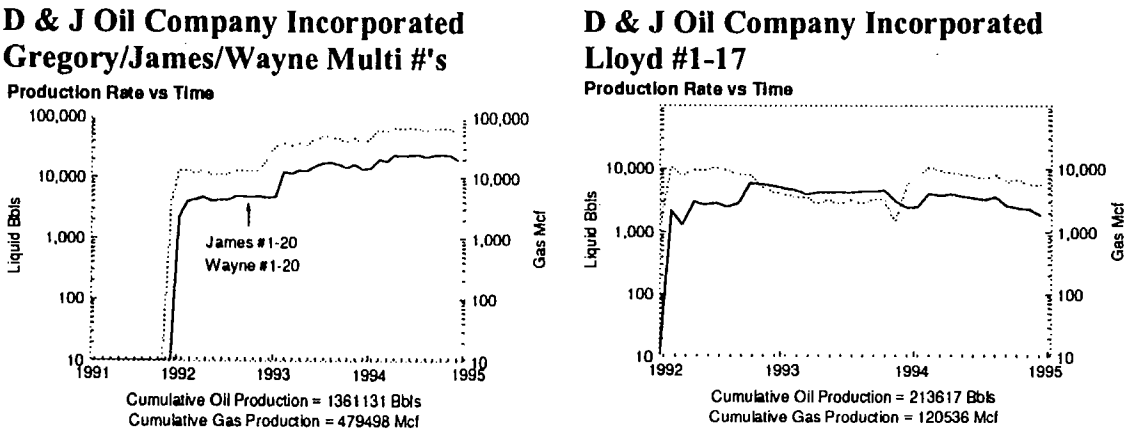

Figure 5. Decline curves for three groups of wells on the Gregory horst; oil production is shown as the dashed line, and gas production is shown as the solid line. The decline curves and geological analysis suggest that the best production comes from the rhyolite and that faults within horst blocks act as seals to hydrocarbon migration. Gregory is the initial well with production; subsequent wells drilled on the lease are identified with their names and an arrow. Dorothy and Marita have one tank battery, and so production is reported to State as one entity, but is really from two wells. Subsequent wells on Gregory lease also reported to State as one entity, but production comes from three wells.

Mustang Field

Mustang Field was discovered in April of 1991 with the drilling of the DLB no. 27-4 Cecil. There are six wells in the field, all producing from Arbuckle dolomite; no rhyolite is present. Mustang Field is unique because within a relatively small areal extent there are five separate trapping mechanisms within five distinct reservoirs (Fig. 6).

The discovery well produces from a bioclastic grainstone reservoir that is not present to the south and west. In a northeasterly direction, the reservoir is structurally low and wet. Upon initial completion the DLB no. 27-4 Cecil produced 170 BOPD and had a decline rate of 20%. In September 1991, the DLB no. 28-9 Bierig was drilled, encountering Arbuckle dolomite 72 ft high to the no. 27-4 Cecil. A normal fault with 85 ft of displacement is the trapping mechanism for the reservoir in this well. The fault plane is at a depth of 8,737 ft in the Oil Creek sandstone. Orientation of the fault is upthrown to the basin. The no. 28-9 Bierig had an initial potential of 2,355 MCFGPD (million cubic feet of gas per day) and had a decline rate of 13%. The CRI no. 1-22 Mary Ellen was drilled as the north offset to the no. 27-4 Cecil discovery well. The Mary Ellen encountered the Arbuckle dolomite 11 ft low to the no. 27-4 Cecil. The reservoir that is producing in the Cecil was found 71 ft low and wet in the Mary Ellen. The operator attempted to make a completion in the cave-fill chaotic-breccia facies, but could only recovery uneconomic quantities of oil. A 38-ft-thick dolomite, which is absent in the wells to the south, was perforated for an initial completion of 1,300 MCFGPD.

The transition from a nonproductive cave-fill chaotic-breccia to a highly fractured collapse-breccia reservoir is illustrated in a cross section from the CRI no. 1-22 Mary Ellen to the CRI no. 1-34 Terry (Fig. 6). Both the no. 1-34 Terry and the no. 27-4 Cecil drill-stem test revealed economic quantities of natural gas from the upper 150 ft of Arbuckle dolomite. These intervals correlate into nonproductive chaotic breccia cored in the no. 1-22 Mary Ellen. The no. 1-34 Terry was perforated in the collapse-breccia facies and initially produced at the rate of 3,688 MCFGPD. Unfortunately, the well had a decline rate of 100%, suggesting that the paleokarst reservoirs are the least significant from an economic perspective (Fig. 7).

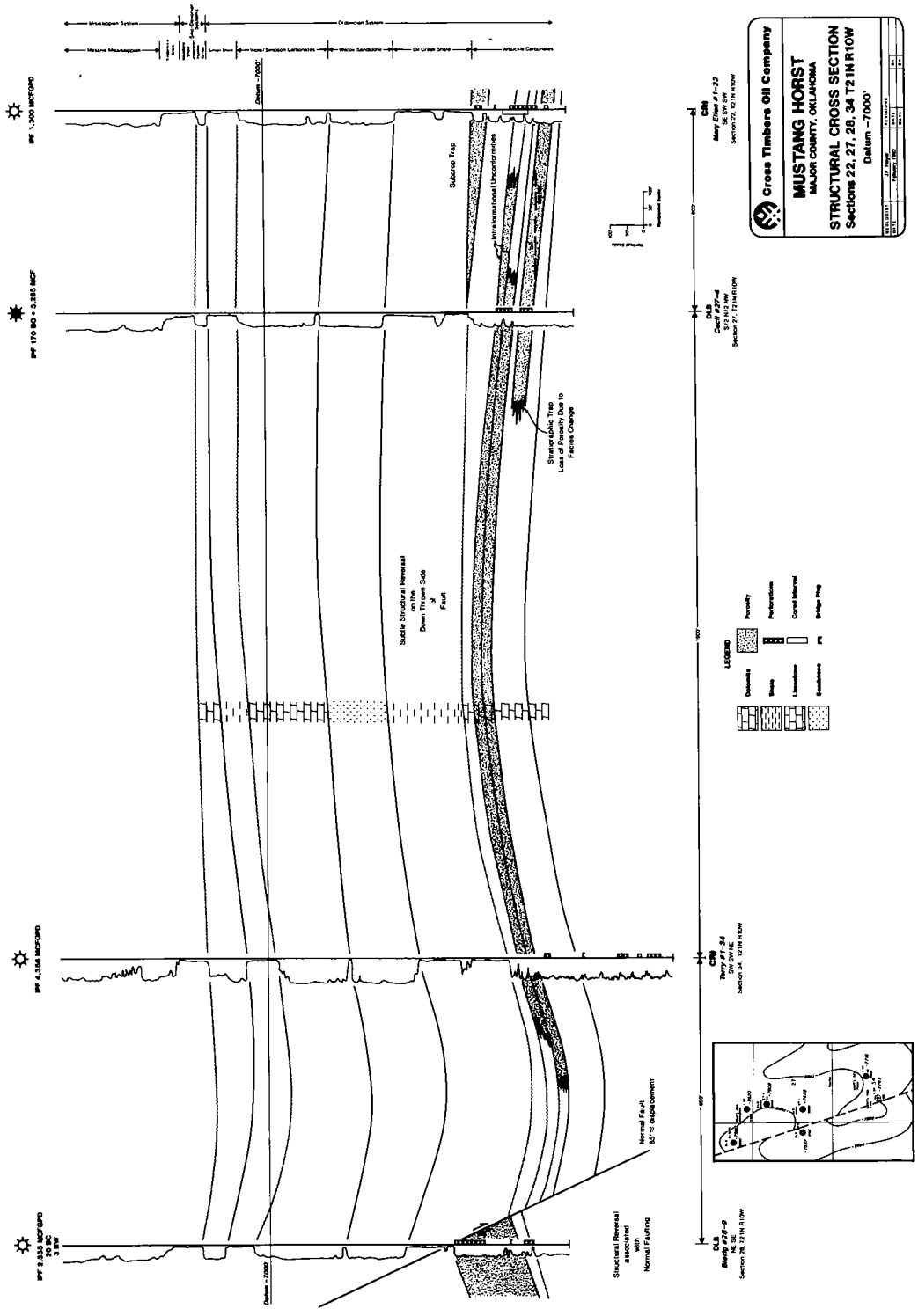

Figure 6. Structural cross section of the Mustang horst. The multiple trapping mechanisms on the crest of the Mustang horst are illustrated.

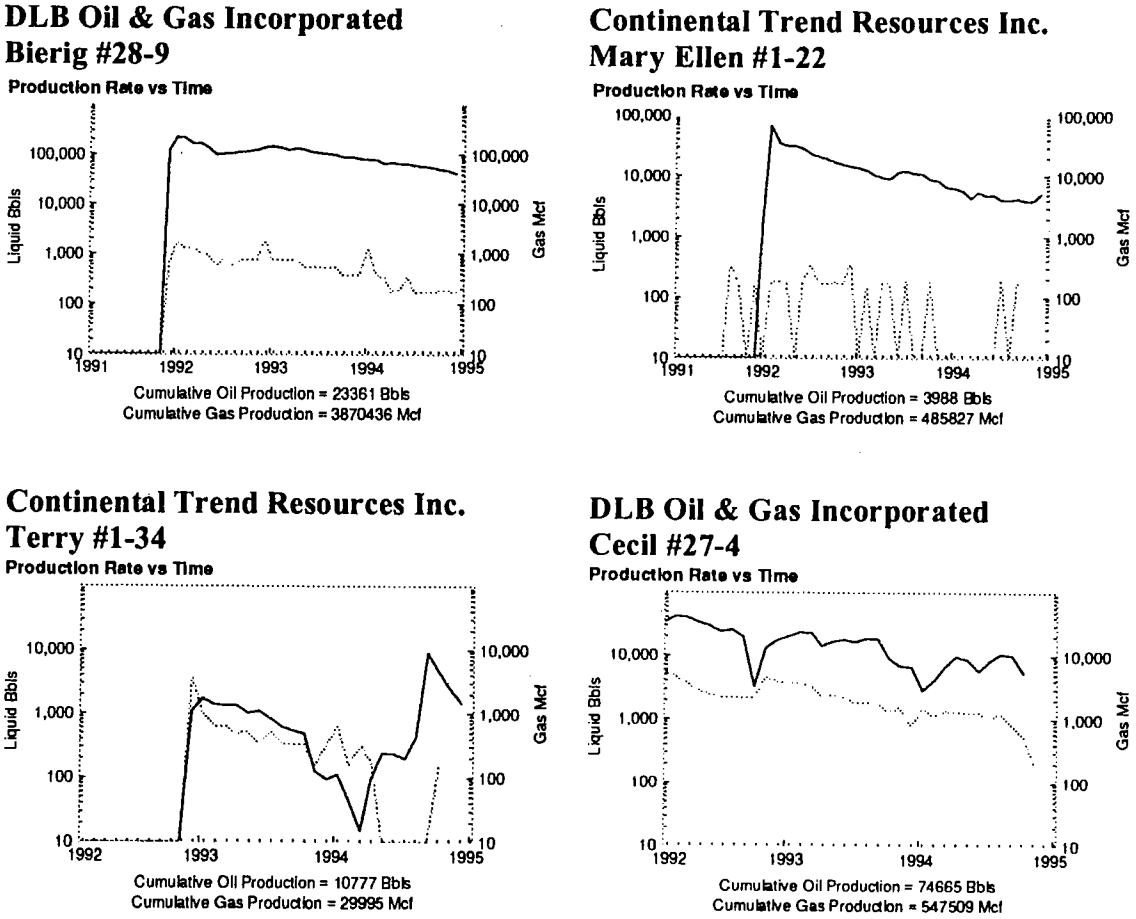

Figure 7. Decline curves for the four wells in the Mustang horst cross section (Fig. 6.). The no. 28-9 Bierig is the most productive well, followed by the no. 27-4 Cecil, no. 1-22 Mary Ellen, and the no. 1-34 Terry.

REFERENCE CITED

Ragland, D. A.; and Donovan, R. N., 1991, Sedimentology and diagenesis of the Arbuckle Group in outcrops of southern Oklahoma, *in* Johnson, K. S. (ed.), Arbuckle Group core workshop and field trip: Oklahoma Geological Survey Special Publication 91-3, p. 9–29.

The Nicor No. 18-4 Chestnut Core, Ames Structure, Oklahoma: Description and Petrography

J. Fritz Fischer
Fischer Petrologic
Arvada, Colorado

ABSTRACT.—The Ames structure, 9,000 ft in the subsurface below Ames, Oklahoma, is a buried crater 8 mi across with an associated debris blanket inside and outside the structure. Although a few people have interpreted the structure as a volcanic feature, the overwhelming evidence is in favor of an origin by impact of a meteor or comet. The discovery of oil and gas in the debris blanket has resulted in numerous drill holes into and through the structure, making it one of the most thoroughly drilled impact structures in the world.

A core from the Nicor No. 18-4 Chestnut well starts in the shale above the debris blanket and penetrates about one third of the way through the blanket. Detailed petrographic study of the rocks in the core reveals numerous mineralogical changes to quartz that can be explained only by forces one to two orders of magnitude larger and 10 orders of magnitude shorter in duration than anything created internally within the Earth. These changes are mosaic texture (mosaicism), planar deformation features, and diaplectic glass, along with lechatelierite (the last two now devitrified to chert). There is also a melt phase that has no phenocrysts, an inordinate amount of Precambrian clasts, and a stratigraphic sequence that is unlike any volcanic sequence, but that can be explained by an impact.

The impactor struck into middle to upper Simpson Group dolomitic clay on a shelf in a marine environment. It created a complex crater with an outer rim and inner ring that are still preserved. The fallback ejecta formed a deposit similar to a spatter cone around a basaltic vent, covered by thick graded beds formed from turbidites thought to have been generated by tsunamis washing over the ejecta rim. The final deposit created by the disturbance was a dolomite-rich sequence of thin graded beds of dolomite and clay reworked from the sediments surrounding the impact. These dolomitic beds, called the dolomite caprock, are completely conformable with the overlying shale. This shale is euxinic, especially within the crater, and is the likely source for the oil found in the ejecta debris.

INTRODUCTION

The location and history of discovery of the Ames structure and its petroleum reserves are discussed in other articles in this volume. The crater is approximately 8 mi across and as much as 600 ft deep inside two concentric structures (the outer rim and inner ring) that are high relative to the regional trend of the surrounding subcrop. There is also a central uplift composed of fractured Precambrian granite that stands approximately 2,000 ft above the normal basement level.

Although most workers agree that the Ames structure probably has an impact origin (Hamm and Olsen, 1992; Roberts and Sandridge, 1992; Shirley, 1992; Carpenter and Carlson, 1992,1997; Koeberl and others, 1994,1997; and most other authors in this volume), others maintain strong doubts and prefer to interpret the structure as having a volcanic origin (Roemer and others, 1992; Coughlon and Denny, 1993,1997; Bridges, 1997). Other papers in this volume offer evidence of the structure's origin on the basis of crater geometry, geochemistry, etc.

The purpose of this paper is to describe a core through the upper third of the stratigraphic sequence unique to the Ames structure and its immediate surroundings. The core was drilled in the Nicor No. 18-4 Chestnut well, located in the northern part of the crater (Fig. 1). Detailed study of the

J. Fritz Fischer, Fischer Petrologic, 16858 W. 73rd Place, Arvada, CO 80007.

Fischer, J. F., 1997, The Nicor No. 18-4 Chestnut core, Ames structure, Oklahoma: description and petrography, *in* Johnson, K. S.; and Campbell, J. A. (eds.), Ames structure in northwest Oklahoma and similar features: origin and petroleum production (1995 symposium): Oklahoma Geological Survey Circular 100, p. 223–239.

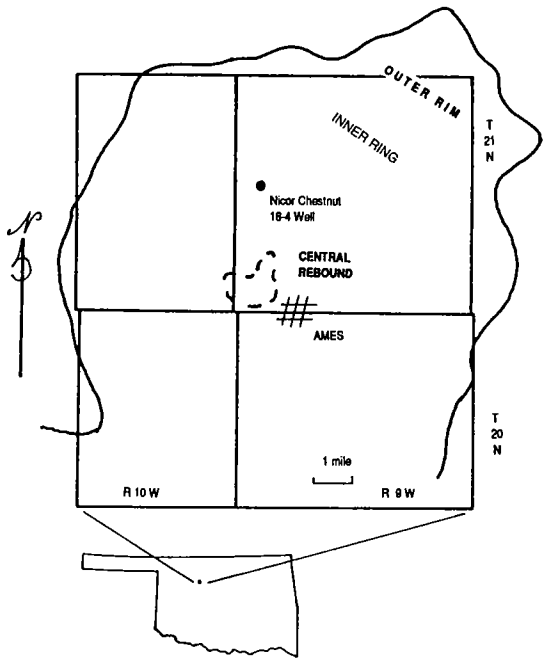

Figure 1. Location map for the Nicor No. 18-4 Chestnut well in the Ames structure (in part after Kuykendall and others, 1997).

units and their petrography provides some strong evidence concerning the genesis of the crater itself.

Roberts and Sandridge (1992) characterize the crater and ejecta subcrop as composed mostly of Arbuckle dolomite; in several places, however, the crater fill rests directly on the Precambrian granite central high (originally reported as glass, and still occasionally referred to as such), which is granite approximately 2,000 ft above the regionally expected contact with basement. Roberts and Sandridge also describe two sedimentary units within the crater itself. The lower one is a breccia, characterized by pebble- to block-sized clasts of Precambrian granite. The breccia has a matrix that was once dominantly a vesicular melt and is known colloquially as the "magic rock"; it is referred to herein as the *melt breccia*. The other unit is what Roberts and Sandridge call "granite wash" and was presumably formed by subaerial weathering of uplifted parts of the crater; it is called the *diamictite* herein. Above their granite wash, Roberts and Sandridge report a euxinic shale that has been correlated on logs with the Oil Creek shale (of the Oil Creek Formation, Simpson Group); however, this shale is apparently younger than the Oil Creek shale, on the basis of conodonts (part of the McLish Formation–Bromide Formation interval or Tyner Formation of the Simpson Group; see Repetski, 1997). This shale is as much as 600 ft thicker in some places within the crater than it is outside the crater (Coughlon and Denny, 1993, fig. 16) and will be referred to informally in this paper as the *crater shale*. There is also a thin layer, known informally as the *dolomite caprock*, which occurs at the base of the crater shale above the diamictite.

The Nicor No. 18-4 Chestnut well was drilled in what Kuykendall and others (1997, fig. 4) refer to as the crater anticline, well inside the inner ring (see Fig. 1). Two consecutive cores were taken. The first starts in the crater shale at 8,969 ft depth, and the second finishes at 9,037 ft. The rocks of greatest interest in terms of the origin of the Ames structure are the rocks that occur from 9,002.8 ft, i.e., the top of the dolomite caprock, to the bottom of the core at 9,037 ft.

The core was described carefully, from 8,990 ft to total depth (TD). Selected samples throughout the interval from 9,002.8 to 9,037 ft were taken from the core and thin sections were prepared. After doing the petrographic work, the core was reexamined numerous times to try to understand better some of the confusing things seen in both the thin sections and in the megascopic examination. Several samples were collected for more detailed mineralogical work, primarily detailed examination of quartz grains for the presence of planar deformation features (PDFs) by both optical and scanning electron microscopy (SEM courtesy of B. Bohor, U.S. Geological Survey, Denver, Colorado). Magnetic susceptibility was also measured (courtesy of R. Reynolds, U.S. Geological Survey, Denver, Colorado), but the samples have uniformly low susceptibilities and show no trends or values that seem significant (see Fig. 2).

PREVIOUS WORK IN SHOCK METAMORPHISM

Experimental and investigative work into the sorts of pressures, time frames, and mineralogical changes resulting from meteorite impacts and into the processes that occur during impacts began with the discovery by Coes (1953) of the high-pressure silica polymorphs. Since that time, a significant amount of work has been done; geologists understand far more today than they did when Bucher (1936) presented his dilemma on "cryptovolcanic" features. One of the important realizations is that the mineralogical changes by meteorite impact take place under pressures that can exceed 50 GPa (gigapascals) and within times of 10^{-6} to 10^{-9} s (seconds). This style of metamorphism has come to be known as shock metamorphism and can be contrasted with regional metamorphism, which has pressures of less than 1 GPa and occurs over times greater than 10^{6} s. Rather than drag the reader through a history of the relevant literature, the interested reader is invited to examine two review papers, Stöffler and Langenhorst (1994) and Grieve and others (1996). These two papers are discussions of shock phenomena in

quartz as understood at this time and of the recognition and geologic significance of such phenomena. Some of their points are summarized in the following paragraphs.

There are several changes in quartz that are common in meteorite impacts; other minerals are affected as well, but the phenomena in quartz are the easiest to see and interpret. These changes include the development of mosaicism, planar deformation features (PDFs), diaplectic glass, and lechatelierite. Of these, only lechatelierite is known from occurrences other than meteorite impacts or features produced by high shock, i.e., artificially caused explosions. The following discussion is taken primarily from the two papers mentioned above.

The lowest-pressure shock effect on quartz is *mosaicism*. This is the initial disruption of the crystal structure of a single grain, breaking it into small domains that are slightly rotated with respect to each other, resulting in a "mottled" appearance. The product is not the same as the smooth change in orientation found in undulatory extinction in quartz.

PDFs, nondecorated and decorated, are the next stage, produced at the lower end of the pressures commonly found in impacts, i.e., 5 to 35 GPa. *Nondecorated PDFs* are lamellae that are highly planar, range from <1 to 5 μm thick, and are composed of glass; they occur as multiple parallel planes in a quartz crystal and have specific orientations with respect to the crystal lattice ({10$\bar{1}$3}, {10$\bar{1}$2}, {10$\bar{1}$1}, etc.). At least 13 different orientations have been measured in quartz; as many as 5 or even more different sets may be found crossing each other in a single grain. *Decorated PDFs* are planes of bubbles remaining after partial annealing of nondecorated PDFs. None of these features is characteristic of Böhm lamellae, the common deformation lamellae found in strained quartz in regional metamorphic environments and rarely in ash-flow tuff. Bruce Bohor with the U.S. Geological Survey has been studying PDFs in quartz, in an attempt to define other criteria for their recognition besides numerous sets of straight lamellae. With the scanning electron microscope (SEM), he has found that the PDFs are remarkably straight, planar features no wider than 0.5 μm, whereas Böhm lamellae are diffuse, broad, and curving (B. Bohor, personal communiation, 1995). An interesting aspect to the PDFs is that they virtually always have columnar structures across the lamellae. The lamellae themselves are composed of silica glass, which has been etched out with HF prior to examination under the SEM (see Fig. 10).

Throughout the pressure range of the formation of the PDFs there is a progressive destruction of the quartz crystal lattice. At 35 GPa a stage is reached at which the lattice is completely destroyed. At this point the quartz is said to have been amorphized or made amorphous; the term used commonly today is *diaplectic glass*. In this condition the quartz grain has not been melted and still retains its original shape; it has, however, assumed a glasslike internal structure even though no liquid was formed. It is important to note here that although the crystalline lattice has been destroyed, the units that go into forming that lattice have not been rotated with respect to each other or randomized; in other words, the silica tetrahedra exist in nearly their original orientation, but bonds between the tetrahedra have been broken. Recrystallization will thus partially preserve the original crystallographic and optical orientation.

When pressure exceeds 50 GPa, quartz begins to form a true melt, which can then solidify into the silica glass known as *lechatelierite*. Lechatelierite was known earlier as the main material in fulgurites, the rocks that form as a result of a lightning strike. Recognition of lechatelierite by itself is therefore not sufficient cause to interpret an impact origin; however, the field relations are so strikingly different that there should be no confusion between the two origins.

At a pressure above 100 GPa, quartz is vaporized. Although it can be shown that it is quite within the realm of possibility in larger impacts that there could be vaporized quartz that would recongeal into droplets of silica liquid or melt, geologists have no concept at this time of what to look for petrographically to recognize this process.

At pressures near the upper end of the formation of PDFs and into the formation of lechatelierite, two definite minerals, *coesite* and *stishovite*, can also form from the quartz. These minerals, first synthesized in the laboratory in the 1950s, were found at Meteor Crater in Arizona in 1960, along with both diaplectic glass and lechatelierite (Chao and others, 1960). To date, these two minerals have been found outside the laboratory only in meteorite impacts and rocks subjected to high explosions, both TNT and nuclear.

A final point in the interpretation of shock-generated glass is that in time, glass recrystallizes or devitrifies, so that in older structures (such as Ames) no glass remains. A characteristic texture that forms during devitrification of silica glass is termed ballen texture and is seen in thin section as a series of successive botryoidal surfaces. These are composed of low quartz, but are thought to have crystallized originally as cristobalite. Differing degrees of optical continuity in the resulting quartz are thought to reflect differing stages in the shock degradation of quartz through diaplectic glass to lechatelierite, in turn thought to reflect differing intensities of shock.

Tektites are another form of glass generated by shock metamorphism, but are more complicated chemically, having full rock chemistries, rather than just silica. The criteria by which tektites are recognized have become quite sophisticated and will not be dealt with further here.

Most of the features listed herein have been

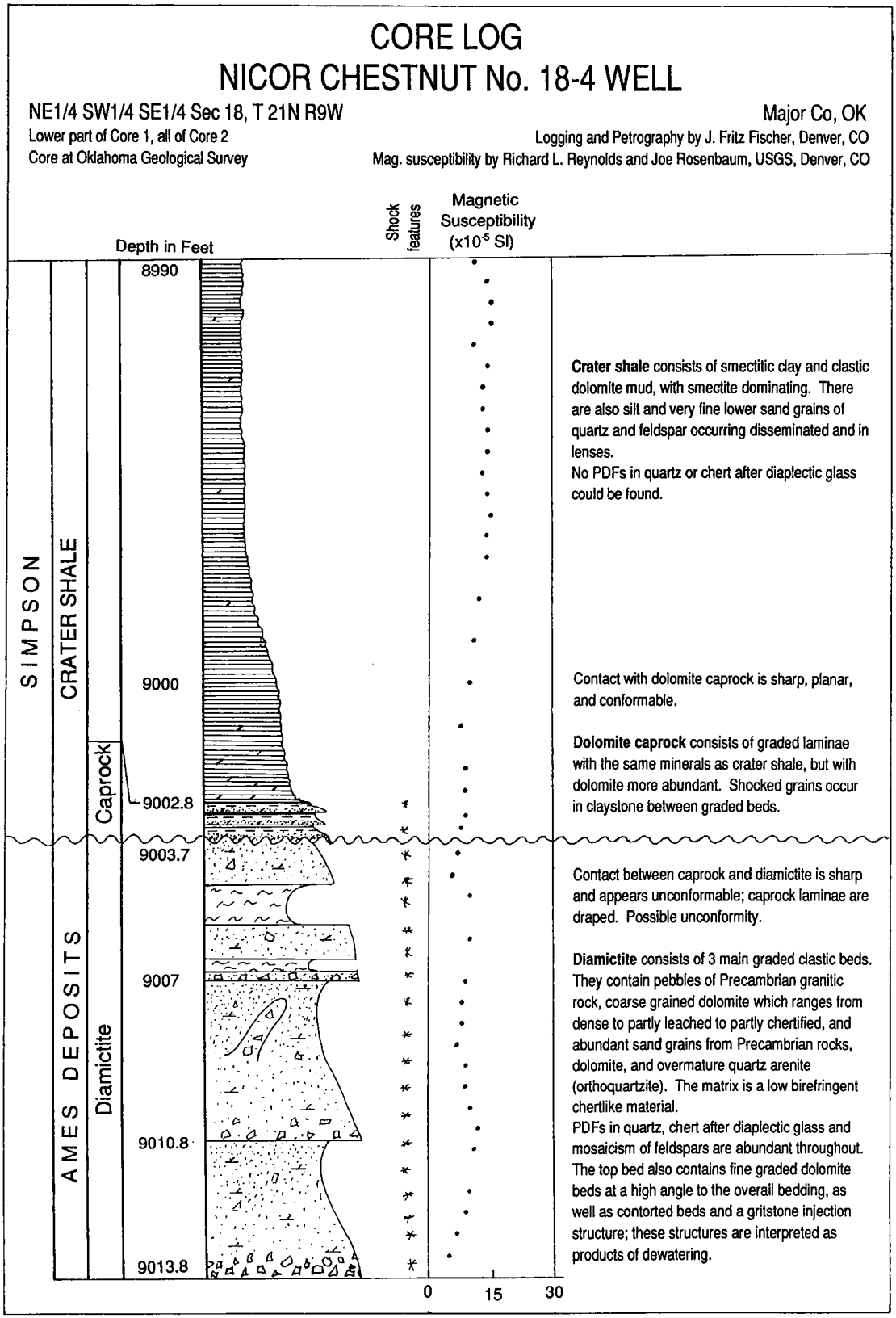

Figure 2 *(above and facing page).* Lithologic log of the relevant parts of the Nicor No. 18-4 Chestnut core.

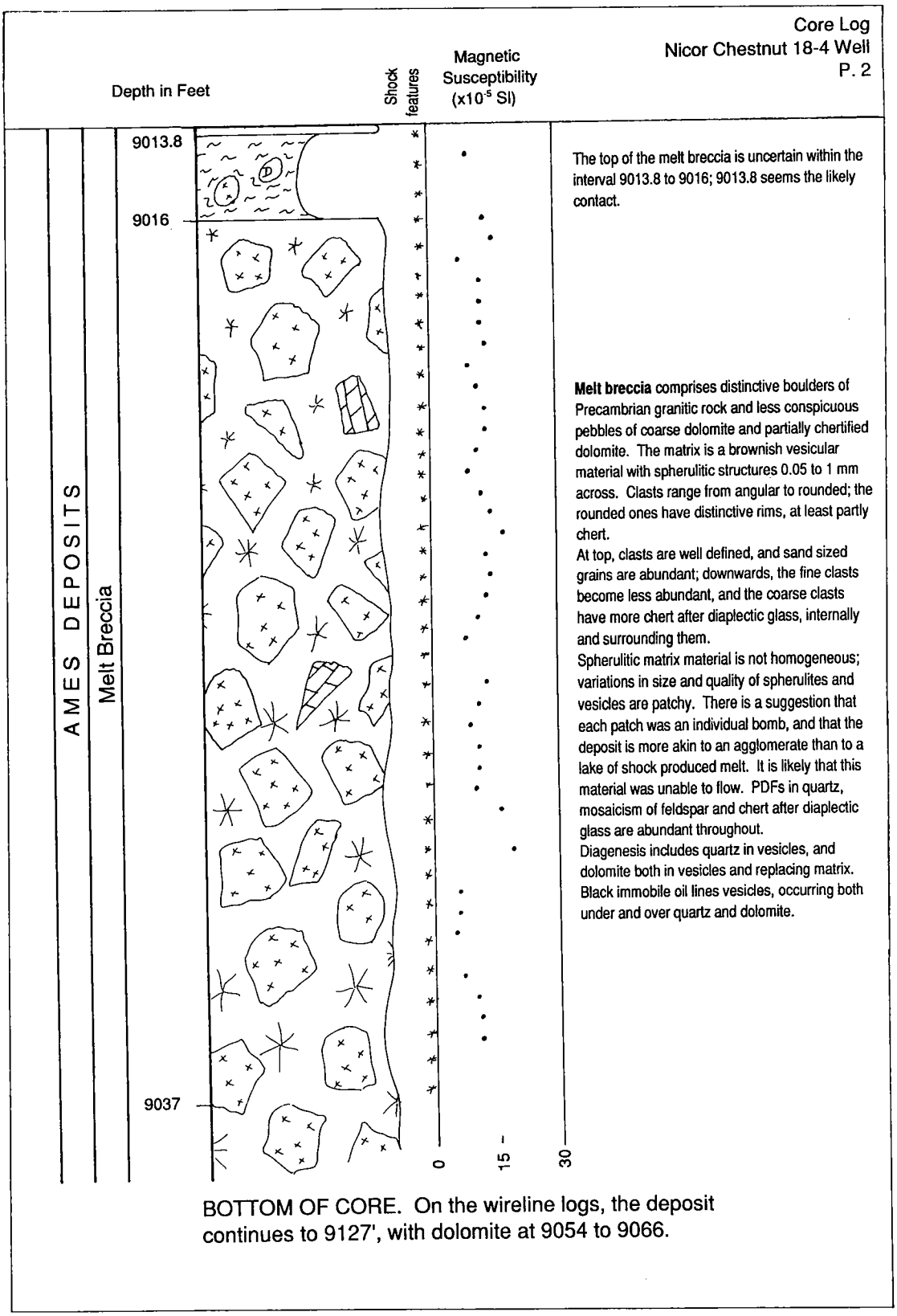

Figure 2 *(continued).*

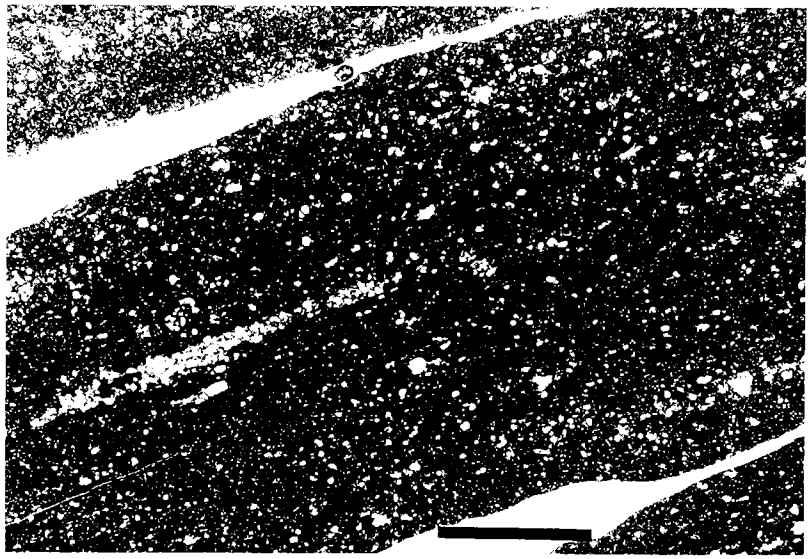

Figure 3. The crater shale is dominated by smectitic clay and dolomite, poorly laminated but with good alignment of elongate grains. The distinct lenses of terrigenous material and coarse dolomite provide the lamination visible in the hand samples. There is no hint of graded bedding. This field of view has three slivers of shale, separated by fractures. Scale bar represents 1 mm. Plane light.

found in the rocks from Ames. Specifically, mosaicism in quartz (see Fig. 8), plagioclase, and K-feldspar is common. Quartz grains with PDFs can be found from the dolomite caprock down to the lowest samples from the melt breccia (see Figs. 9,10). Diaplectic glass and lechatelierite are inherently unstable and so could not be seen directly in the Ames rocks. But there is abundant chert ranging from parts of quartz grains to complete grains to veinlets in the thin sections. Some of this chert appears totally disorganized and is considered to be derived from lechatelierite (see Figs. 12,13); other chert patches have all of the minute chert grains in similar orientation, suggesting that the original material was diaplectic glass (see Fig. 12). Some blebs of quartz are also considered to have been silica liquid at one time (see Fig. 11). Ballen texture is also common (see Fig. 13).

CORE DESCRIPTION

Two cores were actually cut from the Nicor No. 18-4 Chestnut well, but since they are continuous one with the other, no distinction between them is made here. The coring started at 8,969 ft and finished at 9,037 ft. The rock of interest has its top at 9,002.8 ft and continues below the core to 9,127 ft (as interpreted from wireline logs); thus only about the top third of the deposit created by the cratering process is actually represented in the core. To date, the cuttings from this well have not been found and are feared lost. The core was described from 8,990 ft to the bottom. From top to bottom, the units encountered are (1) crater shale, (2) dolomite caprock, (3) diamictite, and (4) melt breccia. A graphic log of the core is presented in Figure 2.

The crater shale appears to be a relatively monotonous sequence of euxinic claystone with thin siltstone and sandstone laminae. At 9,002.8 ft is the contact between the crater shale and the dolomite caprock. At 9,003.7 ft is the contact with strata dominated by sand-sized material, with scattered breccia clasts; Roberts and Sandridge (1992) referred to this unit as the granite wash, but it is called diamictite here to avoid a genetic connotation. Between 9,013.8 and 9,016 ft is the contact with the top of the melt breccia or "magic rock." Wireline logs indicate that the breccia unit continues to 9,127 ft depth, with dolomite present from 9,054 to 9,066 ft.

The topmost unit is the crater shale. It is a very dark brown, finely laminated dolomitic shale. It is highly fissile and contains discontinuous lamellae of siltstone to very fine grained sandstone. The unit was correlated originally to the Oil Creek shale, but conodonts indicate that it is younger than the Oil Creek Formation, "falling somewhere in the McLish Formation–Bromide Formation interval or Tyner Formation of the Simpson Group" (Repetski, 1997); it is much thicker within the crater than without, indicating that the crater was a significant hole at the time the shale was deposited. It is called *crater shale* informally here to avoid assigning an incorrect stratigraphic correlation.

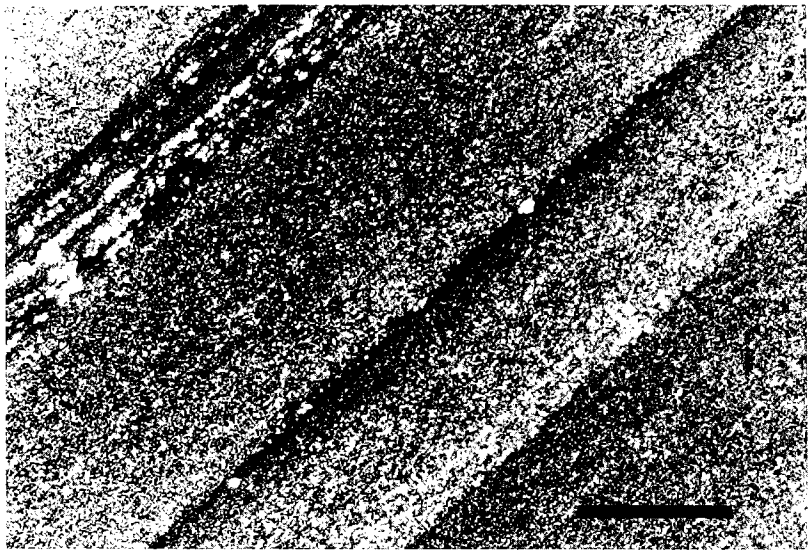

Figure 4. Sharply graded beds in the dolomite caprock. The grading is primarily due to change in the size of the dolomite grains, which in turn indicates that they are clasts. Note that the quartz and feldspar are more abundant in the shale partings between graded beds than in the graded beds. Top is toward the upper left; the sample is from nearly the very top of the unit. Compare with the crater shale (Fig. 3). Scale bar represents 1 mm. Cross-polarized light.

At 9,002.8 ft is a sharp, flat, conformable contact between the crater shale and the underlying dolomite caprock. There is a distinct color change at the contact, from the dark brownish black of the euxinic shale to the gray of the underlying dolomite caprock. The dolomite caprock is finely laminated, graded, dolomitic mudstone containing veins and pods of pyrite. The laminae become fainter and thicker downward, and the rock becomes more indurated.

The contact between the dolomite caprock and the underlying diamictite is also sharp, but does not seem conformable in the 5-in.-diameter core. There is a strong sense that the laminae of the dolomite caprock are draped over what was an underlying irregular, lithified surface at about 45° to the core axis. This underlying unit is dominantly dolomitic sandstone, but is probably best characterized as a diamictite. It consists of three main graded units marked by breccia at their bases, grading through poorly sorted sandstone to siltstone; there is internal graded bedding within the units. Millimeter- to centimeter-scale bedding at 9,005 ft is tilted about 45° to the core axis and is truncated; at 9,007.5 ft a lobe of sandstone 3 cm across is present in the siltstone, oriented nearly vertically, and is interpreted as an injection that occurred during dewatering. Both of these structures, along with contorted bedding (see Fig. 5), are considered to be products of soft-sediment deformation and to indicate that the main mass of this material was deposited in a very short period of time by mass flow, rather than by traction currents.

The lithic pebbles present in the diamictite are dominantly of two types. One type is white and has a pumiceous or tuffaceous appearance; hence it could be interpreted as volcanic. The other type consists of small clasts of granitic material.

The contact between the diamictite and the underlying melt breccia is not well marked in the core. It occurs somewhere in the interval between 9,013.8 and 9,016 ft, which is also an interval of intense shearing. This lowest unit is distinctive in various ways. It has abundant blocks of granitic material and could easily be called a granite breccia. These blocks range to at least 8 in. in length, and some are wider than the core diameter (5 in.). The breccia is porous, whereas the overlying diamictite is not. This porosity consists of clasts of apparent pumice in a tighter, more dolomitic matrix. It contains chert not found in the overlying unit and is host to dead oil in the vesicles.

In the wireline logs, the dolomite caprock and the diamictite have a significantly lower gamma-ray response than the overlying crater shale. The underlying melt breccia, however, has much higher response, so is quite easily identified on the logs; the higher response is thought to be due to the abundance of granitic clasts present. At 9,054 to 9,066 ft is a definite interval of dolomite. Below the dolomite, the breccia has a lower, but variable, gamma signature than above it.

A puzzling aspect of the core is that the diamic-

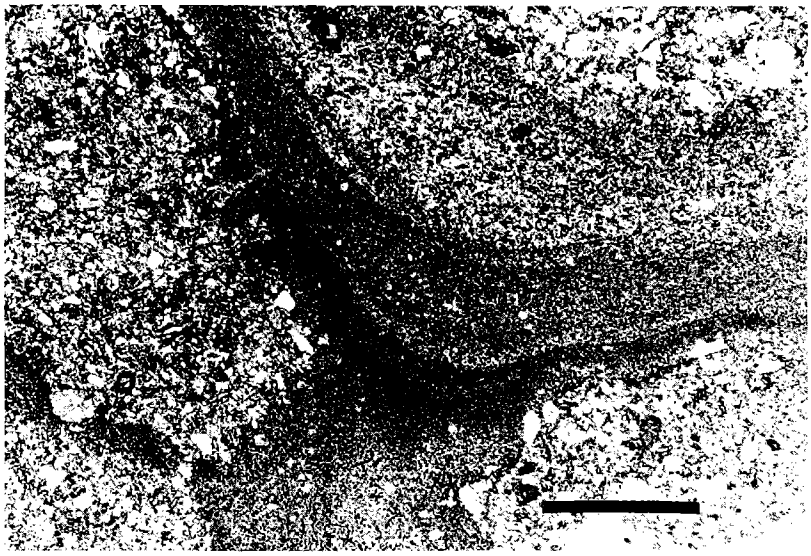

Figure 5. Contorted graded beds in the upper part of the diamictite. The beds are almost entirely dolomite, identical to the graded dolomite beds in the overlying dolomite caprock. The beds are included in gravelly sandstone composed of quartz, feldspars, dolomite, and lithic clasts of devitrified melt. PDFs are common in the quartz. Scale bar represents 1 mm. Plane light.

tite and melt breccia are crossed by numerous shear zones that are not found in the overlying shale. It is not at all clear why this should be. The shears are obvious in the macroscopic examination of the core, yet there is no definite shearing in the thin sections from these zones, so it is possible that they are more apparent than real.

PETROGRAPHY

The section above on the previous work in shock metamorphism indicates numerous features produced by shock that should be unique to rocks affected by an extraterrestrial impact. All of these features can be found in the Ames rocks, but with a difference: any amorphous or glass phases formed during the original event have since recrystallized. Thus, material interpreted as a rock melt is in fact a mass of radial sprays of finely crystalline material, mostly sanidine. There is no diaplectic glass in the rocks; there is, however, abundant "chert" in which all of the fine microscopic and submicroscopic grains of quartz that form the chert are subparallel to each other in their optic (crystallographic) orientation. This chert is called "chert after diaplectic glass" here, to indicate the interpretation that it formed from preexisting quartz grains that had been made amorphous, i.e., shocked to a diaplectic glass. There are also clasts, veins, and fine veinlets of chert in which the individual grains are at random orientations to each other. Since this chert shows a close affinity with granite clasts and still-crystalline quartz, it is thought to have been lechatelierite that has since degraded to chert.

The Crater Shale

The crater shale consists of approximately 50% brown smectitic clay, 30% fine clastic dolomite, 10% silt, 5% organic matter, and 5% diagenetic pyrite, decreasing upward. These proportions vary, as there are fine laminae of siltstone consisting of nearly pure quartz and feldspar and even fine-grained sandstone with carbonate cement (Fig. 3) and other laminae that are mostly dolomite. The dolomite occurs in distinct grains that look like they are transported clasts, rather than authigenic crystals grown in place. Lamination away from the lenses of siltstone and very fine sandstone is poorly developed, in spite of the fact that the core has split repeatedly into thin cylindrical slivers ("hockey-puck shale"). Examination of numerous grain mounts of material from the crater shale failed to find a single grain of quartz with PDFs or chert after diaplectic glass.

The Dolomite Caprock

The contact between the crater shale and the underlying dolomite caprock is sharp and conformable. There are three strong differences between the units, as well as a fourth more subtle one.

1. The style of sedimentation is distinctly differ-

ent. The dolomite caprock has distinct graded bedding, with shale partings between graded beds; the graded beds are thickest at the base of the unit and thin upward (the unit is therefore doubly graded). The shale partings, in contrast, are thicker and more abundant near the top (Fig. 4). The grading is almost entirely from changes in the grain size of the dolomite, which indicates clearly that the dolomite is clastic. Terrigenous minerals including quartz, feldspars, and chert are concentrated in the shale partings, not in the graded beds themselves. There is a particularly pronounced concentration of terrigenous minerals at the contact between the caprock and crater shale.

2. There is also a difference in proportions of minerals. The dolomite caprock is composed of about 90% clastic dolomite, along with 2% smectitic clay, 2% terrigenous silt (quartz, feldspar, chert, etc.), and 6% diagenetic pyrite. An interesting corollary of the difference in the mineral proportions is the similarity in the minerals themselves: the *same* minerals are present in both the caprock and the shale, changed only in proportion. I have the sense that the dolomite caprock is a layer composed of the same minerals as the overlying shale, but with the fines winnowed out. This is my strongest evidence to argue that the crater shale is merely the result of continued deposition of a stratigraphic unit that had started before the impact and continued afterward. The impact created nearly instantaneous deposits of melt rock and diamictite and reworked the existing sediment to form the dolomite caprock (see Conclusions).

3. There is a strong contrast in oxidation state between the two units. The caprock is gray and bears no evidence of organic matter; this unit was deposited under strongly oxidizing conditions. The crater shale, in contrast, has abundant organic matter and was clearly deposited in a reducing environment.

4. A more subtle but no less important difference is that quartz with PDFs and chert after diaplectic glass were found in the caprock, but not in the clay lamina at the contact with the crater shale nor within the crater shale itself. It would appear that the ejecta were exposed and providing detritus to the dolomite caprock deposit when it was being laid down, but were covered by the time the crater shale formed, in spite of the evidence that the crater was still a negative feature during deposition of the crater shale.

The above observations of the relationships between the dolomite caprock and the crater shale carry the following implications. The dolomite caprock is a discrete depositional unit created by the impact; the caprock is the final layer formed by a catastrophically disturbed ocean as it returned to normal marine conditions. The composition of the caprock indicates derivation primarily from reworking of a mud sea bottom that existed at the time of impact, with slight but significant addition of material created by the impact itself (especially quartz with PDFs). The high energy at the time of reworking caused complete oxidation of the transported material, as well as effective separation of silt-sized from clay-sized material. Graded beds indicate deposition by turbidites, whether tsunami-generated or not. Decreasing thickness of beds upward indicates decreasing availability of material in the source or reduced energy of tsunami waves as the disturbance died down. Conformity with the overlying crater shale suggests continuity of deposition, but changing from a turbidite, oxidizing mode to a euxinic, static-water mode, and loss of exposure of impact debris.

Diamictite

The unit below the dolomite caprock is a diamictite. It has graded beds, with granite pebbles at the base of each bed, grading up to sandstone and siltstone. Petrographically, the rocks vary from 30% to 70% or more dolomite, mostly in the matrix. The matrix includes siliceous phases, which near the base of the unit form a continuous chert-like matrix of unknown origin. The clasts are a wide variety of lithologies including dolomite, granite, devitrified glassy rocks with vesicular textures, and individual quartz, feldspar, and dolomite grains, including very well rounded quartz grains. There are abundant quartz grains with PDFs and chert after diaplectic glass.

The rock is composed of a mixture of all of the lithologies to be found down to and including basement: dolomite of the Arbuckle Group, well-rounded quartz grains out of the Arbuckle orthoquartzites, and basement granite are mixed together, along with volcanic-appearing clasts. The presence of the quartz with PDFs and the chert after diaplectic glass are unequivocal evidence of an impact; the formerly glassy rocks are therefore interpreted as bits of impact melt; they may or may not represent true tektites.

Although the contact is sharp and unconformable, the uppermost part of the diamictite has some layers remarkably similar to the dolomite caprock, in that they are thin, graded beds, composed mostly of dolomite (Fig. 5). Except for the apparent angular unconformity in the core, which may be just a local variation in the surface, it is tempting to consider that the depositional environment of the diamictite is similar to that of the caprock, but with a much greater volume of impact material being transported and deposited and a much higher proportion of rocks derived from the basement. This material is thought to be turbidites from the mass flows of ejecta material reworked by powerful tsunamis that had to have wracked the region as the ocean driven away by the impact returned to normal. A variation on this theme is that these deposits are wash-back formed by flooding as sea water broke through the barrier of the built-up ejecta rim and flooded back into the

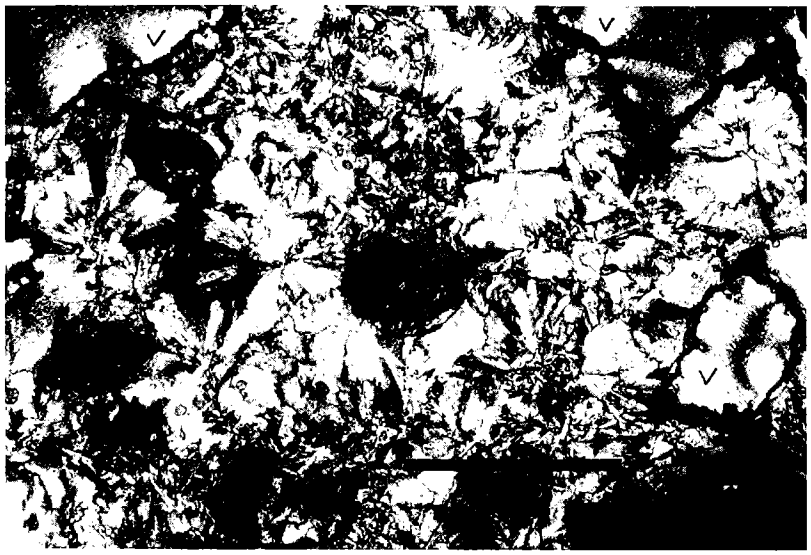

Figure 6. Spherulitic texture between vesicles (V) is evidence of a former melt. Scale bar represents 0.5 mm. Cross-polarized light.

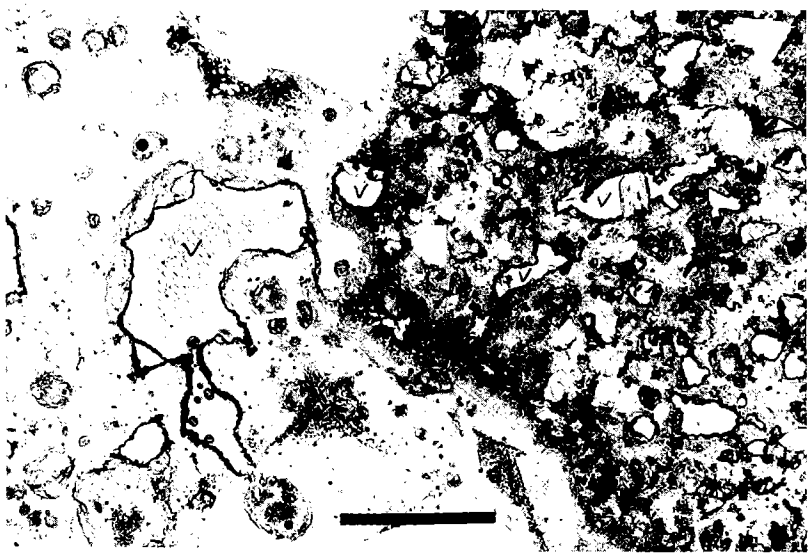

Figure 7. Sample of melt breccia. Differences in the texture of discrete areas of the spherulitic matrix, such as between the right and left sides of this field of view, suggest that the deposit is more similar to a spatter cone than to a lava flow. The material must have been ejected as individual blebs of melt with lithic inclusions and must have solidified penecontemporaneously with contact; thus it should not be considered as a true melt sheet or a "lake" of melt in low-lying topography. V—vesicle. Scale bar represents 1 mm. Plane light.

crater. The force of the water returning after the impactor struck would almost certainly overwhelm the elevation of the rim. Both of these hypotheses require that the impactor strike in a shallow sea, rather than on dry land. (See discussion of the origin of the dolomite caprock under the heading Dolomite Caprock.)

Melt Breccia

The lowest unit present in the core is the melt breccia. In thin section this rock is most distinguished by a matrix that contains abundant radial fibrous growths in material with abundant vesicles (Fig. 6). In the core, and to a lesser extent in

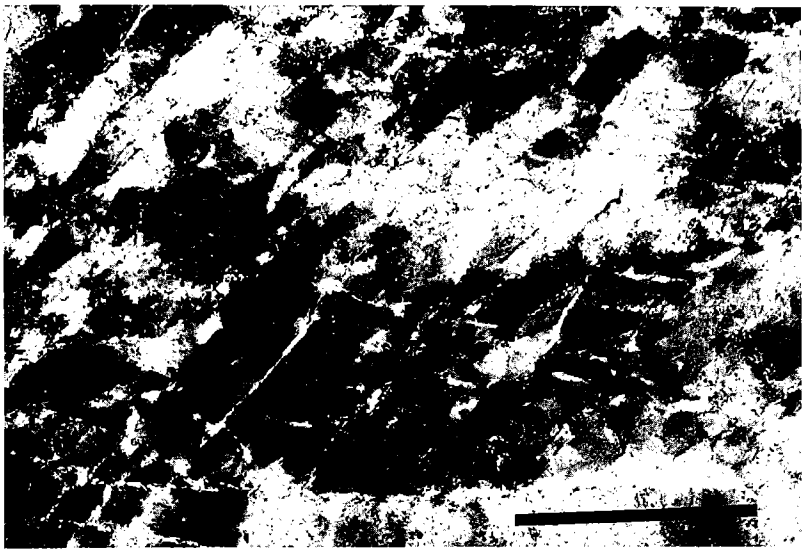

Figure 8. Mosaicism in quartz from the edge of a granite clast in the melt breccia. The *c*-axis is north-south and nearly in the plane of the slide. The quartz has two sets of PDFs (not visible at this scale; see enlargement in Fig. 9); the chert in the mosaic fractures has nearly the same orientation as the main grain, suggesting formation and devitrification of diaplectic glass. Scale bar represents 0.5 mm. Cross-polarized light.

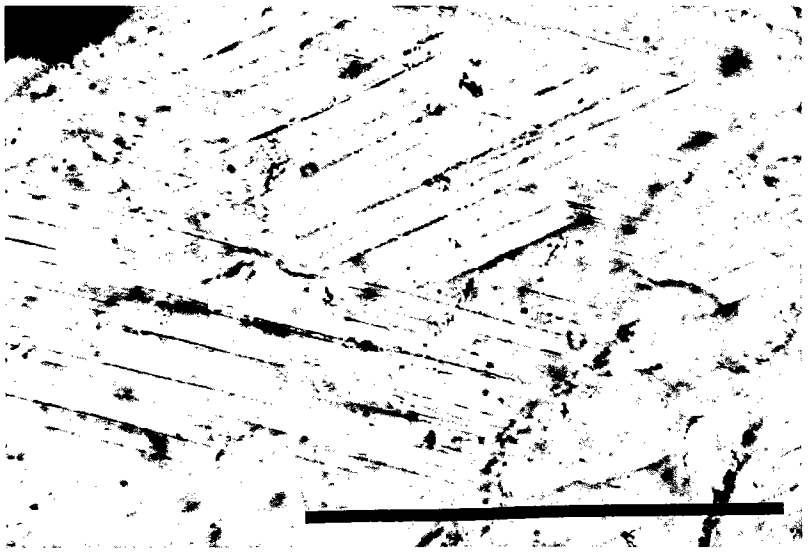

Figure 9. Two well-developed sets of PDFs in the mosaic-textured grain of Figure 8. In other parts of the grain, at least two more sets can be found. Scale bar represents 0.1 mm. Plane light.

the thin sections, one gets the impression that this matrix is not a continuous material, but rather that it was in discrete blebs. Adjacent blebs may have different sizes of radial fibers, different sizes of vesicles, and different orientations of elongated vesicles (Fig. 7). There is also abundant dolomitic material that appears to be interstitial to the vesicular material.

It is my experience that the radial sprays (which take a strong yellow K-feldspar stain and have a low $2V$ and so are thought to be dominantly sanidine) are the devitrification product of a former glass, devitrified while it was still hot, producing spherulites. The apparently clastic nature, or discrimination into discrete blebs (Fig. 7), suggests that this material was not a single mass of melt

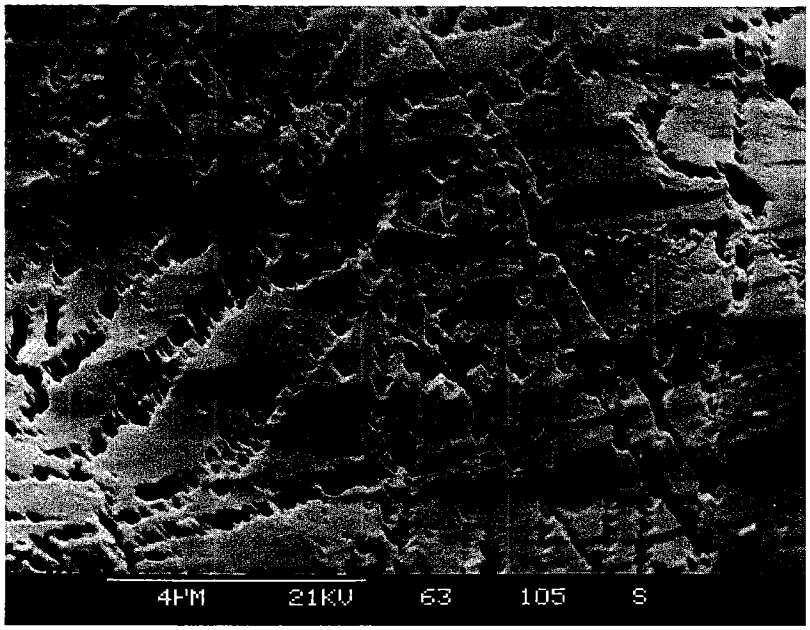

Figure 10. An SEM photograph (bar at bottom represents 4 μm) of a quartz grain from the Ames melt breccia. The photograph indicates four sets of planar features in the quartz that, after etching with HF, are open space, planar, and thin (less than 1 μm) and have columnar structures across them. These are criteria by which shock-induced PDFs are recognized. Photograph by Bruce Bohor.

such as one might find in a lava lake or flow, but was rather a pile of material similar to a pile of scoria bombs building a spatter cone around a basalt vent, in which the bombs are still hot and weld together into an agglomerate instead of remaining loose as in a cinder cone. Throughout all of the rocks studied that have this vesicular spherulitic structure, not a single phenocryst of any sort was found. There are, however, various accessory grains, probably mostly zircon, in some of the rocks. The lack of phenocrysts argues strongly against a volcanic source for this melt.

The breccia also has abundant clasts of granite showing evidence of extreme shock. The quartz ranges from showing strong mosaic texture (see Fig. 8) to having abundant PDFs (see Fig. 9) to being partly converted to chert after diaplectic glass to being chert that forms veinlets throughout the clasts; there are also rims of chert that are thought to have been quartz melt about the clasts. Plagioclase grains show abundant deformation of twin lamellae as well as partial mosaicism; although plagioclase can also show PDFs, I was not confident enough to try to separate features that might be PDFs from the twinning. K-feldspar also has strong mosaicism.

Figure 10 is an SEM photograph taken by Bruce Bohor, U.S. Geological Survey. The photograph shows four distinct sets of thin, planar features in quartz. The lamellae are planar, have thicknesses of far less than 1 μm, and have distinct columnar structures across them; these are features that Bohor (personal communication) has found consistently only in PDFs.

There are numerous blebs of material that are essentially pure quartz today, but that have shapes and internal flow lines suggesting that they were once molten material. Some of these are now coarsely crystalline quartz (Fig. 11), and others are fine-grained chert or microcrystalline quartz. There are also former quartz grains that are now partly chert after diaplectic glass and partly still the original quartz. Other grains that are now chert have the chert near the margins in fair optical continuity (indicating derivation from diaplectic glass), but cores of totally disorganized chert (indicating formation from lechatelierite) (Fig. 12). Virtually all of the chert after diaplectic glass and chert (and microcrystalline quartz) derived from lechatelierite have the faint botryoidal textures known as ballen texture (Fig. 13).

Diagenetic Features

The diagenesis of the rocks has been dominated by growth of authigenic quartz, dolomite, and migration of oil. Almost all permutations of one mineral growing on top of another one can be found, with both quartz and dolomite covering oil in places (Fig. 14), but covered by oil in others. It

Figure 11. Clear patch is crystalline quartz now. The shape leaves little doubt that it was a liquid at one time. The pure quartz composition suggests that it was a pure silica liquid that cooled to form silica glass—i.e., lechatelierite. Scale bar represents 0.1 mm. *A*—Plane light. *B*—Cross-polarized light.

appears that there were numerous periods of formation of quartz, alternating with formation of dolomite, and that some preceded the oil migration whereas others followed it. It does not look like the diagenesis can be reduced to a simple diagram.

CONCLUSIONS

The first conclusion to be drawn from the petrography is that there is abundant evidence of shock metamorphism in the pressure range from formation of shock mosaicism to lechatelierite, which is to say somewhere in the range from 5 GPa to above 50 GPa. These pressures far exceed any known pressures to be found in regional metamorphic, faulting, or volcanic phenomena (all less than 1 GPa) and therefore are considered as incontrovertible evidence for an impact origin of the Ames structure by scientists who have been working with shock phenomena.

The interpretation of the origin of individual layers is a little less certain. The lowermost layer

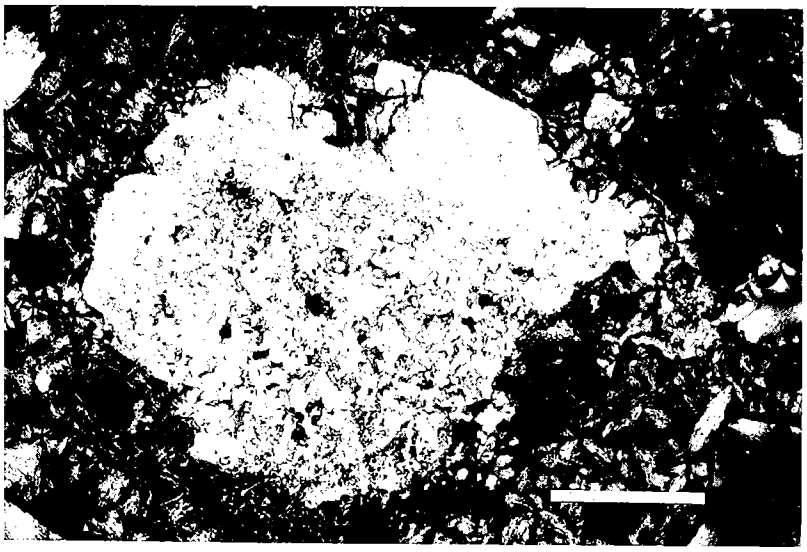

Figure 12. Grain of apparent chert has a rim that is reasonably close to being in optical continuity, although composed of chert. The interior is actually disorganized microcrystalline quartz. In both materials, ballen texture is well developed, although not visible at this scale. The interpretation is that this was a grain of quartz that went to diaplectic glass at the rim, but lechatelierite in the center. The surrounding matrix is a mixture of quartz, feldspar, and dolomite. Scale bar represents 0.5 mm. Cross-polarized light.

(i.e., melt breccia) present in the core has been called suevite informally, although it contains a higher proportion of melt rock than the original suevite does. It contains a large amount of melt material, but as described above, the suggestion of discrete blebs indicates that it was probably not a true melt sheet in the sense of a lava lake filling lows within the crater. Instead, it appears to be a buildup of impact-melt material. The location within the inner ring indicates that this is fallback material.

The wireline logs indicate fairly clearly that beneath the level to which the core sampled there is an 11-ft-thick interval of dolomite, below which is more of the melt breccia overlying Arbuckle dolomite. Although this dolomite interval has been used as an argument that the breccia represents at least two discrete volcanic events separated in time (Coughlon and Denny, 1993), an impact creates forces that can easily lift blocks tens of feet in diameter and redeposit them as part of the ejecta.

Details of the boundary between the melt breccia and the diamictite are lost in a shear zone. The diamictite has three distinct graded beds, along with finer beds (at least near the top) that are deformed and contain penetration structures suggestive of dewatering. I interpret this layer to be a wash-back layer, formed subaqueously as the ejecta on the rim of the crater was washed back into the crater as turbidites, probably driven by tsunamis. This interpretation, in turn, would indicate that the meteor or comet struck while the area was a shallow sea, rather than dry ground.

The contact between the diamictite and the dolomite caprock is a bit of a puzzle. The contact is irregular, at about 45° to the core axis. The laminae in the caprock appear to be draped over this contact. The implication is that the underlying surface was hard and irregular, which is not what one would expect if deposition of both were effectively continuous in a subaqueous environment. Instead, there is the suggestion of lithification and erosion, indicating that this is an unconformable surface. On the other hand, the similarities in mineral constituents and depositional environments and the presence of graded dolomite layers within the diamictite similar to the layers in the caprock argue for a short time interval between units, measurable in days or less rather than millions of years. The arguments either way here are speculative because of lack of data; more work needs to be done. My personal preference is for the latter interpretation.

The dolomite caprock shares some similarities with the overlying crater shale, but has some strong differences as well. Their similarities include (1) being composed of minerals that are identical in composition and grain aspect and (2) being conformable. Their differences are in (1) the style of sedimentation, (2) the proportion of dolomite to clay, (3) the change from oxidation to reduction and the concomitant preservation of organic matter in the crater shale, and (4) the presence of shock-related grains in the caprock, but not in the

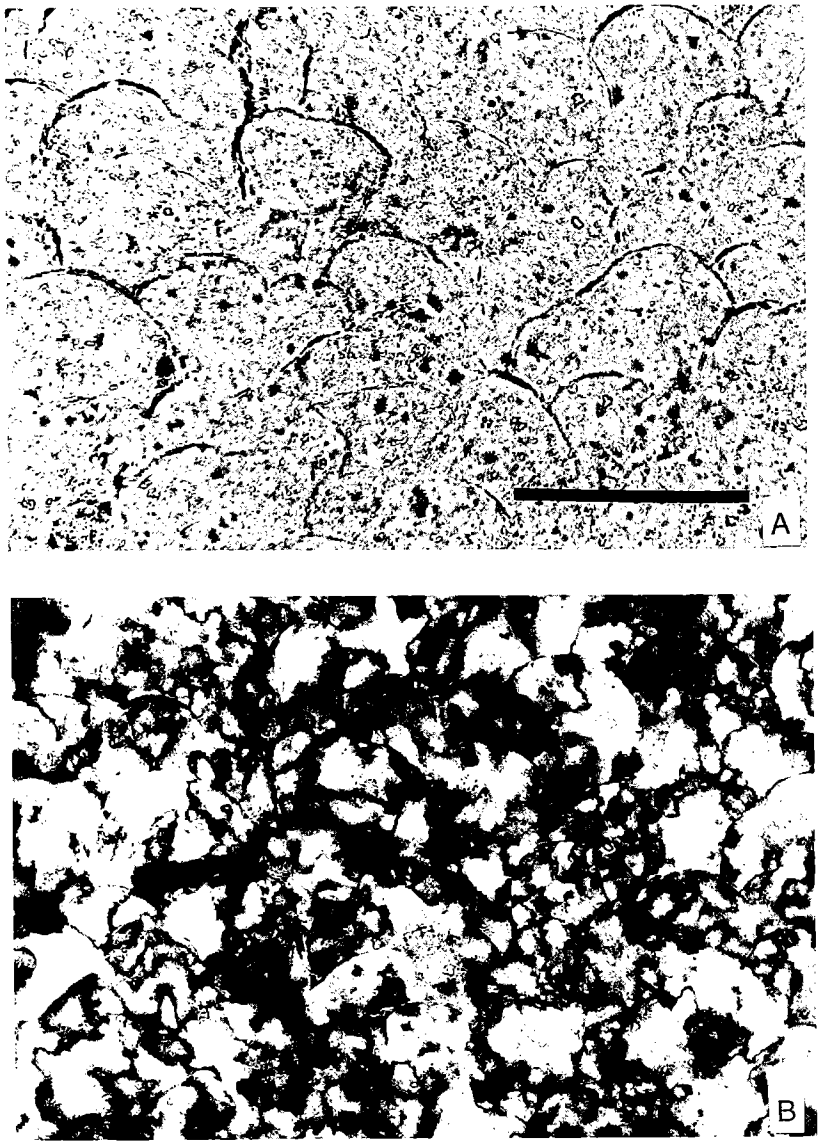

Figure 13. Botryoidal surfaces in a clast that otherwise looks somewhat like chert are the characteristic expression of ballen texture. In this case, the chert is in random optical orientation, indicating that the precursor was lechatelierite, i.e., a true quartz melt. These textures are also found in chert after diaplectic glass and microcrystalline quartz. Scale bar represents 0.2 mm. *A*—Plane light. *B*—Cross-polarized light.

shale. I suggest that the dolomite caprock and crater shale formed one after the other without a significant hiatus. It would appear that the dolomite caprock formed mostly from dolomite-bearing smectite mud identical to the crater shale, but existing on the sea bottom prior to impact; there is a small contribution of quartz with PDFs, indicating that the ejecta blanket was still being eroded and the resulting detritus was being transported and redeposited.

I interpret the dolomite caprock as a transitional unit formed between the chaotic, nearly instantaneous deposition of the diamictite and the slow, orderly deposition of the clay and silt of the crater shale. The dolomite caprock was deposited by turbidity currents of decreasing energy and load, indicating either decreasing slope instability as the ejecta blanket was removed by repeated turbidites or decreasing energy of tsunamis as the disturbed ocean returned to normal; it is likely

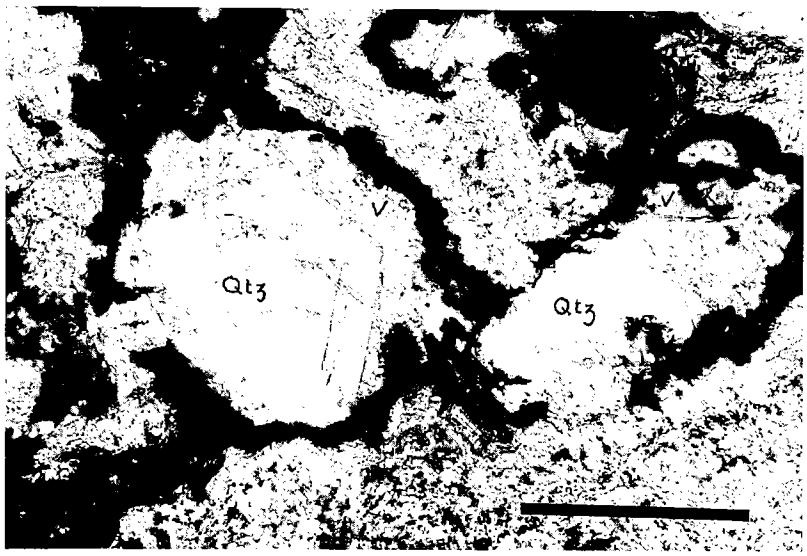

Figure 14. Authigenic quartz crystals (Qtz) in vesicles (V) formed after the migration of the oil, which forms a black rim lining the vugs and is covered by the quartz. Scale bar represents 0.2 mm. Plane light.

that both factors were effective here. The source of material for the dolomite caprock was dominantly reworked preexisting mud rather than ejecta; as the turbidites ceased and the ocean returned to quiescence, the depositional environment returned to euxinic deposition of smectite clay, containing dolomite and terrigenous silt, presumably of windblown origin.

As in the case with the contact between the melt breccia and diamictite, there are weaknesses in the argument concerning the origin of the caprock. A crucial factor is whether the impactor hit in a shallow sea during late deposition of the dolomite (now the upper part of the Arbuckle Group) or early deposition of the clay (now the crater shale, part of the McLish Formation–Bromide Formation interval or Tyner Formation of the Simpson Group [Repetski, 1997]), or whether it hit when the area was high and dry during the formation of the unconformity between the Arbuckle and Simpson. On the basis of (1) the fact that the Ames depression was 400 to 600 ft deep when the postimpact mud that now forms the crater shale was deposited and (2) the apparent gradations from the diamictite to the dolomite caprock and the apparent continuity from the dolomite caprock to the crater shale, I contend that the impactor struck a shallow shelf during the early phase of primarily clay deposition on the Arbuckle unconformity. In the Ames area, this clay was entirely removed by the impact and/or resuspended and redeposited by tsunamis. The dolomite caprock was the early result, followed by the conformable deposition of the more clay-rich but still dolomite-clast–bearing unit that formed the crater shale.

ACKNOWLEDGMENTS

My first examination of the Nicor No. 18-4 Chestnut core was done at the request of Rich Bottjer of Amoco Production Company, who was interested in knowing more about the Ames play and the nature of the main reservoir rock. My contribution was to study the rocks petrographically and give Amoco an interpretation. I thank Amoco for allowing me to use the proprietary data and present it in a public forum. The presentation in this paper was aided greatly by the careful and thorough editing of Mary Eberle. I owe her a debt of gratitude; of course, I take full responsibility for any errors or omissions.

The initial study was done with little knowledge of the rich literature on cratering and shock phenomena. The conclusions, after I presented them to Amoco, shifted with time, thanks to the influence of Glen Izett, whom I met after the initial study was finished. Glen, now retired but then with the U.S. Geological Survey in Denver, Colorado, introduced me to two wonderful worlds at the same time: the fraternity of impact researchers and their work, and the versatility of a remarkably simple but effective microscope tool, the Wilcox spindle stage. Thank you, Glen, for opening my eyes and enriching my life.

REFERENCES CITED

Bridges, L. W. D., 1997, Ames depression, Oklahoma: domal collapse and later subsurface solution, *in* Johnson, K. S.; and Campbell, J. A. (eds.), Ames structure in northwest Oklahoma and similar features: origin and petroleum production (1995 sym-

posium): Oklahoma Geological Survey Circular 100 [this volume], p. 153–168.

Bucher, W. H., 1936, Cryptovolcanic structures in the United States: International Geological Congress, 16th, United States 1933, Reports, v. 2, p. 1055–1084.

Carpenter, B. N.; and Carlson, Rick, 1992, The Ames impact crater: Oklahoma Geology Notes, v. 52, p. 208–223.

_____ 1997, The Ames meteorite-impact crater, *in* Johnson, K. S.; and Campbell, J. A. (eds.), Ames structure in northwest Oklahoma and similar features: origin and petroleum production (1995 symposium): Oklahoma Geological Survey Circular 100 [this volume], p. 104–119.

Chao, E. C. T.; Shoemaker, E. M.; and Madsen, B. M., 1960, First natural occurrence of coesite: Science, v. 132, p. 220–222.

Coes, L., 1953, A new dense crystalline silica: Science, v. 118, p. 131–132.

Coughlon, John; and Denny, Paul, 1993, The Ames structural depression: an endogenic cryptoexplosion feature along a transverse shear: Shale Shaker, v. 43, p. 44–58.

_____ 1997, The Ames structure and other North American cryptoexplosion features: evidence for endogenic emplacement, *in* Johnson, K. S.; and Campbell, J. A. (eds.), Ames structure in northwest Oklahoma and similar features: origin and petroleum production (1995 symposium): Oklahoma Geological Survey Circular 100 [this volume], p. 133–152.

Grieve, R. A. F.; Langenhorst, Falko; and Stöffler, Dieter, 1996, Shock metamorphism of quartz in nature and experiment; II. Significance in geoscience: Meteoritics and Planetary Sciences, v. 31, p. 5–35.

Hamm, Harold; and Olsen, R. E., 1992, Oklahoma lime exploration centered on buried astrobleme structure: Oil and Gas Journal, v. 90, p. 113–116.

Koeberl, Christian; Reimold, W. U.; and Powell, R. A, 1994, Ames structure, Oklahoma: an economically important impact crater: Lunar and Planetary Science Conference, v. 25, p. 721–722.

Koeberl, Christian; Reimold, W. U.; Brandt, Dion; Dallmeyer, R. D.; and Powell, R. A., 1997, Target rocks and breccias from the Ames impact structure, Oklahoma: petrology, mineralogy, geochemistry, and age, *in* Johnson, K. S.; and Campbell, J. A. (eds.), Ames structure in northwest Oklahoma and similar features: origin and petroleum production (1995 symposium): Oklahoma Geological Survey Circular 100 [this volume], p. 169–198.

Kuykendall, M. D.; Johnson, C. L.; and Carlson, R. A., 1997, Reservoir characterization of a complex impact crater: Ames crater, northern shelf, Anadarko basin, Oklahoma, *in* Johnson, K. S.; and Campbell, J. A. (eds.), Ames structure in northwest Oklahoma and similar features: origin and petroleum production (1995 symposium): Oklahoma Geological Survey Circular 100 [this volume], p. 199–206.

Repetski, J. E., 1997, Conodont age constraints on the Middle Ordovician black shale within the Ames structure, Major County, Oklahoma, *in* Johnson, K. S.; and Campbell, J. A. (eds.), Ames structure in northwest Oklahoma and similar features: origin and petroleum production (1995 symposium): Oklahoma Geological Survey Circular 100 [this volume], p. 363–369.

Roberts, Craig; and Sandridge, Bob, 1992, The Ames hole: Shale Shaker, v. 42, no. 5, p. 118–121.

Roemer, C. D.; Roemer, Chris; and Williams, Kyle, 1992, Gravity, magnetics point to volcanic origin for Oklahoma's Ames anomaly: Oil and Gas Journal, v. 90, p. 75–80.

Shirley, Kathy, 1992, Overlooked "hole" found: American Association of Petroleum Geologists Explorer, May 1992, p. 1, 12–13.

Stöffler, Dieter; and Langenhorst, Falko, 1994, Shock metamorphism of quartz in nature and experiment; I. Basic observation and theory: Meteoritics, v. 29, p. 155–181.

The Oil Creek–Arbuckle (!) Petroleum System, Major County, Oklahoma

David K. Curtiss and David A. Wavrek
Energy and Geoscience Institute
University of Utah
Salt Lake City, Utah

ABSTRACT.—A petroleum system includes a mature hydrocarbon source rock, genetically related oil and gas accumulations, and the geologic elements and processes responsible for the hydrocarbon deposits to exist. This study defines the Oil Creek–Arbuckle (!) petroleum system. Geochemical analysis correlates the effective source rock of the lower shale member of the Oil Creek Formation to its related hydrocarbons in the underlying Arbuckle Group reservoir. Optical and chemical methods indicate that the section has achieved a maturity level equivalent to 1.2%–1.3% vitrinite reflectance equivalence. A burial-history model defines the critical moment of peak hydrocarbon generation and expulsion to have occurred at 225 Ma. An events chart documents the petroleum system's development through time.

The generation accumulation efficiency (GAE) compares the amount of hydrocarbons generated in the petroleum source rock to the amount trapped in reservoirs. This petroleum system generated 145 MMBO (million barrels of oil), which, combined with current ultimate reserve estimates, establishes a GAE of 37%. The remaining 63% of the hydrocarbons generated were either lost (i.e., not trapped) or represent the potential for future discovery. Thus, the economic implications for future oil exploration in the structure appear to be positive, contingent on a clearer understanding of the Arbuckle reservoir.

INTRODUCTION

This paper describes the elements and processes (defined below) that led to generation and accumulation of hydrocarbons within the Ames feature; a semicircular structural depression of Cambrian–Ordovician Arbuckle sedimentary rocks in the southeast corner of Major County, Oklahoma (Tps. 20–21 N., Rs. 9–10 W.). Much debate surrounds the origin of the Ames feature. The most popular theory is that the feature is an astrobleme or impact crater (Carpenter and Carlson, 1992,1997; Koeberl, 1997; Koeberl and others, 1997), a convenient working hypothesis for the oil and gas industry (Hamm and Olsen, 1992). Other researchers dispute these findings, claiming the Ames feature has a volcanic origin (Roemer and others, 1992; Coughlon and Denney, 1993, 1997). Still others attribute the subsidence to solution collapse on the midcontinental carbonate platform (Bridges, 1997) that dominated the Ordovician Period, analogous to such events displayed in the European Alps (Fruth and Scherreiks, 1984; Köster and others, 1988). For this study (largely taken from Curtiss, 1995), the mode of origin is irrelevant since the subsidence predates the elements (i.e., source rock and hydrocarbons) and processes considered.

David K. Curtiss, EGI, University of Utah, 423 Wakara Way, Suite 300, Salt Lake City, UT 84108; David A. Wavrek, EGI–Geochemistry Unit, University of Utah, 421 Wakara Way, Suite 125, Salt Lake City, UT 84108.

Petroleum-System Framework

This study is set within a petroleum-system framework, according to the standard promoted by Magoon and Dow (1994). The essential elements are a mature hydrocarbon source rock and genetically related oil and gas accumulations. The processes are the generation, expulsion, migration, and entrapment of the petroleum, which includes hydrocarbons in solid, liquid, and gas forms.

Generation refers to the transformation of buried organic matter to kerogen and then petroleum, first through microbial activity and then by ther-

Curtiss, D. K.; and Wavrek, D. A., 1997, The Oil Creek–Arbuckle (!) petroleum system, Major County, Oklahoma, *in* Johnson, K. S.; and Campbell, J. A. (eds.), Ames structure in northwest Oklahoma and similar features: origin and petroleum production (1995 symposium): Oklahoma Geological Survey Circular 100, p. 240–258.

mal stress (Horsfield and Rullkötter, 1994). Thermal stress is usually associated with deeper burial and can be locally influenced by orogenic and/or igneous activity (Lopatin, 1971; Waples, 1980; Tissot and Welte, 1984).

Expulsion describes the movement of hydrocarbons from the petroleum source rock into the carrier bed or migration conduit. A combination of factors drives the expulsion event, including compaction, chemical reactions, source richness, kerogen type, and thermal expansion (Barker, 1972; Momper, 1978; Ungerer, 1990; Burnham and Sweeney, 1991). Source rocks with greater permeability generate small pressure differentials within pore spaces, whereas less permeable source rocks build up pressures sufficient to fracture the rock. Such pressures within a source rock create vertical fractures that provide conduits for hydrocarbon movement across bedding. Where the pressure gradient generated within the homogeneous source rock exceeds hydrostatic pressure, expulsion will be downward and out of the bottom of the source rock, as well as upward through the top. In cases where organic-rich facies are concentrated at the base of the formation, expulsion from the base can be more significant than from the top. Similarly, expulsion from a thick shale section requires more thermal stress (thermal expansion, hydrocarbon generation) than required for expulsion from a section of shales interbedded with sandstones (Wavrek, unpublished data).

Migration describes the movement of oil through a carrier bed or migration conduit until it is physically trapped. Buoyancy and hydrodynamic forces are the primary factors driving migration; they are most effective in highly permeable strata (England and others, 1991; England, 1994). The migration and drainage style within an individual petroleum system (Demaison and Huizinga, 1991,1994) can be characterized by its vertical and/or lateral components. Vertical migration occurs mainly along faults and fractures that breach a seal, whereas lateral migration dominates in systems with stratigraphically continuous seal-conduit pairs.

Entrapment of petroleum depends on the structural and stratigraphic framework of the system as well as the presence of a seal. A trap occurs where the movement of petroleum toward the surface ceases, usually where a structure has an effective seal prohibiting further migration (Demaison and Huizinga, 1994).

Once identified and described, these elements and processes are placed within a stratigraphic, geographic, and temporal framework. To accomplish the framework definition, Magoon and Dow (1994) suggested the use of four figures and a table: a burial-history chart, map and cross section drawn at the critical moment, an events chart chronicling the kinematic development of the system through time, and a table of related accumulations. The standardized petroleum-system nomenclature is source rock–major reservoir rock followed by punctuation within parentheses indicating a level of certainty for the oil–source-rock correlation: known (!), hypothetical (.), and speculative (?).

In addition to defining the essential elements and processes of the petroleum system, we calculate the petroleum system's generation accumulation efficiency (GAE). The GAE describes what percentage of the hydrocarbons generated accumulated in viable traps. This knowledge is directly applicable to the management of exploration programs (Lewan, 1994).

None of these elements and processes is novel to the petroleum-system concept. The purpose and advantage of this tool is that it reduces exploration risk by insisting on a multidisciplinary, cross-functional approach to exploration. By integrating geology, petroleum, and time into a unified package, the focus shifts from a basinwide emphasis on geology and geophysics to specific oil and gas accumulations within the basin. The objectives are more precise and the decision points more definitive, which in turn lowers the exploration risk (Magoon and Sánchez, 1995).

MATERIALS AND METHODS

Materials

The geochemical database consists of source-rock samples and crude oils. Forty rock samples selected for this study are from the lower shale member of the Oil Creek Formation, a specific facies that is areally confined within the Ames feature. (Repetski [1997] has suggested, on the basis of biostratigraphy, that the "crater shale" may actually correlate to a younger unit. This study, however, retains the "traditional" stratigraphic interpretation.) Thickness ranges from zero at the perimeter to 225 ft in the southern half. Potential source-rock samples came from three wells: the Nicor no. 18-4 Chestnut (n = 21; sec. 18, T. 21 N., R. 9 W.) and the D & J no. 1-20 James (n = 9; sec. 20, T. 21 N., R. 9 W.) in the north-central part of the structure and the DLB no. 5-13 Darin (n = 10; sec. 5, T. 20 N., R. 9 W.) in the south-central half (Table 1). The 30 crude-oil samples analyzed in this study are from wells distributed throughout the feature and represent production from five stratigraphic intervals (Table 2; Fig. 1).

The petrophysical database (Table 3) consists of 30 well logs from wells within the structure. This suite allowed evaluation of several log-based geochemical techniques within the source-rock interval. An isopach map of the source-rock interval (Fig. 1) supplied by DLB was used in conjunction with the well-log techniques to determine the total volume of organic carbon in the lower shale member of the Oil Creek Formation.

TABLE 1.—SOURCE-ROCK SAMPLE INFORMATION

Sample no.	Company	Well name	Depth interval (ft)
MC008R	D & J	no. 1-20 James	8840.3
MC009R	D & J	no. 1-20 James	8858.5
MC010R	D & J	no. 1-20 James	8876.5
MC011R	D & J	no. 1-20 James	8887.5
MC012R	D & J	no. 1-20 James	8891.5
MC013R	D & J	no. 1-20 James	8892.5
MC014R	D & J	no. 1-20 James	8897.1
MC015R	D & J	no. 1-20 James	8902.3
MC016R	D & J	no. 1-20 James	8907.5
MC017R	D & J	no. 1-20 James	8915.9
MC018R	D & J	no. 1-20 James	8919.7
MC019R	D & J	no. 1-20 James	8927.5
MC020R	Nicor	no. 18-4 Chestnut	8969
MC021R	Nicor	no. 18-4 Chestnut	8979
MC022R	Nicor	no. 18-4 Chestnut	8994
MC023R	Nicor	no. 18-4 Chestnut	8970.1
MC024R	Nicor	no. 18-4 Chestnut	8972.1
MC025R	Nicor	no. 18-4 Chestnut	8973.9
MC026R	Nicor	no. 18-4 Chestnut	8975.9
MC027R	Nicor	no. 18-4 Chestnut	8978.1
MC028R	Nicor	no. 18-4 Chestnut	8979.9
MC029R	Nicor	no. 18-4 Chestnut	8982
MC030R	Nicor	no. 18-4 Chestnut	8984.1
MC031R	Nicor	no. 18-4 Chestnut	8985.9
MC032R	Nicor	no. 18-4 Chestnut	8988.1
MC033R	Nicor	no. 18-4 Chestnut	8990.1
MC034R	Nicor	no. 18-4 Chestnut	8991.9
MC035R	Nicor	no. 18-4 Chestnut	8993.9
MC036R	Nicor	no. 18-4 Chestnut	8996
MC037R	Nicor	no. 18-4 Chestnut	8998
MC038R	Nicor	no. 18-4 Chestnut	8999.9
MC039R	Nicor	no. 18-4 Chestnut	9002.1
MC040R	Nicor	no. 18-4 Chestnut	9002.8
MC041R	Nicor	no. 18-4 Chestnut	9003.6
MC042R	Nicor	no. 18-4 Chestnut	9006.7
MC043R	Nicor	no. 18-4 Chestnut	9010.8
MC044R	Nicor	no. 18-4 Chestnut	9013.6
MC045R	DLB	no. 5-13 Darin	9410–9420
MC046R	DLB	no. 5-13 Darin	9440–9450
MC047R	DLB	no. 5-13 Darin	9460–9470
MC048R	DLB	no. 5-13 Darin	9480–9490
MC049R	DLB	no. 5-13 Darin	9500–9510
MC050R	DLB	no. 5-13 Darin	9510–9520
MC051R	DLB	no. 5-13 Darin	9520–9530
MC052R	DLB	no. 5-13 Darin	9530–9540
MC053R	DLB	no. 5-13 Darin	9540–9550
MC054R	DLB	no. 5-13 Darin	9560–9570

Methods

Geochemical Investigation

The analytical methods used in this study were bulk analysis and chromatographic characterization. Bulk analysis included total organic carbon (TOC) and Rock Eval pyrolysis for source-rock samples, as well as API gravity and weight percent sulfur for the crude oils. Both rocks and oils were subjected to carbon isotope analysis.

Chromatographic analysis required the extraction of selected source-rock samples using a Soxhlet apparatus. These rock extracts and the crude oils were then analyzed with gas chromatography–flame ionization detection (GC-FID). Subsequently, rock extracts and selected crude oils ($n = 12$) were split into saturate and aromatic fractions by column chromatography followed by gas chromatography–mass spectrometry (GC-MS) analysis. Two samples were selected and prepared for reflected- and/or transmitted-light microscopy for maturity and depositional-environment analysis.

Burial-History Modeling

The Continental Resources no. 1-19 Chet well was selected for burial-history reconstruction because it penetrates the Arbuckle Group, providing a complete stratigraphic column for calculations, and because it is close to producing oil wells. The model was generated by using BasinMod (Platte River Associates) software, incorporating chronostratigraphic ages for formation tops estimated from Haq and van Eysinga (1987), compaction from Baldwin and Butler (1985), a nominal heat flow of 63 mW/m^2 based on data presented by Gallardo (1989), and no geothermal events or unusually high or low paleo–heat flows (Schmoker, 1986).

Petrophysical Investigation

The sonic and resistivity overlay (Δ log R) technique (Passey and others, 1990) selected for this study is based on the predictable response of the sonic and resistivity tools within an organic-rich interval. Sonic and resistivity traces generally track together in fine-grained rocks lacking appreciable organic matter. In organic-rich intervals, however, the sonic and resistivity curves separate (see Fig. 13 for an example) because of the response of the porosity curve to the low-density, low-velocity kerogen and the resistivity response to the formation fluid. The magnitude of this separation in source rocks can be calibrated to the total organic carbon and maturity, which allows the estimation of organic richness in absence of actual data.

Notations and Calculations

The generation accumulation efficiency (GAE) is defined as the ratio of in-place hydrocarbon re-

TABLE 2.—CRUDE-OIL SAMPLE INFORMATION

Sample	Company	Well name	Producing intervals
A-049C	D & J	no. 1-17 Shelby	Arbuckle
A-050C	D & J	no. 1-18 Peggy	Arbuckle
A-051C	D & J	no. 1-17 Lloyd	Arbuckle
A-052C	D & J	no. 1-20 Gregory	Arbuckle
A-053C	Continental	no. 1-19 Dorothy	Arbuckle
A-054C	Continental	no. 1-19 Heinrich	Arbuckle
A-055C	Continental	no. 1-19 Chet	Arbuckle
A-056C	Continental	no. 1-31 Fred	Arbuckle
A-057C	Continental	no. 1-21 Stansberry	Arbuckle
A-058C	Continental	no. 1-22 Mary Ellen	Arbuckle
A-059C	Continental	no. 1-21 Pacific	Arbuckle
A-060C	Continental	no. 1-34 Terry	Arbuckle
A-061C	White Shield Oil & Gas	no. 1-36 Oliver	Manning, Mississippi, Hunton
A-062C	Petro-Lewis	no. 1-6 Monsees	Mississippi
A-063C	Petro-Lewis	no. 1-27 Oscar	Misener, Mississippi, Manning
A-064C	Hamm Production	no. 1-2 Scott	Mississippi, Manning
A-065C	Staats	no. 1-3 Suit	Mississippi, Manning
A-066C	Petro-Lewis	no. 1-6 Wheeler	Hunton, Mississippi
A-067C	Rodman	no. 1-14 White	Mississippi
A-068C	Petro-Lewis	no. 2-14 White	Mississippi
A-069C	Basin Petroleum	no. 1-5 Bode	Mississippi
A-070C	Getty Oil Co.	no. 1 H. G. Dittmeyer	Hunton
A-071C	Staats	no. 1-21 Detrick	Manning
A-072C	Hamm Production	no. 2-22 Ethel	Hunton, Mississippi, Manning
A-073C	Petro-Lewis	no. 1-16 Fyffe	Mississippi
A-074C	Rodman	no. 1-7 Harvey	Hunton, Mississippi
A-075C	Hamm Production	no. 2-7 Harvey	Hunton, Mississippi, Inola
A-076C	Petro-Lewis	no. 2-7 Hammer	Mississippi
A-077C	Rodman	no. 1-14 Kellogg	Mississippi, Hunton
A-078C	White Shield	no. 1-25 Osborne	Hunton, Mississippi

serves (IHC in kilograms of HC) to hydrocarbons generated (HCG in kilograms of HC) (Magoon and Dow, 1994).

$$GAE = [IHC/HCG] \times 100\% \quad (1)$$

In this study, HCG were calculated whereas IHC were extracted from the literature.

Hydrocarbons Generated (HCG)

Schmoker (1994) presented a calculation method involving four steps. The first step consists of identifying and defining the source-rock interval and then dividing it into sections of approximately equal organic carbon content. Step two involves determining the mass (M, in grams) of organic carbon (TOC, in wt%) in each source-rock section according to the following equation:

$$M = [TOC/100] \times \rho \times V \quad (2)$$

where TOC and density (ρ, in g/cm^3) are averaged over the source-rock section and V (in cm^3), is calculated for the same section (discussed in detail below). The objective of the third step is to determine the mass of hydrocarbons generated per unit mass of organic carbon R (in milligrams of HC per 1 g of TOC), described in equation 3:

$$R = HI_o - HI_p \quad (3)$$

The hydrogen index (HI, in milligrams of HC per 1 g of TOC) indicates the potential of a source rock to produce additional hydrocarbons. Thus, the difference between original HI (HI_o) and present-day HI (HI_p) is the amount of hydrocarbons actually generated. Rock-Eval pyrolysis analysis determines HI_p. Estimating HI_o is possible because of an empirical relationship between hydrogen index and maturity levels (Fig. 2). The

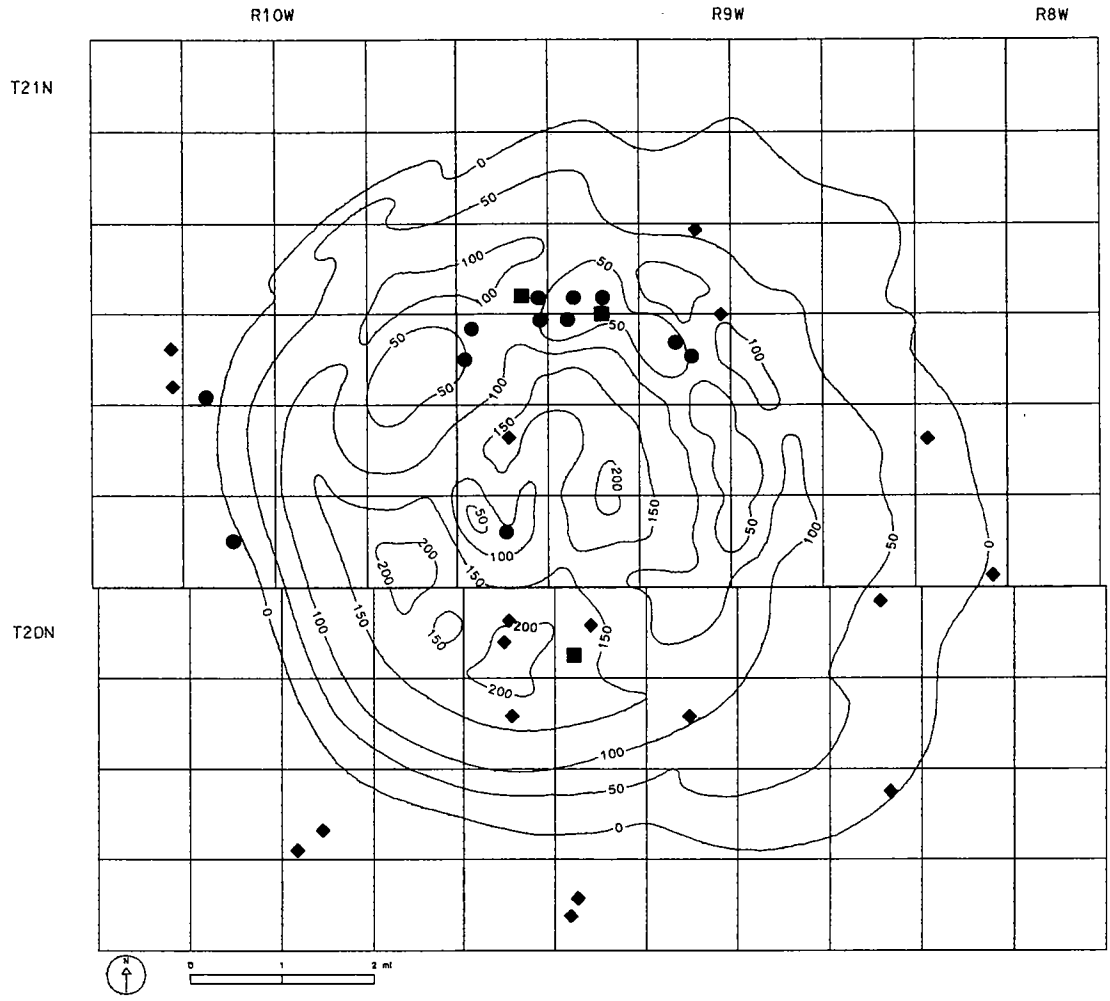

Figure 1. Distribution of crude-oil and source-rock samples throughout the Ames structure. Isopach map of the lower shale member of the Oil Creek Formation (in feet) prepared by M. Kuykendall; used with permission of R. Carlson (DLB).

final step computes the total mass of hydrocarbons generated:

$$HCG = R \times M \times 10^{-6} \quad (4)$$

In this study, calculations 2 through 4 are performed for each distinct source-rock section. The results are then summed to calculate total mass of hydrocarbons generated for the entire structure.

RESULTS AND DISCUSSION

Geochemical Investigation

The crude oils in this study fall into two groups: oils produced from Arbuckle reservoirs and those produced from shallower horizons (Table 2). GC-FID data clearly demonstrate chemical differences between these groups on the basis of relative iso-

TABLE 3.—AVAILABILITY OF PETROPHYSICAL INFORMATION

Operator	Well name	Logs available					Comments
		Gamma ray	Neutron	Micro-log	Latero-log	Sonic	
DLB	no. 28-9 Bierig	X	X	X	X		*
Universal Resources	no. 1-33 Bland	X	X	X	X		
R. E. Blaik	no. 1-14 Bohn	X	X	X	X		*
DLB	no. 20-2 Bullis	X	X	X	X		*
Bogo Energy	no. 3-35 Campbell	X	X	X	X		
Hazelwood	no. 10-1 Carolyn Sue	X	X	X			
DLB	no. 27-4 Cecil	X	X		X		*
Nicor	no. 18-4 Chestnut	X	X	X	X		
Ward	no. 1-1 Cleora	X	X	X		X	
DLB	no. 5-13 Darin	X	X	X			
Continental	no. 1-19 Dorothy	X	X	.	X	X	
Hazelwood	no. 2-2 Edwards	X	X				
DLB	no. 23-3 Elsie	X	X	X			
Continental	no. 6 Fisher	X	X	X	X	X	*
Continental	no. 1-31 Fred	X	X	X			
Miracle	no. 2-16 Fyffe	X	X	X	X	X	
BRG	no. 2-23 Gregory	X	X		X		*
Continental	no. 1-19 Heinrich	X	X	X			
D & J	no. 1-20 Herman	X	X	X	X		
D & J	no. 1-20 James	X	X	X	X		
DLB	no. 27-12 Jesse	X	X	X	X		*
Bromar Oil	no. 26-7 Jim	X	X	X			*
Cross Timbers	no. 1-10 Kennedy	X	X	X		X	
DLB	no. 14-1 Lillie	X	X	X			
D & J	no. 1-17 Mary Helen	X	X				
Continental	no. 2-26 Mason	X	X			X	*
Unknown	no. 36-4 Monsees	X	X	X			
J. L. Thomas	no. 1-9 Munkres	X	X	X	X	X	
Continental	no. 1-21 Stansberry	X	X	X	X	X	
Continental	no. 1-34 Terry	X	X	X	X		*

*Well logs do not penetrate lower member of the Oil Creek shale.

prenoid abundance and carbon-number preference (Figs. 3 and 4). These differences imply that the oils in the Hunton (Devonian) and younger reservoirs are not genetically related to the Oil Creek source facies and consequently not part of the Oil Creek–Arbuckle (!) petroleum system. Therefore, they were excluded from further analysis.

Within the oils in Arbuckle reservoirs, GC-FID analysis differentiates two subtypes (Fig. 5). Genetically, these oils are clearly related although the type A-2 oils have an enhanced abundance of low-molecular-weight (LMW or lower than nC_{15}) compounds and slightly depleted acyclic isoprenoid abundances. Geographically, the A-1 oils accumulated in the interior of the feature, whereas the A-2 oils occur on the rim. The enhanced concentration of the LMW fraction in the A-2 oils likely results from additional thermal stress required for hydrocarbon generation and expulsion. However, the oils appear strikingly similar if the profiles are normalized to the nC_{15} alkane (note internal standard). Noteworthy is the empirical relationship that type A-1 oils are associated with paraffin-related production problems. The reason for these problems is that the LMW compounds act as a natural solvent for these paraffins. When LMW compounds are present in lower abundance, the paraffin is prone to precipitation. In the Ames feature, chemical injectors with carbon disulfide combat these paraffin-

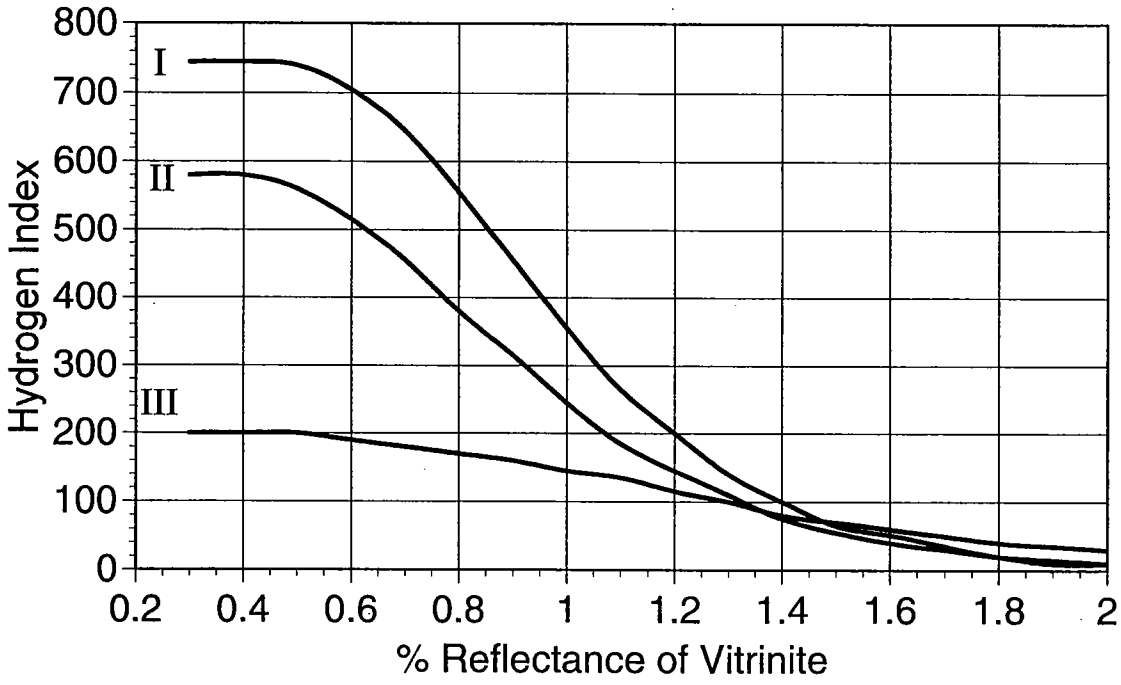

Figure 2. Change of hydrogen index with increasing maturity for types I, II, and III kerogen. (Courtesy of J. Quick; modified after Lo, 1995.)

related production problems (Mike Barnes, personal communication).

Significant features noted in the GC-MS analysis include the distribution of *n*-alkylcyclohexanes that exhibit a mixture of odd- and even-carbon preferences at different carbon numbers. Biomarker analyses indicate a terpane fraction dominated by tricyclic members (C_{23} and C_{24}). The trisnorhopane known as Tm appears to be preferred over Ts, but this apppearance is actually an artifact of a coeluting compound. Pentacyclic terpanes occur in low quantitative abundance, but show enhanced C_{29}Ts and C_{30} diahopanes. The methyl hopanes and demethylated hopanes can be considered absent. Steranes are in low quantitative abundance (sterane concentration average of 35 ppm), although the C_{28} members are relatively enhanced. C_{27} βα rearranged steranes are fairly abundant, and methyl steranes are only present in trace concentrations.

Correlation

The principle of oil–source-rock correlation hinges on the ability to formulate a converging argument by using bulk and specific parameters. Table 4 displays the results of the crude-oil bulk analysis; Table 5 the results of the rock bulk analysis. Chromatographically, the rock extract traces mimic those of the crude oils in the Arbuckle reservoirs. Collectively, the carbon isotopes (Fig. 6), GC-FID (Figs. 3 and 7), and GC-MS (Fig. 8) data support a genetic relationship between the lower shale member of the Oil Creek Formation and the crude oils in the Arbuckle reservoirs.

Maturity Analysis

Accurate assessment of a petroleum system's maturity state is critical to defining the generation and expulsion events and the migration and trapping events. The tools used to quantify maturity include a combination of chemical methods (biomarker-based isomerization reactions, thermal destruction of compound classes, Rock Eval pyrolysis) and optical methods (vitrinite reflectance, fluorescence character, thermal alteration indices). These techniques are integrated in this study to provide a collective maturity value of 1.2–1.3% Ro_{eq} at the base of the Oil Creek Formation. However, true vitrinite is not present in these samples since they predate the evolution of vascular plants. The reflecting particles that could be measured (Ro_{eq} = 1.09, n = 15) were small and sparse. Additional observations that support this maturity are the lack of fluorescence emission from the amorphous kerogen (Stach and others, 1982) and the presence of condensed gray amorphous matter (Castaño, 1995). Native bitumen was also reported to be sparse (J. Quick, personal communication).

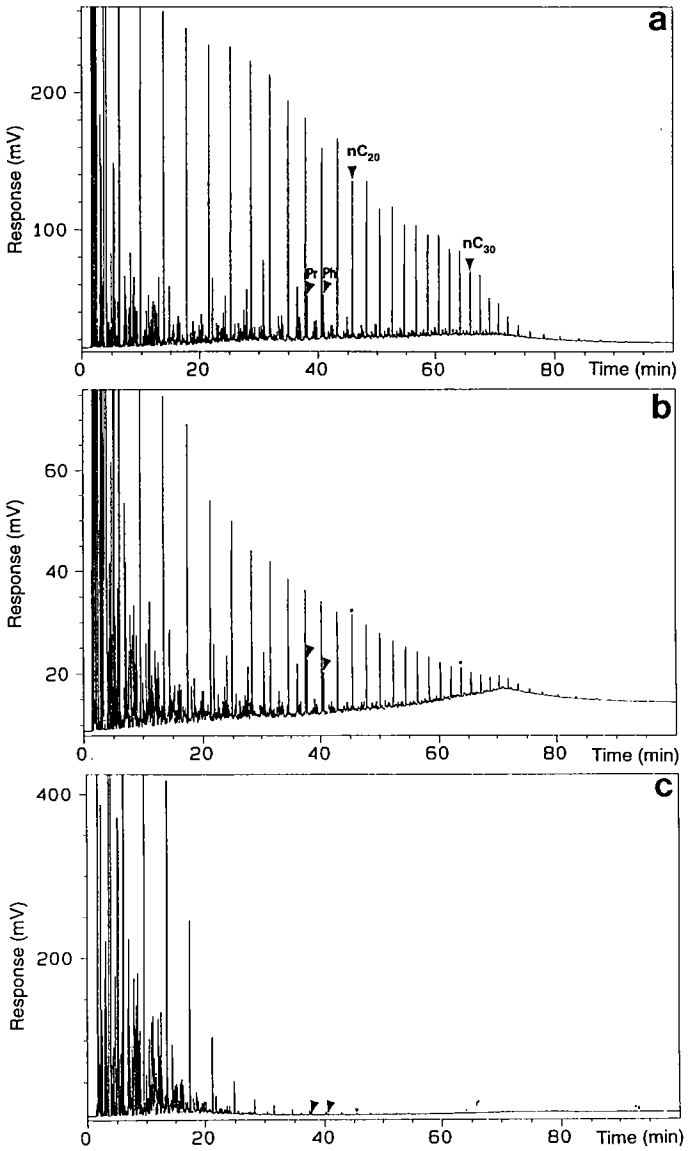

Figure 3. Typical GC-FID traces. *a*—Type A-1 crude oil. *b*—Crude oil in Hunton reservoirs. *c*—Crude oil in younger reservoirs.

Depositional Environment

Debate continues over whether the shale in the Oil Creek Formation is a lacustrine or marine shale. Traditionally, the observed features such as the odd-carbon preference (OCP) in the nC_{23} to nC_{31} range, the enhanced C_{28} steranes, and the enhanced paraffin content (Huang and Meinschein, 1979; Peters and Moldowan, 1993) have signified a lacustrine environment. However, these responses are also observed in marine depositional systems (Wavrek, unpublished), which is consistent with optical observations including abundant amorphous material, marine acritarchs, and skelecodonts (D. Englehardt, personal communication), along with abundant framboidal pyrite (J. Quick, personal communication).

Burial-History Modeling

Effective modeling for the generation and migration of hydrocarbons in the Ames feature requires knowledge of the sedimentation and tectonic and thermal history, as well as the distribution and quality of the organic matter within the feature. Synthesizing these variables generates an integrated basin model. This model establishes the timing of oil generation and expulsion from the major source rocks, documents the orientation of major migration pathways responsible for the hydrocarbon charge, and aids in the recognition of undiscovered oil reserves (Waples, 1980).

Figure 9 shows the burial-history chart for the no. 1-19 Chet well, with oil windows superimposed. The lower shale member of the Oil Creek Formation is located at the bottom of the Simpson Group. This unit entered the early-mature oil window at 280 Ma and remained in it until 254 Ma. From 254 to 206.8 Ma, the source facies remained in the peak oil-generation window, and the critical moment (i.e., when the bulk of the petroleum was generated and expelled from the source rock) was at 225 Ma. Subsequent late oil generation lasted until the present, with a calculated maturity of 1.34% Ro_{eq} at the base of the Oil Creek shale. Although this calculated maturity is consistent with the value observed from actual analyses, it does conflict with other data in the region (Cardott, 1989). The rationale for the discrepancy can be resolved with additional analyses of vertical maturity profiles within the Ames region.

Figure 10 shows a cross section of the Ames feature at the critical moment. Figure 11 shows the geographic extent of the petroleum system at the critical moment. No hydrocarbon accumulations and migration pathways are shown in Figure 11 since expulsion was downward and into the underlying Arbuckle reservoir. The events chart (Fig. 12) chronicles the development of the Oil Creek–Arbuckle (!) petroleum system through time. The table of related accumulations is covered by the summary offered by Evans (1997) of the petroleum

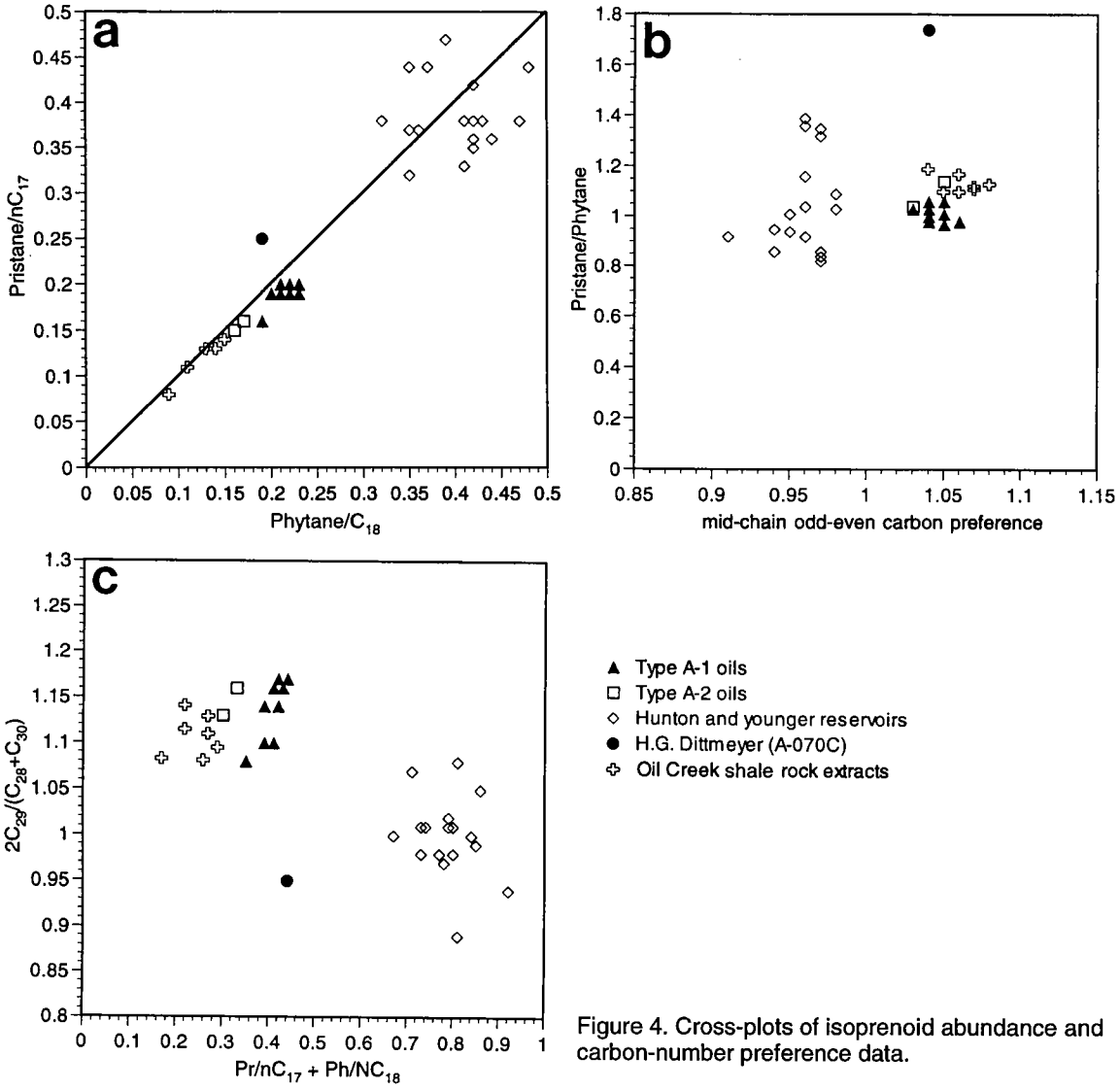

Figure 4. Cross-plots of isoprenoid abundance and carbon-number preference data.

accumulations associated with this petroleum system.

Petrophysical Investigation

Petroleum geologists have long sought a method to identify potential source rocks through well-log analysis. Initial attempts dating back to the mid-1940s concentrated on single logging tool methods (e.g., Schmoker, 1981; Herron and Le Tendre, 1990; Herron and others, 1988; Hester and others, 1990; Schmoker and Hester, 1989,1990; and references therein). Difficulties arose, however, because inherent source-rock characteristics (i.e., sulfur content) adversely affected log response, which limited application. Therefore, several methods using combined logging tools were developed, including the sonic and resistivity overlay method of Passey and others (1990) employed in this study.

The purpose of this investigation is to estimate source-rock volume and organic carbon richness throughout the structure. Units containing significant organic matter display a distinct Δ log R separation (Fig. 13). Unfortunately, this separation could not be calibrated owing to a lack of sonic logs in wells for which TOC data were available for this study. Consequently, the Δ log R response was compared to nearby wells (approximately 2,000 ft away) for which TOC data were available.

Volume Estimates and Organic Richness

The rock samples and well-log response data indicate a systematic variation in organic richness within the Ames feature. Therefore, to proceed

TABLE 4.—SUMMARY OF CRUDE-OIL BULK ANALYSIS DATA

Sample	Relative density	API gravity	wt% sulfur	Carbon isotopes	
				Saturate	Aromatic
A-049C	0.830	38.2	0.05	–31.4	–30.8
A-050C	0.834	37.4	0.00		
A-051C	0.827	38.8	0.05		
A-052C	0.829	38.4	0.05		
A-053C	0.825	39.2	0.04		
A-054C	0.829	38.4	0.04		
A-055C	0.828	38.6	0.03		
A-056C	0.824	39.4	0.00		
A-057C	0.827	38.8	0.02		
A-058C	0.817	40.9	0.02		
A-059C	0.829	38.4	0.06		
A-060C	0.8793	46.1	0.02	–31.0	–30.3

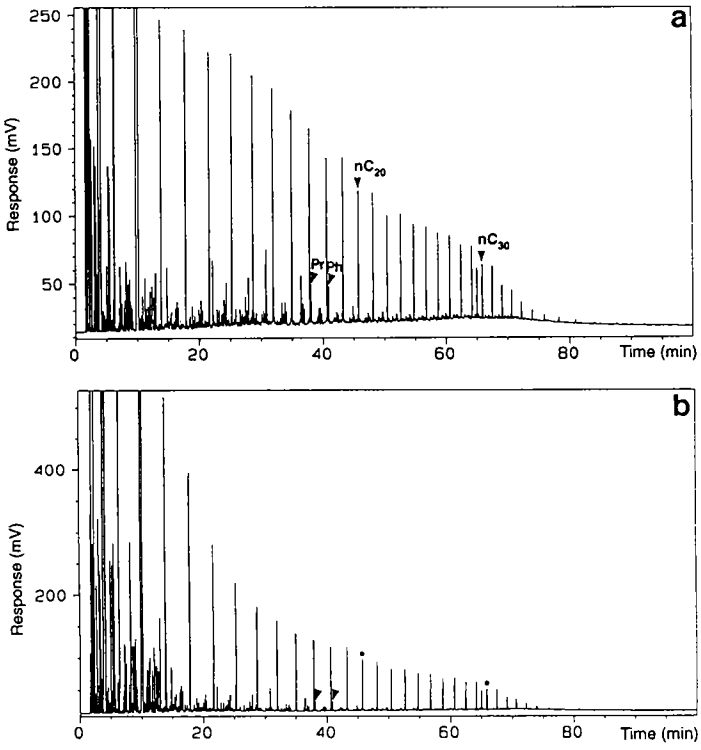

Figure 5. GC-FID traces showing crude oil types. *a*—Type A-1 crude oil. *b*—Type A-2 crude oil, found in the Arbuckle Group reservoirs. The internal standard is the peak eluting prior to nC_{30}.

with the analysis, the source rock was divided into three sections; within each, the TOC was approximately constant (see Fig. 14). In section A (where the source rock has a thickness of 75 to 225 ft), the source rock appears uniformly very lean with an average TOC of 0.3 wt%. In the southern half of the feature, the source rock making up section B (thickness of 0 to 75 ft) has an average TOC of 0.25 wt%. In the northern flank of the feature, section C source rock (also with a thickness of 0 to 75 ft) displays an increased TOC that averages 1.2 wt%.

Generation Accumulation Efficiency

The parameters used to calculate these efficiencies are most easily understood in an organic carbon mass-balance framework. At any given time during hydrocarbon migration from source rock to trap, all of the organic carbon originally deposited in the source rock can be accounted for by totaling (1) the residual hydrocarbons in the source rock after generation and expulsion (Price and others, 1984; Price and Lefever, 1992), (2) the hydrocarbon losses along the migration pathway (England, 1994; England and others, 1987; Mackenzie and Quigley, 1988), and (3) the known and undiscovered hydrocarbon reserves (England, 1994).

Table 6 identifies the lithologically distinct sections and summarizes the calculated HCG values. IHC are the hydrocarbons trapped and approximately equal the reserve estimates. Kuykendall and others (1997) estimated the reserves to be 50 MMBO + 3.1 MMBOeq of gas. From these values, the following efficiency parameters can be calculated:

$$\begin{aligned} GAE &= [IHC/HCG] \times 100\% \\ &= [53.1\ MMBO/145\ MMBO] \\ &\quad \times 100\% \\ &= 36.6 \approx 37\% \end{aligned}$$

The generation accumulation efficiency (GAE) is a particularly useful parameter in economic assessments. By quantifying the efficiency with which a petroleum system accumulates hydrocarbons, the explorationist can better assess a basin's

TABLE 5.—SUMMARY OF SOURCE-ROCK BULK ANALYSIS DATA

Sample no.	TOC	S1	S2	S3	Tmax	HI	OI	S1/TOC	S2/S3	PI*	TGP*	RCI*	Carbon isotopes: Saturate	Carbon isotopes: Aromatic
MC008R	0.50	0.11	0.24	0.37	424 L	48	74	0.22	0.65	0.31	0.35	7.00		
MC009R	0.50	0.11	0.28	0.33	421 L	56	66	0.22	0.85	0.28	0.39	7.80		
MC010R	0.47													
MC011R	0.80	0.31	0.63	0.31	434	79	39	0.39	2.03	0.33	0.94	11.75		
MC012R	1.36	0.79	1.73	0.31	443	127	23	0.58	5.58	0.31	2.52	18.53		
MC013R	1.25	0.81	1.69	0.29	443	135	23	0.65	5.83	0.32	2.50	20.00		
MC014R	1.13	0.88	1.68	0.32	438	149	28	0.78	5.25	0.34	2.56	22.65		
MC015R	1.05	0.75	1.45	0.35	440	138	33	0.71	4.14	0.34	2.20	20.95		
MC016R	1.04	0.70	1.37	0.34	437	132	33	0.67	4.03	0.34	2.07	19.90		
MC017R	1.62	1.14	2.63	0.38	444	162	23	0.70	6.92	0.30	3.77	23.27		
MC018R	1.94	1.59	3.2	0.32	442	165	16	0.82	10.00	0.33	4.79	24.69	–30.7	–30.1
MC019R	1.03	0.40	0.98	0.31	436	95	30	0.39	3.16	0.29	1.38	13.40		
MC020R	1.70	1.56	3.67	0.35	447	216	21	0.92	10.49	0.30	5.23	30.76		
MC021R	1.74	1.35	3.76	0.36	447	216	21	0.78	10.44	0.26	5.11	29.37		
MC022R	1.58	0.57	2.52	0.26	445	159	16	0.36	9.69	0.18	3.09	19.56		
MC023R	1.60	1.60	4.47	0.34	444	279	21	1.00	13.15	0.26	6.07	37.94		
MC024R	1.61	1.58	4.16	0.25	446	258	16	0.98	16.64	0.28	5.74	35.65		
MC025R	1.76	1.78	4.43	0.32	445	252	18	1.01	13.84	0.29	6.21	35.28		
MC026R	1.18	1.24	3.21	0.24	443	272	20	1.05	13.38	0.28	4.45	37.71		
MC027R	1.26	1.08	3.27	0.37	444	260	29	0.86	8.84	0.25	4.35	34.52		
MC028R	1.46	1.06	3.91	0.28	446	268	19	0.73	13.96	0.21	4.97	34.04		
MC029R	1.90	1.15	4.7	0.22	449	247	12	0.61	21.36	0.20	5.85	30.79		
MC030R	0.83	0.72	2.57	0.2	442	247	32	0.89	7.83	0.27	2.45	33.56		
MC031R	0.79	0.71	2.01	0.32	438	254	41	0.90	6.28	0.26	2.72	34.43		
MC032R	0.73	0.65	1.8	0.23	442	247	32	0.89	7.83	0.27	2.45	33.56		
MC033R	0.68	0.69	2.04	0.22	433	300	32	1.01	9.27	0.25	2.73	40.15		
MC034R	0.67	0.57	1.64	0.37	435	245	55	0.85	4.43	0.26	2.21	32.99		
MC035R	0.56	0.42	1.5	0.26	438	268	46	0.75	5.77	0.22	1.92	34.29		
MC036R	2.42	0.81	3.82	0.21	450	158	9	0.33	18.19	0.17	4.63	19.13		
MC037R	0.45													
MC038R	0.36													
MC039R	0.29													
MC040R	0.27													
MC041R	0.12													
MC042R	0.11													
MC043R	0.13													
MC044R	0.07													
MC045R	0.24													
MC046R	0.25													
MC047R	0.23													
MC048R	0.27													
MC049R	0.31													
MC050R	0.29													
MC051R	0.30													
MC052R	0.32													
MC053R	0.31													
MC054R	0.35													

* PI = S1/(S1 + S2)
TGP = S1 + S2
RCI = 10 × (S1 + S2)/TOC

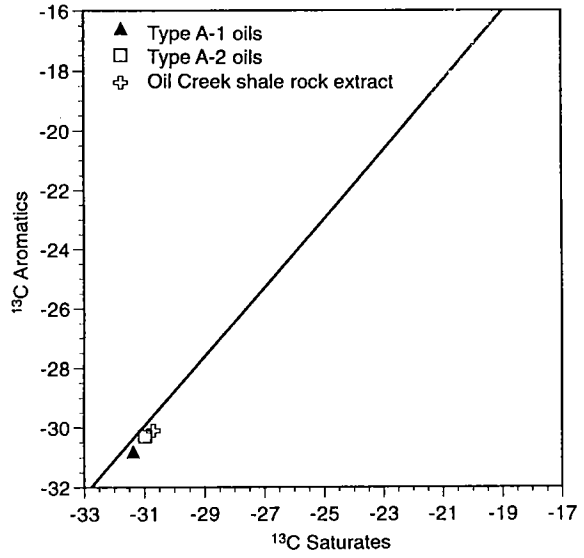

Figure 6. Sofer plot showing $\delta^{13}C$ values (in ‰ relative to PDB [Peedee belemnite] standard) of saturate and aromatic fractions of rock extract and crude oils. Line shows best separation between marine environments (below) and nonmarine environments (above), as established by Sofer (1984). Graph axes represent global variation for crude oils.

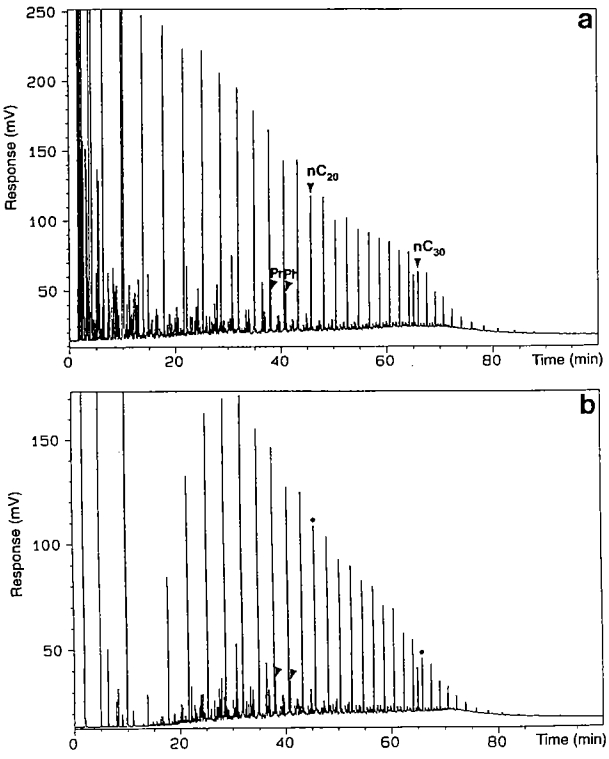

Figure 7. GC-FID traces. *a*—Crude oil in Arbuckle reservoir. *b*—Genetically related source rock from lower shale member of the Oil Creek Formation.

hydrocarbon potential. Large petroleum systems or multiple petroleum systems within a basin increase the likelihood of finding commercial hydrocarbon deposits (Magoon and Dow, 1994). The generation accumulation efficiency calculated shows that 37% (53 MMBO) of the 145 MMBO generated by the lower shale member of the Oil Creek Formation were trapped. The 92 MMBO remnant comprises hydrocarbons that were either not trapped or remain undiscovered (Fig. 15). The calculated GAE appears comparable to similar mass-balance calculations within petroleum systems on a global basis (Hunt, 1996).

The current thought within the petroleum industry is that little new oil will be discovered in the Ames feature (Evans, 1997). In contrast, we view the Ames petroleum system more optimistically, and we anticipate that a clearer understanding of the Arbuckle reservoir will yield additional reserves. This optimism is based upon the limited geographic extent and an advanced knowledge of the elements and processes of this petroleum system. Although this study shows that there was no vertical migration of oils from the Oil Creek source-rock facies, lateral migration was not investigated. Further research on oils updip from the Ames feature may provide insight into the fate of the missing 92 MMBO.

ACKNOWLEDGMENTS

We thank W. H. Kanes of the Energy & Geoscience Institute, University of Utah, for the opportunity to pursue this fundamental research and for one of us (D. K. C.) to attend the Ames workshop in March 1995. Numerous people provided data and welcome suggestions: Richard Bottjer of Amoco Production Company, Denver, Colorado; Michael Kuykendall of Solid Rock Resources, Tulsa, Oklahoma; Ken Johnson of the Oklahoma Geological Survey, Norman, Oklahoma; Rick Carlson of DLB; Jim Evans of Ward Petroleum; Dan Jarvie and Jack Burgess of Humble Instruments and Services, Humble, Texas; Jeff Quick, Jim Collister, and Nic Dahdah of the Energy & Geoscience Institute, University of Utah, Salt Lake City, Utah; Don Englehardt of the University of South Carolina, Columbia, South Carolina; Craig Roberts, Bob Sandridge, and Mike Barnes of Continental Resources; and Bruce Carpenter of Log Experts, among many others. We thank you all. Without your collective cooperation, this type of research would never be achieved.

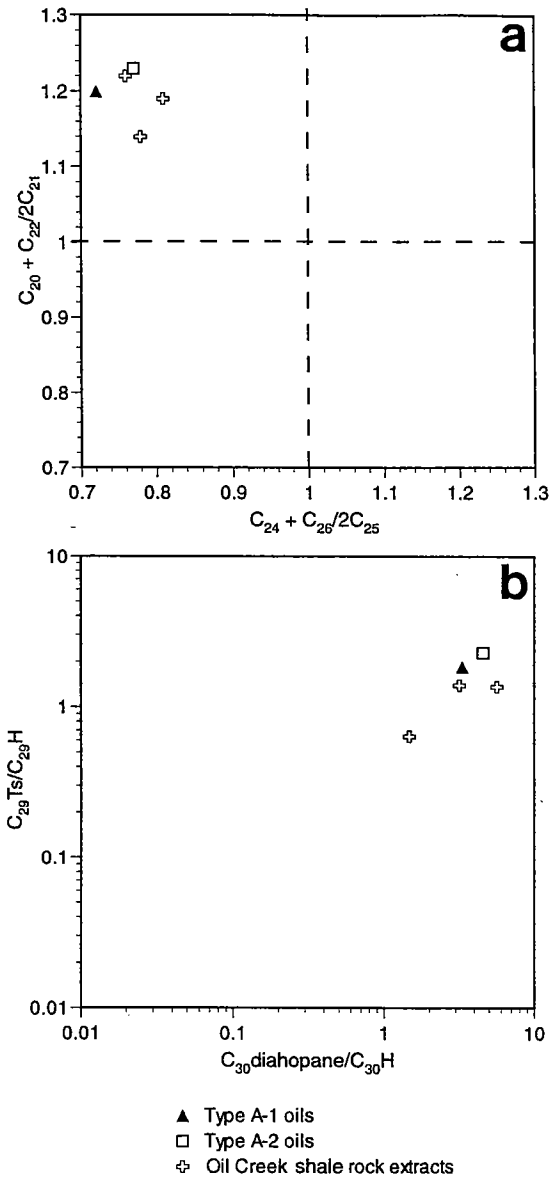

Figure 8. *a*—Cross-plot of the even- vs. odd-carbon preferences for the *n*-alkylcyclohexanes (*m/z* 82) in rock extracts and crude oils. *b*—Cross-plot of the C_{30} diahopane/C_{30} hopane ratio vs. the $C_{29}Ts/C_{29}$ hopane ratio for rock extracts and crude oils. Axes represent range of variation on global basis.

REFERENCES CITED

Baldwin, B.; and Butler, C. O., 1985, Compaction curves: American Association of Petroleum Geologists Bulletin, v. 69, p. 622–626.

Barker, C., 1972, Aquathermal pressuring—role of temperature in development of abnormal pressure zones: American Association of Petroleum Geologists Bulletin, v. 29, p. 1–22.

Bridges, L. W. D., 1997, Ames depression, Oklahoma: domal collapse and later subsurface solution, *in* Johnson, K. S.; and Campbell, J. A. (eds.), Ames structure in northwest Oklahoma and similar features: origin and petroleum production (1995 symposium): Oklahoma Geological Survey Circular 100 [this volume], p. 153–168.

Burnham, A. K.; and Sweeney, J. J., 1991, Modeling the maturation and migration of petroleum, *in* Merrill, R. K. (ed.), Source and migration processes and evaluation techniques: American Association of Petroleum Geologists Treatise of Petroleum Geology, p. 55–63.

Cardott, B. J., 1989, Thermal maturation of the Woodford Shale in the Anadarko basin, *in* Johnson, K. S. (ed.), Anadarko basin symposium, 1988: Oklahoma Geological Survey Circular 90, p. 32–43.

Carpenter, B. N.; and Carlson, Rick, 1992, The Ames impact crater: Oklahoma Geology Notes, v. 52, p. 208–223.

_____ 1997, The Ames meteorite-impact crater, *in* Johnson, K. S.; and Campbell, J. A. (eds.), Ames structure in northwest Oklahoma and similar features: origin and petroleum production (1995 symposium): Oklahoma Geological Survey Circular 100 [this volume], p. 104–119.

Castaño, J. R., 1995, TSOP microscopy workshop, Woodlands, Texas, 27 August, 1995; handouts with lecture.

Coughlon, J. P.; and Denney, P. P., 1993, The Ames structural depression: an endogenic cryptoexplosion feature along a transverse shear: Shale Shaker, v. 43, no. 4, p. 44–58.

_____ 1997, The Ames structure and other North American cryptoexplosion features: evidence for endogenic emplacement, *in* Johnson, K. S.; and Campbell, J. A. (eds.), Ames structure in northwest Oklahoma and similar features: origin and petroleum production (1995 symposium): Oklahoma Geological Survey Circular 100 [this volume], p. 133–152.

Curtiss, D. K., 1995, The Oil Creek–Arbuckle (!) petroleum system, Major County, Oklahoma: University of South Carolina, Earth Sciences and Resources Institute, unpublished Master of Earth Resources Management thesis, 274 p.

Demaison, G. J.; and Huizinga, B. J., 1991, Genetic classification of petroleum systems: American Association of Petroleum Geologists Bulletin, v. 75, p. 1626–1643.

_____ 1994, Genetic classification of petroleum systems, *in* Magoon, L. B.; and Dow, W. G. (eds.), The petroleum system—from source to trap: American Association of Petroleum Geologists Memoir 60, p. 73–89.

England, W. A., 1994, Secondary migration and accumulation of hydrocarbons, *in* Magoon, L. B.; and Dow, W. G. (eds.), The petroleum system—from source to trap: American Association of Petroleum Geologists Memoir 60, p. 211–217.

England, W. A.; Mackenzie, A. S.; Mann, D. M.; and Quigley, T. M., 1987, The movement of entrapment of petroleum in the subsurface: Journal of

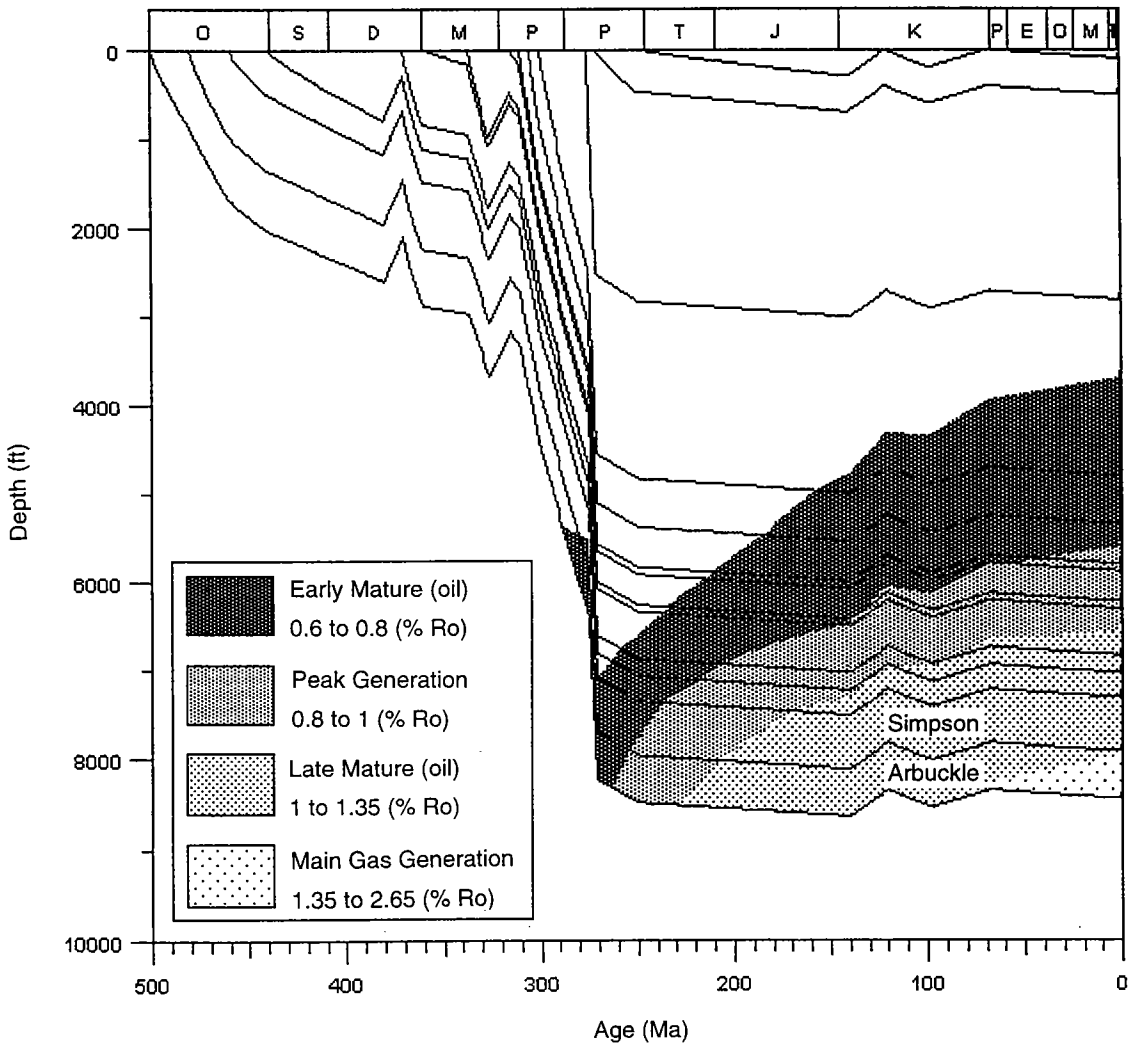

Figure 9. Burial-history reconstruction showing the maturation status for source-rock intervals in the no. 1-19 Chet well. Maturity levels are based on TTI maturity calculations.

the Geological Society (London), v. 144, p. 327–347.

England, W. A.; Mann A. L.; and Mann, D. M., 1991, Migration from source to trap, *in* Merrill, R. K. (ed.), Source and migration processes and evaluation techniques: American Association of Petroleum Geologists Treatise of Petroleum Geology, p. 23–46.

Evans, Jim, 1997, Historical development and production of the Arbuckle and exotic lithologies in the Ames structure, Oklahoma, *in* Johnson, K. S.; and Campbell, J. A. (eds.), Ames structure in northwest Oklahoma and similar features: origin and petroleum production (1995 symposium): Oklahoma Geological Survey Circular 100 [this volume], p. 207–213.

Fruth, I.; and Scherreiks, R., 1984, Hauptdolomit—sedimentary and paleogeographic models: Geologische Rundschau, v. 73, p. 305–319.

Gallardo, J. D., 1989, Empirical model of temperature structure, Anadarko basin, Oklahoma: Southern Methodist University unpublished M.S. thesis, 186 p.

Hamm, H.; and Olsen, R. E., 1992, Oklahoma Arbuckle lime exploration centered on buried astrobleme structure: Oil and Gas Journal, April 20, p. 113–116.

Haq, B. U.; and van Eysinga, F. W. B., 1987, Geological time table [4th edition]: Elsevier, New York, 1 p.

Herron, S. L.; and Le Tendre, L., 1990, Wireline source rock evaluation in the Paris basin, *in* Huc, A. Y. (ed.), Deposition of organic facies: American Association of Petroleum Geologists Studies in Geology, v. 30, p. 57–71.

Herron, S. L.; Le Tendre, L.; and Dufour, M., 1988, Source rock evaluation using geochemical information from wireline logs and cores [abstract]:

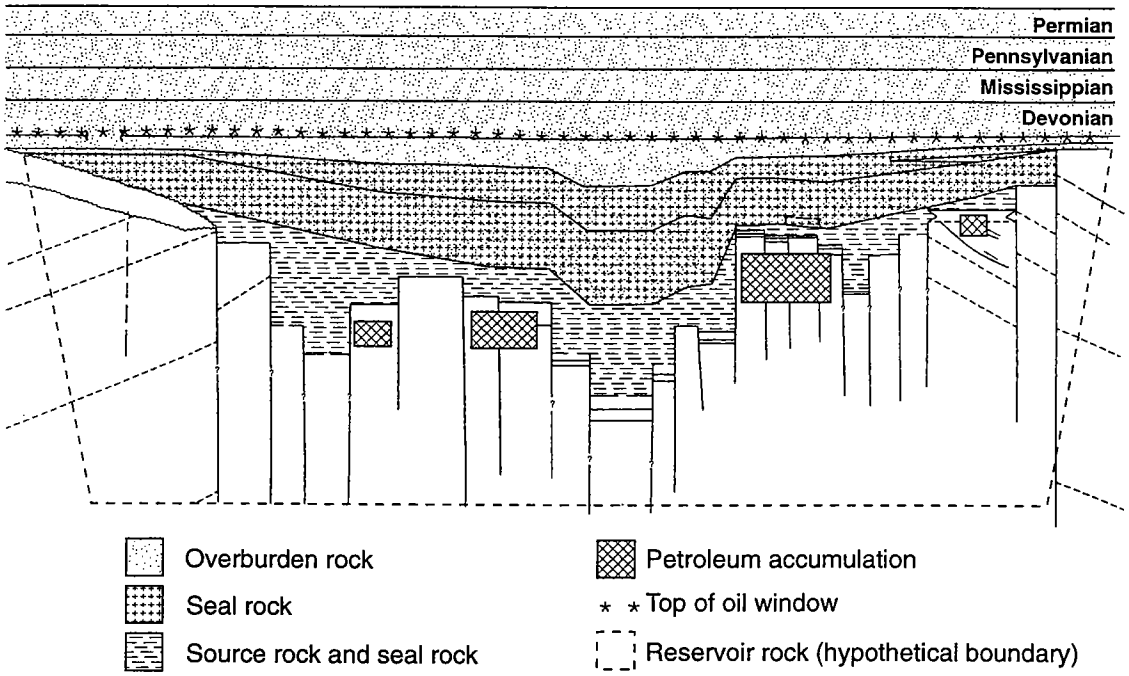

Figure 10. Two-dimensional "time-slice" of the Ames feature at the critical moment (225 Ma). The Devonian and younger section (≈7,000 ft thick) is not to scale. The petroleum accumulations are adjacent to downdropped structures.

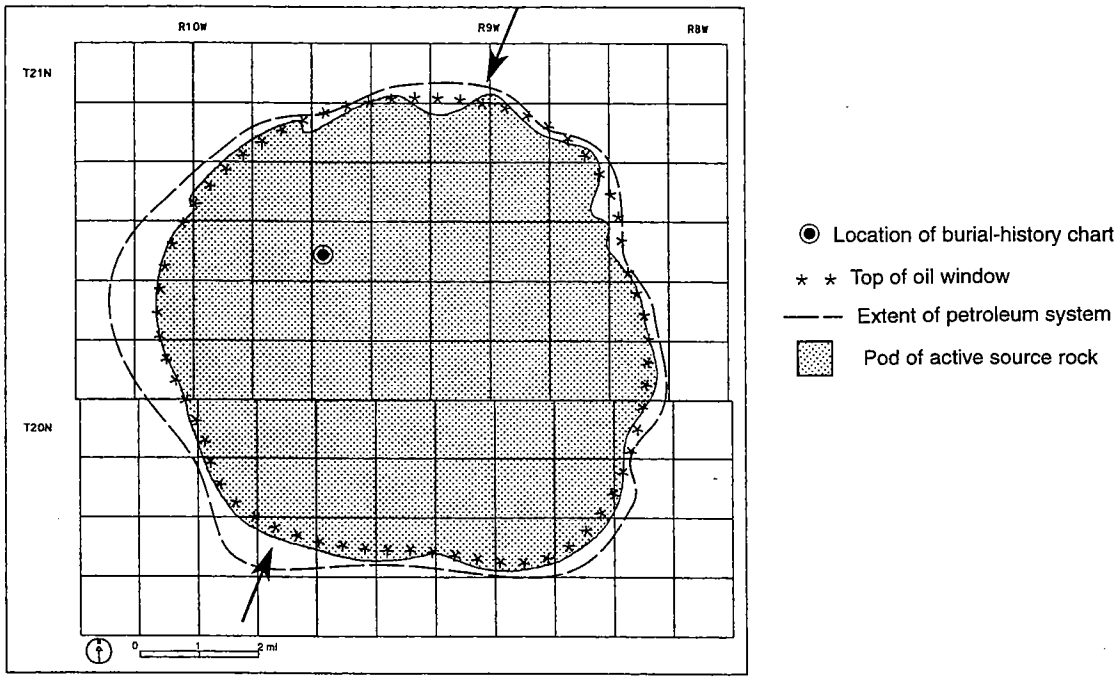

Figure 11. Map showing the geographic extent of the petroleum system at the critical moment.

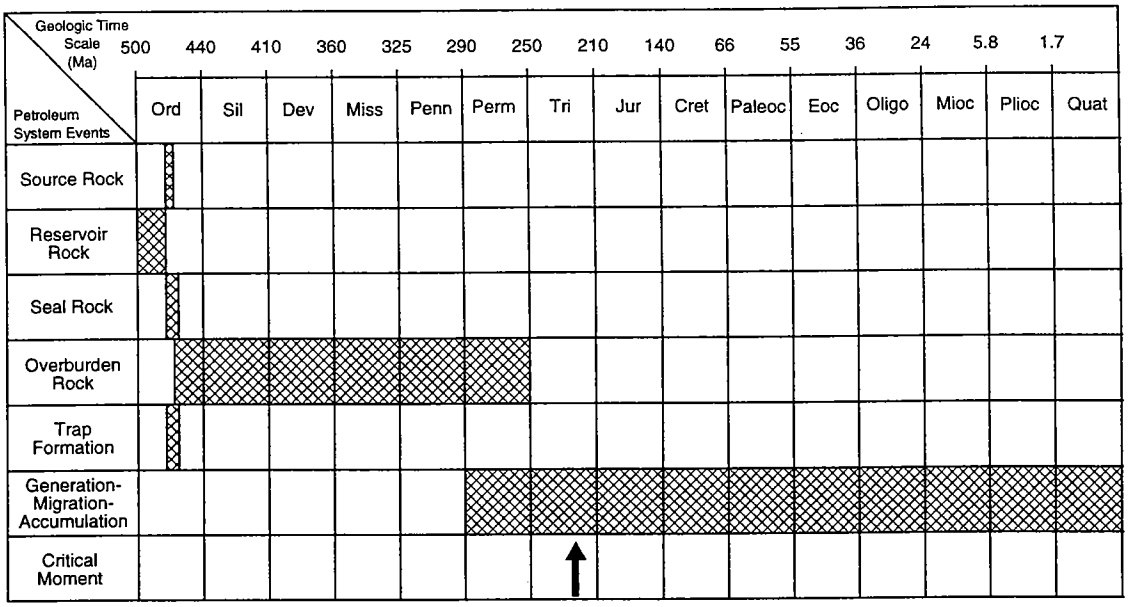

Figure 12. Events chart summarizing the history of the petroleum system.

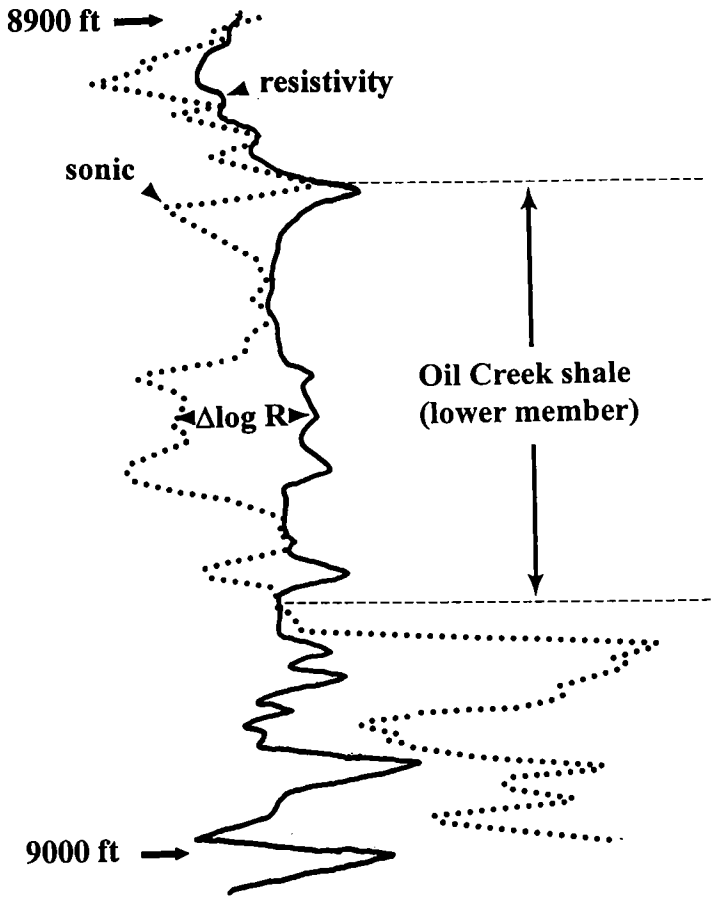

Figure 13. Sonic and resistivity overlay for a section in the Continental Resources Inc. no. 1-19 Dorothy well, showing organic-rich intervals throughout the lower shale member of the Oil Creek Formation.

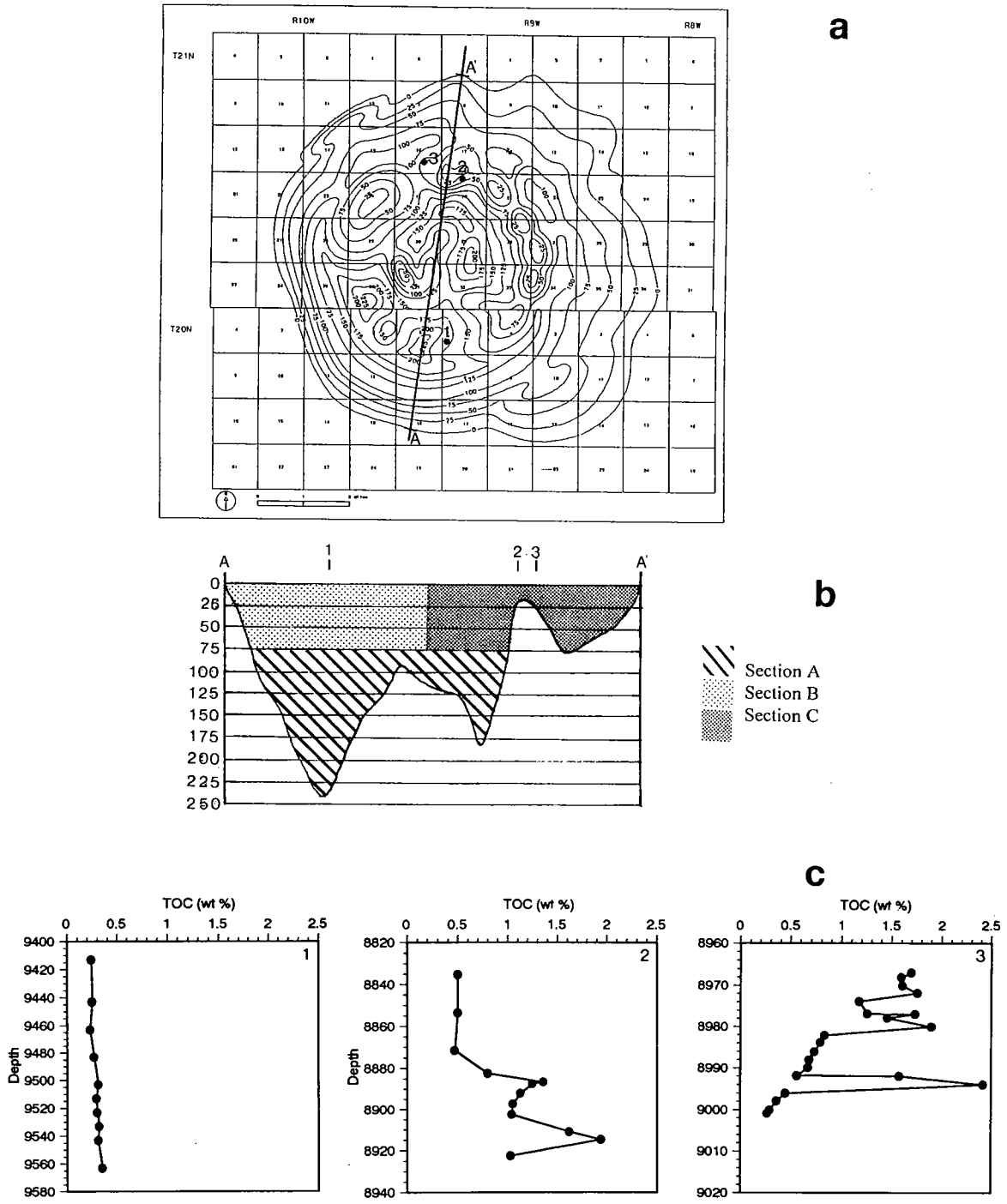

Figure 14. Organic richness distribution in the Ames feature based on a cross section (b) of the Oil Creek Formation (lower shale member) isopach map (a) combined with TOC profiles (c) for the three wells (DLB Darin 5-13 [1], D & J James 1-20 [2], and Nicor Chestnut 18-4 [3]) from which sample suite was obtained.

TABLE 6.—SUMMARY OF PARAMETERS NEEDED FOR CALCULATIONS OF GENERATION ACCUMULATION EFFICIENCY (GAE)

GAE parameters	Lithologic sections			Total
	A	B	C	
Average TOC (wt%)	0.31	0.25	1.18	
Average density (g/cm^3)	2.63	2.62	2.62	
Volume (cm^3)	1.10×10^{10}	1.51×10^{10}	1.09×10^{10}	3.70×10^{10}
M (g TOC)	8.97×10^{12}	9.89×10^{12}	3.37×10^{13}	5.26×10^{13}
HI_o (mg HC/g TOC)	420	400	580	
HI_p (mg HC/g TOC)	107	93.5	171.3	
R (mg HC/g TOC)	313	306.5	408.7	
HCG (kg HC)	2.81×10^9	3.03×10^9	1.38×10^{10}	1.96×10^{10}

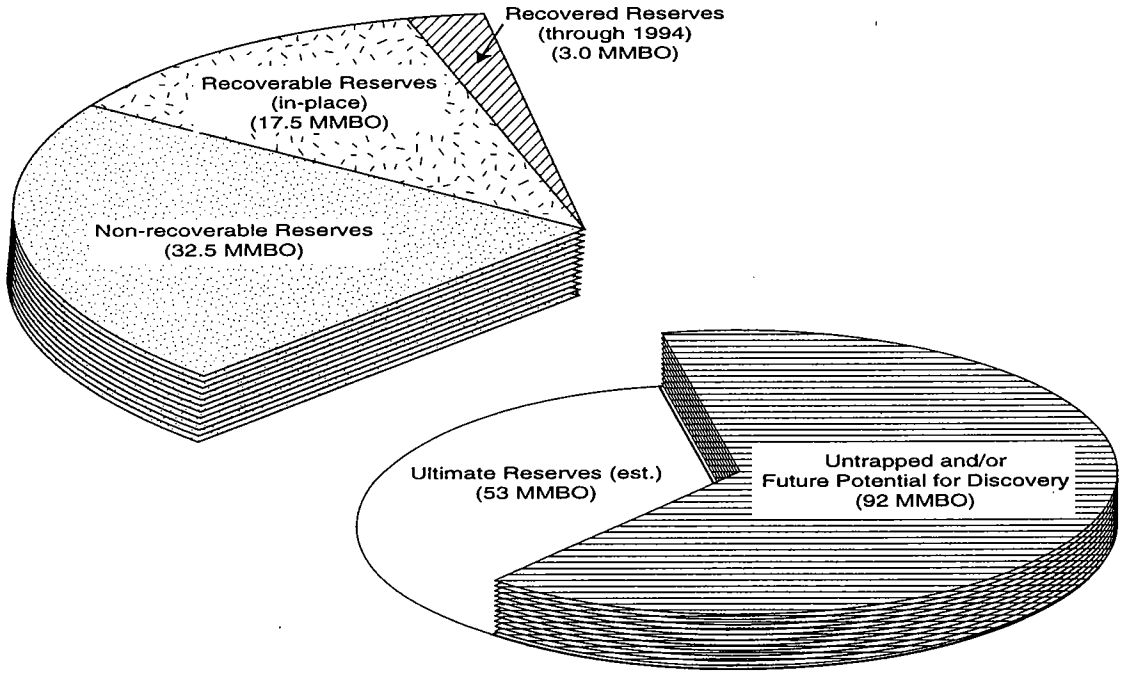

Figure 15. Pie chart showing present distribution of total hydrocarbons generated in the Ames feature.

American Association of Petroleum Geologists Bulletin, v. 72, p. 1007.

Hester, T. C.; Schmoker, J. W.; and Sahl, H. L., 1990, Log-derived regional source-rock characteristics of the Woodford Shale, Anadarko basin, Oklahoma: U.S. Geological Survey Bulletin 1866-D, 38 p.

Horsfield, B.; and Rullkötter, J., 1994, Diagenesis, catagenesis, and metagenesis of organic matter, *in* Magoon, L. B.; and Dow, W. G. (eds.), The petroleum system—from source to trap: American Association of Petroleum Geologists Memoir 60, p. 189–200.

Huang, W.-Y.; and Meinschein, W. G., 1979, Sterols as ecological indicators: Geochimica et Cosmochimica Acta, v. 43, p. 739–745.

Hunt, J. M., 1996, Petroleum geochemistry and geology [2nd edition]: Freeman, New York, 743 p.

Koeberl, Christian, 1997, Impact cratering: the mineralogical and geochemical evidence, *in* Johnson, K. S.; and Campbell, J. A. (eds.), Ames structure in northwest Oklahoma and similar features: origin and petroleum production (1995 symposium): Oklahoma Geological Survey Circular 100 [this volume], p. 30–54.

Koeberl, Christian; Reimold, W. U.; Brandt, Dion; Dallmeyer, R. D.; and Powell, R. A., 1997, Target

rocks and breccias from the Ames impact structure, Oklahoma: petrology, mineralogy, geochemistry, and age, *in* Johnson, K. S.; and Campbell, J. A. (eds.), Ames structure in northwest Oklahoma and similar features: origin and petroleum production (1995 symposium): Oklahoma Geological Survey Circular 100 [this volume], p. 169–198.

Köster, J.; Wehner, H.; and Hufnagel, H., 1988, Organic geochemistry and organic petrology of organic rich sediments within the "Hauptdolomit" formation (Triassic, Norian) of the northern Calcareous Alps: Organic Geochemistry, v. 13, p. 377–386.

Kuykendall, M. D.; Johnson, C. L.; and Carlson, R. A., 1997, Reservoir characterization of a complex impact structure: Ames impact structure, northern shelf, Anadarko basin, *in* Johnson, K. S.; and Campbell, J. A. (eds.), Ames structure in northwest Oklahoma and similar features: origin and petroleum production (1995 symposium): Oklahoma Geological Survey Circular 100 [this volume], p. 199–206.

Lewan, M. D., 1994, Assessing natural oil expulsion from source rocks by laboratory pyrolysis, *in* Magoon, L. B.; and Dow, W. G. (eds.), The petroleum system—from source to trap: American Association of Petroleum Geologists Memoir 60, p. 201–210.

Lo, H. B., 1995, Maturity assessment from suppressed vitrinite reflectance: TSOP microscopy workshop, Woodlands, Texas, 27 August, 1995; handouts with lecture.

Lopatin, N. V., 1971, Temperature and geologic time as factors in coalification [in Russian]: Akademiya Nauk SSSR Izvestiya, Seriya Geologicheskaya, Moscow, no. 3, p. 95–106.

Mackenzie, A. S.; and Quigley, T. M., 1988, Principles of geochemical prospect appraisal: American Association of Petroleum Geologists Bulletin, v. 72, p. 399–415.

Magoon, L. B.; and Dow, W. G., 1994, The petroleum system, *in* Magoon, L. B.; and Dow, W. G. (eds.), The petroleum system—from source to trap: American Association of Petroleum Geologists Memoir 60, p. 3–24.

Magoon, L. B.; and Sánchez, R. M. O., 1995, Beyond the petroleum system: American Association of Petroleum Geologists Bulletin, v. 79, p. 1731–1736.

Momper, J. A., 1978, Oil migration limitations suggested by geological and geochemical considerations, *in* Roberts, W. H.; and Cordell, R. J. (eds.), Physical and chemical constraints on petroleum migration: American Association of Petroleum Geologists Course Note Series, no. 8, p. 1–60.

Passey, Q. R.; Creaney, S.; Kulla, J. B.; Moretti, F. J.; and Stroud, J. D., 1990, A practical method for organic richness from porosity and resistivity logs: American Association of Petroleum Geologists Bulletin, v. 74, p. 1777–1794.

Peters, K. E.; and Moldowan, J. M., 1993, The biomarker guide: interpreting molecular fossils in petroleum and ancient sediments: Prentice-Hall, Englewood Cliffs, New Jersey, 363 p.

Price, L. C.; and LeFever, J. A., 1992, Does Bakken horizontal drilling imply a huge oil-resource base in fractured shales?, *in* Schmoker, J. W.; Coalson, E. B.; and Brown, C. A. (eds.), Geological studies relevant to horizontal drilling: examples from western North America: Rocky Mountain Association of Geologists, Denver, p. 199–214.

Price, L. C.; Ging, T.; Daws, T.; Love, A.; Pawlewicz, M.; and Anders, D., 1984, Organic metamorphism in the Mississippian–Devonian Bakken Shale, North Dakota portion of the Williston basin, *in* Woodward, J.; Meissner, F. F.; and Clayton, J. L. (eds.), Hydrocarbon source rocks of the greater Rocky Mountain region: Rocky Mountain Association of Geologists, Denver, p. 83–133.

Roemer C. D.; Roemer, C.; and Williams, K., 1992, Gravity, magnetics point to volcanic origin for Oklahoma's Ames anomaly: Oil and Gas Journal, June 29, p. 75–80.

Schmoker, J. W., 1981, Determination of organic matter content of Appalachian Devonian shales from gamma-ray logs: American Association of Petroleum Geologists Bulletin, v. 65, p. 1285–1298.

_____ 1986, Oil generation in the Anadarko basin, Oklahoma and Texas: modeling using Lopatin's method: Oklahoma Geological Survey Special Publication 86-3, 40 p.

_____ 1994, Volumetric calculation of hydrocarbons generated, *in* Magoon L. B.; and Dow, W. G. (eds.), The petroleum system—from source to trap: American Association of Petroleum Geologists Memoir 60, p. 323–326.

Schmoker, J. W.; and Hester, T. C., 1989, Oil generation inferred from formation resistivity—Bakken Formation, Williston basin, North Dakota: Transactions of the 30th SPWLA [Society of Professional Well Log Analysts] Annual Logging Symposium, paper H.

_____ 1990, Formation resistivity as an indicator of oil generation—Bakken Formation of North Dakota and Woodford Shale of Oklahoma: The Log Analyst, v. 31, p. 1–9.

Sofer, Z., 1984, Stable carbon isotopic composition of crude oils: applications to source, depositional environments and petroleum alteration: American Association of Petroleum Geologists Bulletin, v. 68, p. 31–49.

Stach, E.; Mackowsky, M.-Th.; Teichmüller, M.; Taylor, G. H.; Chandra, D.; and Teichmüller, R., 1982, Stach's textbook of coal petrology [3rd edition]: Gebrüder Borntraeger, Berlin, 535 p.

Tissot, B. P.; and Welte, D. H., 1984, Petroleum formation and occurrence [2nd edition]: Springer-Verlag, Berlin, 699 p.

Ungerer, P., 1990, State of the art of research in kinetic modeling of oil formation and expulsion: Organic Geochemistry, v. 16, p. 1–25.

Waples, D. W., 1980, Time and temperature in petroleum formation: application of Lopatin's method to petroleum exploration: American Association of Petroleum Geologists Bulletin, v. 64, p. 916–926.

Organic Geochemical Characteristics of Oils and Possible Source Rocks from the Ames Impact Structure

R. Paul Philp and Jon Allen
University of Oklahoma
Norman, Oklahoma

Jane L. Weber
Oklahoma Geological Survey
Norman, Oklahoma

ABSTRACT.—Geologic features and possible modes of formation of the Ames impact structure are covered in great detail by many of the other papers at this symposium. Furthermore, the oil potential and reserves in the structure are also the subject of much discussion. The purpose of this paper is to provide a detailed geochemical characterization of selected oils and selected samples of the Oil Creek Formation collected from the Nicor no. 18-4 Chestnut core taken within the structure.

We illustrate the use of sophisticated geochemical techniques to determine characteristic features of the oils, and we use these features to correlate them with suspected source rocks, possibly from the Oil Creek Formation. In addition, we introduce the concept of reservoir geochemistry and discuss its application within the structure for the purposes of determining lateral and horizontal continuity of the reservoir formation and the possible location of barriers within the reservoirs. This latter information is of course extremely important for the purposes of locating new production wells and ultimately injection wells for secondary and tertiary recovery processes. In addition to the conventional geochemical techniques that have been described at previous OGS Symposia, we utilize the oils and suspected source-rock samples to introduce the relatively new technique of combined gas chromatography–isotope ratio mass spectrometry for the purpose of oil-oil and oil–source-rock correlations.

R. Paul Philp and Jon Allen, School of Geology and Geophysics, University of Oklahoma, Norman, OK 73019; Jane L. Weber, Oklahoma Geological Survey, 100 E. Boyd, Room N-131, Norman, OK 73019.

Philp, R. P.; Allen, Jon; and Weber, J. L., 1997, Organic geochemical characteristics of oils and possible source rocks from the Ames impact structure, *in* Johnson, K. S.; and Campbell, J. A. (eds.), Ames structure in northwest Oklahoma and similar features: origin and petroleum production (1995 symposium): Oklahoma Geological Survey Circular 100, p. 259.

Correlation of Landsat MSS (Multi-Spectral Scanner) and TM (Thematic Mapper) Images with Subsurface Structure, Ames, Oklahoma*

David G. Koger
Koger Remote Sensing
Fort Worth, Texas

Michael A. Wiley
The Consulting Operation
Farmers Branch, Texas

ABSTRACT.—The Ames structure, in southeast Major County, Oklahoma, is the site of more than 20 prolific new oil and gas wells. The wells produce from brecciated and disrupted Precambrian to Ordovician rocks. In the most popular explanation, this brecciation resulted from a large meteorite impact shortly after deposition of the Lower Ordovician Arbuckle carbonate rocks. The reservoirs are very thick, porous, and permeable, but they are difficult to map in the subsurface.

The overlying lower Paleozoic rocks are much thicker than elsewhere in the region. In subsurface studies, geologists had ascribed these anomalous thicknesses to a deep graben formed after Arbuckle deposition and referred to it as the "Ames hole." After several good Arbuckle producers were drilled on local seismic highs, the "graben" was recognized as being a central part of the astrobleme.

There are several subtle geomorphic keys to the presence of the astrobleme, but these had not been noted until recently. Indications of some local subsurface structures are clearly visible in Landsat MSS (Multi-Spectral Scanner) and TM (Thematic Mapper) image data.

Landsat MSS and TM imagery, coupled with the other available data, helps to refine the outline of the astrobleme. The imagery also points out some of the small structures that are prolific producers but are difficult to locate even with three-dimensional seismic surveys.

INTRODUCTION

The Ames feature is a circular structure about 9 mi in diameter. It is located in southeast Major County and southwest Garfield County, Oklahoma. It is on the northern shelf of the Anadarko basin and has a nearly complete Paleozoic section (Fig. 1). Mississippian and Silurian production was well established throughout the area by the late 1970s, thus making this a mature exploration area. However, apart from the recent Ames structure wells, not much well data are available below the base of the Ordovician–Silurian Hunton Group.

Figure 2 is a structure map on the top of the Upper Ordovician Sylvan Shale, the deepest horizon for reliable mapping. The map is from proprietary data obtained from well logs. It was computer contoured by CPS/PC® and was edited prior to final printing. There are 797 control wells in the seven mapped townships, or about three per square mile. Some high-angle, probably normal, faults are known or suspected in the area.

David G. Koger, 3204 Waits Ave., Fort Worth, TX 76109; Michael A. Wiley, The Consulting Operation, 2415 Valley View Lane, Suite 105, Farmers Branch, TX 75324.

*Presented at the Tenth Thematic Conference on Geologic Remote Sensing, San Antonio, Texas, May 9–12, 1994.

Koger, D. G.; and Wiley, M. A., 1997, Correlation of Landsat MSS (Multi-Spectral Scanner) and TM (Thematic Mapper) images with subsurface structure, Ames, Oklahoma, *in* Johnson, K. S.; and Campbell, J. A. (eds.), Ames structure in northwest Oklahoma and similar features: origin and petroleum production (1995 symposium): Oklahoma Geological Survey Circular 100, p. 260–264.

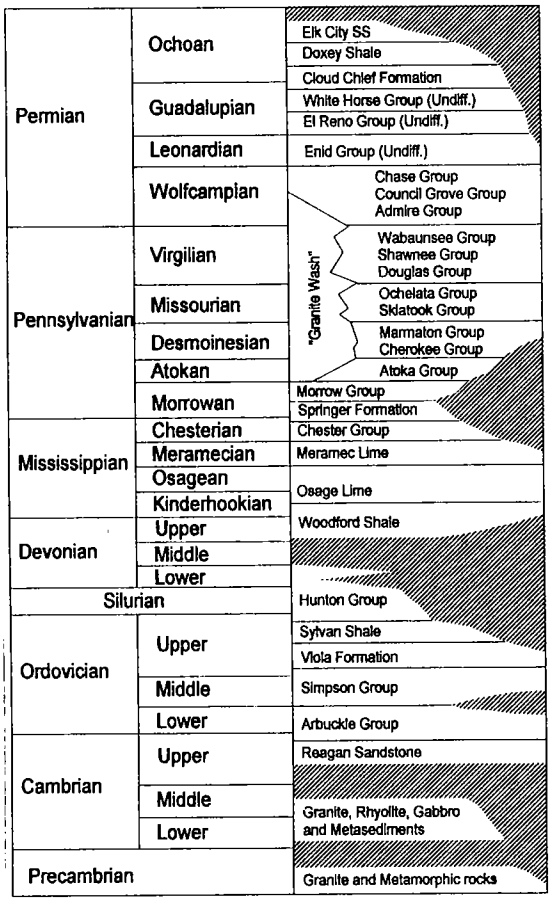

Figure 1. Generalized Paleozoic stratigraphic column for the Ames area (modified from Carpenter and Carlson, 1992).

THE AMES STRUCTURE

The origin of the Ames structure is controversial, but two explanations are favored (Shirley, 1992). One camp believes strongly that the structure is a collapsed caldera structure, and a convincing case for this interpretation can be made with gravity and magnetic data (Roemer and others, 1992). Somewhat more popular is the astrobleme theory of origin with which the mapped structure, stratigraphy, and rock properties agree (Roberts and Sandridge, 1992; Carpenter and Carlson, 1992; Hamm and Olsen, 1992).

The structure's morphology resembles an astrobleme as depicted in Anderson and Hartung (1992). It has an outer rim that is high to regional structure and about 1 to 2 mi wide. The interior low (or crater floor) ranges from 200 to 600 ft low to the regional structure. The higher, central part of the crater floor resembles a rebound structure, with extensively brecciated igneous, metamorphic, and carbonate rock in the stratigraphic position of the Arbuckle Group. According to astrobleme theory, this breccia was blasted out in all directions as the crater was formed by the impact. The material then fell back to form the chaotic jumble that now makes excellent reservoirs.

LOCAL CLOSED HIGHS—EXPLORATION TARGETS

Local closed highs on the outer rim and in the central crater floor are the main Arbuckle exploration targets. At the mapped Sylvan horizon (Fig. 2), the highs are elliptical and range from about 1,000 to 3,000 ft in their longest dimension. Closures range from about 65 to 330 ft. At the depth of the Arbuckle target horizon—500 to 800 ft below the Sylvan—these local closures may be larger, but probably not significantly so. Seismic surveying, using both profiling and three-dimensional techniques, has been the chief method of locating these small targets. Because of the structural chaos, usable seismic data have been difficult to acquire. Seismic interpretation is difficult and often inconclusive. There are few deep well data to provide assistance.

Although the wells on these local closures produce prolific amounts of oil and gas, the small areal extent of the closures restricts the number of wells per prospect. The maximum number of wells allowed on these prospects is generally four or fewer, often one or two. This restriction means that successful wells must be very good producers in order to cover the costs of dry holes or noncommercial wells plus the cost of the seismic program. Many miles of seismic line must be run to find a prospective target. Landsat imagery is an effective, less expensive alternative to regional seismic surveys.

INTERPRETATION OF LANDSAT IMAGERY

Several geomorphic features visible on the Landsat imagery (cf. Koger, 1993) suggest the presence of the Ames structure, most notably the abrupt change of course made by the Cimarron River west of the structure. On the north and northeast side, second-order drainage systems run north rather than in the regional southeast or southerly direction. There is a general absence of third-order drainage in a east-southeast–trending belt over the entire southeast part of Major County. Second-order drainage is much reduced in this belt as well. For this reason, drainage anomalies do not reflect the crater in any detail.

Two MSS scenes and one TM scene were digitally processed and printed in false color at 1:200,000 scale. The TM image was acquired 9 February 1983. Bands 7, 5, and 3 were encoded to RGB (red-green-blue) and then to IHS (intensity-hue-saturation) where a sharpened, weighted-infrared intensity replaced the RGB average. A ratio

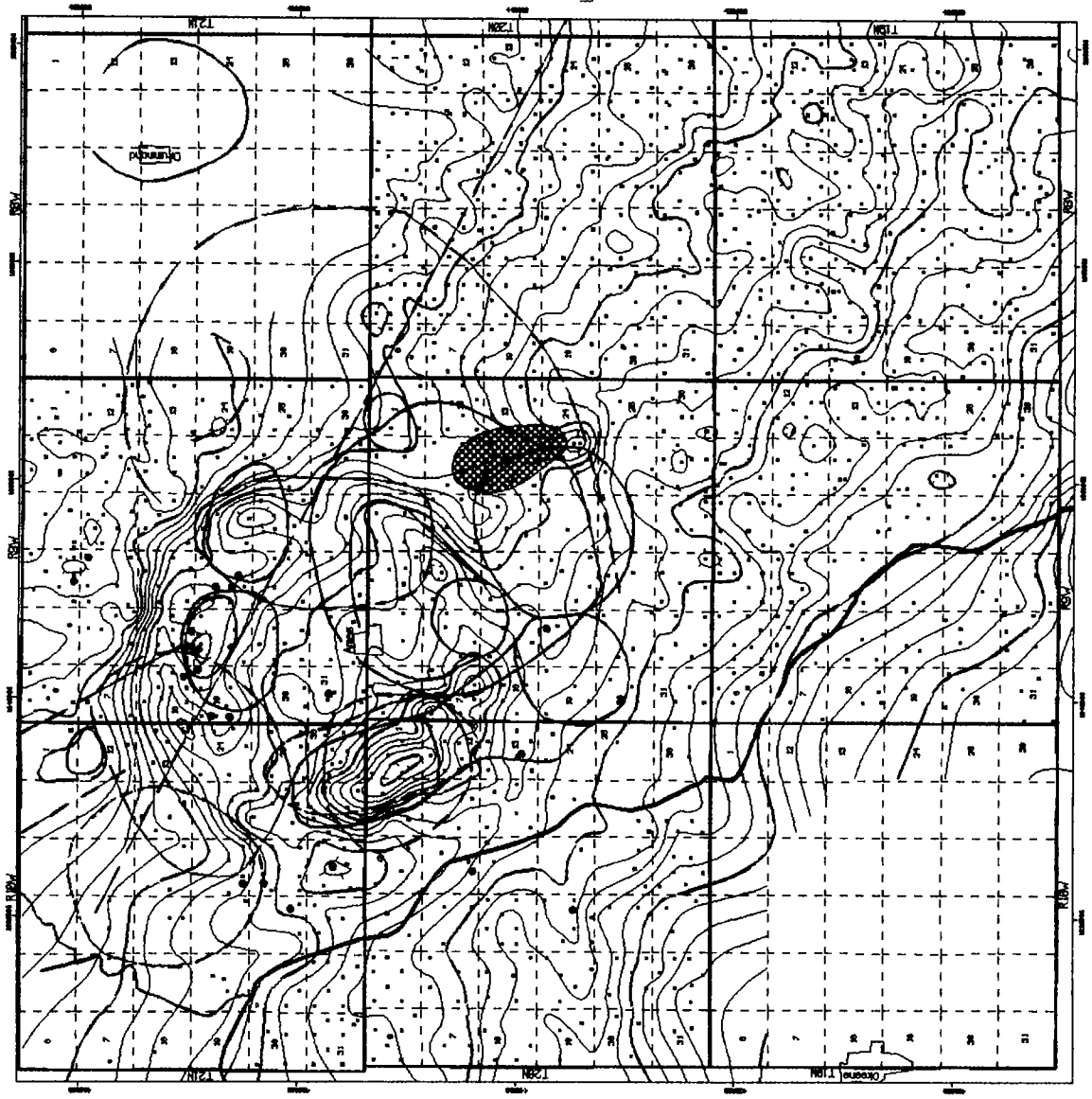

Figure 2. Landsat photogeologic interpretation on top of Sylvan Shale structure map in the Ames structure area. Contour interval 50 ft.

highlighted accumulations of water in low areas, stock tanks, and some rivers. This mask of water features was encoded to blue on the image.

One MSS image was acquired on 11 November 1990. There had been recent moisture and a frost just before acquisition. Winter wheat, which covers much of the area, was up but did not cover the ground entirely. Such conditions aid detection of surface effects of possible hydrocarbon microseepages as well as subtle drainage variations. Low contrast was exhibited between the red and green bands and between the green and infrared bands of the satellite-derived data. The final image is a 4/5 ratio to blue, 5/7 ratio to green, and infrared (band 7) to red. The other MSS image was acquired on 13 April 1976 and is printed with bands 7, 5, and 4 to RGB.

Primary and secondary drainage systems were emphasized on U.S. Geological Survey metric 1:100,000 scale topographic maps that were then reduced to the imagery scale of 1:200,000 for reference. The general area of the crater was noted on the imagery to help focus interpretation. Each image was studied individually and anomalous features were drawn on an overlay to the images.

Winter wheat is grown in this part of Oklahoma on thousands of small plots, mostly about a quarter section (160 acres) in area. The crops are harvested at different times, and not all plots are cultivated. This farming approach results in a cluttered checkerboard of different colors and patterns. The clutter distracts from interpretation because it is difficult to discern or follow trends. In the beginning of the project, we believed that the lower-resolution MSS imagery would be more useful because the small fields would be less sharply defined and produce less clutter. Also, areas of anomalous photographic tone are generally better exemplified in the MSS data (Koger, 1993). However, all three images were of value in the final interpretation. The MSS imagery was best for larger features whereas the TM could resolve some very small, but significant features.

The features detected are mostly elliptical "geomorphic" anomalies that have more or less distinct differences in color, tone, or texture compared to the surrounding areas. The major axes ranges from about 0.9 mi to about 8.5 mi. The median is 2.5 mi. More and smaller features were detected on the TM image than on the two MSS scenes combined. Anomalies detected are shown in Figure 2.

The deepest part of the Ames structure, on the west part of the central low, was detected in all three scenes with near unanimous agreement. The TM scene showed this feature with slightly more detail. It appears to be a slightly wetter, perhaps swampy at times, part of the Cimarron River bed. The north part of the outer rim was detected on the TM scene almost coincident with the two local closures that now produce from the Arbuckle. The east part of the rim was detected on both MSS scenes but not on the TM scene. Two closed highs in the Sylvan are included. The Arbuckle has not been tested on these highs (as of 1995). The south part of the rim was not clearly detected on any of the scenes. A somewhat blurred TM anomaly more or less overlies parts of the south part of the rim.

Parts of the central crater floor were detected on the TM scene and both MSS scenes, but not the same parts. All of these scenes tended to confuse the crater floor with the beginning of the high outer rim to the east. Mostly the lower parts of the crater floor were detected. We believe the crater-floor confusion resulted from (1) blurring of the crater-floor topography by subsequent deposition and compaction, (2) the very small size of the crater-floor structures, and (3) a large amount of vegetative and cultural clutter in this area.

A 1.8-mi-diameter tonal anomaly was detected over a small closed high on the extreme southeast side of the outer rim. This high produces from the Hunton but has not been tested in the Arbuckle (as of 1995). It was apparent only on the November MSS scene.

Several more medium-sized and one very large anomaly were detected on the three scenes. The largest is an incomplete ellipse that generally marks the southeast, east, and northeast outer limits of the outer rim. This anomaly was detected only on the April MSS scene. Although lineaments are not a factor in this study, three were detected on the April MSS scene. The most significant is about 17 mi long and trends east-southeast across the study area.

CONCLUSIONS

The Ames structure is the site of more than 20 prolific new oil and gas wells. They produce from small, difficult-to-map local closures on the outer rim and on the central crater floor. The cost to find these structures with seismic techniques can be extreme and can severely affect the economics of a drilling program.

This study shows that Landsat imagery can (1) detect many of the small structures in advance of seismic data, especially when used with other subsurface data, (2) aid in locating the central low area of the structure, and (3) assist in planning detailed seismic surveys necessary for accurate well-site selection.

No one knows how many astroblemes occur on the planet but, on the basis of lunar geology, the number is probably large. Because astroblemes are random occurrences, they cannot be predicted in the usual regional sense. Inexpensive Landsat MSS and TM imagery, coupled with other data, can aid in the search for more and lead to additional significant oil and gas production.

REFERENCES CITED

Anderson, R. R.; and Hartung, J. B., 1992, The Manson impact structure: its contribution to impact

material observed at the Cretaceous/Tertiary boundary: Proceedings of Lunar and Planetary Science, v. 22, p. 101–110.

Carpenter, B. N.; and Carlson, Rick, 1992, The Ames impact crater: Oklahoma Geology Notes, v. 52, p. 208–223.

Hamm, H.; and Olsen, R. E., 1992, Oklahoma Arbuckle lime exploration centered on buried astrobleme structure: Oil and Gas Journal, v. 90, no. 16, p. 113–116.

Koger, D. G., 1993, Landsat 6 images to provide more remote sensing muscle: Oil and Gas Journal, v. 91, no. 5, p. 51–55.

Roberts, C.; and Sandridge, B., 1992, The Ames hole: Shale Shaker, v. 42, no. 5, p. 118–121.

Roemer, C. D.; Roemer, C.; and Williams, K., 1992, Gravity, magnetics point to volcanic origin for Oklahoma's Ames anomaly: Oil and Gas Journal, v. 90, no. 25, p. 75–80.

Shirley, K., 1992, Overlooked "hole" found: American Association of Petroleum Geologists Explorer, v. 13, no. 5, p. 1, 12–13.

The Wells Creek Structure, Tennessee—From Heaven or Hell?

Herbert A. Tiedemann
U.S. Department of Energy
Bartlesville, Oklahoma

ABSTRACT.—The Wells Creek structure in northwestern middle Tennessee is an anomalous geologic feature whose origin has been the subject of speculation since its discovery. Detailed mapping of Wells Creek by geologists at Vanderbilt University revealed a circular structure, 8 mi in diameter, with a brecciated Lower Ordovician central core surrounded by concentric horst-and-graben rings of Lower Mississippian strata. The dominant relative movements in Wells Creek were downdropping of the grabens, uplift of the central block, and lateral offset along radial faults. Wells Creek is generally considered to be due to a meteorite impact because of its typical impact structure and the presence of shatter cones.

The buried Ames structure in Major County, Oklahoma, another feature with typical impact structure, lacks shatter cones, but contains shocked quartz and has granite basement involved in the structure. I consider Ames and Wells Creek similar enough in size and structural elements—central uplift, horst-and-graben zones, radial faulting, and brecciation—to warrant considering Wells Creek as a structural model for Ames.

INTRODUCTION

In the mid-1960s, the Vanderbilt University Department of Geology, working under a grant from the National Aeronautics and Space Administration, conducted a definitive investigation of the Wells Creek structure in middle Tennessee. The project, comprising comprehensive stratigraphic, structural, and geophysical analyses, was undertaken to determine, in R. G. Stearns's picturesque phrase, whether the forces that formed Wells Creek "came from Heaven or Hell."

In 1993, Michael Kuykendall, Solid Rock Resources, Tulsa (then with Masera Corporation), visited me at the U.S. Department of Energy office in Bartlesville to discuss Wells Creek in relation to Masera's concurrent research on the Ames structure in Major County, Oklahoma. Both structures are considered by many geologists to be the result of meteorite impact. The comparison revealed a number of structural similarities between the two features. This paper presents details of those correlations and suggests that Wells Creek may be a useful model for those working to unravel the structural details buried at Ames.

THE WELLS CREEK STRUCTURE

General Geology

The Wells Creek structure is located in northwestern middle Tennessee, near the town of Erin (Fig. 1). Roughly circular in outline, about 8 mi in diameter, the feature comprises two annular grabens surrounding a central uplift. Strata exposed within the structure range from Lower Ordovician to Mississippian rocks as young as post–Ste. Genevieve (Fig. 2). The surrounding Highland Rim is surfaced by relatively flat lying beds of the Mississippian Fort Payne Formation and Warsaw and St. Louis Limestones. Undisturbed patches of Upper Cretaceous Tuscaloosa gravels on the higher elevations provide a limiting date for the structural event. Evidence that middle Mississippian brecciated rock was not completely lithified when deformation occurred favors a Late Mississippian date.

Early Mapping

The Wells Creek structure was first investigated by Tennessee State Geologist J. M. Safford in the late 1800s; his 1895 geologic map (see Wil-

Herbert A. Tiedemann, Department of Energy, P. O. Box 1398, Bartlesville, OK 74005.

Tiedemann, H. A., 1997, The Wells Creek structure—from Heaven or Hell?, *in* Johnson, K. S.; and Campbell, J. A. (eds.), Ames structure in northwest Oklahoma and similar features: origin and petroleum production (1995 symposium): Oklahoma Geological Survey Circular 100, p. 265–271.

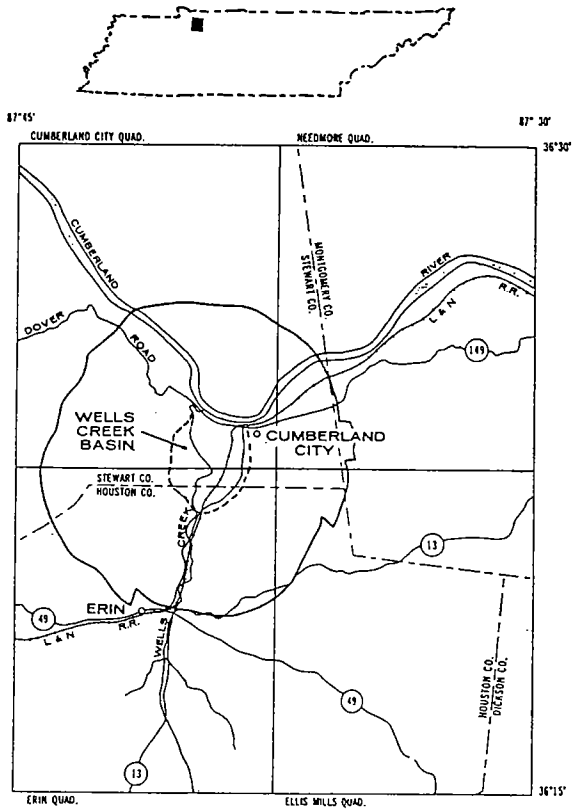

Figure 1. Index map showing location of the Wells Creek structure (Wilson and Stearns, 1968).

son and Stearns, 1966) accurately locates the circumferential faulting (Fig. 3). Walter Bucher, who mapped Wells Creek in the early 1930s as part of a cryptovolcanic study, showed both the circumferential and the radial faulting (Fig. 4). Later work includes studies by C. W. Wilson, Vanderbilt University, who first suggested meteorite impact in 1953 (Wilson, 1953), and J. M. Kellberg, Tennessee Valley Authority, who suggested a tectonic origin in 1965, on the basis of his interpretation of regional structure gained from an analysis of TVA drill cores (Kellberg, 1965).

Vanderbilt University Project

Wells Creek was mapped by the Vanderbilt University Department of Geology under a NASA grant in 1963–1965, when that agency was gathering data on terrestrial craters to study as lunar analogues for the Apollo Program. Under Stearns's direction, and with assistance from Vanderbilt graduate students, I

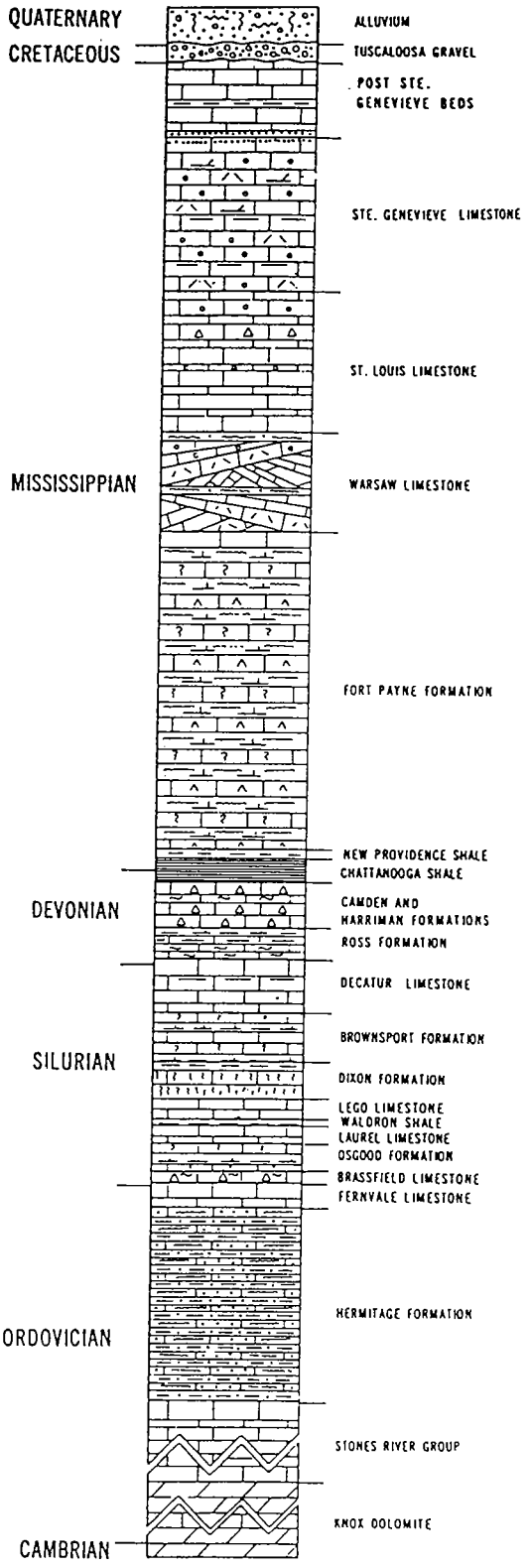

Vertical scale: 1 in. ≈ 160 ft.

Figure 2 *(right)*. Generalized stratigraphic column in the area of the Wells Creek structure (Wilson and Stearns, 1968).

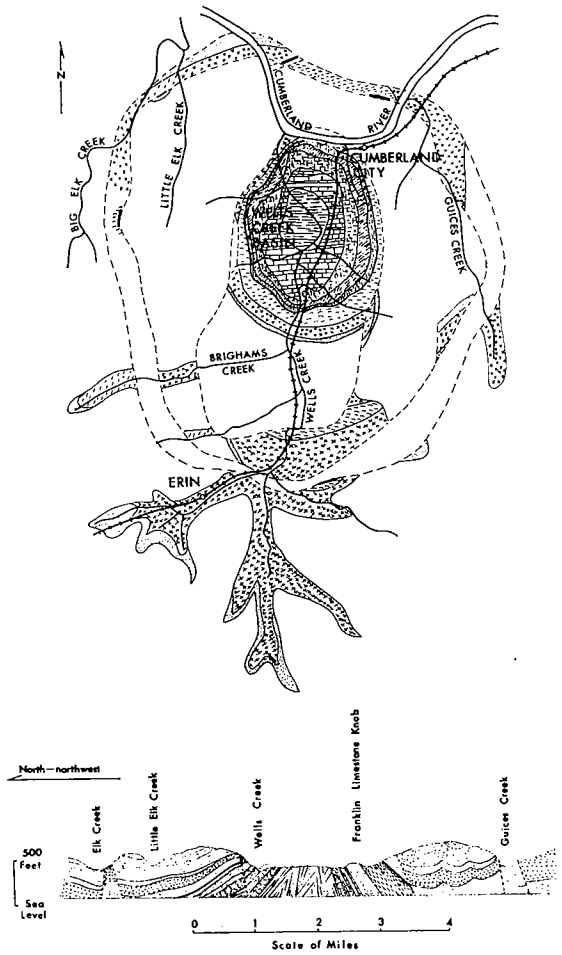

Figure 3. Safford and Lander's geologic map and cross section of the Wells Creek structure, ca. 1895 (Wilson and Stearns, 1966).

conducted the mapping of the structure; Stearns and Wilson assisted in deciphering the structure and stratigraphy in the outer rings and the surrounding Highland Rim. The project was published as Tennessee Division of Geology (TDG) Bulletin 68 (Wilson and Stearns, 1968; now out of print).

Structural Mapping

The Wells Creek structure was mapped at a scale of 1:24,000 on four Tennessee Valley Authority 7.5 minute quadrangles. The final geologic map, published as a single sheet at 1:48,000 (and also as four separate 1:24,000 quadrangles in the TDG series), contains accurate, well-documented geologic detail based on good outcrop control over the entire area. Distinctive thin marker beds in the Silurian and Devonian units helped unravel complex small-scale faulting and folding throughout the central block, and contrasting chert, limestone, and fossils facilitated differentiation of the Mississippian units.

Geologic Structure

The Wells Creek structure comprises an uplifted central block surrounded by two grabens and a horst (Fig. 5). The regional Carlisle fault, tangent on the northwest, disappears a short distance to the northeast. The central block, about 3 mi in diameter, exposes Lower Ordovician to Mississippian strata broken by more than a dozen radial faults (Fig. 6). The outward-dipping central-block rim is capped mostly by resistant cherty beds of the Fort Payne Formation.

The two grabens are surfaced mostly by St. Louis Limestone. The inner graben, up to 1.5 mi wide, has a few small areas of downfaulted post–St. Louis beds. Small radial faults extend into the adjacent horst on the west and north. The outer graben has scattered patches of Warsaw and Fort Payne. The horst and the outer graben, both generally less than 1 mi wide, are broken by radial faulting—two sizable blocks are sharply offset on the east, a left-lateral break occurs on the south, and smaller breaks occur on the west and north.

Structural Movement

The dominant relative movements in Wells Creek were uplift of the central block and downdropping of the grabens (Fig. 7). In the central block, Lower Ordovician Knox Dolomite lies at the regional Mississippian level. Fort Payne contours are low in the grabens, at regional level in the horst, and sharply elevated over the center (Fig. 8). Lateral offset is evident along the numerous radial faults in the circumferential blocks.

The residual structure contour map shows the grabens to be downdropped generally 100–200 ft (Fig. 9). The horst shows essentially no vertical movement except for several small anomalously high spots. The central block is uplifted by 2,500 ft or more.

The movements of the various blocks at or near present surface level can be summarized as follows: The entire mass of central-block material moved inward, either to fill a crater or to form a mound of jumbled rock. The younger rocks at the outer edge of the central block moved 375 ft inward and upward, at least partly by overthrusting. The inner graben moved 200 ft inward and 250 ft down. The horst moved inward without vertical displacement. The outer graben dropped about 200 ft.

Origin

"Shatter breccia," found throughout the Knox Dolomite in the central block and in other surrounding formations, is related to the Wells Creek structural event; other breccias are strictly lithologic, unrelated to structure. (The depiction in Fig.

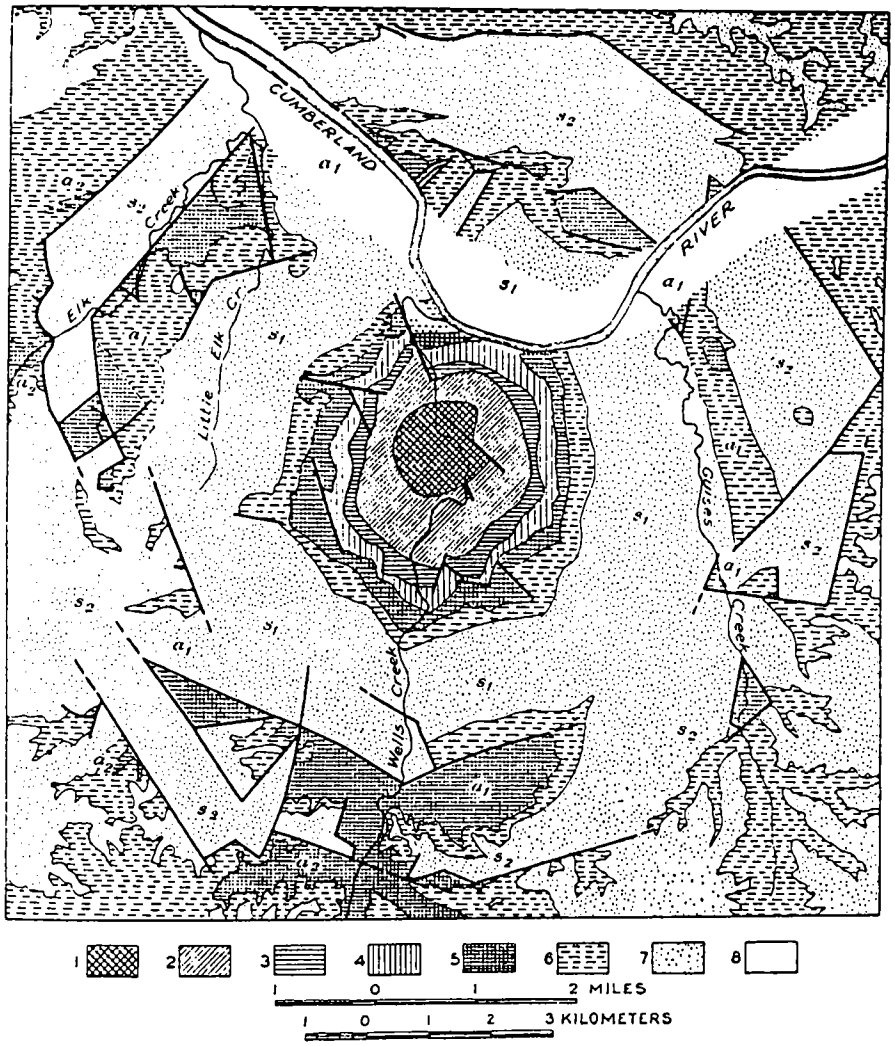

		Feet	
8.	Alluvium.		
7.	St. Louis limestone (may include higher beds locally; thickness estimated, probably more)	200	Middle Mississippian
6.	Warsaw limestone	120	
5.	Fort Payne chert	110	Lower Mississippian
	Ridgetop shale (including Maury member)	35	
	Chattanooga shale	25	
4.	Harriman chert	20	Devonian
	Birdsong formation	20	
	Limestone series	110	Silurian
	Red shales with limestone layers	130	
3.	Hermitage formation	100	Middle Ordovician
2.	Post-Beekmantown, pre-Trenton limestones (estimated, probably more)	500	
1.	Wells limestone (estimated, probably more)	200	Lower Ordovician

s_1, Inner ring depression; a_1, inner ring of the anticlinal bulges; s_2, second depressed zone; a_2, incomplete second marginal zone of anticlinal bulges.

Figure 4. Bucher's geologic map of the Wells Creek structure (Bucher, 1936).

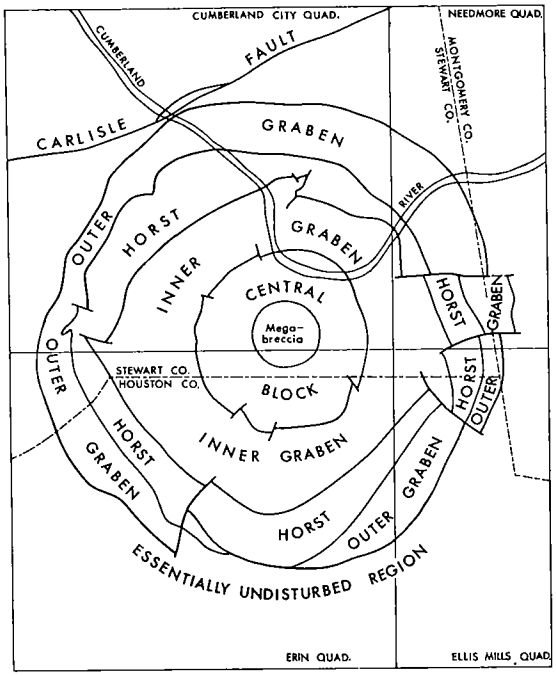

Figure 5. Index map showing major structural features of the Wells Creek structure (Wilson and Stearns, 1968).

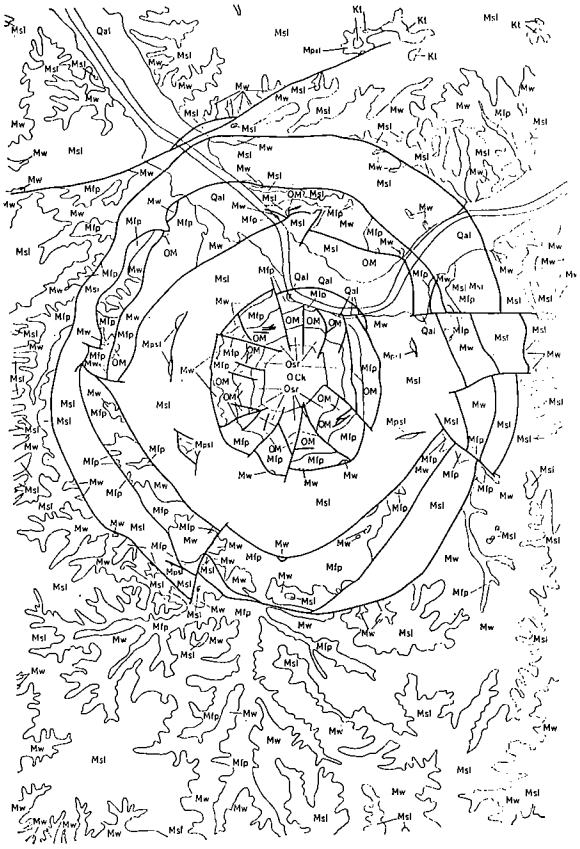

Figure 6. Generalized geologic map of the Wells Creek structure (Wilson and Stearns, 1968).

7 of brecciation in the subsurface of the central block is conjectural and does not reflect accurate knowledge of its complete extent at depth.) Also found in the central-block Knox beds are shatter cones, both in outcrop and in the 2,500 ft core drilled in the central block.

Shatter breccia is characteristic of meteorite-impact structures, and shatter cones are considered to be definitive of impact. Because of these features and the geologic structure typical of impact craters, Wells Creek is generally considered to have been formed by meteorite impact. (The contrasting images of Wells Creek being formed either as a meteorite-impact crater or a "cryptovolcanic" event prompted Stearns's remark characterizing the origin as being "from Heaven or Hell.")

COMPARISON OF WELLS CREEK AND AMES

The Ames structure, discovered in 1991 at a depth of about 9,000 ft on the northern shelf of the Anadarko basin, in Major County, Oklahoma, displays features typical of meteorite impact, including a central rebound peak and concentric horst-and-graben faulting (Kuykendall and others, 1997). The outline of the Ames morphologic zones shows similarities to Wells Creek morphology (Fig. 10). The overall size of both structures is about 8 mi, and in each, an uplifted central area about 3 mi in diameter is surrounded by three circumferential zones 1 mi or so in width. At Ames they are the anticline-syncline-wall zones as interpreted from structural and isopach mapping of the overlying formations (Sylvan Shale) and crater-filling shales (Middle Ordovician Oil Creek or McLish Formations), respectively, that correspond to underlying crater structure; in Wells Creek they are the exposed graben-horst-graben zones. About 3 mi from the Ames central block there is an apparent radial fault that transects the crater syncline and wall zones, which corresponds to similar faults offsetting the Wells Creek horst (Fig. 11).

Two elements not present in Wells Creek but found at Ames are shock-metamorphosed quartz and regional basement granite involved in the central parts of the feature. Shocked quartz, an im-

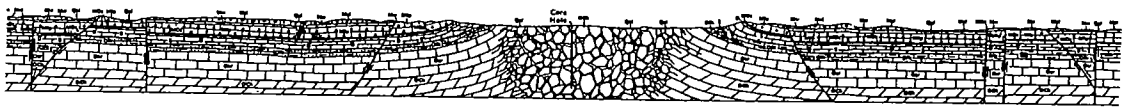

Figure 7. Cross section of the Wells Creek structure; no vertical exaggeration (Wilson and Stearns, 1968).

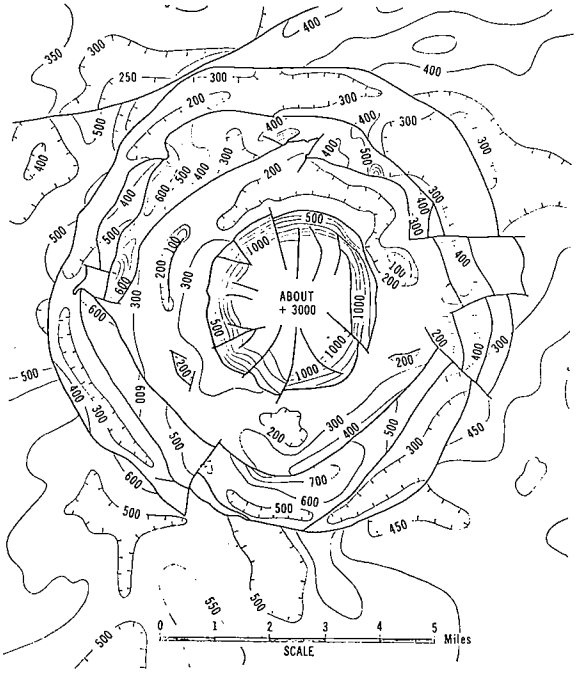

Figure 8. Structure-contour map on top of the Fort Payne Formation (Wilson and Stearns, 1968).

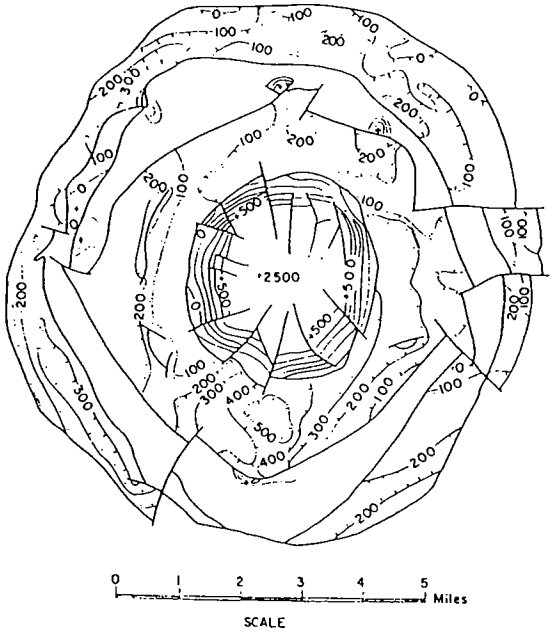

Figure 9. Residual structure-contour map showing vertical movement of Wells Creek structural elements; movement is downward unless marked "+" (Wilson and Stearns, 1968).

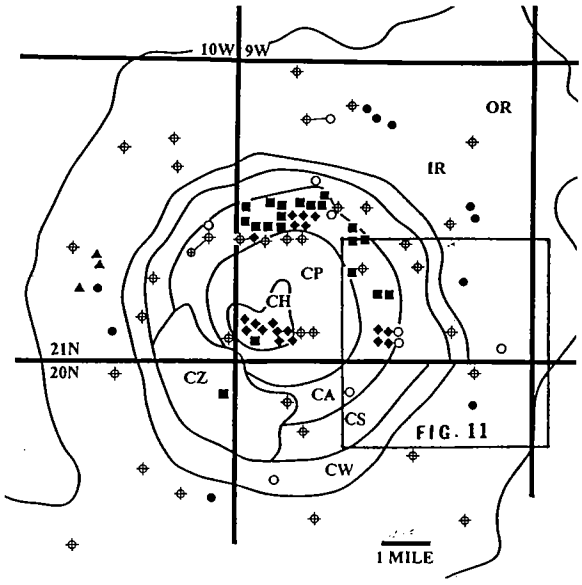

Figure 10 *(left)*. Morphologic zones at the Ames structure: CH—crater high, CP—crater pit, CA—crater anticline, CS—crater syncline, CW—crater wall, IR—inner rim, OR—outer rim. Outlined square is area of Figure 11 (courtesy Masera Corporation and DLB Oil and Gas, Inc.).

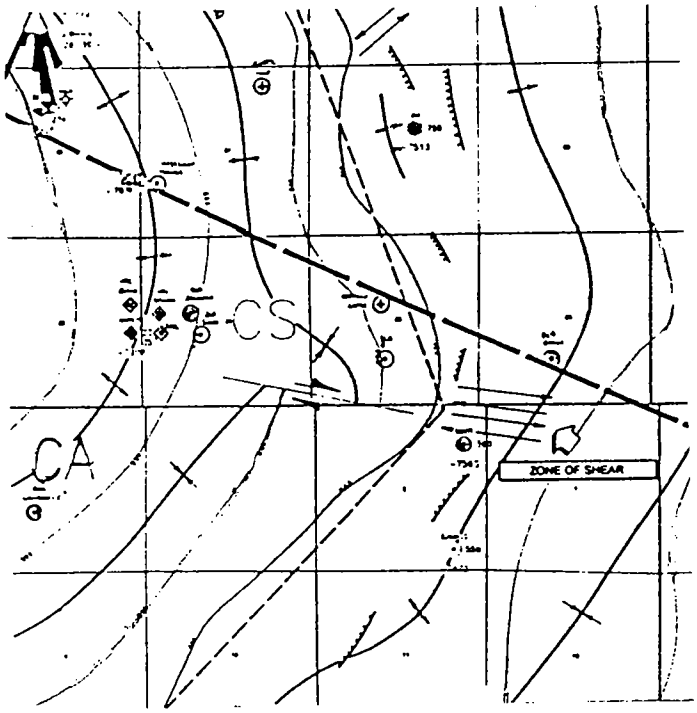

Figure 11. Apparent radial faulting and shear within the syncline and wall zones on the east side of the Ames structure (courtesy Masera Corporation and DLB Oil and Gas, Inc.).

pact criterion, lends weight to an impact origin for Ames; its absence at Wells Creek could be attributed to the lack of sandstones in the Ordovician rocks most subject to impact shock. The absence of granite involved in the structure at Wells Creek is a reflection of age and greater depth to basement. The Wells Creek event was middle Mississippian or later, when basement was 8,000 ft below the surface in Tennessee, whereas Ames was formed in Middle to Early Ordovician, when there was less cover over the granite basement.

CONCLUSIONS

Similarities between Wells Creek and Ames—circularity, size, central uplift, horst-and-graben zones, radial faulting, shock-induced features, and possible similar origin—suggest that the Wells Creek structure may provide a useful model for the structure at Ames. Information on Wells Creek, including cores, samples and logs stored at Vanderbilt, may be obtained by contacting me.

REFERENCES CITED

Bucher, W. H., 1936, Cryptovolcanic structures in the United States: 16th International Geologic Congress, United States 1933, Report, v. 2, p. 1055–1084 (Tennessee: p. 1066–1070, 1074).

Kellberg, J. M., 1965, Possible tectonic origin for "cryptoexplosion" structures: Wells Creek structure, Tennessee: Geological Society of America, Program for 1965, Annual Meeting of Southeastern Section, p. 25.

Kuykendall, M. D.; Johnson, C. L.; and Carlson, R. A., 1997, Reservoir characterization of a complex impact structure: Ames impact structure, northern shelf, Anadarko basin, *in* Johnson, K. S.; and Campbell, J. A. (eds.), Ames structure in northwest Oklahoma and similar features: origin and petroleum production (1995 symposium): Oklahoma Geological Survey Circular 100 [this volume], p. 199–206.

Wilson, C. W., Jr., 1953, Wilcox deposits in explosion craters, Stewart County, Tennessee, and their relations to origin and age of Wells Creek Basin structure: Geological Society of America Bulletin, v. 64, p. 753–768.

Wilson, C. W., Jr.; and Stearns, R. G., 1966, Circumferential faulting around Wells Creek basin, Houston and Stewart Counties, Tennessee—a manuscript by J. M. Safford and W. T. Lander, circa 1895: Tennessee Academy of Science Journal, v. 61, no. 1, p. 37–48.

_____ 1968, Geology of the Wells Creek structure, Tennessee: Tennessee Division of Geology Bulletin 68, 236 p.

"Haswell Hole," A Previously Unknown Impact Structure in Southeast Colorado

S. Parker Gay, Jr.
Applied Geophysics, Inc.
Salt Lake City, Utah

A high-resolution aeromagnetic survey of southeast Colorado flown by Applied Geophysics, Inc., in 1984 showed a circular area of low residual magnetic intensity straddling the border of Bent and Kiowa Counties (see Figs. 1 and 2). The circular feature is 22 mi (35 km) in diameter and is unique among all the survey areas flown by Applied Geophysics, Inc., for oil companies since 1983—an area totaling 273,000 sq mi, slightly larger than the State of Texas. We interpreted this feature—which we named Haswell hole—as a possible meteorite-impact structure, with a deep crater having been excavated in the basement rocks and later infilled by less magnetic sedimentary rocks, hence resulting in the lower magnetic intensities observed in the center. The host Precambrian basement rocks in the area, as deduced by the late Ogden Tweto (1980), are ca. 1.4 Ga granites under the south half and ca. 1.8 Ga quartzites and schists under the north half.

The oldest sedimentary rocks intersected by drilling within this feature belong to the Cambrian–Ordovician Arbuckle Formation, and since no mention is made on well logs of anomalous rocks in any of the wells that intersect the Arbuckle, the circular feature must be earlier than the deposition of the Arbuckle. It may be of Late Proterozoic age and filled with ca. 1.0 Ga "slightly metamorphosed sedimentary and volcanic rocks" that occupy basement grabens 30 mi to the southwest, according to the basement mapping (Tweto, 1983).

By connecting the points of highest residual magnetic intensity around the edges of the magnetic low in the center of Figure 2, an approximate circle was outlined. If the interpretation of the feature as a meteorite-impact structure is correct, this would be location of its rim anticline. This circle is reproduced on two additional data sets that show the circular nature of the feature. Figure 3 is a 2nd-derivative map of the Bouguer gravity data obtained from the State of Colorado and NOAA (National Oceanic and Atmospheric Administration). This low is surrounded by gravity highs around 85% of its circumference; only part of the southwest quadrant shows a breach in the surrounding wall of residual gravity highs.

The interpreted rim anticline superimposed on a drainage map of the area yielded an unexpected result (Fig. 4). The circular area is topographically high, as the drainage is radially away from the feature in nearly all directions. Note that the principal northwest-to-southeast regional drainage is clearly diverted around the feature on the west. Perhaps there has been rebound of the Earth's crust in this area of lower-density rocks following erosion of the overlying sedimentary section.

The great majority of the oil and gas wells have been drilled along the northern and northeast parts of the Haswell hole rim. A structure-contour map of that area (Fig. 5) shows that structurally high noses trending off the closed high on the northeast side coincide closely with the interpreted location of the rim anticline.

Further studies of the overlying sedimentary section are currently being undertaken to determine what effects the ancient impact may still be exerting on oil and gas production. Two types of effects may have occurred: (1) The structure of the sedimentary section may mimic, through gravitational compaction, the underlying basement topography, which could include the interpreted rim anticline and a concentric rim syncline. (2) Recompaction of the infilling Precambrian sedimentary rocks, if they exist, could have occurred in Phanerozoic time, lowering the relative land surface and affecting fluvial, lacustrine, or marine deposition. Four Morrow gas fields—Haswell, Salt Lake, Colt, and Bent's Fort—occupy the area of the supposed ring syncline interior to the interpreted rim and may result from the Morrow fluvial system following Mississippian topographic lows resulting from compaction by either of the two mechanisms mentioned.

S. Parker Gay, Jr., Applied Geophysics, Inc., 675 South 400 East, Salt Lake City, UT 84111.

Gay, S. P., Jr., 1997, "Haswell hole," a previously unknown impact structure in southeast Colorado, *in* Johnson, K. S.; and Campbell, J. A. (eds.), Ames structure in northwest Oklahoma and similar features: origin and petroleum production (1995 symposium): Oklahoma Geological Survey Circular 100, p. 272–276.

REFERENCES CITED

Tweto, Ogden, 1980, Precambrian geology of Colorado, *in* Kent, H. C.; and Porter, K. W. (eds.), Colorado geology: Rocky Mountain Association of Geologists, Denver, p. 37.

_____ 1983, Las Animas Formation (Upper Precambrian) in the subsurface of southeastern Colorado: U.S. Geological Survey Bulletin 1529-G, p. G1–G14.

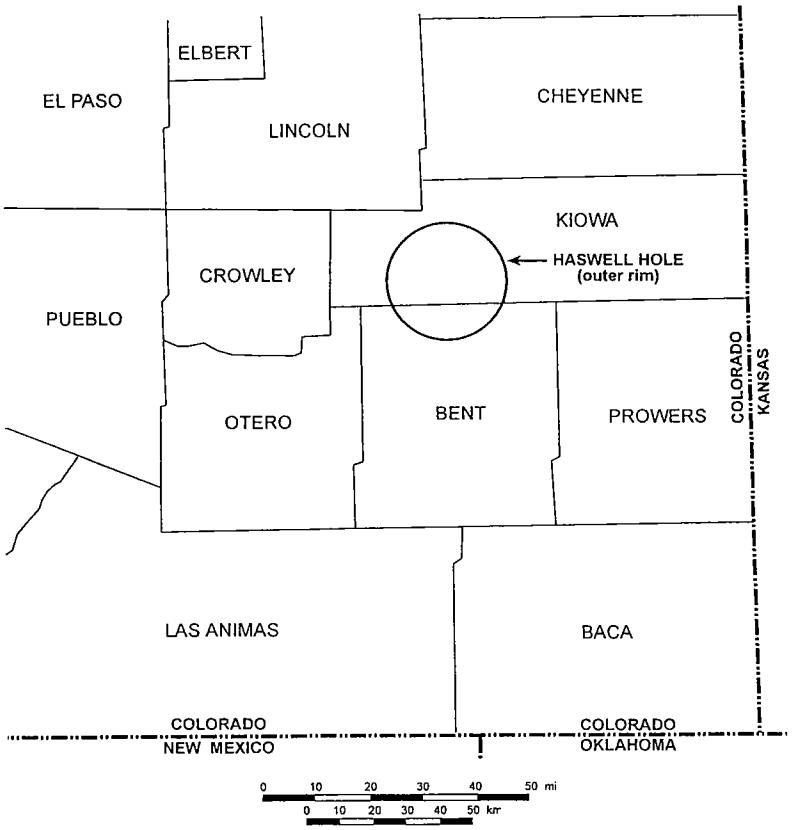

Figure 1. Map showing location of Haswell hole in southeast Colorado. Diameter of outer rim as interpreted from magnetic data is approximately 22 mi (35 km).

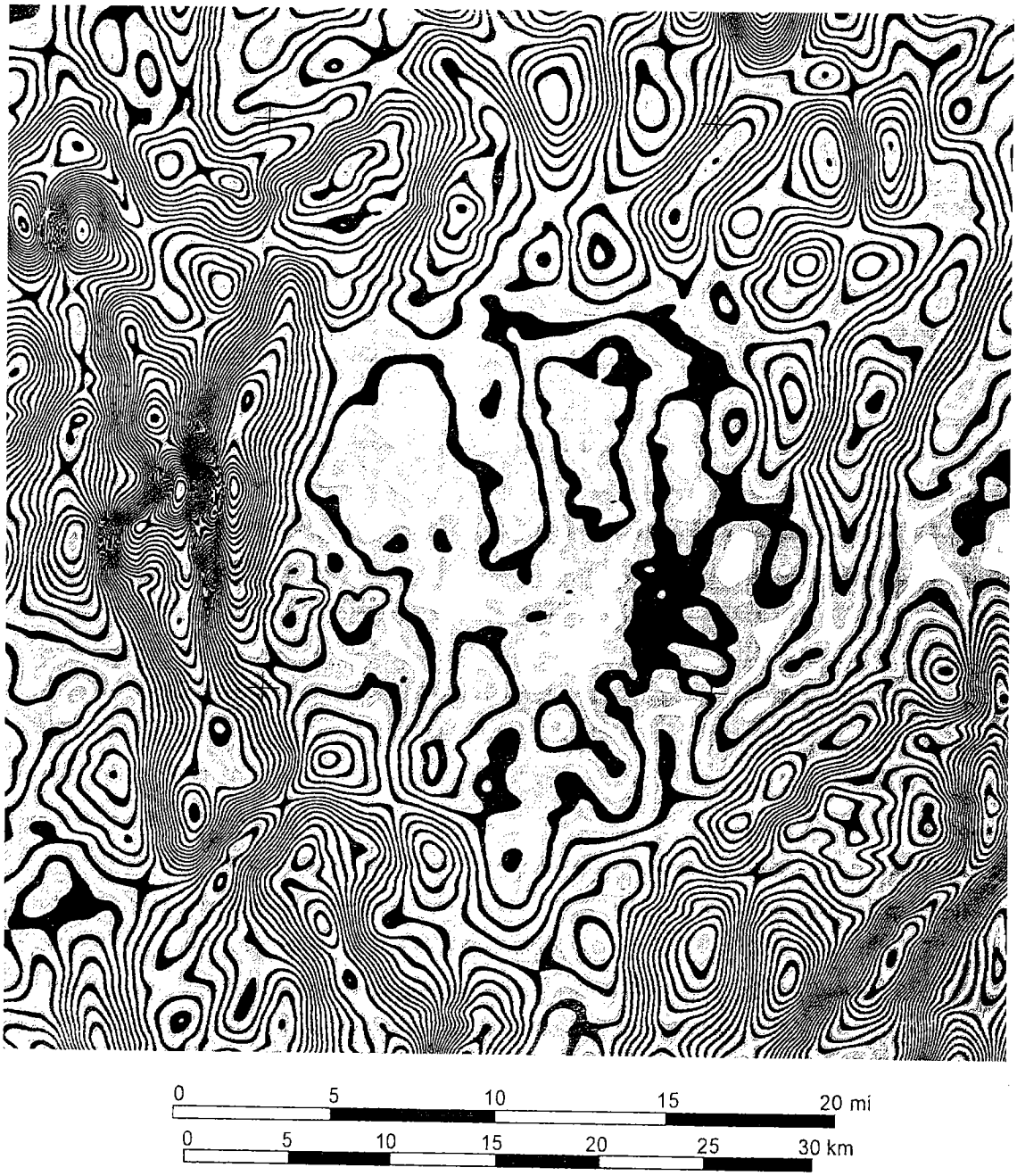

Figure 2. Haswell hole, as it appears on the NewMag® residual magnetic map (unpublished) of southeast Colorado, flown by Applied Geophysics, Inc., in 1984.

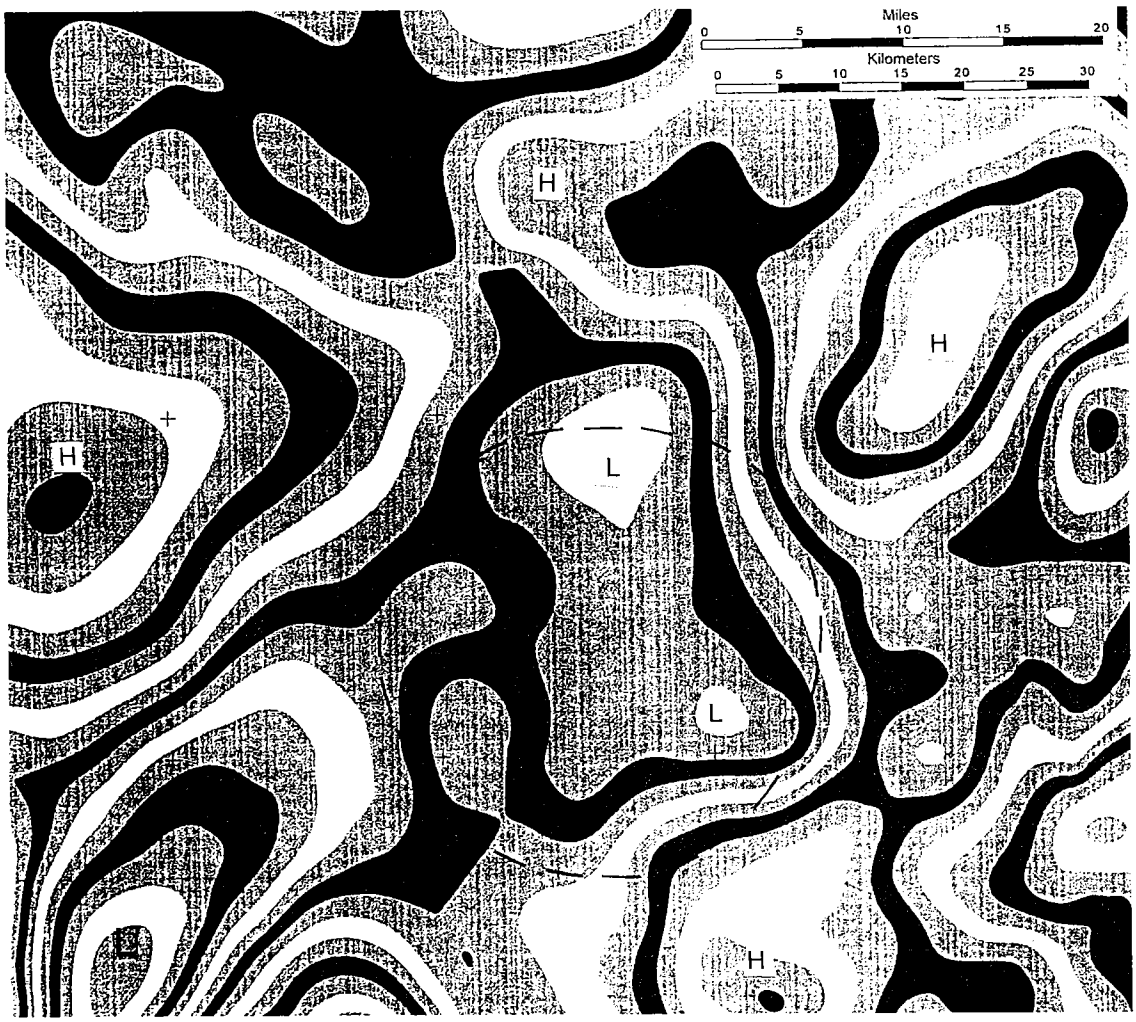

Figure 3. Map of 2nd-derivative of regional gravity data (NOAA). Note that Haswell hole coincides with a gravity low (L) surrounded by gravity highs (H), except for a limited area on the southwest. This finding supports the magnetic interpretation that the impact excavated a hole in the crystalline Precambrian basement that was later infilled with less dense clastic materials.

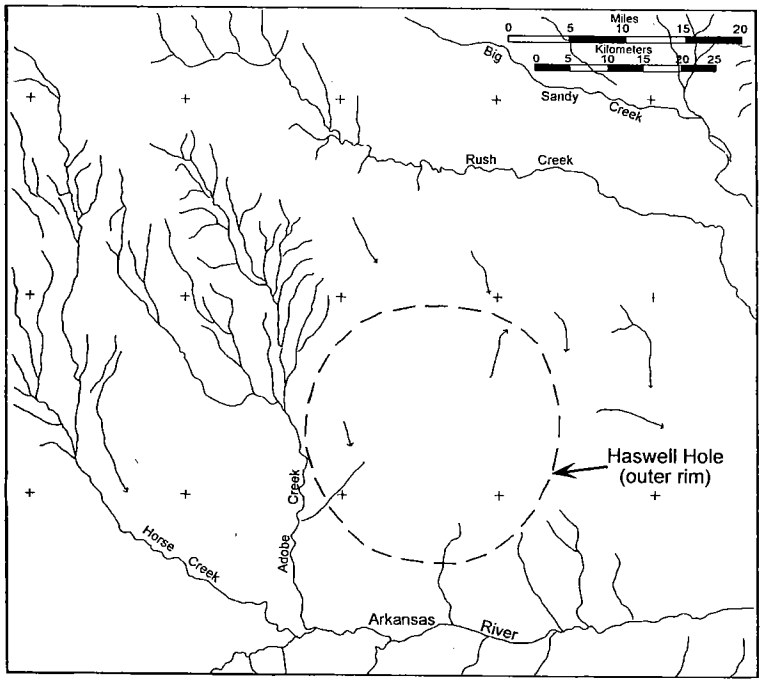

Figure 4. Drainage map of Haswell hole area indicates that the "hole" is anomalously high. Drainages run radially away from the feature in most cases, and the normal northwest to southeast drainage, as shown by Rush Creek and Sandy Creek on the north, are deflected around it to the south (Adobe Creek). The area may be high owing to crustal rebound following erosion of overlying sedimentary rocks.

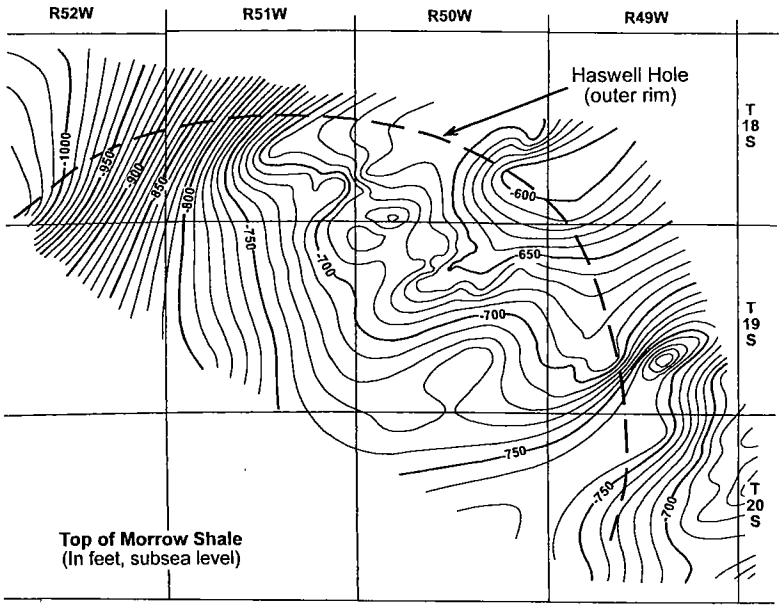

Figure 5. A closed structural high in the northeast quadrant of the Haswell hole has structural noses extending from it that closely follow the interpreted outer rim. However, a lack of data points prevents better definition of these noses.

The Chicxulub Impact Basin, Yucatán, Mexico

V. L. Sharpton
Lunar and Planetary Institute
Houston, Texas

L. E. Marín
Universidad Nacional Autonoma de Mexico
Mexico City, Mexico

ABSTRACT.—The buried Chicxulub impact basin in Northern Yucatán is the source of the worldwide ejecta layer associated with the Cretaceous/Tertiary extinction event. Stratigraphic correlations constructed from eight Pemex exploratory wells indicate a broad basin ~300 km in diameter in which the Mesozoic platform sequence is depressed ~1 km. Reprocessed gravity data over Northern Yucatán reveal an ~300-km-wide multiring basin similar to the largest impact landforms observed on the Moon, Mercury, and Venus. Breccias and melt rocks recovered from three wells in the center of the structure show a diverse suite of classic shock-metamorphic effects including planar deformation features in quartz and feldspar grains, diaplectic glasses, fused mineral glasses, and whole-rock melts. Elevated iridium and osmium abundances indicate a meteoritic component nonuniformly distributed throughout the melt sheet. Melt rocks have experienced varying levels of hydrothermal alteration and albitization; however, ^{40}Ar-^{39}Ar determinations on relatively pristine melt-rock samples from the center of the basin indicate a crystallization age at or very near the K/T boundary. Analysis of the Rb-Sr, O, and Nd-Sm isotopic systems confirm a chemical link between the Chicxulub melt rocks and the impact glasses contained in the K/T boundary deposits at Beloc, Haiti. U-Pb ages of zircons from a Chicxulub breccia sample are ca. 545 Ma and equivalent in age to the zircons contained in the K/T boundary layer in Colorado. Unmelted breccia clasts, representing the silicate basement impacted by the Chicxulub basin-forming event, are medium- to high-grade continental crust similar to the lithic clasts observed within K/T boundary sedimentary deposits around the world. These studies and others leave little doubt that the site of the major collisional event at the K/T boundary is the Chicxulub basin. If and how such an impact event could cause a major collapse in Earth's biosphere is not yet clear. It seems most likely, however, that massive quantities of CO_2 and SO_x compounds were released into the atmosphere when the platform rocks near ground zero were vaporized. Global distribution would be facilitated by the size of this event and its proximity to the equator. Consequently, it seems likely that global temperature shifts and acidification resulting from these pollutants contributed to the K/T biological extinctions.

V. L. Sharpton, Lunar and Planetary Institute, 3600 Bay Area Blvd., Houston, TX 77058; L. E. Marín, Instituto de Geofisica, Universidad Nacional Autonoma de Mexico, Mexico City, Mexico.

Sharpton, V. L.; and Marín, L. E., 1997, The Chicxulub impact basin, Yucatán, Mexico, *in* Johnson, K. S.; and Campbell, J. A. (eds.), Ames structure in northwest Oklahoma and similar features: origin and petroleum production (1995 symposium): Oklahoma Geological Survey Circular 100, p. 277.

The Marquez Crater in Leon County, Texas

Alan C. Wong, Jonathan C. Sadow, Arch M. Reid, and Stuart A. Hall
University of Houston
Houston, Texas

Virgil L. Sharpton
Lunar and Planetary Institute
Houston, Texas

The Marquez dome in Leon County, Texas, is characterized by the exposure of Cretaceous sedimentary rock, in an approximately circular 1.2-km-diameter disturbed zone surrounded by shallowly dipping Tertiary sedimentary strata. This region of local uplift was originally interpreted as the surface expression of a salt dome at depth. Gibson and Sharpton (1989) and Sharpton and Gibson (1990) reinterpreted the structure, explaining the central disturbed zone as the central uplift of a mostly buried, complex impact crater. The presence of continuous flat-lying seismic reflectors beneath the structure indicated that the disturbed zone dies out downward, and well-log information confirmed the absence of a salt dome beneath the uplift. The presence of shatter cones and planar deformation features in quartz in the surface rocks provided further evidence for an impact event. Gibson and Sharpton's estimate of 58 Ma for the age of the event that caused the disturbance was confirmed by apatite fission-track dating (McHone and Sorkhabi, 1994).

We have reexamined the few surface exposures and completed a new gravity survey in and around the structure. These results, along with data derived from a significant number of geophysical well logs in the area, have been utilized in an attempt to define the subsurface nature of the Marquez structure. We were able to compile structure maps for five different stratigraphic horizons that had been disrupted by the impact. The new data define the shape of the central uplift, confirm that the magnitude of the disturbance decreases with depth, and show that there is no evidence of deformation below about 2,000 m depth. The lateral extent of the crater was estimated from the location of the small negative gravity anomaly that surrounds the central uplift.

Gravity and well-log data are in agreement with the hypothesis that the Marquez structure is a buried crater in which the only surface expression is the limited exposure of the central uplift. A three-dimensional model has been constructed of the central uplift to a depth of 2,000 m. The revised model yields a crater diameter estimate of 12.7 km with an uplift in the center of the structure that is at least 1,120 m. In the hope of recovering material from close to the original crater floor, two shallow wells were drilled to depths of 481 m at 3 km from the center and 274 m at 1 km from the center. The scaling laws established for impact craters in crystalline targets predict breccia zones at these depths, but no evidence for a major breccia lens was encountered in either well, from the tailings (taken at 5 ft intervals) or from the very limited coring. The breccia zones characteristic of impact craters in solid targets either did not form at the predicted levels in these water-saturated unconsolidated target materials or were very rapidly eroded, leaving the disturbed central uplift rocks as the only prominent evidence of impact.

REFERENCES CITED

Gibson, J. W., Jr.; and Sharpton, V. L., 1989, Marquez dome: a newly recognized complex impact structure in East Texas [abstract]: EOS (American Geophysical Union, Transactions), v. 70, p. 383.

McHone, J. F.; and Sorkhabi, R. B., 1994, Apatite fission-track age of Marquez dome impact structure, Texas [abstract]: Lunar and Planetary Science, v. 25, p. 881–882.

Sharpton, V. L.; and Gibson, J. W., Jr., 1990, The Marquez dome impact structure, Leon County, Texas [abstract]: Lunar and Planetary Science, v. 21, p. 1136–1137.

Alan C. Wong, Jonathan C. Sadow, Arch M. Reid, and Stuart A. Hall, Department of Geosciences, University of Houston, Houston, TX 77204; Virgil L. Sharpton, Lunar and Planetary Institute, 3600 Bay Area Blvd., Houston, TX 77058.

Wong, A. C.; Sadow, J. C.; Reid, A. M.; Hall, S. A.; and Sharpton, V. L., 1997, The Marquez crater in Leon County, Texas, *in* Johnson, K. S.; and Campbell, J. A. (eds.), Ames structure in northwest Oklahoma and similar features: origin and petroleum production (1995 symposium): Oklahoma Geological Survey Circular 100, p. 278.

Merna Crater—A Young Impact Feature in Loess of Central Nebraska

Wakefield Dort, Jr., Edward J. Zeller, Larry D. Martin, and Ula L. Moody*
University of Kansas
Lawrence, Kansas

ABSTRACT.—The primary eolian depositional surface of loess that composes West Table in central Custer County, Nebraska, is interrupted by a nearly circular depression approximately 1,500 m across and 20 m deep that is surrounded by a discontinuous rim that rises 3–6 m above the general terrain. Centripetal gullies are depositing all of their load on the depression floor, thereby reducing the original depth.

We have considered and rejected possible origins by deflation, piping, solution subsidence, or volcanic or glacial processes. We have concluded that Merna Crater was created by the hypervelocity impact of an extraterrestrial bolide.

Reconnaissance sampling has resulted in recovery of particulates that appear foreign to loess deposits. We have recognized four informal classes: (1) black, magnetic spherules up to 1 mm across composed mainly of iron oxide and titanium oxide in a wide range of proportions, (2) flat to slightly curved silica glass plates, the surfaces of which are pockmarked with innumerable dimples 1–5 μm in diameter, (3) irregular glass fragments, some of which contain magnetic spherules as inclusions, and (4) spherical aggregates, 1–5 mm across, of grains of both magnetic and glassy compositions, found only in the basal part of the proposed ejecta blanket.

Merna Crater is extremely young. It cuts the Peoria Loess, deposition of which concluded about 12,000 yr ago. The relatively slight development of sidewall gullies in the loose silt required even less time. A soil buried by glassy sediment believed to be part of the ejecta blanket yielded a radiocarbon age of 2,860 yr B.P.

INTRODUCTION

The terrain of central Nebraska is characterized by the presence of scattered, isolated loess tablelands. The margins of these uplands are etched by innumerable small "loess canyons" that are being rapidly extended headward (Dort, 1991). These tablelands stand as much as 100 m above flanking lowlands created in the recent past by fault movements and through-flowing streams. Although broadly horizontal, the tables bear numerous low-relief hummocks and hollows that are believed to collectively constitute the final depositional surface formed as loess accumulation terminated. Many of these gentle undulations are shown on topographic maps by only one or two 10-ft contour lines; some are not indicated at all by the published maps. The undulations tend to be elongated in a northwest-southeast direction that is interpreted to express prevailing wind flow at time of deposition. A few of the hollows are somewhat deeper and irregular in outline.

The surface of West Table, located west of the towns of Merna and Broken Bow in Custer County (Fig. 1), is marked by a very prominent depression that is notably different from other hollows either nearby or on distant tables (Fig. 2). It is nearly circular, approximately 1,500 m across and about 20 m deep. It is cut into the Peoria Loess, accumulation of which ended roughly 12,000 yr ago. This depression—occupying almost all of sec. 9, T. 17 N., R. 23 W., and centered on lat 41°27′30″N, long 99°58′30″W—clearly truncates or interrupts

Wakefield Dort, Jr., and Ula L. Moody, Department of Geology, University of Kansas, Lawrence, KS 66045; Larry D. Martin, Museum of Natural History, University of Kansas, Lawrence, KS 66045.

*Deceased.

Dort, Wakefield, Jr.; Zeller, E. J.; Martin, L. D.; and Moody, U. L., 1997, Merna Crater—a young impact feature in loess of central Nebraska, *in* Johnson, K. S.; and Campbell, J. A. (eds.), Ames structure in northwest Oklahoma and similar features: origin and petroleum production (1995 symposium): Oklahoma Geological Survey Circular 100, p. 279–293.

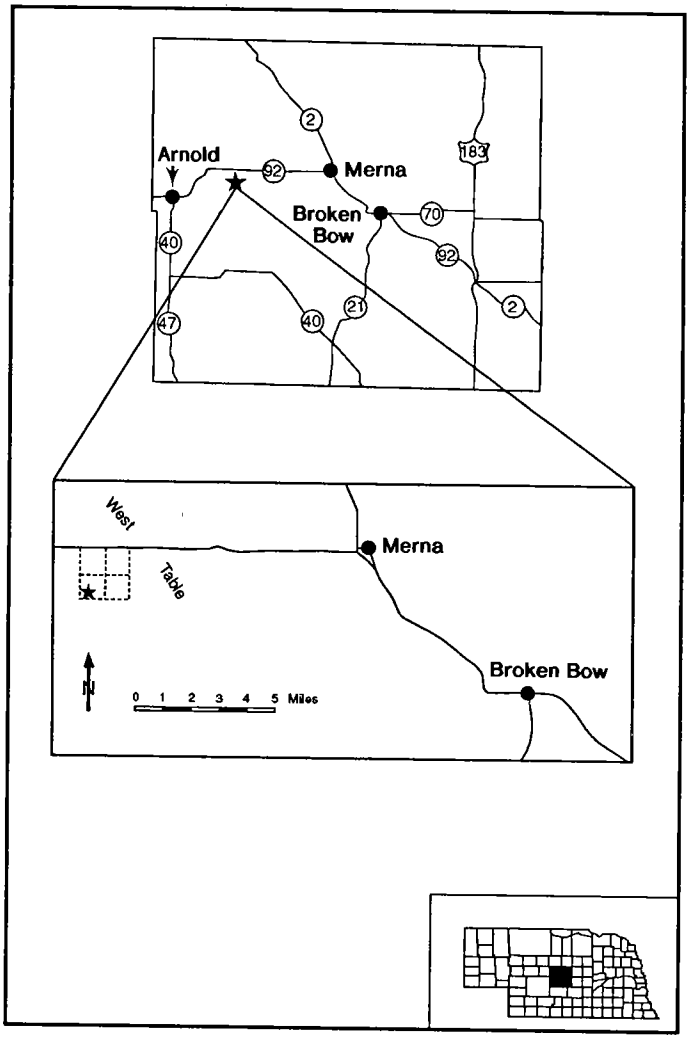

Figure 1. Location of Merna Crater (star) in Custer County, central Nebraska.

the northwest-southeast grain of the general table surface (Fig. 3).

The present flat floor (Fig. 4) of the depression is a secondary depositional surface that is not related to the original formation of the hole. Since the depression first formed, inward flowing (centripetal) gullies have been eroded into the sidewalls. All of the sediment carried by these intermittent streams has been deposited at the center, thereby reducing the original depth, which is believed to have exceeded 50 m. This value is based on computation of the volume of sediment that was removed to create the gullies, then deposited to build up the floor of the depression. The hole is surrounded by a discontinuous rim that rises 3–6 m above the surrounding terrain, which has a general elevation of about 915 m above sea level.

POSSIBLE ORIGIN OF CRATER

This feature has been named the Merna Crater after the town of Merna, located 18 km due east. Because it differs from all other landforms in the area, its origin must have been in some way unique. In an attempt to understand this origin, we have studied the crater on maps and aerial photographs and in the field for more than three years. We describe the origins that we considered below. We conclude that it was most probably created by the hypervelocity impact of an extraterrestrial bolide. No other origin fits all of the observed relationships (Dort and others, 1992,1993).

Eolian Deflation Hollow

Inasmuch as this depression is cut into a plain that is the upper surface of wind-deposited loess, and because it is situated only 8 km from the southern border of the Nebraska Sand Hills, an eolian origin must be considered. Nevertheless, we believe that it is not a deflation hollow. The usual deflation hollow is elongated in the direction of the prevailing wind, not circular, and any raised rim should be restricted to the downwind end of the depression, not extending all the way around it. Furthermore, the depression's original depth as estimated from the apparent thickness of infilling sediment reached below the contact between the Peoria Loess and the underlying Loveland Loess. Regionally this contact is the location of the thick, clay-rich Sangamon Paleosol, a unit that would have retarded, or completely stopped, deflation. The diameter and depth of this depression greatly exceed those of depressions of clear eolian origin located on the loess tables and in the Sand Hills of Nebraska.

Collapse Above Subsurface Solution Void

Drillers' logs for several water wells located within a few kilometers of the crater record the presence of 150 m of clay, silt, sand, and fine gravel, presumably the Peoria and Loveland Loesses and fluvial interbeds. Annotations by an unidentified geologist on the log of a well 10 km to the east located the probable top of the Ogallala Group (gravel) at a depth of 128 m. A deeper well nearby encountered possible Arikaree Group beds (silts and volcanic ash) about 130 m below the top of the Ogallala, the Brule Formation (silt) perhaps 10 m deeper, and estimated the Pierre

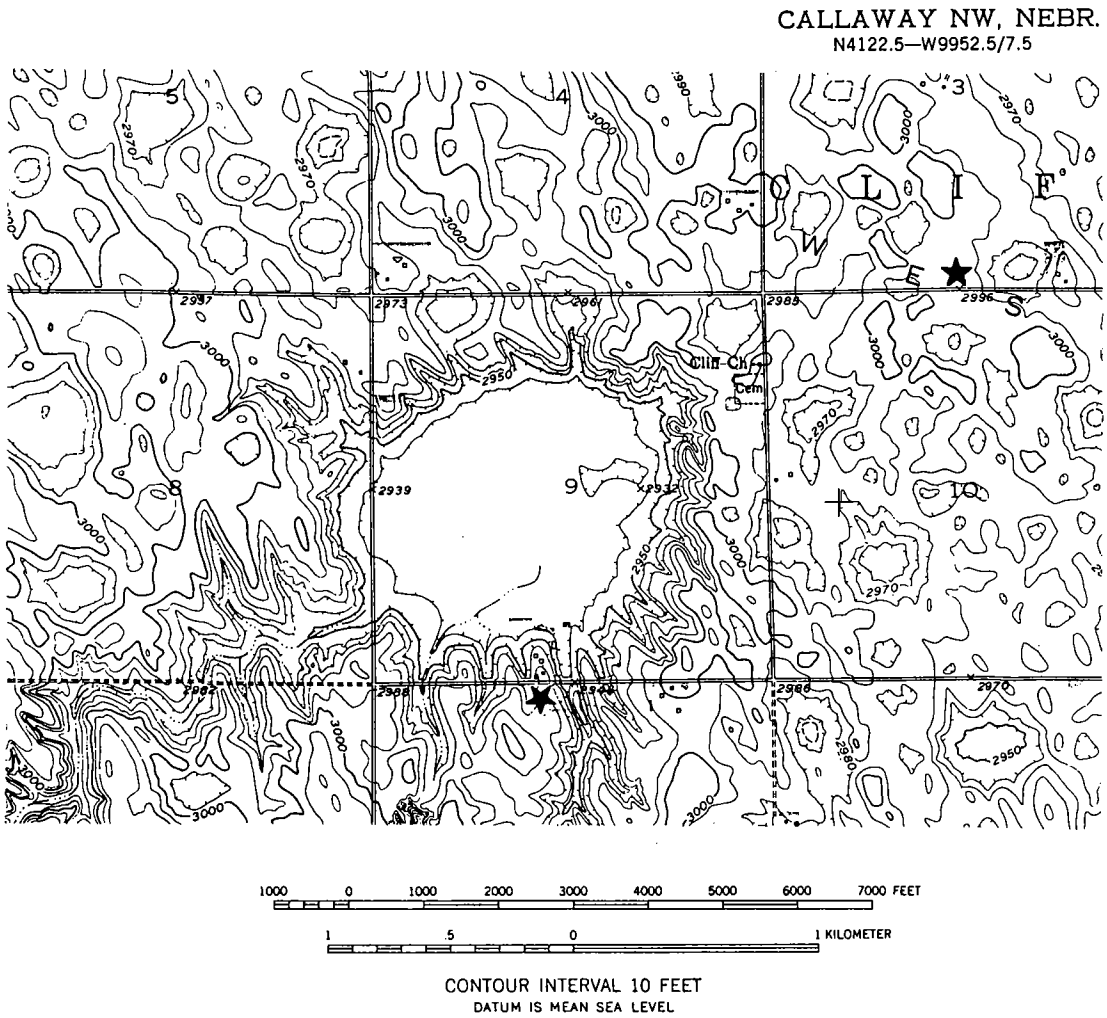

Figure 2. Topographic map of Merna Crater and environs. Two main sampling sites are shown by stars; a third site is located 4 km east of the crater.

Shale 30 m or more below that, followed at even greater depths by the Colorado Group and Dakota Group.

The loesses are composed of quartz grains, and the older formations contain clastic debris derived mainly from erosion of igneous rocks in the mountains to the west, plus a locally high influx of volcanic ash. This means that for more than 300 m below the surface of West Table, there are no sediments soluble enough to produce large voids or significant surface collapse. It appears unlikely that Merna Crater formed in this way. The raised rim would be inexplicable by solution collapse.

Piping

Water descending from the land surface along an animal burrow, decomposing tree root, or desiccation crack can transport sediment, removing it from the near-surface environment and redepositing it beyond some exit orifice at a lower elevation. This process is called "piping," and it is believed by some field workers to be common in areas of loess uplands. Indeed, it has been suggested to us that this was the process by which Merna Crater was formed. However, we believe that piping cannot account for a landform of this size.

To create a circular depression by piping, all of the missing sediment would have to be removed by way of a pipe, or group of pipes, situated in the center. It could be argued that no such conduit is now visible in the middle of Merna Crater because sediment removal occurred at some time in the past and the head of the pipe has since been covered. Perhaps, but another obstacle to application of this theory is more difficult to refute.

Approximately 35×10^6 m^3 of loess must have

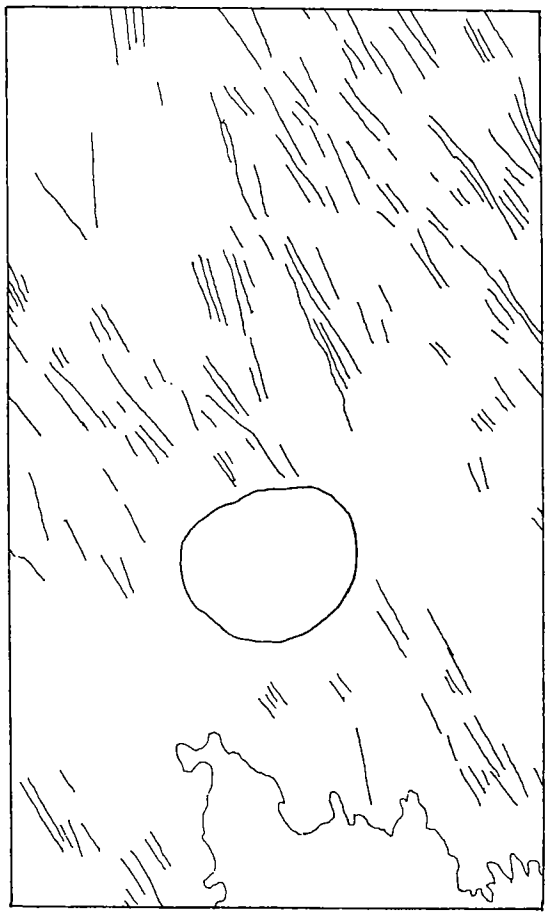

Figure 3. Setting of Merna Crater in field of linear eolian topography. Irregular line in southeast marks limit of headward erosion into West Table by fingertip tributaries of loess canyons.

been removed to create the depression now seen on West Table. Conservative computations based on the volume of loess transported into the original crater by expanding centripetal gullies yield an additional 35×10^6 m^3. Therefore, the original hole was created by the removal of at least 70×10^6 m^3 of silt. If a volume even approximating that magnitude was transported down an underground conduit and spewed out at a lower-elevation orifice into a neighboring creek valley, the resulting depositional mass should be easily recognizable. No such accumulation is seen in adjacent valleys, and we conclude that material transfer by piping did not happen.

Volcanic and Glacial Origins

We reject origins by volcanic action, melt-out of buried glacier ice, or thermokarst developed on melting permafrost. Merna Crater penetrates a very young loess. There is no evidence of recent volcanism within hundreds of kilometers of the site. Furthermore, Pleistocene ice sheets terminated roughly 300 km to the north and 200 km to the east of the crater, at a time long before deposition of the Peoria Loess.

Meteorite Impact

The simplest, most parsimonious explanation for the creation of Merna Crater is by a hypervelocity impact of an extraterrestrial body. Indeed, it is not necessary that an arriving bolide actually strike the Earth's surface. While traversing the atmosphere, a bolide generates an intense shock wave. The wave will strike the surface with great force, and a crater may be formed even if the incoming object itself breaks into fragments or vaporizes completely.

If an impact origin for the depression on West Table is tentatively accepted, closer estimation of the original depth of the crater is possible. The relationship between diameter and depth has been plotted by Baldwin (1949) for craters formed by artificial explosions on Earth and by natural impacts on both Earth and the Moon. Because all crater walls slope inward, measurement of diameter is affected by location in the vertical plane. The crater on West Table is about 1,500 m across at the top, but side slopes must have retreated by slumping and slope wash since they were created. The average diameter at the level of the present depositional surface, the depression floor, is about 1,000 m. According to Baldwin's graph, a crater 1,000 m across should have been about 150 m deep. This value is somewhat greater than indications from more recent publications that are summarized by Grieve (1987,1991), but less than the depth-to-diameter ratio advanced by Pike (1980) and Melosh (1989).

Characteristics of material into which a crater has penetrated will affect the dimensions of the depression, especially through modification by slumping and erosion of the side slopes. All of Baldwin's larger craters, as well as many of the smaller ones, extend into, or even lie entirely within, bedrock. It must be emphasized that in this respect Merna Crater is different. It lies entirely within loose, unconsolidated silt and fine sand. There is no known closely similar crater in the world. The Rio Cuarto craters are in loess, but are elongate; the Campo del Cielo craters, also in loess, are much smaller features. Both of these groups of depressions are in Argentina.

MATERIAL EVIDENCE

As soon as the depression had been tentatively identified as a meteorite-impact crater on the basis of interpretation of the geomorphology, it became incumbent on us to search the area for mate-

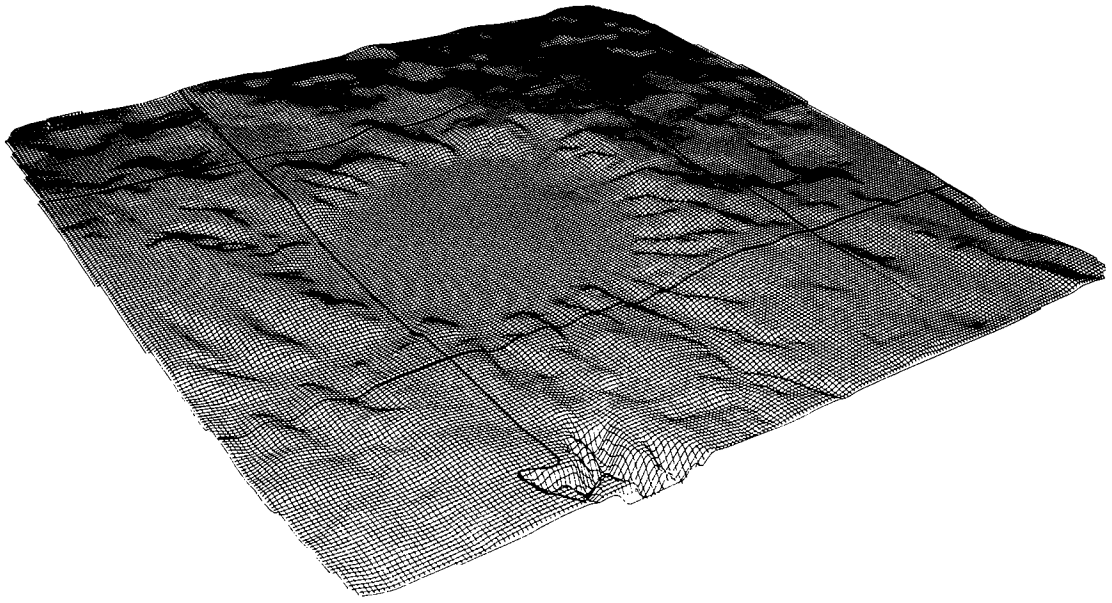

Figure 4. Computer-generated depiction of Merna Crater as viewed toward the northeast. Note discontinuous rim breached by recent gullying. Bold lines are roads on 1-mi grid. (Prepared by Erik Hubl, Lincoln, Nebraska.)

rial evidence. Unfortunately, most of the first-order diagnostic features usually associated with meteorite craters cannot possibly be present here, at least not on the surface. There can be no surface exposure of upturned rock layers, no brecciated or metamorphosed bedrock, no development of shatter cones. Not only is this crater entirely within unconsolidated silt and fine sand, but it is separated from any approximation of solid rock by more than 300 m of loose to very weakly cemented sediments. The force of the impact may well have disrupted deep rocks, but it is highly unlikely that blocks were raised as far as the present land surface.

An impact would, of course, have greatly disturbed near-surface materials. This effect could be detected if there were recognizable and traceable horizons or contacts in those units. It is well known that at some localities in central Nebraska, the Peoria Loess is separated from the underlying Loveland Loess by a paleosol complex called the Gilman Canyon Formation and that the thick Sangamon Soil is developed in the uppermost part of the Loveland Loess. Our reconnaissance has failed to discover exposures of these paleosols anywhere on or near West Table. There is, however, a sand unit at approximately the same stratigraphic level, but it seems to have been discontinuous even before an impact might have occurred, and any subsequent disruption cannot, at present, be identified.

Early in this study we initiated a reconnaissance program aimed at discovering quickly whether or not any unusual substances are present at the land surface in the vicinity of the crater. Remains of a bolide, fragments of impactite, grains of shocked minerals, or an ejecta blanket would all support a meteoritic origin. If, on the other hand, all we could find were angular silt-sized grains of quartz typical of a "normal" loess, then we would be forced to reevaluate our ideas about the origin of Merna Crater.

Grab samples were collected at randomly selected sites within the crater, on its upper sidewall and rim, on the upland to the east and northeast, and in the dissected area to the south. The bulk of each sample was composed of the expected silt-sized grains of quartz. Mixed in, however, were other kinds of particulates that we had not observed in loess samples from other parts of Nebraska and from Kansas (Fig. 5).

Our reconnaissance sampling program has led to recognition of four informal classes of unusual particulates present in the vicinity of Merna Crater: (1) black, magnetic spherules about 1 mm across, composed mainly of iron oxide and titanium oxide; (2) flat to slightly curved silica glass plates, the surfaces of which are pockmarked by innumerable dimples 1–5 μm in diameter; (3) irregularly rounded glass fragments, some of which contain magnetic spherules as inclusions; and (4) spherical aggregates, 1–5 mm across, composed of

Figure 5. Strew of unsorted grains from surface loess sample collected 1 km northeast of Merna Crater. Rounded grains are magnetic Fe-Ti spherules. Arrow in upper left points to glass plate. (Micrograph by Bruce Cutler, SEM Laboratory, University of Kansas.)

numerous tiny grains of both magnetic and glassy material of a wide range of compositions.

Black Magnetic Spherules

Results of microscopic examination of samples of loess collected at several widely separated localities in Nebraska and Kansas suggest the nearly ubiquitous presence of black, magnetic grains. These are typically a small fraction of a millimeter across and highly irregular in form. They occur both as single grains and in small aggregations. Their origin is anecdotally linked to soil-forming processes, although details are lacking.

Tiny grains of this sort occur in the loess near Merna Crater. Also present, however, is a very different population of black, magnetic grains. These are round to somewhat ovoid (Fig. 6). Most are roughly 1 mm in diameter; a few are somewhat smaller, a few larger. Their surfaces, as

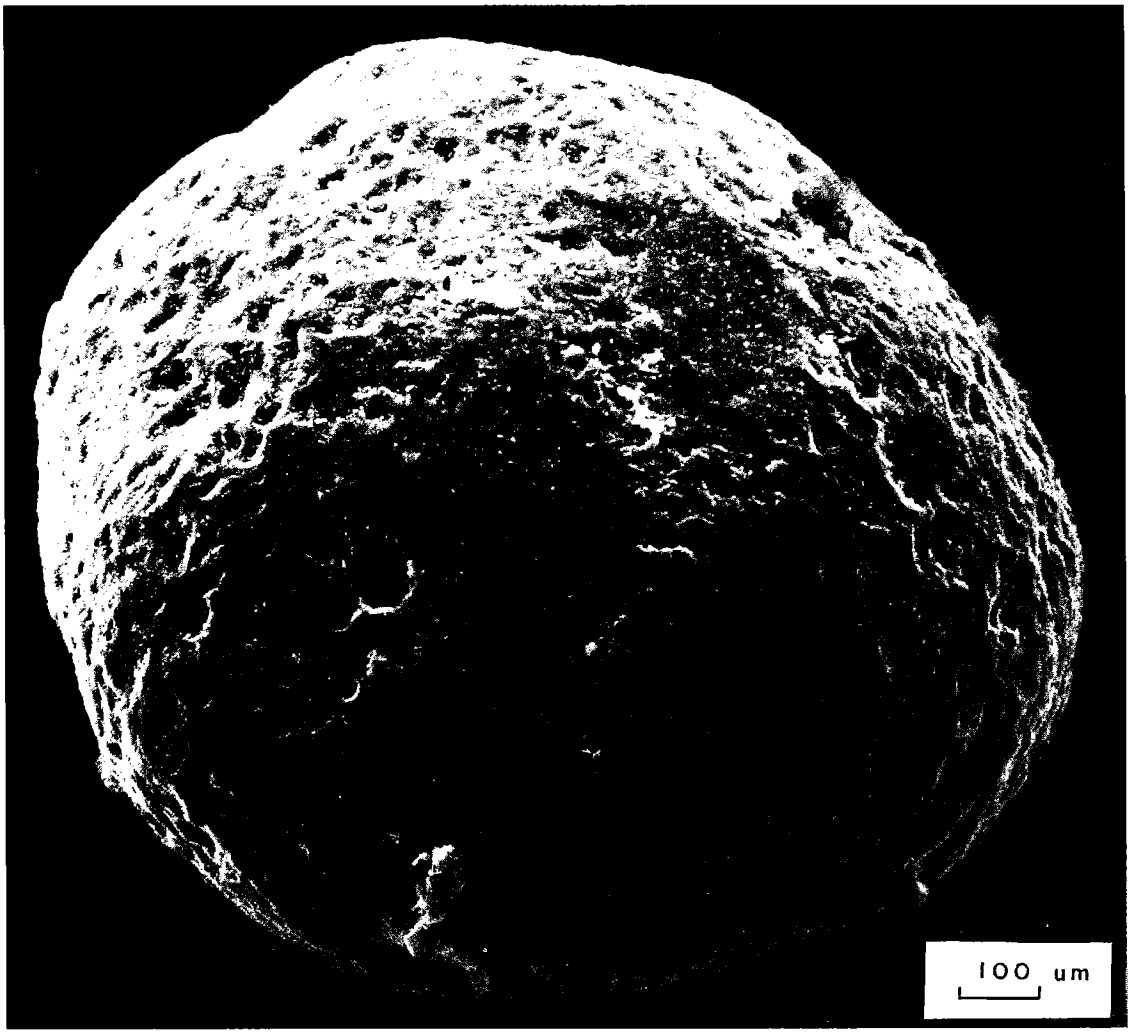

Figure 6. Scanning electron micrograph of magnetic Fe-Ti grain from southern rim of Merna Crater. (Micrograph by Bruce Cutler, SEM Laboratory, University of Kansas.)

shown by scanning electron microscope, are rough and pitted and bear irregular small blobs of white material that is believed, from X-ray analysis, to be silica glass. The compositions of the spherules themselves range from iron oxide with only minor amounts of titanium oxide to approximately 50% iron oxide and 50% titanium oxide (Fig. 7). They are, therefore, not the mineral ilmenite. The X-ray determinations also detected traces of Mg, Al, Si, K, Ca, and Mn; the specific elements and their apparent amounts varied from one spherule to another.

Thousands of these rounded black, magnetic spherules speckle the ground about 1 km northeast of Merna Crater. They appear to have been concentrated on the present surface by rain splash and deflation. This area has been deeply plowed many times for more than 100 yr. Therefore, it is likely that the primary spherule-bearing horizon originally lay at a depth of several tens of centimeters. Spherules of this type have also been recovered from a road cut on the inside of the southern rim of the crater.

Glass Plates

Numerous in a few of our samples are flat to slightly curved plates 100–300 μm across. These grains have conchoidal fracture, appear clear under plane-polarized light, but remain black under cross-polarized light. They are believed to be composed of silica glass. The flat surfaces of all samples studied are pocked with innumerable de-

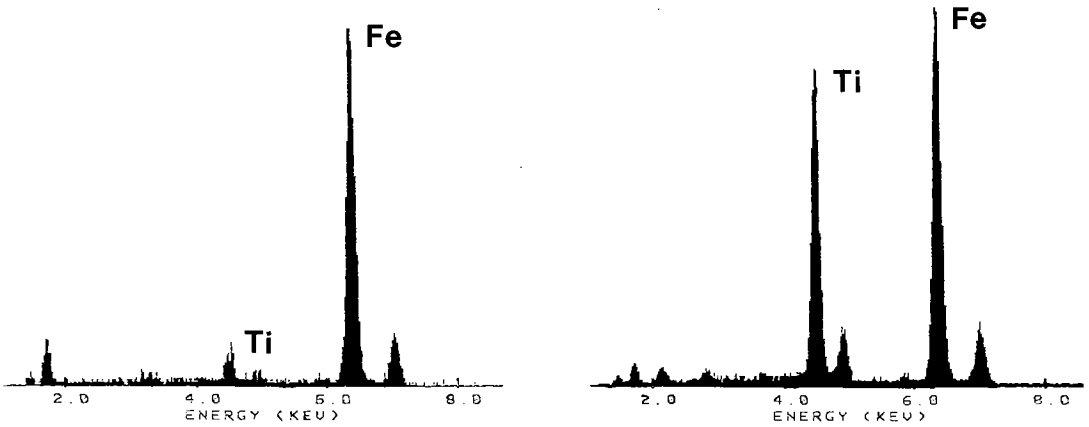

Figure 7. XRF spectra illustrating end members of range in Fe and Ti contents of magnetic spherules, all of which appear physically alike under the SEM. (Analyses by Bruce Cutler, SEM Laboratory, University of Kansas.)

pressions ranging in diameter from slightly more than 2 μm to <0.5 μm (Fig. 8). None of these grains even vaguely resembles shards of volcanic glass.

Fresh dissection 4 km east of Merna Crater has exposed a layer, up to about 30 cm thick, that is a much lighter color than the loess below and above it (Fig. 9). This layer, known to us colloquially as "the white layer," has a high content of the glass plates. X-ray fluorescence analyses of 20 individual plates and one composite bulk sample (Table 1) revealed compositions predominantly of silica with subordinate aluminum and numerous trace elements.

Glass with Magnetic Inclusions

Differing greatly from the glass plates are irregularly rounded clear grains that also remain black under cross-polarized light. A very few of these contain inclusions of rounded, black, opaque, magnetic particles. No analyses have yet been obtained for these specimens.

Spherical Multigrain Aggregates

A fourth type of particulate was found only in the lowermost few centimeters of the white layer that has been exposed by recent erosion 4 km east of Merna Crater. Here occur scattered spherical aggregates, up to 5 mm in diameter, of tens of tiny grains having widely diverse appearances when viewed under a binocular microscope. Some are glassy; others are black and opaque. These grains adhere tightly together to form the spherules; loose, similar grains do not occur in the surrounding loess.

A bulk X-ray analysis of a single one of these multigrain spherules, selected at random, showed it to be composed largely of Si, Al, and Mn, plus an array of trace elements (Table 1). However, electron-microprobe analyses of individual grains within spherules revealed extreme differences in composition. Grains in three spherules were subjectively selected to include as wide a range of physical appearance as possible in the belief that this would yield the widest range of chemical compositions. The results (Table 2) clearly show that bulk analyses provide little information about true compositions of the constituent grains.

INTERPRETATION OF CHEMICAL DATA

Our attention was drawn to Merna Crater because it is a unique landform, one of a kind for Nebraska. Analysis of geomorphic parameters led us to conclude that it is most readily explained as a product of meteorite impact. The circularity, presence of a raised rim, lack of soluble materials at depth, and absence of both piping conduits and deposits all appear to rule out other possible origins. However, our preliminary examination of samples of sediments from within and near the crater has yielded information that is less convincing.

Aside from elusive iridium, the presence of nickel is usually considered to be a key indicator of an extraterrestrial origin of material occurring under unusual circumstances on Earth. Our finds have, in general, been disappointing. The very first analysis, run for us by L. W. McKenna at the University of Kansas on a blend of several black magnetic spherules, recorded 30 wt% Fe_2O_3, 1000 ppm of Cr, and 50 ppm of Ni. This analysis was requested solely to determine the presence of Ni. The Cr was an add-on, the high level a surprise. We were encouraged by the Ni content. However, all subsequent analyses of individual black magnetic spherules, made by X-ray fluorescence linked to a scanning electron microscope and run by B. E.

Figure 8. Scanning electron micrograph of surface of silica glass plate. All examples studied showed similar pockmarking by innumerable round depressions. (Micrograph by Bruce Cutler, SEM Laboratory, University of Kansas.)

Cutler at the University of Kansas, found no Ni within the limits of detection. On the other hand, electron-microprobe analyses of individual particles, made by U. L. Moody at Washington State University, contained in multigrain spherules from the white layer found as much as 0.4 wt% Ni (Table 2), and bulk analysis of all the grains in one spherule recorded 499 ppm Ni (Table 2). Neutron activation analysis of bulk samples of multigrain spherules found 780–900 ppm Ni (Table 3).

Meteoriticists with whom we have discussed our findings have been in general agreement that our analyses show too little Ni and too much Ti for material of extraterrestrial origin. Indeed, Dence (1971, p. 5560) stated that "nickel, being two or three orders of magnitude more abundant in mete-

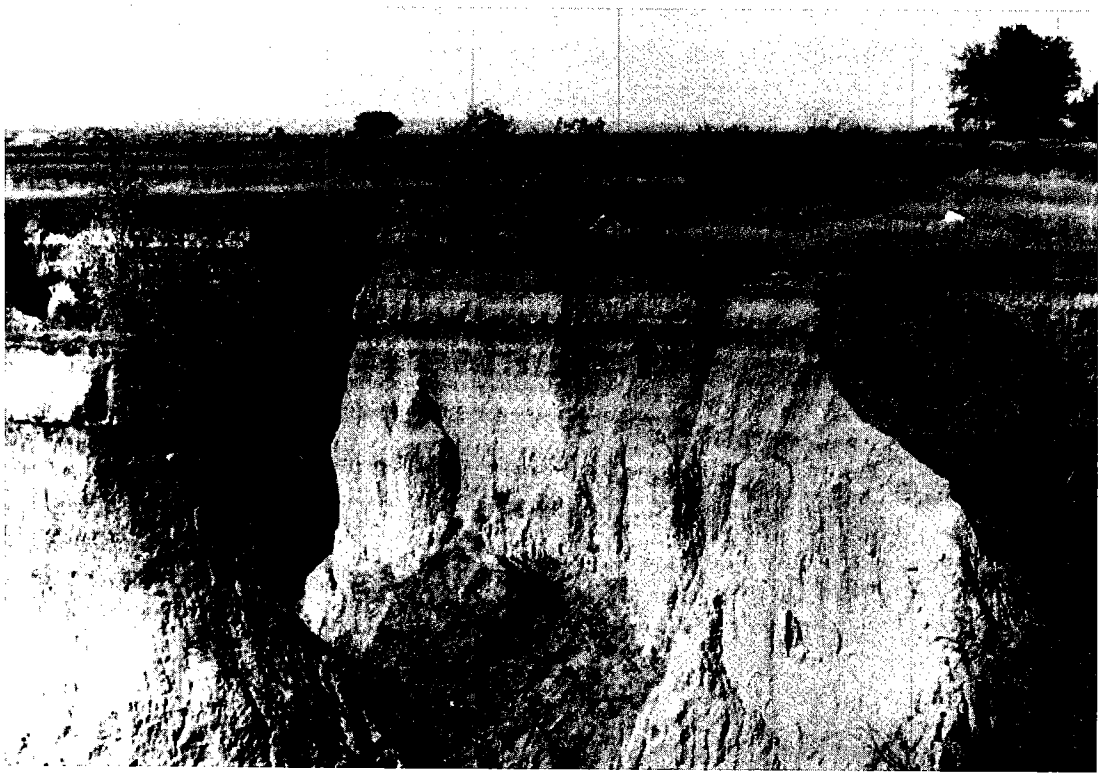

Figure 9. Fresh exposure 4 km east of Merna Crater. The tip of the arrow (right of center) points to the contact between the white layer and the underlying paleosol, which yielded a radiocarbon date of 2860 yr B.P.

orites than in average crustal rocks, is potentially the most useful indicator of meteoritic contamination." Nevertheless, studies made more recently show that Ti is often present, especially in interplanetary dust particles (IDPs). Indeed, in a list of element abundances in 89 IDPs published by Arndt and others (1996), 40 of the specimens contained more Ti than Ni. Greshake and others (1996) reported that inclusions of rutile (TiO_2) were identified in carbonaceous chondrites, and Christoffersen and Buseck (1986) found perovskite ($CaTiO_3$) in an IDP. Zhang and others (1992) detected both Ti and Ni in black magnetic spherules believed to be microtektites.

In this respect, tabulations of chemical constituents of meteorites provided by Dodd (1981, tables 2.1, 8.2, 8.3, 9.1, 9.5) are of interest. Although Ni content (listed in some tables as an element, in others as an oxide) ranges from 14 to 61 times Ti in chondritic meteorites (the most Ni occurs in the enstatite chondrites), these two elements occur in almost equal amounts in ureilites, Ti can exceed Ni in achondrites, and only Ti is recorded in eucrites and diogenites. Wood (1963, table 10) tabulated the presence of TiO_2, but no NiO, in eucrites, howardites, diogenites, ureilites, and nakhlites. Similar results were listed by Jarosewich (1990). Glass (1971, table 2) tabulated TiO_2 content ranging from 0.15 to 8.6% in specimens of lunar debris collected by Apollo 11 and 12 astronauts. Impact glass at the Henbury Craters contains almost 1% TiO_2 (Taylor, 1967, table 1).

Ni contents can range up to nearly 20% in iron meteorites, but similarly high percentages of Ti are unknown. It therefore seems clear that formation of spherules apparently composed of nearly equal amounts of iron oxide and titanium oxide, to the near exclusion of other elements, would require either an unusual source bolide or a peculiar concentration mechanism. We do, however, note that Koeberl (1986, table 3) reported the presence of TiO_2 in all tabulated classes of tektites, although he stated (Koeberl, 1994, p. 133) that these objects are "produced by nonequilibrium shock melting of surficial rocks." Amounts generally range from 0.5% to a little more than 1%, but some basic zhamanshinites exceed 5%, yet have only 10–11% FeO, proportions similar to some of the Merna spherules. It is alternatively possible that the Ti was derived from target material, i.e., the loess. Unfortunately, there is a decided dearth of published analyses of individual grains present in loess. Trace elements reported from analyses of bulk loess samples may indeed be present in

TABLE 1.—X-RAY FLUORESCENCE (XRF) ANALYSES OF SAMPLES FROM WHITE LAYER

Element	1	2	3
SiO_2	80.90	71.05–73.76	66.38
TiO_2	0.41	0.07–0.45	0.49
Al_2O_3	10.76	11.19–12.34	10.69
Fe_2O_3	—	0.71–2.58	—
FeO	1.22	—	6.82
MnO	—	—	10.37
MgO	0.31	0.04–0.22	0.00
CaO	1.46	0.30–1.00	1.68
Na_2O	1.97	0.97–3.29	0.00
K_2O	2.90	4.46–8.00	2.18
P_2O_5	0.02	—	1.39
Cl	—	0.00–0.18	—
Sc	4	—	0
V	29	—	96
Cr	25	—	0
Ni	15	—	499
Cu	30	—	70
Zn	25	—	214
Ga	9	—	0
Rb	88	—	77
Sr	300	—	216
Y	24	—	44
Zr	366	—	243
Nb	14	—	48
Ba	867	—	11,648
La	21	—	0
Ce	92	—	546
Pb	14	—	161
Th	10	—	12

Note: XRF analyses by F. F. Foit, Jr., and U. L. Moody at Washington State University. Major elements in weight percent; trace elements in parts per million. Samples: (1) composite bulk sample, (2) ranges for 20 glass plates, and (3) single multigrain spherule. Samples were collected from white layer exposed about 4 km east of Merna Crater.

grains of the loess itself, or they may conceivably occur in interplanetary dust particles that fell as the loess was accumulating.

The presence and proportions of rare earth elements are used by some researchers to distinguish extraterrestrial materials. Neutron activation analysis of samples from Merna (Table 3) led L. A. Haskins to state, "the bulk of the material in the spherules is not meteoritic, but seems to have come from the loess" (personal communication, 1994), and he suggested that sedimentary processes were involved. It is then frustrating to discover that there is available very little detailed information about either the presence or source of trace elements in loess.

The data presented in Table 2 clearly demonstrate the necessity of analyzing individual grains. Analysis of bulk samples obscures the great range of composition that may be present. Furthermore, the existence of numerous grains of such disparate compositions all adhered together into a single spherical mass would seem to preclude any sedimentary or pedogenic controls in the currently existing environment. Therefore, we must conclude that at this stage of the study, our chemical data neither prove nor disprove meteoritic activity.

AGE OF THE CRATER

Regardless of whether Merna Crater was formed by meteorite impact or by some other, as yet unrecognized process, the time of its creation is of interest. This landform lies wholly within the Peoria Loess, an unconsolidated silt that erodes rapidly when disturbed. For example, in 1992 a 6-ft-deep miniature canyon was cut into the bed of a farm road by runoff from a single unusually heavy spring rain.

The side slopes of the crater are now notched by more than 30 gullies (Figs. 2 and 4). These must have been eroded by intermittent localized runoff since the depression was formed. Early in the course of this research, it was estimated, on the basis of general geomorphic field experience, that a period of about 3,000 yr might have been required to produce the landform pattern existing today. That duration was then used informally as the possible age of the crater.

The so-called white layer that has been exposed by ongoing dissection 4 km east of Merna Crater directly overlies a dark gray unit that is clearly a paleosol (Fig. 9). Organic carbon contained in this buried soil has yielded a radiocarbon age of 2,860 ± 50 yr. If our interpretation is correct that the white layer is the ejecta blanket from the crater, then impact occurred approximately 2,860 yr ago. The close agreement of this measured number with that estimated on geomorphic grounds is gratifying, but perhaps fortuitous.

POTENTIAL VALUE OF STUDY

If further study provides verification of the proposed origin of Merna Crater by hypervelocity impact of an extraterrestrial body, this crater will be the largest (in diameter) impact crater—as opposed to impact structure or eroded astrobleme (Dietz, 1961)—yet identified in North America. Its width is slightly greater than that of Meteor Crater, Arizona, although its depth and the relief of its rim are much less. This contrast is undoubtedly due to the strength of the target material (loess vs.

TABLE 2.—ELECTRON-MICROPROBE ANALYSES OF INDIVIDUAL GRAINS IN MULTIGRAIN SPHERULES FROM WHITE LAYER

Samples	Si	Al	Fe	Mn	Ba	K	Ca	Ti	V	Ni
Spherule 1										
Bright metallic	0.58	0.42	95.65	1.04	0.15	0.05	0.05	2.38	0.08	0.00
Glassy	99.45	0.06	0.40	0.14	0.01	0.00	0.01	0.00	0.01	0.00
Glass, bubbles	71.32	11.92	1.38	0.48	0.20	5.49	1.00	0.10	0.00	0.00
Glassy	65.97	17.94	0.12	0.57	0.02	0.04	0.29	0.01	0.00	0.02
White matrix	64.56	16.38	0.97	2.96	0.47	5.24	3.03	0.36	0.00	0.02
Dark matrix	9.84	1.86	8.07	55.28	5.62	0.56	2.12	0.09	0.20	0.17
White matrix	21.70	8.77	6.71	43.30	4.25	1.61	2.32	0.25	0.12	0.14
Dark matrix	30.31	5.53	5.67	37.41	4.03	1.33	1.93	0.24	0.17	0.16
Dark matrix	14.73	4.37	20.50	19.53	2.55	1.17	1.83	0.23	0.06	0.06
Opaque	45.62	11.08	14.74	0.34	0.48	1.97	1.72	0.39	0.04	0.00
Opaque	16.39	5.08	5.53	18.13	0.06	1.71	1.24	0.22	0.08	0.05
Dark matrix	16.76	1.57	3.12	1.54	0.22	0.55	0.70	1.18	0.06	0.01
Spherule 2										
White matrix	62.70	23.08	2.74	0.85	0.12	0.26	4.74	0.04	0.00	0.00
Bright metallic	0.63	0.92	4.61	70.43	8.66	0.33	1.29	0.09	0.23	0.12
White matrix	1.97	1.47	1.06	72.28	9.37	0.48	1.28	0.13	0.27	0.16
Dark matrix	2.28	0.88	9.59	61.62	6.31	0.65	1.12	0.10	0.19	0.13
Dark matrix	25.99	8.98	8.73	29.13	3.03	1.53	0.76	0.25	0.06	0.24
Glassy	99.13	0.44	0.80	1.68	0.19	0.07	0.05	0.03	0.02	0.00
Dark matrix	28.72	5.26	1.56	31.56	3.48	1.11	0.84	0.04	0.00	0.03
White matrix	1.11	1.51	0.28	73.23	8.59	0.80	1.49	0.11	0.25	0.28
Spherule 3										
Dark matrix	1.34	1.03	12.45	64.65	5.08	1.01	0.93	0.08	0.14	0.11
Glassy	60.55	9.68	3.81	4.61	0.50	5.83	0.70	0.28	0.05	0.00
Quartz	100.72	0.03	0.14	0.32	0.00	0.02	0.01	0.00	0.01	0.00
Glassy	64.70	15.18	3.26	0.14	0.24	5.10	2.05	0.37	0.04	0.00
White matrix	93.70	3.04	0.98	0.14	0.07	0.53	0.08	0.15	0.04	0.00
Dark matrix	26.18	8.49	3.22	38.15	4.12	1.59	2.12	0.23	0.11	0.22
White matrix	85.41	1.56	5.12	3.81	0.41	0.34	0.38	0.33	0.10	0.00
Dark matrix	36.10	13.12	4.86	26.33	2.03	2.29	1.71	0.64	0.12	0.24
White matrix	15.22	6.14	3.73	53.50	4.66	1.46	2.37	0.22	0.22	0.26
Dark matrix	8.00	3.29	2.11	61.97	6.66	0.86	2.32	0.13	0.12	0.41

Note: Analyses by F. F. Foit, Jr., and U. L. Moody at Washington State University. Values in weight percent. Samples were collected from white layer exposed about 4 km east of Merna Crater.

well-indurated bedrock) and probably the nature of the impactor and the vertical location of the explosion on or above the ground surface.

Physical features frequently mentioned as a basis for identification of a meteorite-impact crater—upturned and faulted strata, brecciation, development of shatter cones, evidence of widespread melting—all involve changes imposed on bedrock. Of the 131 impact structures listed by Grieve (1991), the 139 listed by Grieve and Shoemaker (1994), or the 141 briefly described by Hodge (1994), less than a dozen are wholly contained in unconsolidated surficial sediment. Indeed, most of these latter are so small as to be indiscernible from a distance (e.g., Boxhole [Australia], Haviland [Kansas], Snelling [Australia], Veevers [Australia], and individual craters in the Campo del Cielo [Australia], Henbury [Australia], Morasko [Poland], and Sikhote Alin [Russia] groups). Only the Rio Cuarto craters in Argentina closely resemble Merna Crater with respect to size, freshness, and geologic setting; both areas are underlain by thick loess (Schultz and Beatty, 1992; Schultz and Lianza, 1992).

TABLE 3.—INSTRUMENTAL NEUTRON ACTIVATION ANALYSES OF BULK SAMPLES

	White layer*			Loess 70 km	Magnetic spherules	
Element	Spherule 1	Spherule 2	Bulk sample	southwest of Merna Crater	Northeast location*	South location*
Na_2O	0.786 ± 0.008	0.760 ± 0.008	1.536 ± 0.015	1.547 ± 0.015	0.827 ± 0.008	0.067 ± 0.004
K_2O	1.9 ± 0.3	2.0 ± 0.3	2.6 ± 0.3	2.5 ± 0.2	1.7 ± 0.3	<1.0
CaO	1.1 ± 0.4	1.3 ± 0.5	1.25 ± 0.19	2.85 ± 0.14	1.3 ± 0.3	<1.9
FeO	5.68 ± 0.06	5.93 ± 0.06	1.616 ± 0.016	2.39 ± 0.02	33.0 ± 0.3	58.2 ± 0.6
Sc	6.67 ± 0.07	6.87 ± 0.07	5.19 ± 0.05	6.30 ± 0.06	19.06 ± 0.19	58.7 ± 0.6
Cr	32.8 ± 1.0	34.8 ± 1.2	28.8 ± 0.4	38.0 ± 0.4	692 ± 7	783 ± 8
Co	518 ± 5	550 ± 6	5.26 ± 0.05	6.53 ± 0.07	58.6 ± 0.6	76.9 ± 0.8
Ni	780 ± 50	900 ± 60	<21	<23	<160	<300
Zn	210 ± 19	218 ± 9	44.2 ± 1.2	57.2 ± 1.2	533 ± 10	455 ± 12
As	52 ± 0.7	54.9 ± 0.7	2.7 ± 0.2	6.25 ± 0.17	9.9 ± 0.5	2.5 ± 0.8
Se	<1.9	<1.7	<0.4	<0.4	<2.2	<5
Br	1.1 ± 0.2	0.9 ± 0.2	1.52 ± 0.15	0.88 ± 0.09	3.1 ± 0.3	1.1 ± 0.5
Rb	83 ± 6	74 ± 6	89.7 ± 1.4	90.3 ± 1.3	63 ± 7	24 ± 9
Sr	260 ± 50	220 ± 40	229 ± 14	264 ± 11	110 ± 50	<160
Zr	240 ± 50	250 ± 50	318 ± 13	404 ± 12	510 ± 60	600 ± 90
Ag	—	—	<0.5	0.20 ± 0.09	6.9 ± 0.5	–
Sb	3.30 ± 0.07	3.20 ± 0.07	0.516 ± 0.016	0.668 ± 0.015	1.31 ± 0.05	0.64 ± 0.08
Cs	3.79 ± 0.09	3.85 ± 0.10	3.23 ± 0.03	3.65 ± 0.04	2.28 ± 0.10	<0.5
Ba	11,150 ± 200	11,600 ± 200	809 ± 13	766 ± 11	470 ± 20	80 ± 30
La	83.8 ± 0.8	81.6 ± 0.8	38.8 ± 0.4	36.5 ± 0.4	34.9 ± 0.3	33.3 ± 0.3
Ce	982 ± 10	874 ± 9	72.2 ± 0.7	68.9 ± 0.7	64.0 ± 0.7	59.1 ± 0.9
Nd	68 ± 7	71 ± 8	30.8 ± 2.0	30.9 ± 1.8	31 ± 5	34 ± 9
Sm	14.68 ± 0.15	14.35 ± 0.14	6.11 ± 0.06	5.82 ± 0.06	5.75 ± 0.06	5.25 ± 0.05
Eu	2.66 ± 0.06	2.57 ± 0.06	1.137 ± 0.014	1.040 ± 0.012	0.98 ± 0.04	0.80 ± 0.06
Tb	2.20 ± 0.05	2.13 ± 0.06	0.774 ± 0.015	0.709 ± 0.013	0.69 ± 0.04	0.53 ± 0.06
Yb	6.69 ± 0.08	6.76 ± 0.09	2.77 ± 0.03	2.54 ± 0.03	2.56 ± 0.05	1.65 ± 0.08
Lu	0.984 ± 0.019	0.98 ± 0.02	0.404 ± 0.005	0.387 ± 0.005	0.425 ± 0.012	0.279 ± 0.018
Hf	5.96 ± 0.14	6.24 ± 0.15	8.51 ± 0.09	10.06 ± 0.10	12.62 ± 0.20	14.6 ± 0.3
Ta	0.85 ± 0.07	0.88 ± 0.08	0.92 ± 0.02	0.890 ± 0.019	3.49 ± 0.11	12.6 ± 0.3
W	5.1 ± 0.8	4.4 ± 0.7	1.0 ± 0.3	1.2 ± 0.4	<3	<5
Th	10.77 ± 0.12	10.63 ± 0.13	10.84 ± 0.11	11.93 ± 0.12	11.83 ± 0.12	6.18 ± 0.15
U	6.0 ± 0.2	5.1 ± 0.2	3.38 ± 0.09	3.46 ± 0.08	3.64 ± 0.17	1.0 ± 0.3
Ir	<5	<7	<1.1	<0.9	<7	<13
Au	<5	<12	<3	2.9 ± 0.7	275 ± 8	8

Note: Analyses by Trace-Element Geochemistry Laboratory, Washington University, St. Louis. Oxides in weight percent; trace elements in parts per million, except Ir and Au in parts per billion.

* Samples from white layer were collected from an exposure about 4 km east of Merna Crater (see Fig. 9). For locations of samples of magnetic spherules, see Figure 2.

The Rio Cuarto craters are notably elongate, presumably resulting from a very low angle, grazing impact by an object that then broke into fragments that ricocheted farther along the surface. The Merna bolide struck at a higher angle; the crater is almost perfectly circular. However, the loess at the two localities presumably has very much the same physical properties. Therefore, detailed studies of these localities both separately and together will provide theoreticians and modelers much basic data regarding impacts and crater formation in loose material. Furthermore, the craters at both localities are of very recent origin. Schultz and Lianza (1992) suggested an age of "considerably less than 10,000 yr" for Rio Cuarto; at Merna we have an apparent date of 2,860 yr

B.P. In both areas the craters cut into nearly level plains. Geologic processes have changed these surrounding surfaces very little since the time of impact. Therefore, any material either blown out of the crater on impact or condensed from ablation of the bolide during its passage through the atmosphere would still be present on or very close to the land surface. This circumstance provides an unusual opportunity to obtain samples of material, especially particulates, that has long since been eroded away or buried by younger deposits at almost all of the world's impact structures. It is likely that much can be learned of events and processes occurring in the moments immediately preceding and following impact.

A perusal of recent publications, especially the extensive compilation by Melosh (1989), reveals that there remain numerous questions about the mechanics of formation of impact craters. Working concepts and theoretical relationships have been developed almost entirely by study of either large craters formed in solid rock or very small dimples created by artificial explosions. Merna Crater is in an intermediate size class, and it was formed in a different kind of substrate. Here, then, is an opportunity to verify the lower end of scaling laws now in use.

Melosh (1989, p. 14) indicated that the rim-to-floor depth of a simple crater is about one fifth of the rim-to-rim diameter and rim height is about 4% of the diameter. These values imply that Merna Crater would have been about 300 m deep before sidewall collapse and sediment deposition began the infilling process, and its rim would have been about 60 m high. However, it is our belief that remnants of the rim would be more prominent today if its original height had been that great.

Other questions come to mind. Would the rate of decline of the impact shock wave in loose loess be the same as in solid rock, and would excavation flow have proceeded in the same way? There would not have been rock fracturing and ejection of spall plates. Would the resistance afforded by the loess halt the increase in depth at a level different from that determined by characteristics of hard bedrock, and would this difference have produced a variation of the usual width-depth relationship? Grieve (1990) and Grieve and Robertson (1979) suggested that simple craters in crystalline bedrock may be as much as twice as wide as craters formed in sedimentary rocks. Would craters in loose sediment tend to be even narrower and, perhaps, deeper? Would the absence of solid rock permit greater gravitational collapse of the transient crater in the first few minutes after impact and therefore result in a landform of greater than expectable diameter? Close study of Merna Crater, especially in the subsurface, might indicate answers to some of these questions.

PLANS FOR ADDITIONAL STUDIES

Numerous black magnetic Fe-Ti spherules lie on the surface of a plowed field about 1 km northeast of Merna Crater. It is possible that these formed by condensation of vapor from ablation of a bolide traversing the atmosphere from the northeast. However, close examination of sediment samples from an extensive grid is necessary before definitive statements can be made regarding distribution of these particulates. Additional chemical analyses will be run on individual grains from several sampling sites, and the search for shocked grains will continue.

Reconnaissance by portable magnetometer revealed an increasing intensity from southwest to northeast across the crater. Further survey along a grid of closely spaced lines will determine what, if any, definitive pattern is present. Additional data will be sought from remote-sensing records and images (e.g., Garvin and others, 1995; McHone and others, 1995).

The local landowner has reported the presence of about 10 m of "black muck" beneath the present floor of the crater. This section will be sampled by drill to determine the depth and stratigraphic sequence of recent fill to evaluate its organic content and to obtain samples for radiocarbon dating and palynological analysis. Deeper drilling beneath the crater will be attempted.

ACKNOWLEDGMENTS

Merna Crater was discovered during research on an unrelated project funded by National Science Foundation grant EAR-9007029. Support from Robert Bearse and the Research Development Fund of the University of Kansas made possible detailed chemical analyses and radiocarbon dating. We have received enthusiastic assistance from many people in Custer County, especially Brad Bartak, who owns Merna Crater, Jessie McCaslin of Merna, and Linda Henderson of KCNI/KBBN in Broken Bow. We are grateful for the cautious encouragement that has been offered by Christian Koeberl, John McHone, and James Underwood.

REFERENCES CITED

Arndt, Peter; Bohsung, Jorg; Maetz, Mischa; and Jessberger, Elmar K., 1996, The elemental abundances in interplanetary dust particles: Meteoritics and Planetary Science, v. 31, p. 817–833.

Baldwin, R. B., 1949, The face of the Moon: University of Chicago Press, Chicago, 239 p.

Christoffersen, Roy; and Buseck, P. R., 1986, Refractory minerals in interplanetary dust: Science, v. 234, p. 590–592.

Dence, M. R., 1971, Impact melts: Journal of Geophysical Research, v. 76, p. 5552–5565.

Dietz, R. S., 1961, Astroblemes: Scientific American, v. 205, no. 2, p. 50–58.

Dodd, R. T., 1981, Meteorites—a petrochemical synthesis: Cambridge University Press, Cambridge, 368 p.

Dort, Wakefield, Jr., 1991, Aligned streams, tablelands, and upland closed depressions [abstract]: Association of American Geographers, Annual Meeting Abstracts, p. 51.

Dort, Wakefield, Jr.; Zeller, E. J.; and Martin, L. D., 1992, Holocene meteorite impact crater, Nebraska: youngest in North America? [abstract]: Geological Society of America Abstracts with Programs, v. 24, no. 7, p. 196.

_____ 1993, Particulates verify meteorite impact origin of Merna crater, Custer County, Nebraska [abstract]: Eos (Transactions, American Geophysical Union), v. 74, p. 388.

Garvin, J. B.; Grieve, R. A. F.; and Schnetzler, C. C., 1995, Satellite remote sensing signatures of impact structures [abstract]: Meteoritics, v. 30, p. 509.

Glass, B. P., 1971, Investigation of glass recovered from Apollo 12 Sample 12057: Journal of Geophysical Research, v. 76, p. 5649–5657.

Greshake, A.; Bischoff, A.; Putnis, A.; and Palme, H., 1996, Corundum, rutile, periclase, and CaO in Ca,Al-rich inclusions from carbonaceous chondrites: Science, v. 272, p. 1316–1318.

Grieve, R. A. F., 1987, Terrestrial impact structures: Annual Review of Earth and Planetary Sciences, v. 15, p. 245–270.

_____ 1990, Impact cratering on the Earth: Scientific American, v. 262, no. 4, p. 66–73.

_____ 1991, Terrestrial impact: the record in the rocks: Meteoritics, v. 26, p. 175–194.

Grieve, R. A. F.; and Robertson, P. B., 1979, The terrestrial cratering record; 1. Current status of observations: Icarus, v. 38, p. 212–229.

Grieve, R. A. F.; and Shoemaker, E. M., 1994, The record of past impacts on Earth, *in* Gehrels, Tom (ed.), Hazards due to comets and asteroids: University of Arizona Press, Tucson, p. 417–462.

Hodge, Paul, 1994, Meteorite craters and impact structures of the Earth: Cambridge University Press, Cambridge, 124 p.

Jarosewich, Eugene, 1990, Chemical analysis of meteorites: a compilation of stony and iron meteorite analysis: Meteoritics, v. 25, p. 323–337.

Koeberl, Christian, 1986, Geochemistry of tektites and impact glasses: Annual Review of Earth and Planetary Sciences, v. 14, p. 323–350.

_____ 1994, Tektite origin by hypervelocity asteroidal or cometary impact: target rocks, source craters, and mechanisms, *in* Dressler, B. O.; Grieve, R. A. F.; and Sharpton, V. L. (eds.), Large meteorite impacts and planetary evolution: Geological Society of America Special Paper 293, p. 133–151.

McHone, J. F.; Blumberg, D. G.; Greeley, R.; and Underwood, J. R., Jr., 1995, Space shuttle radar images of terrestrial impact structures: SIR-C/X-SAR [abstract]: Meteoritics, v. 30, p. 543.

Melosh, H. J., 1989, Impact cratering: a geologic process: Oxford University Press, Oxford, 245 p.

Pike, R. J., 1980, Control of crater morphology by gravity and target type: Mars, Earth, Moon: Proceedings of the 11th Lunar and Planetary Science Conference, p. 2159–2189.

Schultz, P. H.; and Beatty, J. K., 1992, Teardrops on the Pampas: Sky and Telescope, v. 83, p. 387–392.

Schultz, P. H.; and Lianza, R. E., 1992, Recent grazing impacts on the Earth recorded in the Rio Cuarto crater field, Argentina: Nature, v. 355, p. 234–237.

Taylor, S. R., 1967, Composition of meteorite impact glass across the Henbury Strewnfield: Geochimica et Cosmochimica Acta, v. 31, p. 961–968.

Wood, J. A., 1963, Physics and chemistry of meteorites, *in* Middlehurst, B. M.; and Kuiper, G. P. (eds.), The Moon, meteorites, and comets: University of Chicago Press, Chicago, p. 337–401.

Zhang Bao-min; Li Rong-quan; You Chang-jiang; and Jia Tie-fei, 1992, A study on the black microspherules with magnetism in soil from Dongling Mountain, Beijing: Chinese Science Bulletin, v. 37, p. 1647–1652.

PART II

ABSTRACTS AND SHORT PAPERS RELATED TO POSTER PRESENTATIONS

Drilling and Oil and Gas Production History at the Ames Feature, Major County, Oklahoma

Robert A. Northcutt
Independent Geologist
Oklahoma City, Oklahoma

David P. Brown
Geo Information Systems
Norman, Oklahoma

ABSTRACT.—The discovery of oil and gas production from Arbuckle (Cambrian–Ordovician) rocks in the area of Ames, Oklahoma, during 1990 and 1991 caused an active exploration effort that resulted in the development of significant oil and gas reserves below the previously established productive reservoirs. This newly developed area is located in four townships within the Ringwood field and Sooner Trend in Major County, a mature producing area. The Ames structural feature, or Ames hole as it soon became known, has now been found to be oil and gas productive from sedimentary rocks correlative with the Simpson and Arbuckle Groups and from brecciated Precambrian igneous rocks.

INTRODUCTION

The Ames feature, in southeastern Major County, Oklahoma, is located on the Anadarko shelf in northwestern Oklahoma. This structural feature covers an area of 57 sq mi in a four-township area and is believed by most to be a meteorite-impact crater. Figure 1 shows the location of the Ames feature and its relationship to the Ringwood field and Sooner Trend. The Sooner Trend is a group of combined fields in a designated geographic area that produce from many separate units or reservoirs.

DRILLING AND COMPLETION HISTORY

The first well completed to produce oil and gas from the Arbuckle in the Ames feature was the J. L. Thomas Energy no. 1-4 Ott. This well is located in the S½SW¼SE¼ sec. 4, T. 21 N., R. 9 W., and was completed on July 7, 1990. The no. 1-4 Ott was the only well completed from the Arbuckle in 1990. The next Arbuckle oil well was completed June 15, 1991, also by J. L. Thomas Energy. Figure 2 is a well-location map of the four-township area that includes the Ames feature. Shown on this map is the approximate location of the rim anticline that delineates the location of the Ames feature. The location of the discovery well is also shown on the map. Previously drilled wells in the area (small symbols) and wells drilled to test the Arbuckle (large symbols) are shown.

There were 95 wells drilled and completed between July 1, 1990, and August 1, 1994, that tested the Arbuckle at depths ranging from 8,500 to 9,500 ft in the four-township area of the Ames feature (Fig. 2). Table 1 lists these wells in chronological order of their completion and identifies the operator, well name and number, location, completion date, and result. These data were obtained from the Well History File in the Natural Resources Information System (NRIS) at the University of Oklahoma, and, in some instances, from the well-completion records of Petroleum Information Corporation.

OIL PRODUCTION AT THE AMES FEATURE

The fast-paced drilling activity at the Ames feature resulted in rapid development of leases and a dramatic increase in oil production in this mature

Robert A. Northcutt, 11422 Red Rock Road, Oklahoma City, OK 73102; David P. Brown, Geo Information Systems, 1818 W. Lindsey, Suite A105, Norman, OK 73069.

Northcutt, R. A.; and Brown, D. P., 1997, Drilling and oil and gas production history at the Ames feature, Major County, Oklahoma, *in* Johnson, K. S.; and Campbell, J. A. (eds.), Ames structure in northwest Oklahoma and similar features: origin and petroleum production (1995 symposium): Oklahoma Geological Survey Circular 100, p. 297–301.

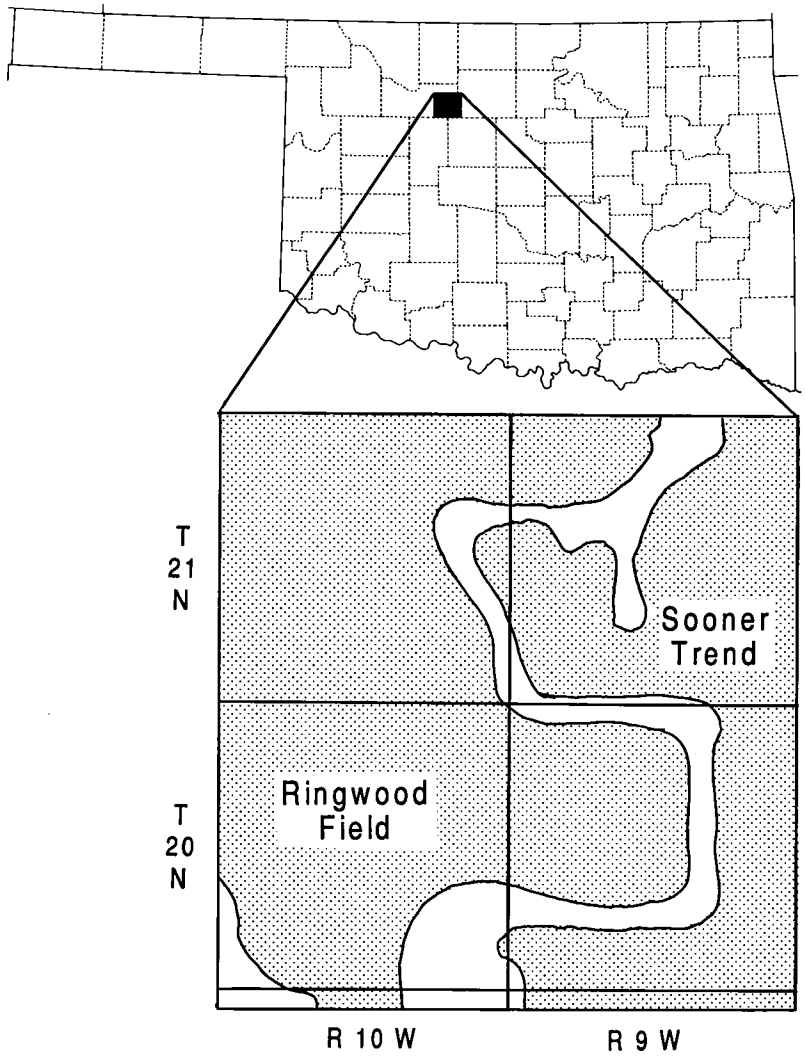

Figure 1. Map of Oklahoma showing the location of the area of the Ames feature with inset map of the four-township area showing the outlines of the Ringwood field and Sooner Trend.

producing area. Monthly oil production for the area of the Ames feature is shown on the production graph (Fig. 3). The oil production from the deeper Arbuckle interval is plotted separately on top of the previously developed production from shallower Pennsylvanian, Mississippian, and Silurian–Devonian rocks. The new, deeper production from both the Cambrian–Ordovician Arbuckle rocks and the Precambrian igneous rocks found at the Ames feature is classified as being Arbuckle, since this is the stratigraphic unit named as the common source of supply in the Oklahoma Corporation Commission spacing and pooling orders.

Cumulative production from the Arbuckle (as defined above) at the Ames feature through 1994 was 3.7 million barrels of oil and 10.8 billion cubic feet of gas.

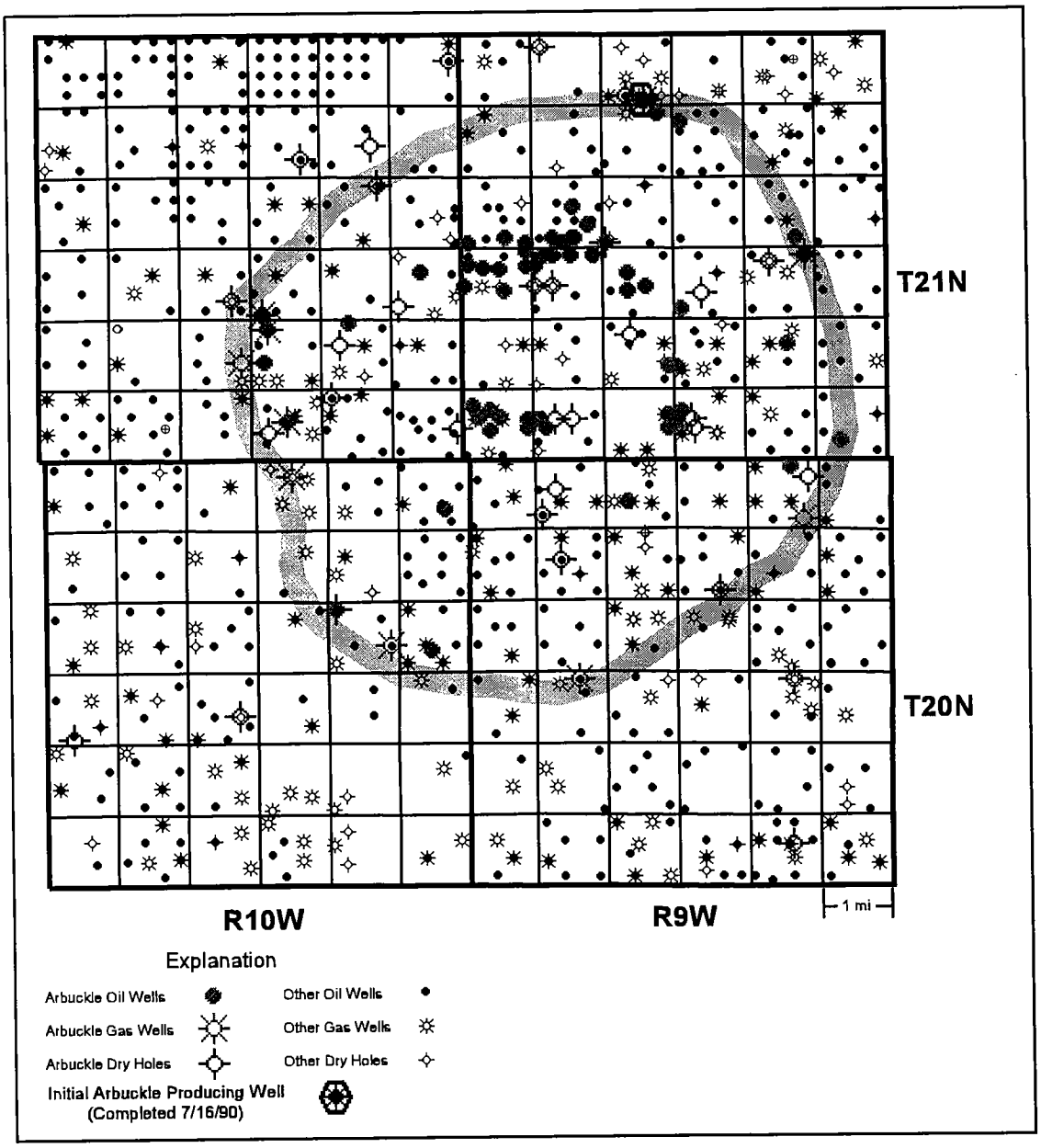

Figure 2. Well-location map of Ames feature area showing the approximate location of the rim anticline (nearly circular pattern), wells that penetrated into or through Arbuckle rocks (large symbols), and wells shallower than Arbuckle (small symbols). Wells that penetrated Arbuckle rocks but were completed in shallower zones are shown by a small symbol inside the large symbol. Table 1 lists well type and completion zone.

TABLE 1.—CHRONOLOGICAL LISTING OF ARBUCKLE TEST WELLS COMPLETED IN THE AMES FEATURE AREA (TPS. 20–21 N., RS. 9–10 W.), MAJOR COUNTY, OKLAHOMA, FROM JULY 1, 1990, TO AUGUST 1, 1994

Operator	Well Name	Well No.	Twp	Rge	Sec	Location	Completion Date			Well Type
							Yr	Mo	Day	
J.L. Thomas Energy	Ott	# 1-4	21 N	09 W	4	SH SW SE	1990	07	16	Arbuckle gas & oil
J.L. Thomas Energy	Ott	# 2-4	21 N	09 W	4	CT SE SW	1990	12	3	Arbuckle dry - Vi oil
J.L. Thomas Energy	Munkres	# 1-9	21 N	09 W	9	WH NE NE	1991	06	15	Arbuckle oil
D L B O&G	Henry	# 21-10	20 N	10 W	21	EH NW SE	1991	08	5	Arbuckle dry
D L B O&G	Cecil	# 27-4	21 N	10 W	27	SH NH NW	1991	08	9	Arbuckle oil & gas
D L B O&G	Bierig	# 28-9	21 N	10 W	28	CT NE SE	1991	11	10	Arbuckle gas
D & J Oil	Gregory	# 1-20	21 N	09 W	20	WH NE NW	1991	11	23	Arbuckle oil
D L B O&G	Allen	# 13-11	20 N	10 W	13	SE NE SW	1991	12	22	Arbuckle oil (directional)
D & J Oil	Peggy	# 1-18	21 N	09 W	18	SE SE SE	1991	12	24	Arbuckle oil
Continental Res	Mary Ellen	# 1-22	21 N	10 W	22	SE SW SW	1991	12	24	Arbuckle oil & gas
D & J Oil	Herman	# 1-20	21 N	09 W	20	NW NE SW	1991	12	30	Arbuckle dry
Continental Res	Dorothy	# 1-19	21 N	09 W	19	NE NE NE	1992	01	3	Arbuckle oil
D & J Oil	Lloyd	# 1-17	21 N	09 W	17	CT SW SE	1992	01	28	Arbuckle oil
Continental Res	Heinrich	# 1-19	21 N	09 W	19	CT WH NW	1992	01	30	Arbuckle oil
Continental Res	Terry	# 1-34	21 N	10 W	34	SW SW NE	1992	03	17	Arbuckle gas & oil
D L B O&G	Bullis	# 20-2	20 N	09 W	20	CT NW NE	1992	03	24	Arbuckle gas - Osw & Mssp oil
D L B O&G	Dehaas	# 21-11	21 N	09 W	21	CT NE SW	1992	04	9	Arbuckle oil
D & J Oil	Shelby	# 1-17	21 N	09 W	17	WH SE SW	1992	04	11	Arbuckle oil
R. E Blaik	Buckles	# 1-A-2	21 N	09 W	23	NE NE	1992	05	1	Arbuckle oil
Continental Res	Fred	# 1-31	21 N	09 W	31	SW SW NE	1992	05	6	Arbuckle oil
Continental Res	Pacific	# 1-21	21 N	09 W	21	NH NW SE	1992	05	8	Arbuckle oil
Continental Res	Stansberry	# 1-21	21 N	09 W	21	SE NW	1992	05	8	Arbuckle oil
Continnetal Res	Chet	# 1-19	21 N	09 W	19	NW NW SW	1992	05	12	Arbuckle oil
Continental Res	Fisher	# 6-3	20 N	10 W	3	WH WH NE	1992	06	1	Arbuckle dry
Bromar Oil	Jim	# 26-7	21 N	09 W	26	SW NE	1992	06	18	Arbuckle oil
Coastal Oil (Blaik)	Lillie	# 14-1	21 N	10 W	14	WH NE NE	1992	07	14	Arbuckle dry
D L B O&G	Elsie	# 23-6	21 N	09 W	23	SH NE NW	1992	07	24	Arbuckle dry - Oil Creek gas
R. E. Blaik	Bohn	# 1-14	21 N	09 W	14	WH SE	1992	07	30	Arbuckle oil
D L B O&G	Jimmy	# 31-11	21 N	09 W	31	NE NE SW	1992	08	1	Arbuckle oil
D & J Oil	Mary Helen	# 1-17	21 N	09 W	17	SW NE SE	1992	08	15	Arbuckle oil
Miracle Prod	Fyffe	# 2	21 N	09 W	16	SE SW SE	1992	08	23	Arbuckle dry
Bogo Energy	Campbell	# 3-35	21 N	10 W	35	EH NW NW	1992	09	2	Arbuckle dry - Osw & Hn oil
D L B O&G	Ruby	# 11-10	21 N	10 W	11	NH NH SE	1992	09	4	Arbuckle dry
B R G Petroleum	Gregory	# 2-23	20 N	09 W	23	EH NW NE	1992	09	15	Arbuckle dry - Mssp gas
Shelly Engr	Monsees	# 36-4	21 N	10 W	36	NE NE SE	1992	09	24	Arbuckle dry
D L B O&G	Campbell	# 21-9	21 N	10 W	21	CT SE	1992	10	6	Arbuckle dry
J.L. Thomas Energy	Farber	# 1-10	21 N	09 W	10	CT WH NW	1992	10	12	Arbuckle oil
Continental Res	Federal	# 1-14	20 N	10 W	14	SE NE SE	1992	10	15	Arbuckle gas
Universal	Dixon	# 2-18	21 N	09 W	18	SH SW SW	1992	10	21	Arbuckle oil
D & J Oil	James	# 1-20	21 N	09 W	20	WH NW NE	1992	11	10	Arbuckle oil
D & J Oil	Wayne	# 1-20	21 N	09 W	20	EH NW NW	1992	12	15	Arbuckle oil
Nicor Prod	Chestnut	# 18-4	21 N	09 W	18	NE SW SE	1993	01	8	Arbuckle oil
Ward Petroleum	Cleora	# 1	20 N	10 W	1	SE NW SE	1993	01	16	Arbuckle oil
D L B O&G	Darin	# 5-13	20 N	09 W	5	NH SW SW	1993	01	21	Arbuckle dry - Mssp oil
NICOR Expl	Scott	# 1-2	20 N	09 W	2	CT EH NE	1993	01	27	Arbuckle dry
Hazelwood	Edwards	# 2-2	20 N	09 W	2	WH SE SE	1993	02	1	Arbuckle gas
Cross Timbers	J J Kennedy	# 1-10	21 N	10 W	10	CT SE	1993	02	12	Arbuckle dry - Hn oil
Continental Res	Lydia	# 1-14	20 N	10 W	14	NW NW	1993	03	8	Arbuckle dry
Sho-Bar Energy	Mears	# 1-11	21 N	09 W	11	NW NE SE	1993	03	11	Arbuckle dry - Marshall oil
D L B O&G	Jesse	# 27-12	21 N	10 W	27	EH NW SW	1993	03	16	Arbuckle oil
Cross Timbers	Sherman	# 2-5	21 N	09 W	5	SE NW NW	1993	03	24	Arbuckle dry
D L B O&G	Marilyn	# 33-9	21 N	09 W	33	NE NE SE	1993	03	24	Arbuckle oil
Hazelwood	Carolyn Sue	# 10-1	20 N	09 W	10	SW SE	1993	03	26	Arbuckle dry
Continental Res	Floyd	# 1-19	20 N	10 W	19	SE SE SW	1993	04	12	Arbuckle gas
Continental Res	Donna	# 1-31	21 N	09 W	31	SE SW NW	1993	04	14	Arbuckle oil
Latigo	Dorothy	# 1-20	21 N	09 W	20	NW NW SW	1993	04	15	Arbuckle dry
Continental Res	Gerald	# 1-31	21 N	09 W	31	SE SE NE	1993	04	20	Arbuckle oil
Continental Res	Wayne	# 1-32	21 N	09 W	32	SW SW NW	1993	04	21	Arbuckle oil
D L B O&G	Della	# 28-6	21 N	09 W	28	EH EH NW	1993	04	24	Arbuckle dry
Ward Petroleum	Orin	# 1	20 N	09 W	35	SH SW NE	1993	05	3	Arbuckle dry
Continental Res	Christina	#1-31	21 N	09 W	31	SE NW NW	1993	05	16 *	Arbuckle oil
D L B O&G	Turner	# 28-9	21 N	09 W	28	SE NE SE	1993	06	3	Arbuckle oil
L R French	Bowles	# 1-31	21 N	09 W	31	NE NE SE	1993	06	12	Arbuckle oil

TABLE 1.—*CONTINUED*

Operator	Well Name	Well No.	Twp	Rge	Sec	Location	Completion Date Yr	Mo	Day	Well Type
Bogo Energy	Dillman	# 1-1	21 N	10 W	1	CT SE NE	1993	07	14	Arbuckle dry - Mssp oil
Universal	Bland	# 1-33	21 N	09 W	33	EH SE NE	1993	07	15	Arbuckle oil
D L B O&G	Chestnut	# 16-13	21 N	09 W	16	SW SW SW	1993	07	23	Arbuckle dry
Continental Res	Charles	# 1-32	21 N	09 W	32	SW SW NE	1993	08	19	Arbuckle dry
Continental Res	Earl Dean	# 1-31	21 N	09 W	31	NE SE NW	1993	09	16	Arbuckle oil
D L B O&G	Delores	# 8-3	21 N	09 W	8	S2 NE NW	1993	10	1	Arbuckle dry (Horiz)
Continental Res	Nellie	# 1-22	21 N	09 W	22	CT SW SW	1993	10	2	Arbuckle oil
Continental Res	Marita	# 1-19	21 N	09 W	19	NE SE NE	1993	10	10	Arbuckle oil
D L B O&G	Hammer	# 5-6	20 N	09 W	5	SW SE NW	1993	10	11	Arbuckle dry
D L B O&G	Detrick	# 19-10	21 N	09 W	19	CT NW SE	1993	10	17	Artbuckle dry
Continental Res	Sam	# 1-19	21 N	09 W	19	NW SE NW	1993	10	20	Arbuckle oil
Continental Res	Bisel	# 1-32	21 N	09 W	32	NE NW SW	1993	10	21	Arbuckle oil
D L B O&G	Patricia	# 24-13	21 N	10 W	24	NH SW SW	1993	10	30	Arbuckle dry
D & J Oil	E	# 1-17	21 N	09 W	17	SE SE SW	1993	11	22	Arbuckle oil
D L B O&G	Carl	# 34-12	21 N	09 W	34	NW NW SW	1993	12	16	Arbuckle oil
Continental Res	Viola	# 1-32	21 N	09 W	32	SW SE NW	1993	12	21	Arbuckle dry
Universal	Gammon	# 1-34	21 N	09 W	34	SW SW NW	1993	12	22	Arbuckle oil
Continental Res	Marjorie	# 1-19	21 N	09 W	19	NW SW NE	1993	12	29	Arbuckle oil
Continental Res	Marjorie	# 1-19	21 N	09 W	19	NW SW NE	1993	12	29	Arbuckle oil
D & J Oil	J D	# 1-20	21 N	09 W	20	C NW	1993	12	22	Arbuckle oil
D & J Oil	H W	# 1-20	21 N	09 W	20	WH WH NW	1994	01	19	Arbuckle oil
Continental Res	Mason	# 2-26	21 N	10 W	26	WH SE NW	1994	01	23	Arbuckle dry
Hazelwood	Mackie	# 27-3	21 N	09 W	27	SW NW SW	1994	02	17	Arbuckle oil
Cirrus Production	Uvah	# 1	21 N	09 W	17	SW SW NE	1994	02	19	Arbuckle oil
Continental Res	Laverne	# 1-22	21 N	09 W	22	SE NE SW	1994	03	8	Arbuckle dry
Continental Res	Tina	# 1-34	21 N	10 W	34	NW NE SW	1994	03	21	Arbuckle dry
D & J Oil	Marvin	# 1-20	21 N	09 W	20	CT NE NE	1994	05	7	Arbuckle oil
Continental Res	Gladys	# 1-24	21 N	10 W	24	NE SE NW	1994	05	10	Arbuckle oil
D L B O&G	Jennifer	# 34-6	21 N	09 W	34	SW SE NW	1994	05	22	Arbuckle dry
DLB O&G	Emma	# 36-14	21 N	09 W	36	C E2 SW	1994	05	16	Arbuckle oil
EOG Oklahoma Inc	Laubhans	# 2	20 N	09 W	4	WH NE SW	1994	07	13	Arbuckle oil
DLB O&G	Roger	# 34-5	21 N	09 W	34	NH SW NW	1994	07	1	Arbuckle oil

* Spud date.

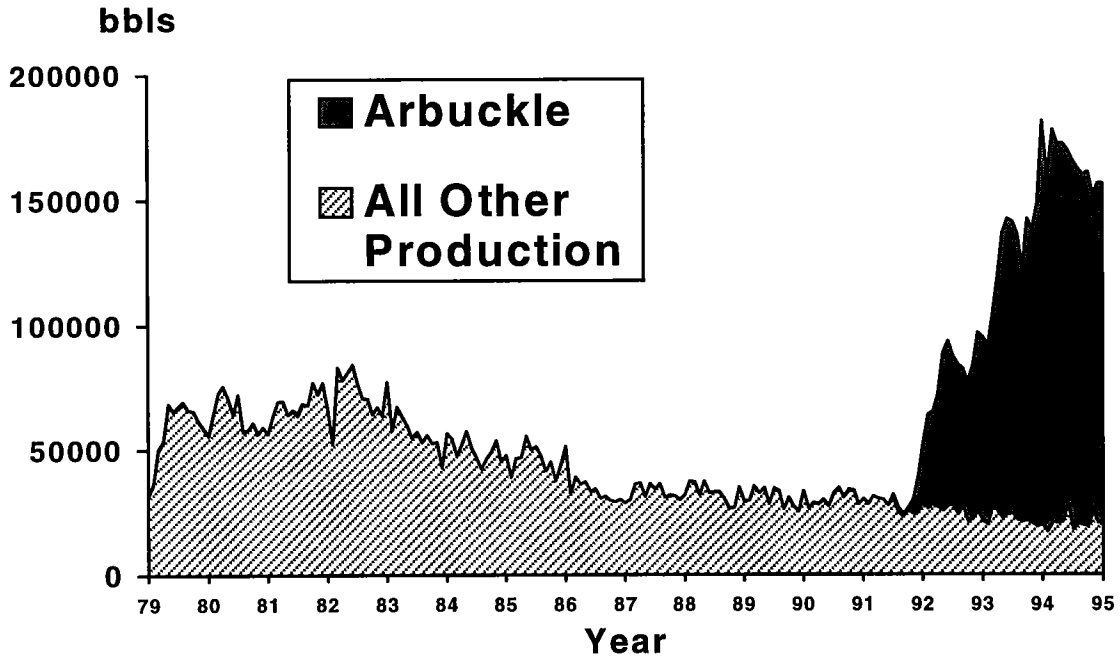

Figure 3. Graph of Arbuckle and all other oil production for the four-township Ames feature area.

Petrology of Enigmatic Rocks from 2.75 Km Depth in the Ames Structural Anomaly, Major County, Oklahoma, and Their Relationship to Suevite from the Ries Crater, Nördlingen, Bavaria

Clifford P. Ambers
University of Oregon
Eugene, Oregon

Peter Brändlein
LGA Services
Nürnberg, Germany

M. Charles Gilbert
University of Oklahoma
Norman, Oklahoma

ABSTRACT.—Petrology of core from the Nicor no. 18-4 Chestnut (9,003–9,037 ft), Universal Resources Corporation no. 1-33 Bland (9,191–9,193 ft), and Continental Resources, Inc., no. 1-22 Mary Ellen (8,993.6 ft and 9,001.0 ft) wells in southeastern Major County, Oklahoma, reveals features that place important constraints on the origin of the Ames structure. Clear and abundant evidence of shock-induced deformation and melting occurs throughout the interval of the Nicor no. 18-4 Chestnut core studied. Comparison of rocks from the Chestnut well to suevite from the Ries Crater in Bavaria, a well-documented Miocene impact site, provides a compelling argument for a common mechanism of origin of the Ries and Chestnut well rocks. Alteration of the Chestnut well rocks complicates their interpretation. Fluid-inclusion analysis of late void-filling quartz and dolomite shows that these minerals are products of ordinary burial-diagenetic processes. On the basis of our observations and published data, we conclude that the Ames and Ries structures and their associated rocks have similar histories. The most simplistic and direct interpretation for the Ames structure that incorporates all of the available information is that it is a deeply buried, Ordovician astrobleme.

INTRODUCTION

The Ames structure, located in southeastern Major County, Oklahoma, is a 10-km-diameter, circular structure containing a series of concentric, inward-dipping faults. The structure is overlain by thickened sections of Ordovician–Permian rocks that illustrate compaction of the structure through much of Paleozoic time (Roberts and Sandridge, 1992; Carpenter and Carlson, 1992). Locations of wells from which cores studied here were taken include Nicor no. 18-4 Chestnut—sec. 18, T. 21 N., R. 9 W.; Universal Resources Corporation no. 1-33 Bland—sec. 33, T. 21 N., R. 9 W.; and Continental Resources, Inc., no. 1-22 Mary Ellen—sec. 22, T. 21 N., R. 10 W. The Bland and Chestnut wells are located on the Ringwood SW, Oklahoma, 7.5′, topographic quadrangle. The Mary Ellen well is located on the Fairview SE, Oklahoma, 7.5′, topographic quadrangle.

Clifford P. Ambers, Dept. of Geological Sciences, 1272 University of Oregon, Eugene, OR 97403; Peter Brändlein, Tillystr. 2, 90431, Nürnberg, Germany; M. Charles Gilbert, School of Geology and Geophysics, University of Oklahoma, Norman, OK 73019.

Ambers, C. P.; Brändlein, Peter; and Gilbert, M. C., 1997, Petrology of enigmatic rocks from 2.75 km depth in the Ames structural anomaly, Major County, Oklahoma, and their relationship to suevite from the Ries crater, Nördlingen, Bavaria, *in* Johnson, K. S.; and Campbell, J. A. (eds.), Ames structure in northwest Oklahoma and similar features: origin and petroleum production (1995 symposium): Oklahoma Geological Survey Circular 100, p. 302–309.

The Ries Crater is one of the most extensively studied and well-documented impact sites on Earth (Stöffler and Ostertag, 1983). The impact occurred during Miocene time (14.7 Ma), and the structure has never been buried, limiting burial diagenetic alteration of the rocks. The size and general geologic setting of the Ries Crater (Hörz and others, 1983) are very similar to the size and setting of the buried Ames structure (Roberts and Sandridge, 1992; Carpenter and Carlson, 1992). As such, the Ries Crater is an excellent candidate for comparison of its impact-generated rocks with the enigmatic rocks at the top of the Arbuckle Group in the Ames structure. Six samples were collected from deposits of impact melt ejected from the Ries Crater at four separate locations: a road cut north of Zipplingen, a quarry at Aumühle, a quarry at Polsingen, and a quarry at Otting. Thin sections were prepared from the samples for comparison to the Nicor no. 18-4 Chestnut rocks.

PETROLOGY OF THE AMES ROCKS

Polished thin sections were prepared at 2 ft intervals through the densely dolomitized upper part of the Nicor no. 18-4 Chestnut core and at 1 ft intervals through the vesicular lower part. X-ray diffraction scans were performed on all the sections, and selected samples were analyzed with the electron microprobe employing backscattered-electron imaging, energy-dispersive X-ray spectral analysis, and wavelength-dispersive spectral analysis.

Rock Fragment Types

Rock fragment types in the Nicor no. 18-4 Chestnut core include altered granite, dolostone, shale, chert, strongly altered diabasic rock, and isolated, very well rounded quartz grains from sandstone. Microbreccia in granite from the Universal Resources, Inc., no. 1-33 Bland well at a similar depth also contains diabase and dolostone fragments. Dolostone, shale, sandstone, and chert from the upper Arbuckle Group in the Continental Resources, Inc., no. 1-22 Mary Ellen well are petrographically identical to the fragments mixed in the no. 18-4 Chestnut rocks and no. 1-33 Bland microbreccias, indicating that the sedimentary fragments may have all originated in the Arbuckle Group. Granite fragments are undoubtedly from the basement below the Ames structure. The diabase is probably also from the basement, as shown by the presence of a diabase dike in at least one deep well near Ames (R. E. Denison, personal communication).

Shock Deformation Features

Shock deformation features in quartz and feldspar are common in the Nicor no. 18-4 Chestnut core below 9,002.7 ft. Deformation microstructures in the rocks include pervasive brecciation, multidirectional planar lamellae in quartz and feldspar, relict isotropic patches (diaplectic glass) in quartz grains, kinking of micas, intense microcracking of accessory apatite (Fig. 1A) and zircon in granitic fragments, and contortion of shale fragments. Titanite and magnetite relicts in granite fragments have distorted forms and are replaced by microcrystalline rutile and pyrite, respectively.

Evidence of Melting

Microstructures indicative of syndeformational melting of the Nicor no. 18-4 Chestnut rocks include (1) vesiculation and flow fabrics (compositional streaking, vesicle elongation) in quartz; (2) anomalous microcrystalline quartz (AMQ) grains having relict perlitic cracks (Fig. 1E), delicately folded lens shapes with internal flow lines (Fig. 2A,C), curvilinear and straight cracks containing opaque minerals and very fine grained quartz, and complex anisotropism showing arcuate bands and swirled textures; (3) relict vesicular isotropic material (feldspathic glass) at the edges of granite fragments; and (4) flow fabrics in vesicular, devitrified, feldspathic glass defined by rare-earth phosphate, apatite, iron oxide, rutile, zircon, K-feldspar fragments, and microporosity (Figs. 1C and 2E,F). Much of the feldspathic glass has crystallized as felted mats of microlitic, plumose, or spherulitic orthoclase (Figs. 1C and 2E,F). A distinct lack of sodic phases was noted during electron-microprobe analysis of the rocks.

COMPARISON OF THE AMES AND RIES ROCKS

Comparison of rocks in the Nicor no. 18-4 Chestnut well with suevite (melt rock formed by meteorite impact) from the Ries Crater in Bavaria, Germany, shows close similarities and indicates precursors to petrographic components of the Chestnut rocks.

All of the shock features found in the Ames rocks are also found in the Ries suevite, in identical abundance. Also, the general natures of the Ames and Ries rocks are the same, both without an igneous analogue. Because the Ries suevite is a proven by-product of impact metamorphism, a similar origin for the Ames suevite logically follows. A particularly strong piece of evidence along this line is the apatite observed in diaplectic glass after quartz in the Ries rocks that shows the exact same deformation style as in the Chestnut core (Fig. 1A,B). In our collective experience with thousands of igneous and metamorphic rocks in thin section, we have never observed this microdeformational feature. Its occurrence in both the Ames and Ries rocks is not trivial and strongly supports their genetic equivalence.

Melt fabrics in the Ames and Ries suevites are also remarkably similar, further supporting the contention of genetic equivalence. Flow fabrics

found in felted orthoclase replacing vesicular, feldspathic glass in the Chestnut core also occur in the Ries rocks where they are marked by varicolored glasses. Flow microstructures in AMQ bodies from Ames are marked by streaks of slightly different refractive index in attenuated parts of the bodies (Fig. 2A,C). These features are perfectly analogous to streaking in lechatelierite (silica glass) lenses that occur in impact melt from the Ries (Fig. 2B,D). AMQ bodies in the Chestnut core also exhibit vesiculation, flow fabrics, and perlitic cracks (Fig. 1E) identical to diaplectic glass after quartz (containing stishovite and coesite) and silica glass (lechatelierite) in the Ries suevite (Fig. 1F). These occurrences further suggest that AMQ in the Chestnut core is crystallized from diaplectic glass after quartz and flowed lechatelierite. Coesite and stishovite may still be present in the Chestnut core, but will require concentration by HF digestion of the host rock before they can be detected by X-ray diffraction. X-ray scans run in this study showed that peaks from the dominant minerals (quartz, orthoclase, dolomite, pyrite) overlap the peak positions of coesite and stishovite, making identification of coesite and stishovite impossible.

All of the shock and melt features found in the Chestnut rocks are represented in the Ries suevite. The Ries suevite samples represent both bulk impact-melt ejecta and fragmented airborne fallout, the former bearing strong resemblance to the vesicular material in the lower Chestnut core and the latter being very similar to the dolomitized clastic rock above the vesicular rock. Comparison of the Chestnut and Ries rocks confirms identification of the Chestnut melt rocks as suevite.

With the strong evidence for genetic equivalence of the Ries and Ames suevites, we interpret the lower suevite in the Chestnut core (9,022.7–9,037 ft; Figs. 1C and 2E,F) to be identical in origin to the "red suevite" from Polsingen in the Ries Crater (Fig. 1D). The radial position of the Nicor no. 18-4 Chestnut well in the Ames structure and radial position of Polsingen in the Ries Crater are also very similar. Stöffler and Ostertag (1983, p. 111) interpreted the Polsingen "red suevite" as "lumps of impact melt mixed with crystalline fragments and ejected from the central part [of the transient crater] to the rim of the [transient] crater." We interpret the upper, normally graded, clastic suevite in the Chestnut core (9,003–9,022.7 ft) as the fallout suevite that accumulated from debris raining out of the ejecta plume, as did most of the suevite surrounding the Ries Crater, including that at Aumühle, Otting, and Zipplingen studied here. We do not believe the fallout suevite in the Chestnut core was water-laid except for the top few feet, which is laminated, contains ripple structures, and contains small-scale graded beds. Hypothesized deposits formed by oceanic impacts are, by necessity of the chaotic influx of water back into the water crater, jumbled and unsorted, not graded like the upper suevite at Ames (McKinnon, 1982). This concept leads us to believe that the impact at Ames occurred on land or in very shallow water such that the rim debris prevented swash back into the crater. The water-laid material in the top few feet of the clastic suevite could have easily been deposited in a lake environment within the crater after impact or during early stages of the following marine incursion.

The granite in the Universal Resources Corporation no. 1-33 Bland well that is apparently unshocked and much fresher than the granite in the Nicor no. 18-4 Chestnut well is also easily explained by the Ries analogue. Coarse deposits (containing kilometer-scale megablocks) of low-shock materials, excavated from the transient crater during impact, are exposed in the inner ring of the Ries Crater (Hörz and others, 1983; Stöffler and Ostertag, 1983; Von Engelhardt, 1990) at a radial position very similar to that of the Bland well in the Ames structure. As the rock in the Chestnut well was shock melted, it is no surprise that it is now more altered than the comparatively undeformed Bland granite, especially after at least 250 m.y. of deep burial.

ALTERATION OF THE AMES SUEVITE

Diagenetic alteration has overprinted the deformed and melted rocks in the Ames structure and complicates, but does not completely obscure,

Figure 1 *(facing page).* Key petrographic features of suevite from the Nicor no. 18-4 Chestnut core and corresponding fabrics in suevite from the Ries Crater. *A*—Shattered apatite from 9,016.9 ft in the Chestnut core. Plane-polarized light; bar length represents 25 μm. *B*—Shattered apatite in diaplectic glass after quartz from Otting in the Ries Crater. Note the similarity with *A*. Plane-polarized light; bar length represents 25 μm. *C*—General view of melt suevite from 9,031.7 ft in the Chestnut core showing vesicles filled with quartz, plumose orthoclase, and anomalous microcrystalline quartz (top right). Cross-polarized light; bar length represents 200 μm. *D*—Melt suevite from Polsingen in the Ries Crater. Note the similarity of the vesiculation, orthoclase, and recrystallized diaplectic glass (AMQ at top right) to the features shown in *C*. Cross-polarized light; bar length represents 200 μm. *E*—Perlitic cracks in AMQ from 9,025.3 ft in the Chestnut core. Plane-polarized light; bar length represents 50 μm. *F*—Perlitic cracks in diaplectic glass in a biotite-quartz-plagioclase schist fragment in the suevite collected from Otting in the Ries Crater. Note the similarity to *E*. Plane-polarized light; bar length represents 200 μm.

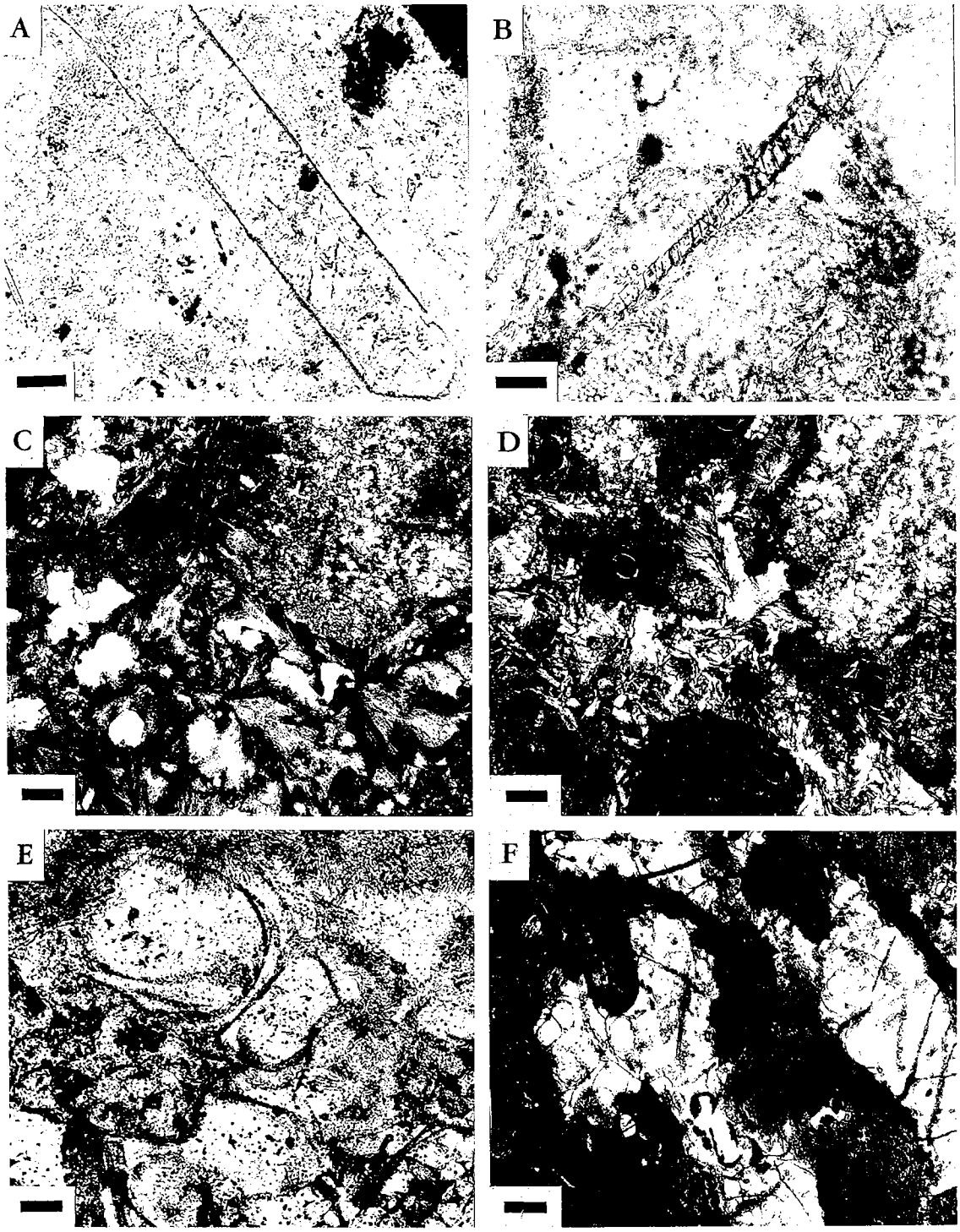

Figure 1.

evidence of the deformation and melting event. Postimpact alteration includes crystallization of orthoclase from feldspathic glasses; argillization of glass along faults to illite-smectite; isochemical recrystallization of silica glass to microcrystalline quartz; pore filling by dolomite, quartz, chlorite, pyrite, rutile, orthoclase, and bitumen; and replacement of early silicate minerals and glasses by dolomite. Alteration of granite and suevite in the Nicor no. 18-4 Chestnut core is not easily overlooked, or even "looked through," when studying the rocks.

Observation of the Ries samples (which have never been buried) shows that some of the alteration and crystallization products in the no. 18-4 Chestnut suevite probably formed during the initial cooling and hydrothermal alteration of the rock, but others are the products of deep burial. On the basis of published work (Newsom and others, 1986) and our observations on the Ries suevite, both plumose, microlitic, and spherulitic feldspar replacing feldspathic glass and AMQ replacing silica glass are very early crystallization products formed during initial cooling of suevite from about 600 °C (Fig. 1D). The same is true for vesicular suevite in the lower no. 18-4 Chestnut core (Fig. 1C). Similarly, early hydrothermal alteration produced clay linings in vesicles, clay replacement (smectitization) of glass, and chalcedony precipitation in vesicles in both the Ries and Ames suevites. Burial diagenetic effects in the Ames suevite include dolomite and euhedral quartz fillings of vesicles and conversion of early clay linings of vesicles to chlorite. Early-glass replacements of smectite were converted to illite during deep burial.

Results of Fluid-Inclusion Microthermometry

Fluid inclusions in quartz and dolomite that fill pores were analyzed microthermometrically to help constrain the conditions under which quartz and dolomite formed. Homogenization temperature (T_h) data were collected during heating experiments. Eutectic (T_{eu}) and melting (T_m) temperatures were determined by melting experimentally frozen inclusions. Both dolomite and quartz exhibit growth-zone–restricted inclusions that support interpretation of inclusion entrapment during growth. This finding allows use of the T_h data as a minimum temperature for mineral growth (Goldstein and Reynolds, 1994).

Although the number of fluid inclusions measured for dolomite is small, a clear distinction between the homogenization temperatures for quartz and dolomite is observed (Fig. 3A). The main cluster of homogenization temperatures ranges from 75 to 115 °C for inclusions in quartz and from 115 to 145 °C for inclusions in dolomite. Quartz and dolomite inclusions with homogenization temperatures above 115 °C and 145 °C, respectively, all show evidence of necking down (which precludes their use in any interpretation based on T_h). Lack of petroleum in the cores of pore-filling quartz grains coupled with low homogenization temperatures for fluid inclusions in the grains suggests that quartz growth began before the local source rocks entered the oil window and continued growth through migration of oil to the suevite. Relative to quartz, the higher homogenization temperatures for dolomite inclusions, the later paragenesis of dolomite, and lack of petroleum in the dolomite all suggest that the dolomite precipitated later and at greater burial depths than quartz, after the mobile, light fraction of the petroleum was driven off.

Low melting temperatures show the brine in the fluid inclusions in both quartz and dolomite (Fig. 3B) to be very saline. Low eutectic temperatures determined for the inclusions in the quartz (–53 °C) are interpreted to indicate a dominantly NaCl-$CaCl_2$ brine, whereas higher eutectic temperatures for inclusions in the dolomite (40 to 25 °C) are believed to show an increase in magnesium in the brine (Fig. 3C), on the basis of calibrations presented by Goldstein and Reynolds (1994). If we use a NaCl-$CaCl_2$ model composition, we estimate salinities of the included fluids at 20–23 wt% solids (>50% $CaCl_2$). Changing ion chemistry of the brine with increased temperature is indicated without major changes in total dissolved solids (Fig. 3B,D). This is easily accounted for by evolution of the basinal brine in the Ames structure through time as a result of progressive mineral reactions during burial.

Figure 2 *(facing page).* Aspects of devitrified glasses in Ames suevite and of lechatelierite in Ries suevite. *A*—Lensoid AMQ exhibiting flow lines from 9,023.4 ft in the Chestnut core. Plane-polarized light; bar length represents 50 μm. *B*—Lechatelierite lens in suevite from the Aumühle Quarry in the Ries Crater. Note the similarity to *A*. Plane-polarized light; bar length represents 50 μm. *C*—Lensoid AMQ exhibiting flow lines from 9,025.3 ft in the Chestnut core. Plane-polarized light; bar length represents 200 μm. *D*—Lechatelierite lens in suevite from Otting in the Ries Crater. Note the similarity to *C*. Plane-polarized light; bar length represents 50 μm. *E*—Devitrified feldspathic glass from 9,031.7 ft in the Chestnut core exhibiting flow banding and vesicles partly filled with authigenic quartz. Backscattered-electron image. *F*—Devitrified feldspathic glass from 9,018.2 ft in the Chestnut core containing delicately deformed vesicles partly filled with orthoclase. The matrix is made of porous illite and finely divided orthoclase. Backscattered-electron image.

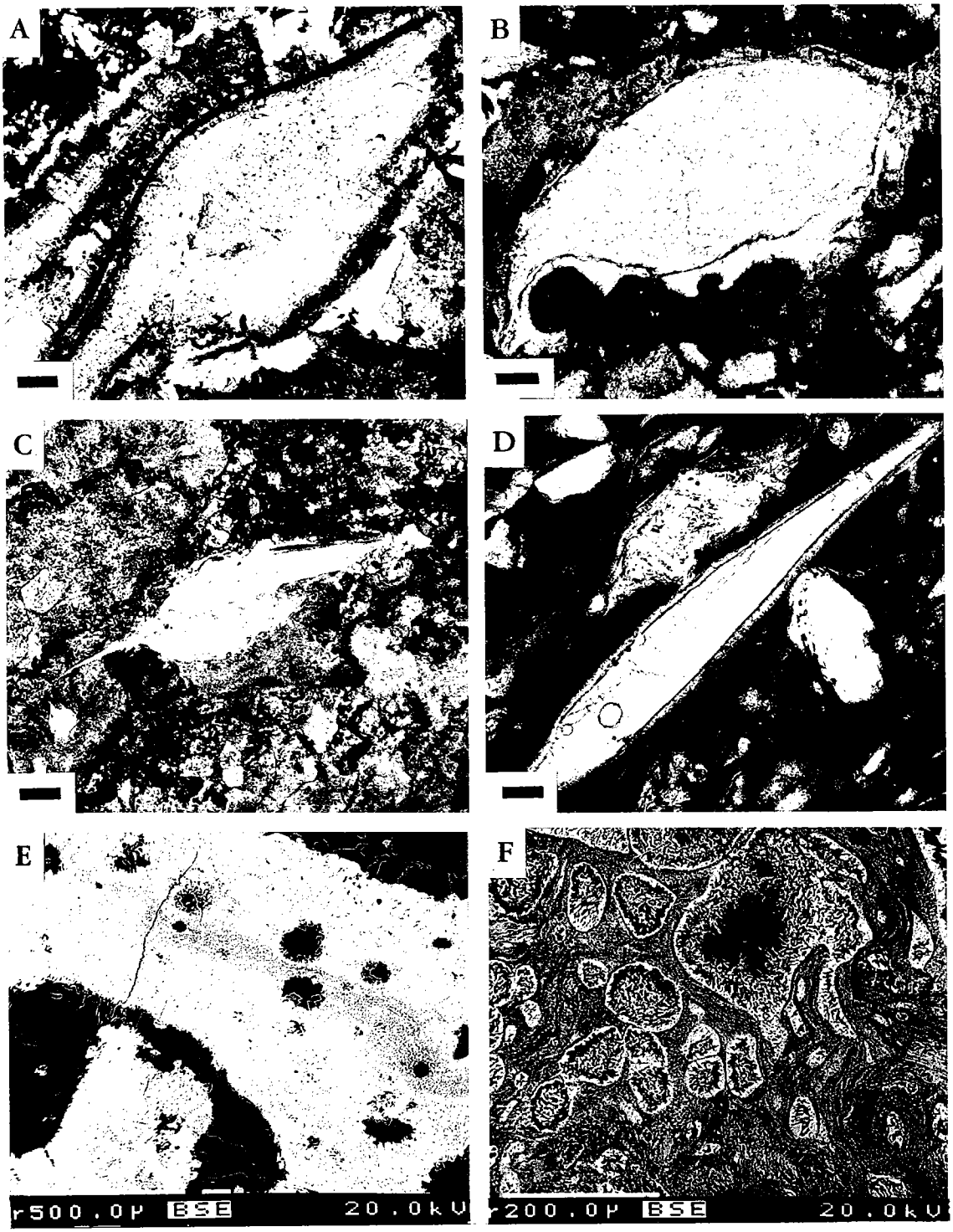

Figure 2.

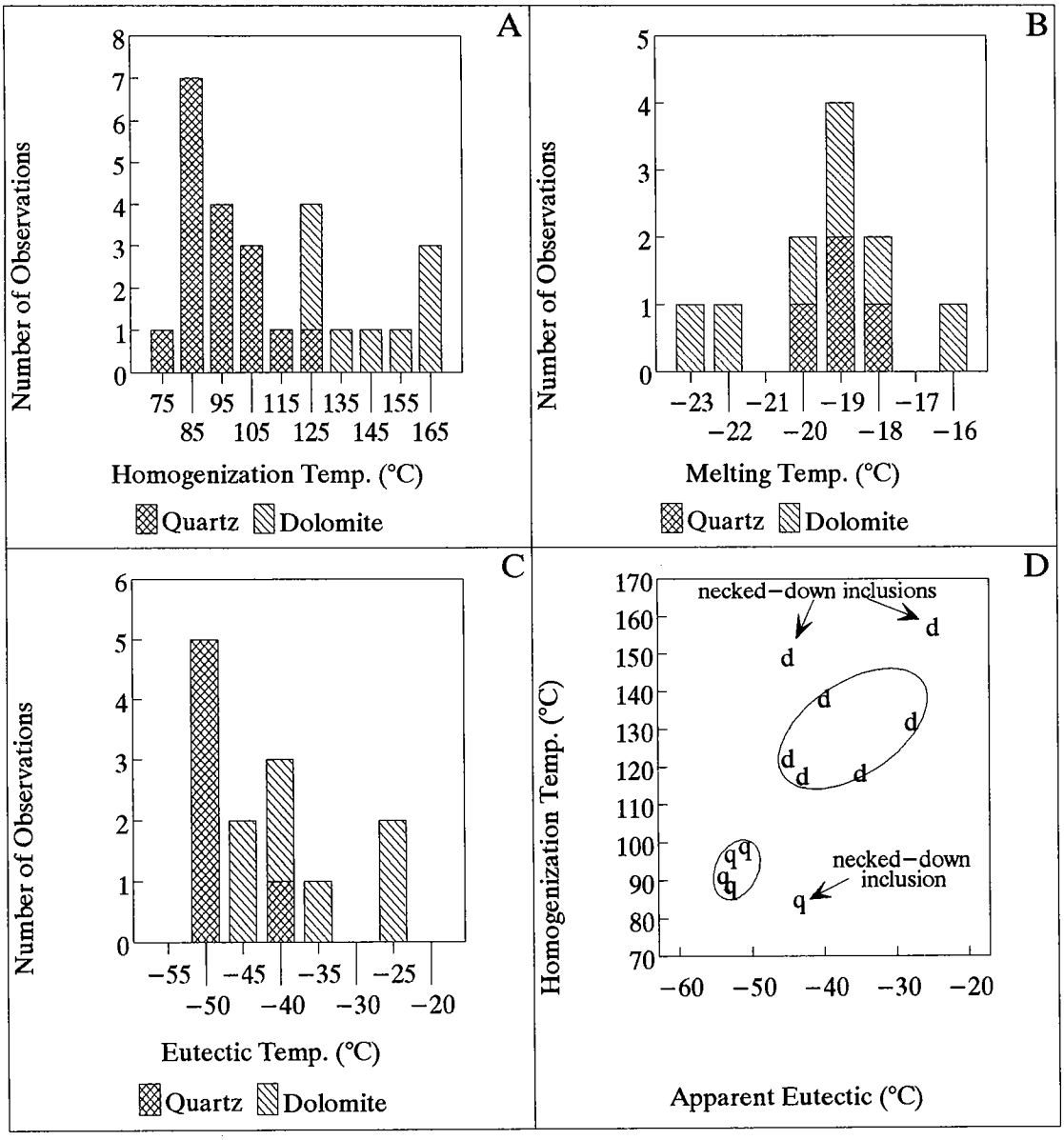

Figure 3. Fluid-inclusion microthermometry results for quartz and dolomite that fill vesicles in the lower Nicor no. 18-4 Chestnut core. *A*—Homogenization temperatures for all fluid inclusions measured in quartz and dolomite. *B*—Melting temperatures for experimentally frozen inclusions in quartz and dolomite. *C*—Eutectic temperatures estimated for fluid inclusions in quartz and dolomite. *D*—Cross plot of homogenization temperature vs. eutectic temperature for inclusions in quartz (q) and dolomite (d) for which both measurements could be made. Note the clustering of quartz inclusions at lower homogenization and eutectic temperatures than inclusions in dolomite.

These results are compatible with normal basinal brines and argue against high-temperature fluids (such as those that circulate around igneous intrusions) having been involved in dolomite and quartz precipitation.

CONCLUSIONS

With Occam's razor in hand, the overwhelming similarity of the Ames structure's and Ries Crater's geologies, coupled with identical rock fab-

rics, rock microfabrics, and mineral microstructures, leads us to no other conclusion than that the Ames structure is a deeply buried, Middle Ordovician astrobleme containing shocked and melted rocks produced by the meteorite impact. Acceptance of the Ries Crater as a model for the Ames structure allows identification of the lower melt rocks in the Nicor no. 18-4 Chestnut core as part of an impact-melt body spattered onto the transient crater rim, whereas the overlying, normally graded, clastic material is fallout from the impact-generated debris plume. Reworking of the upper few feet of fallout in a subaqueous environment seems plausible, but hypothesizing the catastrophic emplacement of the entire upper clastic interval by closure of a water crater is not warranted. Fresh granite in the Universal Resources Corporation no. 1-33 Bland well represents unshocked granite excavated as a block during initial impact.

Alteration of glasses in the Ames suevites began immediately upon deposition with crystallization of felted orthoclase from feldspathic glass and AMQ from diaplectic glass after quartz and lechatelierite. Hydrothermal alteration during later cooling and interaction with surface waters initiated argillization and perhaps sulfide precipitation. Burial diagenesis modified early-formed clays and led to emplacement of vesicle-filling quartz and vesicle-filling and replacement dolomite. Compaction phenomena, including vesicle collapse, silicate stylolitization, and microfaulting have all contributed to reduction of porosity during deep burial.

SPECULATION

The results of Attrep and others (1997) show only slightly elevated iridium levels in a few Ames samples. Given the conclusive evidence for the impact origin of the structure presented at the 1995 workshop in Norman, Oklahoma (see various papers in this volume), the low iridium abundances probably suggest that the Ames impactor was stony as opposed to iron rich (Morgan and others, 1979). If this conclusion is correct, and assuming a density of 2.9 for the Ames impactor, then the body is estimated to have weighed approximately 1.8×10^{10} to 7.2×10^{10} kg (2,080 million tons) and was 100–200 m in diameter (Weissman, 1982). In comparison to what is known about the debris ejected from the Ries Crater (Von Engelhardt, 1990), it is quite certain that decimeter-scale blocks were hurled as far away as the present location of Oklahoma City from the Ames structure (approximately 100 km). It is possible that a bed containing such debris is exposed in the upper Arbuckle Group along the north flank of the Wichita Mountains and in the Arbuckle Mountains. Such material would be comparable to Reuter Blocks found in Miocene strata south of the Ries Crater.

ACKNOWLEDGMENTS

We thank the School of Geology and Geophysics at the University of Oklahoma for financial support of the photomicrography included in the poster presented at the Ames Workshop that this paper was extracted from. The school also provided thin-sectioning supplies and facilities for the study. Special thanks is also extended to David London in the School of Geology and Geophysics at the University of Oklahoma, who made available the facilities for the electron-microprobe analysis, backscattered-electron imaging, and fluid-inclusion analysis included in this paper. George B. Morgan VI graciously assisted with the electron-microprobe operation. The Oklahoma Geological Survey, through its representatives Jock Campbell and Ken Johnson, made the cores included in this study available for analysis.

REFERENCES CITED

Carpenter, B. N.; and Carlson, Rick, 1992, The Ames impact crater: Oklahoma Geology Notes, v. 52, p. 208–223.

Goldstein, R. H.; and Reynolds, T. J., 1994, Systematics of fluid inclusions in diagenetic minerals: Society for Sedimentary Geology (SEPM) Short Course 31, 199 p.

Hörz, F.; Ostertag, R.; and Rainey, D. A., 1983, Bunte breccia of the Ries: continuous deposits of large impact craters: Reviews of Geophysics and Space Physics, v. 21, no. 8, p. 1667–1725.

McKinnon, W. B., 1982, Impact into the Earth's ocean floor: preliminary experiments, a planetary model, and possibilities for detection, *in* Silver, L. T.; and Schultz, P. H. (eds.), Geological implications of impacts of large asteroids and comets on the Earth: Geological Society of America Special Paper 190, p. 129–142.

Morgan, J. W.; Janssens, M. J.; Hertogen, J.; Gros, J.; and Takahashi, H., 1979, Ries impact crater, southern Germany: search for meteoritic material: Geochimica et Cosmochimica Acta, v. 43, p. 803–815.

Newsom, H. E.; Graup, G.; Sewards, T.; and Keil, K., 1986, Fluidization and hydrothermal alteration of the suevite deposit at the Ries Crater, West Germany, and implications for Mars: Journal of Geophysical Research, v. 91, p. E239–E251.

Roberts, C.; and Sandridge, B., 1992, The Ames hole: Shale Shaker, v. 42, no. 5, p. 118–121.

Stöffler, D.; and Ostertag, R., 1983, The Ries impact crater: Fortschritte der Mineralogie, Beiheft, v. 61, no. 2, p. 71–116.

Von Engelhardt, W., 1990, Distribution, petrography and shock metamorphism of the ejecta of the Ries Crater in Germany: a review: Tectonophysics, v. 171, p. 259–273.

Weissman, P. R., 1982, Terrestrial impact rates for long- and short-period comets, *in* Silver, L. T.; and Schultz, P. H. (eds.), Geological implications of impacts of large asteroids and comets on the Earth: Geological Society of America Special Paper 190, p. 1524.

Shock-Induced Microstructures and Experimental Constraints on the Formation of the Ames Impact Structure

Alan R. Huffman
Conoco, Inc.
Ponca City, Oklahoma

ABSTRACT.—The occurrence in a silicate mineral of planar deformation features (PDFs), shock mosaicism, and high-pressure polymorphs has long been accepted as sufficient evidence to indicate the microstructures' origin by impact of an extraterrestrial object. The uniqueness of this association was challenged in the context of the K/T boundary extinction debate during the 1980s after single sets of PDFs and shock mosaicism were identified in the products of explosive volcanism. As a result of this debate, a significant volume of new experimental data on the development of shock-induced microstructures has become available over the past 10 years. These data can be used to better constrain the physical and thermodynamic parameters that control the development of shock-induced microstructures. The experimental data reveal that factors such as preshock temperature, pulse duration, and crystallography of target minerals have a primary influence on how these microstructures develop.

Microstructural evaluation of samples from conventional core from the Nicor no. 18-4 Chestnut well reveals that the dolomitic and felsic breccia units encountered in the core between 9,004 and 9,037 ft contain a variety of shock-induced microstructures including planar fractures, single and multiple sets of PDFs, shock mosaicism, and partial melting of the target rock. The upper unit (9,004 to 9,014 ft) is dominated by a fine dolomitic matrix containing clastic, dolomitic, and granitic fragments. The silicic fragments contain multiple and single sets of PDFs, planar fractures, and shock mosaicism. Large granitic fragments in this interval occasionally show quench textures including dendritic to spherulitic feldspar crystals. The lower unit (9,014 to 9,037 ft) is dominated by a fine-grained, mostly spherulitic to dendritic groundmass of feldspar that is indicative of very rapid cooling. Granitic fragments in this interval commonly contain multiple and single sets of PDFs, planar fractures, and shock mosaicism. The intensity and ubiquitous nature of the shock deformation in the Nicor no. 18-4 Chestnut core support the thesis that these rocks have been shocked to pressures in excess of 20 GPa during an impact event. On the basis of limited observational data, the upper interval may be an ejecta-fallback deposit, and the lower interval appears to be an impact breccia or melt rock that was rapidly quenched after the shock event. The microstructural evidence also excludes the possibility that these rocks are of volcanic origin. The experimental database indicates that the pressures required to produce some of the features observed in the no. 18-4 Chestnut core are well beyond the range of pressures believed to occur in volcanic detonation events, which are limited to peak pressures of well below 10 GPa, as determined by current models.

INTRODUCTION

The origin of the Ames structure in Major County, Oklahoma, has been the subject of significant recent debate. Proposed causes for the Ames structure have included meteorite impact (Hamm and Olsen, 1992; Roberts and Sandridge, 1992; Shirley, 1992; Carpenter and Carlson, 1992), a volcanic or "cryptoexplosion" event (Roemer and others, 1992; Coughlon and Denney, 1993), and domal collapse and later subsurface dissolution (Bridges, 1997). The discovery of significant oil and gas reserves within the Arbuckle and basement rocks of the Ames structure has stimulated this

Alan R. Huffman, Conoco, Inc., 5 RWA, 1000 South Pine, P.O. Box 1267, Ponca City, OK 74602.

Huffman, A. R., 1997, Shock-induced microstructures and experimental constraints on the formation of the Ames impact structure, *in* Johnson, K. S.; and Campbell, J. A. (eds.), Ames structure in northwest Oklahoma and similar features: origin and petroleum production (1995 symposium): Oklahoma Geological Survey Circular 100, p. 310–325.

debate over the origin of the structure. New data from wells have now provided some very convincing evidence for an impact origin of the structure.

Conventional core data from the Nicor Production Company's no. 18-4 Chestnut well, SW¼SE¼ sec. 18, T. 21 N., R. 9 W., has provided a unique opportunity to evaluate the microstructural evidence that supports an impact origin for the Ames structure. The purposes of this paper are (1) to document some of the observed microstructures in the dolomitized and felsic breccia and melt-rock units from the Nicor no. 18-4 Chestnut well and (2) to discuss the conditions under which these microstructures form and their unique relationship to an origin for the Ames structure by impact of an extraterrestrial object.

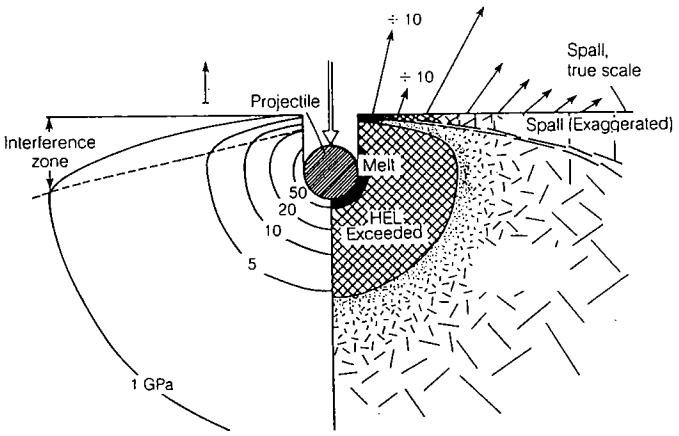

Figure 1. Illustration of the intensity of shock deformation along a radial traverse from the impact epicenter and of spalling during the compressional phase of an impact event. The projectile velocity is 10 km/s, which produces a throw velocity on the free surface of the target of 200 m/s. Below the target, which is assumed to be a homogeneous, isotropic silicate material, the pressure contours are roughly hemispherical and grade outward from the vaporized and melted target, to plastic shock deformation above the HEL, and finally to shock states below the HEL dominated by fracturing and cataclasis. Tension waves produced by rarefaction off the free surface produce a spall sheet that is expelled as high-velocity ejecta. Diagram after Melosh (1989).

MICROSTRUCTURES ASSOCIATED WITH IMPACT EVENTS

Considering the primary role that impact craters have played in understanding shock deformation, a brief discussion of the relationship between impact structures and shock-induced microstructures is appropriate. Early work on the Ries Crater, Germany (Engelhardt and Stöffler, 1968) and Canadian craters (Dence, 1968) revealed a clear relationship between the intensity of deformation and proximity to the center of a crater. This relationship was confirmed by hypervelocity-impact studies in the laboratory (Gault and others, 1968; Stöffler and others, 1975). In general, the central uplift of most structures shows the strongest deformation, in comparison with the more outlying parts of the crater floor and rim, with intense melting and dissociation of nearly all minerals. Farther from the central uplift, but still within the crater, intense deformation—including partial melting, phase transformation in the forms of high-pressure polymorphs, and formation of PDFs (planar deformation features), diaplectic glasses, and intense mosaicism—predominates. Farther from ground zero and at greater depths, the level of deformation decreases until only fracturing of the target rocks is observed (Fig. 1). It is important to note that the volume of material that is shocked to states above the Hugoniot elastic limit (HEL) is quite small compared to the total volume of material that is affected by an impact event. In addition, very little of this highly shocked material is ejected from the crater, which explains why distal impact deposits are often difficult to recognize. In fact, the largest portion of distal deposits from impacts are probably a mixture of spall from surface effects of the event, along with vaporized impactor and vaporized and melted target rock that is jetted out of the crater during the excavation phase. Therefore, the diagnostic feature for identifying distal impact deposits would be the presence of tektites and microtektites, along with evidence of shock-induced microstructures in silicate minerals.

SHOCK-INDUCED DEFORMATION IN SILICATES

Microstructures induced by natural and artificial shock deformation were studied extensively during the mid-1960s to early 1970s (e.g., the symposium proceedings edited by French and Short, 1968; Stöffler, 1972,1974) following the discovery by McIntyre (1962) of shock-induced planar deformation features (PDFs, also called planar elements or shock lamellae) in quartz from the Clearwater Lake structures in Quebec. This flurry of activity was stimulated initially by the Bucher-Dietz controversy concerning the impact vs. volcanogenic origin of certain enigmatic structures ("cryptoexplosion structures") and was accelerated subsequently by the Apollo program, resulting in the recovery of shock-metamorphosed samples from the Moon. Studies related to cratering dynamics (Roddy and others, 1977) and shock meta-

morphism subsided somewhat during the 1970s until the bolide theory to explain the K/T boundary mass extinction was proposed by Alvarez and others (1980). Most of the early work on shock-induced microstructures in silicates was carried out on the common target minerals quartz and feldspar, and this discussion will focus on these minerals. For detailed discussions of shock effects in other silicate minerals, the reader is referred to Chao (1968), Stöffler (1972,1974), and Stöffler and others (1988,1991).

Shock damage in silicate rocks is a function of many material properties, including bulk density, porosity, modal mineral composition, mineral compressibility, shock impedance variations between adjacent minerals, variations in volatile content, and macroscopic and microscopic textural features (e.g., grain size, primary fabric, etc.). Shock deformation in known impact structures (e.g., Melosh, 1989) historically has been divided into four general types: (1) brittle response characterized by fracturing and cataclasis; (2) plastic deformation including formation of PDFs, shock mosaicism, and hydrodynamic bulk flow; (3) phase transformations to high-pressure polymorphs, such as coesite and stishovite; and (4) thermal dissociation, melting, and vaporization (e.g., Stöffler, 1972,1974). The general progression of these features is from 1 to 4 as the intensity of shock deformation increases; however, any combination of these types of deformation may occur in a single specimen because of the heterogeneous nature of shock deformation in multicomponent rocks (components may be individual crystals in a polycrystalline rock or several mineral constituents). Similarly, the peak pressure at which specific types of deformation occur is a complex function of the material properties coupled with the character of the shock event.

Planar Deformation Features

Since their initial discovery, the nature, properties, and orientations of shock-induced PDFs have been described and discussed by many workers (Chao, 1968; Engelhardt and Stöffler, 1968; Engelhardt and Bertsch, 1969; Dence, 1968; Short, 1968; Hörz, 1968; Robertson and others, 1968; Carter, 1968; Sclar and others, 1968; Stöffler, 1972,1974, Christie and Ardell, 1976; Huffman, 1990; Langenhorst and Deutsch, 1994, Stöffler and Langenhorst, 1994, and Leroux and others, 1994). Like tectonic deformation or Böhm lamellae, naturally formed PDFs are commonly partly healed or annealed, are frequently decorated with minute bubbles, voids, or inclusions, and are often only recognizable as planar trails of inclusions. Unlike tectonic lamellae, they are typically straight, sharp, and continuous and possess optical signatures that are very different and distinctive (e.g., Carter, 1968; Alexopoulos and others, 1988). Transmission electron microscopy (TEM) studies show that fresh PDFs consist of thin zones of glass, separated by nearly dislocation-free quartz (Christie and Ardell, 1976; Gratz and others, 1988; Huffman, 1990; Huffman and others, 1993; Langenhorst, 1994), along which very small apparent shear displacements may have taken place (<0.1 μm, Carter, 1968). In sharp contrast, tectonically produced lamellae are composed primarily of dislocation tangles or minute elongate subgrains. PDFs commonly occur in two or more intersecting sets whose number, densities, and orientations are an increasing function of peak shock pressure (Hörz, 1968; Müller and Defourneaux, 1968; Robertson and others, 1968; Robertson and Grieve, 1977).

PDFs can be divided into four classes based on their morphology, including (1) nondecorated, fine optical discontinuities that are barely resolvable with the optical microscope (except in phase-contrast illumination), but easily resolved by TEM; (2) homogeneous PDFs that differ slightly in optical orientation from the host crystal and show decreased refractive index; (3) PDFs filled with glass and high-pressure polymorphs, and (4) decorated PDFs containing vesicles or inclusions of fluid and gas caused either by thermal annealing after the shock event or by emplacement of gas into the shocked grains during the shock event (Engelhardt and Bertsch, 1969). Optically visible PDFs are usually oriented along lattice planes with the shortest Bravais vectors and are spaced 2 to 10 μm apart. They form at pressures above the HEL in the mixed-phase region of the Hugoniot (Grady and others, 1974) and increase in number as a function of increasing shock pressure. In room-temperature experiments on quartz, it is observed that the ω PDFs are the first to form at 15 to 17 GPa, followed by π PDFs at about 20 GPa. Above 20 GPa, the π PDFs are the most common type, along with other forms such as *s*, *a*, *m*, $\{11\bar{2}2\}$, $\{21\bar{3}1\}$, and $\{51\bar{6}1\}$.

To achieve unification of shock terminology, an ad hoc workshop on shock deformation was held in March 1989 at the Lunar and Planetary Institute (Grieve and others, 1990). At this workshop, it was agreed that the term *planar deformation feature* (PDF) would be used in place of previously introduced terms such as *shock lamellae, planar features,* and *planar elements* to eliminate future confusion in the literature.

Equation-of-State Experiments on Quartz and Feldspar

The Hugoniot equation of state of quartz is well characterized (Wackerle, 1962; Ahrens and Rosenberg, 1968). Results for single-crystal quartz and Arkansas Novaculite (Fig. 2) reveal that the HEL for quartz shocked from a room-temperature initial condition lies between 10 and 15 GPa. Above about 35 GPa, shocked states of quartz have specific volumes near those expected for the high-

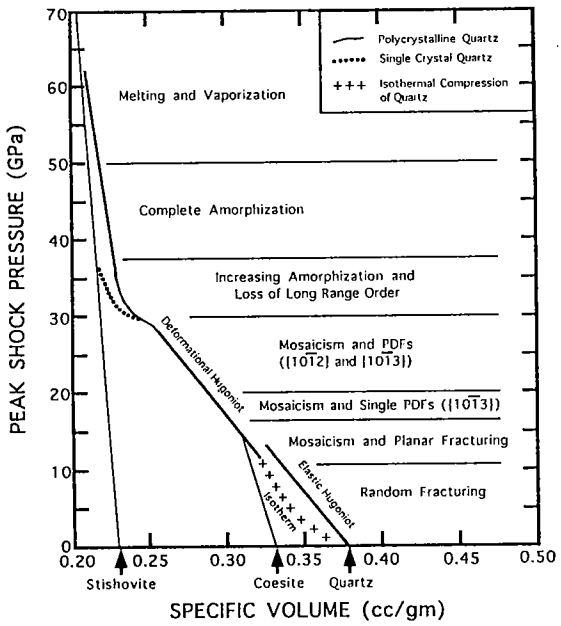

Figure 2. Onset pressures for specific shock-induced microstructures in quartz and quartzite. This plot is a synopsis of the data available from previous shock-recovery experiments at room temperature. PDFs in the {0001} plane are not included in this diagram, but are believed to form at pressures above 9 GPa. Arrows at the base of the diagram represent the specific volumes at room pressure for quartz, coesite, and stishovite. The deformational Hugoniot for polycrystalline quartz was determined from final shock-state data for Arkansas Novaculite, Eureka Quartzite, and Sioux Quartzite. The elastic Hugoniot was determined by elastic limit shocks for the same rocks. Diagram after Ahrens and Rosenberg (1968).

pressure polymorph stishovite. Complete conversion to stishovite-like state appears to occur at lower pressures in single-crystal quartz than in polycrystalline material. It is important to note here that the possible dependence of the HEL on the initial target temperature has not been investigated to date. It is possible that the HEL may decrease at elevated temperatures, as plastic deformation behind the shock front occurs at lower pressures owing to the more energetic state of the quartz crystal.

For shock states at or below the HEL, the release adiabats follow the quartz compression curve. However, for shock states exceeding the HEL, up to 30 GPa, release curves suggest decompression of a dense phase with a specific volume similar to that of coesite. Above 30 GPa, the release paths reflect nearly isothermal decompression of a phase with a specific volume similar to that of stishovite, followed by reversion to quartz as the release curve crosses the lower stability pressure of 9 GPa for stishovite. Thus, the presence of both high-pressure polymorphs of quartz is suggested in the shock-state data. The shock-release data for quartz imply that coesite and stishovite can be preserved only in materials shocked to peak pressures between 15 and 30 GPa. The back conversion to the low-pressure phase during release from shock states above 30 GPa suggests that postshock temperatures are too high to permit preservation of the high-pressure polymorphs.

HELs for feldspars range from 3.5 to 4.5 GPa (Grady and Murri, 1976; Ahrens and others, 1973; Borg, 1972). Above the HEL, the Hugoniot data also suggest that feldspars undergo a progressive conversion to a denser high-pressure phase. Since no high-pressure polymorphs for feldspars have been discovered in shock-deformed rocks, the resulting structure has been assumed to be a short-range-order glass with higher density than that of the unshocked material (Kitamura and others, 1977). However, it is also possible that the final state is similar to that of the high-pressure polymorph of the germanate orthoclase analogue reported by Kume and others (1966) or that of a hollandite-type structure in which silicon changes from tetrahedral to hexagonal close packing with oxygen (Ringwood and others, 1967).

Shock-Recovery Experiments

The progressive development of shock-induced deformation with increasing peak shock pressure in many common rock-forming minerals has been calibrated by using shock-recovery experiments at room temperature (Stöffler, 1972,1974; Stöffler and others, 1988). The general progression of shock-induced microstructures varies as a function of the physical properties of the target mineral, and specific microstructures may or may not occur in a specific mineral. For example, shocked olivine develops planar fractures and mosaicism at 10 to 15 GPa, followed by intergranular brecciation at about 30 GPa, and finally by formation of glass, annealing, and melting above 50 GPa. In contrast, pyroxenes develop mechanical twinning at 5 to 10 GPa, followed by mosaicism and PDFs at about 20 to 25 GPa, and finally by formation of glass, melting, and recrystallization above 75 GPa.

Shock-recovery experiments performed at room temperature with a powder gun (e.g., Hörz, 1968; Kleeman and Ahrens, 1973; Reimold and Hörz, 1986a,b) or with high-explosive methods (e.g., Grothues and others, 1989; Huffman, 1990; Huffman and others, 1993; Stöffler and Langenhorst, 1994) document that a general progression of shock-induced microstructures in quartz that was initially at room temperature can be calibrated to specific ranges of shock pressure (Fig. 2). Only brittle deformation in the form of fracturing occurs below the HEL. With increasing pressure, the progression is from planar fractures and mosaicism to

mosaicism and PDFs, followed by amorphization and development of a short-range-order diaplectic glass at still higher pressures. At even higher pressures, partial, and finally complete, mineral melting (fusion) is observed.

Laboratory data are in accord with the observed progression of shock-induced microstructures from known impact structures (e.g., Engelhardt and Stöffler, 1968; Engelhardt and Bertsch, 1969; Kieffer and others, 1976; Stöffler and Langenhorst, 1994). Kleeman and Ahrens (1973) detected stishovite in all of their samples of Brazilian quartz shocked from 9 to 26 GPa; preservation of stishovite decreased at shock states above 23.4 GPa. Kieffer and others (1976) observed that stishovite was not preserved at shock states above 28 to 30 GPa at Barringer (Meteor) Crater, Arizona.

Detailed measurements of the changes in refractive index of recovered quartz samples, shocked parallel to *m* at room temperatures (Grothues and others, 1989), revealed that the entire change from normal quartz to isotropic quartz occurs between 30 and 35 GPa. However, refractive-index data from naturally shocked quartz from the Ries and Lappajärvi structures (Xie and Chao, 1987) indicate onset of the development of amorphization at pressures from 10 to 15 GPa, with total change being accomplished at pressures below 30 GPa. The naturally shocked samples were calibrated to shock pressures by using cell-expansion parameters. If this calibration is valid, then the data imply that parameters other than peak shock pressure are also important for the constraint of deformation and high-pressure phase regimes.

MECHANISMS FOR DEVELOPMENT OF SHOCK-INDUCED MICROSTRUCTURES

The available experimental data indicate that shock-induced deformation occurs in four modes including brittle failure, plastic yielding above the HEL, amorphization, and phase transformation including PDF formation, and pressure-release melting. The brittle response of the material includes the formation of random and planar fractures during compression, along with additional fracturing that occurs during the release phase as the sample decelerates from the shocked state. The plastic response of the samples also occurs during the compressional phase of a shock event and includes shock mosaicism and, possibly, bulk flow along grain boundaries after the initial compression to the shocked state is achieved. Phase transformations occur heterogeneously in the shock transition at low pressures by collapse of the crystal structure parallel to specific planes to form PDFs containing short-range-order silica or high-pressure polymorphs, followed by complete amorphization at higher pressures. Melting occurs primarily during the pressure-release phase, but can also occur in compression at the very highest temperatures and pressures.

The results from shock experiments with preheated samples (Reimold and Hörz, 1986a,b; Langenhorst and others, 1992; Huffman and others, 1993) suggest that the development of PDFs is partly controlled by the initial temperature of the sample. Development of primarily single sets of thick PDFs at the TEM (transmission electron microscopy) scale in high-temperature experiments suggests that the kinetics of glass formation relative to formation of new PDFs may be increased at high temperatures. Increased temperatures may also suppress collapse of the less compressible planes so that the resulting strains are localized on sets of thicker features, in contrast to the multiple sets of thin PDFs that are observed at the same shock pressures without preheating.

The change from heterogeneous to homogeneous phase transformation, as reflected in the onset of amorphization, is also a function of preshock temperature. The progression from single to multiple sets of PDFs and, then, to amorphization at low initial temperatures is replaced by mostly single sets of PDFs with a dominance of ω forms, followed directly by a broad range of PDFs leading to complete amorphization at high temperatures. This change in behavior suggests that silicates begin to respond by homogeneous phase transformation at high temperatures, before the transformation can become localized along optically visible sets of PDFs. This change in response may be due, in part, to the fact that quartz starts out in the β form in the higher-temperature experiments, as suggested by Langenhorst and others (1992).

The apparent lack of coesite or stishovite in high-temperature experiments results from postshock residual temperatures that are much too high to permit preservation of either polymorph. The most thorough study of high-pressure polymorphs in shocked Coconino Sandstone from Barringer Crater (Kieffer and others, 1976) reveals that coesite and stishovite are probably formed directly from quartz or from a hot precursor phase, such as amorphous silica. The absence of either phase in low-temperature experiments suggests that the transformation must have nucleation and growth rates that are too slow to preserve domains of sufficient size to be identified at the scales of observation used. The large differences in duration of loading between the laboratory (10^{-6} to 10^{-5} s) and the Barringer Crater shock event (10^{-3} to 10^{-2} s) and the size of the largest grains of coesite (~5 μm) and stishovite (~1 μm) preserved at Barringer Crater vs. their absence in the laboratory suggest that the kinetics of crystallization for coesite and stishovite are slow relative to the durations of loading in the laboratory. For a detailed discussion of the mechanism of formation of shock-induced microstructures and their relationship to

environmental conditions, the reader is referred to Huffman and Reimold (1996).

THE NICOR NO. 18-4 CHESTNUT WELL

The Nicor no. 18-4 Chestnut well was drilled to a total depth of 9,500 ft and penetrated the upper 130 ft of the Kindblade Formation (upper Arbuckle Group, Ordovician) before drilling stopped. In the interval from 8,969 to 9,150 ft, the well penetrated a section that included the base of the Oil Creek shale (Simpson Group, Ordovician), which lies conformably above the breccia and melt-rock units associated with the Ames event (Fig. 3). The lowermost breccia unit lies unconformably on the West Spring Creek Formation (upper Arbuckle Group), which was penetrated at 9,121 ft. This entire interval from 8,969 to 9,150 ft was also evaluated by using a Western Atlas borehole image log, which shows the entire sequence from the Oil Creek shale to the West Spring Creek Formation. The operator also retrieved conventional core in the interval from 8,969 to 9,037 ft. The cored interval included about 34 ft of Oil Creek shale, 11 ft of dolomitized clastic rock, and 23 ft of felsic-rich breccia containing abundant granitic xenoliths. The zone of interest, called the Chestnut volcanics by Coughlon and Denney (1993), consists of four layers of interbedded dolomitized and felsic breccia units. The upper two units were sampled by the conventional core.

Microstructural Observations

Thin sections of selected samples from the cored interval (denoted on the borehole image in Fig. 3) were evaluated by using a petrographic microscope, and the observed microstructures were documented photographically. The samples were taken at measured depths of 9,003, 9,005, 9,007, 9,010.8, 9,014, 9,015.5, 9,020, 9,024, 9,025, 9,028, 9,034, and 9,036 ft. The samples fall into two groups: (1) the upper section from 9,004 to 9,014 ft is made up of a dolomitized clastic bed containing clastic and granitic fragments, and (2) the lower section from 9,014 to 9,037 ft is made up of felsic-rich breccia containing abundant granitic xenoliths in a partially melted, quenched groundmass of felsic material.

Character of Deformation in Upper Section

The upper section from 9,004 to 9,014 is characterized by the samples at 9,007 and 9,010.8 ft. At 9,007 ft (Fig. 4), occasional grains of quartz and feldspar appear in a fine-grained dolomitic groundmass. The quartz grains show the first signs of hypervelocity-impact deformation in the form of planar fractures, shock mosaicism (Fig. 4A), and PDFs (Fig. 4B). The uppermost part of the section has fewer large fragments, and the level of shock damage is not as pronounced as deeper in the section. In contrast to the sample from 9,007 ft, the sample at 9,010.8 ft shows significantly more granitic fragments and a larger clastic fraction, with much more pronounced shock-induced deformation. In this sample, large numbers of individual quartz and feldspar grains (Fig. 5) show the effects of peak shock stresses in excess of 20 GPa. Granitic fragments also show strong evidence of shock. In particular, individual quartz grains (Fig. 5B,C) show classic multiple intersecting sets of PDFs, some sharp and well defined, and others decorated by inclusions. Single grains may contain up to five sets of PDFs with up to three sets visible in a single grain orientation (Fig. 5B). Feldspars also show the ubiquitous effects of the shock event, with well-developed PDFs, planar fractures, and significant loss of birefringence (Fig. 5A,D) due to the volume of crystalline material that has been transformed to diaplectic glass. Single quartz grains contained in the dolomitized, clastic matrix (Fig. 6) show the full range of features associated with the peak stresses during the impact event. At low magnification, a 200 μm quartz grain (Fig. 6A) shows evidence of fracturing and recrystallization. At high magnification (Fig. 6B,C), the same grain shows multiple sets of PDFs, and their relationship to the fractures becomes more visible. The zones of fracturing are actually filled with melted quartz that has recrystallized after the shock event. Part of the recrystallized area is also related to a zone in the grain where several sets of PDFs intersect each other (Fig. 6B) and partial melting of the crystal followed by recrystallization has occurred. Other quartz grains (Fig. 6D) show only single sets of PDFs.

The general character of the upper section suggests that this unit may be an ejecta-fallback deposit that settled in the crater after the shock event had ended and the breccias had already been emplaced. The paucity of shock features in the upper part of the section grading into progressively more common, intensely shocked grains and fragments in the lower part of the unit supports this contention, as those larger fragments would tend to settle out more rapidly than the finer fraction that occurs higher in the unit.

Character of Deformation in Lower Section

The lower unit encountered in the core from 9,014 to 9,037 ft is characterized by a felsic-rich groundmass containing large granitic fragments with ubiquitous evidence of intense shock-induced deformation in the pressure range from 20 to 50 GPa. The textures in this section are indicative of an intense shock event, followed by rapid cooling. The groundmass (Fig. 7A) shows a range of dendritic and spherulitic textures indicative of rapid cooling. The groundmass crystals grow rapidly from seed crystals in this setting and grow chaotically into each other as the temperature drops rap-

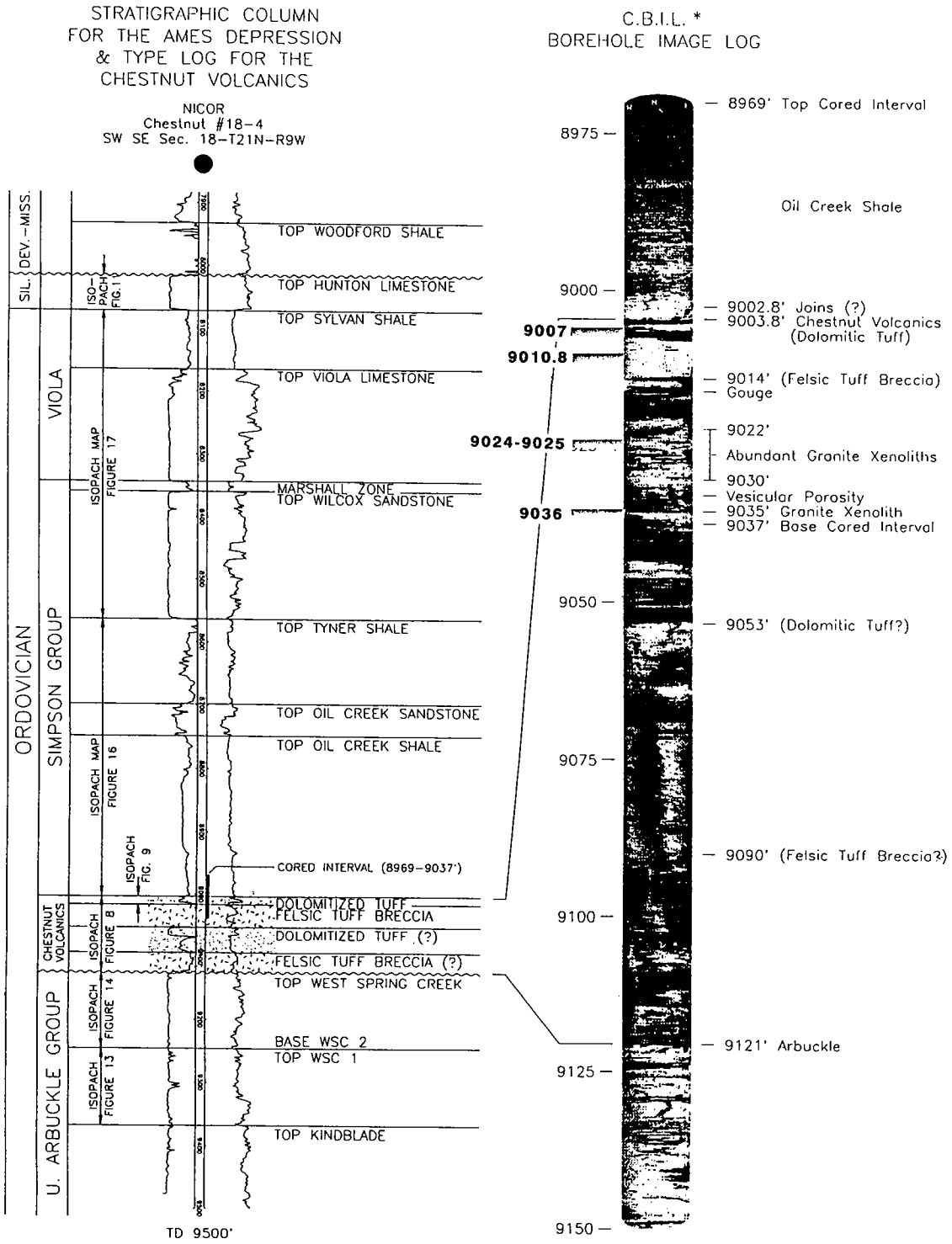

Figure 3. Stratigraphic column with borehole-image log for the cored interval from 8,975 to 9,150 ft in the Nicor no. 18-4 Chestnut well. The expanded interval on the stratigraphic cross section represented by the borehole image includes the rocks that were subjected to the Ames impact event. The depths identified by the heavy markers and boldface labels were analyzed in thin section.

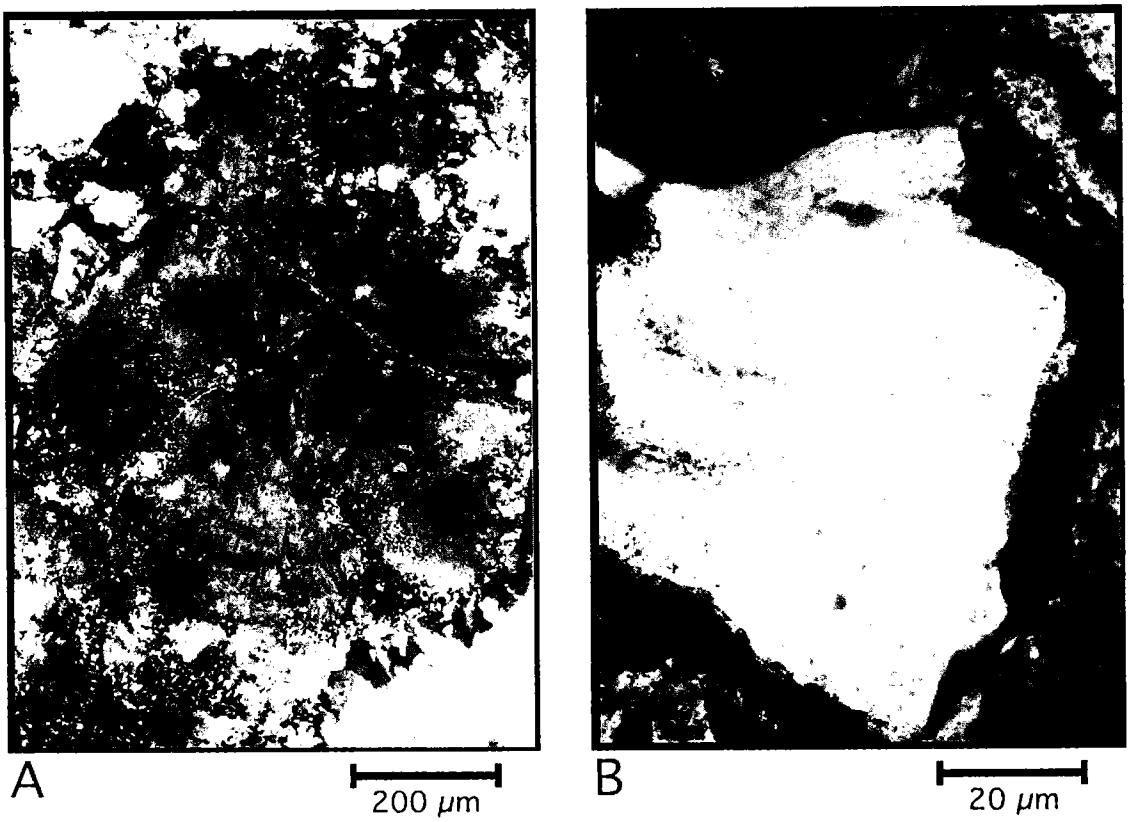

Figure 4. Photomicrographs of shock-induced deformation in quartz from 9,007 ft. *A*—Large quartz grain showing shock mosaicism, loss of birefringence, and multiple sets of PDFs. *B*—Quartz grain showing a single set of PDFs.

idly following the shock event. Within the groundmass, single grains of quartz still display single and multiple sets of PDFs, shock mosaicism, and loss of birefringence (Fig. 7C,D). Some grains also display single sets of clean and decorated PDFs (Fig. 7B). Specific quartz and feldspar grains in this interval show deformation that is so intense that the crystals are near the point of melting. Feldspar grains (Fig. 8A) often display severe disruption including intense mosaicism, planar fractures, crystallographically controlled faulting, and PDFs. Individual quartz grains (Fig. 8B) often show similar disruption with intense mosaicism and planar fracture (Fig. 8C) and multiple sets of PDFs (Fig. 8D). In some of the granitic fragments, deformation in feldspar grains is so intense that the original crystal is difficult to recognize (Fig. 9A). Such grains often display bulk flow during shock compression, so that they appear to be distorted. The most intensely deformed grains show much smaller domains of shock mosaicism that are also disrupted by intense fracturing, partial melting, and subsequent recrystallization that nearly destroys the original crystal. Other feldspar crystals show greatly reduced birefringence, intense mosaicism, and PDFs (Fig. 9B).

The general character of the lower section suggests that this unit represents a impact breccia or melt rock, also known as suevite. The predominance of shock-induced microstructures such as multiple sets of PDFs, loss of birefringence, intense mosaicism, significant partial melting, and spherulitic textures indicative of rapid cooling in the samples studied suggests that this unit was subjected to stresses from 20 to 50 GPa. Therefore, it is believed that this unit represents basement and crustal rocks that were remobilized by the impact event, but never left the crater.

DISCUSSION

The character of the shock-induced deformation observed in the core samples from the Nicor no. 18-4 Chestnut well strongly supports that contention that the Ames structure was formed by im-

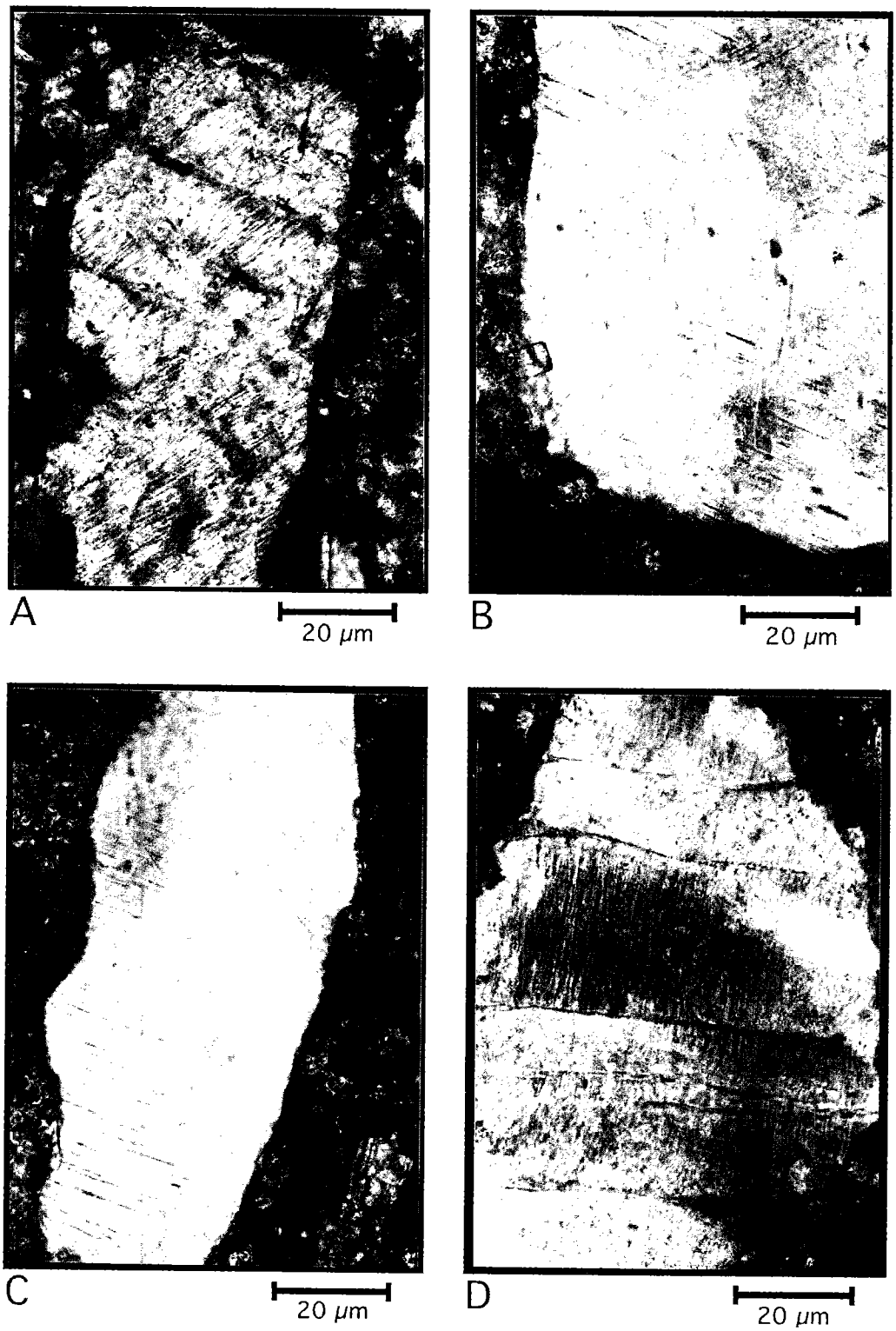

Figure 5. Photomicrographs of shock-induced deformation in quartz and feldspar from 9,010.8 ft. *A*—Feldspar grain displaying planar fractures and PDFs. *B*—Quartz grain showing three sets of PDFs; some are decorated by inclusions. *C*—Quartz grain showing two sets of PDFs. *D*—Feldspar grain showing planar fractures, PDFs, and loss of birefringence.

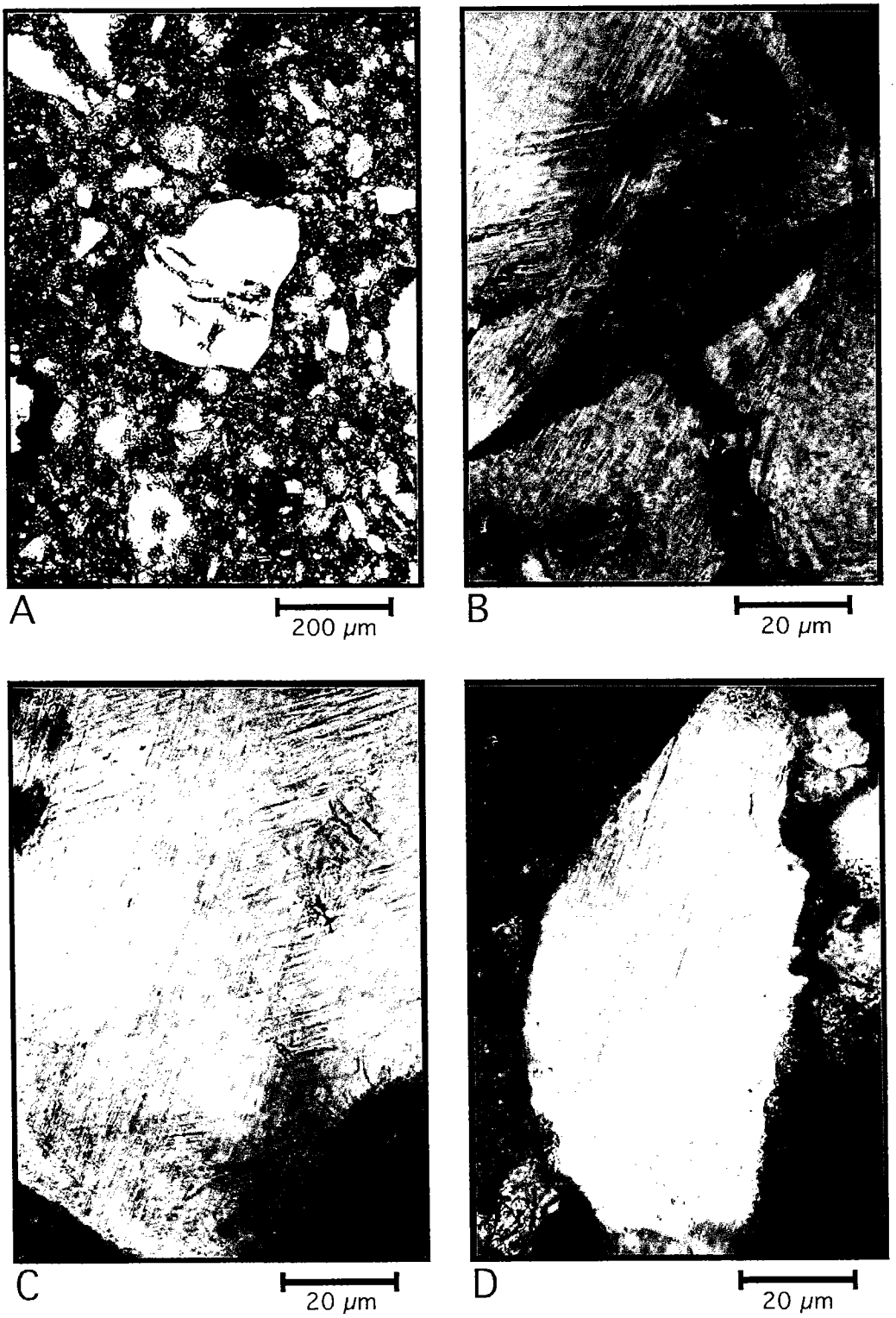

Figure 6. Photomicrographs of shock-induced deformation in quartz from 9,010.8 ft. *A*—Quartz fragment in fine groundmass of glass and dolomite, showing multiple sets of PDFs and fractures containing recrystallized melt. *B*—Same grain as in *A* showing multiple sets of PDFs and fractures with recrystallized melt. *C*—Same grain as in *A* showing multiple sets of PDFs. *D*—Quartz fragment with single set of PDFs.

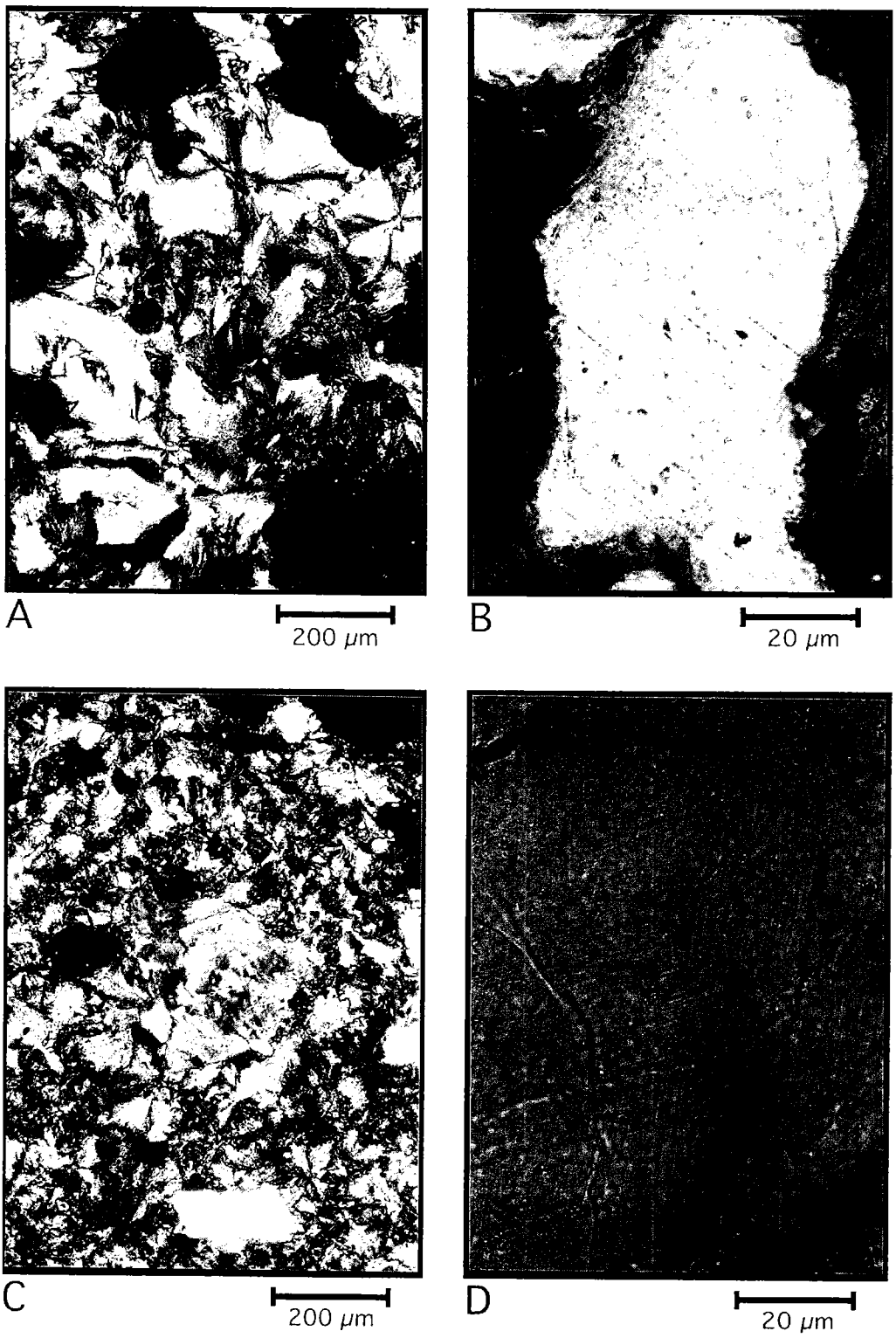

Figure 7. Photomicrographs of shock-induced deformation of quartz and spherulitic textures from 9,024 to 9,025 ft. *A*—Spherulitic textures in groundmass indicative of rapid cooling following the shock event. *B*—Quartz grain showing single set of decorated PDFs. *C*—Quartz grain in spherulitic groundmass showing shock mosaicism and PDFs. *D*—Same grain as in *C* showing multiple sets of PDFs.

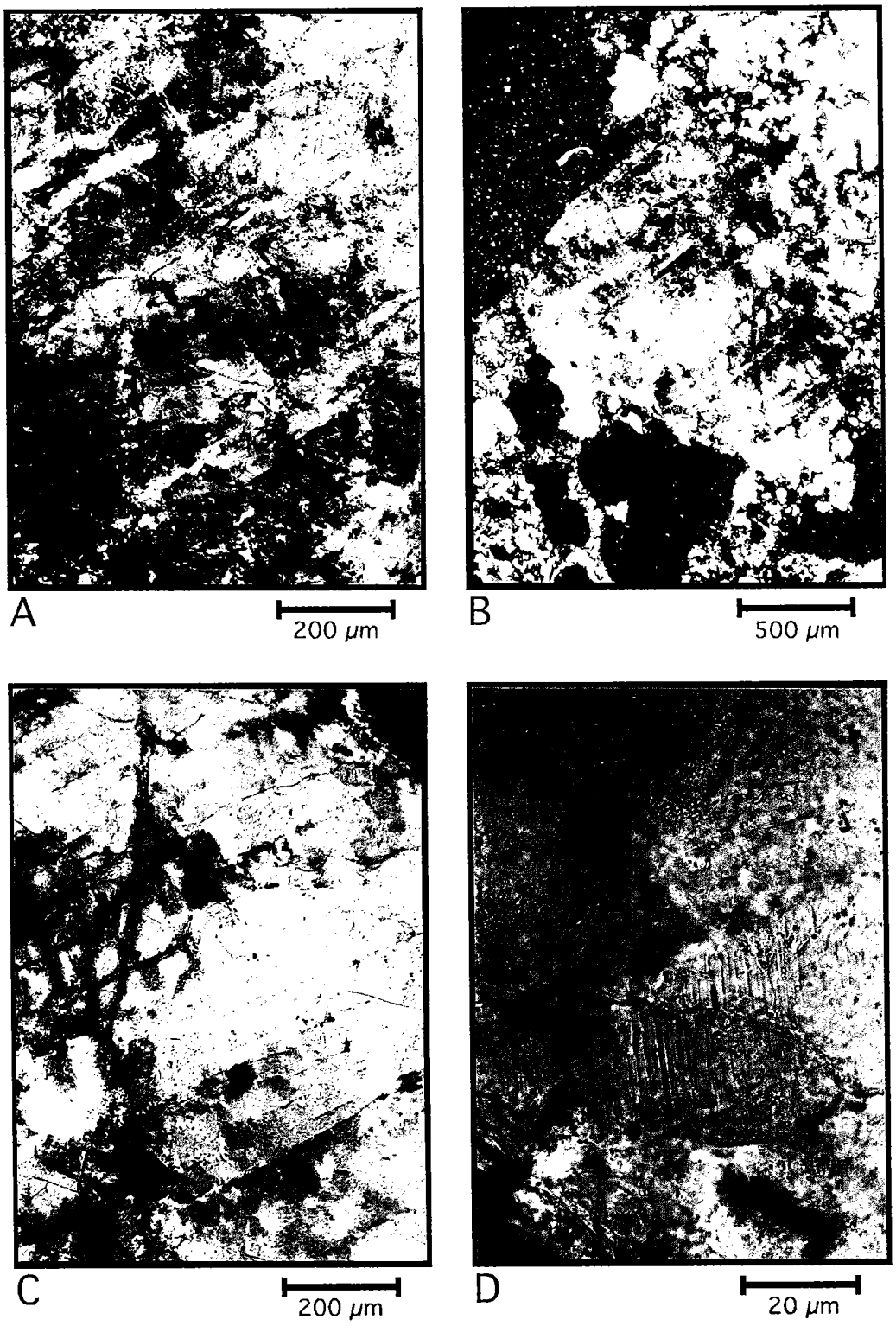

Figure 8. Photomicrographs of shock-induced deformation of K-feldspar and quartz from 9,024 to 9,025 ft. *A*—Feldspar grain showing intense mosaicism, PDFs, and planar fractures. *B*—Quartz grain in fine-grained to glassy matrix showing mosaicism, planar fractures, and PDFs. *C*—Same grain as in B showing recrystallized melt zones, planar fractures, and PDFs. *D*—Same grain as in C showing multiple sets of PDFs.

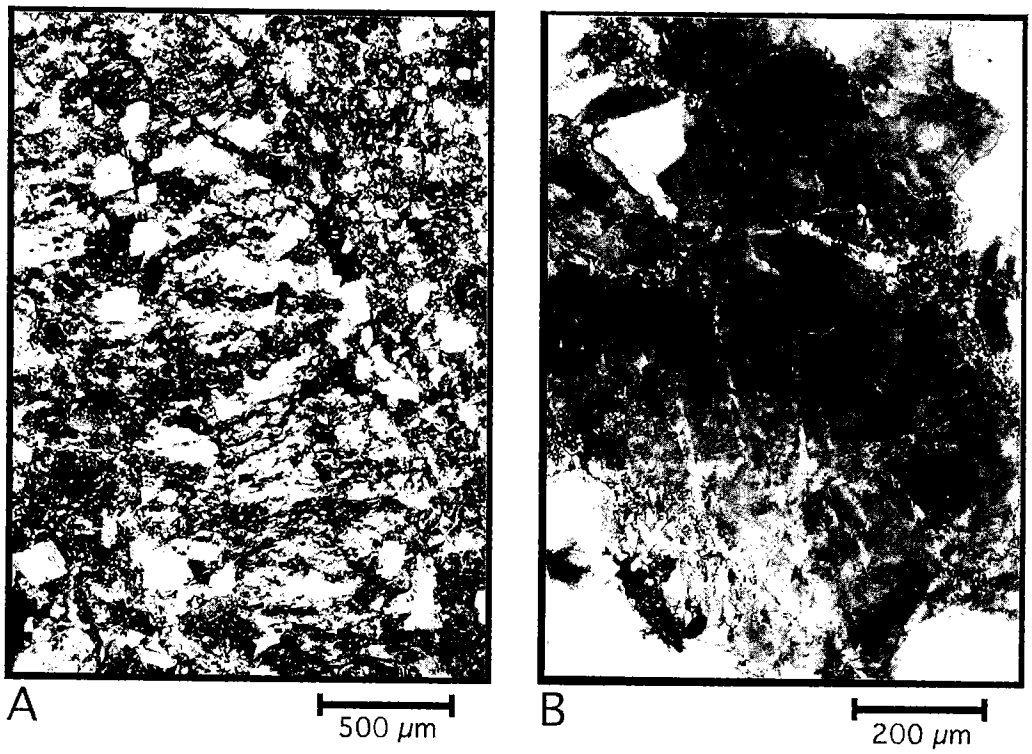

Figure 9. Photomicrographs of shock-induced deformation of feldspar at 9,036 ft. *A*—Severely fractured, mosaic-textured, and partially melted K-feldspar showing fine-grained recrystallized material in melt zones. *B*— Feldspar with intense mosaicism, reduced birefringence, and PDFs.

pact of an extraterrestrial object. This conclusion is supported by the database from hypervelocity-impact, diamond-anvil-cell, and friction experiments that constrain the conditions under which such microstructures may form (Huffman and Reimold, 1996). Although it is beyond the scope of this paper to discuss in detail the differences between hypervelocity-impact, volcanic detonation, and friction-deformation regimes, it is clear from the core evidence that the Ames event produced pressures that exceeded 20 GPa and may have reached 50 GPa or greater. The microstructural evidence—especially the presence of multiple sets of PDFs, loss of birefringence, and partial melting—limits the possible range of conditions to which the Ames rocks were subjected to pressures from 20 to 50 GPa, temperatures less than about 500 °C, and strain rates greater than 10^6 s^{-1}. These conditions exclude the possibility of a volcanic or other terrestrial origin for the structure, as endogenous processes are generally constrained to pressures less than 10 GPa and strain rates less than 10^6 s^{-1} (Huffman and Reimold, 1996). In addition to the observations made herein, other authors have reported similar shock-induced microstructures for samples from the Universal Resources Corporation no. 1-34 Gammon, Universal Resources Corporation no. 2-18 Dixon, and Continental Resources, Inc., no. 1-19 Dorothy wells (Koeberl and others, 1997).

Additional work that would further verify the impact origin for these rocks should include identification of coesite and stishovite (the high-pressure polymorphs of quartz) and detailed optical and transmission electron microscope measurements of the PDFs and partial melt structures to confirm the presence of diaplectic glass and lechatelierite in the melt rocks.

CONCLUSIONS

The microstructural evidence from the Nicor no. 18-4 Chestnut well conventional core reveals that the Ames structure was formed by the impact of an extraterrestrial object into Arbuckle dolomites and Precambrian granites. The dolomitized and felsic breccia units are believed to represent an impact fallback deposit overlying an impact

breccia or melt rock. The observed microstructures and their correlation to the database of shock-recovery experiments suggest that the Ames rocks were subjected to shock-induced stresses from 20 to 50 GPa and strain rates greater than 10^6 s^{-1}.These observations preclude the possibility that the Ames structure was formed by an endogenous process.

ACKNOWLEDGMENTS

I gratefully acknowledge John Coughlon of AMOCO who introduced me to the Ames debate and who kindly shared his thin sections and literature on the Nicor no. 18-4 Chestnut well and the Ames area.

REFERENCES CITED

Ahrens, T. J.; and Rosenberg, J. T., 1968, Shock metamorphism: experiments on quartz and plagioclase, *in* French, B. M.; and Short, N. M. (eds.), Shock metamorphism of natural materials: Mono Book Corp., Baltimore, p. 59–82.

Ahrens, T. J.; O'Keefe, J. D.; and Gibbons, R. V., 1973, Shock compression of a recrystallized anorthosite rock from Apollo 15: Proceedings, Lunar and Planetary Science Conference, v. 4, p. 2575–2590.

Alexopoulos, J. S.; Grieve, R. A. F.; and Robertson, P. B., 1988, Microscopic lamellar deformation features in quartz: discriminative characteristics of shock-generated varieties: Geology, v. 16, p. 796–799.

Alvarez, L. W.; Alvarez, W.; Asaro, F.; and Michel, H. V., 1980, Extraterrestrial cause for the Cretaceous/Tertiary extinction: Science, v. 208, p. 1095–1108.

Borg, I. Y., 1972, Some shock effects in granodiorite to 270 kilobars at the Piledriver site, *in* Heard, H. C., and others (eds.), Flow and fracture of rocks: American Geophysical Union, Geophysical Monograph Series, v. 16, p. 293–311.

Bridges, L. W. D., 1997, Ames depression, Oklahoma: domal collapse and later subsurface solution, *in* Johnson, K. S.; and Campbell, J. A. (eds.), Ames structure in northwest Oklahoma and similar features: origin and petroleum production (1995 symposium): Oklahoma Geological Survey Circular 100 [this volume], p. 153–168.

Carpenter, B. N.; and Carlson, Rick, 1992, The Ames impact crater: Oklahoma Geology Notes, v. 52, p. 208–223.

Carter, N. L., 1968, Dynamic deformation of quartz, *in* French, B. M.; and Short, N. M. (eds.), Shock metamorphism of natural materials: Mono Book Corp., Baltimore, p. 453–474.

Chao, E. C. T., 1968, Pressure and temperature histories of impact-metamorphosed rock based on petrographic observations, *in* French, B. M.; and Short, N. M. (eds.), Shock metamorphism of natural materials: Mono Book Corp., Baltimore, p. 135–158.

Christie, J. M.; and Ardell, A. J., 1976, Deformation structures in minerals, *in* Wenk, H. R. (ed.), Electron microscopy in mineralogy: Springer-Verlag, New York, p. 374–403.

Coughlon, J.; and Denney, P., 1993, The Ames structural depression: an endogenic cryptoexplosion feature along a transverse shear: Shale Shaker, v. 43, no. 4, p. 44–58.

Dence, M. R., 1968, Shock zoning at Canadian craters: petrography and structural implications, *in* French, B. M.; and Short, N. M. (eds.), Shock metamorphism of natural materials: Mono Book Corp., Baltimore, p. 169–184.

Engelhardt, W. v.; and Bertsch, W., 1969, Shock-induced planar deformation structures in quartz from the Ries Crater, Germany: Contributions to Mineralogy and Petrology, v. 20, p. 203–234.

Engelhardt, W. v.; and Stöffler, D., 1968, Stages of shock metamorphism in the crystalline rocks of the Ries basin, Germany, *in* French, B. M.; and Short, N. M. (eds.), Shock metamorphism of natural materials: Mono Book Corp., Baltimore, p. 159–168.

French, B. M.; and Short, N. M. (eds.), 1968, Shock metamorphism of natural materials: Mono Book Corp., Baltimore, 644 p.

Gault, D. E.; Quaide, W. L.; and Oberbeck, V. R., 1968, Impact cratering mechanics and structures, *in* French, B. M.; and Short, N. M. (eds.), Shock metamorphism of natural materials: Mono Book Corp., Baltimore, p. 87–100.

Grady, D. E.; and Murri, W. J., 1976, Dynamic unloading in shock-compressed feldspar: Geophysical Research Letters, v. 3, p. 472–474.

Grady, D. E.; Murri, W. J.; and Fowle, G. R., 1974, Quartz to stishovite: wave propagation in the mixed-phase region: Journal of Geophysical Research, v. 29, p. 332–338.

Gratz, A. J.; Tyburczy, J.; Christie, J. M.; Ahrens, T. J.; and Pongratz, P., 1988, Shock metamorphism of deformed quartz: Physics and Chemistry of Minerals, v. 16, p. 221–233.

Grieve, R. A. F.; Sharpton, V. L.; and Stöffler, D., 1990, Shocked minerals and the K/T controversy: EOS (Transactions, American Geophysical Union), v. 71, p. 1792.

Grothues, J.; Hornemann, U.; and Stöffler, D., 1989, Mineralogical shock wave barometry I: calibration of refractive index data of experimentally shocked alpha quartz [abstract]: Lunar and Planetary Sciences, v. 20, p. 365–366.

Hamm, H.; and Olsen, R. E., 1992, Oklahoma Arbuckle lime exploration centered on buried astrobleme structure: Oil and Gas Journal, April 20, p. 113–116.

Hörz, F., 1968, Statistical measurements of deformation structures and refractive indices in experimentally shock-loaded quartz, *in* French, B. M.; and Short, N. M. (eds.), Shock metamorphism of natural materials: Mono Book Corp., Baltimore, p. 243–254.

Huffman, A. R., 1990, Shock deformation and volcanism across the Cretaceous-Tertiary transition:

Texas A&M University unpublished Ph.D. dissertation, 347 p.

Huffman, A. R.; and Reimold, W. U., 1996, Experimental constraints on shock-induced microstructures in naturally deformed silicates: Tectonophysics, v. 256, p. 165–217.

Huffman, A. R.; Brown, J. M.; and Carter, N. L., 1990, Temperature dependence of shock-induced microstructures in tectosilicates, *in* Schmidt, S. C.; Johnson, J. N.; and Davison, L. W. (eds.), Shock compression of condensed matter 1989: Elsevier, New York, p. 649–652.

Huffman, A. R.; Brown, J. M.; Carter, N. L.; and Reimold, W. U., 1993, The microstructural response of quartz and feldspar under shock loading at variable temperatures: Journal of Geophysical Research, v. 98, B12, p. 22171–22197.

Kieffer, S. W.; Phakey, P. R.; and Christie, J. M., 1976, Shock processes in porous quartzite: transmission electron microscope observations and theory: Contributions to Mineralogy and Petrology, v. 59, p. 41–93.

Kitamura, M.; Goto, T.; and Syono, Y., 1977, Intergrowth textures of diaplectic glass and crystal in-shock-loaded P-anorthite: Contributions to Mineralogy and Petrology, v. 61, p. 299–304.

Kleeman, J. D.; and Ahrens, T. J., 1973, Shock-induced transition of quartz to stishovite: Journal of Geophysical Research, v. 78, p. 5954–5960.

Koeberl, Christian; Reimold, W. U.; Brandt, Dion; Dallmeyer, R. D.; and Powell, R. A., 1997, Target rocks and breccias from the Ames impact structure, Oklahoma: petrology, mineralogy, geochemistry, and age, *in* Johnson, K. S.; and Campbell, J. A. (eds.), Ames structure in northwest Oklahoma and similar features: origin and petroleum production (1995 symposium): Oklahoma Geological Survey Circular 100 [this volume], p. 169–198.

Kume, S.; Matsomoto, T.; and Koizumi, M., 1966, Dense form of germanate orthoclase ($KAlGe_3O_8$): Journal of Geophysical Research, v. 71, p. 4999–5000.

Langenhorst, F., 1994, Shock experiments on alpha- and beta-quartz; II. X-ray and TEM investigations: Earth and Planetary Science Letters, v. 128, p. 683–698.

Langenhorst, F.; and Deutsch, A., 1994, Shock experiments on alpha- and beta-quartz; I. Optical and density data: Earth and Planetary Sciences Letters, v. 125, p. 407–420.

Langenhorst, F.; Deutsch, A.; Stöffler, D.; and Hornemann, U., 1992, Effect of temperature on shock metamorphism of single crystal quartz: Nature, v. 356, p. 507–509.

Leroux, H.; Reimold, W. U.; and Doukhan, J.-C., 1994, A TEM investigation of shock metamorphism in quartz from the Vredefort dome, South Africa: Tectonophysics, v. 230, p. 223–239.

McIntyre, D. B., 1962, Impact metamorphism at Clearwater Lake, Quebec: Journal of Geophysical Research, v. 67, p. 1647.

Melosh, H. J., 1989, Impact cratering, a geologic process: Oxford University Press, New York, 245 p.

Müller, W. F.; and Defourneaux, W., 1968, Deformations-strukturen in quartz als indikator fur stosswellen: eine experimentelle untersuchung an quartzein kristallen: Zeitschrift für Geophysik, v. 34, p. 483–504.

Reimold, W. U.; and Hörz, F., 1986a, Experimental shock metamorphism of Witwatersrand quartzite, *in* Geo-Congress '86: Geological Society of South Africa, p. 53–57.

_____1986b, Textures of experimentally-shocked (5.1 GPa–35.5 GPa) Witwatersrand quartzite [abstract]: Proceedings, Lunar and Planetary Science Conference, v. 17, p. 703–704.

Ringwood, A. E.; Reid, A. F.; and Wadsley, A. D., 1967, High-pressure transformation of alkali aluminosilicates and aluminogermanates: Earth and Planetary Sciences Letters, v. 3, p. 38–40.

Roberts, C.; and Sandridge, B., 1992, The Ames hole: Shale Shaker, v. 42, no. 5, p. 118–120.

Robertson, P. B.; and Grieve, R. A. F., 1977, Shock attenuation at terrestrial impact structures, *in* Roddy, D. J., and others (eds.), Impact and explosion cratering: Pergamon Press, New York, p. 687–702.

Robertson, P. B.; Dence, M. R.; and Vos, M. A., 1968, Deformation in rock forming minerals from Canadian craters, *in* French, B. M.; and Short, N. M. (eds.), Shock metamorphism of natural materials: Mono Book Corp., Baltimore, p. 433–452.

Roddy, D. J.; Pepin, R. O.; and Merrill, R. B. (eds.), 1977, Impact and explosion cratering: planetary and terrestrial implications: Pergamon Press, New York, 1229 p.

Roemer, C. D.; Roemer, C.; and Williams, K., 1992, Gravity, magnetics point to volcanic origin for Okahoma's Ames anomaly: Oil and Gas Journal, June 29, p. 75–80.

Sclar, C. B.; Short, N. M.; and Cocks, G. C., 1968, Shock wave damage in quartz as revealed by electron and incident light microscopy, *in* French, B. M.; and Short, N. M. (eds.), Shock metamorphism of natural materials: Mono Book Corp., Baltimore, p. 483–494.

Shirley, K., 1992, Overlooked "hole" found: American Association of Petroleum Geologists, AAPG Explorer, v. 13, no. 5.

Short, N. M., 1968, Experimental microdeformation of rock materials by shock pressures from laboratory-scale impacts and explosions, *in* French, B. M.; and Short, N. M. (eds.), Shock metamorphism of natural materials: Mono Book Corp., Baltimore, p. 219–242.

Stöffler, D., 1972, Deformation and transformation of rock-forming minerals by natural and experimental shock processes; I. Behavior of minerals under shock compression: Fortschritte der Mineralogie, v. 49, p. 50–113.

_____ 1974, Deformation and transformation of rock-forming minerals by natural and experimental processes; II. Physical properties of shocked minerals: Fortschritte der Mineralogie, v. 51, p. 256–289.

Stöffler, D.; and Langenhorst, F., 1994, Shock metamorphism of quartz in nature and experiment; I. Basic observation and theory: Meteoritics, v. 29, p. 155–181.

Stöffler, D.; Gault, D. E.; Wedekind, J.; and Polkowski, G., 1975, Experimental hypervelocity impact into quartz sand: distribution and shock metamorphism of ejecta: Journal of Geophysical Research, v. 80, p. 4062–4077.

Stöffler, D.; Bischoff, A.; Buchwald, V.; and Rubin, A. E., 1988, Shock effects in meteorites, *in* Kerridge, J. F.; and Matthews, M. S. (eds.), Meteorites and the early solar system, p. 165–202.

Stöffler , D.; Keil, K.; and Scott, E. R. D., 1991, Shock metamorphism of ordinary chondrites: Geochimica et Cosmochimica Acta, v. 55, p. 3845–3867.

Wackerle, J., 1962, Shock-wave compression of quartz: Journal of Applied Physics, v. 33, p. 922–937.

Xie, X.; and Chao, E. C. T., 1987, Studies on the lattice distortion and substructures of shocked lamellae in naturally shocked quartz: Geochemistry, v. 6, p. 19–32.

Production and Structural Features Identified by Surface Geochemical Techniques, Ames Impact Structure, Oklahoma

James D. Tucker, Daniel C. Hitzman, and Brooks A. Rountree
Geo-Microbial Technologies, Inc.
Ochelata, Oklahoma

ABSTRACT.—Anomalous hydrocarbon microseepage was measured by a microbial soil survey; the survey results identified specific production and structural features of the Ames impact structure. These features were identified by a 30 mi reconnaissance microbial survey designed to test the microseepage properties of deeper productive strata within the Ames impact structure. Three straight east-west traverses containing 101 soil samples each (10 per mile sampling density) were collected along section roads. The profiles were designed to cross both outer-rim and inner-ring structural features, the D. & J. no. 1-20 Gregory well, and the locations of recent deeper producing wells.

Microbial measurements indicate that strong hydrocarbon microseepage occurs throughout the area of the Ames impact structure and that anomalously high microbial values are associated with newer producing wells. The highly pressured D. & J. no. 1-20 Gregory well still exhibited a very positive microseepage signature after approximately three years of production. Other deeper and more pressured wells demonstrate a very positive microseepage signature. Conversely, structural lows and locations with older, shallower production exhibit weaker microseepage signatures. Used in conjunction with geophysical and geologic data, geochemical microseepage measurements are an effective exploration tool for the Ames impact structure.

INTRODUCTION

Microseepage from hydrocarbon accumulations is detected by observing the concentrations and distributions of hydrocarbon-indicating microorganisms found in shallow soils. More specifically, when upward-migrating light hydrocarbon gases from hydrocarbon reservoirs enter the shallow soil environment, they are utilized by a specific group of microorganisms. There is a direct, positive relationship between the hydrocarbon concentrations in the soils and these microbial populations (Beghtel and others, 1987). The specific microorganism populations are measured from shallow soil samples collected from depths of between 6 and 8 in. The soils are analyzed by microbiological screening techniques for hydrocarbon-indicating microbes (Hitzman and others, 1994b). The process used in this survey screened for only those microorganisms that indicate the presence of light hydrocarbons, particularly butane.

Sample patterns and sample density are selected to best define the hydrocarbon potential of the target area, subject to considerations of terrain and accessibility. Reconnaissance and more detailed surveys of acreage or prospects may be completed in this manner. The predictive value of this technology has been demonstrated by extensive field surveys (e.g., Sundberg and others, 1994; Hitzman and others, 1994a,1996). Microbial surveys are highly effective when used in conjunction with geologic and geophysical data.

SURVEY STRATEGY

GMT personnel collected 303 shallow soil samples in August 1994 and February 1995 on the undisturbed sides of fence lines along section

James D. Tucker, Daniel C. Hitzman, and Brooks A. Rountree, Geo-Microbial Technologies, Inc., P.O. Box 132, Ochelata, OK 74051.

Tucker, J. D.; Hitzman, D. C.; and Rountree, B. A., 1997, Production and structural features identified by surface geochemical techniques, Ames impact structure, Oklahoma, *in* Johnson, K. S.; and Campbell, J. A. (eds.), Ames structure in northwest Oklahoma and similar features: origin and petroleum production (1995 symposium): Oklahoma Geological Survey Circular 100, p. 326–329.

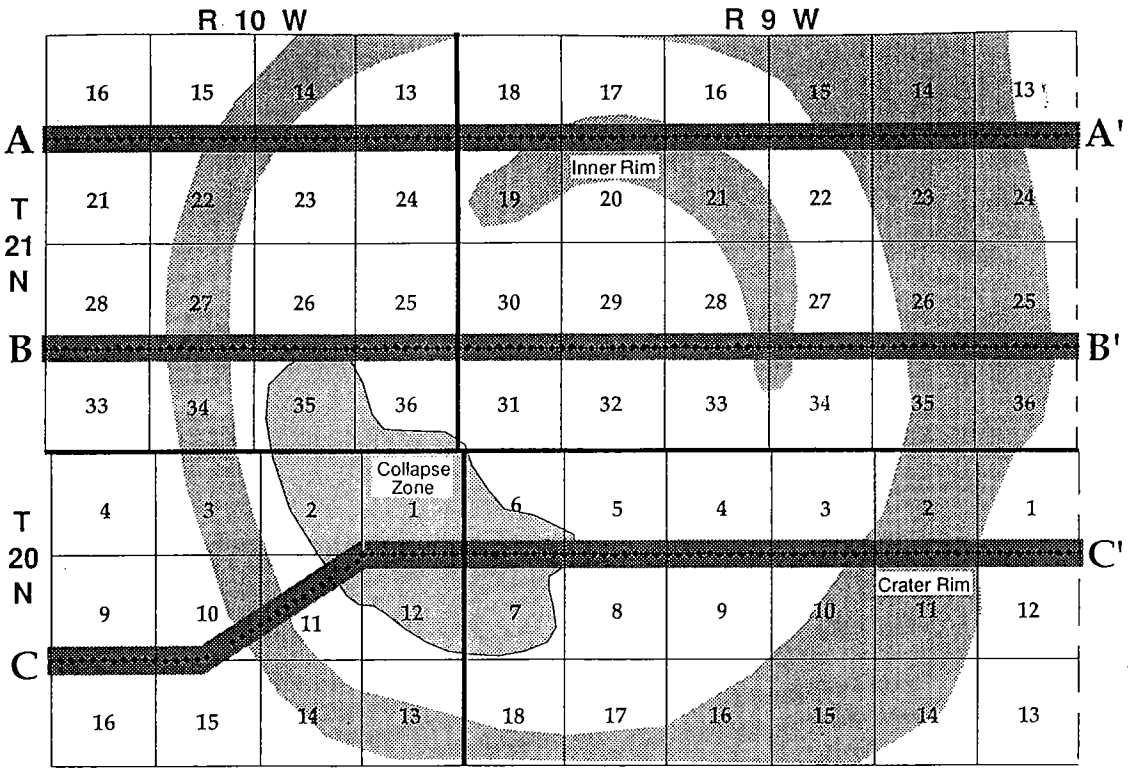

Figure 1. Three 10-mi reconnaissance traverses, A–A′, B–B′, and C–C′, crossed the Ames impact structure along east-west section roads. Shallow soil samples were collected every 0.1 mi.

roads. Samples were spaced every 0.1 mi along three east-west traverses that crossed the Ames structure (Fig. 1) for a total of 30 mi. This microbial reconnaissance program was designed to evaluate large structural and production parameters of the Ames impact structure. Both the outer rim and inner ring of the crater area were traversed. All samples were collected approximately 6–8 in. deep and analyzed at GMT's Ochelata, Oklahoma, laboratory.

Microbial Plots

Profile plots were constructed for each of the three east-west traverses to demonstrate the correlation between the microbial microseepage signatures and the structural and productive elements of the Ames impact structure (Fig. 2). These microbial data can be directly compared to geophysical profiles. Statistical values of the microbial population signatures are presented. The statistical microbial values were calculated by using a five-point weighted moving average formula in which each sample is averaged with the two adjacent sample point values on each side. This function reduces noise in the data and delineates clusters of both anomalously high and low values. Structural and production features are identified along the microbial population plots.

The first and most northern line, A–A′, was sampled in August 1994 and passed near the D. & J. no. 1-20 Gregory well location. The Gregory area shows the strongest microseepage signature of the 10-mi traverse. Without knowledge of deeper potential or seismic data, this reconnaissance survey could have narrowed a 10-mi line down to the best 1-mi prospect. Other microbial signatures along this line also demonstrate exploration potential. The second and third lines, B–B′ and C–C′, respectively, were collected in February 1995 and evaluated the rebound area and additional rim area features. Strong groupings of microbial samples correspond to Arbuckle production and indicate other undrilled areas with good Arbuckle potential. As a reconnaissance survey, the microbial results proved very encouraging. Undrilled and still-pressured Arbuckle targets should send a positive hydrocarbon microseepage signature to the surface. If samples were collected with a tighter density and in a grid pattern, even stronger correlation between deep, pressured production and hydrocarbon microseepage would be anticipated.

Frequency-Distribution Data

A frequency-distribution histogram displays the trend of the microbial data (Fig. 3). The histogram has a distinct right-hand skewed distribu-

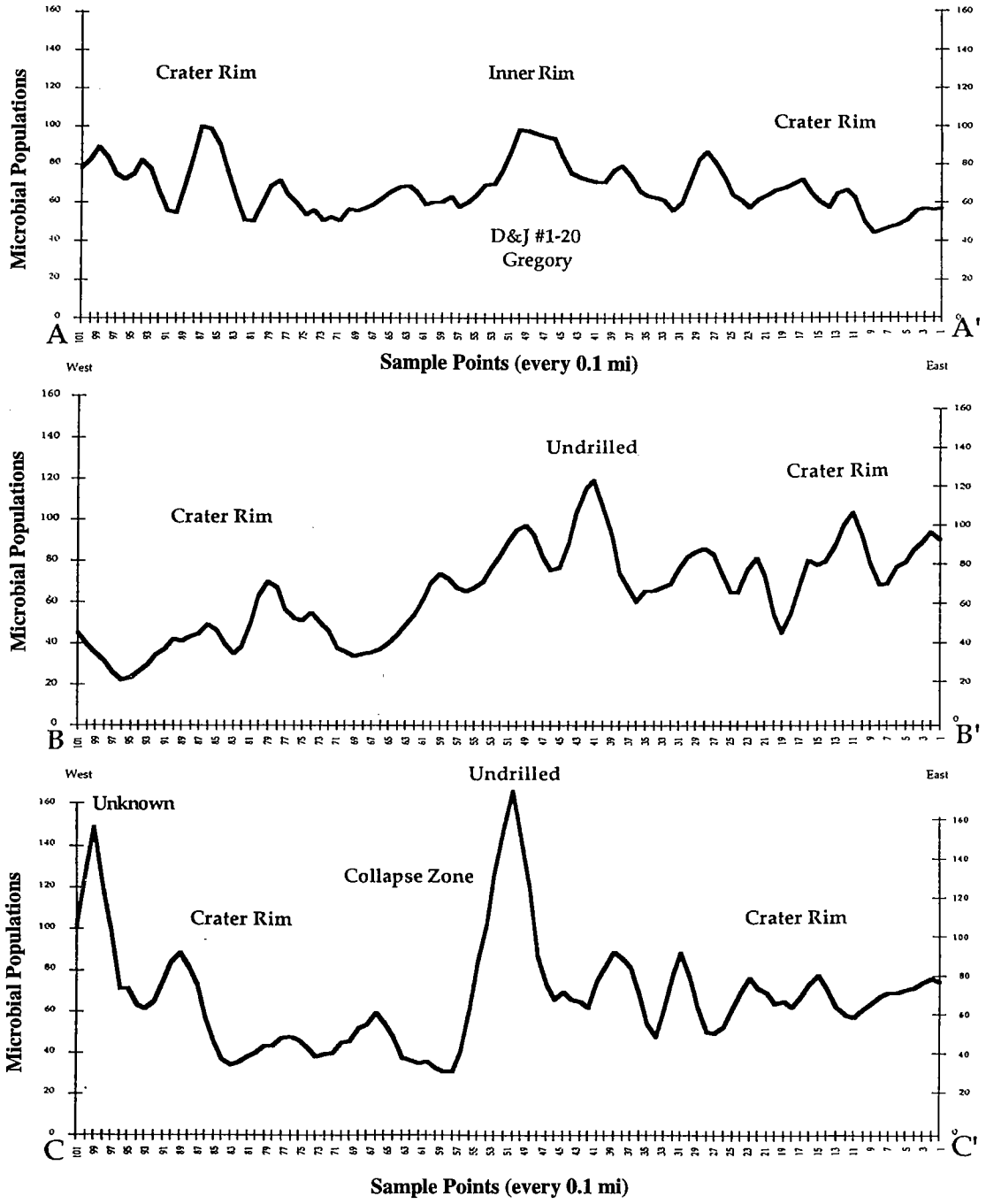

Figure 2. Microbial plots highlight anomalous microseepages that correspond to Ames area structural and production features.

tion common for producing areas. Background values are reflected in a normal bell-shaped curve that can be extrapolated through the left side of the data. Population breaks indicate distinct value cutoffs that are significant for distinguishing between background values and microseepage-indicating microbial values. Anomalously high values distinctly skew the data distribution to the right and indicate a high microseepage and high probability of production. With enough samples it may be possible to distinguish deeper, pressured, and undrilled reservoirs from shallower, depleted, and

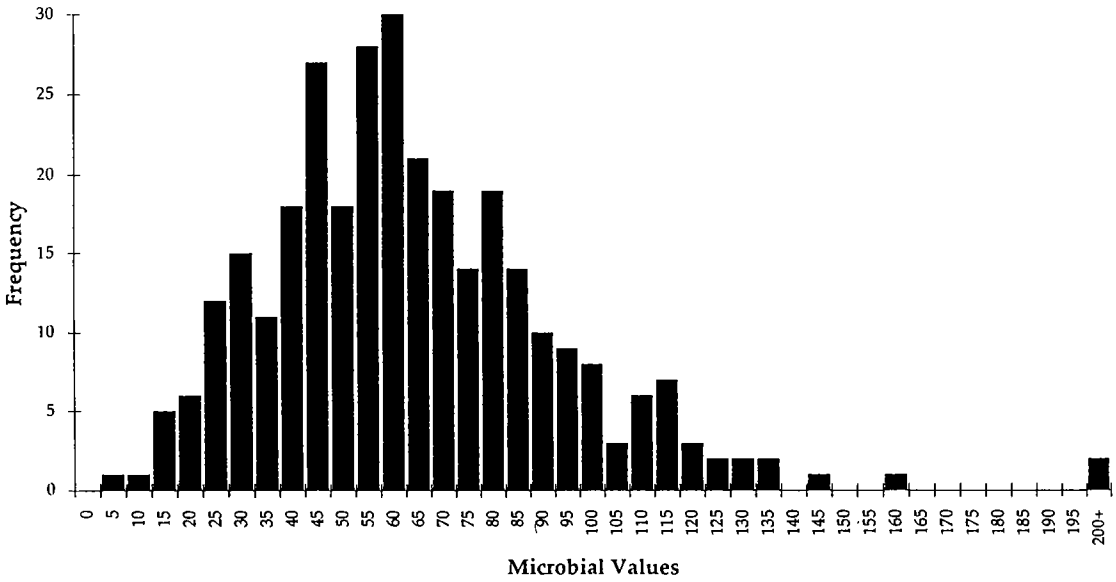

Figure 3. Microbial frequency-distribution histogram for all three traverses. Population breaks at values of 105 and 80 show microbial thresholds corresponding to anomalous microseepage and features of the Ames impact structure.

mature hydrocarbon traps. This data set has a higher than normal average for central Oklahoma and exhibits right-hand skewness that can be extrapolated through the right side of the histogram.

CONCLUSIONS

1. Hydrocarbon microseepage signatures as measured by a reconnaissance microbial survey correspond directly to general production and structural features of the Ames impact structure.

2. A reconnaissance microbial traverse 10 mi long shows that the D. & J. no. 1-20 Gregory well has a very positive microseepage signature reflecting strong, deep pressures.

3. Deeper Arbuckle exploration targets exhibit anomalous microbial activity that is apparent in occurrence vs. distance plots, frequency distribution of microorganism population values, and mapped microbial data. Some Arbuckle features remain undrilled.

4. Used in conjunction with geophysical and geologic data, microbial microseepage measurements are an effective exploration tool for the Ames impact structure and possibly for other deeper target plays.

REFERENCES CITED

Beghtel, F. W.; Hitzman, D. O.; and Sundberg, K. R., 1987, Microbial oil survey technique (MOST) evaluation of new field wildcat wells in Kansas: Association of Petroleum Geochemical Explorationists Bulletin, v. 3, no. 1, p. 1–14.

Hitzman, D. C.; Tucker, J. D.; and Heppard, P. D., 1994a, Offshore Trinidad survey identifies hydrocarbon microseepage: Houston, Offshore Technology Conference.

Hitzman, D. C.; Tucker, J. D.; and Rountree, B. A., 1994b, Development drilling in correlation with hydrocarbon microseepage signatures, *in* Proceedings: American Association of Petroleum Geologists, annual meeting, Denver.

_____ 1996, Surface geochemical hydrocarbon signatures of the eastern Colorado and western Kansas Morrow Group, *in* Johnson, K. J. (ed.), Deltaic reservoirs in the southern Midcontinent, 1993 symposium: Oklahoma Geological Survey Circular 98, p. 255–262.

Sundberg, K. R.; Hitzman, D. C.; Tucker, J. D.; Rountree, B. A.; and Hitzman, D. O., 1994, Surface hydrocarbon microseepage detection by microbial survey of the Sorrento–Mt. Pearl field area, Cheyenne County, Colorado, *in* Proceedings: American Association of Petroleum Geologists, annual meeting, Denver.

Gravity and Magnetic Investigation of the Ames Structure, North-Central Oklahoma

Judson L. Ahern
University of Oklahoma
Norman, Oklahoma

ABSTRACT.—The origin of the Ames structure in Oklahoma is uncertain. Analysis and modeling of gravity and magnetic data collected over the Ames structure place constraints on hypotheses for its origin.

A negative residual Bouguer gravity anomaly surrounded by an annular high mimics the subsurface structure of the Ames feature. The amplitude, shape, and character of the gravity data over the Ames structure are consistent with observations of other structures believed to be caused by meteorite impact. A magnetic low over the Ames structure is also consistent with magnetic field observations over (most) other impact craters.

The 2½-D gravity and magnetic models and a 3-D gravity model yield a density and magnetization structure typical of known meteorite-impact craters.

INTRODUCTION

The Ames structure is a circular depression located near Ames, Oklahoma, in eastern Major County (Fig. 1). It is buried under about 3,000 m of Ordovician and younger sedimentary rocks and is the site of significant oil and gas production (Carpenter and Carlson, 1992; Hamm and Olsen, 1992). Its origin has been variously attributed to meteorite impact, volcanic activity, dissolution collapse, and other causes. Geologic arguments for an impact origin have been based on geomorphology, rock textures, mineral deformation, and stratigraphic relationships (e.g., Hamm and Olsen, 1992; Carpenter and Carlson, 1992; Nick, 1994). The purpose of this study was to determine whether the gravity and magnetic fields in the vicinity of the Ames structure are consistent with an impact origin.

DATA ACQUISITION, REDUCTION, AND PROCESSING

Gravity data were collected at 40 stations on December 17–18, 1994, with a Lacoste and Romberg model G gravimeter. These data were combined with data from the National Geophysical Data Center (1994) and Roemer and others (1992). Where applicable, data were corrected for instrument drift and for latitude, free-air, and Bouguer effects.

Aeromagnetic data were collected by Applied Geophysics, Inc., Salt Lake City, along 2,130-m-spaced east-west flight lines from June through August 1982 at a flight altitude of 762 m, sampling rate of 1.0 s, and sensitivity of 0.25 nT. Diurnal corrections were made and effects of cultural features were removed.

Residual Bouguer gravity was produced by removal of a third-order regional field; similarly, a third-order regional field was removed from magnetic data following reduction to pole (Fig. 2).

DESCRIPTION AND INTERPRETATION

Gravity

The residual Bouguer field reveals a circular negative anomaly of about 2 mgal that is almost perfectly coincident with the central structural depression as defined by structure contours on the Sylvan Shale (Fig. 2). This gravity low is surrounded by an annular gravity high with a radius of 6 km and an amplitude of about 0.5 mgal; this positive anomaly ring coincides with the structural high composing the rim of the Ames structure.

The gravity signature of impact craters is relatively distinctive, and the relationship between impact effects and density is somewhat straight-

Judson L. Ahern, School of Geology and Geophysics, University of Oklahoma, Norman, OK 73019.

Ahern, J. L., 1997, Gravity and magnetic investigation of the Ames structure, north-central Oklahoma, *in* Johnson, K. S.; and Campbell, J. A. (eds.), Ames structure in northwest Oklahoma and similar features: origin and petroleum production (1995 symposium): Oklahoma Geological Survey Circular 100, p. 330–333.

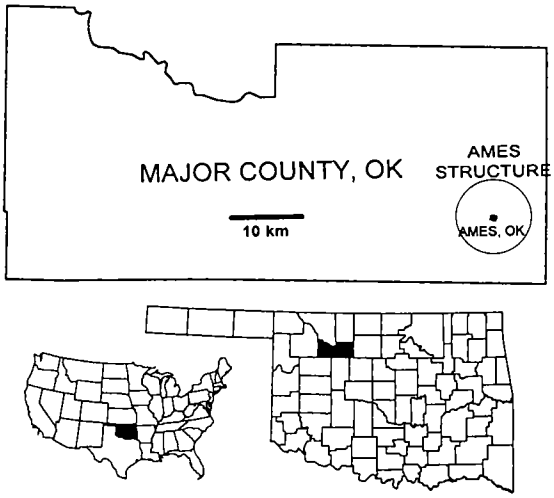

Figure 1. The Ames structure is located beneath the town of Ames, Oklahoma, in Major County. Its approximate position and extent are shown by the open circle.

forward. In fact, since about one fifth of known impact craters on Earth are covered with sedimentary deposits, gravity is the major tool for investigation of these structures (Grieve and Pesonen, 1992; Pilkington and Grieve, 1992). The amplitude, shape, and character of gravity over the Ames structure are consistent with observations of other structures believed to have been caused by meteorite impact. Impact craters formed in sedimentary rocks with a diameter similar to the Ames structure (≈15 km) generally produce negative gravity anomalies that extend to or slightly beyond the rim of the crater (Grieve and Pesonen, 1992). The amplitude of the Ames anomaly is similar to that of other similar-sized astroblemes.

Magnetic Data

Although there is a large (≈100 nT) negative anomaly centered about 8 km northeast of the center of the Ames structure, its position suggests that it may not directly relate to the Ames structure. On the other hand, the residual reduced-to-pole magnetic field reveals a 60 nT low nearly coincident with the gravity low and Sylvan structural low (Fig. 2). The radius of the magnetic anomaly is similar to the radius of the subsurface structural feature and to the radius of the gravity anomaly.

The magnitude and shape of the magnetic low over the Ames structure is similar to those of negative magnetic anomalies observed over other impact craters (generally between tens to hundreds of nanoteslas); the anomalies may be due to shock demagnetization, shock remagnetization, and thermal and chemical remanent magnetization (TRM, CRM) effects (Pilkington and Grieve, 1992). However, the magnetic field associated with impact craters is more variable and typically less diagnostic than their gravity field (Grieve and Pesonen, 1992).

GRAVITY AND MAGNETIC MODELS

The 2½-D gravity and magnetic models are based on a west–east profile through the center of the Ames structure (heavy line, Fig. 2) and have been constructed with the impact model in mind (Fig. 3). The 2½-D designation means that the model consists of polygons with finite extent into and out of the plane of the cross section (in this case, ±5 km).

Gravity

A gravity model that gives good agreement to observed gravity includes a thin, 5-km-radius, low-density (–0.3 g/cm^3) layer about the same radius as the Sylvan structural low. This layer might represent low-density fallback breccia composed of basement granite and Arbuckle dolomite (Carpenter and Carlson, 1992) or clastic sediment infill. Beneath this layer is a zone of low density (–0.2 g/cm^3) with a maximum thickness, under the center of the structure, of about 900 m. Crater-fill sedimentary deposits, authigenic breccia, and a melt sheet might present such a contrast (Henkel, 1992). Thin, low-density layers on the flanks of the structure (–0.2 g/cm^3) might represent fallback breccia and ejecta blanket.

A simple 3-D gravity model was also constructed consisting of a region with a negative density contrast (–0.2 g/cm^3), which could be interpreted as low-density sedimentary fill, ejecta, and brecciated Arbuckle dolomite and granite. The upper boundary of the region is a plane at a depth of 2.8 km below the surface. The lower boundary is an irregular surface determined by iterative inverse modeling of the residual gravity field (Cordell and Henderson, 1968). The maximum depth of the low-density region is about 3.5 km, in good agreement with the 3.6 km maximum depth of low-density material as determined from the 2½-D model. The position and diameter of the low-density region mimic the Ames structural depression.

Magnetic Data

To model the observed magnetic low, a region of lowered magnetic susceptibility (–0.005 emu) about 14 km wide and with a maximum thickness of 400 m was constructed near the center of the structure. It should be noted that an equally valid magnetic model could be obtained by placing the anomalously low magnetization deeper, in basement rocks, where preimpact susceptibilities and remanent magnetizations would be expected to be larger and hence the de- or remagnetization effect larger. The magnetic model is less well con-

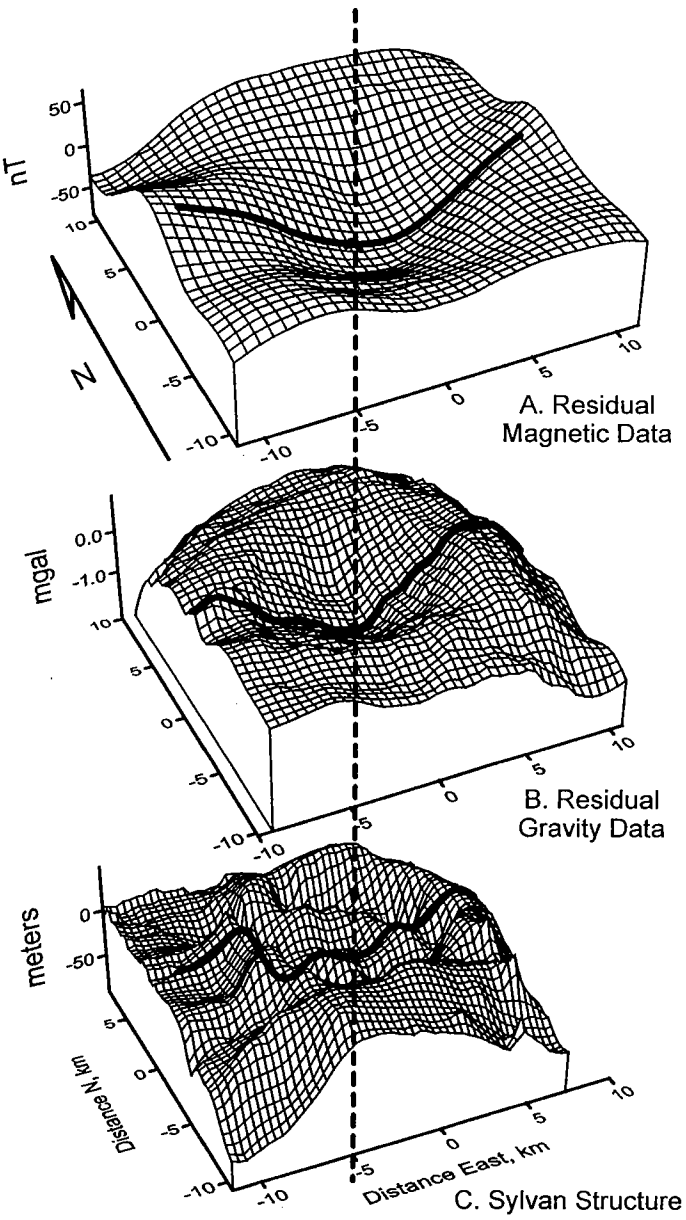

Figure 2. Perspective views: *A*—(third-order polynomial) residual, reduced-to-pole magnetic anomaly; *B*—(third-order polynomial) residual Bouguer gravity anomaly; *C*—Sylvan structure. Dashed line intersects each "surface" at lat 36.260°N, long 98.187°W, taken to be the center of the Sylvan structure ($x = 0$ km, $y = 0$ km), and passes close to the center of the gravity and magnetic lows. Heavy lines show the west–east line of cross section used to construct profiles and models in Figure 3.

strained than the gravity model because susceptibility can vary over several orders of magnitude and pre- and postimpact remanent magnetization magnitudes and directions are largely undetermined.

CONCLUSIONS

A negative residual Bouguer anomaly and a negative residual magnetic anomaly are almost perfectly coincident with the Ames structural depression defined by Sylvan structure contours. The 2½-D and 3-D gravity models, consisting of low-density material at a depth appropriate for the Ames structure, can explain the gravity low. The low-density regions, which extend from 2.8 to 3.5 km below the surface, may be interpreted as brecciated country rock overlain by low-density infill.

A 2½-D magnetic model consisting of low-susceptibility material, at a depth appropriate for the Ames structure, can explain the magnetic low. The low-susceptibility material may be the result of shock effects on basement rocks or magnetic sedimentary deposits.

Although the generally good agreement of the models to the data does not rule out other origins for the Ames structure, the observed gravity and magnetic fields are similar to those observed for confirmed complex meteorite-impact craters. The density and magnetization models derived from the data are similar to structures obtained from geophysical surveys, geologic data, and modeling of known and presumed meteorite-impact craters. Alternative models for the origin of the Ames structure must take into account these geophysical observations.

ACKNOWLEDGMENTS

I thank Donald Preston for assistance with field work. Aeromagnetic data were generously donated by Applied Geophysics, Inc., Salt Lake City.

REFERENCES CITED

Carpenter, B. N.; and Carlson, Rick, 1992, The Ames impact crater: Oklahoma Geology Notes, v. 52, p. 208–223.

Cordell, L.; and Henderson, R. G., 1968, Iterative three-dimensional solution of gravity anomaly data using a digital computer: Geophysics, v. 33, p. 596–601.

Grieve, R. A. F.; and Pesonen, L. J., 1992, The terrestrial impact crater-ing record: Tectonophysics, v. 216, p. 1–30.

Hamm, Harold; and Olsen, R. E., 1992, Oklahoma Arbuckle lime exploration centered on buried

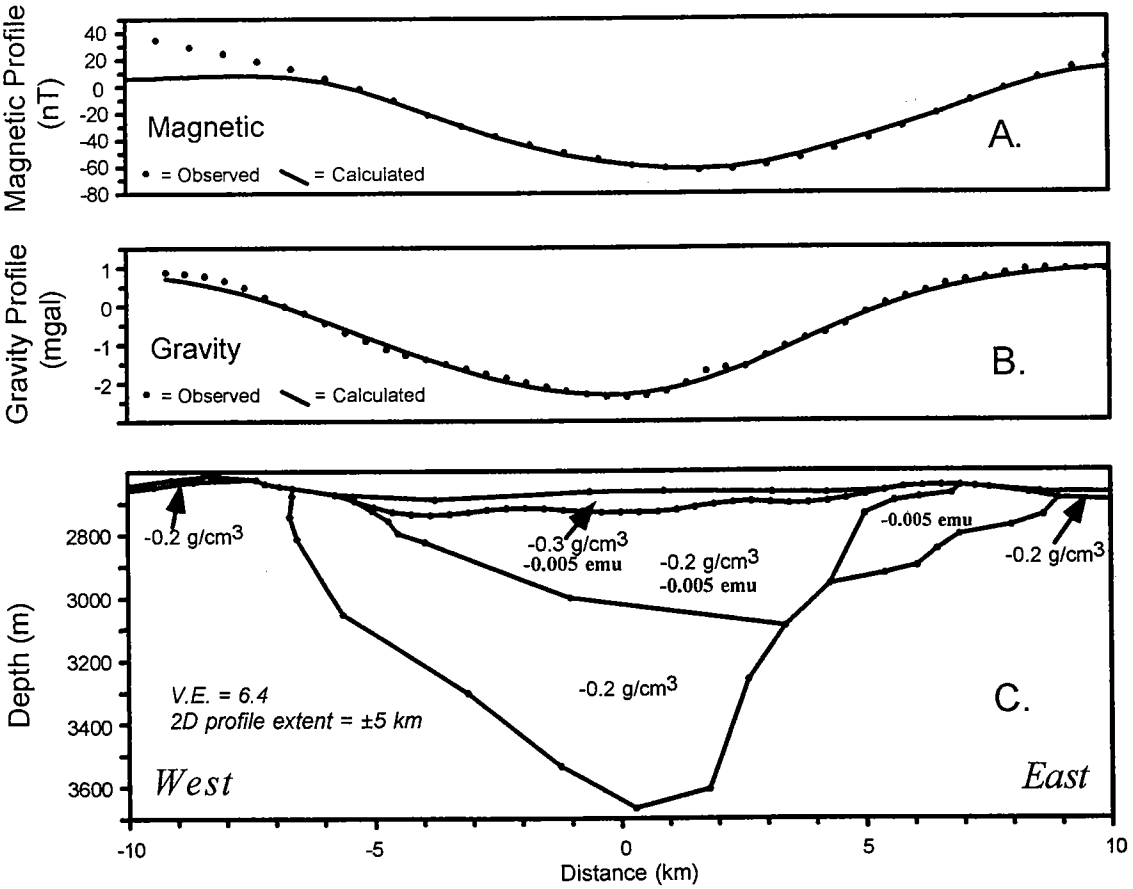

Figure 3. Profiles along the west–east cross section shown in Figure 2: *A*—magnetic profiles, *B*—gravity profiles. Results of 2½-D magnetic modeling (*A*, solid line) and gravity modeling (*B*, solid line) agree well with observed profiles (solid circles). *C*—Polygonal regions used in the modeling and their gravity and magnetic susceptibility contrasts. Polygons extend 5 km into and out of the plane of the cross section. Origin of the distance axis is lat 36.260°N, long 98.187°W.

astrobleme structure: Oil and Gas Journal, v. 90, p. 113–116.

Henkel, H., 1992, Geophysical aspects of meteorite impact craters in eroded shield environment, with special emphasis on electrical resistivity: Tectonophysics, v. 216, p. 63–89.

National Geophysical Data Center, 1994, Gravity CD-ROM [1994 edition]: National Geophysical Data Center, Boulder, Colorado.

Nick, K. E., 1994, Lithologic and stratigraphic evidence for the impact origin of a buried Ordovician age crater and reservoir near Ames, Major County, Oklahoma: American Association of Petroleum Geologists 1994 Annual Convention Official Program, p. 224.

Pilkington, M.; and Grieve, R. A., 1992, The geophysical signature of terrestrial impact craters: Reviews of Geophysics, v. 30, p. 161–181.

Roemer, C. D.; Roemer, C.; and Williams, K., 1992, Gravity, magnetics point to volcanic origin for Oklahoma's Ames anomaly: Oil and Gas Journal, v. 90, p. 75–80.

Basement Rocks in the Ames Area

Rodger E. Denison, Robert J. Stern, and Chih-Hsien Sun
University of Texas at Dallas
Richardson, Texas

INTRODUCTION

The Ames structure in Major County, Oklahoma, lies in the south-sloping northern shelf of the Anadarko basin. There are only a handful of wells that have drilled to basement in this general area. None reached basement rocks at Ames. The Ordovician impact that caused the Ames structure penetrated to the basement and ejected fragments of the Precambrian over a substantial but undetermined area. Wells drilled to the Ordovician in search of oil and gas have penetrated layers of widely distributed basement clasts that occur in Lower Ordovician carbonates, a breccia matrix, or an impact-generated melt rock.

The Precambrian of Major County is included in the Southern Granite-Rhyolite province (Van Schmus and others, 1993). This province is characterized by undeformed granite and rhyolites between 1300 and 1500 Ma in age. The Precambrian of north-central Oklahoma and southern Kansas is composed mostly of mesozonal granite and rhyolites with ages of 1,300 to 1400 Ma. There are no published descriptions of the Precambrian rocks in northwest Oklahoma west of the Nemaha uplift, and very little information has been published on the Precambrian in adjacent southwest Kansas.

FRAMEWORK

Wells into the Precambrian basement along the Nemaha uplift in north-central Oklahoma penetrate medium- to coarse-grained two-feldspar granites. These undeformed granites yield Rb-Sr ages near 1300 Ma and are part of the Central Oklahoma Granite Group (Denison, 1981). To the north, Bickford and others (1979) showed a sprinkling of wells to Precambrian basement in southwest Kansas.

Rodger E. Denison, Robert J. Stern, and Chih-Hsien Sun, Department of Geosciences, University of Texas at Dallas, Box 830688, Richardson, TX 75083.

The location of 13 known wells to basement (west ranges, north of T. 14 N.) and the Ames structure is shown in Figure 1. Samples from eight of these wells have been examined and another has a published rock identification (Table 1). Several lithologic types were recovered. Six of the wells we examined penetrated the expected undeformed granite (one of which contained a diabase dike), another drilled rhyolite, and the remaining well recovered a banded granitic gneiss. The basement clearly does not consist of only the simple, massive, undeformed granites found to the east on the Nemaha uplift, and it could be much more complex than the scattered wells suggest.

BASEMENT AT AMES

Samples from a number of the deeper wells in the Ames area penetrated zones where basement clasts were abundant enough to be identified in cuttings. In addition, several wells cored intervals in which the clasts of the Precambrian were not only abundant but large enough for meaningful petrographic and isotopic analytical studies.

All of the identifiable basement clasts are composed of a distinctive medium-grained two-feldspar granite. The degree of alteration varies greatly. Those clasts caught in the melt formed during impact are scarcely recognizable because of extensive mineralization and hydration of feldspars (e.g., the IMF no. 18-1 Chestnut, sec. 18, T. 21 N., R. 9 W.). Those clasts found either in the cold ejecta or a carbonate matrix are both undeformed and remarkably fresh.

The granite is pale pinkish to white. It is composed almost entirely of microcline perthite, intermediate oligoclase, and quartz. The accessory minerals include biotite, iron oxides, zircon, carbonate, sphene, rutile, fluorite, and apatite. Biotite, where present, is mostly altered to chlorite and white mica. Accessory minerals represent less, in some samples much less, than 2% of the rock volume in every sample large enough to be point counted. The microcline perthite is generally fresh and accounts for about 40% of the rock volume. Quartz represents about one third of the granite, is mildly

Denison, R. E.; Stern, R. J.; and Sun, C.-H., 1997, Basement rocks in the Ames area, *in* Johnson, K. S.; and Campbell, J. A. (eds.), Ames structure in northwest Oklahoma and similar features: origin and petroleum production (1995 symposium): Oklahoma Geological Survey Circular 100, p. 334–338.

TABLE 1.—REPORTED WELLS TO BASEMENT IN NORTHWEST OKLAHOMA (WEST RANGES, NORTH OF T. 14 N.)

County No.	Well name	Location	Depth to basement (ft subsea)	Rock type
Alfalfa				
Af-1	Good no. 2 Singree	1-23N-12W	9437 –8102	Undetermined
Af-2	Phillips no. 1 Weber	21-24N-11W	9170 –7745	Granite gneiss
Af-2	E&B Cox no. 1 Florence	22-26N-11W	7520 –6330	Undetermined
Af-4	Champlin no. 1 Smith	1-27N-10W	7239 –6076	Granite[1] 1380 Ma (z) 1.55 Ga (s)
Garfield				
Gf-1	Sinclair no. 19 Hartley	18-22N-2W	5461 –4346	Granite[2]
Gf-2	Cameron (Hoke) no. 3 Ford	31-23N-3W	6595 –5458	Granite[2]
Grant				
Gr-1	Basin no. 1 Mulhey	7-25N-4W	7428 –6265	Undetermined
Harper				
Hp-1	Marlin no. 1 Gaddis	2-28N-24W	9342 –7230	Undetermined
Hp-2	Ran Ricks no. 27A Selman	27-27N-21W	8812 –7070	Rhyolite porphyry
Kingfisher				
Kf-1	Marlin no. 1 Grishow	14-16N-7W	11510 –10427	Granite
Kf-2	Harper no. 1 Buford	11-19N-9W	10025 –9850	Granite and diabase
Noble				
Nb-1	Shell no. 1 Magney	17-20N-2W	7062 –5793	Granite[2]
Nb-3	Oklahoma Natural Gas no. 1 Hardrow	15-23N-2W	5464 –4496	Granite[2] 1305 Ma (r)[3]

[1] Rock name and ages from Van Schmus and others (1993).
[2] Data from Denison (1981).
[3] Data recalculated from Denison and others (1966).

Note: z = zircon U-Pb age, s = Sm-Nd model age, r = Rb-Sr age.

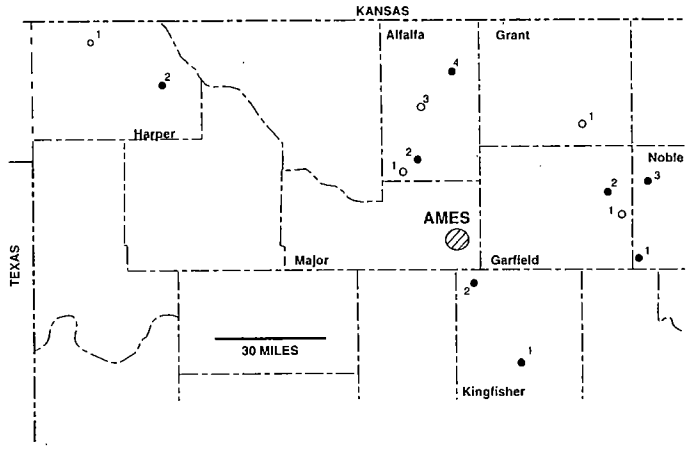

Figure 1. Map showing the location of the Ames structure and wells reported to have reached basement in northwest Oklahoma. Filled symbols indicate wells from which samples have been examined (Table 1 lists references). No samples were examined from wells marked by open circles. The county well numbers are keyed to Table 1.

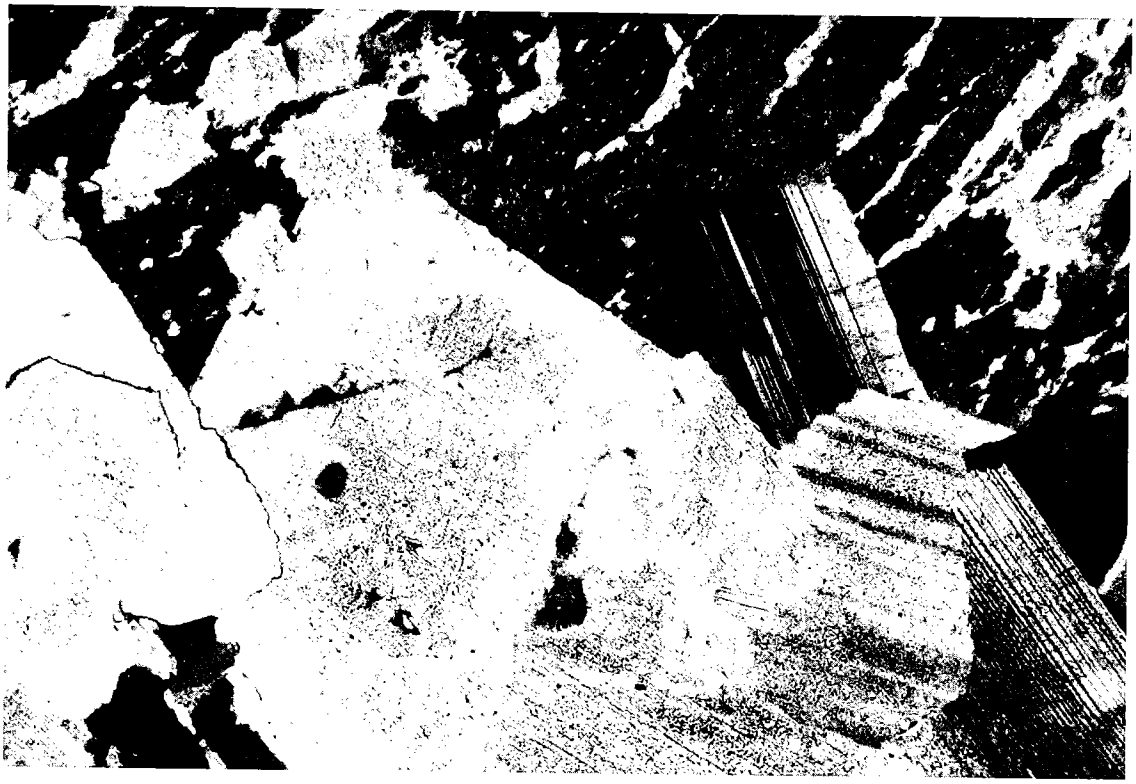

Figure 2. Photomicrograph of typical unaltered granite ejected at Ames. Microcline perthite (upper), moderately clouded oligoclase (lower), and unstrained quartz (left) make up almost the entire rock. Granite clast from the Universal Resources Corporation no. 1-33 Bland at 9,193 ft (My-7). Cross-polarized light; field width represents 3.1 mm.

strained to unstrained, and contains bubble inclusions and some fine rutile needles. Plagioclase occurs as well-twinned, larger primary crystals and in late and secondary myrmekite crystals. Plagioclase accounts for about one fourth of the rock and is unzoned to mildly zoned with undisturbed twinning. Sericite is developed as tiny scattered flakes in the larger plagioclase crystals (see Fig. 2). The later plagioclase is remarkably fresh and clear. The grain size averages a fairly uniform 3 to 4 mm. The texture is hypidiomorphic and does not appear to have been modified since initial magmatic crystallization. The clasts in a breccia or carbonate matrix show absolutely no evidence of the rough handling that scattered them across the Ordovician landscape.

ISOTOPE RESULTS

Four Rb-Sr and two Nd-Sm analyses were made on clasts from two wells, using the facilities at University of Texas at Dallas and techniques outlined in Stern and Kröner (1993). The results offer no surprises. The Rb-Sr analytical results are presented in Table 2 and the isochron calculations in Table 3. The isochron resulting from pooling all of the feldspar and whole-rock data is shown in Figure 3. The two whole-rock Rb-Sr analyses define an age of 1321 ± 62 Ma with a reasonable and low initial $^{87}Sr/^{86}Sr$ (0.7025). All three of the other isochrons are within error of this value, although the Mj-7 whole-rock–feldspar pair defines an age and initial $^{87}Sr/^{86}Sr$ that is most consistent with resetting at about 1200 Ma.

Can isotopic results from basement clasts ejected during an Ordovician impact be trusted? We think the results are both consistent and regionally reasonable. The analyzed granite clasts came from different settings. One clast (Mj-8) was in an ejecta breccia matrix, and the other (Mj-7) was in a carbonate matrix. It could be argued that the two originated in different parts of the impact area and potentially have a different thermal history; certainly they ended 2 mi apart in a totally different sedimentary context. Yet the samples are petrographically identical and isotopically consistent. We interpret the whole-rock isochron age of 1321 ± 62 Ma as approximating the crystallization age of the granite pluton that now underlies the Ames area.

This value is in agreement with the isotopic ages reported from the nearest wells that reach

TABLE 2.—RB-SR ANALYTICAL DATA FOR GRANITE CLASTS AT AMES

Well no.	Well name	Location, depth (ft)	Rb ppm	Sr ppm	$^{87}Rb/^{86}Sr$	$^{87}Sr/^{86}Sr$
Mj-7W	Universal Res.	33-21N-9W	202	26.7	22.91	1.1365
Mj-7F	no. 1-33 Bland	9193	471	28.9	51.38	1.6231
Mj-8W	D&J	20-21N-9W	147	59.1	7.28	0.8404
Mj-8F	no. 1-29 Wayne	9258	269	78.5	10.07	0.8914

Note: W = whole rock, F = feldspar. Rb and Sr contents of all samples were determined by isotope dilution and were analyzed for $^{87}Sr/^{86}Sr$ using the Finnigan MAT instrument at University of Texas at Dallas; accuracy on $^{87}Sr/^{86}Sr$ for these is ±0.00004.

TABLE 3.—RB/SR ISOCHRON CALCULATIONS

Analyses used	$^{87}Sr/^{86}Sr$ intercept (±2σ)	Age (±2σ) (Ma)
Mj-7W, Mj-8W	0.7025 ± 0.0086	1321 ± 62
Mj-7W, Mj-7F	0.7449 ± 0.0300	1194 ± 71
Mj-8W, Mj-8F	0.7073 ± 0.0204	1276 ± 172
All F & W	0.7084 ± 0.0059	1270 ± 37

Note: W = whole rock, F = feldspar.

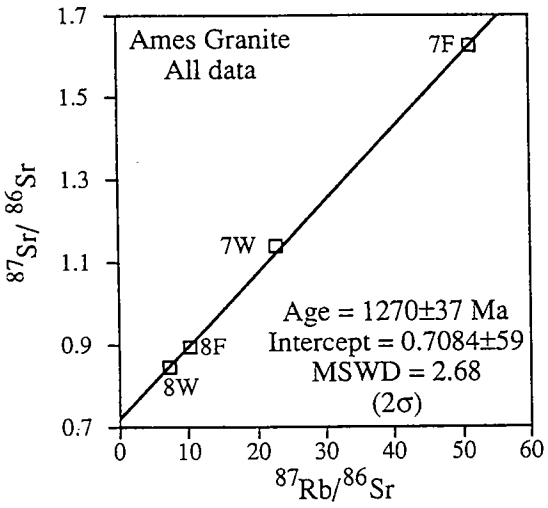

Figure 3. Isochron plot of all Rb-Sr analyses on granite clasts from the Ames area. Numerical data are presented in Table 2.

Precambrian basement. To the east, along the Nemaha uplift, Denison and others (1966) calculated a three-point Rb-Sr isochron age of 1305 ± 30 Ma from a granite in the Oklahoma Natural Gas no. 1 Hardrow (sec. 15, T. 23 N., R. 2 W.) in Noble County. To the north of Ames, Van Schmus and others (1993, p. 241) reported a zircon age (but no analytical data) of 1380 ± 21 Ma from a granite penetrated in the Champlin no. 1 Smith (sec. 1, T. 27 N., R. 10 W.) in Alfalfa County. A Sm-Nd T_{DM} model age of 1550 Ma was also reported from the same granite.

Sm-Nd results can be used to determine the age of crustal formation in the Ames area, i.e., when did the components in these 1300–1400 Ma granites originally separate from the mantle to form this part of the North American craton? Our determined separation ages of 1,660 to 1740 Ma (Table 4) are close to results reported by Nelson and DePaolo (1985) on samples to the north and south of Ames but are somewhat older than the closest determinations given in Van Schmus and others (1993, p. 247). We conclude that our Sm-Nd determination from the granite at Ames fits within the regional pattern of older crustal formation ages.

CONCLUSIONS

Examination of regional wells to basement and petrography and isotopic analysis of two clasts of basement ejected from the Ames impact can be used to reach the following conclusions.

1. The basement in the Ames area is composed of granite, unusual only because of a very low accessory mineral content. Carbonate-enclosed granite clasts are remarkably unaltered and show no petrographic evidence of the Ordovician impact. The exception is the highly altered granite clasts found in a matrix of the melt rock formed during the impact.

2. The Rb-Sr age of granite samples give a

TABLE 4.—SM-ND ANALYTICAL DATA

Sample	Sm (ppm)	Nd (ppm)	$^{147}Sm/^{144}Nd$	$^{143}Nd/^{144}Nd$	T_{DM} (Ga)
Mj-7-1W	3.17	15.98	0.1199	0.51203 ± 0.00006	1.66 ± 0.10
Mj-8-1W	8.11	39.3	0.1247	0.512037 ± 0.000021	1.74 ± 0.01

Note: $^{143}Nd/^{144}Nd$ for six analyses of UCSD Nd = 0.511861 ± 0.000011 (total range). $^{143}Nd/^{144}Nd$ for one analysis of BCR = 0.512647.

whole-rock isochron age near 1320 Ma. The age fits into the regional Precambrian framework. The isotopic systems of the samples examined do not appear to have been disturbed during the impact event.

3. The Sm-Nd ages of about 1700 Ma for the Ames ejection clasts a fits into an older group of crustal separation ages in Kansas and Oklahoma.

4. Most wells to basement in northwestern Oklahoma encountered a undeformed two-feldspar granite. Two other wells penetrated rocks that raise questions: (1) Is the rhyolite in Harper County (from well Hp-2 in Table 1; well 2 in Fig. 1) of Cambrian age, part of the southern Oklahoma aulacogen, or (more likely) part of the 1300–1400 Ma volcanic field? (2) The granite gneiss drilled in Alfalfa County is probably the oldest rock known in Oklahoma. The gneiss clearly underwent a regional metamorphic event that is unrecorded in the 1400 Ma granites. How much older is it? It is unlikely to be older than the oldest rocks in Kansas, 1700 Ma or so.

ACKNOWLEDGMENTS

The samples were obtained with the cooperation of Jock Campbell and Ken Johnson of the Oklahoma Geological Survey. Their efforts made our work go smoothly. Thin sections from the IMF no. 18-1 Chestnut well were made available early in our study by John Hogan and Cliff Ambers. This examination profoundly affected the direction of our isotopic and petrographic work. Finally, this study was initiated with the financial support of Dan Bridges, which is gratefully acknowledged.

REFERENCES CITED

Bickford, M. E.; Harrower, K. L.; Nusbaum; R. L., Thomas, J. J.; and Nelson, G. E., 1979, Preliminary geologic map of the Precambrian rocks of Kansas: Kansas Geological Survey Map M-9, scale 1:500,000, with accompanying note, 9 p.

Denison, R. E., 1981, Basement rocks in northeastern Oklahoma: Oklahoma Geological Survey Circular 84, 84 p.

Denison, R. E.; Hetherington, E. A., Jr.; and Kenny, G. S., 1966, Isotopic-age dates from basement rocks in Oklahoma: Oklahoma Geology Notes, v. 26, p. 170–176.

Nelson, B. K.; and DePaolo, D. J., 1985, Rapid production of continental crust, 1.7–1.9 b.y. age; Nd isotopic evidence from the basement of the North American Midcontinent: Geological Society of America Bulletin, v. 96, p. 746–754.

Stern, R. J.; and Kröner, A., 1993, Late Precambrian crustal evolution in NE Sudan: isotopic and geochronologic constraints: Journal of Geology, v. 101, p. 555–574.

Van Schmus, W. R.; and others, 1993, Transcontinental Proterozoic provinces, *in* Reed, J. C.; and others (eds.), Precambrian: Conterminous U.S.: Geological Society of America, Geology of North America, Boulder, Colorado, v. C-2, p. 171–334.

Arcuate Faults Help to "Relax" and Explain the Ames Structure

Richard Banks
Scientific Computer Applications, Inc.
Tulsa, Oklahoma

Michael D. Kuykendall
Solid Rock Resources
Tulsa, Oklahoma

The Ames structure (Ts. 20–21 N., Rs. 9–10 W., Major County, Oklahoma) can be segregated into several distinct regions or zones: these are the crater wall, crater syncline, crater anticline, central pit, and central high. Of these zones, the crater wall is most clearly defined. We model the crater wall as a nearly circular, normal growth fault that intersects all surfaces below the Woodford Shale. We illustrate the results using a series of maps and cross sections.

To pursue this project, we originally purchased data from Natural Resource Information Systems (NRIS) in Norman, Oklahoma. The data consisted of locations and formation tops for about 770 wells in a four-township area (144 sq mi). Formation tops ranged from the Pennsylvanian Tonkawa unit to the Cambrian–Ordovician Arbuckle Group. Since NRIS data come from many diverse sources, the data set contained many inconsistencies. These inconsistencies were so numerous that we decided to abandon the NRIS data.

Geological Data Services Inc. (GDS), Dallas, agreed to furnish data to us if we would give them credit on all exhibits that were made by using their data. We agreed to do this. The error rate in GDS data was about 0.1%, which was acceptable and easily corrected.

We first made a series of structure maps and cross sections by stacking 17 surfaces from the Tonkawa through the Arbuckle. Figures 1 through 6 show contour maps of Tonkawa, Oswego, Mississippian, Woodford, Simpson, and Arbuckle in the Ames area. Note that continued slumping has made the Ames structure evident in formations as shallow as the Tonkawa. In fact, the structure is evident even in the Permian strata.

Figures 7 through 13 show pairs of various radial cross sections across the Ames structure. The upper cross section in each figure shows an interpretation of the structure without consideration of any faults around the crater rim; the lower cross section of each pair shows the structure with the circular growth faults. In the upper cross sections of Figures 7–13, note that the structure is evident at all levels from the Tonkawa through the Arbuckle (cf. Figs. 1–6). Formations shown in the cross sections, in stratigraphic order from upper to lower units, are as follows:

Tonkawa
Cottage Grove
Hogshooter
Checkerboard
Oswego
Redfork
Atoka
Mississippian (Chester)
Meramec
Woodford
Hunton
Sylvan
Viola
Simpson
McLish
Oil Creek
Arbuckle

To model the crater wall, we created a nearly circular, normal growth fault that started just above the Woodford Shale with zero vertical displacement and that increased in vertical displacement to 300 ft below Arbuckle level. The dip of the fault was assumed to be about 80°. This circular

Richard Banks, Scientific Computer Applications, Inc., 810 Petroleum Club Bldg., Tulsa, OK 74119; Michael D. Kuykendall, Solid Rock Resources, 1408 So. Delaware Place, Tulsa, OK 74104.

Banks, Richard; and Kuykendall, M. D., 1997, Arcuate faults help to "relax" and explain the Ames structure, *in* Johnson, K. S.; and Campbell, J. A. (eds.), Ames structure in northwest Oklahoma and similar features: origin and petroleum production (1995 symposium): Oklahoma Geological Survey Circular 100, p. 339–356.

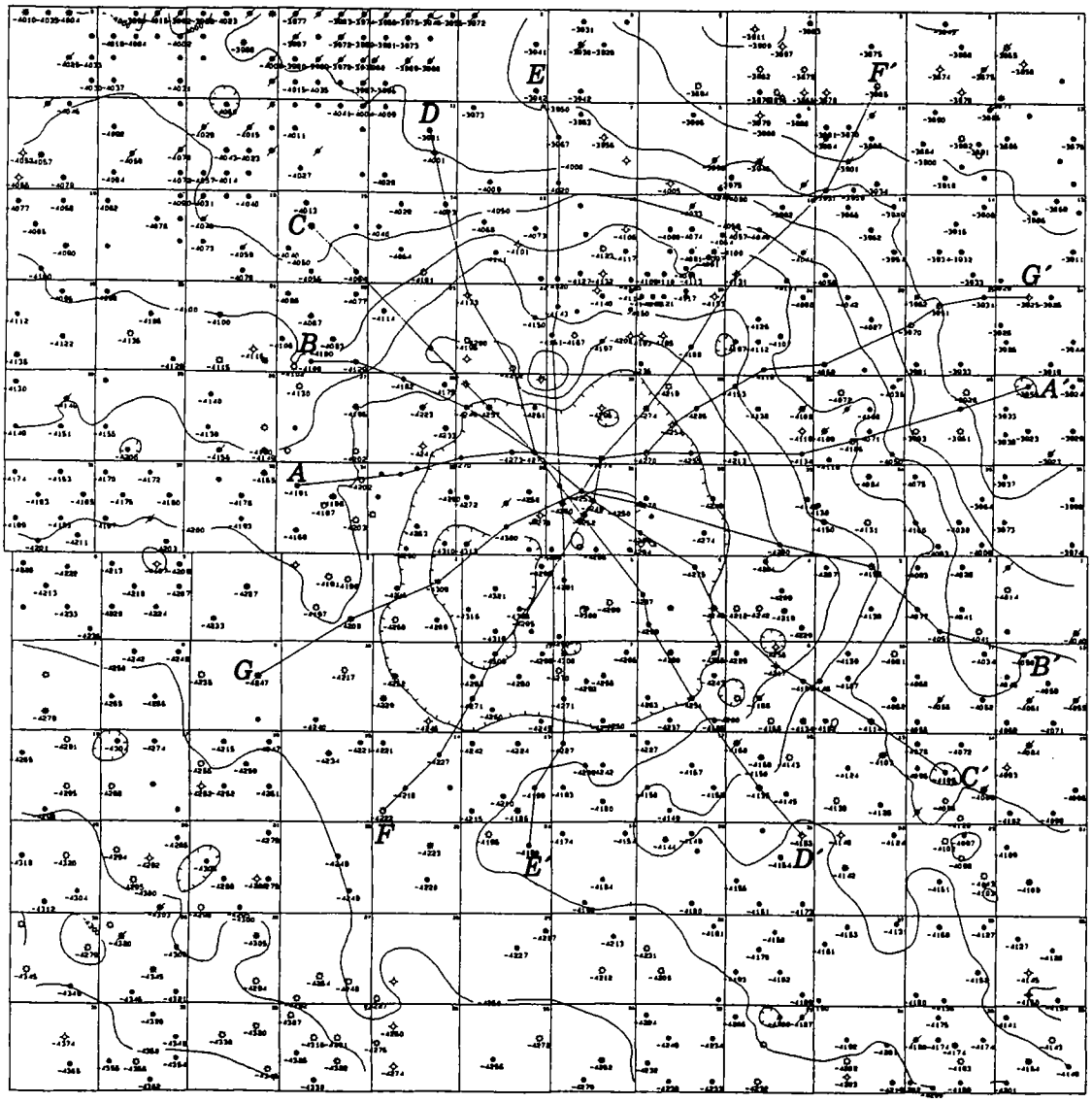

Figure 1. Structure map on top of the Tonkawa; contour interval 50 ft. Data courtesy of Geologic Data Services, Inc. (GDS), Dallas, Texas. Cross-section locations are for the cross sections shown in Figures 7–13.

growth fault is shown in Figure 14, along with its elevation and its vertical displacement values (both in feet; e.g., –8753/300).

Faulted systems are treated as what they are: sets of three-dimensional fault blocks containing geologic markers (formation tops) that once were continuous surfaces. Faulted systems are processed in the following three steps that are designed to honor continuity of shapes across faults: (1) Move fault blocks to their prefaulted positions, together with contained formation tops; i.e., do a sequential vertical palinspastic restoration to paleosurfaces. (2) Having restored the continuous surface attribute to the geologic markers, perform all the stacking and interpolation needed to obtain smooth maps and cross sections. (3) Rebreak the faults (i.e., reverse the first step), and return fault blocks to their faulted positions.

The crater-wall normal growth fault is a model of the crater wall at Arbuckle time, but also it models the discontinuities due to later slumping in shallower horizons. We let vertical displacement go from zero at Woodford level to 300 ft below the Arbuckle.

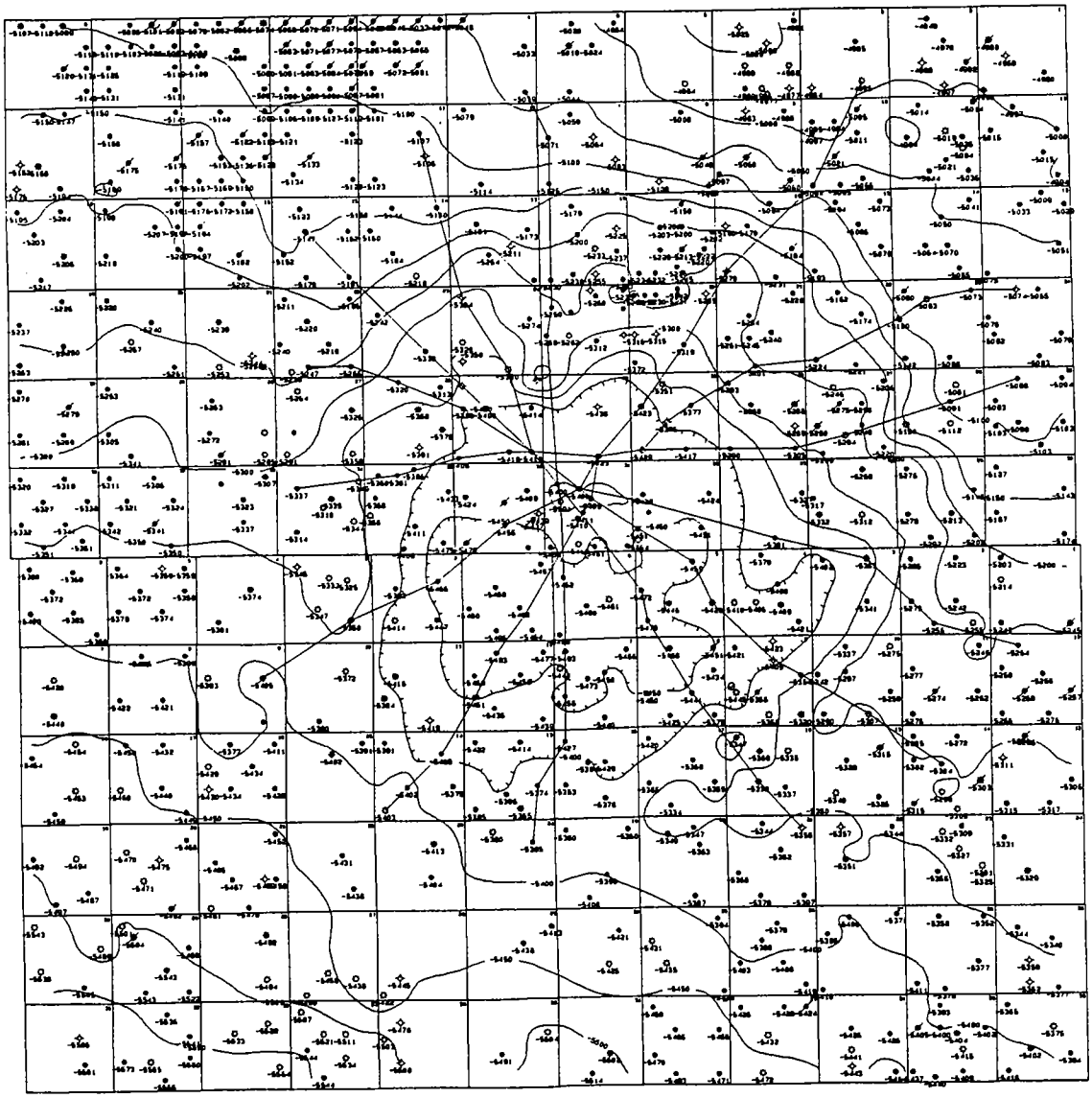

Figure 2. Structure map on top of the Oswego; contour interval 50 ft. Data courtesy of GDS.

Figure 15 is a structure map on top of the Simpson that shows an average fault displacement of 50 ft. Figure 16 is a structure map on top of the Arbuckle. Compare Figure 16 with Figure 6 and notice that the nearly circular growth fault allows the contours' "relaxation," i.e., an easing of the apparent steepness of the formation-top contours along the crater-wall fault. ("Relaxation" is used in the sense—taken from physics—of adjustment of the system to equilibrium following abrupt change; the contours do not show tight contortion against the crater wall where the faults are modeled.) Also compare Figure 5 with Figure 15 (Simpson structure maps).

The lower halves of Figures 7–13 show various radial faulted cross sections across the Ames structure. In Figures 7–13, compare the lower cross section (faulted) with the upper cross section (unfaulted) and note how the crater-wall fault relaxes the contour of the Arbuckle surface.

Additional smaller, arcuate normal growth faults could be added to model the crater syncline, the crater anticline, the central pit, and the central high.

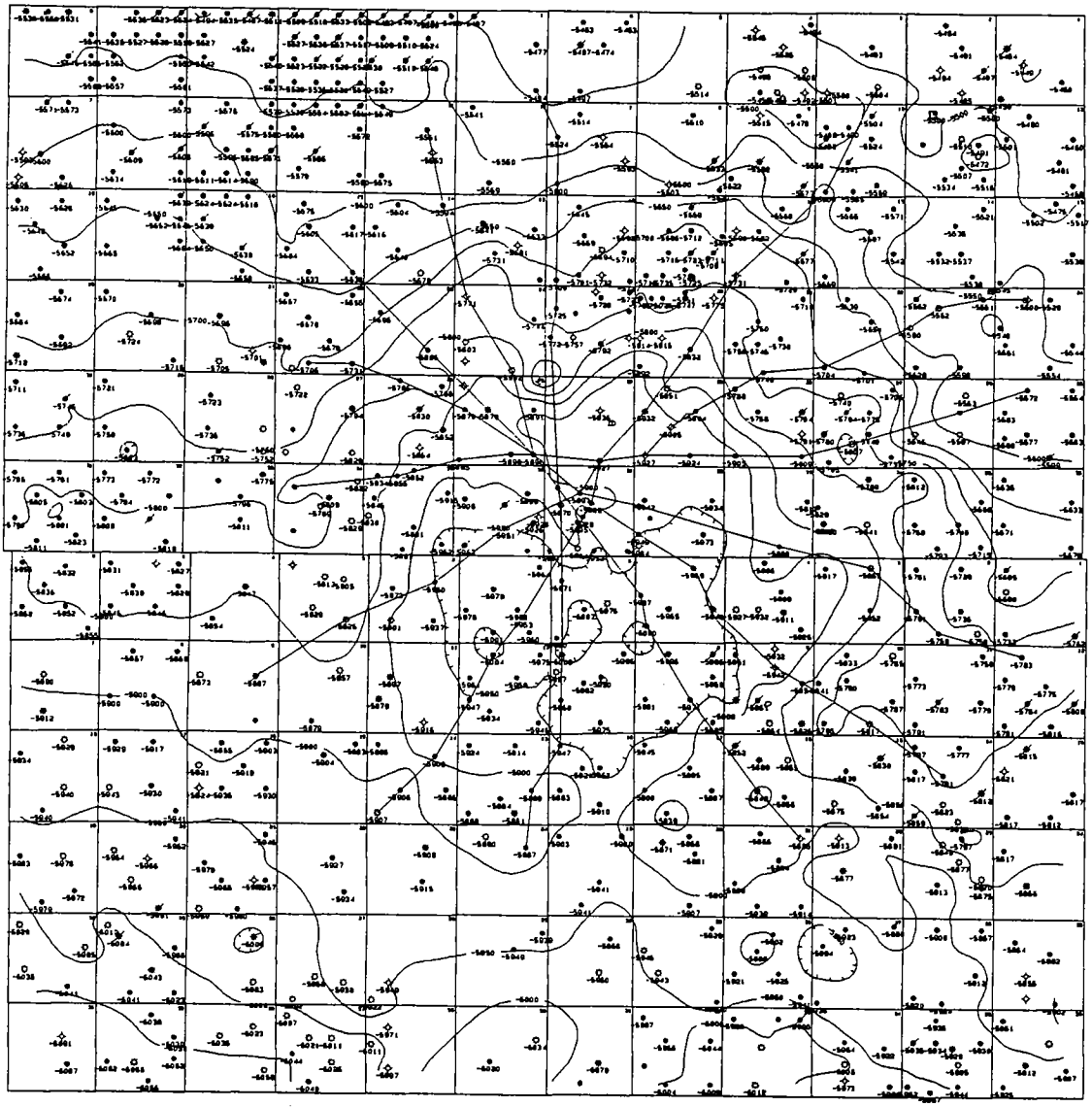

Figure 3. Structure map on top of the Mississippian (Chester); contour interval 50 ft. Data courtesy of GDS.

Figure 17 is a posted location map that shows API well numbers.

SELECTED REFERENCES

Banks, Richard; and Sukkar, Joseph, 1992, Computer processing of multiple 3-D fault blocks containing multiple surfaces: Geobyte, August, p. 58–62.

Kuykendall, M. D.; Johnson, C. L.; and Carlson, R. A., 1997, Reservoir characterization of a complex impact structure: Ames impact structure, northern shelf, Anadarko basin, *in* Johnson, K. S.; and Campbell, J. A. (eds.), Ames structure in northwest Oklahoma and similar features: origin and petroleum production (1995 symposium): Oklahoma Geological Survey Circular 100 [this volume], p. 199–206.

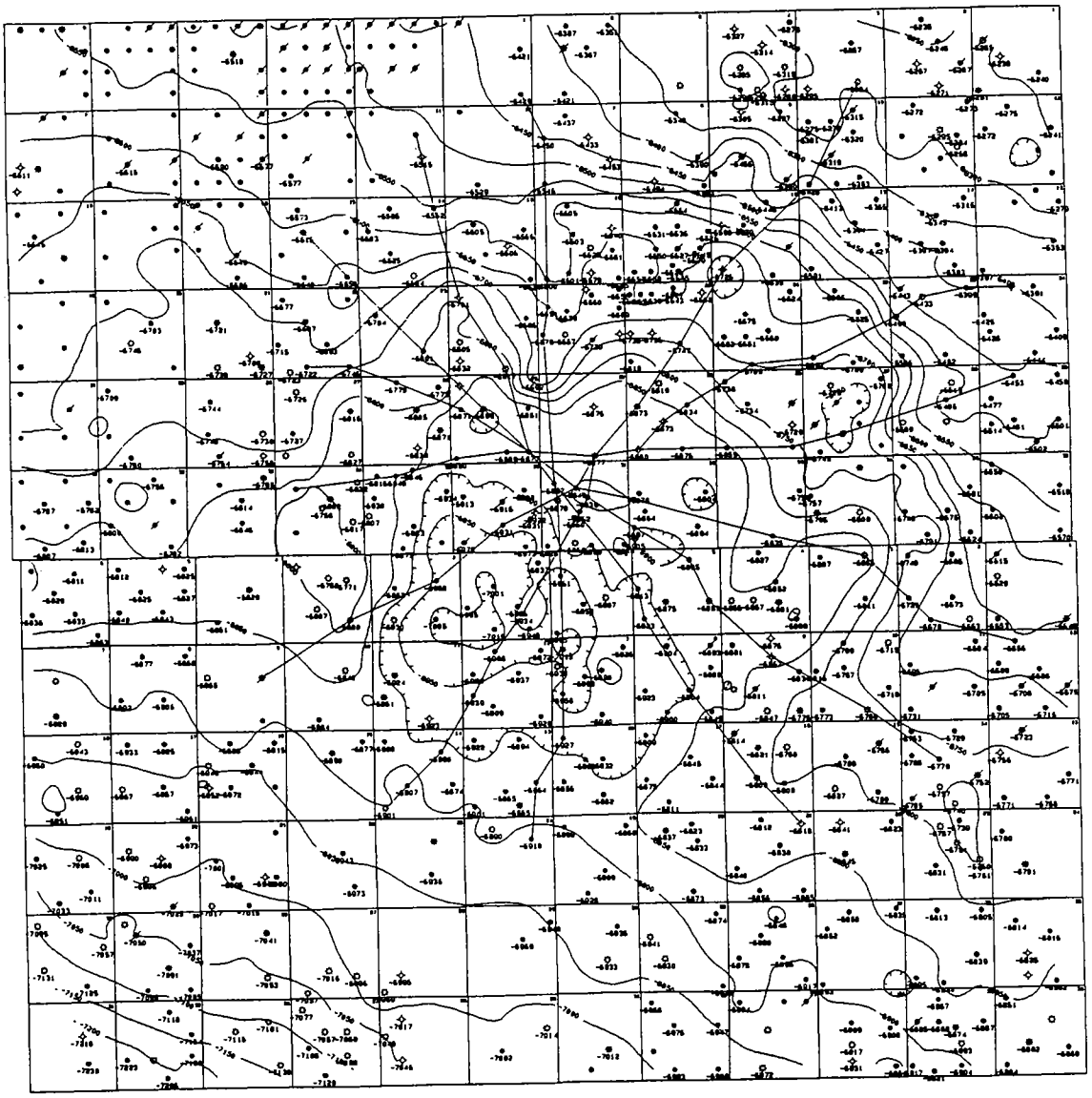

Figure 4. Structure map on top of the Woodford; contour interval 50 ft. Data courtesy of GDS.

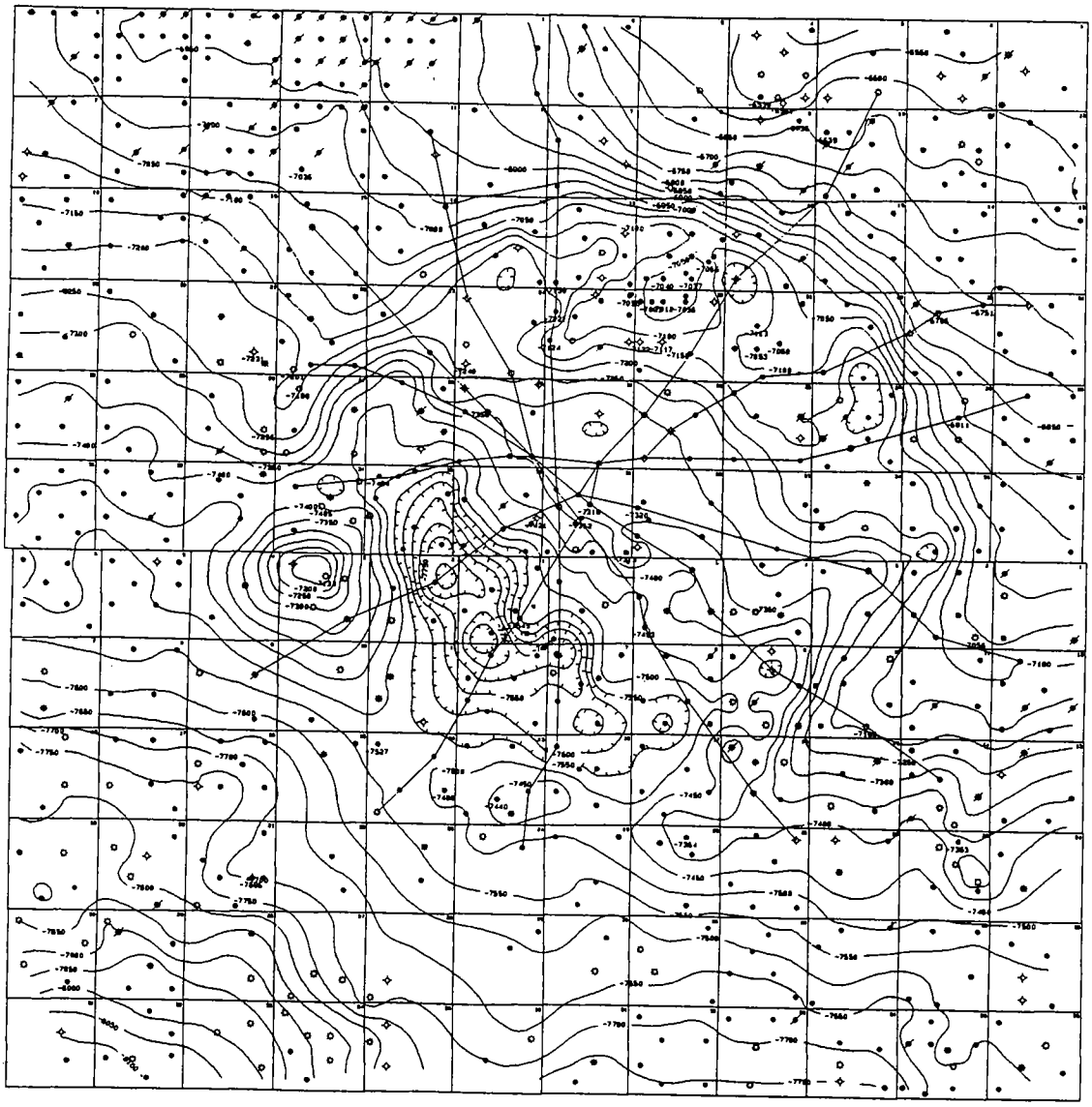

Figure 5. Structure map on top of the Simpson; contour interval 50 ft. Data courtesy of GDS.

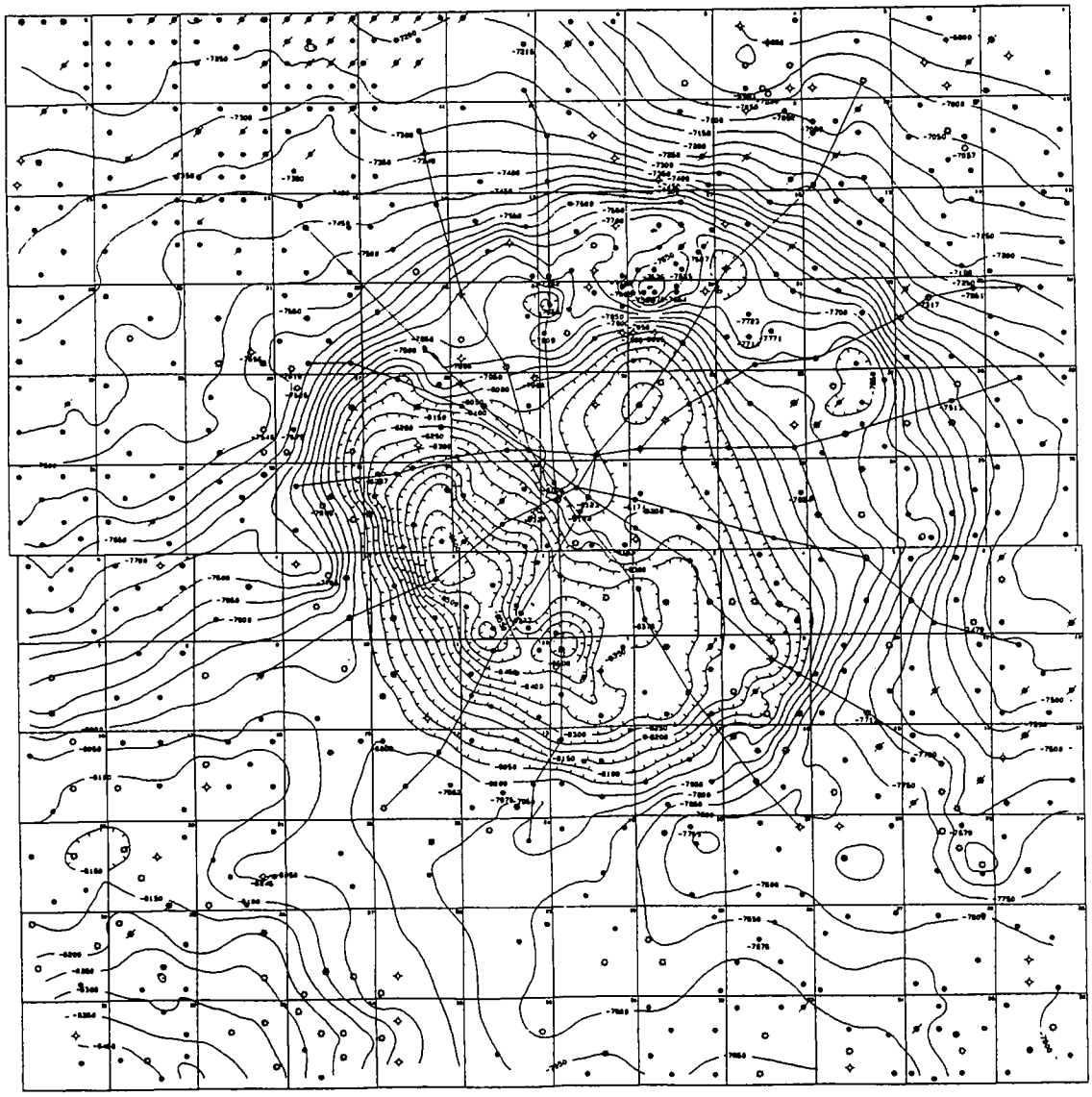

Figure 6. Structure map on top of the Arbuckle; contour interval 50 ft. Data courtesy of GDS.

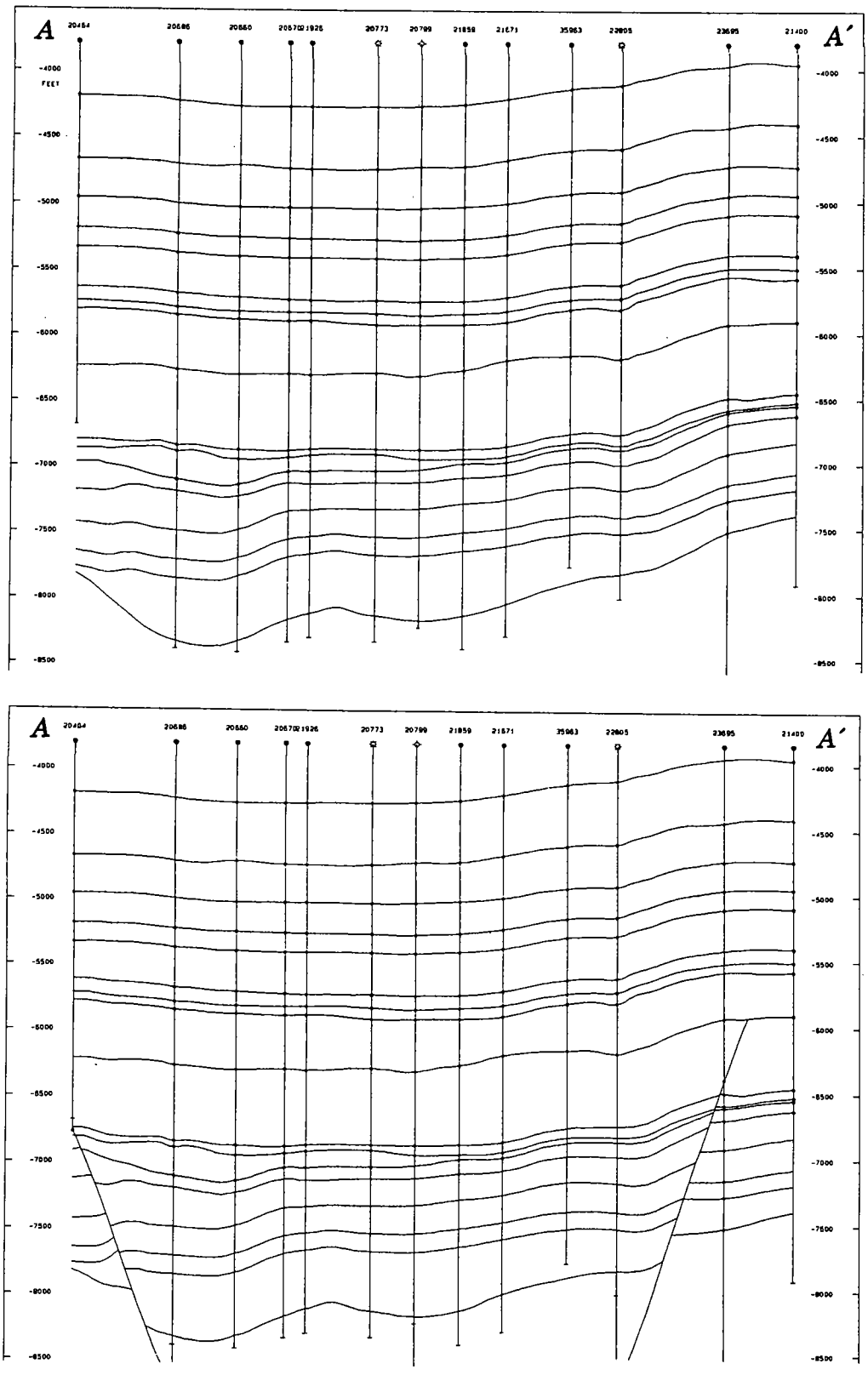

Figure 7. Cross section A–A´ (see Figs. 1 and 14 for location).

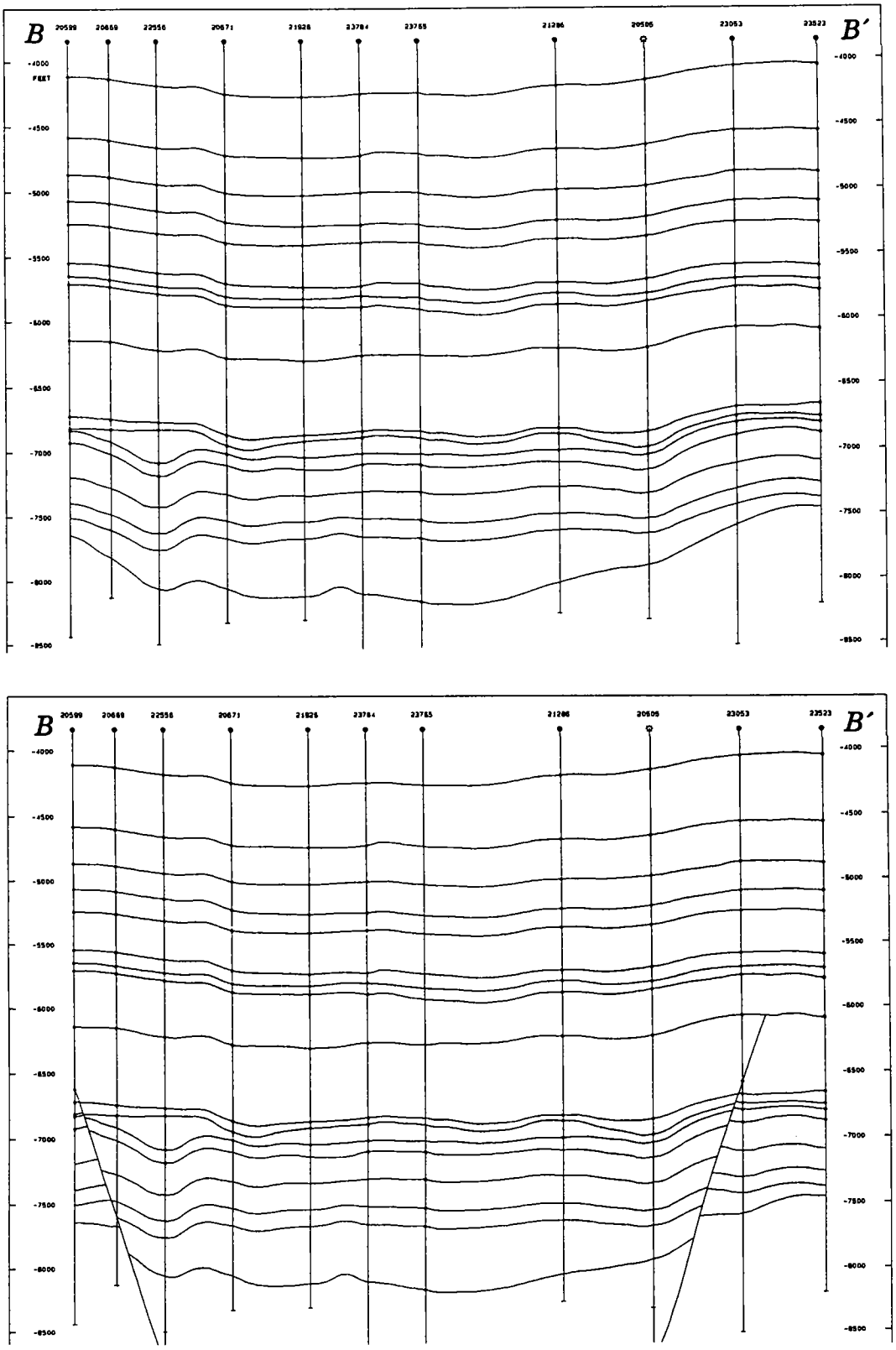

Figure 8. Cross section B–B′ (see Figs. 1 and 14 for location).

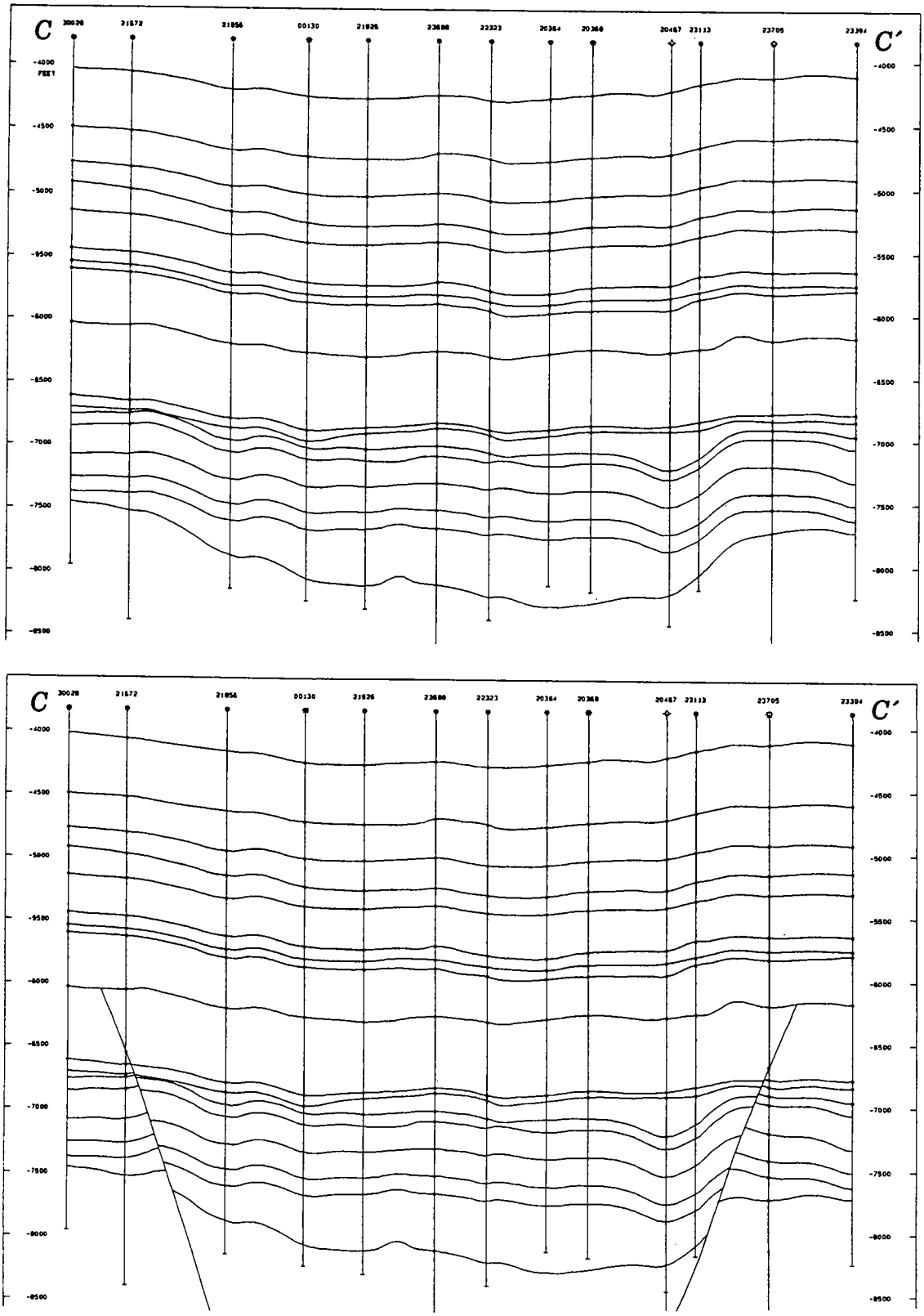

Figure 9. Cross section C–C′ (see Figs. 1 and 14 for location).

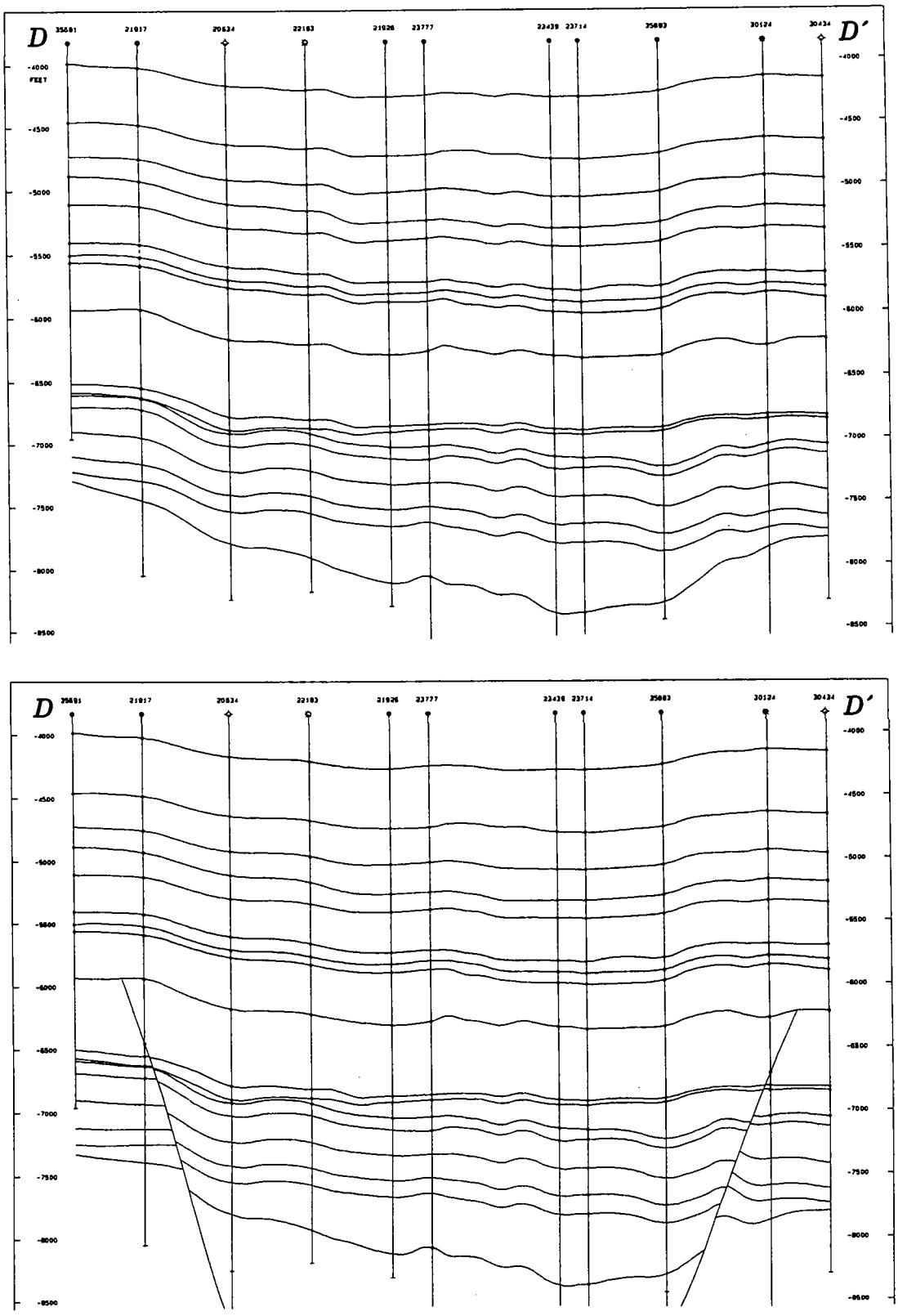

Figure 10. Cross section D–D′ (see Figs. 1 and 14 for location).

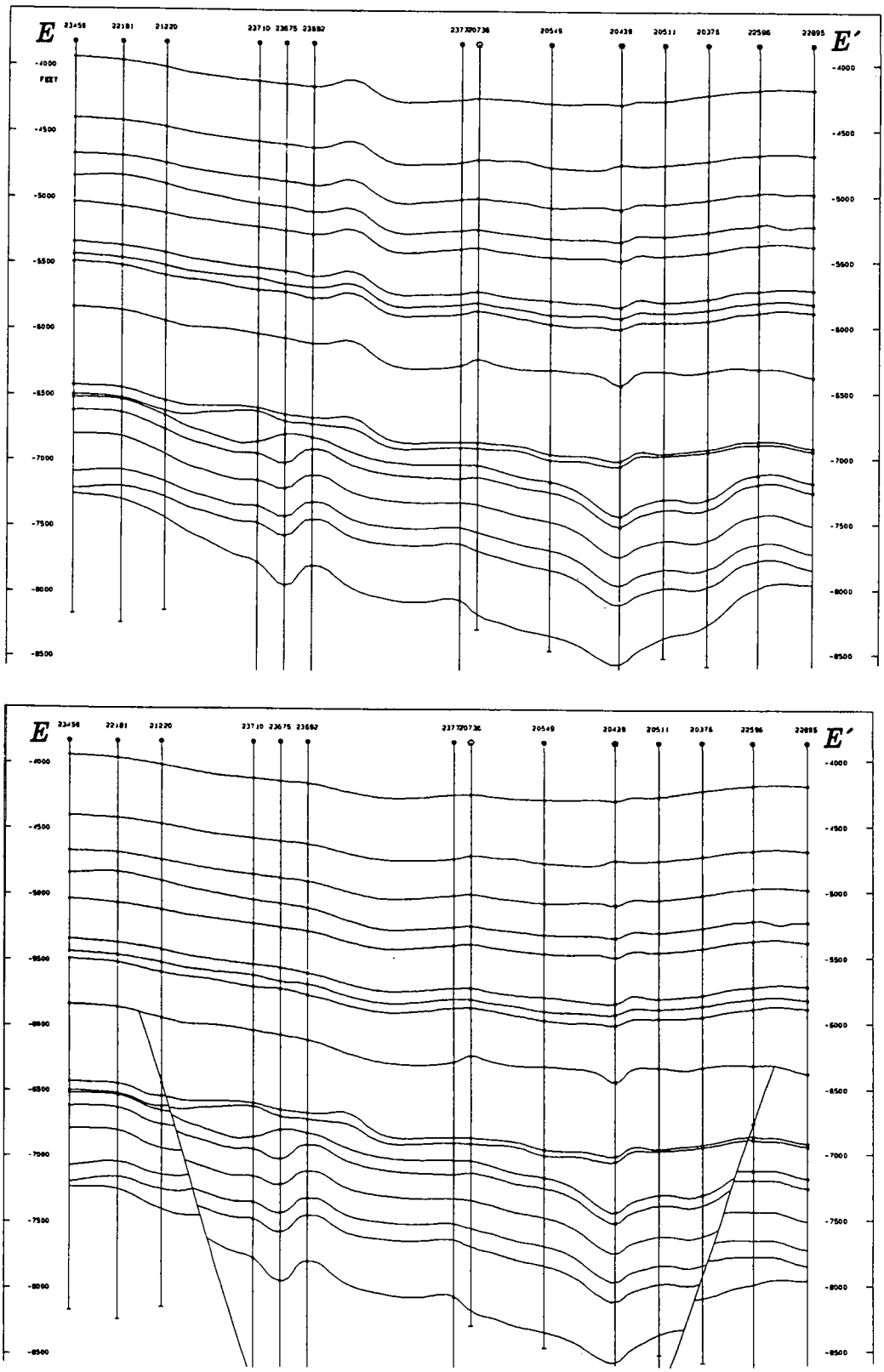

Figure 11. Cross section E–E′ (see Figs. 1 and 14 for location).

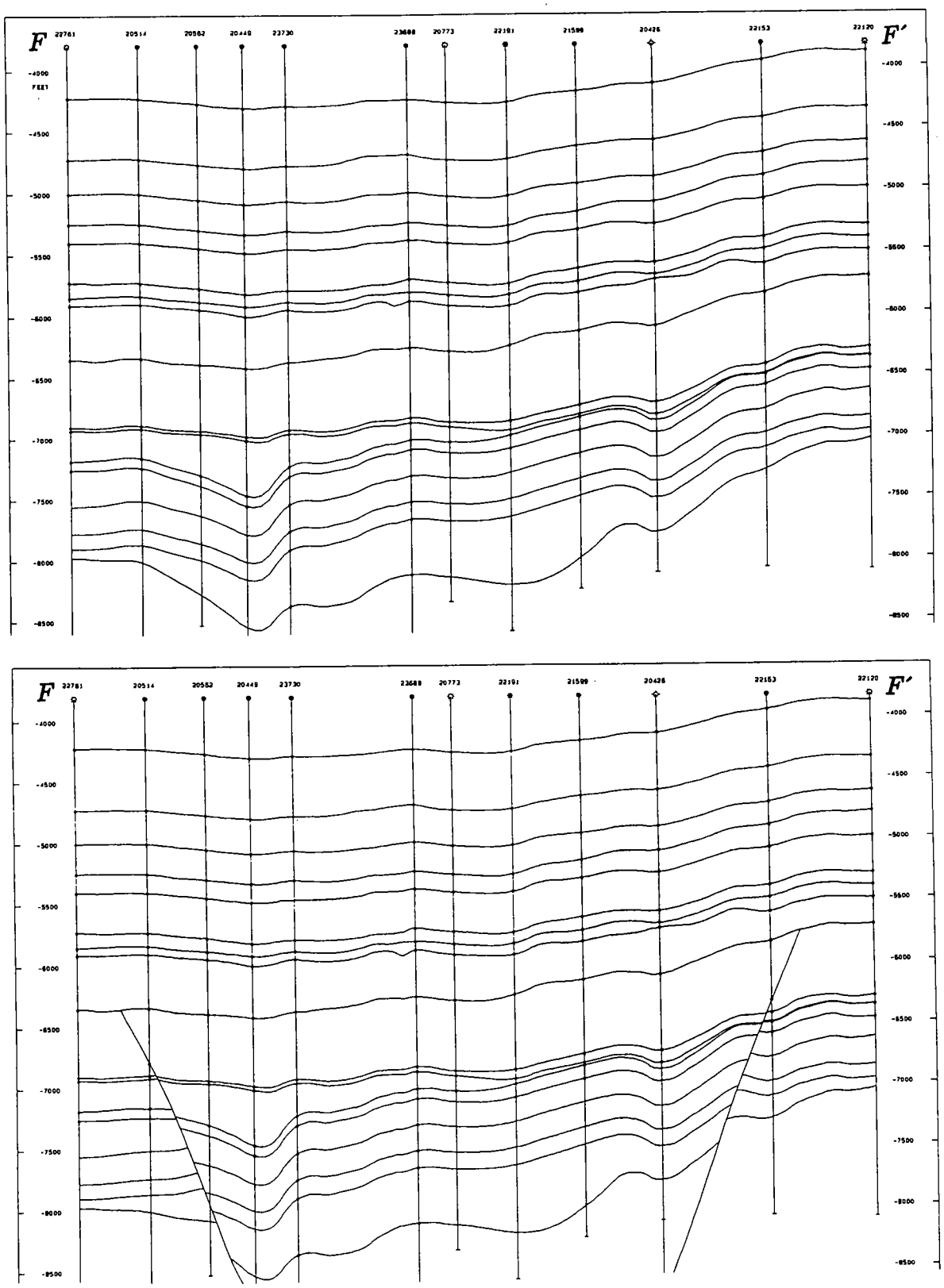

Figure 12. Cross section F–F′ (see Figs. 1 and 14 for location).

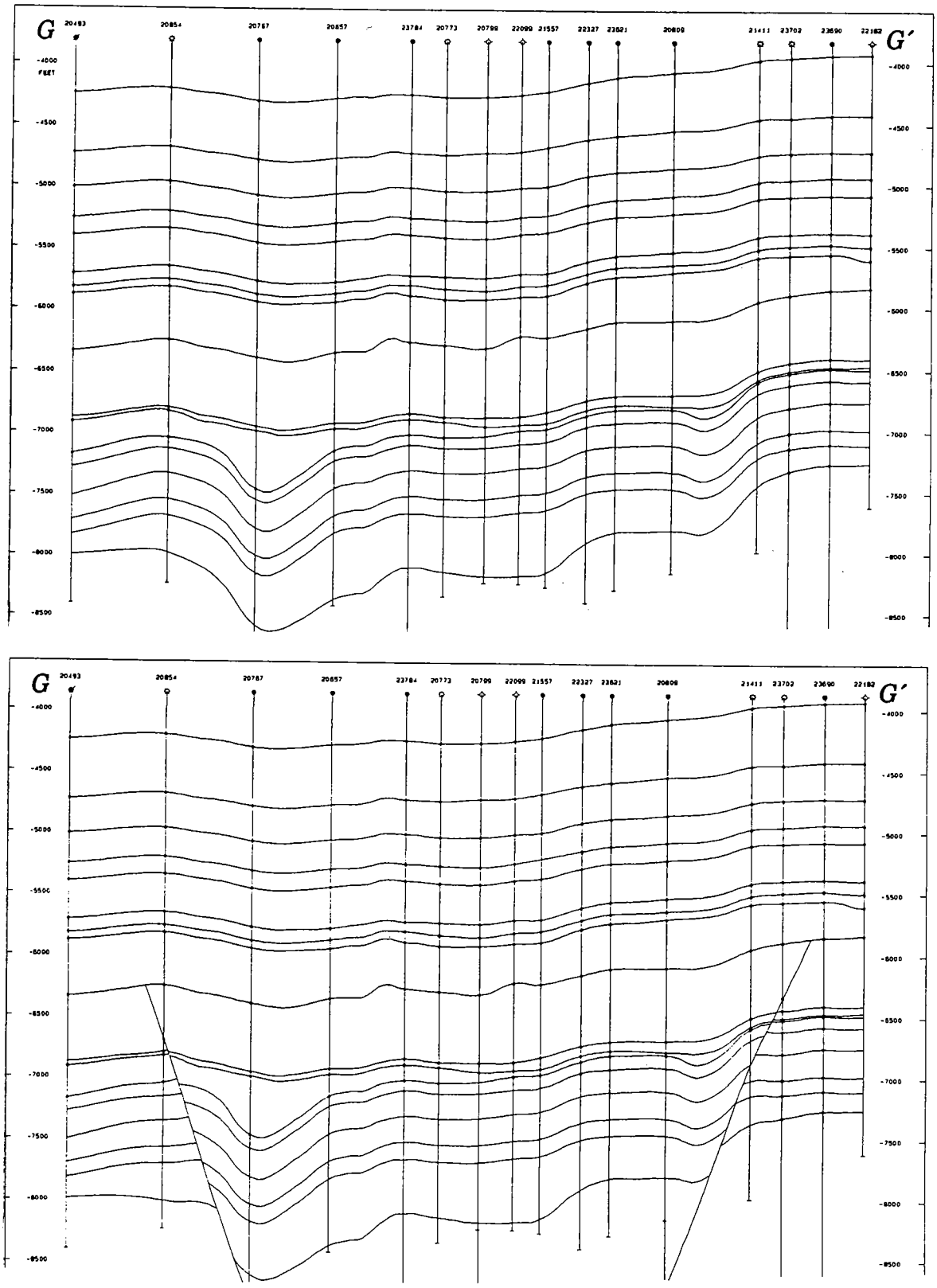

Figure 13. Cross section G–G′ (see Figs. 1 and 14 for location).

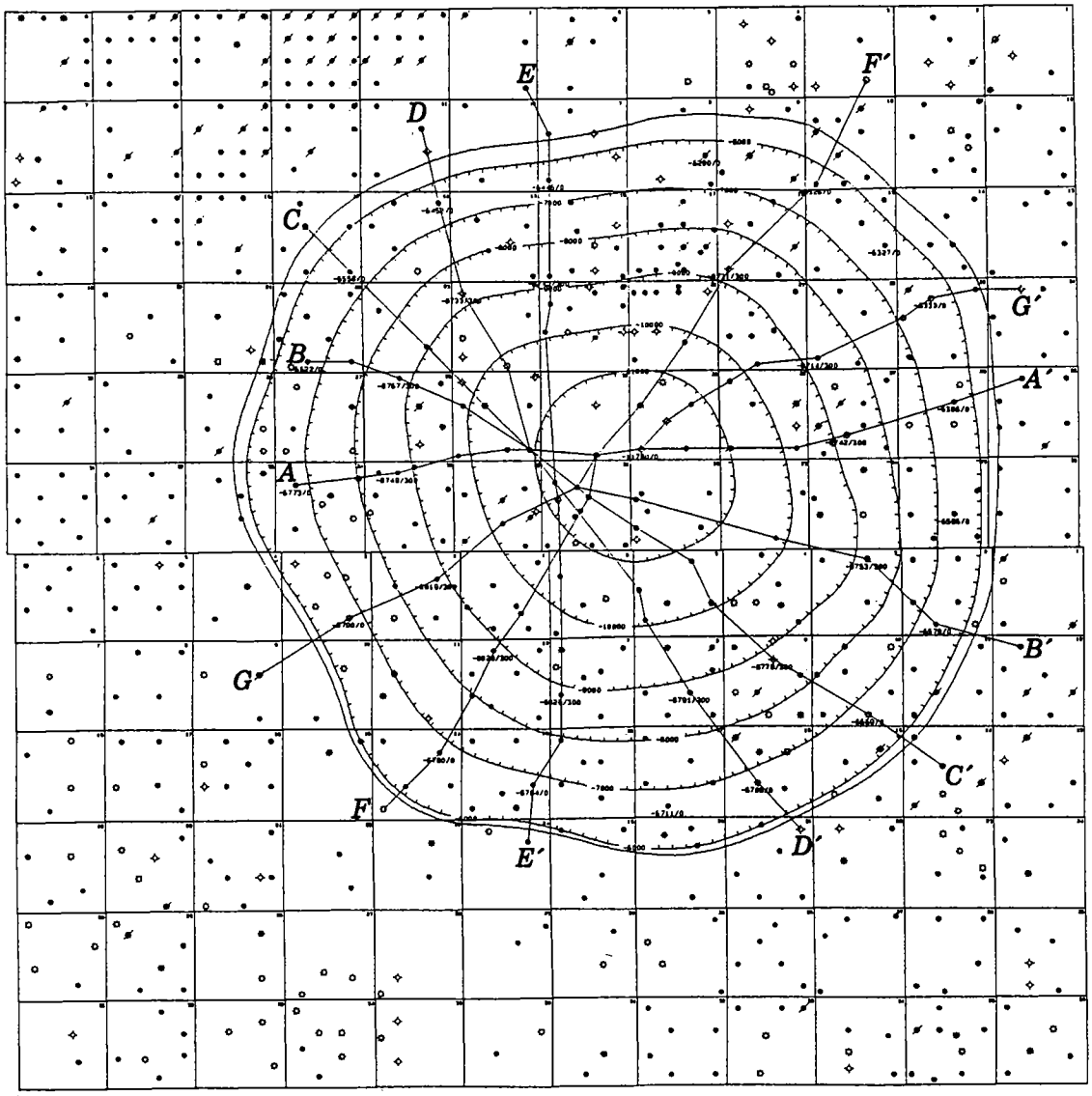

Figure 14. Map of Ames area showing assumed circular growth fault intersecting the top of the Woodford Shale and structure contours on the fault plane; contour interval, 1,000 ft.

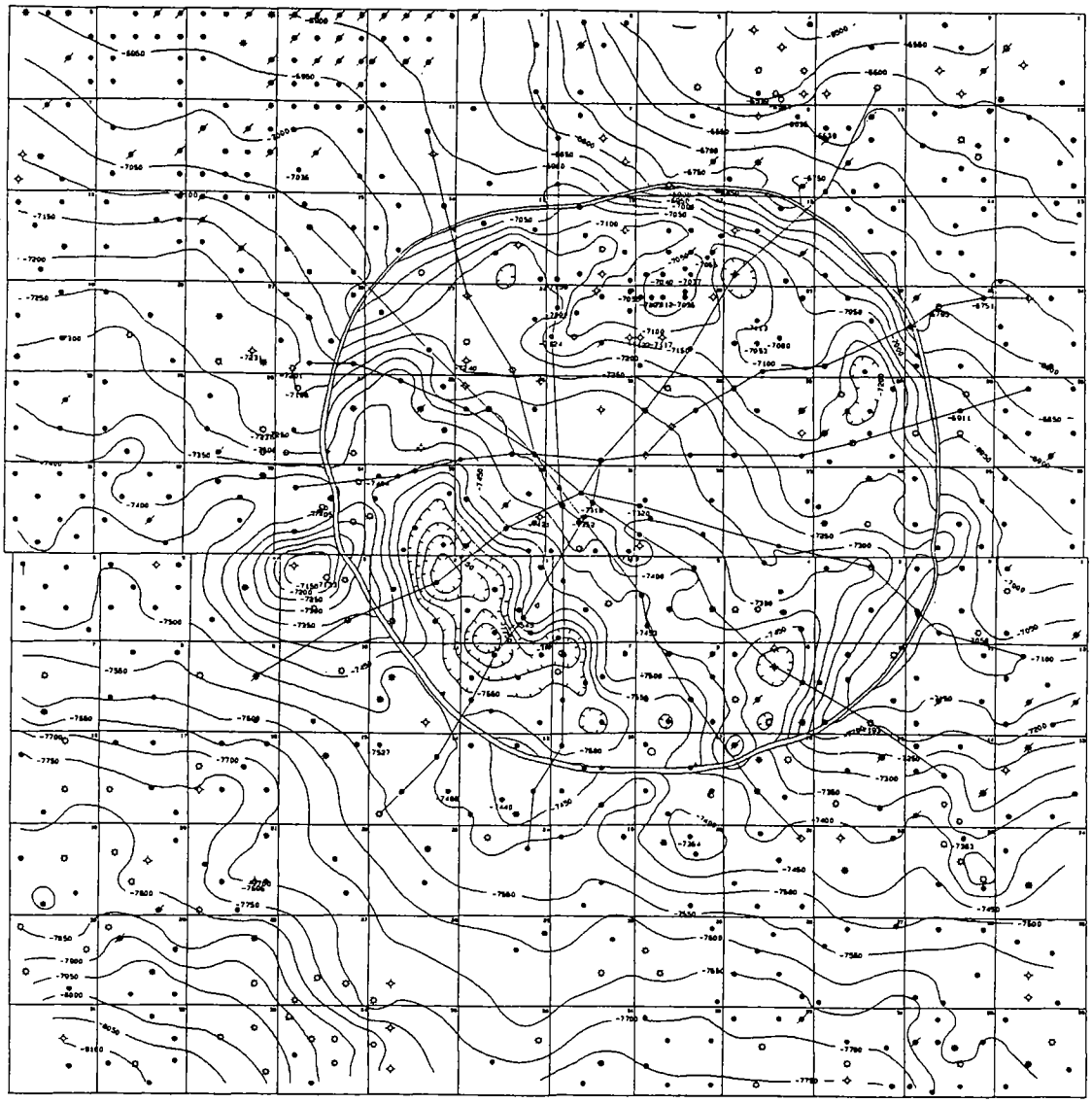

Figure 15. Structure map on top of the faulted Simpson Group; contour interval 50 ft. Data courtesy of GDS.

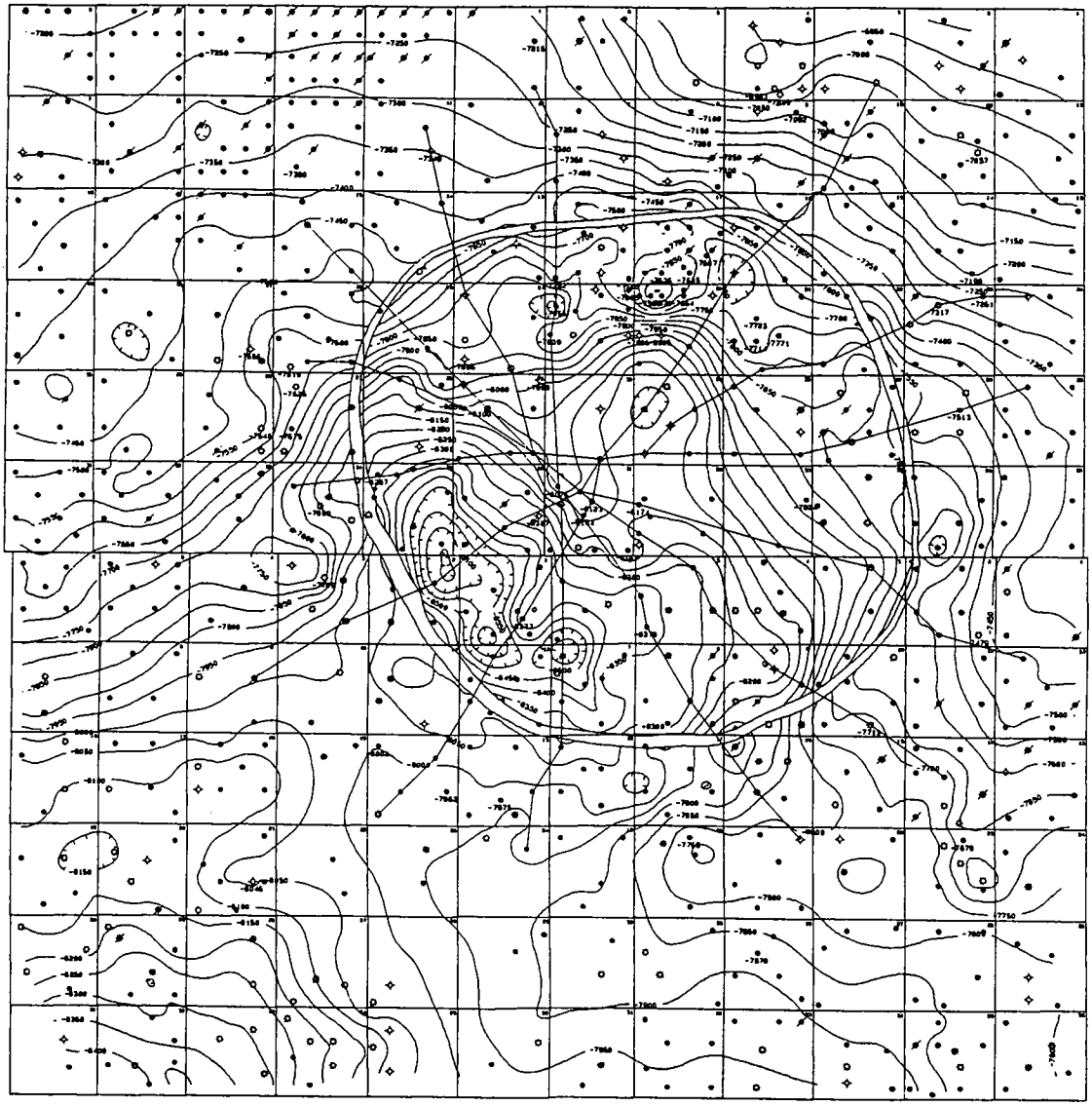

Figure 16. Structure map on top of the faulted Arbuckle Group; contour interval 50 ft. Data courtesy of GDS.

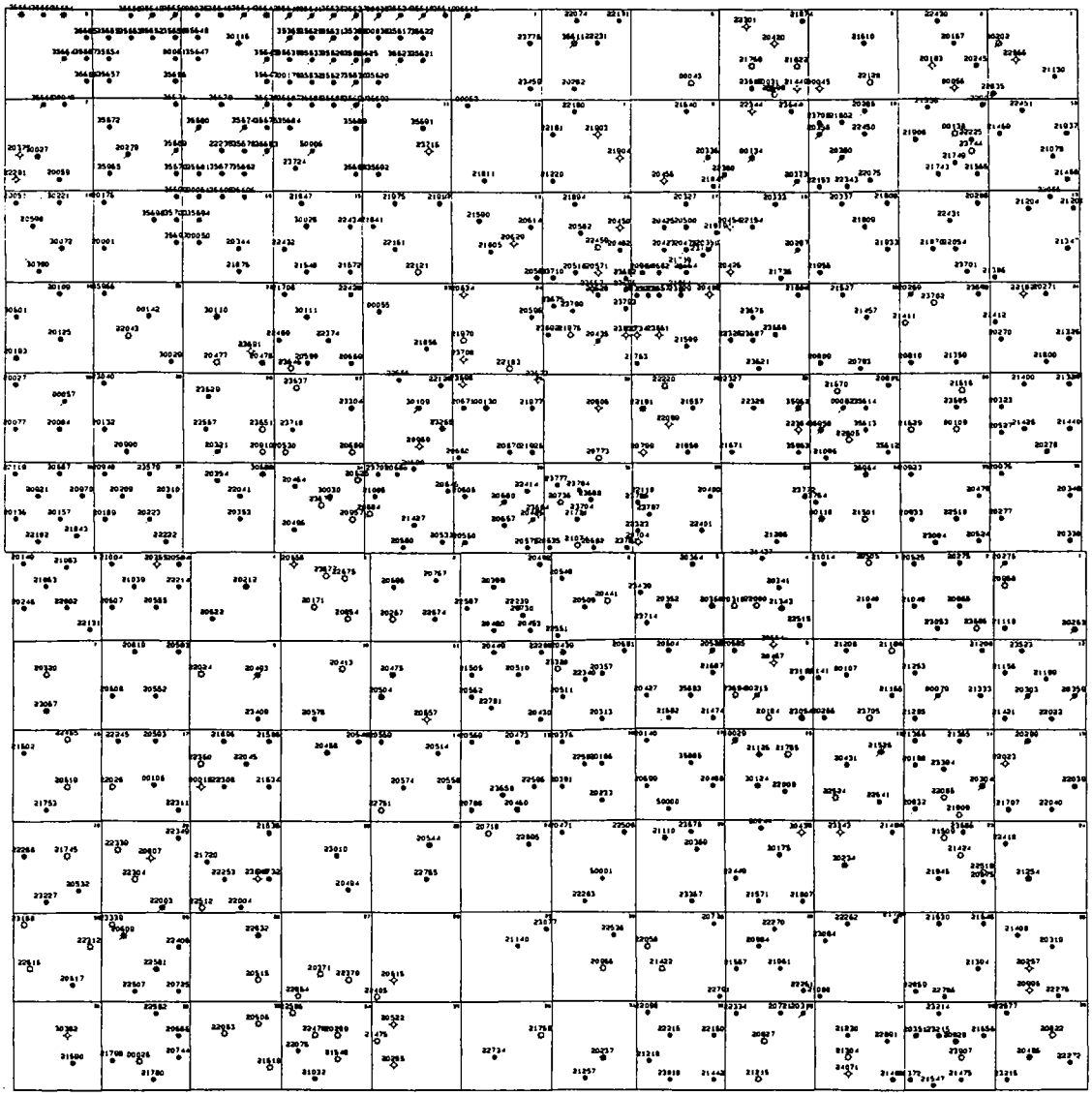

Figure 17. Map of Ames area (Ts. 20–21 N., Rs. 9–10 W., Major County, Oklahoma) showing wells used in study. Data courtesy of GDS.

Ames Structure of Northwestern Oklahoma Is Reflected in Overlying Permian Strata

Kenneth S. Johnson and Dorothy Smith
Oklahoma Geological Survey
Norman, Oklahoma

INTRODUCTION

The Ames structure is a deep-seated circular depression, buried beneath more than 9,000 ft of Paleozoic sedimentary rocks on the northern shelf of the Anadarko basin in northwestern Oklahoma (Fig. 1). It has been interpreted most commonly as a meteorite-impact crater, although some workers interpret it as a volcanic caldera or a dissolution and collapse feature. The structure was formed in Early or Middle Ordovician time (during deposition of the upper Arbuckle or lower Simpson Groups) and is reflected in the structure of all overlying rocks, up to, and including, the near-surface Permian strata. The structure probably also would be seen in Permian outcrops (red beds of the Cedar Hills Sandstone), except that the land surface is mantled mostly with 50–100 ft of Quaternary terrace deposits (the Cimarron River terrace) (Morton, 1980). Surface elevations above the crater are about 1,150–1,300 ft above sea level. The deep-seated structure has a diameter of about 7 mi, from rim to rim, and a structural relief of about 300–600 ft from the crater floor to the surrounding rim of Arbuckle Group rock. Rock immediately beneath the present crater floor consists of perhaps 1,000 ft of brecciated Arbuckle Group carbonates and Precambrian granite that settled into the crater after the impact.

METHODS OF STUDY

We conducted a reconnaissance study of the shallow Permian Wellington Formation evaporites that overlie the deep-seated Ames structure to determine the structural influence of the deep-seated structure on these shallow strata. The Wellington here consists of 700–800 ft of interbedded anhydrite, shale, and halite (Fig. 2): above the central depression, or crater area, the Wellington top is about 1,650 ft deep (below land surface) and the base is about 2,400 ft deep. Regional studies of the Permian evaporites (Jordan and Vosburg, 1963) established that the Wellington is a widespread sequence of evaporites, and individual beds (5–20 ft thick) can be correlated over all of northwestern Oklahoma. The Wellington evaporites at Ames are overlain, successively, by the Hennessey Group (red-bed shales and siltstones) and the Cedar Hills Sandstone (red-bed sandstones, siltstones, and shales); both these units are Permian in age. The Cedar Hills, in turn, is mantled by Quaternary terrace deposits in most parts of the Ames structure.

Our data base consists of the geophysical logs of about 275 wells (typically, 2 wells per section of land) wherein we can determine the top and base of the Wellington evaporites (Fig. 2). Although there are many more well logs in the area that contain data on the Wellington, we felt that this sample was adequate to determine whether the deep-seated crater affects, and is reflected in, shallow Permian strata.

The top and base of the Wellington are readily correlated in all wells, and the Wellington evaporites are the youngest (shallowest) subsurface unit in the area that contains conspicuous marker beds suitable for structure mapping. The elevation of the base of the Wellington was plotted (Fig. 3) to show its structure, and the thickness of the Wellington also was plotted (Fig. 4) to determine if there is any thickness variation in the Wellington across the deeply buried crater. The base of the Wellington was selected for structure mapping in order to remove any possibility that salt dissolution and collapse in underlying strata might affect the shallow-structure map; there are no salt beds or other evaporites beneath the base of the Wellington. Three cross sections were made (Fig. 5) to further examine structure of the Wellington.

Kenneth S. Johnson and Dorothy Smith, Oklahoma Geological Survey, 100 E. Boyd, Rm. N-131, Norman, OK 73019.

Johnson, K. S.; and Smith, Dorothy, 1997, Ames structure of northwestern Oklahoma is reflected in overlying Permian strata, *in* Johnson, K. S.; and Campbell, J. A. (eds.), Ames structure in northwest Oklahoma and similar features: origin and petroleum production (1995 symposium): Oklahoma Geological Survey Circular 100, p. 357–362.

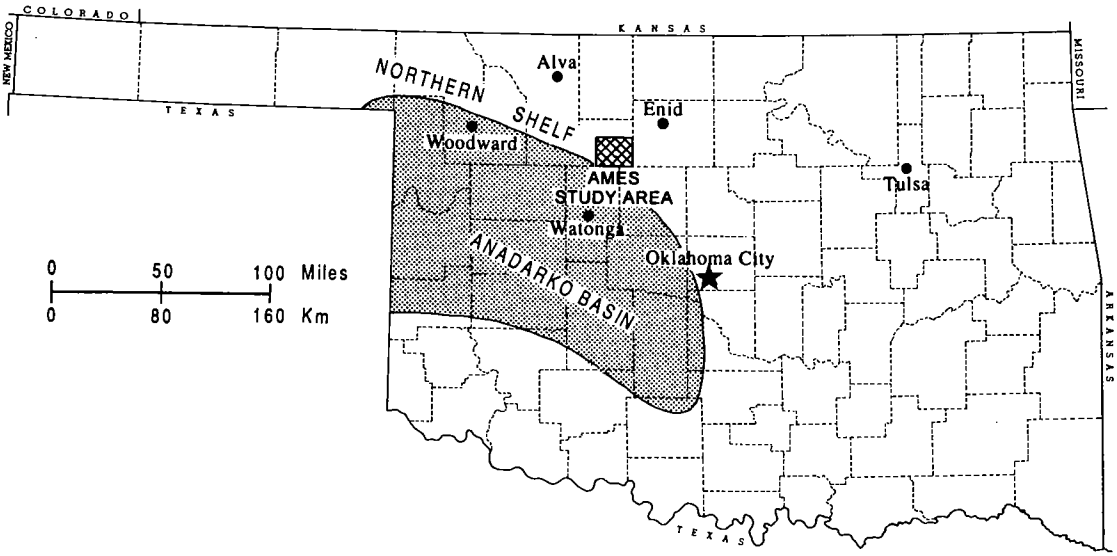

Figure 1. Location of Ames study area in Major County, northwestern Oklahoma.

DISCUSSION

The structure map and the cross sections (Figs. 3,5) clearly show that Permian strata reflect or mimic the deep-seated structure. The position of the deeply buried crater rim, as shown in Figures 3, 4, and 5, is based upon third-order residual structural mapping on top of the Upper Ordovician Sylvan Shale, prepared by Geological Data Services, Inc., of Dallas, Texas, and provided by Richard Haines; the top of the Sylvan is at a depth of about 8,000 ft in the crater area.

The structure map (Fig. 3) does not show a closed depression for the entire structure, because the Wellington has a regional dip of about 20 ft/mi toward the southwest (see Fig. 5, A–A′). The only closed depression is in the southwest part of the structure, above what is commonly called the "Hunton graben" (a depression, identified through early structure mapping on top of the Silurian–Devonian Hunton Group); here there is at least 40 ft of negative closure at the base of the Wellington.

Cross sections B–B′ and C–C′ (Fig. 5) are drawn along the regional north-northwest strike, and they show that, within the crater, the base of the Wellington is dropped down as much as 140 ft below its elevation just outside of the crater. And if data on the structure map were manipulated to create a third-order residual-structure map, we are confident that the resulting structure of Wellington strata would show a striking circular depression, with as much as 140 ft of negative closure (the lowest point being in the "Hunton graben").

The structure map and cross sections show that Wellington strata above the crater floor are, in general, structurally 75–140 ft lower than those above the rim and outside of the crater. Thus these Permian strata do reflect the presence of the deep-seated crater, but the structural depression is only about one-third or one-fourth as deep as that present in the Simpson and Sylvan strata that immediately overlie the crater. This structural relief in Wellington strata results (1) from post-Wellington differential compaction of Paleozoic strata that overlie the Ames structure and (2) possibly from late-stage compaction and settling of the crater-floor breccia. The pre-Wellington sedimentary units, which include many thick shales, have greater thicknesses above the crater than outside it; and these greater thicknesses resulted in a greater amount of compaction and subsidence of those same strata above the crater. Other examples of surface structures in Permian rocks reflecting deep-seated structures are documented in southwestern Oklahoma by Johnson (1995); those surface structures result from a combination of differential compaction and late-stage (post-Permian) tectonic adjustment along preexisting major basement-rock faults.

Thickness of the Wellington evaporites increases fairly uniformly across the Ames structure, ranging from 700 ft in the east to about 800 ft in the west; an increase of about 15 ft/mi (Fig. 4). However, the Wellington thins from 800 ft within the crater to less than 780 ft just west of the west crater rim, indicating that there may have been a small amount of sedimentary thickening of the Wellington within the crater area. Such thickening can be explained as resulting from a greater amount of compaction and subsidence of all underlying rock units within the crater, compared to

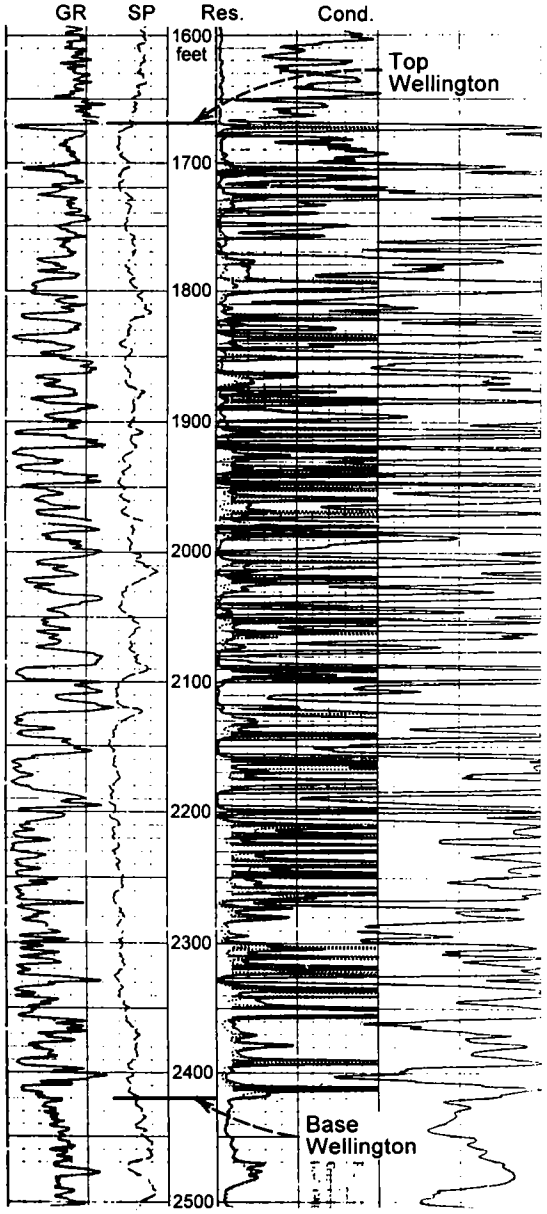

Figure 2. Typical geophysical log of the Wellington Formation evaporites that overlie the deep-seated Ames crater. The well is the Continental Resources, Inc., no. 1–32 Charles, sec. 32, T. 21 N., R. 9 W.; surface elevation, 1,229 ft; depths are in feet below land surface. Logs are gamma ray (GR), spontaneous potential (SP), resistivity (Res.), and conductivity (Cond.).

those just to the west, *during* deposition of Wellington strata. It appears that there may have been about 10–20 ft of differential compaction and subsidence within the crater during Wellington time.

SUMMARY

We conclude, therefore, that the deep-seated Ames crater affects, and is reflected in, near-surface Permian Wellington evaporites, and that it undoubtedly also is evident in still-younger Permian strata that subcrop beneath the mantle of Quaternary terrace deposits. The amount of subsidence or settling of the Wellington base within the crater, when compared to the area just outside the crater, is as much as 140 ft. The subsidence of Wellington strata within the crater is due to differential compaction, mostly after deposition of the Wellington: a greater thickness of Paleozoic sedimentary units above the crater, and the presence of the crater-floor breccia, allowed more compaction and subsidence within the crater than outside. This differential compaction also occurred throughout the Paleozoic Era; each younger rock unit above the Sylvan (the Hunton, Woodford, Mississippian, and Pennsylvanian strata) shows less structural relief than the underlying unit (Banks and Kuykendall, 1997). And it appears that about 10–20 ft of the differential compaction may have occurred even during Wellington deposition. An alternate explanation for this shallow structure in the Wellington is that it results from post-Wellington tectonic adjustment (i.e., tectonic dropping of basement rocks or younger strata within the crater, in comparison to the rim and surrounding area), but there is no evidence of post–Middle Ordovician tectonic activity in or near the Ames structure, much less any evidence of post-Permian tectonic activity; therefore, this alternative explanation is rejected.

REFERENCES CITED

Banks, Richard; and Kuykendall, M. D., 1997, Arcuate faults help to "relax" and explain the Ames structure, *in* Johnson, K. S.; and Campbell, J. A. (eds.), Ames structure in northwest Oklahoma and similar features: origin and petroleum production (1995 symposium): Oklahoma Geological Survey Circular 100 [this volume], p. 339–356.

Johnson, K. S., 1995, Surface structures in Permian strata of southwestern Oklahoma as indicators of deep-seated structures, *in* Johnson, K. S. (ed.), Structural styles in the southern Midcontinent, 1992 symposium: Oklahoma Geological Survey Circular 97, p. 288–292.

Jordan, Louise; and Vosburg, D. L., 1963, Permian salt and associated evaporites in the Anadarko basin of the western Oklahoma–Texas Panhandle region: Oklahoma Geological Survey Bulletin 102, 76 p.

Morton, R. B., 1980, Reconnaissance of the water resources of the Woodward quadrangle, northwestern Oklahoma: Oklahoma Geological Survey Hydrologic Atlas 8, scale 1:250,000, 4 sheets.

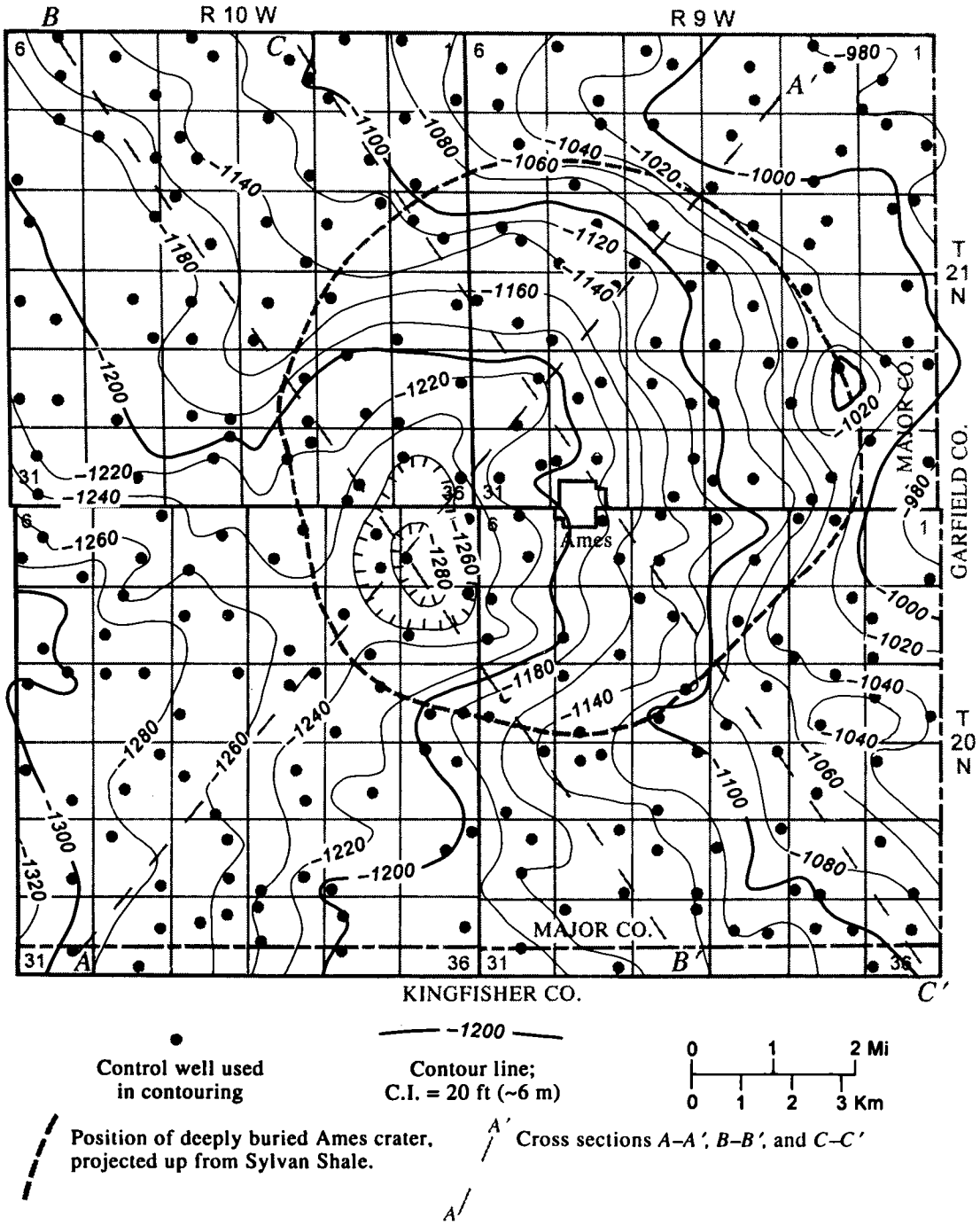

Figure 3. Map of Ames area showing structure contours on base of Permian Wellington Formation evaporites; datum is sea level (see Fig. 5 for cross sections).

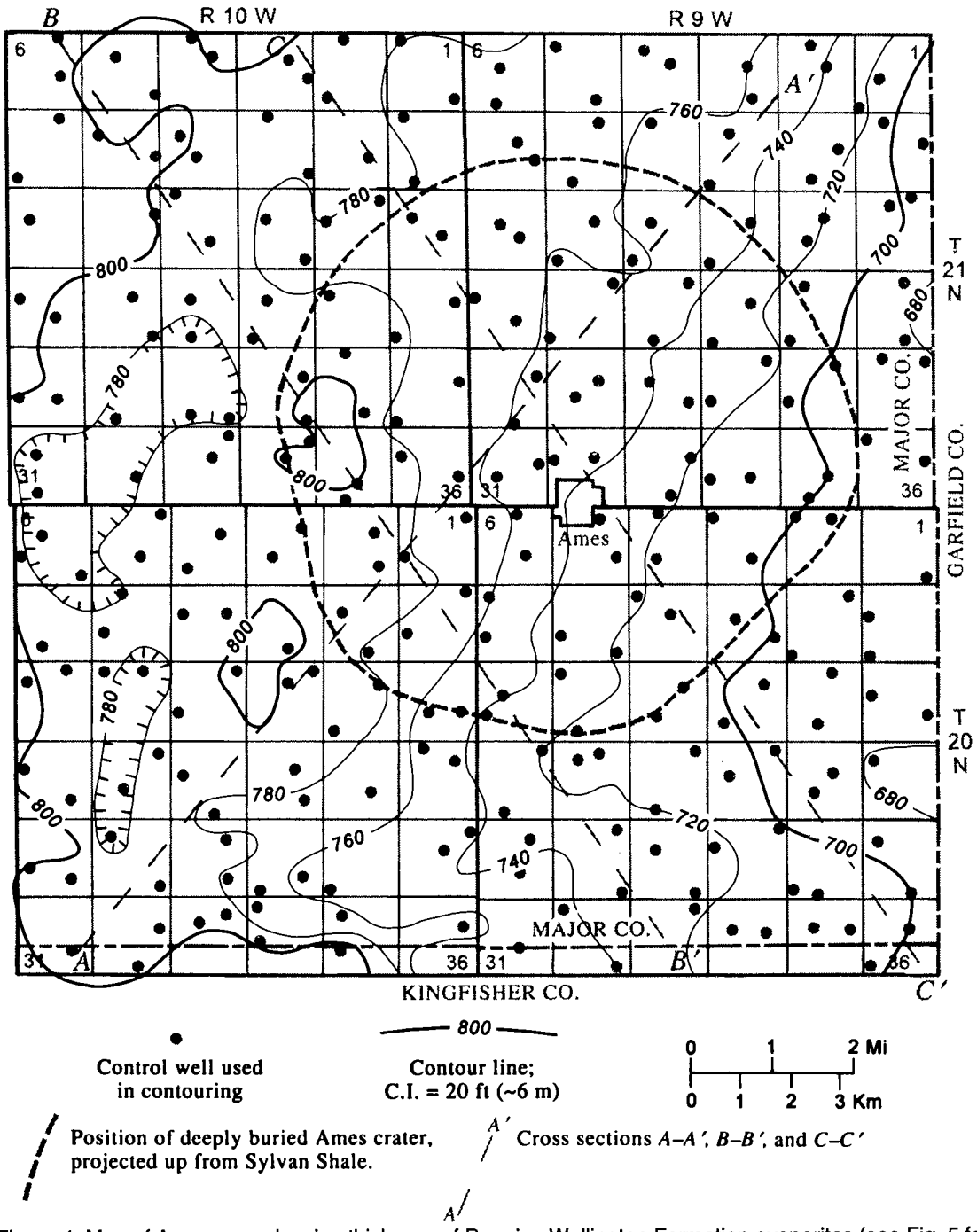

Figure 4. Map of Ames area showing thickness of Permian Wellington Formation evaporites (see Fig. 5 for cross sections).

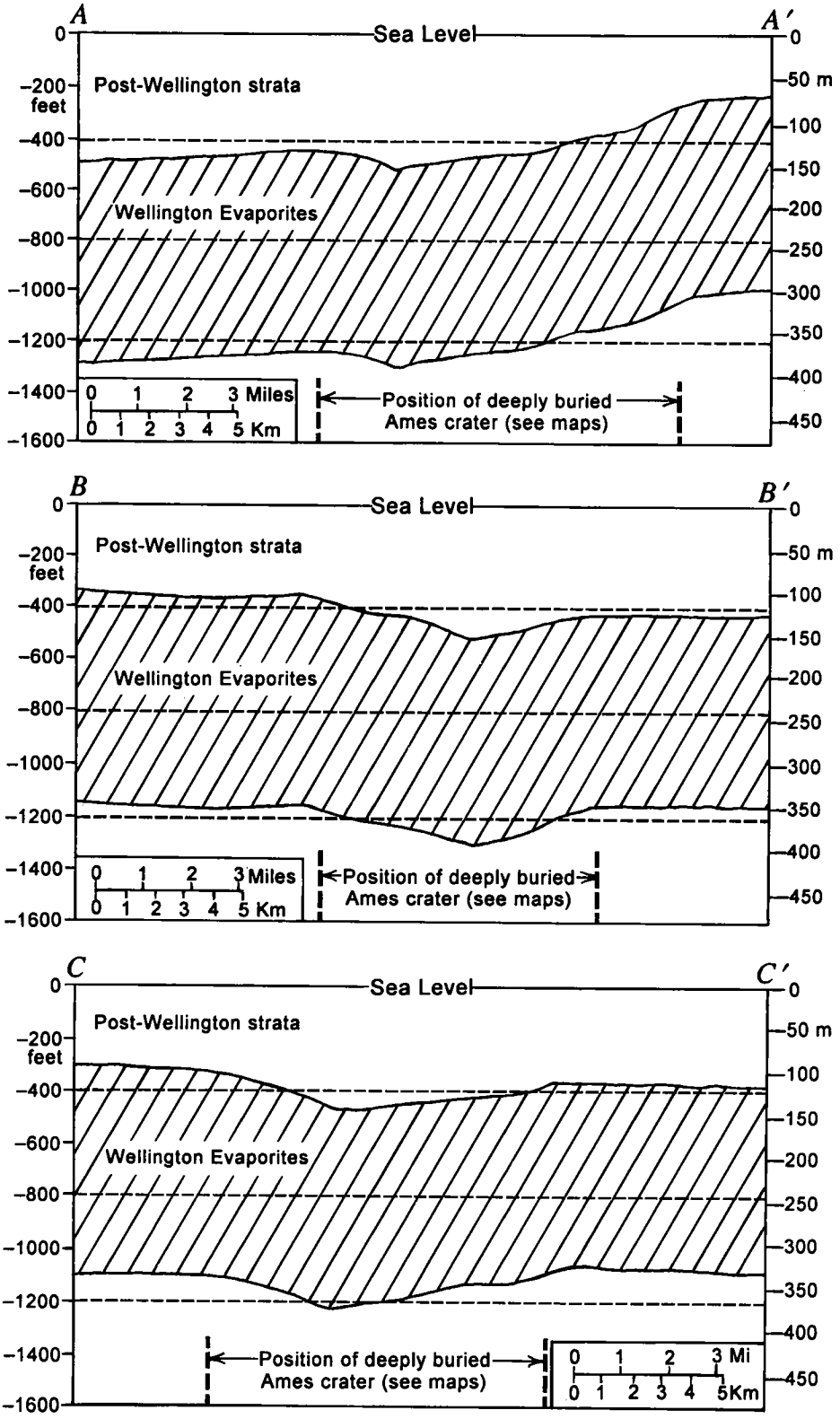

Figure 5. Cross sections showing structure of Permian Wellington Formation evaporites above the deeply buried Ames crater; vertical exaggeration 30:1 (see Figs. 3,4 for location of cross sections).

Conodont Age Constraints on the Middle Ordovician Black Shale Within the Ames Structure, Major County, Oklahoma

John E. Repetski
U.S. Geological Survey
Reston, Virginia

ABSTRACT.—Numerous conodont elements found on core chips of the black shale that fills the now-buried Ames impact crater, from the D. & J. no. 1-20 James and the Nicor no. 18-4 Chestnut wells, Major County, Oklahoma, date that shale as middle Middle Ordovician and constrain the age of both the impact event and its infilling. Both individual elements with preserved basal attachment structures and bedding-plane assemblages of oriented elements are present, the latter giving evidence of the lack of significant current activity, oxidation, scavenging, and bioturbation in the local depositional environment. The host rock is a noncalcareous black shale that contains other indicators of gentle, dysaerobic or anaerobic bottom conditions such as abundant carbonaceous and pyritized phyllocarid fragments. Preliminary study of the conodonts recovered thus far shows the presence of *Erismodus* species and at least one species of *Phragmodus*, either a species of the *Ph. flexuosus* plexus or *Ph. inflexus*. These taxa indicate that the host black shale is no older than the upper part of the late middle Whiterockian *Ph.* "pre-*flexuosus*" Zone and indeed may be as young as middle Blackriveran. Stratigraphic implications of these finds are that at least this part of the Ames "crater shale" is best correlated with the McLish Formation–Tulip Creek Formation–Bromide Formation interval (middle Middle Ordovician) in the Simpson Group of southern Oklahoma and with the McLish Formation and the upper part of the middle Tyner Formation in northeastern Oklahoma (Conodont Association II of J. A. Bauer) rather than with any part of the Oil Creek Formation (early Middle Ordovician), as has been the convention in earlier papers on the Ames structure. These age data, if applicable to the entire "crater shale" succession, are consistent with the scenario of the Ames structure being filled by sediments of the initial marine transgression of the Tippecanoe I sequence locally.

INTRODUCTION

The Ames structure, a roughly circular depression with raised rim and central uplift in the subsurface of west-central northern Oklahoma, is widely believed to be an impact crater (e.g., Carpenter and Carlson, 1992), although there are those who hold that it is of volcanic origin (e.g., Coughlin and Denney, 1993). The evidence—including details of the structure (Roberts and Sandridge, 1992; Carpenter and Carlson, 1992) and the presence of shocked quartz with planar deformation features (Koeberl and others, 1997)—strongly favors an impact origin. The crater is approximately 16 km in diameter and was about 100 m deep; it is buried at nearly 3,000 m. The crater is located on the northern shelf area of the Anadarko basin (Fig. 1); it was excavated into dolomitic rock of the upper part of the Arbuckle Group and is overlain by presumed Middle Ordovician marine rocks assigned by most workers to the Simpson Group. The crater itself is filled, above the basal breccia, slump, and wash-back deposits, with up to 225 ft of organic-rich black shale of marine or marginal marine origin. The Ames structure is an extensively explored target for both oil and gas, with more than 100 wells already having been drilled in and immediately around the crater. Productive plays are in highly fractured host rock,

John E. Repetski, U.S. Geological Survey, 926-A National Center, Reston, VA 20192.

Repetski, J. E., 1997, Conodont age constraints on the Middle Ordovician black shale within the Ames structure, Major County, Oklahoma, *in* Johnson, K. S.; and Campbell, J. A. (eds.), Ames structure in northwest Oklahoma and similar features: origin and petroleum production (1995 symposium): Oklahoma Geological Survey Circular 100, p. 363–369.

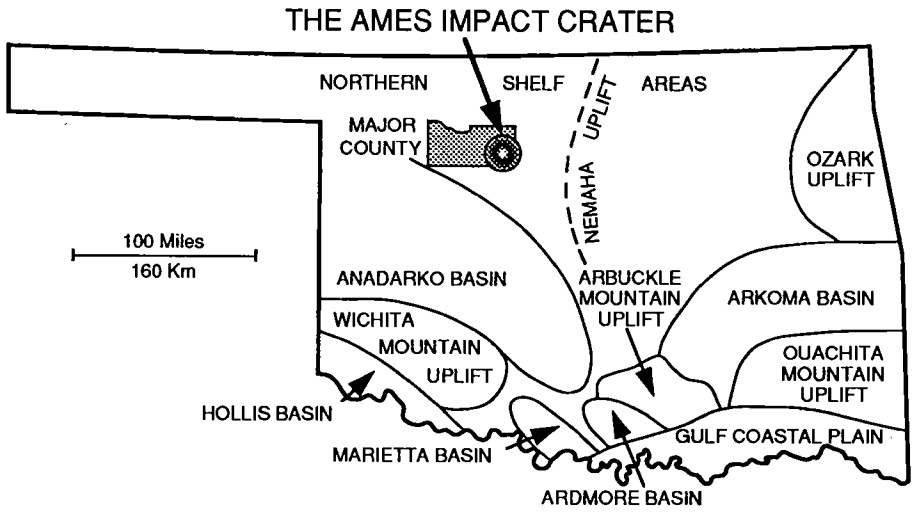

Figure 1. Location of Ames structure and major geologic provinces of Oklahoma (modified from Johnson and others, 1980, and Johnson, 1989).

and the crater-filling black shale is believed to be a major source for the hydrocarbons.

Previously, no biostratigraphic data were available to constrain the age of the rocks below, in, or above the crater. Therefore, the discovery of fossils in some cores gives the opportunity not only to date these stratigraphic units but also to improve regional correlations and better define the context of the history of this structure. Fossils known thus far include well-preserved phyllocarid arthropods and a few brachiopods (Hannibal and Feldmann, 1997) and conodonts, the subject of this paper.

Conodont elements are the calcium-phosphatic hard parts that functioned, most likely as teeth, in the food-gathering organ at the anterior end of the group of Cambrian through Triassic marine animals called conodonts. Each conodont animal had several to more than a dozen elements making up an apparatus. Analogous, and arguably homologous, to teeth in vertebrates, each apparatus comprised elements of several (typically six or seven) specialized morphologies arranged bilaterally symmetrically within the apparatus. Characteristic element shapes (related to common function) can be classified according to their presumed location in the apparatus; herein, I follow the element location notation scheme of Sweet (1981).

MATERIAL

The conodonts examined for this preliminary report are from chips of Ames crater–filling black shale from two wells, both drilled into the north side of the crater proper. The host rock is fine-grained, organic-rich, fissile black shale that also contains intervals with abundant well-preserved phosphatic and pyritized phyllocarid arthropod remains. Some isolated conodont elements were found (Figs. 2,5), but most of the elements seen thus far are in bedding-plane assemblages, or clusters (Figs. 3,4). Conodont elements can be concentrated on bedding planes by physical (e.g., current winnowing) or biogenic means. Biogenic clusters can represent either coprolitic accumulations or in-place preservation of the elements of decaying individual conodont animals not scavenged or otherwise disaggregated and dispersed before burial. The latter are the most rare of occurrences, requiring that the apparatuses be spared the dispersing actions caused by scavengers, widespread bioturbation of the bottom sediment, oxidizing bottom conditions, and currents strong enough to scatter the elements. The Ames clusters fall into this rare category.

Each of the few dozen clusters found thus far comprise elements of a single species, and in most of the assemblages the constituent elements are oriented nonrandomly, i.e., they reflect the original orientation of the elements in the biological apparatus of the animal, modified somewhat by decay and compression postmortem (Figs. 3,4). Each cluster is surrounded by, and some are thinly covered by, films of shiny black organic matter, presumed to be remains of, or at least derived from, the animals' soft tissue. Preliminary examination has not thus far identified any organized structural detail within this matter.

D. & J. No. 1-20 James Well

A single 1- to 2-cm-thick chip of core from 8,908.9 ft depth in the D. & J. no. 1-20 James well, USGS collection locality 11365-CO (E½NW¼NE¼ sec. 20, T. 21 N., R. 9 W.), yielded a few dozen bedding-plane assemblages, each consisting wholly of elements of a single species (Figs. 3,4), and a few

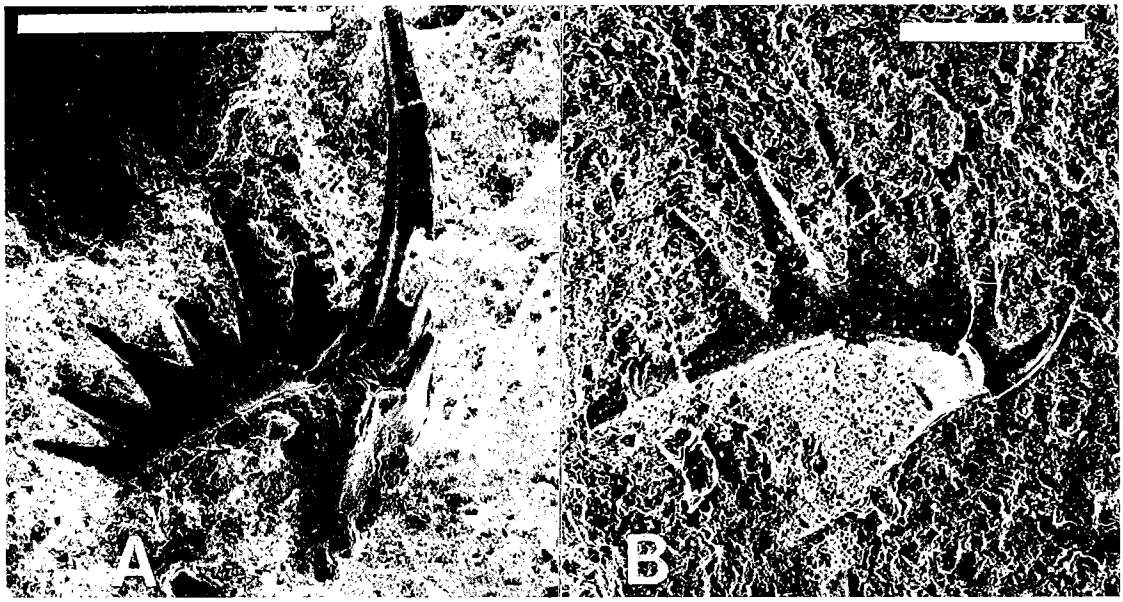

Figure 2. Scanning electron microscope (SEM) photomicrographs of isolated conodont elements from the crater-filling black shale in the D. & J. James no. 1-20 well, depth 8,908.9 ft. *A—Erismodus* near *E. asymmetricus*, posterolateral view of an Sb(?) element, scale bar represents 500 μm, USNM 489620. *B*—Lateral view of Sc element of a species of *Phragmodus*, scale bar represents 200 μm, USNM 489621. Both specimens are part actual element and part mold or impression of element; both also preserve impressions of their basal attachment structures. These and the other illustrated specimens herein are reposited in the type collections of the Paleobiology Department, U.S. National Museum (USNM), Washington, D.C.

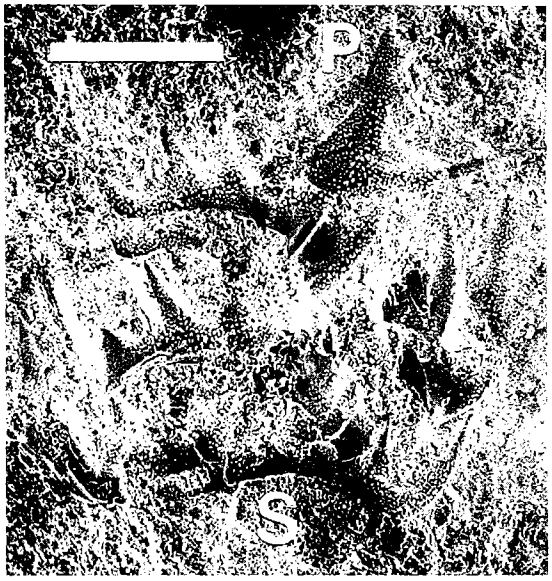

Figure 3. Bedding-plane assemblage of nonrandomly oriented elements of a *Phragmodus* species, belonging either to the *Ph. flexuosus* plexus or to *Ph. inflexus*. Most elements appear to be S elements, but one is an outer lateral view of a P element. D. & J. no. 1-20 James well, depth 8,908.9 ft, scale bar represents 200 μm, USNM 489622.

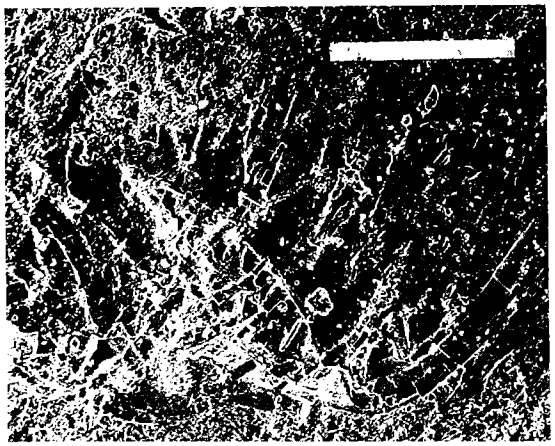

Figure 4. Bedding-plane assemblage of a *Phragmodus* species, consisting of laterally juxtaposed oriented S elements, presumably of an individual apparatus. D. & J. James well, depth 8,908.9 ft, scale bar represents 200 μm, USNM 489623.

isolated elements (Fig. 2). Most of the assemblages contain elements oriented nonrandomly, indicating that they were most likely from individual animals. The remaining clusters consist of ele-

ments of essentially the same size, indicating that these also probably represent collections of elements from individuals.

All of the elements found as clusters are assignable to species either of the *Phragmodus flexuosus* Moskalenko plexus or *Phragmodus inflexus* Stauffer. All of the isolated specimens are elements of a species of *Erismodus* near *E. asymmetricus* (Branson and Mehl).

Core-chip surfaces from three additional horizons in this well also yielded specimens. A sample at 8,904.5 ft (USGS colln. loc. 11366-CO) shows two isolated *Phragmodus* sp. S elements, with basal attachment structures intact. This chip also contains a linguloid brachiopod valve. A chip from 8,898.5 ft (USGS colln. loc. 11367-CO) exposes one assemblage of at least five or six elements and three isolated S elements, all assignable to *Phragmodus* species. A sample from 8,894.5 ft (USGS colln loc. 11368-CO) exposes five *Phragmodus* assemblages and three isolated *Phragmodus* S elements.

One isolated S element of *Phragmodus* from the chip at 8,908.9 ft was extracted mechanically from the surface for determination of its color alteration index (CAI), a method of assessing the organic metamorphism of the host rock (Epstein and others, 1977). This specimen exhibits a CAI value of 1 to 1.5, indicating host-rock heating approximately in the range of 50° to 90° C, a range consistent with the burial depth given a normal geothermal gradient.

Nicor No. 18-4 Chestnut Well

A small chip, 0.5 to 1 cm thick, of somewhat silty black shale from 8,972.2 ft depth in the Nicor no. 18-4 Chestnut well, USGS collection locality 11369-CO (NE¼SW¼SE¼ sec. 18, T. 21 N., R. 9 W.), exposes molds of two isolated conodont specimens (Fig. 5). Both of these elements belong to a species of *Erismodus*. Incomplete preservation prevents assignment to species, but the most likely possibilities are *E. asymmetricus, E. arbucklensis* Bauer, and *E. typus* Branson and Mehl.

AGE

The conodonts leave no doubt that the Ames crater–filling black shale hosting them is medial Middle Ordovician, with a possible range of late middle Whiterockian to early Blackriveran (Fig. 6). Both conodont genera *Phragmodus* and *Erismodus* appear in the late middle Whiterockian *Ph.* "pre-*flexuosus*" Zone, with species of the latter appearing above the base of that zone. Lack of diagnostic elements and incomplete preservation of the recovered ones limits the identification of the *Erismodus* elements below the genus level. As pointed out by Bauer (1987,1989) and other workers, within-species element variability and interspecific similarity of most elements of the apparatus make it difficult to diagnose to species level without well-preserved collections that include the

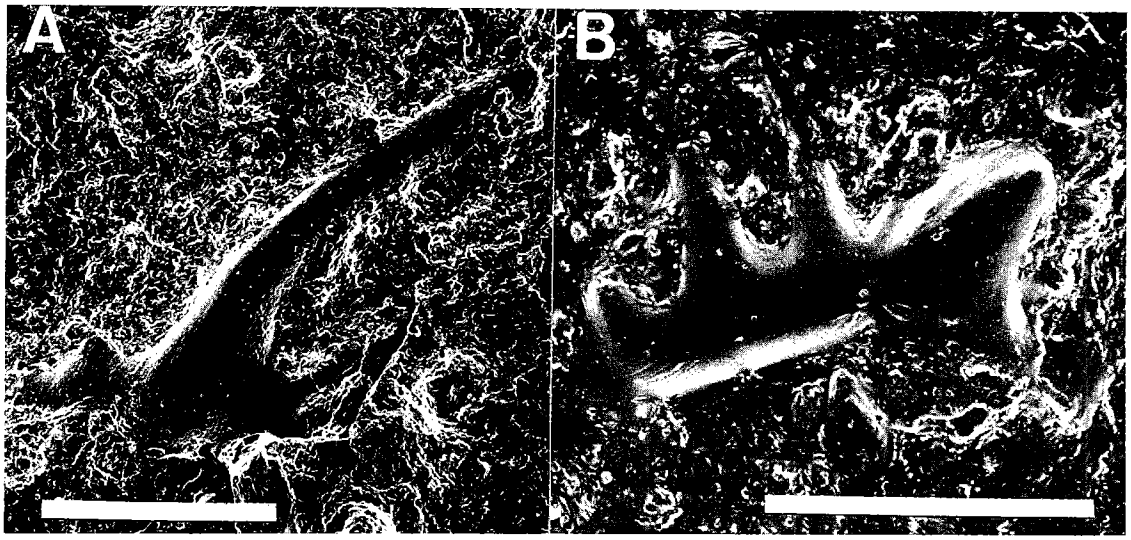

Figure 5. Isolated elements of *Erismodus* species from the Nicor Chestnut no. 18-4 well, depth 8,972.2 ft. *A*—Mold of outer surface of a P or Sb element. *B*—Latex cast of outer surface of a P or Sb element. Scale bars represent 200 μm, USNM 489624 and 489625.

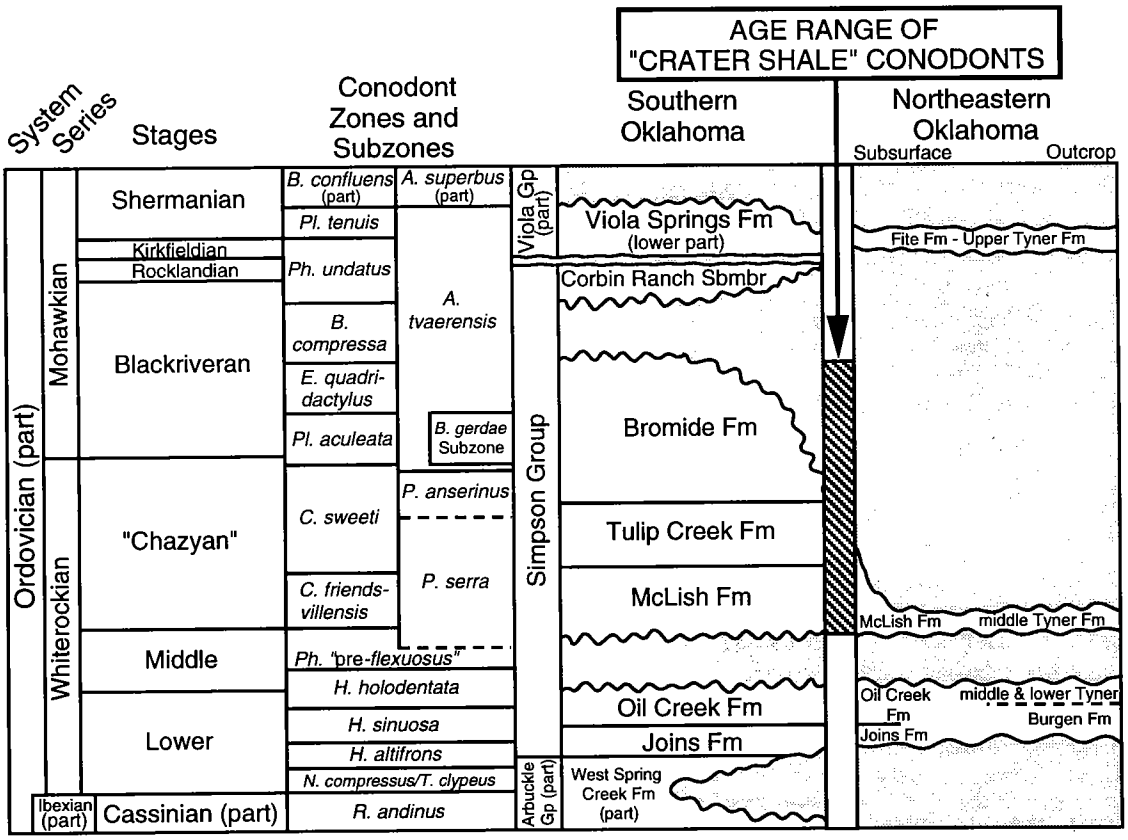

Figure 6. Stratigraphic correlation chart and conodont zonation for Middle Ordovician rocks of southern and northeastern Oklahoma, showing total possible age range for the conodont-bearing black shale filling the Ames structure (modified from Derby and others, 1991).

more rare M and Sa elements. The few specimens found in the Ames crater shale appear to fit best the oldest-known species of the genus.

Even though the studied *Phragmodus* specimens from the crater shale have not been identified to species, it is clear that they belong to species that have a possible range of high in the *Ph.* "pre-*flexuosus*" Zone through the *Belodina compressa* Zone. The S elements show the laterally alternating flexing of their posterior processes that characterizes the several species of the *Ph. flexuosus* plexus (*Ph.* "pre-*flexuosus*" [including ?*Ph. flexuosus* of Ethington and Clark, 1981, *Ph. polystrophos* Watson, *Ph. harrisi* Bauer, 1989, and *Ph. polonicus* Dzik, *sensu* Dzik, 1994], *Ph. flexuosus* Moskalenko, *sensu* Bauer [1994], and *Ph. ambiguus* Bauer, 1994), and *Ph. inflexus* Stauffer, *sensu* Sweet (in Ziegler, 1981; p. 258–263). Posteriorly denticulate dolabrate M elements have been identified, indicating the presence of one, or more, of the last three of these species, but the P elements, necessary for diagnosis among these three, have not been distinguished because of their rarity, small size, and only partial exposure on the bedding planes. It will require eventual disaggregation of some conodont-bearing crater shale or some fortuitous additional bedding-plane exposures to further refine these species identifications. Regardless, the lowest appearance of *Ph. flexuosus*, the oldest of these three species, is high in the *Ph.* "pre-*flexuosus*" Zone, and so the maximum age is essentially the same based on both genera found thus far.

CORRELATION

The Ames structure conodonts reported herein clearly point to correlation of the crater shale with the middle to upper (but not uppermost) part of the Simpson Group of the main part of the Anadarko basin to the south of Major County. Bauer's (1987,1990,1994) studies of middle and upper Simpson Group faunas in the Arbuckle Mountains demonstrate that the species of *Phragmodus* and *Erismodus* represented in the Ames crater shale first appear in the lower part of the McLish For-

mation and have a mutual range through the Bromide Formation.

In the thinned Middle Ordovician succession of eastern Oklahoma, the middle part of the Simpson Group of the Arbuckle Mountains correlates with strata of the McLish Formation in the subsurface (J. R. Derby, personal communication, 1995) and with part of the Tyner Formation in outcrop in Cherokee County (Bauer, 1989). Bauer (1989) found that *Phragmodus* of the *Ph. flexuosus* plexus occurs there only in the upper part of the middle Tyner, with physical and faunal evidence of unconformity both below and above these strata.

DISCUSSION AND SUMMARY

Derby and others (1991) summarized biostratigraphic data for the Cambrian and Ordovician of southern Oklahoma. One of their conclusions was that the major regional unconformity between the Oil Creek and overlying McLish Formations represents the Sauk-Tippecanoe sequence boundary of Sloss (1982). Thus, the black shale filling the Ames crater appears to represent deposits of the initial marine transgression of the Tippecanoe sequence onto this part of the northern shelf of Oklahoma, as the crater is presumed to have formed by meteorite impact into (Sauk sequence) upper Arbuckle Group rocks (Carpenter and Carlson, 1992). The conodont data require reconsideration of the stratigraphic framework of the post–Arbuckle Group rocks in the vicinity of the Ames structure. Most previous papers, e.g., Roberts and Sandridge (1992), assign the crater shale to the Oil Creek Formation. With the recognition, based on the conodont data reported herein, that the age of the crater shale places it above the major unconformity between the Oil Creek and McLish Formations, it is more reasonable now to assign this unit to the middle part of the Simpson Group (McLish Formation–Tulip Creek Formation–Bromide Formation interval) rather than to the lower part of the Simpson (i.e., the Oil Creek Formation).

Additional biostratigraphic work in and around the Ames crater is needed and could greatly clarify our knowledge of the geologic history related to that structure and of the Ordovician of the northern shelf area in general. For example, it is not known whether the youngest rocks predating the impact are Lower or Middle Ordovician. And, the actual age range (rather than the total possible range) of the crater shale itself can still be narrowed. This biostratigraphic refinement should be feasible, given the material available from the recent intensive drilling activity in the area.

Finally, it should be noted that the Ames structure is but one of numerous Ordovician impact craters now known (Lindström and others, 1992; Puura and others, 1994; Grieve and others, 1995). One of these, the Brent crater in Ontario, Canada, has been dated by using conodonts and chitinozoans (Grahn and Ormö, 1995). Interestingly, both *Erismodus* and *Phragmodus inflexus* were reported from the Brent crater–filling deposits. Thus, at least the infilling of the Ames and Brent craters, if not the impact events as well, could have been nearly, or actually, contemporaneous.

ACKNOWLEDGMENTS

I thank S. C. Finney and J. T. Hannibal for providing material from the Ames crater shale for conodont study and D. & J. Oil Company and Nicor Production Company for making this core material available for study through the Oklahoma Geological Survey. J. R. Derby, M. D. Kuykendall, and J. A. Bauer shared ideas about the local and regional stratigraphy. D. J. Weary ably helped with the illustrations. The manuscript was improved by reviews by R. L. Ethington, R. C. Orndorff, and J. A. Bauer.

REFERENCES CITED

Bauer, J. A., 1987, Conodonts and conodont biostratigraphy of the McLish and Tulip Creek Formations (Middle Ordovician) of south-central Oklahoma: Oklahoma Geological Survey Bulletin 141, 58 p.

_____ 1989, Conodont biostratigraphy and paleoecology of Middle Ordovician rocks in eastern Oklahoma: Journal of Paleontology, v. 63, p. 92–107.

_____ 1990, Stratigraphy and conodont biostratigraphy of the upper Simpson Group, Arbuckle Mountains, Oklahoma, *in* Ritter, S. M. (ed.), Early to middle Paleozoic conodont biostratigraphy of the Arbuckle Mountains, southern Oklahoma: Oklahoma Geological Survey Guidebook 27, p. 39–53.

_____ 1994, Conodonts from the Bromide Formation (Middle Ordovician), south-central Oklahoma: Journal of Paleontology, v. 68, p. 358–376.

Carpenter, B. N.; and Carlson, Rick, 1992, The Ames impact crater: Oklahoma Geology Notes, v. 52, p. 208–223.

Coughlin, J.; and Denney, P., 1993, The Ames structural depression: an endogenic cryptoexplosion feature along a transverse shear: Shale Shaker, v. 43, no. 4, p. 44–58.

Derby, J. R.; Bauer, J. A.; Creath, W. B.; Dresbach, R. I.; Ethington, R. L.; Loch, J. D.; Stitt, J. H.; McHargue, T. R.; Miller, J. F.; Miller, M. A.; Repetski, J. E.; Sweet, W. C.; Taylor, J. F.; and Williams, Mark, 1991, Biostratigraphy of the Timbered Hills, Arbuckle, and Simpson Groups, Cambrian and Ordovician, Oklahoma: a review of correlation tools and techniques available to the explorationist, *in* Johnson, K. S. (ed.), Late Cambrian–Ordovician geology of the southern Midcontinent, 1989 symposium: Oklahoma Geological Survey Circular 92, p. 15-41.

Dzik, Jerzy, 1994, Conodonts of the Mójcza Limestone: Palaeontologia Polonica, no. 53, p. 43–128, Pls. 11–24.

Epstein, A. G.; Epstein, J. B.; and Harris, L. D., 1977, Conodont color alteration—An index to organic metamorphism: U.S. Geological Survey Professional Paper 995, 27 p.

Ethington, R. L.; and Clark, D. L., 1981, Lower and Middle Ordovician conodonts from the Ibex area, western Millard County, Utah: Brigham Young University Geology Studies, v. 18, 155 p.

Grahn, Y.; and Ormö, J., 1995, Microfossil dating of the Brent meteorite crater, southeast Ontario, Canada: Revue de Micropaléontologie, v. 38, no. 2, p. 131–137.

Grieve R.; Rupert, J.; Smith, J.; and Therriault, A., 1995, The record of terrestrial impact cratering: Geological Society of America, GSA Today, v. 5, p. 189, 194–196.

Hannibal, J. T.; and Feldmann, R. M., 1997, Phyllocarid crustaceans from a Middle Ordovician black shale within the Ames structure, northwest Oklahoma, *in* Johnson, K. S.; and Campbell, J. A. (eds.), Ames structure in northwest Oklahoma and similar features: origin and petroleum production (1995 symposium): Oklahoma Geological Survey Circular 100 [this volume], p. 370–373.

Johnson, K. S., 1989, Geologic evolution of the Anadarko basin, *in* Johnson, K. S. (ed.), Anadarko basin symposium, 1988: Oklahoma Geological Survey Circular 90, p. 3–12.

Johnson, K. S.; Luza, K. V.; and Roberts, J. F., 1980, Disposal of industrial wastes in Oklahoma: Oklahoma Geological Survey Circular 80, 82 p.

Koeberl, Christian; Reimold, W. U.; Brandt, Dion; Dallmeyer, R. D.; and Powell, R. A., 1997, Target rocks and breccias from the Ames impact structure, Oklahoma: petrology, mineralogy, geochemistry, and age, *in* Johnson, K. S.; and Campbell, J. A. (eds.), Ames structure in northwest Oklahoma and similar features: origin and petroleum production (1995 symposium): Oklahoma Geological Survey Circular 100 [this volume], p. 169–198.

Lindström, M.; Flodén, T.; Puura, V.; and Suuroja, K., 1992, The Kärdla, Tvären, and Lokne craters—possible evidences of an Ordovician asteroid swarm: Proceedings of the Estonian Academy of Sciences, Geology, v. 41, no. 2, p. 45–53.

Puura, V.; Lindström, M.; Flodén, T.; Pipping, F.; Motuza, G.; Lehtinen, M.; Suuroja, K.; and Murnieks, A., 1994, Structure and stratigraphy of meteorite craters in Fennoscandia and the Baltic region: a first outlook: Proceedings of the Estonian Academy of Sciences, Geology, v. 43, no. 2, p. 93–108.

Roberts, C.; and Sandridge, B., 1992, The Ames hole: Shale Shaker, v. 42, no. 5, p. 118–121.

Sloss, L. L., 1982, The Midcontinent province: United States, *in* Palmer, A. R. (ed.), Perspectives in regional geological synthesis: Geological Society of America, Decade of North American Geology, Special Publication 1, p. 27–39.

Sweet, W. C., 1981, Macromorphology of elements and apparatuses, *in* Clark, D. L.; and others (eds.), Conodonta, Supplement 2, *Part W of* Robison, R. A. (ed.), Treatise on invertebrate paleontology: Geological Society of America, Boulder, Colorado (and University of Kansas Press), p. W5–W20.

Ziegler, W. (ed.), 1981, Catalogue of conodonts, v. IV: E. Schweitzerbart'sche Verlagsbuchhandlung, Stuttgart.

Phyllocarid Crustaceans from a Middle Ordovician Black Shale Within the Ames Structure, Northwest Oklahoma

Joseph T. Hannibal
Cleveland Museum of Natural History
Cleveland, Ohio

Rodney M. Feldmann
Kent State University
Kent, Ohio

ABSTRACT.—Phyllocarid crustaceans are found in abundance in cores from a Middle Ordovician black shale taken from the D. & J. no. 1-20 James well and the Nicor no. 18-4 Chestnut well, Major County, Oklahoma. These wells penetrate the Ames structure. At least two taxa of phyllocarids are present; one is similar to *Ceratiocaris*. Conodonts, brachiopods, and other fossils are also present in the same black shale. The fossils imply that the shale is a marine unit, probably deposited in dysaerobic conditions.

INTRODUCTION

Fossil-bearing sections of a Middle Ordovician black shale are known from cores taken from the D. & J. Drilling Company no. 1-20 James well (sec. 20, T. 21 N., R. 9 W.) and the Nicor no. 18-4 Chestnut well (sec. 18, T. 21 N., R. 9 W.), Major County, Oklahoma (Carpenter and Carlson, 1992, fig. 6A; Fischer, 1997). These wells penetrate the Ames structure. Phyllocarid crustaceans are found in abundance within the 8,886 to 8,913 ft interval of core taken from the D. & J. no. 1-20 James well and the 8,969 to 8,994 ft interval of the Nicor no. 18-4 Chestnut well. Other macro- and microfossils are also present. The cores of these intervals are mainly grayish black, laminated, fissile shale. These intervals are part of a black shale unit that has usually been designated as belonging to the Oil Creek Formation (Carpenter and Carlson, 1992; but see Repetski, 1997). This black shale overlies a dolomitic layer and a microbreccia containing dolomite and granite fragments (Carpenter and Carlson, 1992; Fischer, 1997; Kevin E. Nick, personal communication).

Joseph T. Hannibal, Cleveland Museum of Natural History, 1 Wade Oval Dr., University Circle, Cleveland, OH 44106; Rodney M. Feldmann, Department of Geology, Kent State University, Kent, OH 44242.

FAUNA

The fauna found in the shale at the two wells contains phyllocarid crustaceans (Figs. 1,2), which are abundant along many bedding planes; conodonts (Repetski, 1997); and rare brachiopods, including rhynchonellids. The fauna also contains large (ranging up to 5.4 cm long or more), pyritized cone-shaped body fossils; pyritized, ribbonlike fossils (ranging in width to more than 1 mm) of undetermined affinity; and small phosphatic masses, some of which might represent fish remains.

The phyllocarids, for the most part, are represented by aggregations of carapaces, abdomens, and telsons. They are preserved as phosphatic and pyritic replacements. The specimens are generally small, with carapace lengths ranging between 4 and 20 mm. The total body lengths of larger specimens approach 3 cm. Some specimens exhibit both abdominal and thoracic segmentation.

At least two taxa of phyllocarids are present; one common form is similar to *Ceratiocaris*. This form (Fig. 1) has an elongate carapace that covers the anterior of the abdomen. There is an anterodorsal projection of the carapace (?rostral plate). The furcal rami (lateral telson spines) of this form,

Hannibal, J. T.; and Feldmann, R. M., 1997, Phyllocarid crustaceans from a Middle Ordovician black shale within the Ames structure, northwest Oklahoma, *in* Johnson, K. S.; and Campbell, J. A. (eds.), Ames structure in northwest Oklahoma and similar features: origin and petroleum production (1995 symposium): Oklahoma Geological Survey Circular 100, p. 370–373.

Figure 1. Phyllocarids resembling *Ceratiocaris* from the 8,886 to 8,913 ft interval of the D. & J. no. 1-20 James well, Major County, Oklahoma. Material is in the invertebrate paleontology repository of the Oklahoma Museum of Natural History (OU). Photographed under alcohol to enhance contrast between the specimens and matrix. *A*—OU9658, one well-preserved specimen is seen in side view, with the carapace on the right and abdomen and telson on the left. Portions of a second, less well-preserved specimen are seen below and to the left. *B*—OU9659, consisting of carapace, abdomen, and telson material. The best-preserved carapace in this photograph is seen on the upper right; several well-preserved abdomina with elongate swordlike axial telson spines can also be seen. Scale bars represent 1 cm.

Figure 2. Phyllocarids from the D. & J. no. 1-20 James well, Major County, Oklahoma, OU 9660. This slab is from 8,887 ft. Two fairly complete specimens are seen in side view, the one on the top is upside down; the one on the bottom is right side up. Parts of additional specimens are scattered on the slab. The phyllocarids shown here each have a prominent ventral spine located along the midlength of the carapace. Scale bar represents 1 cm.

however, are not long and spinelike as are those of typical *Ceratiocaris*. The ornamentation of the abdomen also differs from that of typical *Ceratiocaris*. The other common type of phyllocarid (Fig. 2) has a broader carapace with a prominent ventral spine located along its midlength. The posterior of the carapace is concave, and the anterodorsal projection of the carapace (?rostrum) is less pronounced than that of the other form. Both taxa of phyllocarids are preserved laterally flattened, indicating that they probably were higher than wide in life. Upon death, organisms typically assume a position of repose on their broadest side.

DISCUSSION

Phyllocarids are rare in the lower Paleozoic rocks of Oklahoma. Although Ruedemann (1935) described the phyllocarid *Caryocaris* from the Henryhouse Shale (Silurian) of Oklahoma, his report was based on very poor material that was subsequently rejected as belonging to the Phyllocarida (Churkin, 1966, p. 379; Branson, 1967). There is a possible phyllocarid specimen from the Henryhouse Shale in Carter County, Oklahoma, however. That specimen, deposited in the U.S. National Museum of Natural History (USNM 114535), is labeled *Caryocaris*. Although it may be a phyllocarid, it is too fragmentary for more specific identification. Phyllocarids such as *Ceratiocaris* and *Caryocaris*, however, are known from dark, lower Paleozoic rocks in other areas of North America.

Phyllocarids are generally accepted to be confined to marine environments (Rolfe, 1969, p. R308). Therefore, the presence of phyllocarids and rhynchonellid brachiopods implies that the shale is a marine unit. Like some other Ordovician phyllocarids, the phyllocarids found in this core were probably pelagic. Obligatory bottom-dwelling organisms are poorly represented in the phyllocarid-rich intervals. Thus, this shale resembles other shales generally thought to have been deposited in a dysaerobic environment.

ACKNOWLEDGMENTS

We thank Kevin E. Nick, Stim-Lab, Inc., Duncan, Oklahoma, and Patrick K. Sutherland,

Oklahoma Museum of Natural History, Norman, Oklahoma, who collected the initially examined specimens; and J. Fritz Fischer, Fischer Petrologic, Denver, and Kenneth S. Johnson and his colleagues at the Oklahoma Geological Survey who facilitated study of additional core material. Jann Thomson provided access to the U.S. National Museum of Natural History collections. Photographs were taken by Bruce Frumker, the Cleveland Museum of Natural History, and a manuscript version of this paper was critiqued by John E. Repetski, U.S. Geological Survey.

REFERENCES CITED

Branson, C. C., 1967, *Caryocaris* removed from Oklahoma faunal list: Oklahoma Geology Notes, v. 27, p. 44.

Carpenter, B. N.; and Carlson, Rick, 1992, The Ames impact crater: Oklahoma Geology Notes, v. 52, p. 208–223.

Churkin, Michael, Jr., 1966, Morphology and stratigraphic range of the phyllocarid crustacean *Caryocaris* from Alaska and the Great Basin: Palaeontology, v. 9, p. 371–380.

Fischer, J. F., 1997, The Nicor no. 18-4 Chestnut core, Ames structure, Oklahoma: description and petrography, *in* Johnson, K. S.; and Campbell, J. A. (eds.), Ames structure in northwest Oklahoma and similar features: origin and petroleum production (1995 symposium): Oklahoma Geological Survey Circular 100 [this volume], p. 223–239.

Repetski, J. E., 1997, Conodont age constraints on the Middle Ordovician black shale within the Ames structure, Major County, Oklahoma, *in* Johnson, K. S.; and Campbell, J. A. (eds.), Ames structure in northwest Oklahoma and similar features: origin and petroleum production (1995 symposium): Oklahoma Geological Survey Circular 100 [this volume], p. 363–369.

Rolfe, W. D. I., 1969, Phyllocarida, *in* Moore, R. C. (ed.), Treatise on invertebrate paleontology, Part R, Arthropoda 4: Boulder, Colorado, Geological Society of America (and University of Kansas Press), p. R296–R331.

Ruedemann, Rudolf, 1935, Silurian phyllocarid crustaceans from Oklahoma: Journal of Paleontology, v. 9, p. 447–448.

Comparison of Sylvan Structure Residual Maps of the Ames Feature, Using Control as of December 1990 and December 1994

Richard A. Haines
Geological Data Services
Dallas, Texas

ABSTRACT.—As early as 1986, Geological Data Services (GDS) was generating structure maps of the Ames feature, Major County, Oklahoma, by using digital data from the GDS Formation Tops File and the CPS-3 contouring software from GeoQuest. Maps were generated for many horizons from the Heebner Shale to the Viola limestone, all of which expressed a circular depression. For several years, opinions on the origin and mechanics of the structural formation were discussed and debated, with very little thought given to possible production.

With the discovery of gas in the DLB no. 1 Cecil (sec. 27, T. 21 N., R. 10 W.) and oil at the D. & J. no. 1 Gregory (sec. 20, T. 21 N., R. 9 W.), the interest in this feature exploded. Having no direct interest in production, GDS began an intensive mapping program to provide materials to the industry to study and discuss the origin and mechanics of the feature. At that time (December 1990), there were only three Arbuckle wells in the vicinity. GDS therefore concluded that the best map possible to express the geometry of the deeper horizons was a third-order trend residual map of the Sylvan Shale structure.

GDS has shown by generating the Sylvan residual maps with addition of over 80 new control points as of December 1994 that the expressions of all the major features of the Ames structure are essentially unchanged. All the major rebound highs were obvious on the earlier maps. A residual map can be a useful tool for predicting deeper structure in many situations, not just over unique features like the Ames structure.

Richard A. Haines, Geological Data Services, 4951 Airport Pkwy., #600, Dallas, TX 75248.

Haines, R. A., 1997, Comparison of Sylvan structure residual maps of the Ames feature, using control as of December 1990 and December 1994, *in* Johnson, K. S.; and Campbell, J. A. (eds.), Ames structure in northwest Oklahoma and similar features: origin and petroleum production (1995 symposium): Oklahoma Geological Survey Circular 100, p. 374.

Iridium in Samples from the Ames Structure

Moses Attrep, Jr., Leonard R. Quintana, and Michael R. Cisneros
Los Alamos National Laboratory
Los Alamos, New Mexico

ABSTRACT.—Eighteen rock samples from four wells in the Ames structure were analyzed for iridium. Three samples showed iridium concentrations of >100 ppT (parts per trillion); the range was ≤3 ppT to 173 ppT. The elevated iridium values in the three samples together with the presence of shocked quartz provide additional support for the bolide hypothesis for the origin of the Ames structure.

INTRODUCTION

The Ames structure is located near the town of Ames, in Major County, Oklahoma. Study of the Ames structure has revealed many features that convincingly indicate that it was created by the impact of a meteorite or some other extraterrestrial object. The structure is a circular feature with a diameter of approximately 8 mi; its paleotopography resembles an impact crater (Roberts and Sandridge, 1992). Shocked quartz of the type identified in and around high-energy-release impact structures is found within the Ames structure. There is also stratigraphic evidence of backwash deposits with graded breccia to support such a scenario.

Iridium (and other platinum-group element) abundances can be an extremely useful tool for indicating the presence of extraterrestrial material in terrestrial rock samples. There are several classes of meteorites that contain high concentrations of iridium. Terrestrial background levels of iridium in most rocks are only a few tens of parts per trillion (10^{-15} g/g; ppT); therefore, only a small amount of an iridium-rich source introduced into the rock would increase the iridium's apparent abundance.

In support of the efforts to provide additional information concerning the origin of the Ames structure, we determined iridium in 18 rock samples from the structure. Our interpretation of the iridium results are made in the context of all the other evidence known about the structure and with knowledge of the major mechanisms for iridium enrichments in geologic samples.

Moses Attrep, Jr., Leonard R. Quintana, and Michael R. Cisneros, MS-J514, Los Alamos National Lab, Los Alamos, NM 87545.

EXPERIMENTAL PROCEDURES

The four wells sampled from the Ames structure are Nicor no. 18-4 Chestnut (NE¼SW¼SE¼ sec. 18, T. 21 N., R. 9 W.; 10 samples); Continental Resources, Inc., no. 1-19 Dorothy (NE¼NE¼NE¼ sec. 19, T. 21 N., R. 9 W.; 6 samples); DLB Oil and Gas no. 21-11 DeHaas (NE¼SW¼ sec. 21, T. 21 N., R. 9 W.; 1 sample); and D. & J. Oil Company no. 1-20 James (W½NW¼NE¼ sec. 21, T. 21 N., R. 9 W.; 1 sample). Sidewall samples were provided to us for analysis.

The determination of iridium by radiochemical neutron activation analysis provides one of the most sensitive and unambiguous methods to determine this rare element. The neutron absorption cross section of ^{191}Ir is large and makes this element particularly suitable for low-level neutron activation analysis. The analysis consists of irradiating whole-rock samples, performing radiochemical purifications, and counting the samples on a gamma spectrometer. Our limit of detection is a few parts per trillion. The details of the procedure are given as follows.

Rock samples were crushed to a powder under careful conditions as to not contaminate or cross-contaminate the samples with iridium from other sources. The sample was loaded into ultrapure quartz vials, the mass of rock sample was measured (≈0.5 g), and the vial was sealed. Rock standards for iridium were also prepared in a similar manner. The samples were irradiated at the Uni-

Attrep, Moses Jr.; Quintana, L. R.; and Cisneros, M. R., 1997, Iridium in samples from the Ames structure, *in* Johnson, K. S.; and Campbell, J. A. (eds.), Ames structure in northwest Oklahoma and similar features: origin and petroleum production (1995 symposium): Oklahoma Geological Survey Circular 100, p. 375–378.

TABLE 1.—IRIDIUM IN ROCK SAMPLES FROM WELLS AT THE AMES STRUCTURE

Sample Location	Depth (ft)	Ir concentration (ppT)
Nicor no. 18-4 Chestnut	9,006.9	48.1
	9,009.7	25.3
	9,014.0	121.0
	9,016.8	65.3
	9,021.0	15.9
	9,024.1	51.6
	9,028.2	43.5
	9,033.0	31.5
	9,034.4	83.7
	9,036.3	29.4
Continental Resources, Inc. no. 1-19 Dorothy	8,978.5	37.2
	9,003.0	127.0
	9,038.5	173.4
	9,041.5	10.9
	9,054.0	≤5
	9,157.0	20.8
DLB Oil & Gas no. 21-11 DeHaas	8,982	15.1
D & J Oil Co. no. 1-20 James	8,885	≤5

versity of Missouri Research Reactor (Columbia, Missouri) for 6 h at a flux of 2.5×10^{12} neutrons/(s·cm^2).

Following irradiation, the rock samples were allowed to radioactively decay for a week or more. The samples were then removed from the vials, iridium carrier was added, and strong mineral acids were added (HF, HNO_3, and $HClO_4$) for dissolution. The iridium was isolated and purified by two cation-exchange columns and finally precipitated as Cs_2IrCl_6. The chemical yield was determined by the amount of recovered iridium. The samples were counted for 200–300 min on a lithium-drifted germanium gamma ray spectrometer where the characteristic gamma rays were identified and quantified. The amount of iridium in the rock sample was determined by comparison to the iridium standards irradiated and treated in the same manner.

RESULTS AND DISCUSSION

The results of the iridium determinations for the 18 rock samples are given in Table 1. The iridium concentrations are plotted as a function of depth for the two sets of core samples where multiple samples were analyzed (Figs. 1,2). Concentrations of iridium are given in parts per trillion in all cases.

Iridium has a naturally low abundance in most sedimentary rocks and deposits. When an impact crater is investigated geochemically, a mixture of the extraterrestrial object and the remaining target rocks may be revealed. Although this mixture usually contains much less than 1% of the projectile, the platinum-group elements can play a crucial role in determining the nature of the impactor. Their presence in the debris (melt rock and glasses) mixed with the host rock can be a strong signal indicating such an event.

The iridium values observed in the Ames samples, even the three that are most iridium enriched, cannot alone provide conclusive evidence that the iridium is associated with the impact of an extraterrestrial object. The three most iridium-enriched samples that we observed contained only weak anomalies of iridium: 127.0 and 173.4 ppT in the Continental Reserve samples and 121.0 ppT in the Nicor Chestnut section. In addition to these three anomalies, the value of 83.7 ppT in the Nicor Chestnut well suggests a slight enrichment. In such cases in which the iridium anomalies are very weak, caution must be exercised in relying totally on the iridium values to interpret whether there has been a meteorite impact. Usually, to be more convincing of an impact origin, an iridium anomaly would be at the parts per million (μg/g) level.

In the Nicor Chestnut no. 18-4 well, the iridium enrichment of 121.0 ppT is found below rocks that are interpreted (according to the impact theory) as back-wash deposits. There are three graded clastic beds between approximately 9,003 and 9,013 ft (Fischer, 1997). The high iridium sample in this well occurs at 9,014.0 ft, which corresponds approximately to the bottom of the lowermost graded bed. We do not have a stratigraphic correlation of the iridium samples from the Continental Reserve well.

There are three explanations of why we did not observe higher iridium signals. (1) The samples that we analyzed were not continuous throughout the breccia section, and we may have missed extremely high elevated iridium signatures. (2) The impactor may not have been an iridium-rich object. (3) The iridium levels we observed are at the same level we would observe from an enriched terrestrial source.

Terrestrial Sources of Iridium

To expand on the third explanation, there are several other mechanisms and sources for anomalous iridium to be found in the geologic record. A brief description of the more important mechanisms provides a basis of comparison of the results

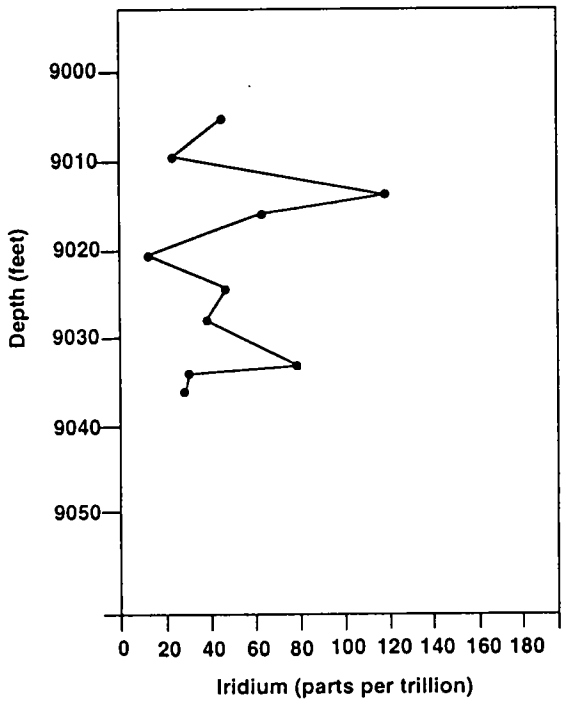

Figure 1. Iridium values in samples from the Nicor no. 18-4 Chestnut well.

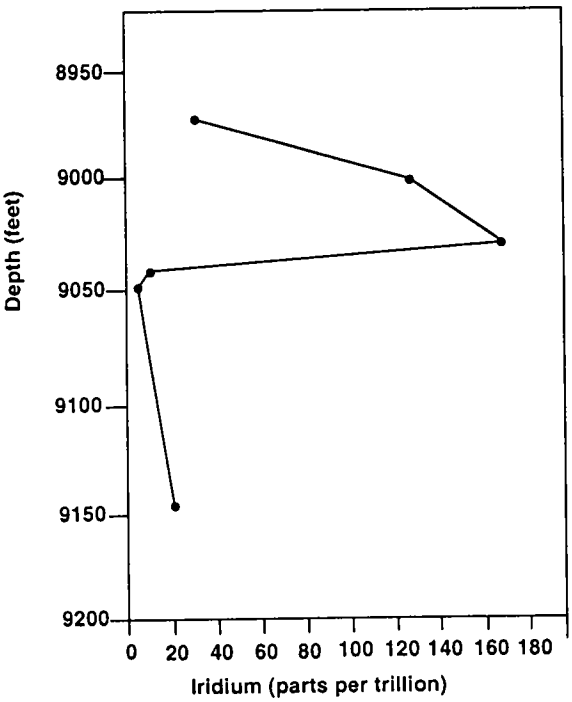

Figure 2. Iridium values in samples from the Continental Resources, Inc., no. 1-19 Dorothy well.

given here and shows what might be anticipated from other mechanisms.

The source of background iridium is primarily the constant shower of micrometeorites containing high iridium levels. As sediments are deposited in the oceans, the micrometeorite dust is incorporated into the sediment. If the sediment rate is very high, then the iridium signal is low, as seen in rapidly deposited carbonates. However, if the rate of sedimentation is low, then there is an appearance of an iridium enrichment. This phenomenon is observed at the Ordovician–Silurian boundary in China (Wang and others, 1992) where iridium signals reach 230 ppT.

It was reported by Playford and others (1984) that specialized bacteria appear to concentrate iridium from their marine environment, as seen in the Devonian rocks of Australia. This iridium anomaly is associated with high iron concentrations that were observed in the fossil remains of the bacteria colonies.

In addition to the above sources, there are terrestrial sources for the elevated iridium values. For example, gases from Kilauea volcano are elevated in iridium (Olmez and others, 1986); however, the quantities cannot provide an explanation for the global anomalies.

At the Cenomanian/Turonian boundary studied by Orth and others (1993), up to three weak iridium peaks were observed in sections in the Western Hemisphere. These were thought to be associated with continental rifting and subsequent undersea activities at the rift zones that released siderophile elements. This boundary was studied at nearly 30 sites worldwide; the signals were varied, and iridium enrichments at the Cenomanian/Turonian boundary are clustered geographically in the southern area of the North American continent and in Colombia, South America.

Iridium from a Meteorite

However, if we consider the possibility that the iridium observed was from an impact that caused the Ames structure, then one of the most important supporting pieces of evidence for meteorite impact is the presence of shocked quartz in the rocks associated with the impact. Multiple sets of lamellae in quartz are found throughout the graded beds of the Ames breccia (Fischer, 1997). Shocked quartz is associated with many known impact structures. The combination of shocked quartz and the presence of iridium anomalies offers a stronger position for an impact scenario.

The iridium-rich clay layer deposited worldwide at the Cretaceous/Tertiary (K/T) boundary (Alvarez and others, 1980) is well known. This layer is attributed to fallout resulting from the impact of an asteroid or comet on the Yucatán peninsula (Hildebrand and others, 1991). Because the iridium signal for this event is global, the iri-

dium-rich material is associated with an extremely large impact event (the crater diameter is estimated to be ≈200 km). Also it has been found that iridium values for samples in the breccia of the K/T boundary impact crater are elevated several orders of magnitude over background iridium values (Sharpton and others, 1992). Shocked quartz is found around the world at the K/T boundary. If we had observed an iridium anomaly of this magnitude in the Ames structure, it would have been more convincing that it was an extraterrestrial impact.

Iridium Source in Ames Structure

On the basis of the iridium values determined in these samples alone, there is no conclusive evidence to confirm that the Ames structure is the result of an extraterrestrial object's hitting the Earth. Likewise, there are no indications that the iridium observed in the Ames structure is due to a slow deposition rate, a biological source, or other terrestrial sources. However, the anomalous iridium values that we report, together with the compelling implications of shocked quartz in the breccia zone, provide further positive indication of a meteorite-impact origin for the Ames structure.

ACKNOWLEDGMENTS

This work was supported by the Geosciences Research Program in the U.S. Department of Energy's Office of Basic Energy Sciences. We thank Ken Johnson, Bob Sandridge, and Paul Mescher for their help in supplying and describing the samples.

REFERENCES CITED

Alvarez, L. W.; Alvarez, W.; Asaro, F.; and Michel, H. V., 1980, Extraterrestrial cause for the Cretaceous-Tertiary extinction: Science, v. 208, p. 1095–1108.

Carpenter, B. N.; and Carlson, Rick, 1992, The Ames impact crater: Oklahoma Geology Notes, v. 52, p. 208–223.

Fischer, J. F., 1997, The Nicor no. 18-4 Chestnut core, Ames structure, Oklahoma: description and petrography, *in* Johnson, K. S.; and Campbell, J. A. (eds.), Ames structure in northwest Oklahoma and similar features: origin and petroleum production (1995 symposium): Oklahoma Geological Survey Circular 100 [this volume], p. 223–239.

Hildebrand, A. R.; Penfield, G. T.; Kring, D. A.; Pilkington, M.; Camargo, A. Z.; Jacobeson, S. B.; Boyton, W. V., 1991, Chicxulub crater: a possible Cretaceous/Tertiary boundary impact crater on the Yucatán Peninsula, Mexico: Geology, v. 19, p. 867–871.

Olmez, I.; Finnegan, D. L.; and Zoller, W. H., 1986, Iridium emissions from Kilauea Volcano: Journal of Geophysical Research, v. 91, p. 653–663.

Orth, C. J.; Attrep, M., Jr.; Quintana, L. R.; Elder, W. P.; Kauffman, E. G.; Diner, R.; and Villamil, T., 1993, Elemental abundance anomalies in the late Cenomanian extinction interval: a search for the source(s): Earth and Planetary Science Letters, v. 117, p. 189–204.

Playford, P. E.; McLaren, D. J.; Orth, C. J.; Gilmore, J. S.; and Goodfellow, W. D., 1984, Iridium anomaly in the Upper Devonian of the Canning basin, Western Australia: Science, v. 226, p. 437–439.

Roberts, Craig; and Sandridge, Bob, 1992, The Ames hole: Shale Shaker, v. 42, no. 5, p. 118–121.

Sharpton, V. L.; Dalrymple, G. B.; Marin, L. E.; Ryder, G.; Schuaytz, B. C.; and Urrutia-Fucugauchi, J., 1992, New links between the Chicxulub impact structure and the Cretaceous/Tertiary boundary: Nature, v. 359, p. 819–312.

Wang, K.; Chatterton, B. D. E.; Attrep, M., Jr., and Orth, C. J., 1992, Iridium abundance maxima at the latest Ordovician mass extinction horizon, Yangtze basin, China: terrestrial or extraterrestrial?: Geology, v. 20, p. 39–42.

Gamma-Ray Marker in Arbuckle Dolomite, Wilburton Field, Oklahoma—A Widespread Event Associated with the Ames Impact Structure

Paul K. Mescher
Geological Resources Company
Plano, Texas

Douglas J. Schultz
ARCO International Oil and Gas Company
Plano, Texas

ABSTRACT.—A regionally correlative, distinctive, gamma-ray electric-log marker occurs in the Lower Ordovician carbonate rocks of the Arbuckle (Oklahoma), Ellenburger (Texas), and Knox (southeastern United States) Groups. The marker represents a widespread unconformity surface formed by tsunami-generated bottom erosion and subsequent tsunami-derived sediments. The tsunami resulted from the impact of a meteorite near the location of Ames, Major County, Oklahoma, and its effects are preserved in shallow-shelf carbonate sedimentary rocks throughout the region.

In core samples, the distinctive gamma-ray marker interval consists of dark gray laminated dolomudstone; it includes 23% potassium feldspar (responsible for the high gamma-ray response) as well as shocked quartz, siliceous particles representing former lechatelierite(?), and pyrite. This stratigraphic unit occurs approximately 100 ft below the top of the Arbuckle dolomite in the subsurface of the Arkoma basin, southeastern Oklahoma, where it was first recognized and used as a stratigraphic marker in the Wilburton Field, Latimer County, Oklahoma. The unit has also been recognized in outcrop in southeastern Oklahoma. The interval is limited by the geographical extent of the carbonate shelf and is not recognized in equivalent basinal facies.

Besides the distinctive gamma-ray log response that is correlative on a regional scale, evidence supporting a meteorite impact and tsunami origin for the unconformity and related overlying sedimentary deposits includes the sharp erosional boundary at the base of the interval, the presence of tsunami deposits in the Ames area and their correlative units on the shelf, two faunal extinction events, and anomalous iridium concentrations in one well from the Ames impact structure.

INTRODUCTION

A regionally correlative, distinctive, gamma-ray electric-log marker occurs in the Lower Ordovician Arbuckle (Oklahoma), Ellenburger (Texas), and Knox Group (southeastern United States) carbonate rocks (see Fig. 1); the marker represents a widespread unconformity surface formed by tsunami-generated bottom erosion and subsequent tsunami-derived and related dust cloud sediments. The tsunami resulted from the impact of a meteorite near the present location of Ames, Major County, Oklahoma, and its effects are preserved in shallow-shelf carbonates throughout the region. This distinctive marker has been recognized in wells and outcrop throughout the southern Midcontinent and as far away as Indiana (Fig. 1).

Paul K. Mescher, Suite 175, Box 172, 3131 Custer Road, Plano, TX 75075; Douglas J. Schultz, ARCO International, 2300 W. Plano Pkwy., Plano, TX 75075.

Mescher, P. K.; and Schultz, D. J., 1997, Gamma-ray marker in Arbuckle dolomite, Wilburton Field, Oklahoma—a widespread event associated with the Ames impact structure, *in* Johnson, K. S.; and Campbell, J. A. (eds.), Ames structure in northwest Oklahoma and similar features: origin and petroleum production (1995 symposium): Oklahoma Geological Survey Circular 100, p. 379–384.

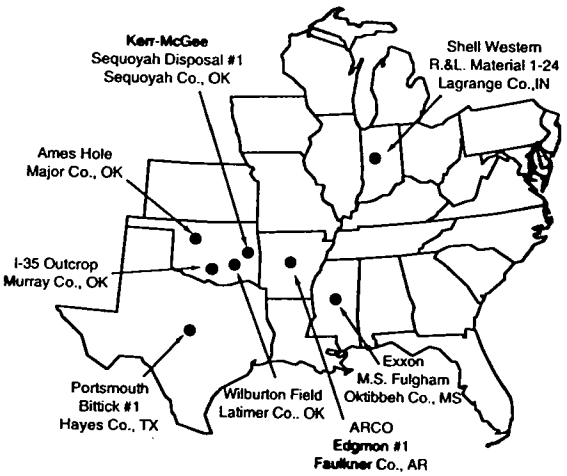

Figure 1. Location map showing site of Ames impact structure and wells studied for this paper.

GAMMA-RAY MARKER LITHOLOGY AND PETROGRAPHY

The lithology of this marker interval consists of dark gray laminated dolomudstone containing abundant potassium feldspar, quartz, and pyrite. The high gamma-ray response is largely due to the basement-derived potassium feldspar; X-ray diffraction (XRD) analysis of samples from the ARCO No. 2-16 Kilpatrick well (Wilburton Field) shows that potassium feldspar constitutes up to 23% of the marker interval (Table 1). This stratigraphic unit occurs approximately 100 ft below the top of the Arbuckle dolomite in the subsurface of the Arkoma basin, where it was first recognized and used as a stratigraphic marker in the Wilburton Field, Latimer County, Oklahoma (Mescher and others, 1993). The interval is limited by the geographical extent of the carbonate shelf and is not recognized in basinal facies. The electric-log marker is illustrated in Figure 2, with log displays from the ARCO No. 2-16 Kilpatrick (Wilburton Field), Continental Trend Resources No. 1-22 Mary Ellen (Ames structure), and Nicor No. 18-4 Chestnut (Ames structure).

In thin section, this marker interval contains unusual detrital quartz particles, consisting of quartz with shock lamellae, and siliceous particles representing former lechatelierite (?)—elongated, straight to gently curved fragments with a hollow tube–like central core that extends the length of the particles. Petrographic photographs showing a comparison of similar fragments from the Nicor No. 18-4 Chestnut well (impact site) and the ARCO No. 2-16 Kilpatrick well are shown in Figure 3.

EVIDENCE FOR METEORITE IMPACT AND TSUNAMI ORIGIN OF UNCONFORMITY AND RELATED OVERLYING ROCKS

1. The distinctive gamma-ray log response that is correlative on a regional scale was discussed and illustrated above (Table 1; Figs. 1,2).

2. There is a sharp erosional boundary at the base of the interval that is seen in wireline logs, Formation Micro-Scanner and Formation Micro-Imager electric logs, whole core, and outcrops. The boundary commonly abruptly truncates the ooid and skeletal grainstone deposits.

3. The sedimentary rocks at the level of the gamma-ray marker in the Kerr-McGee No. 1 Sequoyah disposal well contain detrital feldspar dated in 1989 by Krueger Enterprises, Inc. (Cambridge Massachusetts), at 1,226 ± 42 Ma, indicating that it originated from basement rocks whose age is similar to that of the granite found in the Ames structure area (Denison and others, 1997).

4. Two faunal extinctions have been noted from biostratigraphic studies of the I-35 outcrops (Fig. 1). Derby and others (1991) showed that nearly all of the West Spring Creek Formation (Ordovician Arbuckle Group) macrofauna were abruptly terminated approximately 100 ft below the top of the West Spring Creek Formation. Dresbach and Ethington (1991) showed that nearly all of the long-ranging conodont fauna disappeared also at the same stratigraphic level and, in addition, that conodonts present above this level are significantly abraded, indicating turbulent deposition at shallow depth.

5. Sedimentary rocks in the gamma-ray marker interval correspond in part to the tsunami deposits reported by Fischer (1997; J. F. Fischer and G. A. Izett, personal communication, 1995) in the Nicor No. 18-4 Chestnut core from the Ames structure, Major County, Oklahoma.

6. Anomalously high values of iridium have been determined in the No. 1-22 Mary Ellen well of the Ames structure (M. Attrep, Jr., personal communication, 1995). Analysis of samples from the Wilburton area, however, was inconclusive.

7. It is our interpretation that the "dolomite caprock" (9,002.8–9,003.7 ft) in the Nicor No. 18-4 Chestnut well of the Ames structure corresponds to the gamma-ray marker, suggesting that some of the West Spring Creek Formation carbonates (Arbuckle Group) were "blown out" of the crater during impact. The 18-4 location remained a positive structural element (impact rebound structure?), ending the West Spring Creek deposition there, and was later buried by Simpson Group shales (Repetski, 1997). In basinward areas, "normal" West Spring Creek deposition resumed at the end of the tsunami event, as shown by the West Spring Creek carbonates preserved above the gamma-ray log marker on a regional scale.

TABLE 1.—WHOLE-ROCK MINERAL CONTENT OF CORE SAMPLES FROM GAMMA-RAY MARKER ZONES BY X-RAY DIFFRACTION ANALYSIS

Ames Structure, Major County, Oklahoma

	CRI No. 1-22 Mary Ellen[a]		Nicor No. 18-4 Chestnut[a]			
Sample no.:	9024.4	9025.4	9001.8	9002.8	9004.2	9034.8
Quartz	24.6	16.8	37.1	34.7	34.2	34.0
K-feldspar	16.8	13.6	8.1	6.3	21.6	35.5
Plagioclase	0.0	1.1	0.0	0.0	0.0	0.0
Calcite	0.0	0.0	0.5	0.0	0.0	0.0
Mg-bearing calcite	1.1	0.7	0.9	0.8	0.0	0.0
Dolomite	47.0	55.6	43.7	50.7	2.8	29.0
Siderite	0.3	0.3	0.4	0.0	0.0	0.0
Pyrite	3.9	7.6	2.6	2.1	4.1	0.3
Halite	—	—	0.0	0.0	0.0	0.5
Illite + illite/smectite	5.3	3.2	5.6	4.8	37.3	0.8
Kaolinite or chlorite	1.0	1.2	1.1	0.6	0.0	0.0
Total	100.0	100.0	100.0	100.0	100.0	100.0

Wilburton Field, Latimer County, Oklahoma

	ARCO No. 2-16 Kilpatrick[b]							
Sample no.:	12939	12940	12941	12942	12943	12944	12945	12946
Quartz	5	6	3	14	17	11	12	14
K-feldspar	3	4	5	16	23	10	15	23
Plagioclase	0	0	0	0	0	0	0	0
Calcite	1	0	0	0	3	2	3	4
Dolomite	91	90	92	64	48	73	63	52
Pyrite	0	0	0	2	3	3	3	2
Illite + illite/smectite	0	0	0	2	3	1	2	2
Kaolinite or chlorite	0	0	0	2	3	0	2	3
Total	100	100	100	100	100	100	100	100

	Quantification of Insoluble Residue				
Sample no.:	12939	12940	12941	12942	12943
Quartz	59	47	51	42	45
K-feldspar	40	41	46	49	49
Plagioclase	1	0	0	0	0
Calcite	0	1	0	0	0
Dolomite	0	0	0	0	0
Pyrite	0	0	1	3	1
Illite + illite/smectite	0	11	2	6	5
Kaolinite or chlorite	0	0	0	0	0
Total	100	100	100	100	100

Note: Sample numbers correspond to well depth in feet. XRD analysis courtesy of MaxRay, Fredericksburg, Texas. Values are percentages. Illite/smectite (R3) is approximately 10% expandable.

[a]The percentages of detrital quartz and potassium feldspar are high compared to detrital quartz and potassium feldspar contents of normal Arbuckle rocks. The deeper sample from the Nicor No. 18-4 Chestnut well (9,034.8 ft) is from within the "ejecta blanket" of J. F. Fischer and G. A. Izett (personal communication, 1995; Fischer, 1997).

[b]There is a sharp increase in the percentages of detrital quartz and potassium feldspar within the marker zone (samples from 12,942 to 12,946 ft) compared to the values in the samples above it.

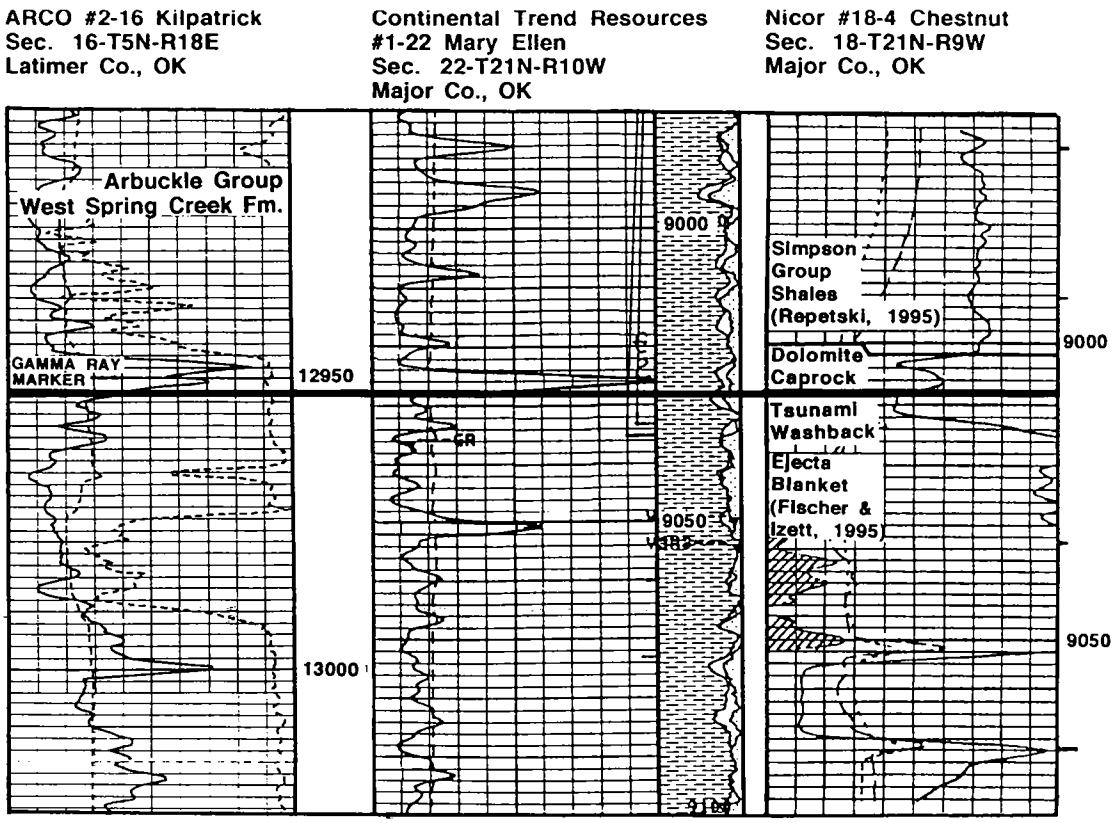

Figure 2. Gamma-ray marker zone illustrated with electric-log gamma-ray tracks from the ARCO No. 2-16 Kilpatrick in the Wilburton Field and the Continental Trend Resources No. 1-22 Mary Ellen and Nicor No. 18-4 Chestnut wells of the Ames area. The anomalous gamma-ray zone has been cored in all of these wells.

REFERENCES CITED

Denison, R. E.; Stern, R. J.; and Sun, C.-H., 1997, Basement rocks in the Ames area, *in* Johnson, K. S.; and Campbell, J. A. (eds.), Ames structure in northwest Oklahoma and similar features: origin and petroleum production (1995 symposium): Oklahoma Geological Survey Circular 100 [this volume], p. 334–338.

Derby, J. R.; Bauer, J. A.; Creath, W. B.; Dresbach, R. I.; Ethington, R. L.; Loch, J. D.; Stitt, J. H.; McHargue, T. R.; Miller, J. F.; Miller, M. A.; Repetski, J. E.; Sweet, W. C.; Taylor, J. F.; and Williams, M., 1991, Biostratigraphy of the Timbered Hills, Arbuckle, and Simpson Groups, Cambrian and Ordovician, Oklahoma: a review of correlation tools and techniques available to the explorationist, *in* Johnson, K. S. (ed.), Late Cambrian–Ordovician geology of the southern Midcontinent, 1989 symposium: Oklahoma Geological Survey Circular 92, p. 15–41.

Dresbach, R. I.; and Ethington, R. L., 1991, Conodont biostratigraphy of Lower Ordovician rocks, Arbuckle Group, southern Oklahoma, *in* Johnson, K. S. (ed.), Late Cambrian–Ordovician geology of the southern Midcontinent, 1989 symposium: Oklahoma Geological Survey Circular 92, p. 215–216.

Figure 3 *(facing page)*. Comparison of siliceous, tubelike fragments (shown by arrows) from stratigraphically equivalent intervals at Ames and Wilburton (locations in Fig. 1). Scale bars represent 100 μm. A—Sample from 9,004.2 ft depth in the Nicor No. 18-4 Chestnut well in the Ames area (Major County, Oklahoma), which is the site of the impact structure and of the formation of the lechatelierite [?] fragments. B—Sample from 12,945 ft depth in the ARCO Kilpatrick No. 2-16 well in the Wilburton Field (Latimer County, Oklahoma). Sample consists of tsunami deposits associated with the gamma-ray marker interval of the Wilburton Field area. Note the similar size and unusual morphology of the detrital fragments (after lechatelierite?) in the two occurrences.

A

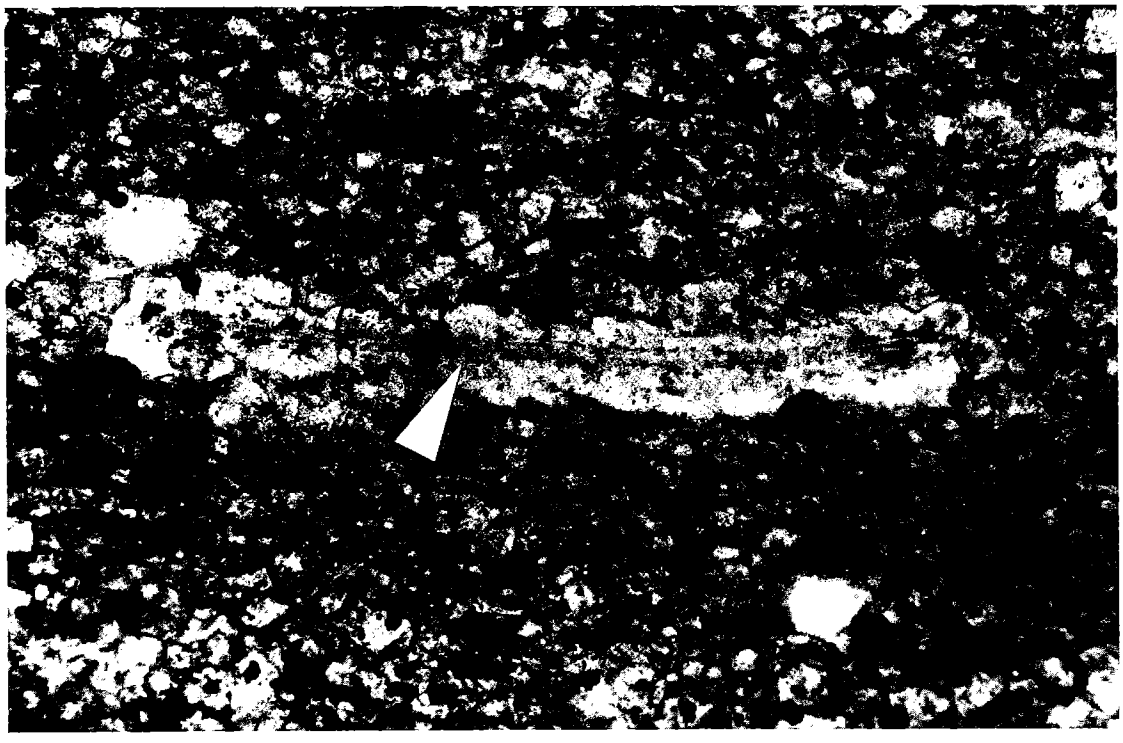

B

Figure 3.

Fischer, J. F., 1997, The Nicor No. 18-4 Chestnut core, Ames structure, Oklahoma: description and petrography, *in* Johnson, K. S.; and Campbell, J. A. (eds.), Ames structure in northwest Oklahoma and similar features: origin and petroleum production (1995 symposium): Oklahoma Geological Survey Circular 100 [this volume], p. 223–239.

Mescher, P. K.; Schultz, D. J.; Hendrick, S. J.; Ward, M. A.; and Schwarz, J. A., 1993, Lithology and reservoir development of the Arbuckle dolomite, Wilburton Field, Latimer County, Oklahoma, *in* Johnson, K. S.; and Campbell, J. A. (eds.), Petroleum-reservoir geology in the southern Midcontinent, 1991 symposium: Oklahoma Geological Survey Circular 95, p. 240–245.

Repetski, J. E., 1997, Conodont age constraints on the Middle Ordovician Black Shale within the Ames structure, Major County, Oklahoma, *in* Johnson, K. S.; and Campbell, J. A. (eds.), Ames structure in northwest Oklahoma and similar features: origin and petroleum production (1995 symposium): Oklahoma Geological Survey Circular 100 [this volume], p. 363–369.

The Steen River Structure, Alberta, Canada: Subsurface Identification and Hydrocarbon Occurrences

Gordon A. Robertson
Mercantile Canada Energy, Inc.
Calgary, Alberta

INTRODUCTION

The Steen River megastructure is located in the shallow northeastern part of the Western Canada Sedimentary basin approximately 435 mi north-northwest of the city of Edmonton, Alberta (Fig. 1). The area is remote, suffers from a lack of oil and gas infrastructure, and is consequently underexplored. It is one of the only remaining lightly explored but highly prospective areas with hydrocarbon potential that may yield significant reserves of Middle Devonian oil and gas within the Western Canada Sedimentary basin. The Steen River structure has no surface expression; the structure is defined by seismic and subsurface well data as a giant elliptical anomaly approximately 18 by 16 mi. Subsurface well control from approximately 25 wells, 2-D seismic data, and microscopic examination of rocks from the boreholes suggest that this megafeature is a meteorite-impact structure, the basement rocks of which have undergone severe shock metamorphism and fracturing. Age of the Steen River structure has been placed at 95 ± 10 Ma, which approximates the Lower Cretaceous/Upper Cretaceous boundary.

The Steen River structure consists of a central uplift (rebound feature) surrounded by an annular ring syncline that passes laterally into an outer concentric ring of semicontinuous fault-defined rim-anticline features that to date have yielded several Middle Devonian hydrocarbon discoveries at relatively shallow drilling depths (Fig. 2). The central uplifted area consists of a basement rebound feature that is now 3,600 ft above the regional strike. The rocks of the ring syncline are depressed some 650 to 1,950 ft below their regional level. The rocks of the rim anticline are uplifted approximately 65 to 160 ft relative to their regional level (Fig. 3).

Geophysical seismic data and aeromagnetic surveys have played an integral part in unraveling the structural complexity of the Steen River structure. To date, faulted structures have formed the key trapping mechanism for the various reservoirs that are sealed by overlying or lateral impermeable anhydrites, carbonates, and shales.

The purposes of this paper are (1) to offer an update on the latest phase of exploration being undertaken on the Steen River megastructure, the exploration activity of which has been dormant for a decade (1986–1995), and (2) to summarize for the first time the series of significant hydrocarbon discoveries and shows that have been encountered since serious exploration commenced in 1963 on the giant feature.

RECENT ACTIVITY

The principals of Mercantile Canada Energy, Inc., have believed that the Steen River megastructure on the northeastern fringe of the Western Canada Sedimentary basin may be a sleeping giant from a hydrocarbon perspective. During the last quarter of 1994, Mercantile purchased the Steen River oil and gas assets of the Kerr-McGee Corporation's Canadian affiliate. Consequent to this purchase, Mercantile encouraged Bearspaw Petroleum, Ltd., to join as a joint venture partner to further explore and exploit the hydrocarbon potential of the Steen River structure. The Mercantile Bearspaw Group then posted eight Petroleum and Natural Gas Licenses comprising some 48,000 acres for Crown sale (public auction) during November–December 1994. All of the acreage was purchased by various corporate entities, and the Mercantile Group acquired two Key Licenses (11,200 acres) immediately adjacent to and contiguous with their oil-producing properties.

Gordon A. Robertson, Mercantile Canada Energy, Inc., 717 7th Ave. S.W., Suite 500, Calgary, Alberta, Canada T2P0Z3.

Robertson, G. A., 1997, The Steen River structure, Alberta, Canada: subsurface identification and hydrocarbon occurrences, *in* Johnson, K. S.; and Campbell, J. A. (eds.), Ames structure in northwest Oklahoma and similar features: origin and petroleum production (1995 symposium): Oklahoma Geological Survey Circular 100, p. 385–390.

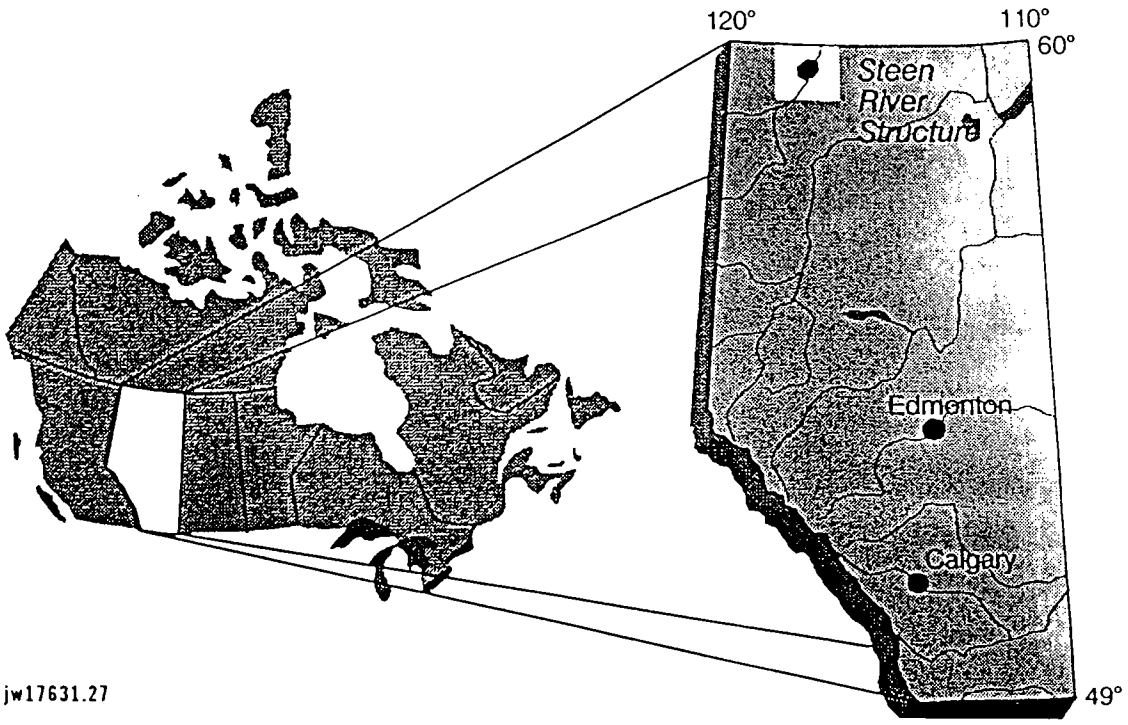

Figure 1. Location map Steen River structure in northern Alberta.

During the first quarter of 1995, Spectra Exploration Geoscience Corporation of Calgary undertook a proprietary speculative high-resolution aeromagnetic survey to further delineate the intricacies of this giant feature.

Three licenses comprising 14,080 acres were posted and sold at a November 1995 Crown auction and a development well, Bearspaw et al. Marlowe 16-21 (Lsd 16, 21-122-22 W5 [Canadian land-division designation: legal subdivision 16, Section 21, Township 122, Range 22 west of the 5th meridian; each Lsd is 40 acres, and there are 16 Lsds per section, which is 1 sq mi]), was drilled on the northern extremity of the rim anticline of the Steen River feature. The no. 16-21 well is an indicated Keg River Formation oil well and is scheduled for completion in early 1997.

In January 1996, Pennzoil Canada, Inc., drilled an exploratory well on the eastern part of the Steen River structure on the rim anticline. That company has not released any data pertaining to this test well (information is kept confidential for a 12-month period from rig release of the well).

A 10 km^2 3-D seismic survey was shot by the Mercantile Bearspaw Group in February 1996. This survey was the first attempt to gather 3-D seismic data on the Steen River structure. The survey evaluated the step-out potential of the northern Keg River Formation oil pool. The 3-D seismic survey results were favorable; consequently, Bearspaw Petroleum Ltd. located and drilled an offset development well, Bearspaw et al. Marlowe 4-27 (Lsd 4, 27-122-22 W5M) in December 1996. The well is an indicated Keg River Formation oil well and is scheduled for completion in mid-January 1997.

In addition, Pennzoil Canada, Inc., conducted a seismic survey during the first quarter of 1996 on the Steen River structure.

RESULTS OF EXPLORATION IN MIDDLE DEVONIAN ROCKS, STEEN RIVER STRUCTURE

Light gravity (34°API) oil has been discovered in dolomites within the Keg River Formation, the Sulphur Point Member of the Muskeg Formation, and the Zamma Member of the Muskeg Formation at separate and diverse locations on the rim anticline of the Steen River structure. In addition, the structure has yielded two gas discoveries from the Slave Point Formation, an indicated gas discovery in the Sulphur Point Member of the Muskeg Formation, and a minor show of gas in the Keg River Formation (Fig. 4).

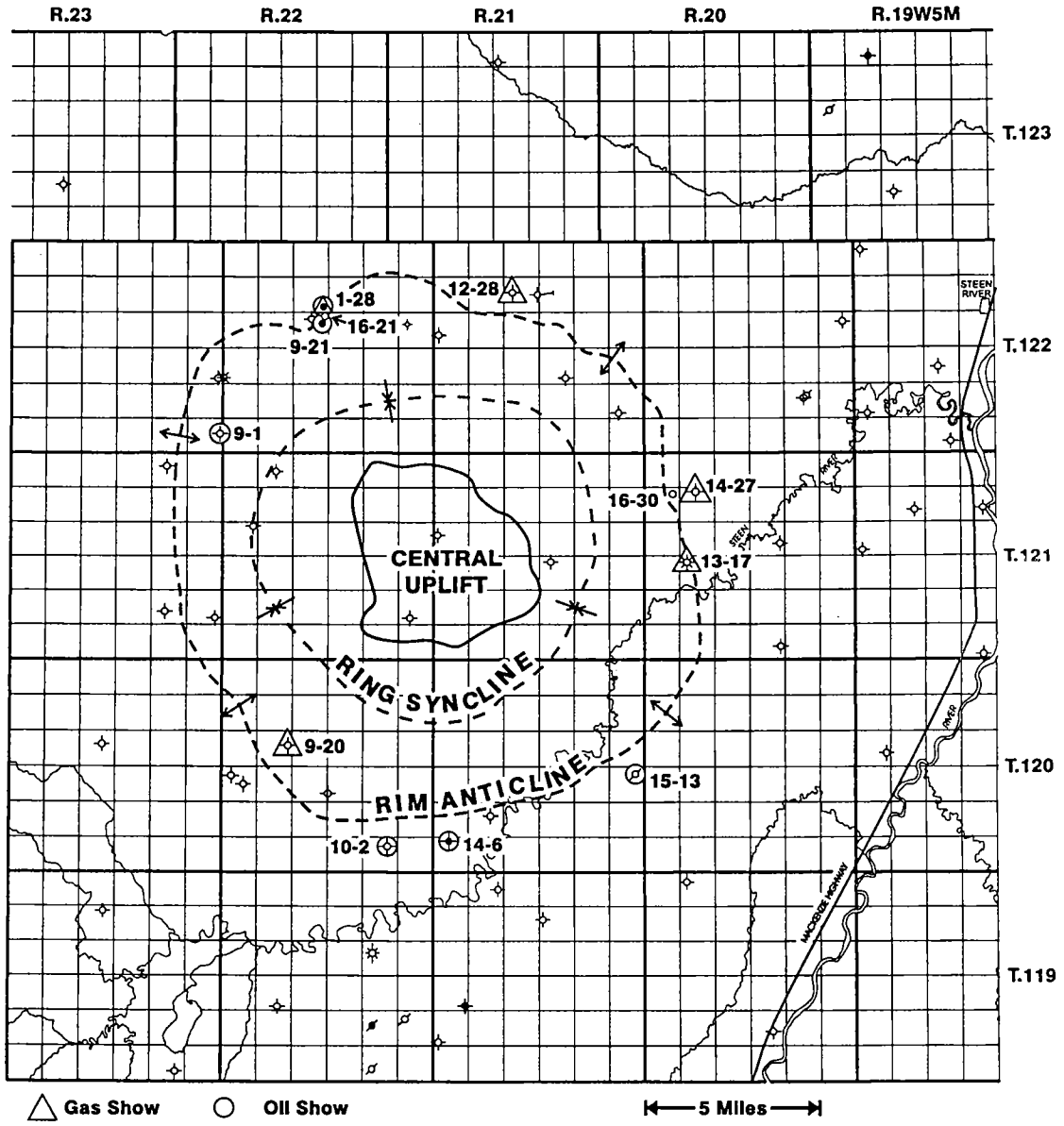

Figure 2. Sketch indicating structural components of the Steen River impact feature. Hydrocarbon-show wells are identified.

OIL DISCOVERIES

Keg River Formation

Keg River Formation oil was discovered on the northern rim of the feature in 1968 by the drilling and testing of Mobil Steen 1-28 (Lsd 1, 28-122-22 W5M). The well encountered 305 ft of oil-stained, fractured Keg River dolomite over the interval 4,263–4,568 ft, which was subsequently drill-stem tested and production tested through perforations at the rate of 312 barrels of fluid per day with a 5% water cut. Drill-stem test data suggest evidence of an oil/water contact on electrical logs at 4,890 ft (–2,509 ft subsea).

Because of its remote location and the lack of pipeline infrastructure, the Mobil Steen 1-28 discovery well remained shut-in until 1990 when it was purchased from Mobil Oil Canada by Kerr-McGee Canada Ltd. The no. 1-28 well was recompleted in March 1990 as a pumping Keg River oil well at rates approximating 300 BOPD (barrels of oil per day) with a water cut of 15%. Cumulative

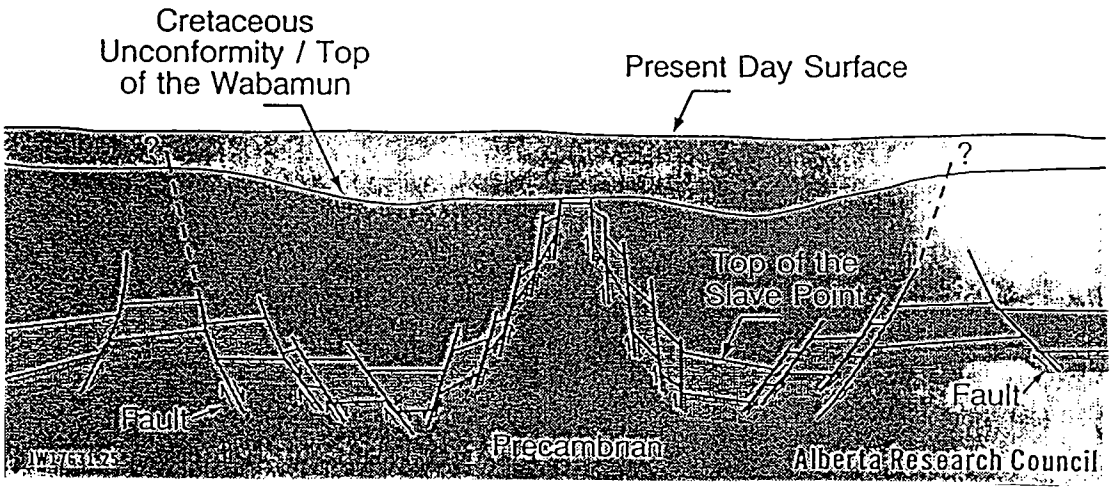

Figure 3. Diagrammatic cross section through the Steen River structure.

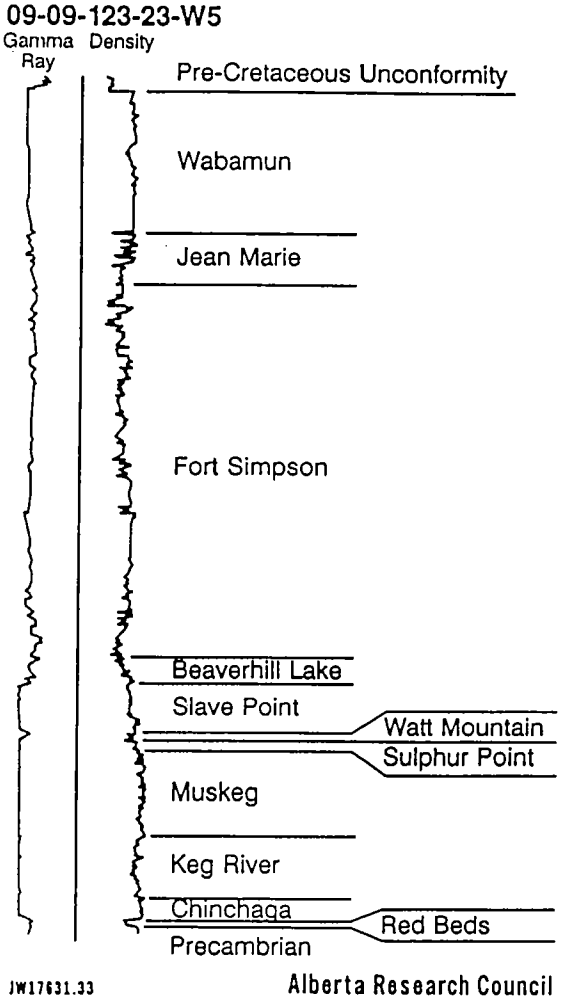

Figure 4. Stratigraphic section, Steen River area, Alberta.

production through November 1996 is 232,380 barrels of oil, 49,238 barrels of water, and 103,465 MCF (thousand cubic feet) of gas (the gas is flared). The most recent production rate (November 1996) after a pump workover in 1995 was 526 BOPD with an 18% water cut. This discovery well was followed up in 1968 by the Mobil Steen 15-21 (Lsd 15, 21-122-22 W5M), an abandonment, and by Diamond Shamrock Marlowe 9-21 (Lsd 9, 21-122-22 W5M), a Keg River oil well drilled in 1986. Through November 1, 1996, the two wells (9-21 and 1-28) in the Keg River pool have produced 425,000 barrels of oil.

The Keg River reservoir consists of highly fractured dolomite that exhibits poor to fair intercrystalline and small vug porosity. Core data indicate severe deformation and brecciation of the rock that in places show dips as steep as 45°. Fracturing of the rock is common and considerably enhances permeability of the reservoir dolomites.

Because of the lack of pipeline infrastructure and severe muskeg (boglike) conditions, the wells can produce for only four months per year (December through March) when the surface is frozen. This situation will prevail until there is sufficient daily production to justify the building of an 18-mi pipeline to the main highway immediately east of the oil pool. It is estimated that 2,000 to 3,000 BOPD production and attendant reserves are required to justify the line and convert the operation to a year-round status.

Mobil Oil Canada drilled Mobil W. Steen 9-1 (Lsd 9, 1-122-23 W5M) on the western part of the rim anticline in mid-1968. The well drill-stem tested the Keg River Formation over the interval 4,780–4,820 ft and recovered 456 ft of gassy 30°API oil and 119 ft of salt water. A completion was attempted, but the well was suspended in 1969 and finally abandoned in 1990. There is no record of production from the well.

Sulphur Point Member of the Muskeg Formation

In January 1987, Diamond Shamrock drilled and completed Diasham Russet 15-13 (Lsd 15, 13-120-21 W5M) on the southeastern side of the Steen River structure. This well was located on the rim anticline and resulted in a Middle Devonian Sulphur Point Member oil discovery from a 23-ft pay zone at 3,023–3,046 ft. Production test data indicate that the no. 15-13 well flowed 2,084 barrels of 31°API oil and 1,660 barrels of water in a 30-day period (February–March 1987). Because of the relatively low productivity and the remote location of the well, it was shut-in and suspended and remains so to date. Engineering data indicate that this well has a pumping potential of approximately 90 BOPD with associated water production.

Zamma Member of the Muskeg Formation

The first indication that the Zamma Member of the Muskeg Formation is oil bearing came from a production test in the Mobil Steen 1-28 (Lsd 1, 28-122-22 W5M) Keg River oil well. The Zamma Member yielded oil at the swab rate of 1 barrel per hour from perforations at 4,182–4,186 ft. This zone was then squeezed off, and the well was completed in the Keg River Formation.

Two exploratory wells drilled on the rim anticline at the south end of the Steen River structure—the Gardiner et al. Steen R. 14-6 (Lsd 14, 6-120-21 W5M) drilled in 1981 and the Gardiner et al. Russet 10-2 (Lsd 10, 2-120-22 W5M) drilled in 1982—encountered oil in the Zamma Member of the Muskeg Formation. The no. 14-6 well was completed in the Zamma Member and produced on pump 3,530 barrels of oil and 643 barrels of water from a depth of approximately 3,700 ft. The well was suspended in 1983 and subsequently abandoned in 1991. In the no. 10-2 well there was an attempted completion in the Zamma Member, but the completion failed; the well was suspended in 1982 and abandoned in 1991.

GAS DISCOVERIES AND SHOWS

Slave Point Formation

The Mobil Steen 1-28 (Lsd 1, 28-122-22 W5M) Keg River oil well also was the initial Middle Devonian Slave Point gas discovery well on the astrobleme. A drill-stem test of the lower Slave Point over the interval 3,598–3,698 ft yielded gas at 500 MCFGPD (thousand cubic feet of gas per day). The zone was subsequently perforated, acidized, and tested gas at rates up to 10,600 MCFGPD with a strong water spray at rates in excess of 4,000 MCFGPD. The pay zone is 54 ft thick with a possible further 18 ft of Upper Slave Point gas pay, which was not tested.

Natomas et al. Marlowe 13-17 (Lsd 13, 17-121-20 W5M) was drilled in 1978 and completed in 1979 as a suspended Slave Point Formation gas discovery. The well is located on the eastern side of the megafeature on the rim anticline. A drill-stem test of the interval 2,658–2,675 ft flowed gas at the stabilized rate of 1,063 MCFGPD. Production tests through perforations at the base of a 45 ft pay zone gave flows up to 3,100 MCFGPD without any acid treatment. The well is shut-in and awaiting a pipeline connection.

Several other wells drilled on the rim anticline of the Steen River structure yielded gas flows from the Slave Point Formation. Shell Steen River 14-29 (Lsd 14, 29-121-20 W5M) on the east side of the structure flowed gas at the rate of 60 MCFG from a drill-stem test of a 30 ft porous zone. Imperial Russet Cr. 9-20 (Lsd 9, 20-120-22 W5M) on the southwest side of the megafeature's rim anticline flowed gas from the Slave Point Formation over the interval 2,991–3,006 ft at the rate of 124 MCFGPD with a recovery of 150 ft of sulfurous salt water.

Sulphur Point Member of the Muskeg Formation

Gulf AEC Marlowe 12-28 (Lsd 12, 28-122-21 W5M) was drilled in 1984 on the northwest side of the Steen River structure on its rim anticline. A drill-stem test of the Sulphur Point interval from 3,028 to 3,091 ft yielded 1,673 MCFGPD and a recovery of 105 ft of salt water. The well was subsequently abandoned.

Keg River Formation

There has been one minor show of gas associated with the Steen River structure from the Middle Devonian Keg River Formation. Natomas et al. Marlowe 13-17 (Lsd 13, 17-121-20 W5M) drill-stem tested the interval 3,505–3,575 ft and had gas to surface immediately at a very strong rate that could not be measured owing to a heavy mud and water spray. The rising water in the drill-stem shut off the gas flow and the DST recovered 3,400 ft of salt water.

CONCLUSIONS

Interest in the Steen River megastructure was reactivated with the latest phase of exploration activity, which commenced in late 1994. Since November 1994, 81,280 acres (127 sections) have been leased over the feature. It is interesting to note that some 25 to 30% of the rim anticline of the Steen River structure remains unleased and available for future Alberta Petroleum and Natural Gas Crown postings. This unleased part of the megastruture that has been relatively underexplored is believed to have excellent hydrocarbon potential.

The high rates of production that have been achieved from vertical wells penetrating these

highly fractured reservoirs may be enhanced considerably by horizontal-drilling techniques. To date, no horizontal drilling has been undertaken on the Steen River structure.

In late winter of 1997 (March or April), a new natural gas line is being constructed by the Nova Corporation. This line will tie the northwestern Bistcho gas fields to the Alberta Nova system for the first time. The Bistcho field terminus will be located in Twp 122-2 W6M, approximately 20 mi due west of the Bearspaw et al. 1-28 (Lsd 1-28-122-22 W5M) potential Slave Point Formation shut-in gas well. This gas line should act as a catalyst to renew natural gas exploration interest in the Steen River area.

ACKNOWLEDGMENTS

I thank the Alberta Research Council, the Alberta Geological Survey, and the following authors for allowing me to reproduce several of the diagrams included in this paper (Figs. 1, 3, 4). The diagrams accompanied an unpublished internal proposal by the Alberta Geological Survey, 1989, entitled "Proposal for Scientific Drilling on the Steen River Structure, Northwest Alberta" by John Wilson, Willem Langenberg (Alberta Geological Survey), Lynn Jeffries (Husky Oil), Jeff Tooth (Maxus Energy), Richard Grieve (Geological Survey of Canada), and Zoltan Berkes (University of Alberta).

SELECTED REFERENCES

Garrigy, M. A., 1968, Evidence of shock metamorphism in rocks from the Steen River structure, Alberta, *in* French, B. M.; and Short, N. M. (eds.), Shock metamorphism of natural materials: Mono Books Corp., Baltimore, p. 367–378.

Winzer, S. R, 1972, The Steen River astrobleme, Alberta, Canada: 24th International Geological Congress, Montreal, section 15, p. 148–156.

The Calvin Impact Structure, Cass County, Michigan: Identification and Analysis of a Subsurface Ordovician Astrobleme

Randall L. Milstein
Oregon State University
Corvallis, Oregon

The Calvin impact structure is an isolated, nearly circular subsurface structure of Late Ordovician age centered 1.4 km south of the village of Calvin Center, Cass County, Michigan (Fig. 1). Owing to the severity of subsurface disruption observed at the Calvin structure, as well as questions surrounding the structure's origin, the Michigan Geological Survey considers it the most anomalous and enigmatic subsurface geologic feature in the Michigan basin (Milstein, 1988). At Upper Cambian and Lower Ordovician levels, the structure consists of a central domal uplift bounded by an annular depression and an encircling anticlinal rim (Figs. 2,3). These structural characteristics are reflected, to some degree, throughout the entire overlying stratigraphy, appearing as subtle surface expressions. The structure has a rim-to-rim diameter of 6.3 km and an overall dimensional diameter of 8.5 km.

Exploration and development of three Devonian oil fields associated with this structure have provided all available data. Of the 110 wells drilled into the three oil fields, 72 were oil wells, 5 were nonproducing gas wells, and 33 were dry holes. As of January 1997, all production is from the Middle Devonian Traverse Limestone with the exception of one well producing from the Sylvania Sandstone.

The Calvin structure involves large-scale and intense structural deformation within a limited area of circular shape. Lithologic and structural evidence suggests that the feature was the result of a single explosive event resulting in a sudden, highly localized release of tremendous energy. Speculation as to the possible origin of such a large-scale explosive structure includes both endogenetic and exogenetic processes. Summaries of both arguments for the origin of the Calvin structure are given by Milstein (1986,1994).

Nine characteristics of the Calvin structure lend support to its origin by impact:

1. The Calvin structure exhibits morphological characteristics consistent with those of a complex impact structure in a sedimentary target: an overall circular shape, with a central uplift, surrounding annular depression, and a peripheral anticline.

2. The Calvin structure is an isolated feature involving intense localized, large-scale deformation in otherwise flat-lying strata, with the structural and lithologic deformation decreasing with depth beneath and distance away from the structure.

3. The Calvin structure exhibits recognized relationships between overall structural diameter, observable stratigraphic displacement, and final crater form commonly used in the identification of surface impact craters.

4. Reflection seismic profiles, gravity and magnetic signatures, and resistivity data suggest that Calvin's subsurface structural morphology results in geophysical patterns analogous to those observed at recognized impact structures with similar lithologic components (Figs. 3,4).

5. A polymictic microbreccia is present within the disturbed zone of the Calvin structure. The microbreccia is composed of fractured and unfractured, subrounded to rounded, floating quartz grains imbedded in a carbonate matrix or floating shardlike carbonate fragments cemented in a carbonate matrix.

6. Individual quartz grains recovered from within the disturbed zone of the Calvin structure exhibit single and multiple sets of decorated shock lamellae, Böhm lamellae, rhombohedral cleavage, and radiating concussion fractures. The identification of shock-metamorphosed quartz, a characteristic considered indicative of impact-cratering

Randall L. Milstein, Oregon State University, College of Science, Corvallis, OR 97331.

Milstein, R. L., 1997, The Calvin impact structure, Cass County, Michigan: identification and analysis of a subsurface Ordovician astrobleme, *in* Johnson, K. S.; and Campbell, J. A. (eds.), Ames structure in northwest Oklahoma and similar features: origin and petroleum production (1995 symposium): Oklahoma Geological Survey Circular 100, p. 391–393.

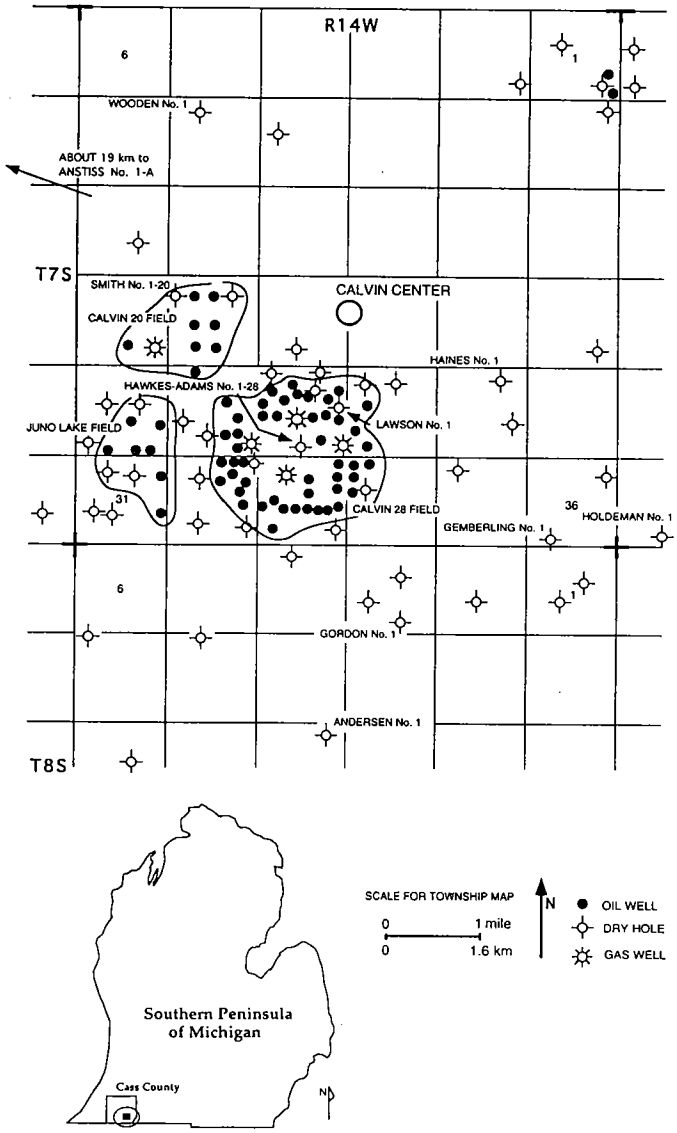

Figure 1. Location map of the Calvin impact structure, Cass County, Michigan.

events, strongly confirms the Calvin structure as an Ordovician astrobleme.

7. No igneous material is associated with the Calvin structure. Mineralization attributable to hydrothermal or known volcanic processes has not been recognized in well samples. The microbreccias associated with the structure contain no volcanic material.

8. The event responsible for the Calvin structure's origin is estimated to have released at least 5.9×10^{18} J of energy, without the development of magma or production of any true volcanic or igneous material.

9. Black metallic microspherules similar to those associated with meteoritic ablation and impact ejecta were identified in sample cuttings from test wells located in close proximity to the Calvin structure. The particles were recovered from a restricted stratigraphic interval of the Ordovician Richmond Group that is isochronous with the genesis of the Calvin structure. The surface textures and interior structures of the black metallic microspherules resemble those characteristics for numerous other extraterrestrial microspherules recovered from later geologic ages by other workers, as reported in the literature; however, the major element ratios of the Calvin microspherules, determined by neutron activation and electron-microprobe analyses, differ significantly. In addition to the black metallic microspherules, a second population of pyrite microspherules was recovered from the same stratigraphic interval. The pyrite microspherules closely resemble pyrite particles associated with extraterrestrial-component-rich layers identified in sedimentary units at the K/T boundary in western Europe and at the Permian/Triassic boundary in China.

The identification of astroblemes in the subsurface is rare. Comparison of the Calvin structure to known or suspected astroblemes suggests consistent structural and physical analogues. Although a considerable body of interpretive geophysical and structural data favors an impact origin for the Calvin structure, it is the identification of shock-metamorphosed quartz that most strongly confirms the structure as an Ordovician astrobleme. On the basis of the available data, I conclude that the subsurface Calvin structure is a buried complex impact structure and suggest that it be formally recognized as the Calvin impact structure.

REFERENCES CITED

Milstein, R. L., 1984, Impact origin of the Calvin 28 cryptoexplosive disturbance, Cass County, Michigan: University of Northern Colorado unpublished M.A. thesis, 87 p.

_____ 1988, Impact origin of the Calvin-28 cryptoexplosive disturbance, Cass County, Michigan: Michigan Geological Survey Report of Investigation 28, 33 p.

_____ 1994, The Calvin impact crater, Cass County, Michigan: identification and analysis of a subsurface Ordovician astrobleme: Oregon State University unpublished Ph.D. dissertation, 114 p.

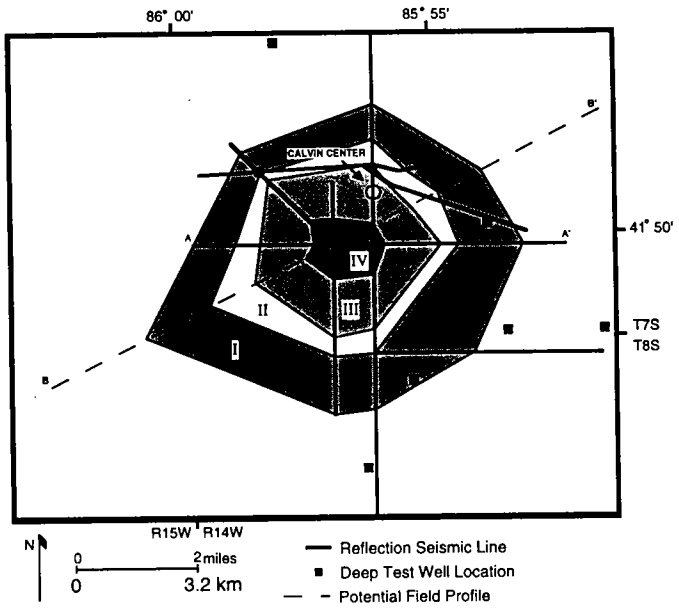

Figure 2 *(left)*. Areal extent and radial zonation of the Calvin impact structure at the Upper Cambrian level. I—anticlinal rim zone, II—terrace, III—annular basin, IV—central uplift.

Figure 3 *(below)*. Interpretive structural cross section along seismic profile A–A′ through the Calvin impact structure (location shown in Fig. 2).

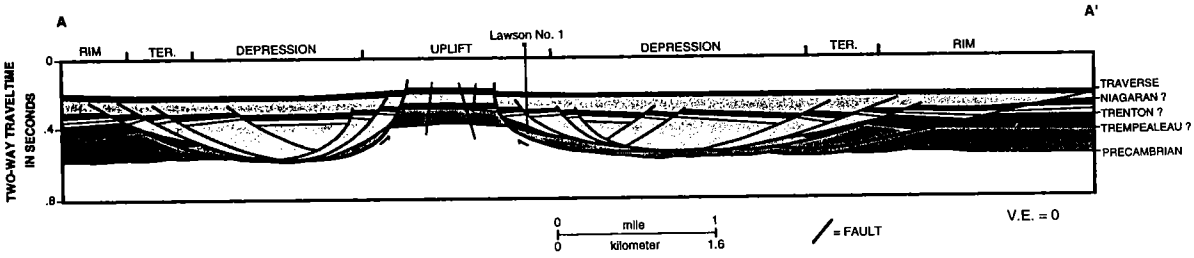

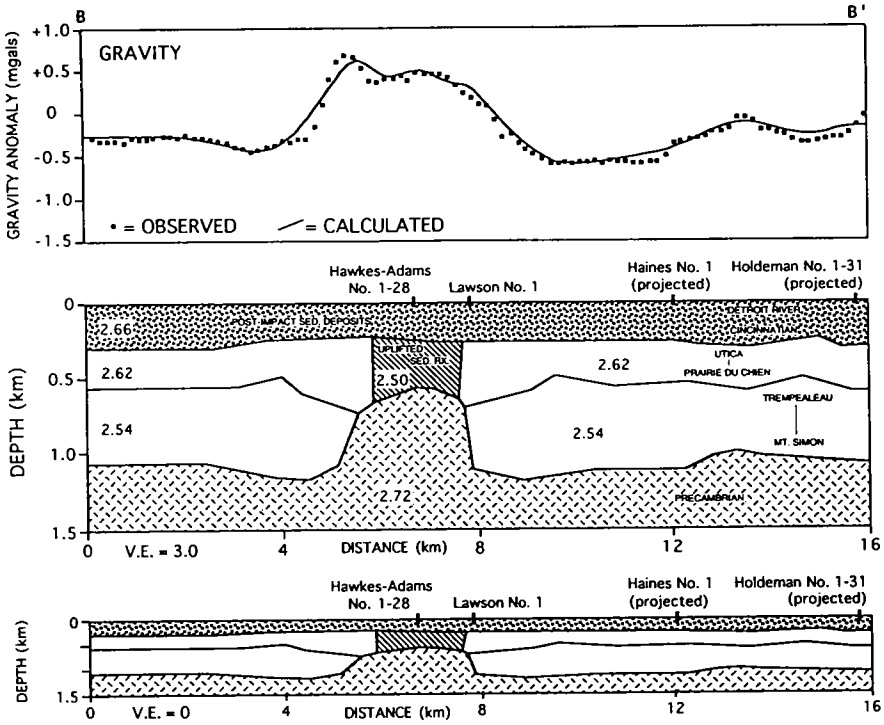

Figure 4 *(left)*. Two-dimensional residual gravity anomaly along profile B–B′ through the Calvin impact structure (location shown in Fig. 2). Density values for the model are given in g/cm^3 and are values derived from geophysical well logs.

Red Creek Impact (Precambrian), Eastern Uinta Mountains, Northeast Utah: 125 Years of Mistaken Identity

Howard R. Ritzma
Consulting Geologist
Salt Lake City, Utah

The contact between high-grade metamorphic rocks, the Red Creek Quartzite (or Red Creek Complex where it includes various rock types), and a thick (>7,700 m) sequence of metasedimentary rocks, the Uinta Mountain Group, was viewed by J. W. Powell in 1868 and 1871. Powell (1876) envisioned this contact as an unconformity involving younger sediments (the Uinta Mountain Group—ferruginous sandstone and shale with an interbedded massive sequence of conglomerate, composed of quartzite cobbles cemented by ferruginous sandstone, siltstone, and claystone) deposited against a gigantic headland of ancient metamorphic rocks (the Red Creek Quartzite—white, vitreous, nearly pure quartzite where Powell observed it). Although in some places, this contact is diffuse over a few to 30 m, it is a knife-edge where Powell saw it. At that location, the bedding of the Uinta Mountain Group is 75° to nearly vertical, and the contact actually cuts across individual Uinta Mountain Group cobbles and boulders. There are relict masses of Uinta Mountain Group rocks within the Red Creek Quartzite in some places along the contact. The conglomerate at the Powell "classic" section has been named the Jesse Ewing Canyon Formation (Sanderson and Wiley, 1986).

Powell's eloquent and inventive explanation for the highly unusual juxtaposition of these rock groups has endured. As detailed mapping began, an intricate and largely nonexistent tracery of faults was contrived to support Powell's concept (Hansen, 1965; and other publications).

There are other views, however (Marsh, 1871; Weeks, 1907; Hinds, 1935–36; Ritzma, 1959,1960, 1987; Ritzma, unpublished, 1992). Weeks, Hinds, and Ritzma recognized the contact as metamorphic, not an unconformity. I now propose that the metamorphism and resulting contact were formed by meteorite impact. The contact represents the point at which the quartzitic melt being violently driven into the conglomerate and other sediments chilled and suddenly stopped.

The scenario: a large meteorite struck a surface on which the Uinta Mountain Group was exposed about 1,500–1,550 Ma (whole-rock K-Ar dates; Hansen, 1965; Ritzma, unpublished). A crater 1.6 to possibly >3 km deep and >10 to possibly >25 km in diameter was excavated in Uinta Mountain Group ferruginous sandstones and shales. Target rocks (Uinta Mountain Group) were shattered, vaporized, melted, and reconstituted via this impact metamorphism into quartzite, schist, amphibolite, granite, and other rocks (Red Creek Complex). The relict masses of Uinta Mountain Group rocks within the Red Creek Complex along the contact represent only partially melted and assimilated material.

Only the upper, youngest part of the Uinta Mountain Group was metamorphosed by the impact, i.e., the upper 1,600–3,000 m out of the total 7,700 m (or thicker) section. The remarkable process is displayed over about 35 km² of Red Creek Complex outcrops along the north flank of the Uinta Mountains in the vicinity of Flaming Gorge Dam and Reservoir (Flaming Gorge National Recreation Area) and extending for a short distance into Colorado to the east. The most diagnostic crater-wall contact between the Red Creek Complex and the Uinta Mountain Group is exposed along the east wall of Jesse Ewing Canyon, 25 km east of Flaming Gorge Dam and 6.5 km southeast of Clay Basin gas field, Daggett County, Utah. The chaotic, variable contact zone at this location is replete with impact features including baked and recrystallized Uinta Mountain Group rocks along the metamorphic contact as well as undigested

Howard R. Ritzma, P.O. Box 58736, Foothill Station, Salt Lake City, UT 84158.

Ritzma, H. R., 1997, Red Creek impact (Precambrian), eastern Uinta Mountains, northeast Utah: 125 years of mistaken identity, *in* Johnson, K. S.; and Campbell, J. A. (eds.), Ames structure in northwest Oklahoma and similar features: origin and petroleum production (1995 symposium): Oklahoma Geological Survey Circular 100, p. 394–395.

fragments of Uinta Mountain Group floating as xenoliths in Red Creek Quartzite. Abundant shocked quartz is present in thin sections. Although much evidence has been eroded, presumably even more lies at depth beneath younger strata along the overthrust north flank of the Uinta Mountain arch.

Recognition that this contact was formed by meteorite impact makes profound changes in the interpretation of the geology of the Uinta Mountains and the surrounding region. The Uinta Mountain Group is the oldest Precambrian unit in the Uinta Mountains, and its base is not seen (Marsh, 1871). It may be as old as early Proterozoic or late Archean.

REFERENCES CITED

Hansen, W. R., 1965, Geology of the Flaming Gorge area, Utah-Colorado-Wyoming: U.S. Geological Survey Professional Paper 490, 196 p.

Hinds, N. E. A., 1935, Ep-Archean and Ep-Algonkian intervals in western North America: Carnegie Institution of Washington Publication 463, p. 1–52.

_____ 1936, Uncompahgran and Beltian deposits in western North America: Carnegie Institution of Washington Publication 463, p. 53–136.

Marsh, O. C., 1871, On the geology of the eastern Uinta Mountains: American Journal of Science, 3rd ser., v. 1, p. 191–198.

Powell, J. W., 1876, Report on the geology of the eastern portion of the Uinta Mountains, and the region of the country adjacent thereto: U.S. Geological and Geographical Survey of the Territories, 218 p.

Ritzma, H. R., 1959, Geologic atlas of Utah, Daggett County: Utah Geological and Mineralogical Survey Bulletin 66, 111 p.

_____ 1960, Precambrian rocks of the eastern Uinta Mountains, Utah-Colorado, a new concept [abstract]: Geological Society of America Bulletin, v. 71, p. 2039–2040.

_____ 1987, Basement in the Uintas: an enigma? [abstract]: American Association of Petroleum Geologists Bulletin, v. 71, p. 1014.

Sanderson, I. D.; and Wiley, M. T., 1986, The Jesse Ewing Canyon formation, an interpreted alluvial fan deposit in the basal Uinta Mountain group (middle Proterozoic), Utah: The Mountain Geologist, v. 23, p. 77–89.

Weeks, F. B., 1907, Stratigraphy and structure of the Uinta Range: Geological Society of America Bulletin, v. 18, p. 427–448.

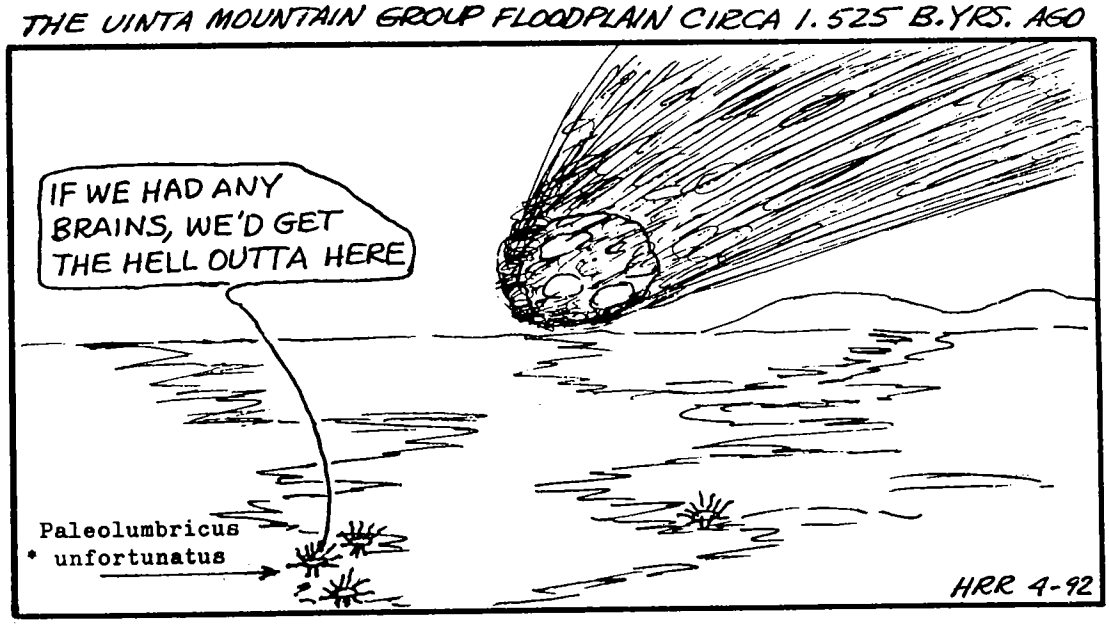

*An ambitious, advanced tubeworm that became extinct 1.525 billion yrs. ago

The Big Basin Impact Craters of Western Kansas

P. Jan Cannon
Planetary Data
Tecumseh, Oklahoma

ABSTRACT.—A sharply defined basin, 1,300 m in diameter, 35 m deep, and with internal drainage, is located 35 mi south of Dodge City, Kansas. This feature is named Big Basin on topographic maps of the region. It has been considered to be of solution origin.

Remote-sensing investigations of the area revealed that the feature had two small satellite pits approximately 300 m in diameter. This cluster of holes is an isolated phenomenon in this area. However, the cluster of one large crater and two nearby smaller ones is similar to numerous primary impact-crater clusters found on other planets. This type of clustering is not found in areas of karst.

The remote-sensing data further indicated prominent radial fracture sets and a polygonal shape that reflects the regional fractures.

Subsequent field work revealed that the strata on the rim of the larger hole dip radially away from the center of the feature. The rim and wall materials are intensely fractured.

These observations are indicative of impact features and not solution features.

When, the Big Basin Crater is physically compared with Meteor Crater, Arizona, and Upheaval Dome, Utah, it shows a close similarity to Meteor Crater, Arizona. This similarity is indicated by polygonal shape, size, and radial features. Big Basin appears to be partially filled with wall and rim materials. It is more eroded than Meteor Crater, Arizona. Based on the extent of erosion and the slight difference in climate, I estimate the age of the Big Basin Crater to be between 80,000 and 100,000 yr.

The walls of the Big Basin Crater contain cherts that appear to have been partially extracted by early man for tools. Tektites are found beyond the rim area.

P. Jan Cannon, Planetary Data, 302 East Locust,
Tecumseh, OK 74873.

Cannon, P. J., 1997, The Big Basin impact craters of western Kansas, *in* Johnson, K. S.; and Campbell, J. A. (eds.), Ames structure in northwest Oklahoma and similar features: origin and petroleum production (1995 symposium): Oklahoma Geological Survey Circular 100, p. 396.